THE JOURNAL OF CHEMICAL PHYSICS

Volume 23 Number 10

OCTOBER, 1955

Published by the
AMERICAN INSTITUTE OF PHYSICS
Lancaster Press, Inc., New York, N.Y.

...TORS

...Editor

...

...

...

THE JOURNAL
OF
CHEMICAL PHYSICS

VOLUME 23, NUMBER 10 OCTOBER, 1955

Anomalous Dielectric Dispersion in Polar Macromolecular Solutions*

W. G. HAMMERLE AND J. G. KIRKWOOD
Sterling Chemistry Laboratory, Yale University, New Haven, Connecticut
(Received January 17, 1955)

The Kirkwood and Fuoss theory of dielectric dispersion in polymer solutions is recalculated by including the Oseen hydrodynamic interactions in the polymer's diffusion tensor. The theoretical results agree with experiment where comparison is possible. The recalculation gives root-mean-square molecular dimensions consistent with values calculated from viscosity and light scattering.

I

POLAR macromolecular solutions exhibit an anomalous dielectric dispersion quite different from the dispersion in solutions of small polar molecules. For polymers, the frequency of maximum dispersion is generally lower than for simple molecules, and the loss depends upon the polymer's concentration and molecular weight as well as upon the temperature and frequency. The dielectric loss extends over several decades of frequency and cannot be explained by a single Debye relaxation time, a distribution of relaxation times being necessary.

A theoretical treatment of the dielectric dispersion has been given by Kirkwood and Fuoss.[1] In this theory (hereafter referred to as *I*), it is assumed that the bond lengths and bond angles of each polymer molecule are constant, but that the azimuth angles are free to rotate. When no external field is applied to the solution, the macromolecule forms a random coil in which the azimuth angles are continually changing under the thermal agitation of the solution. In the presence of an electric field, the azimuth angles tend to rotate so as to align the individual dipoles with the direction of the field. The dielectric dispersion accompanying this process may be calculated from the configurations of the molecules, which in turn are obtained from a solution of the appropriate diffusion equation. Because the rotations of the azimuth angles are coupled together by the constraints of constant bond lengths and bond angles, the diffusion equation must necessarily treat the entire macromolecule as a single system. Solution of the diffusion equation indicates that the molecular chain moves in sections of various length, with each section acting as a mechanical and electrical unit. The distribution of possible section lengths within a single molecule leads to the distribution of electrical relaxation times.

No interactions between polymer molecules are included in the theory, and it is directly applicable only to very dilute solutions. In a semiquantitative way, however, it agrees with the experimental behavior of polar macromolecules in fairly concentrated solutions.

More recently, a general theory of irreversible processes in macromolecular solutions has been developed which includes the dielectric dispersion as a particular case.[2] In applying the general theory to the mechanical properties of macromolecules,[3] it was found that the Oseen hydrodynamic interactions between segments of the polymer chain are quite important in determining the irreversible properties of the solution. For very long polymer chains, the hydrodynamic interactions become the overwhelming terms in the molecular diffusion tensor. However, the hydrodynamic interactions were not included in *I*. It is the purpose of this article to recompute the dielectric dispersion, including in the derivation the more complete diffusion tensor.

The experimental dielectric behavior of a solution is generally expressed in terms of the complex dielectric constant $\epsilon'-i\epsilon''$, where ϵ', the real dielectric constant, and ϵ'', the loss factor, are dependent upon the frequency $\omega/2\pi$ of the applied electric field. The results of

* This work was supported by the U. S. Office of Naval Research, under Contract Nonr 410(00) with Yale University.

[1] J. G. Kirkwood and R. M. Fuoss, J. Chem. Phys. **9**, 329 (1941).

[2] J. G. Kirkwood, J. Polymer Sci. **12**, 1 (1954).

[3] J. G. Kirkwood and J. Riseman, J. Chem. Phys. **16**, 565 (1948).

the theoretical derivation will be given in terms of $Q(\omega)$, the reduced dielectric polarization. $Q(\omega)$ is equal to $P(\omega)/P(0)$, where $P(\omega)$ is the polarization at frequency $\omega/2\pi$ and $P(0)$ is the polarization at zero frequency. The relationship between the dielectric constant and $Q(\omega)$ has been given previously and will not be reproduced here.[1,4]

II

The reduced polarization $Q(\omega)$ may be expressed in terms of a distribution of relaxation times $G(\tau)$:

$$Q(\omega)=\int_0^\infty \frac{G(\tau)d\tau}{1+i\omega\tau}. \tag{1}$$

For a polymer with unrestricted rotation of the azimuth angles, $G(\tau)$ is given by the following series of equations:

$$G(\tau)=\left[\lambda^2\frac{d\Omega(\lambda)}{d\lambda}\right]_{\lambda=1/\tau},$$

$$\Omega(\lambda)=\frac{1}{\langle(\boldsymbol{\mu}\cdot\mathbf{e}_3)^2\rangle}\sum_{\lambda'<\lambda}\mu_{\lambda'}\mu_{\lambda'}^*,$$

$$\mu_\lambda=f_0^{\frac{1}{2}}\int\boldsymbol{\mu}\cdot\mathbf{e}_3\psi_\lambda^*\sqrt{g}\prod_{\alpha=1}^{\nu}dq^\alpha, \tag{2}$$

$$L\psi_\lambda+\lambda\psi_\lambda=0,$$

$$L=\sum_{\alpha,\beta=1}^{\nu}\frac{1}{\sqrt{g}}\frac{\partial\sqrt{g}}{\partial q^\alpha}\left(D^{\alpha\beta}\frac{\partial}{\partial q^\beta}\right).$$

The total dipole moment of the molecule is $\boldsymbol{\mu}$, while $\mathbf{e}_3$ is the unit vector in the direction of the electric field. The normalization constant for $\Omega(\lambda)$ is the average of $(\boldsymbol{\mu}\cdot\mathbf{e}_3)^2$ over all possible configurations of the polymer molecule. L is a second-order differential operator in the coordinates $q^1,\cdots,q^\nu$ specifying the configuration of the macromolecule. The $D^{\alpha\beta}$ are the contravariant components of the diffusion tensor, and are given by

$$D^{\alpha\beta}=kT(g^{\alpha\beta}/\zeta+T^{\alpha\beta}),\quad T^{\alpha\beta}=\sum_{l,s=1}^{2n}T_{ls}{}^{\alpha\beta},$$

$$T_{ls}{}^{\alpha\beta}=\frac{1}{8\pi\eta_0|\mathbf{R}_{ls}|}\sum_{\sigma,\tau=1}^{\nu}g^{\alpha\sigma}g^{\beta\tau}\frac{\partial\mathbf{R}_l}{\partial q^\sigma}\cdot\left[1+\frac{\mathbf{R}_{ls}\mathbf{R}_{ls}}{|\mathbf{R}_{ls}|^2}\right]\cdot\frac{\partial\mathbf{R}_s}{\partial q^\tau}, \tag{3}$$

where the $g^{\alpha\beta}$ are the contravariant components of the metric tensor in the ν-dimensional space $q^1,\cdots,q^\nu$; ζ is the friction constant of an isolated structural element of the molecule, η_0 is the viscosity of the solvent, and the $T^{\alpha\beta}$ are the components of the Oseen hydrodynamic interaction tensor. $\mathbf{R}_l$ is a three-dimensional vector specifying the position of the lth structural element relative to some external coordinate system, and $\mathbf{R}_{ls}=\mathbf{R}_l-\mathbf{R}_s$. These equations are the same as were used in I to find $Q(\omega)$ except that $T^{\alpha\beta}$ is now included in the diffusion tensor.

We shall apply the equations for $Q(\omega)$ to the same type of linear polymer molecule as was considered in I. This polymer is of the form $(CH_2-CHX)_n$, in which X is a monatomic dipolar sidegroup. The chain may be divided into 2n elements each consisting of a skeletal carbon atom and its substituents; the elements are numbered from one end of the chain. $\mathbf{a}_k$ denotes the unit vector in the direction of the carbon bond from element $k-1$ to element k. If the bond lengths and bond angles are constant, the q^α specifying the configuration of the molecule are the azimuth angles along the chain:

$$\cos q^\alpha=\begin{cases}\dfrac{(\mathbf{a}_\alpha\times\mathbf{a}_{\alpha+1})\cdot(\mathbf{a}_{\alpha+1}\times\mathbf{a}_{\alpha+2})}{|\mathbf{a}_\alpha\times\mathbf{a}_{\alpha+1}|\,|\mathbf{a}_{\alpha+1}\times\mathbf{a}_{\alpha+2}|} & 2\leqslant\alpha\leqslant n-1\\[2ex] \dfrac{(\mathbf{a}_n\times\mathbf{a}_{n+1})\cdot(\mathbf{a}_{n+1}\times\mathbf{e}_3)}{|\mathbf{a}_n\times\mathbf{a}_{n+1}|\,|\mathbf{a}_{n+1}\times\mathbf{e}_3|} & \alpha=n\\[2ex] \dfrac{(\mathbf{a}_{n+2}\times\mathbf{a}_{n+1})\cdot(\mathbf{a}_{n+1}\times\mathbf{e}_3)}{|\mathbf{a}_{n+2}\times\mathbf{a}_{n+1}|\,|\mathbf{a}_{n+1}\times\mathbf{e}_3|} & \alpha=n+1\\[2ex] \dfrac{(\mathbf{a}_{\alpha+1}\times\mathbf{a}_\alpha)\cdot(\mathbf{a}_\alpha\times\mathbf{a}_{\alpha-1})}{|\mathbf{a}_{\alpha+1}\times\mathbf{a}_\alpha|\,|\mathbf{a}_\alpha\times\mathbf{a}_{\alpha-1}|}. & n+2\leqslant\alpha\leqslant 2n-1\end{cases}$$

In addition, two coordinates θ and ϕ are necessary to describe the rotation of the molecule relative to an external coordinate system $(\mathbf{e}_1,\mathbf{e}_2,\mathbf{e}_3)$:

$$\cos\theta=\mathbf{e}_3\cdot\mathbf{a}_{n+1},\ \cos\phi=\frac{(\mathbf{e}_3\times\mathbf{a}_{n+1})\cdot\mathbf{e}_2}{|\mathbf{e}_3\times\mathbf{a}_{n+1}|}.$$

The chain has three other degrees of freedom involving translation of the entire molecule relative to $(\mathbf{e}_1,\mathbf{e}_2,\mathbf{e}_3)$, but these coordinates may be neglected if the magnitude of the electric field is everywhere the same within the solution.

The covarient components of the metric tensor are given by

$$g_{\alpha\beta}=\sum_{l=1}^{2n}\frac{\partial\mathbf{R}_l}{\partial q^\alpha}\cdot\frac{\partial\mathbf{R}_l}{\partial q^\beta}. \tag{4}$$

If the molecule is very large ($n\gg1$), the center of the chain is almost stationary relative to the surrounding solvent. $\mathbf{R}_l$ may then be measured from the center of the $(n+1)$th bond, so that

$$\mathbf{R}_l\cong\begin{cases}a\sum_{k=n+2}^{l}\mathbf{a}_k & l\geqslant n+2\\ -a\sum_{k=l+1}^{n}\mathbf{a}_k & l\leqslant n-1,\end{cases} \tag{5}$$

[4] R. M. Fuoss and J. G. Kirkwood, J. Am. Chem. Soc. **63**, 385 (1941).

where a is the bond length. From the geometry of the chain it follows that

$$\frac{\partial \mathbf{R}_l}{\partial q^\alpha}=\begin{cases}\mathbf{a}_\alpha\times(\mathbf{R}_l-\mathbf{R}_\alpha) & n+1\leqslant\alpha\leqslant l\\ -\mathbf{a}_\alpha\times(\mathbf{R}_l-\mathbf{R}_\alpha) & l\leqslant\alpha\leqslant n\\ 0 & \alpha>l\geqslant n+1\\ 0 & \alpha<l\leqslant n,\end{cases} \tag{6}$$

$$\frac{\partial \mathbf{R}_l}{\partial\theta}=\mathbf{a}_\theta\times\mathbf{R}_l,\quad \frac{\partial \mathbf{R}_l}{\partial\phi}=\mathbf{e}_3\times\mathbf{R}_l,$$

where $\mathbf{a}_\theta$ is the unit vector in the direction of $\mathbf{e}_3\times\mathbf{a}_{n+1}$. Also, it may be shown that

$$\mathbf{a}_k=\begin{cases}\mathbf{A}(\theta,\phi)\cdot\mathbf{A}(\gamma,q^{n+1})\cdot\mathbf{A}(\gamma,q^{n+2})\cdot\ldots\cdot\mathbf{A}(\gamma,q^{k-1})\cdot\mathbf{e}_3 & k\geqslant n+1\\ \mathbf{A}(\theta,\phi)\cdot\mathbf{A}(\gamma,q^{n})\cdot\mathbf{A}(\gamma,q^{n-1})\cdot\ldots\cdot\mathbf{A}(\gamma,q^{k+1})\cdot\mathbf{e}_3 & k\leqslant n,\end{cases} \tag{7}$$

where γ is the supplement of the bond angle and

$$\mathbf{A}(\theta,\phi)=\begin{bmatrix}\cos\theta\cos\phi & -\sin\phi & \sin\theta\cos\phi\\ \cos\theta\sin\phi & \cos\phi & \sin\theta\sin\phi\\ -\sin\theta & 0 & \cos\theta\end{bmatrix}. \tag{8}$$

From (4), (5), (6), (7), and (8), $g_{\alpha\beta}$ may be expressed in terms of the q^α. In theory, the contravariant components $g^{\alpha\beta}$ may be obtained from

$$g^{\alpha\beta}=|g|_{\alpha\beta}/g, \tag{9}$$

$|g|_{\alpha\beta}$ being the appropriate minor of the determinant g. ${T_{ls}}^{\alpha\beta}$ and $D^{\alpha\beta}$ then follow from (3). In practice, however, inversion of the metric tensor is impossibly complicated and some approximation to $g_{\alpha\beta}$ is necessary. We shall employ the same approximation as was used in I: $g_{\alpha\beta}$ is replaced by $\langle g_{\alpha\beta}\rangle$, its average over all configurations of the molecule. To facilitate the computations, γ is assumed to be 90°. By the averaging process described in Appendix I of I, it is found that $\langle g_{\alpha\beta}\rangle$ is diagonal, and

$$\begin{aligned}&g^{\alpha\beta}=\langle g_{\alpha\beta}\rangle^{-1}=3\delta_\alpha{}^\beta/a^2(n-|n-\alpha|)^2,\\ &g^{\theta\theta}=g^{\phi\phi}=\langle g_{\theta\theta}\rangle^{-1}=3/2n^2a^2,\\ &g^{\theta\phi}=g^{\theta\alpha}=g^{\phi\alpha}=0.\end{aligned} \tag{10}$$

This metric tensor may be substituted into (3) to find ${T_{ls}}^{\alpha\beta}$ and $D^{\alpha\beta}$. However, the resultant diffusion tensor is still too complicated for solution of (2), and ${T_{ls}}^{\alpha\beta}$ must also be replaced by its average over all configurations:

$${T_{ls}}^{\alpha\beta}=\frac{1}{8\pi\eta_0}\left\langle\sum_{\sigma,\tau=1}^{\nu}\langle g_{\alpha\sigma}\rangle^{-1}\langle g_{\beta\tau}\rangle^{-1}|\mathbf{R}_{ls}|^{-1}\frac{\partial \mathbf{R}_l}{\partial q^\sigma}\cdot\times\left[1+\frac{\mathbf{R}_{ls}\mathbf{R}_{ls}}{|\mathbf{R}_{ls}|^2}\right]\cdot\frac{\partial \mathbf{R}_s}{\partial q^\tau}\right\rangle. \tag{11}$$

The errors in the dielectric dispersion resulting from the above approximations are unknown.

Replacement of ${T_{ls}}^{\alpha\beta}$ by its average leads to the following diffusion tensor (Appendix I):

$$\begin{aligned}&D^{\alpha\beta}=A\left(1-\left|\frac{\alpha-n}{n}\right|\right)^{-2}\delta_\alpha{}^\beta+B\left(1-\left|\frac{\alpha-n}{n}\right|\right)^{-\frac{1}{2}}\delta_\alpha{}^\beta,\\ &D^{\theta\theta}=D^{\phi\phi}=(A+B)/2,\\ &D^{\theta\phi}=D^{\theta\alpha}=D^{\phi\alpha}=0,\\ &A=\frac{3kT}{\zeta a^2n^2},\quad B=\frac{16kT}{15\pi a^3\eta_0 n^{\frac{1}{2}}}\left(\frac{6}{\pi}\right)^{\frac{1}{2}}.\end{aligned} \tag{12}$$

From the last equation of (2) we find that

$$\begin{aligned}L=\tfrac{1}{2}(A+B)\Bigg[&\frac{1}{\sin\theta}\frac{\partial}{\partial\theta}\left(\sin\theta\frac{\partial}{\partial\theta}\right)+\frac{1}{\sin^2\theta}\frac{\partial^2}{\partial\phi^2}\Bigg]\\ &+A\sum_{i=2}^{2n-1}\left(1-\left|\frac{i-n}{n}\right|\right)^{-2}\frac{\partial^2}{\partial q^{i2}}\\ &+B\sum_{i=2}^{2n-1}\left(1-\left|\frac{i-n}{n}\right|\right)^{-\frac{1}{2}}\frac{\partial^2}{\partial q^{i2}}.\end{aligned} \tag{13}$$

The eigenfunctions and eigenvalues of this operator are

$$\begin{aligned}\psi_\lambda=&\left[\frac{(2K+1)(K-|m|)!}{4\pi(K+|m|)!}\right]^{\frac{1}{2}}(2\pi)^{-n+1}\\ &\times P_K{}^m(\cos\theta)e^{\sqrt{-1}m\phi}\prod_{i=2}^{2n-1}\exp(\sqrt{-1}m_iq^i)\\ \lambda=&\tfrac{1}{2}(A+B)K(K+1)+A\sum_{i=2}^{2n-1}\left(1-\left|\frac{i-n}{n}\right|\right)^{-2}m_i{}^2\\ &+B\sum_{i=2}^{2n-1}\left(1-\left|\frac{i-n}{n}\right|\right)^{-\frac{1}{2}}m_i{}^2.\end{aligned} \tag{14}$$

The ratio of A to B is proportional to $n^{-\frac{1}{2}}$, and becomes small as the molecule increases in length. In the following equations, we shall neglect the terms proportional to A, a procedure which gives the asymptotic approximation to $Q(\omega)$ for large n. The importance of the hydrodynamic interactions may be seen directly here, because the terms proportional to B are due solely to the interactions. What are now the asymptotically negligible terms were the only ones to appear in the derivation in I.

The next step in finding the dielectric dispersion is to evaluate $\mu_\lambda\mu_\lambda{}^*$ from the third equation of (2). Introduction of the hydrodynamic interactions into the diffusion tensor has changed the eigenvalues λ but has not altered the eigenfunctions ψ_λ. It follows that the μ_λ are

the same as in I:

$$\mu_\lambda\mu_\lambda^*=\mu_X^2(\tfrac{1}{2})^{2\sigma}Y^2(K,m,m_i)\prod_{i=n+s+1}^{2n-1}\delta_{m_i}{}^0\prod_{i=2}^{n}\delta_{m_i}{}^0,$$

$$\sigma=\sum_{i=2}^{2n-1}m_i^2,$$

$$Y(K,m,m_i)=\delta_m{}^0(1)_{n+s}\prod_{i=n+2}^{n+s-1}[(1)_i+(1)_{i+1}(1)_{i-1}\delta_{m_i}{}^0] \quad (15)$$

$$\times\left[\frac{1}{\sqrt{3}}\delta_K{}^1\delta_{m_{n+1}}{}^0(1)_{n+2}+\sum_{\beta=0}^{\infty}\frac{c_\beta}{(2\beta+1)^{\frac{1}{2}}}\delta_K{}^\beta(1)_{n+1}\right],$$

$$(1)_i=\delta_{m_i}{}^1+\delta_{m_i}{}^{-1}.$$

μ_X is the dipole moment associated with each C−X bond, and the c_β are the expansion coefficients of $\sin\theta$ in Legendre polynomials of $\cos\theta$:[5]

$$c_0=\pi/4,\quad c_1=0,$$
$$c_{\beta+2}=\frac{(\beta-1)(\beta+1)(2\beta+5)}{(\beta+2)(\beta+4)(2\beta+1)}c_\beta. \quad (16)$$

Equation (15) applies only when $s>0$; a corresponding equation may be written when the nonzero m_i lie in the lower half of the chain. The foregoing $Y(K,m,m_i)$ is not quite the same as the $Y(m',m)$ given in I. This difference arises because the order of the matrices in (7) is reversed from the order used in I, which is erroneous. The change in $Y(m',m)$ does not affect the final results for the dispersion.

It might be pointed out that the above $\mu_\lambda\mu_\lambda^*$ applies to a polymer chain in which the C−X bond on the ith carbon atom is perpendicular to $\mathbf{a}_i$ and 120° from $\mathbf{a}_{i+1}$. The average dipole moment of such a model differs slightly from the moment of a tetrahedral chain.[6]

The $\mu_\lambda\mu_\lambda^*$ may now be substituted into the second equation of (2) to find $\Omega(\lambda)$. To do this, let us consider the set of nonzero expansion coefficients corresponding to a specific σ, s, and K. From (15) it follows that μ_λ either is zero or has an absolute magnitude dependent only upon σ, s, and K, i.e., the set of $\mu_\lambda\mu_\lambda^*$ under consideration all are equal. Furthermore, from (14) it may be seen that the corresponding eigenvalues are not very widely distributed in magnitude. Thus the contribution of the set to $\Omega(\lambda)$ may be approximated by a single term of magnitude $N(\bar\lambda)\mu_{\bar\lambda}\mu_{\bar\lambda}^*$, where $N(\bar\lambda)$ is the total number of nonzero μ_λ consistent with the specified σ, s, and K. This contribution occurs at λ equal to $\bar\lambda(\sigma,s,K)$, the average of all the corresponding eigenvalues. In other words,

$$\Omega(\lambda)\cong\frac{1}{\langle(\mathfrak{y}\cdot\mathbf{e}_3)^2\rangle}\sum_{\bar\lambda<\lambda}N(\bar\lambda)\mu_{\bar\lambda}\mu_{\bar\lambda}^*. \quad (17)$$

This approximation is the same as was used in I.

As an example of the calculation for $\Omega(\lambda)$ let us consider the case where $K=1$; from (15) it follows that the only contribution to $\Omega(\lambda)$ occurs when $m_{n+1}=0$ and $|m_{n+2}|=1$. The method for counting the eigenvalues is described in I, and gives

$$N(\bar\lambda)=2^{\sigma+1}\binom{\sigma-1}{s-\sigma-1}. \quad (18)$$

The additional power of two appears when both sides of the chain are included in $N(\bar\lambda)$. From (14), neglecting the term in K, we have

$$\bar\lambda=B\sum_{i=2}^{2n-1}\left(1-\left|\frac{i-n}{n}\right|\right)^{-\frac{1}{2}}\overline{m_i^2}. \quad (19)$$

The average value of m_i^2 consistent with the requirement that $Y(K,m,m_i)$ be nonzero is σ/s. By approximating the sum for $\bar\lambda$ by an integral over i, it follows that

$$\bar\lambda=\frac{2B\sigma n^{\frac{1}{2}}}{s}[(n-s)^{-\frac{1}{2}}-n^{-\frac{1}{2}}]. \quad (20)$$

In addition $\langle(\mathfrak{y}\cdot\mathbf{e}_3)^2\rangle$ equals $n\mu_X^2/3$. Combining (15), (17), (18), and (20) we find that the contribution to $\Omega(\lambda)$ for $K=1$ is

$$\Omega(\lambda)|_{K=1}=\frac{2}{n}\sum_{\sigma,s}(\tfrac{1}{2})^\sigma\binom{\sigma-1}{s-\sigma-1}. \quad (21)$$

The limits on this sum are $0\leqslant s\leqslant n$, $s/2\leqslant\sigma\leqslant s$, s even, and

$$\sigma\leqslant\lambda s\{2Bn^{\frac{1}{2}}[(n-s)^{-\frac{1}{2}}-n^{-\frac{1}{2}}]\}^{-1}. \quad (22)$$

For large σ and s, the sum may be evaluated quite accurately by replacing the binomial coefficient with its asymptotic approximation:

$$\Omega(\lambda)|_{K=1}=\frac{1}{n}\int_{s=0}^{n}\int_{\sigma=s/2}^{s}(2\pi\sigma)^{-\frac{1}{2}}\times\exp\left[-\frac{(2s-3\sigma)^2}{2\sigma}\right]d\sigma ds, \quad (23)$$

with (22) still to be added as a limit. The integral over σ is approximately $1/3$ if the limits include $2s/3$, and zero if they do not. Since the right side of (22) is a monotone decreasing function of s from 0 to n, we have

$$\Omega(\lambda)|_{K=1}=\frac{1}{3n}\int_0^{s_0}ds,$$
$$\frac{2s_0}{3}=\lambda s_0\{2Bn^{\frac{1}{2}}[(n-s_0)^{-\frac{1}{2}}-n^{-\frac{1}{2}}]\}^{-1}. \quad (24)$$

[5] W. E. Byerly, *Fourier Series and Spherical, Cylindrical, and Ellipsoidal Harmonics* (Ginn and Company, New York, 1893), p. 184.

[6] P. Debye and F. Bueche, J. Chem. Phys. **19**, 589 (1951).

Integration over s and substitution for s_0 give

$$\Omega(\lambda)|_{K=1}=\frac{1}{3}\left[1-\frac{(4Bn/3)^2}{(\lambda+4Bn/3)^2}\right]. \tag{25}$$

In order to find the total $\Omega(\lambda)$, it is necessary to add up the contributions from all values of K. When n is large, the dependence of $\bar{\lambda}$ upon K may be neglected, and $\Omega(\lambda)$ turns out to be three times the contribution from $K=1$:

$$\Omega(\lambda)=1-\frac{(4Bn/3)^2}{(\lambda+4Bn/3)^2}. \tag{26}$$

The distribution of relaxation times $G(\tau)$ is obtained from (26) and the first equation of (2):

$$G(\tau)=\frac{2\tau\tau_0}{(\tau+\tau_0)^3}$$
$$\tau_0=\frac{45\pi}{64}\left(\frac{\pi}{6}\right)^{\frac{1}{2}}\frac{a^3\eta_0 n^{\frac{1}{2}}}{kT}. \tag{27}$$

We note that $\Omega(\infty)$ is unity and $G(\tau)$ is properly normalized:

$$\int_0^\infty G(\tau)d\tau=1.$$

Due to the approximation involved in (17), the above formula for $G(\tau)$ is valid only when $\tau_0/n\ll\tau\ll\tau_0 n$. For large n, these limits do not appreciably change the dielectric dispersion and may be neglected.

The reduced polarization $Q(\omega)$ may now be obtained by integration over τ in (1):

$$J(x)=(1+x^2)^{-3}\times[2x^2(x^2-3)\log x-(3x^2-1)(x^2-\pi x+1)],$$
$$H(x)=(1+x^2)^{-3}\times[2x(3x^2-1)\log x+x(x^2-3)(x^2-\pi x+1)], \tag{28}$$
$$x=\omega\tau_0,$$

where $J(x)$ and $H(x)$ are, respectively, the real and imaginary parts of the reduced polarization:

$$Q(\omega)=J(x)-iH(x). \tag{29}$$

In Fig. 1 the reduced dispersion $H(x)$ is plotted as a function of ω/ω_m, where ω_m is 2π times the frequency of maximum dispersion. Also plotted in Fig. 1 is the dispersion previously calculated in I without the hydrodynamic interactions. The uncorrected and corrected dispersions differ very little in shape, the new $H(x)$ being slightly more peaked and somewhat asymmetric about its maximum. The corrected dispersion has a maximum value, H_m, of 0.315. This peak is only slightly larger than 0.285, the maximum dispersion obtained in I.

The important difference between the corrected $H(x)$ and the $H(x)$ derived in I occurs in the frequency scale. H_m is reached when x equals 0.44. From (28) it follows

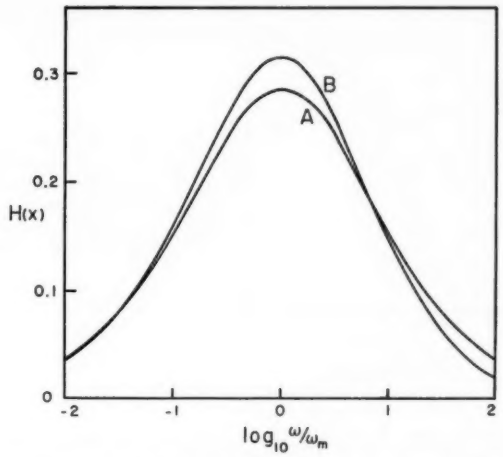

FIG. 1. Reduced dielectric dispersion of polymer solutions. Curve A: theory of Kirkwood and Fuoss; curve B: corrected for hydrodynamic interactions.

that f_m, the frequency of maximum dispersion, is equal to

$$f_m=0.044kT/a^3\eta_0 n^{\frac{1}{2}}. \tag{30}$$

Thus the frequency of maximum dispersion varies as the inverse one-half power of the degree of polymerization n. Without the hydrodynamic interactions f_m varies as n^{-1}. Furthermore, the dispersion is independent of the resistance constant ζ of the polymer elements, depending instead on the viscosity of the solvent. From measurements of f_m and the viscosity η_0, it therefore should be possible to estimate the effective bond length a without making any assumption as to the magnitude of ζ.

In the calculation of the diffusion tensor in Appendix I, the excluded volume of the polymer chain is neglected and $\langle|\mathbf{R}_{ls}|^{-1}\rangle$ is taken as proportional to $|l-s|^{-\frac{1}{2}}$. Because of the excluded volume, it has been suggested that $\langle|\mathbf{R}_{ls}|^{-1}\rangle$ may vary instead as $|l-s|^{-p}$, where p is somewhat larger than $\frac{1}{2}$ but smaller than unity.[7] For any p within these limits, the dispersion would fall between the two curves in Fig. 1 and consequently would vary in shape only slightly with p. However, from Appendix I it may be shown that f_m would depend upon n^{-p} rather than $n^{-\frac{1}{2}}$. Careful measurements of f_m for dilute solutions might be used to determine p.

All the foregoing results are appropriate to a monodisperse polymer solution. In I, $H(x)$ is calculated for an exponential distribution of molecular weights by carrying out an integration over n. The resultant dispersion differs only slightly from $H(x)$ for a single molecular weight. Because the change in the dispersion is so small, it does not seem worth while to correct the present results for polydispersity.

III

No experiments have been found in the literature which are ideally suited for comparison with the theo-

[7] P. J. Flory, J. Chem. Phys. 17, 303 (1949).

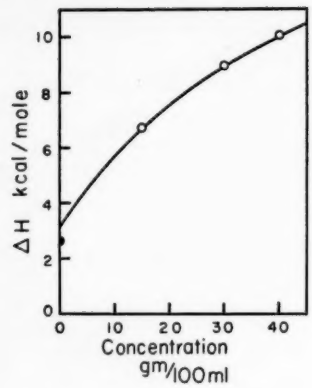

FIG. 2. The activation energy for the frequency of maximum dispersion. ○ polyvinyl acetate in toluene; ● activation energy for the viscosity of toluene.

retical results, the principal disparity arising from the theory's restriction to very dilute solutions. The best experiments for comparison were made fairly recently by Funt and Mason on polyvinyl acetate dissolved in toluene.[8] The dielectric constant was measured for solutions containing 15, 30, and 40 grams of polymer per 100 ml of solvent. Both ϵ' and ϵ'' were determined at 1, 3, and 10×10^6 cps over a temperature range from -80°C to 60°C.

When ϵ' is much larger than ϵ'', as is the case for the solutions investigated, the reduced dispersion $H(x)$ is proportional to ϵ''.[4] The ratio is dependent upon the value of ϵ' at high temperatures. Unfortunately, the data are not spread over a large enough temperature range to determine the absolute magnitude of $H(x)$. To eliminate the unknown ratio in comparing ϵ'' with the calculated $H(x)$, the data for ϵ'' may be divided by the polymer concentration and all results for the three concentrations simultaneously normalized to a maximum of 0.315. This normalization assumes that the observed H_m equals its theoretical value.

Because the experimental ϵ'' is reported as a function of temperature at constant frequency, the $H(x)$ obtained by the above normalization is still not directly comparable with theory. It is necessary also to relate the variation of temperature to a change in the variable x. For this purpose, it may be assumed that the viscosity of the solution is proportional to $\exp(\Delta H/RT)$, where ΔH may depend upon the concentration but does not vary rapidly with T. Using (30), the reported variation of f_m with T (Table III of reference 8) may be used to calculate ΔH. For a molecular weight of 15 000, ΔH is plotted *versus* concentration in Fig. 2. The limit as the concentration approaches zero is about 3 kcal/mole, a value appropriate to a temperature range centered at 220°K. The viscosity of toluene at this temperature has an effective ΔH of 2.7 kcal/mole, in agreement with the extrapolated value. This result indicates that the dispersion is correctly related to the viscosity of the solvent.

Once ΔH is known, it is possible to change a plot of the dispersion *versus* temperature to one *versus* frequency at constant temperature. The observed ϵ'', normalized to 0.315, may in this way be graphed against ω/ω_m. The data for a molecular weight of 15 000 (Fig. 3 of reference 8) are shown here in Fig. 3 together with the theoretical dispersion given by (28). The theoretical curve fits the data excellently near the maximum and at the lower frequencies. At relatively high frequencies the experimental points fall slightly above the curve. Considering the possible inaccuracies in the method of comparison, the agreement is satisfactory.

A second check of the theory is possible by computing the effective bond length a. The logarithm of the observed f_m may be plotted against the polymer concentration and extrapolated to zero concentration. For a molecular weight of 15 000, this gives an f_m of 1.7×10^7 cps at 220°K. From (30) and the viscosity of toluene at this temperature, it follows that a^3n^1 equals 3.6×10^{-21} cm^3. Using the known molecular weight ($n=175$) we obtain an effective bond length of 6.5 A.

This calculation is valid only for the theoretical model of the polymer molecule, a chain having 90° bond angles, no excluded volume, and no hindrance to rotation of the azimuth angles. One way to compare this model with the actual polymer is to calculate the root-mean-square length of the molecule. A tetrahedral carbon chain with a molecular weight of 15 000 and no restricted rotation has a length of 41 A. The model chain has a length of 121 A, a factor of three larger. This same factor has been obtained previously in other types of experiments, and indicates that the polymer is somewhat more extended in solution than would be the case if its bonds were randomly oriented.

Another way to compare the calculated bond length with the actual chain is to note that

$$a^2=\frac{(1+\langle\cos q^\alpha\rangle)(1+\cos\gamma)}{(1-\langle\cos q^\alpha\rangle)(1-\cos\gamma)}a_0^2, \tag{31}$$

where $\langle\cos q^\alpha\rangle$ is the average value of $\cos q^\alpha$ including the restricted rotation, γ is the supplement of the bond angle, and a_0 is the actual length of a C—C bond. To obtain an effective bond length of 6.5 A for a tetrahedral carbon chain, it is necessary that $\langle\cos q^\alpha\rangle$ be 0.80. This value agrees quite well with results obtained from mechanical properties of polymer solutions and from light scattering.[3]

It is not possible to check the theory on several important points. Experimental values of f_m are reported in reference 8 for two molecular weights larger than 15 000, but the data are too scattered to demonstrate any particular variation with n. As discussed above, it is also not possible to evaluate H_m from the reported dielectric measurements. Until further experiments on dilute solutions are performed, comparison between the theory and experiment must remain limited.

[8] B. L. Funt and S. G. Mason, Can. J. Research **28B**, 182 (1950).

APPENDIX I. DIFFUSION TENSOR INCLUDING HYDRODYNAMIC INTERACTIONS

From (10) and (11) we have

$$T_{ls}^{\alpha\beta}=\frac{1}{8\pi\eta_0}g^{\alpha\alpha}g^{\beta\beta}\left\langle\frac{1}{|\mathbf{R}_{ls}|}\frac{\partial\mathbf{R}_l}{\partial q^\alpha}\cdot\left[1+\frac{\mathbf{R}_{ls}\mathbf{R}_{ls}}{|\mathbf{R}_{ls}|^2}\right]\cdot\frac{\partial\mathbf{R}_s}{\partial q^\beta}\right\rangle. \quad (32)$$

By substituting for $\mathbf{R}_l$ from (5) and $\partial\mathbf{R}_l/\partial q^\alpha$ from (6), and defining $\mathbf{a}_{ls}$ as the unit vector in the direction of $\mathbf{R}_{ls}$, it follows that

$$T_{ls}^{\alpha\beta}=\frac{a^2}{8\pi\eta_0}g^{\alpha\alpha}g^{\beta\beta}\sum_{p=\alpha+1}^{l}\sum_{q=\beta+1}^{s}$$
$$\times\left\langle\frac{1}{|\mathbf{R}_{ls}|}[(\mathbf{a}_\alpha\cdot\mathbf{a}_\beta)(\mathbf{a}_p\cdot\mathbf{a}_q)-(\mathbf{a}_\alpha\cdot\mathbf{a}_q)(\mathbf{a}_\beta\cdot\mathbf{a}_p)\right.$$
$$\left.+(\mathbf{a}_\alpha\cdot\mathbf{a}_p\times\mathbf{a}_{ls})(\mathbf{a}_\beta\cdot\mathbf{a}_q\times\mathbf{a}_{ls})]\right\rangle \quad (33)$$

provided l and s are both greater than n. A corresponding equation may be written when l and s are less than n. The average value of each term within the summation is zero unless $\alpha=\beta$ and $p=q$. These restrictions permit the separation of the average into two parts, to give

$$T_{ls}^{\alpha\beta}=\begin{cases}\dfrac{a^2}{9\pi\eta_0}(g^{\alpha\alpha})^2\{(l,s)-\alpha\}\langle|\mathbf{R}_{ls}|^{-1}\rangle\delta_\alpha{}^\beta & \\ & n+1\leqslant\alpha\leqslant(l,s)-1\\ -\dfrac{a^2}{9\pi\eta_0}(g^{\alpha\alpha})^2\{[l,s]-\alpha\}\langle|\mathbf{R}_{ls}|^{-1}\rangle\delta_\alpha{}^\beta & \\ & n\geqslant\alpha\geqslant[l,s]+1\\ 0 & \alpha\geqslant(l,s)\geqslant n+1\\ 0 & \alpha\leqslant[l,s]\leqslant n\end{cases} \quad (34)$$

where (l,s) is the lesser of l and s, and $[l,s]$ is the greater. For the case in which the excluded volume of the polymer chain is neglected, the average of $|\mathbf{R}_{ls}|^{-1}$ has been determined[3]:

$$\langle|\mathbf{R}_{ls}|^{-1}\rangle=\left(\frac{6}{\pi}\right)^{\frac{1}{2}}a^{-1}|l-s|^{-\frac{1}{2}}. \quad (35)$$

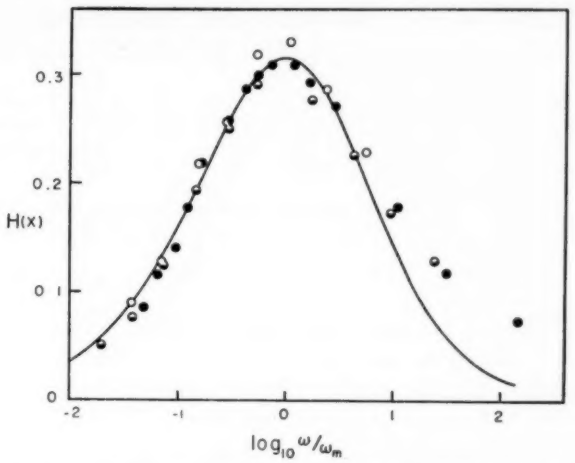

FIG. 3. Reduced dielectric dispersion of polyvinyl acetate in toluene. Polymer concentration: ○ 15 g/100 ml; ◒ 30 g/100 ml; ● 40 g/100 ml. —— theoretical curve.

Substituting this expression into (34) and summing over l and s, we have

$$T^{\alpha\beta}=\frac{16a(g^{\alpha\alpha})^2}{135\pi\eta_0}\left(\frac{6}{\pi}\right)^{\frac{1}{2}}(n-|n-\alpha|)^{5/2}\delta_\alpha{}^\beta. \quad (36)$$

By introducing the value of $g^{\alpha\alpha}$, $D^{\alpha\beta}$ in (12) follows immediately. The terms of D involving θ and ϕ may be obtained in much the same manner as above.

Due to the excluded volume of the polymer chain, $\langle|\mathbf{R}_{ls}|^{-1}\rangle$ may not vary exactly as $|l-s|^{-\frac{1}{2}}$. If $\langle|\mathbf{R}_{ls}|^{-1}\rangle$ were given by $(c/a)|l-s|^{-p}$, where c and p are constants, the nonzero terms of the diffusion tensor (neglecting A) would become:

$$D^{\alpha\alpha}=B'\left(1-\left|\frac{\alpha-n}{n}\right|\right)^{-(1+p)}$$
$$D^{\theta\theta}=D^{\phi\phi}=B'/2 \quad (37)$$
$$B'=\frac{2ckT}{\pi(1-p)(2-p)(3-p)\eta_0a^3n^{1+p}}.$$

Chemical and Photochemical Studies on 6,8-Thioctic Acid and 1,2-Dithiolane (Trimethylene Disulfide)*

R. B. WHITNEY† AND MELVIN CALVIN
Department of Chemistry and Radiation Laboratory, University of California, Berkeley, California
(Received December 9, 1954)

Quantum yields have been determined in the photolysis of thioctic acid and trimethylene disulfide by ultraviolet light under a variety of conditions. The order of magnitude of the quantum yield is unity.

THE hypothesis of the primary conversion of light quanta in photosynthesis by the thioctic acid disulfide link[1] has made it desirable to obtain more detailed information about the interaction of photons with this linkage, both in the model compound, trimethylene disulfide, and in thioctic acid itself. Barltrop, Hayes, and Calvin[2] observed the decrease in the 3300 A absorption maximum of trimethylene disulfide when it was exposed to radiation from a "black light" fluorescent lamp. We have developed a method for exposing the substance to essentially monochromatic radiation of 3130 and 3650 A wavelengths and for measuring the quantum yield of the reaction in which the disulfide link is broken.

EXPERIMENTAL

Light from a 275-watt General Electric sun lamp type RS (100 watt mercury arc at 2 atmos pressure) was used. The relative intensities of the 100 A bands in the ultraviolet are known[3]; most of the energy comes from the 3130 and 3650 A mercury lines. The lamp was mounted as shown in Fig. 1, inside a bright aluminum tube, with an air jet playing on the tube in such a way that the blast came out both in front and in back. Cooling was effected by water flowing through a Lucite tank of $1\frac{1}{4}$ in. inner diameter with quartz windows, and a black brass plate with a 2 in. hole to absorb excess radiation. (A T-tube placed in the water exit line 1 inch away from the tank completely eliminated difficulties of overflowing due to entrapped air.) The light then passed into a wooden box, black inside, containing filters, the reaction cell held in a spring clip in a quartz-walled vessel (Fig. 2) through which water circulated at 25°C, and the Kurlbaum bolometer which measured the energy transmitted by the system. A brass mask with a hole $\frac{1}{4}$ by $\frac{3}{4}$ in. was held in place against the wall of the reaction cell.

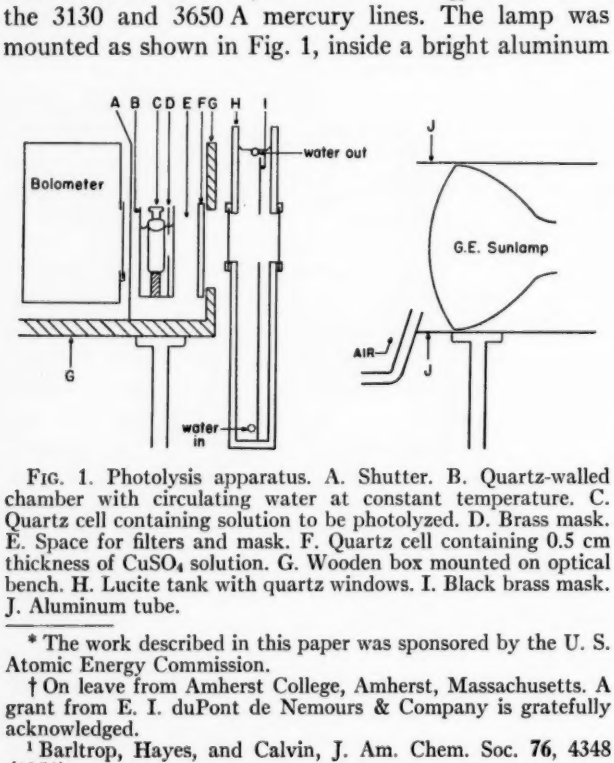

FIG. 1. Photolysis apparatus. A. Shutter. B. Quartz-walled chamber with circulating water at constant temperature. C. Quartz cell containing solution to be photolyzed. D. Brass mask. E. Space for filters and mask. F. Quartz cell containing 0.5 cm thickness of $CuSO_4$ solution. G. Wooden box mounted on optical bench. H. Lucite tank with quartz windows. I. Black brass mask. J. Aluminum tube.

The first filter was a thin-walled quartz cell containing a 0.5 cm layer of a copper sulfate solution (5.7 g of pentahydrate per 100 ml) which absorbed almost totally from 7600 to 20 000 A. This was not used in the earlier experiments. A 3 mm Corning No. 9863 glass ultraviolet filter absorbed totally from 4000 to 6800 A, almost totally from 12 000 to 30 000 A, and transmitted over 63% of the radiation between 3120 and 3800 A. For the 3650 A line, a Baird interference filter No. 7-1900 A, was used, and for the 3130 A line a 1 cm quartz cell containing 10 g $NiSO_4 \cdot 7H_2O$ and 35 g $CuSO_4 \cdot 7H_2O$ per 100 ml of solution. Extinction curves for these filters are shown in Fig. 3.

The Kurlbaum large-area bolometer, whose sensitive surface consists of two frames of ten blackened platinum foils (each foil $36 \times 1.8 \times 0.001$ mm) with an area of 13 cm^2, was calibrated against a National Bureau of Standards 50-watt lamp. While the calibration was done with the quartz window removed, the bolometer was used with it in place so that a small correction for ultraviolet light absorbed by quartz was made. It should be noted, however, that the quartz absorbs about 15% of the light from the standard lamp (mostly infrared). The most commonly used setting had a sensitivity of 1.88×10^{-4} watt per galvanometer scale division. The bolometer drifted very slowly, and readings were taken in sets of five, as with balance swings.

Samples were contained in 1 cm square quartz Beckman cells of 3.3 ml capacity. Such a cell with 95% alcohol was used as a reference, to determine the total energy transmitted to the bolometer in the absence of the absorbing substance (I_0). The absorbed energy was

* The work described in this paper was sponsored by the U. S. Atomic Energy Commission.
† On leave from Amherst College, Amherst, Massachusetts. A grant from E. I. duPont de Nemours & Company is gratefully acknowledged.
[1] Barltrop, Hayes, and Calvin, J. Am. Chem. Soc. **76**, 4348 (1954).
[2] See reference 1, page 4356.
[3] G. E. Lamp Bulletin, LD-1, October, 1950, p. 49.

taken as the difference (I_0-I) between this value and the energy recorded by the bolometer with the solution of the sample in place (I). Readings of the reference cell were taken at intervals of 15 min for rapid reactions, half an hour or an hour for slower reactions, short enough so that the change of absorption for three successive intervals was linear within the limits of experimental error. Fluctuations of lamp intensity were usually less than 3%. The reaction cell was shaken each time that it was removed for a reading of the reference cell. Readings before and after shaking differed usually by less than 2%.

The contents of the cell were analyzed by running the spectrum in a Cary recording spectrophotometer, Model 11. The previously measured extinction coefficients[1] of 147 for the 3300 A peak of trimethylene disulfide and 154 for the 3320 A peak of the thioctic acid were used to calculate the composition. Dilution experiments showed that the optical density at the maximum was proportional to the concentration up to a density of 1.6. It was

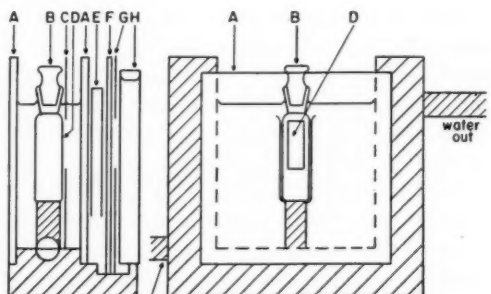

FIG. 2. Constant temperature chamber for photolysis cell. A. Quartz windows. B. Quartz Beckman photolysis cell. C. Brass mask. D. Slot in mask, $\frac{1}{4}$ in.$\times\frac{3}{4}$ in. E. Interference filter. F. Glass filter. G. Mask. H. Quartz cell with copper sulfate solution.

of interest that in the latter half of the experiments where all residual and visible and infrared radiation had been filtered out, the optical density at the wavelength used as measured by the Cary spectrophotometer agreed with 0.01 or 0.02 optical density units with that calculated from the bolometer readings (o.d.$=-\log I/I_0$).

Several samples of trimethylene disulfide were used. They were redistilled with alcohol under a pressure of 20 in. No difficulty was experienced with polymerization of solutions in 95% ethanol if the concentration was under 0.05 *M*. The thioctic acid was a crystalline sample, kindly supplied by Dr. T. H. Jukes of the Lederle Laboratories. Nitrogen, purified by bubbling through chromous chloride solution and then through 95% ethanol, was bubbled through the solutions in the quartz Beckman cells for 20 min. The ground tops were lubricated at the top with silicone high vacuum grease. Usually the cells remained closed, but when it was necessary to transfer material, nitrogen was introduced with a capillary tube and material was added or withdrawn by a syringe and a micropipette, the latter flushed out with nitrogen.

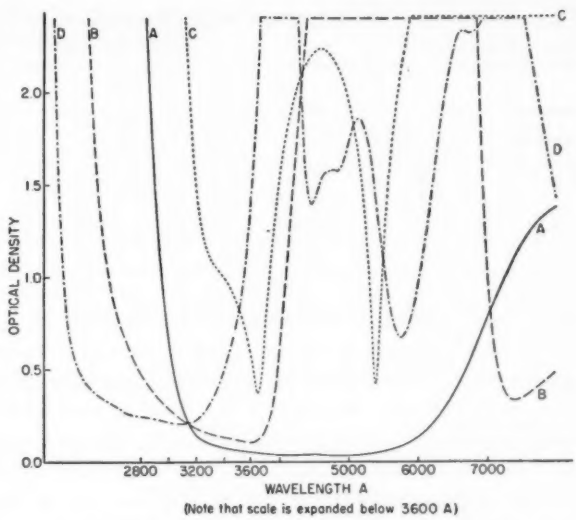

FIG. 3. Absorption curves for filters used. —— A. $CuSO_4$ (5.7 g per 100 ml), 0.5 cm. — — B. Corning No. 9863 filter. ---- Baird interference filter No. 7-1990-C. — - — D. $NiSO_4-CoSO_4$ filter 1.0 cm.

METHOD OF CALCULATION

The number of micromoles of substance reacted was calculated using the equation

$$\mu\text{moles}=\frac{\text{change in o.d.}\times\text{volume }(\mu\text{l})}{\text{extinction coefficient}}.$$

The number of micromoles of photons absorbed per hour was found by multiplying the observed bolometer reading by $\lambda/hc\times 1/6.02\times 10^{23}\times 3600\times 10^{13}\times$ watts per scale division $\times$ correction for absorption by quartz window (1.10). (The optical density toward ultraviolet light of the thickness of quartz in the bolometer window plus the rear wall of the chamber in Fig. 2 was 0.04, representing 91% transmission. Thus approximately 10% more light was passing through the reaction cell than was registered by the bolometer.) For example, when 3650 A light and the second bolometer setting (one division $=1.88\times 10^{-4}$ watt) were used, a value of 2.26 μmoles of photons per hour per scale division was obtained.

RESULTS

Trimethylene Disulfide

A representative family of spectrophotometer curves is shown in Fig. 4. Tables I and II show the details of the data and the calculations.

The quantum yields obtained with trimethylene disulfide under a variety of conditions are given in Table III. The first eleven were carried out without the copper sulfate filter for the red and infrared, so that a third or more of the radiation going through the cell was

TABLE I. Quantum yield in a photolysis of trimethylene disulfide. (7.2×10^{-3} *M* TMDS, 3×10^{-3} *M* HCl in 95% ethanol, 3650 A light, intensity 7.7 μmoles of photons per hr, vol 3.3 ml.)

Original concn $\times10^3$ *M*	Time (hr)	Change in o.d. at ϵ_{max}	μmoles lost	Average bolometer reading	Average fraction of light absorbed	O.d. from final bolometer reading	O.d. at 3650 obs. by spectrometer	μmoles photons absorbed	Quantum yield
7.2	1.0	0.155	3.26	2.47	0.69	0.48	0.48	5.55	0.58
6.1	1.55	0.225	4.75	2.19	0.63	0.37	0.36	7.68	0.62
4.6	2.0	0.22	4.65	1.74	0.50	0.24	0.21	7.81	0.595
3.1	3.0	0.225	4.75	1.14	0.32	0.12	0.11	7.75	0.61

unabsorbed and made the readings less accurate. During these runs also the Lucite cooling tank had not had quartz windows installed, so that the ultraviolet radiation, although not filtered by the 3650 A interference filter, was very largely 3650 A light and this value was used in calculating the quantum yield. The first eleven were also corrected by a factor of 25% for loss of light due to faulty spacing of the lamp and bolometer. Since conditions were identical in all eleven, the results are useful for comparison purposes.

These comprise all of the determinations which were made, excepting that one experiment was performed in alkaline solution, where by rapid operation it was possible to obtain a decrease in optical density of 0.23 at the 3300 A maximum, with only a rise of 0.03 at 4000 A due to turbidity. (Turbidity due to polymerization in alkaline solution had previously prevented such a measurement.) Correcting for this turbidity a quantum yield of 0.54 is obtained (0.94×10^{-2} *M*, 1.6 hours, 3650 interference filter).

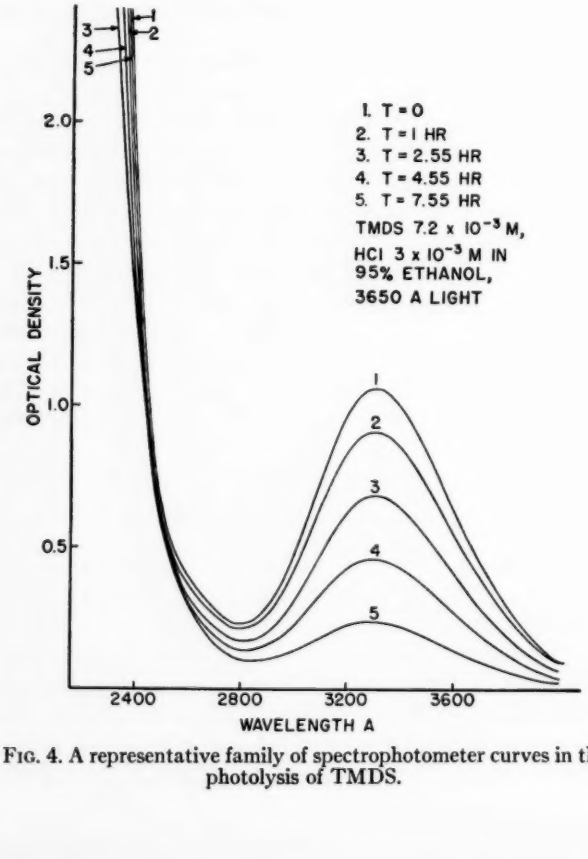

FIG. 4. A representative family of spectrophotometer curves in the photolysis of TMDS.

Thioctic Acid

Table IV and Fig. 5 show the results of the most complete photolysis experiment with thioctic acid. In addition, a single photolysis was run with 1.07×10^{-2} *M* thioctic acid in 95% ethanol containing HCl, 3×10^{-3} *M*. A yield of 0.476 was obtained.

Figure 6 shows the effect of excess NaOH (150λ of 0.1 *N* NaOH, or 15 μmoles, with 3.0 ml of 3.1×10^{-3} *M* thioctic acid, or 9.3 μmoles) upon the absorption spectrum. The decrease in optical density is due to dilution, and no shift in wavelength is detectable. It also shows that complete photolysis produces a product with considerable absorption in the vicinity of 3300 A. The calculation of an accurate quantum yield is thus not possible, but if one assumes that the base line for zero thioctic acid concentration is curve 4, the loss of thioctic acid during the first 3½ hr photolysis will be 3.3 μmoles. From the bolometer readings, 12.3 μmoles of photons were absorbed. If one assumes that the extinction coefficient of the product is one-half of that for thioctic acid, and that on the average five-sixths of the absorbing material was thioctic acid (since one-third of it disappeared), 11.2 μmoles of photons were absorbed by thioctic acid, giving a quantum yield of 0.30, not very different from that in acid solution.

Discussion of Results

The chief significance of these results lies in the fact that under varied conditions of concentration, light intensity, wavelength, and acidity, the number of

TABLE II. Detailed calculations of an average bolometer reading. (A bolometer reading is the difference in the galvanometer deflection with and without a shutter.)

Reference cell (95% ethanol)	3.57	(averaging three times open, twice closed)
Reaction cell, first minute	0.97	
Initial absorption reading		2.60
Reaction cell, 15th minute	1.03	
Reaction cell, 30th minute	1.08	
Reference cell, after 30th minute	3.54	
Half-hour absorption		2.46
Reaction cell, 45th minute	1.10	
Reaction cell, 60th minute	1.19	
Reference cell, after 60th minute	3.54	
Absorption after one hour		2.35
Average absorption, first hour		2.47

TABLE III. Summary of quantum yields with TMDS.

Experiment	Solvent	Original TMDS concn $\times 10^2$	Fraction photolyzed	Type of light	Intensity I_0 μmoles per hr	Quantum yield (duration of each photolysis in hr given in parentheses)		
I	95% EtOH 3×10^{-3} *M* HCl	1.25	0.96	Chiefly 3650 Å	31	0.67 (0.33) 0.64 (1.00)	0.64 (0.50) 0.58 (2.00)	0.61 (0.50) 0.68 (3.67)
II	95% EtOH 1.5×10^{-3} *M* HCl	0.46	0.34	Chiefly 3650 Å	31	0.595(1.00)		
III	95% EtOH 9×10^{-3} *M* HCl	0.81	0.67	Chiefly 3650 Å	29 (1st & 4th) 2.9 (2nd & 3rd)	0.48 (1.00) 0.48 (2.05)	0.425(1.25) 0.51 (1.00)	
IV	90% EtOH 3.2×10^{-2} *M* HCl	0.75	0.80	Chiefly 3650 Å	29	0.48 (1.00)	0.48 (3.07)	
V	30% EtOH, 70% H_2O 3×10^{-2} *M* HCl	0.33	0.40	Chiefly 3650 Å	27.5	0.21 (4.07)		
VI	65% EtOH 2×10^{-3} *M* HCl	0.51	0.75	Chiefly 3650 Å	28	0.34 (1.00)	0.34 (3.57)	
VII[a]	27% EtOH, 73% H_2O 3×10^{-3} *M* HCl	0.43	0.60	Chiefly 3650 Å	32	0.34 (1.00)	0.18 (3.00)	
VIII	90% EtOH	0.75	0.78	Chiefly 3650 Å	25	0.61 (0.50)	0.535(1.00)	0.57 (2.37)
IX	80% EtOH	0.68	0.85	Chiefly 3650 Å	23	0.51 (0.50)	0.51 (1.00)	0.51 (3.00)
X	31% EtOH 69% benzene	0.59	0.29	Chiefly 3650 Å	*ca* 25	*ca* 0.55 (1.00)		
XI	95% EtOH	0.73	0.81	3650 A	4.9	0.58 (2.0)	0.52(3.0) 0.51(3.0)	0.48 (5.0)
XII	95% EtOH	0.67	0.88	3130 A	4.1 (1st) 7.0 (2nd & 3rd)	0.865(13.4)	0.75 (2.00)	0.64 (6.33)
XIII	90% EtOH	2.10	0.50	3130 A	7.0	0.725(1.75)	0.765(6.67)	
XIV	95% EtOH	1.10	0.34	3130 A	3.9	0.81 (1.75)	0.75 (2.92)	
XV	95% EtOH	0.99	0.40	3650 A	8.0	0.74 (1.00)	0.65 (2.08)	
XVI	95% EtOH	0.73	0.32	3650 A	1.9	0.58 (9.87)		
XVII[b]	95% EtOH 3×10^{-3} *M* HCl	1.13	0.24	3650 A	8.0 (1st) 42 (2nd)	0.66 (1.00)	0.57 (0.33)	
XVIII	95% EtOH 3×10^{-3} *M* HCl	0.72	0.78	3650 A	8.0	0.59 (1.00) 0.59 (2.00)	0.615(1.55) 0.614(3.00)	
XIX	95% EtOH	1.11	0.11	3650 A	8.0	0.605(1.00)		
XX[c]	95% EtOH 3×10^{-3} *M* HCl	0.71	0.41	3000–4000 Chiefly 3650	25 (1st) 4.7 (2nd) 18 (3rd)	0.61 (0.50)	0.50 (3.17)	0.58 (0.50)
XXI	95% EtOH	1.10	0.41	3650 3130 3650	8.0 (1st) 2.6 (2nd) 25 (3rd)	0.61 (1.00)	0.795(2.7)	0.595(0.50)

[a] This solution began to polymerize when prepared (usual when much water is present). After a short irradiation it was centrifuged at 40 000 rpm. The resulting clear solution, under nitrogen, did not polymerize for 12 hr.
[b] The second yield was determined without the interference filter.
[c] Three different extreme geometrical situations were used.

photons required to break the S—S bond is of the order of unity. This makes reasonable the presumption of a repulsive excited state from which energy is efficiently transferred. The molecule cannot store energy, but must react rapidly. These are conditions which must be met if thioctic acid is indeed the substance to which chlorophyll transfers solar energy for the oxidation of water and the reduction of CO_2.

We have conducted several experiments, details of which are given in a University of California Radiation

TABLE IV. Quantum yields in a photolysis of thioctic acid. (1.10×10^{-2} *M* in 95% ethanol, 3650 A light, intensity 7.8 μmoles of photons per hr.)

Original concn. $\times10^3$ *M*	Time (hr)	Change in o.d.	μmoles lost	Average bolometer reading	Average fraction of light absorbed	O.d. from final bolometer readings	O.d. at 3650 obs by spectrometer	μmoles photons absorbed	Quantum yield
11.0	1.5	0.19	3.95	3.15	0.86	0.84	0.82	7.8	0.48
9.7	2.12	0.25	5.2	2.92	0.82	0.675	0.67	14.0	0.37
8.1	3.58	0.37	7.7	2.53	0.71	0.45	0.47	20.4	0.37
5.7	5.82	0.42	8.7	1.87	0.52	0.22	0.22	24.5	0.35
2.7[a]	3.43	0.32	6.45	2.8	0.23	0.05	0.04	21.6	0.30

[a] Without interference filter, $I_0=27.5$ μmoles of photons per hr.

Laboratory Report[4] attempting to observe a photolysis of the disulfide link by quanta of visible light transferred to it from a dye. No such transfer has been detected under the conditions used (see Table V). In each case, the absorption spectrum of the dye showed no shift of wavelength of absorption maxima, such as would have been observed if there were an interaction between the dye-stuff and the disulfide.

A detailed consideration of Table III shows that a quantum yield of around 60% is obtained initially in neutral or slightly acidic ethanol, with 3650 A light (I, II, VIII, XI, XVI–XXI). Experiment XV represents a deviation from this but is included in order that the data may be complete. When HCl is present the yield remains essentially constant (I, III, XVIII), but in the absence of acid a decrease is noted (XI, XII).

Any excess acid decreases the yield markedly (III, IV), although a larger excess does not cause further decrease. Water also causes a decrease in the yield (IV, IX, VI, V, VII), which becomes more pronounced with increasing concentration of water. These results were surprising, as previous work[5] had indicated the probability that photolysis produced a biradical which could either recombine or polymerize, and it was expected that water by reducing solubility would promote polymerization in incipient micelles by a chain mechanism so that after a certain critical concentration of water had been reached the quantum yield would increase rapidly. We have conducted a number of exploratory experiments on the relation between water concentration, *p*H, and polymerization.[4] These indicate that polymer formation is undoubtedly not a simple consequence of the fission of the S—S bond; that ultraviolet light, after causing slight polymerization then actually inhibits it; and that polymerization occurs less readily in quartz than in glass. The failure of the biradicals produced by the primary action of photons to polymerize in ethanol solution is consistent with recently

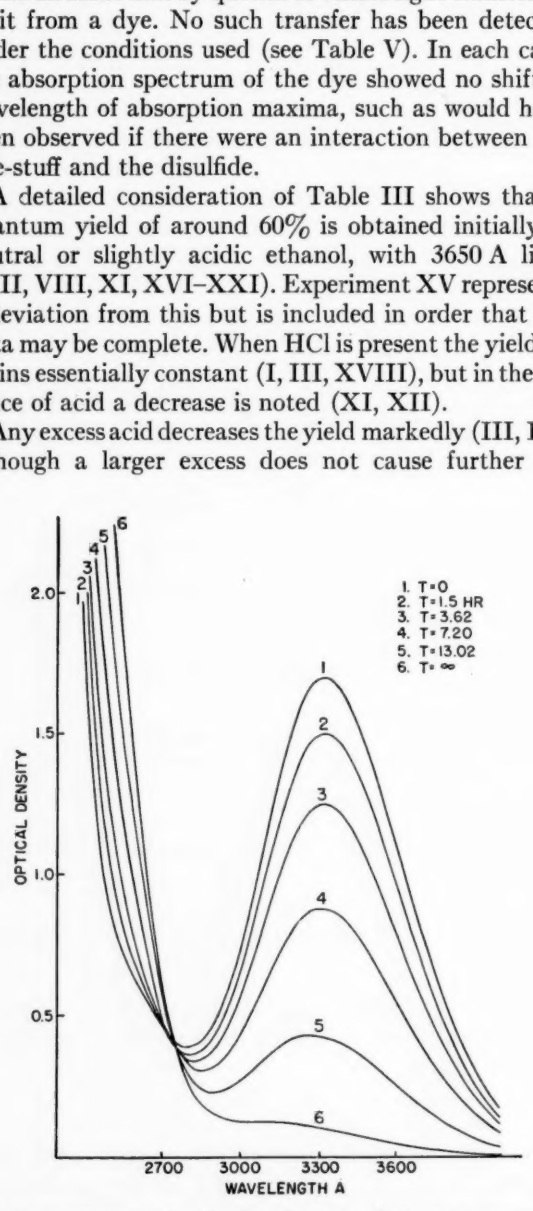

FIG. 5. A representative family of spectrophotometer curves in the photolysis of 6,8-thioctic acid.

[4] R. B. Whitney, UCRL-2755.

TABLE V. Energy transfer experiments.

Dye used, and wavelength	Composition	Number of equivalents of photons used	Minimum quantum requirement
Zinc tetraphenylporphin (ZnTPP) 5600 A	95% ethanol HCl 3×10^{-3} *M* ZnTPP 4×10^{-4} *M* TMDS 6.6×10^{-3} *M*	112	7400
Zinc tetraphenylporphin 5600 A	65% ethanol HCl 2×10^{-3} *M* TMDS 4.5×10^{-3} *M* ZnTPP suspension of 1 μmole solid	74	4950
Copper tetraphenylporphin 5600 A	50% benzene 48% ethanol 2% water TMDS 7×10^{-3} *M* 10 μmoles ZnTPP, mostly in solution	286	3170
Chlorophyll *a* and *b*[a] 6700 A	95% ethanol TMDS 8×10^{-3} *M* Chlorophyll 3.3×10^{-4} *M*	390	3500

[a] Kindly prepared fresh by Professor G. MacKinney, to whom we are much indebted.

[5] Reference 1, page 4350.

expressed views on the improbability of biradicals forming long chains.[6]

Perhaps the most striking variation among the quantum yields is the increase observed with 3130 A light (XII, XIII, XIV, XXI). This fits in with the concept of the entirely repulsive excited state; the higher energy results in a lower probability of back reaction.

From the experimental part it is seen that thioctic acid, whether in the form of the free acid alone or in the presence of HCl, or in the form of the anion, gives quantum yields very similar to those for the model compound, trimethylene disulfide. A comparison of the photolysis curves for thioctic acid (Fig. 5) and for TMDS (Fig. 4) sheds some light on the behavior of the photolysis products. Further studies on these are in progress,[7] but it appears from the fact that a good isobestic point is observed that thioctic acid itself (or its anion) proceeds to a definite set of products immediately, while trimethylene disulfide forms products which undergo continual change, even in the dark in the absence of oxygen, as evidenced by the fact that the absorption curves of photolyzed material remain constant at 3300 A but rise with time at 2500–2800 A.

Rate Calculations

The quantum yields reported in Table III were all determined by dividing the average number of photons absorbed during a time Δt into the number of molecules reacting during that time; that is

$$\phi=\frac{-\Delta x}{(I_0-I)\Delta t}.$$

It was noted (Table I) that the optical density at 3650 A as determined by the bolometer agreed closely with that measured by the spectrophotometer. This led to the idea that the rate equation

$$-\frac{dx}{dt}=\phi(I_0-I)$$

could be integrated, since $I=I_0 10^{-\epsilon x}$ (ϵ=extinction coefficient for 3650 A, x=concentration in moles per liter).

$$\int\frac{dx}{1-10^{-\epsilon x}}=-\phi I_0 t+\text{constant}$$

or

$$x+\frac{1}{\epsilon}\log_{10}(1-10^{-\epsilon x})=-\phi I_0 t+x_0+\frac{1}{\epsilon}\log_{10}(1-10^{-\epsilon x_0}).$$

From this it is apparent that if ϕ is a constant, a plot of $x+1/\epsilon\log(1-10^{-\epsilon x})$ against time should give a straight line whose slope is $-\phi I_0$. In Experiment XVIII the data were thought to be extensive enough to warrant a trial of this method.‡ Figure 7 shows the plot, and Table VI the data. Since the thickness of the Cary cell was 1 cm, the optical density, D, at 3650 A is equal to ϵx.

The values of the integral plotted against the time lie on a fairly good straight line whose slope determined graphically is -1.55×10^{-3} and by the method of least squares is -1.54×10^{-3}, giving a value of $\phi=0.597$, in

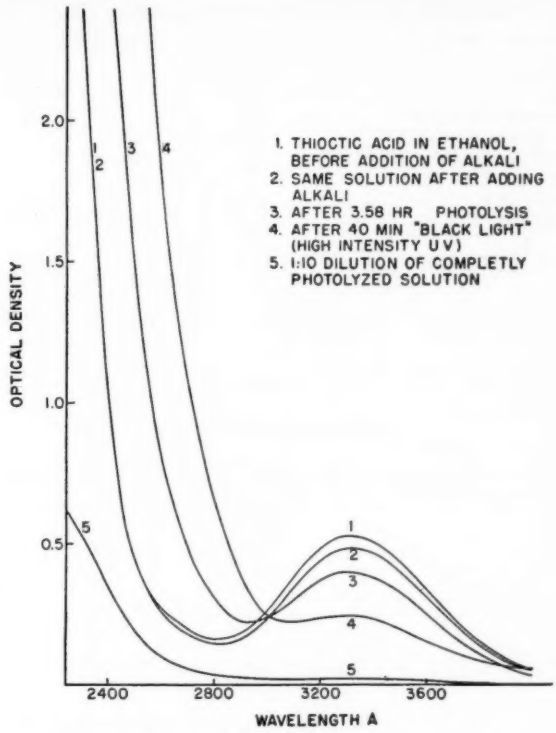

FIG. 6. Alkaline photolysis of 6,8-thioctic acid.

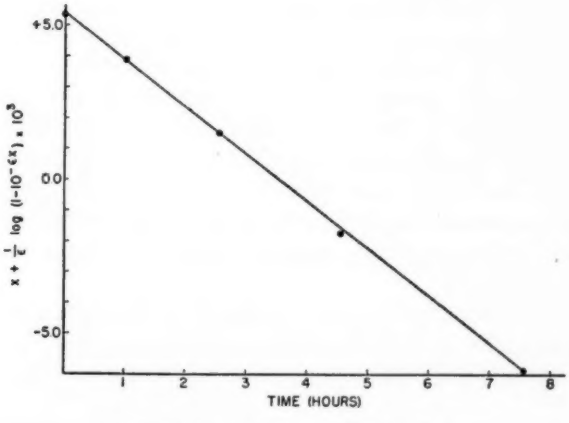

FIG. 7. Integral rate equations *vs* time.

[6] B. H. Zimm and J. K. Bragg, J. Polymer Sci. 9, 476 (1952).

[7] See reference 1, page 4356 for previous work on these, and UCRL-2755 for a report of the current work.

‡ Even though the reaction cell was exposed for only 40% of its area, shaking at 15 to 30 min intervals seemed to produce the needed mixing, as shown by the very small change in optical density before and after shaking.

TABLE VI. Methods of calculating quantum yield in Experiment XVIII. ($\epsilon_{3650}=76.8$, $I_0=2.57\times10^{-3}$ moles/liter/hour.)

t (hours)	0		1		2.55		4.55		7.55
D_{3650}	0.553		0.475		0.355		0.240		0.125
x (moles/liter)$\times10^3$	7.21		6.15		4.62		3.13		1.60
Δx (moles/liter)$\times10^3$		1.06		1.53		1.49		1.53	
I_0-I (moles/liter/hr)$\times10^3$		1.80		1.60		1.27		0.831	
$\phi=-\Delta x/(I_0-I)\Delta t$		0.589		0.615		0.586		0.614	
$(I_0-I)\times10^3$	1.895		1.720		1.466		1.085		0.620
$I_0(1-10^{-\epsilon x})\times10^3$	1.856		1.715		1.44		1.093		0.645
$\left(x+\frac{1}{\epsilon}\log(1-10^{-\epsilon x})\right)\times10^3$	5.35		3.88		1.42		−1.73		−6.21

agreement with the determinations by the integral method.

ACKNOWLEDGMENTS

The authors would like to acknowledge much valuable help from Mr. Paul M. Hayes in the design and construction of apparatus and in carrying out the spectrophotometric measurements. We are indebted to Professor G. K. Rollefson, Professor D. S. McClure, and Professor K. Shibata, and to Dr. Dan F. Bradley for helpful suggestions and discussion.

THE JOURNAL OF CHEMICAL PHYSICS VOLUME 23, NUMBER 10 OCTOBER, 1955

Dielectric Properties of Liquid Ethanol and 2-Propanol

F. X. HASSION* AND R. H. COLE
Metcalf Chemical Laboratories, Brown University, Providence, Rhode Island
(Received January 5, 1955)

Dielectric constants and loss were measured from room temperature to −160°C for the pure liquids and mixtures with small amounts of water to facilitate supercooling. Two distinct dispersion regions were found below −100°C in the experimental frequency range from 1 cy/sec to 5 Mc/sec. The temperature dependences are similar and described by rate laws of the form found for similar measurements in 1-propanol. An explanation of the multiple dispersions in terms of hydrogen bond breaking to permit reorientation of alkyl and hydroxyl groups is discussed.

I. INTRODUCTION

PREVIOUSLY reported work on 1-propanol and related glycols[1] showed that definitive measurements of their dielectric dispersion and loss were possible in the audio- and radio-frequency range by working at sufficiently low temperatures. These measurements in the case of 1-propanol revealed the existence of three experimentally distinct dispersion regions[2] all exhibiting the exponential temperature dependence characteristically associated with dielectric relaxation and other rate processes. In the present work, similar studies were undertaken on the related alcohols, ethanol and 2-propanol.

The available frequency range of accurate and convenient bridge and transient methods, extending from 1 cy/sec to 5 Mc/sec, was adequate for reasonably definitive measurements only if temperatures of the supercooled liquids could be studied. This necessity was a matter of some difficulty for the present cases. While a substantial amount of information was obtained for both ethanol and 2-propanol before the onset of freezing, it was not possible from the data obtained to confirm with any great assurance the existence of secondary, higher frequency dispersions previously defined in 1-propanol. However, addition of small amounts of water to absolute ethanol to facilitate supercooling permitted study of alcohol-rich solutions over a sufficiently wide temperature range. The properties of the anhydrous alcohols at low temperatures could then be obtained by extrapolation in a manner consistent with the concentration dependence observed at higher temperatures.

By this indirect approach, measurements of dielectric dispersion and loss were made in the range 120–200°K for 2-propanol, and in the range 110–160°K for ethanol. Equilibrium dielectric constants were determined from the lowest temperature to 300°K in both cases.

* Now at Bell Telephone Laboratories, Murray Hill, New Jersey. This work was supported by the Office of Naval Research.
[1] D. W. Davidson and R. H. Cole, J. Chem. Phys. **19**, 1484 (1951).
[2] R. H. Cole and D. W. Davidson, J. Chem. Phys. **20**, 1389 (1952).

II. EXPERIMENTAL METHODS

A. Purification of Materials

2-propanol (Eimer and Amend, Tested Purity Reagent) was dried by refluxing over calcium hydride. Upon distillation, the fraction boiling at 82.4°C was collected, and the average room temperature specific conductance for all samples reported was 5.8×10^{-8} ohm^{-1} cm^{-1}.

A 13 weight percent mixture of water (specific conductance less than 3×10^{-7} ohm^{-1} cm^{-1}) in 2-propanol was prepared. The lower boiling fraction (80.4°C; $n_D^{15}=1.3795$), corresponding to the azeotropic mixture (12.1% water), was collected. A 99 weight percent mixture of 2-propanol in water ($n_D^{15}=1.3792$–3; 24:1 molecular ratio) was then prepared from the constant boiling mixture and dry 2-propanol. The average room temperature conductance for all samples reported was 5.4×10^{-8} ohm^{-1} cm^{-1}.

Absolute ethanol was refluxed over calcium hydride, and the fraction distilling at 78.3°C ($n_D^{25}=1.3594$) was collected. The average room temperature specific conductance for all samples reported was 8.2×10^{-8} ohm^{-1} cm^{-1}.

A 95 weight percent mixture of ethanol in water was distilled, and the lower boiling fraction (78.2°C; $n_D^{25}=1.3611$), corresponding to the azeotropic mixture (4.4% water; 8:1 molecule ratio), was collected. The average room temperature conductance for all samples reported was 4.1×10^{-7} ohm^{-1} cm^{-1}.

A 99 weight percent mixture of ethanol in water ($n_D^{25}=1.3598$; 39:1 molecule ratio) was prepared from the constant boiling mixture and dry ethanol. The average room temperature conductance for all samples reported was 1.1×10^{-7} ohm^{-1} cm^{-1}.

B. Dielectric Cells and Cooling Systems

Two cells were employed in the measurements, both embodying coaxial cylindrical electrodes. The first was a three terminal guarded electrode arrangement of nickel-plated brass with Teflon insulation and is shown in Fig. 1 in cross section. The air capacitance was 2.60 $\mu\mu$f, reproducible to one percent on reassembly.

The second cell, of nickel and glass construction, from J. C. Balsbaugh of Cambridge, Massachusetts, employed three coaxial nickel cylindrical tubes, the inner and outermost connected together to serve as the low potential electrode. The lead wires through a supporting glass press had unavoidable direct capacitance, which, however, was kept to a minimum by grounded shielding of the leads from the press to the bridge. The resulting residual capacitance was 1.50 $\mu\mu$f and the "replaceable" capacitance 4.81 $\mu\mu$f.

The first cell had the advantage of requiring only a small volume of sample (4 cc) and permitting direct admittance measurements without correction for stray capacitances. The second could be cooled more rapidly,

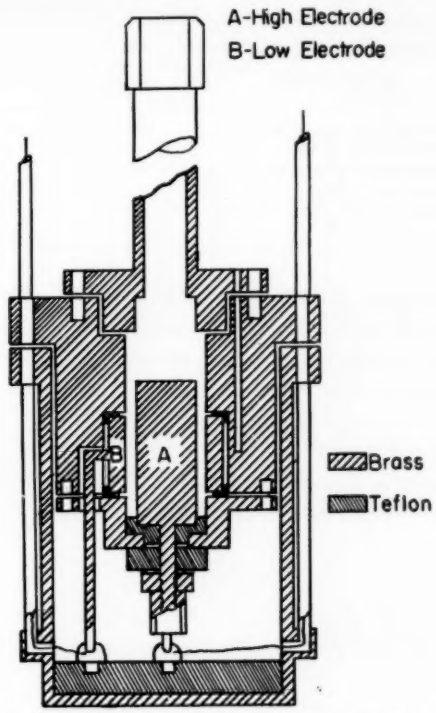

FIG. 1. Experimental guarded electrode cell for dielectric measurements.

and was useful for measurements of the supercooled pure alcohols. Comparable measurements were in good agreement. Cooling of both cells to temperatures as low as 120°K was effected by passing liquid nitrogen through cooling coils immersed in a bath liquid devised by Kanolt[3] to be nonflammable and fluid at low temperature. Temperature control of the first cell was obtained by adjustment of current in a six watt heating coil, and in the second cell by judicious addition of liquid nitrogen to a small annular trough partially immersed in the bath liquid. Ordinarily, constancy to $\pm0.1°$ could be realized, but variations of $\pm0.2°$ were tolerated when rapid measurements were necessary to avoid errors from freezing.

Copper-constantan couples calibrated at the freezing point of mercury, sublimation point of CO_2, and by comparison with an oxygen vapor pressure thermometer were employed for temperature measurement, their emf being read by a Leeds and Northrup Type K potentiometer.

C. Electrical Measurements

The frequency range 15 cy/sec to 5 Mc/sec was covered by a bridge described elsewhere,[4] and studies to times of a second or more were made by a special transient apparatus.[5] With the two methods, a range of

[3] C. W. Kanolt, Natl. Bur. Standards Scientific Paper No. 520, March, 1926.
[4] R. H. Cole and P. M. Gross, Jr., Rev. Sci. Instr. **20**, 252 (1949).
[5] Cole, Auty, and Davidson, Rev. Sci. Instr. **22**, 678 (1951).

TABLE I. Temperature ranges of measurement.

Alcohol (Wt %)	EtOH 100%	EtOH 99%	EtOH 95.6%	2-PrOH 100%	2-PrOH 99%
Temperature range of equilibrium data	130–300°K	110–300°K	117–300°K	178–300°K	123–300°K
Temperature range of relaxation data	130–160°K	110–154°K	117–160°K	178–200°K	123–200°K
Number of spectra	23	16	14	12	37

seven decades in rate of the dielectric relaxation processes could be studied. In the bridge range, values were obtained at fifteen to twenty frequencies if these were in regions of dispersion.

III. EXPERIMENTAL DATA

Data were obtained for five different systems in all, at temperatures as summarized in the table below.

A. Equilibrium Data

The equilibrium dielectric constants ϵ_0 were found to be accurately described by the simple equation

$$\epsilon_0 = -A + B/T, \qquad (1)$$

where T is temperature in °K. Equation (1) reproduces the individual measurements of different series, over the ranges indicated by Table I, to within $\pm 1\%$. The values of A and B for best fit of the data are listed in Table II.

B. Low-Frequency Dispersion Data

For all the systems studied, it was found that the first dispersion encountered with increasing frequency was quantitatively described by the familiar Debye equations characteristic of a simple first-order rate process.

These relations require that the locus of ϵ'' *versus* ϵ' be a semicircle in the complex plane,[6] with intercepts on the real axis (ϵ') at values ϵ_0 and ϵ_1, representing the limiting low and high frequency dielectric constants. Typical examples in Figs. 2–4 show the excellent agreement.

The values of ϵ_0, ϵ_1, and relaxation frequencies f_1 of maximum absorption were determined by analytical methods described elsewhere.[7]

Representative results are listed in Table III, together with parameters ϵ_2 and f_2 of the higher frequency dispersion (as discussed below).

TABLE II. Constants of the equilibrium dielectric constant equation.

System	EtOH 100%	EtOH 99%	EtOH 95.6%	2-PrOH 100%	2-PrOH 99%
A	18.60	21.09	24.20	21.53	23.65
$B\times 10^3$	12.80	13.68	15.26	12.20	12.78

[6] K. S. Cole and R. H. Cole, J. Chem. Phys. **9**, 341 (1941).
[7] R. H. Cole, J. Chem. Phys. **23**, 493 (1955).

C. High-Frequency Dispersion Data

For all five systems studied, the dispersion data give conclusive evidence that a further dispersion exists at higher frequencies. This is illustrated by data for 99% ethanol at 115°K, plotted in Fig. 5. In this figure, only the high-frequency portion of the complete complex plane locus is shown, in order to exhibit the departures from the semicircle with asymptotes at $\epsilon_0 = 98.2$ and $\epsilon_1 = 8.5$.

TABLE III. Parameters of dispersion in ethanol and 2-propanol. (Values in parentheses by considerable extrapolation, data at starred temperatures by transient measurements.)

A. Ethanol

T°K	ϵ_0	ϵ_1	f_1 (kc/sec)
159.4	62.6	...	1850
155.6	63.9	(6.0)	1460
148.4	67.3	6.5	755
137.3	74.2	7.6	180
130.6	79.0	8.0	60

B. 99% Ethanol

T°K	ϵ_0	ϵ_1	ϵ_2	f_1 (kc/sec)	f_2 (kc/sec)
153.7	68.7	...	...	780	...
138.9	77.8	(7.6)	...	125	...
126.0	87.4	8.5	5.1	11.4	1500
120.4	91.7	8.5	4.7	2.67	225
115.3	98.2	8.6	4.7	0.203	14.0
110.1	(102.0)	8.6	4.1	0.0168	0.52

C. 95% Ethanol

162.3	70.0	...	...	1240	...
153.1	75.4	(7)	...	425	...
141.9	83.7	8.2	...	76	...
133.7	90.1	8.6	(4.9)	14.6	4900
126.0	96.1	9.2	4.7	1.84	460
116.8	(104)	10.6	4.5	0.029	3.1

D. 2-Propanol

T°K	ϵ_0	ϵ_1	f_1 (kc/sec)
200.0	39.5	(2.6)	1330
190.4	42.7	3.8	603
183.2	44.5	3.9	335
177.5	47.1	4.0	156

E. 99% 2-Propanol

T°K	ϵ_0	ϵ_1	ϵ_2	f_1 (kc/sec)
199.5	40.8	(3.0)	...	1450
189.5	44.2	(3.2)	...	514
179.1	47.5	4.2	...	179
138.1	67.1	5.2	3.3	0.058
132.2*	72.7	5.7	2.7	0.0032
128.1*	75.8	5.7	2.8	0.00048
122.9*	80.0	5.9	3.0	0.00002

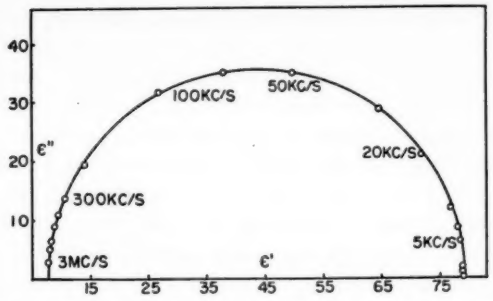

FIG. 2. Complex dielectric constant of ethanol at 130°K.

The analytical procedure found to yield a reasonable resolution of the similar dispersion in 1-propanol[2] was applied to the present results also. This consists in assuming that the observed complex dielectric constant is a sum of overlapping dispersions:

$$\epsilon^* = \epsilon_1^* + \epsilon_2^*.$$

In this expression $\epsilon_1^* = (\epsilon_0 - \epsilon_1)/(1 + if/f_1)$ is the Debye function for the low-frequency dispersion and ϵ_2^* is the further dispersion of interest here. Since the constants representing ϵ_1^* are known accurately, the necessary real and imaginary parts of ϵ_2^* to fit the data can be obtained from the measured values of ϵ^*.

In the example of Fig. 5, the results of this numerical process are indicated by the dashed lines from the upper locus of ϵ^* to the lower locus of ϵ_2^*. The latter is not fitted by a semicircle, but conforms to a circular arc with slightly depressed center until frequencies of the order 100 kc/sec are reached. At higher frequencies, the analysis thus suggests still further dispersion but the data are too limited in extent and too sensitive to errors in differences for a further analysis into overlapping dispersions to be of quantitative significance.

All data extending to sufficiently high frequencies showed the behavior illustrated in Fig. 5, except, of course, for scale and range of frequencies. In particular, the secondary dispersions (corresponding to the data between 100 kc/sec and 2 kc/sec in the example) were in all cases fitted reasonably well by a circular arc, but not by a semicircle. The exact depression angle of the radius vector characterizing this form of locus,

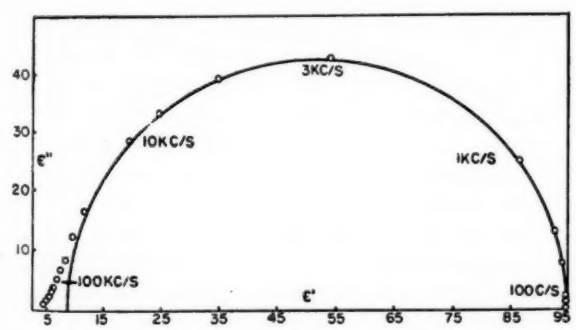

FIG. 3. Complex dielectric constant of 95% ethanol-water solution at 128°K.

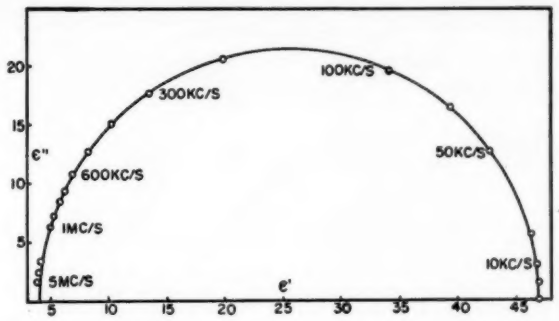

FIG. 4. Complex dielectric constant of 2-propanol at 178°K.

which has been found to describe many dielectrics,[7] is not accurately determinable because of sensitivity of the derived data to small errors, but is of the order 10°–15°. This corresponds to values of 0.11–0.17 for the parameter α of the empirical arc dispersion function:

$$\epsilon_2^* = \epsilon_2 + (\epsilon_1 - \epsilon_2)/1 + (if/f_2)^{1-\alpha}.$$

The center frequency f_2 of this arc dispersion and the values ϵ_1 and ϵ_2 from the intercepts on the ϵ' axis are listed in Table III.

IV. DISCUSSION

A. Equilibrium Dielectric Constants

The values for both alcohols are larger than for normal polar liquids and increase at lower temperatures in the fashion expected from decreasing effect of thermal energy on net orientation. The extent of these effects is conveniently expressed by the values of Kirkwood's correlation factor g necessary to secure agreement between his equation and the measured values. This equation and the question of proper choice of the dielectric constant ϵ_∞ for induced polarization are discussed in

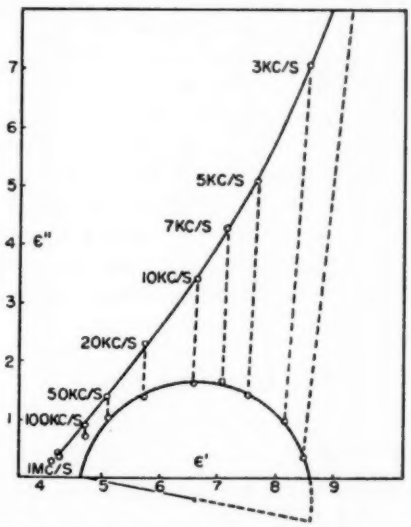

FIG. 5. High-frequency dispersion in 99% ethanol-water solution at 115°K. Dashed lines indicate the contribution of the low-frequency dispersion to the observed complex dielectric constant.

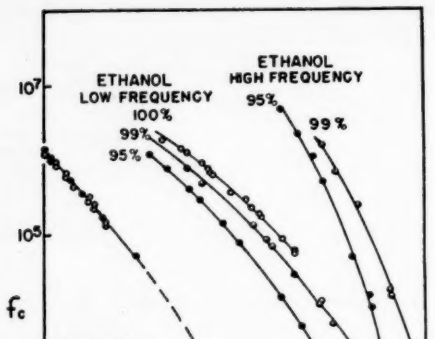

FIG. 6. Rate plots of log relaxation frequency *versus* reciprocal temperature. Hollow circles for 2-propanol are for the pure liquid, filled circles for the 99% 2-propanol-water solution.

the second paper of this group.[8] We have calculated the values of g given in Table IV for two possible choices of ϵ_∞: the value n^2 corresponding to the optical refractive index n, and the corresponding value at the far infrared wavelength of 50μ. For either, the empirical g values are substantially larger than Oster and Kirkwood's figure 2.39[9] for a model of infinite hydrogen bonded chains of alcohol molecules with free rotation about the OH—O bonds, and the values increase at lower temperatures with indications of approaching limiting values. The parameter g is in Kirkwood's theory a measure of correlation of neighboring dipoles by short-range forces, and the results thus indicate greater correlation at lower temperatures than is predicted by the free rotation model. Measurements of isomeric butyl alcohols discussed in the next paper[8] define a similar behavior over still wider ranges of temperature, and it is shown there that a model of chains with varying lengths and neighbor correlations is capable of accounting for the observed properties.

It should be pointed out that Eq. (1) for the temperature dependence of ϵ_0 is purely empirical, and the parameters A and B have no simple theoretical significance. The negative values predicted for high temperatures have no physical meaning and indicate the limited range for which (1) is valid.

B. The Relaxation Processes

For the pure alcohols, the relaxation frequencies f_1 can be approximately represented by Arrhenius expressions, as shown by the plots in Fig. 6 of log f_1 *versus* $1/T$. The average slope of the curve for ethanol from 130° to 160°K corresponds to an activation energy of 4.9 kcal/mole, and of the curve for 2-propanol from 178 to 200°K to a value of 6.2 kcal/mole, which may be compared with a figure of 7.1 kcal/mole for 1-propanol at 160°K. It is to be emphasized, however, that for both alcohols the data show definite curvature on the conventional rate plot, especially in the case of ethanol, and attempts at interpretation of these apparent activation energies solely in terms of potential barriers for molecular displacements are correspondingly doubtful.

A second important aspect of the data for the pure alcohols is the fact that in both cases the high-frequency limit ϵ_1 of the principal dispersion is significantly larger than n^2, where n is the optical refractive index. For ethanol at 148°K, the values are $\epsilon_1=6.5$ and $n^2=2.0$ (as estimated from the room temperature value with correction for density by the Clausius-Mossotti formula); for 2-propanol at 190°K, ϵ_1 is 3.8 whereas $n^2=2.1$. There were also small but definite indications of further dispersion at the highest frequencies available, thus suggesting the existence of further relaxation processes similar to those previously found in 1-propanol.[2]

Measurements of the solutions with small amounts of water show that, as in the pure alcohols, there is a principal dispersion, and at the much lower temperatures possible the frequency measurements extend far enough to define a region of further dispersion. The principal dispersion is in all cases accurately described by a Debye function, and the relaxation frequencies f_1 are plotted in Fig. 6.

The principal effect found on adding water to ethanol is the considerable decrease in relaxation frequency for the one percent solution and the significant but proportionately smaller further decrease for the 5% ethanol-water solution. The curvatures of the rate plots are, however, similar for the different concentrations and resemble closely the results for 1-propanol.[1] For these reasons, we believe that the general behavior is characteristic of alcohol molecule interactions which are influenced but not changed in kind on addition of water. The disproportionately large decreases in frequency suggest that water molecules inhibit the alcohol relaxation process by forming bonds between chains.

The temperature dependences of the frequencies f_1 can as for 1-propanol be represented by the equation $\ln f_1=A-B/R(T-T_\infty)$ for suitable choice of the constants A, B, and T_∞, and the necessary values of T_∞ to fit the data are all of the order 70–75°K. Whether this particular empirical description of the low-temperature behavior has a simple theoretical explanation is questionable, but it is significant that the value of T_∞ corresponds approximately to completion of the transformation from supercooled liquid to a glass and thus suggests a "freezing-in" in this range of the molecular reorientations responsible for f_1.

The second dispersions in the two ethanol-water

[8] W. Dannhauser and R. H. Cole, J. Chem. Phys. **23**, 1762 (1955).
[9] G. Oster and J. G. Kirkwood, J. Chem. Phys. **11**, 175 (1943). In this paper, the result $g=2.57$ is given, which is apparently obtained using 0.8 debye for the O—R group moment rather than the usual value of 1.2 debye. The latter gives $g=2.39$ from their formula.

solutions are very similar, the amplitude of the dispersion being the same or a little larger in the 95% solution, while the characteristic frequency range is significantly lower. This dispersion is thus, like the principal one, to be explained in terms of the alcohol molecule interactions modified by the presence of water in small quantities. The central frequency f_2 is higher than f_1 by a factor 10 to 100 depending on concentration and temperature, and has a temperature dependence similar to that of f_1 as shown in Fig. 6. A second similarity is that the amplitude of this dispersion increases at low temperatures at the same rate, so far as can be judged, as does the amplitude of the first dispersion. There is no indication of a relative decrease which Magat and co-workers[10] inferred for other alcohols by comparisons which involved less complete data at temperatures of 0°C and higher.

The continuing similar increase in amplitude of the two dispersions at low temperatures has been found also for 1-propanol and for other alcohols.[8] This behavior is important because it is inconsistent with Magat's proposal that the second dispersion arises from reorientation of unbonded molecules, the number of which for any reasonable bond energy would decrease rapidly at the lower temperatures of the present work.

C. Mechanism of the Dispersions

If one accepts the general viewpoint of Kirkwood's theory, it is necessary to conclude from the magnitude and temperature dependence of the static dielectric constant that extensive correlation of the dipole moments of the molecules exists in liquid alcohols. It is further reasonable to suppose that this takes the form of linear OH—O bonds as surmised from the observed x-ray scattering, and that the average lengths and numbers of molecules in the transient chains so formed are increasingly large at low temperatures.

In an earlier communication[11] about some of the work reported here, a model consistent with this viewpoint was proposed. In this model, the principal dispersion is attributed to reorientation of a molecule's OH moment by breaking of its intermolecular hydrogen bond and subsequent forming of a bond to the oxygen of another molecule. The second, higher frequency, dispersion is interpreted as the result of reorientation of the oxygen-alkyl group moment during the shift of the hydrogen bond from one electron orbital of the bridged oxygen atom to the other of the two which is not used by the alkyl group and the proton of the alcohol molecule.

[10] Brot, Magat, and Remisch, Kolloid Z. **134**, 101 (1953).
[11] F. X. Hassion and R. H. Cole, Nature **172**, 212 (1953).

TABLE IV. Calculated correlation factors to give agreement with measured dielectric constants.

	Ethanol			2-Propanol		
(a) ϵ_∞ from refractive indices (calculated from n^2 at room temperature by the Clausius-Mossotti formula)						
t°C	22.0	−49.3	−101.1	21.5	−49.1	−101.8
ϵ_∞	1.80	1.88	1.94	1.84	1.93	1.99
g	3.32	3.55	3.66	3.33	3.82	4.11
(b) ϵ_∞ from infrared dispersion $n^2=2.2$ at 50μ and room temperature						
ϵ_∞	2.20	2.33	2.44	2.20	2.33	2.43
g	2.68	2.83	2.86	2.77	3.12	3.32

This model is consistent with the facts that the second dispersion is much faster, as the cooperation of another molecule is not immediately required, with the similar temperature dependences, as both involve partial breaking and reforming of a hydrogen bond, and with the much smaller amplitude of the second dispersion. The small amplitude is expected because only the component of the O—R bond moment perpendicular to the plane of the two hydrogen bonds is reoriented and because correlation of this component with the moments of neighboring hydrogen bonded molecules is ineffective.

On this picture, one might expect the same activation energy, equal to the hydrogen bond energy, for the dispersions in different alcohols, whereas actually the temperature dependences of relaxation frequencies are stronger for the propyl alcohols than for ethanol, are greater for the second dispersion than the first,† and both dispersions fail to conform to a simple rate law. These complications suggest the need to consider both the energy requirements in the local environment and the frequency of arrangements of alkyl groups and bonding neighbors which are compatible with rebonding. After completion of the present work, studies of other normal and branched chain alcohols and of alcohol solutions have been completed which give evidence bearing on these questions. These results, which make possible some amplification of the model proposed on the basis of data for ethyl and propyl alcohols, are discussed in the following papers.

† It may be noted that this difference is the opposite of that inferred by Magat[10] on the basis of available data near room temperature.

Dielectric Properties of Liquid Butyl Alcohols

WALTER DANNHAUSER* AND ROBERT H. COLE
Metcalf Chemical Laboratories, Brown University, Providence, Rhode Island

(Received January 5, 1955)

Measurements of static dielectric constant were made for all except *t*-butyl alcohol from the boiling points to −140°C; dispersion and loss were measured below 0°C in the range 20 cy/sec to 2 Mc/sec. Multiple dispersions were found as in other alcohols. The temperature dependences of static values are examined in terms of finite extent of chainwise molecular coordination by hydrogen bonding, and the rate laws of the dispersions are discussed.

I. INTRODUCTION

THE present work is in continuation of previously reported investigations of ethyl[1] and propyl[2] alcohols. Extensive studies were made for three of the four isomers, the exception being *t*-butyl alcohol. For the others, the dispersions occur at lower frequencies than in the lower alcohols. Because of this and the low melting points, measurements at the available frequencies were adequate to define the dispersion processes for temperatures from −150°C to −60°C or higher and measurements of static dielectric constants extended nearly to the boiling points in the vicinity of 100°C. These wide ranges permitted a better definition of the rate laws for the relaxation processes, and especially in the case of the static behavior revealed significant isomeric effects. In the discussion, these results are examined in relation to the model previously proposed for the dispersions[1] and in relation to nature and extent of chainwise association.

II. EXPERIMENTAL METHODS

A. Purification of Materials

n-Butyl alcohol (Baker's A.R.) was refluxed over calcium hydride and distilled; density 0.8056 (25/4), $n_D^{20}=1.3994$, specific conductance 1.0×10^{-7} mho/cm at 25°C. *Iso*-butyl alcohol (Eastman Kodak White Label) was stored over calcium hydride and distilled with a Vigreaux column; density 0.7972 (25/4), $n_D^{25}=1.3939$, specific conductance 1.6×10^{-8} mho/cm at 25°C. *Sec*-butyl alcohol was dried over calcium hydride and distilled; specific inductance $<1.0\times10^{-7}$ mho/cm at 25°C.

TABLE I. Static dielectric constants of butyl alcohols above 273°K.

n-Butyl		*iso*-Butyl		*sec*-Butyl	
T°K	ϵ_0	T°K	ϵ_0	T°K	ϵ_0
386.1	8.7	376.8	8.2	365.3	8.3
379.1	9.2	364.5	9.2	354.8	9.2
363.7	10.5	352.5	10.3	342.8	10.3
353.6	11.4	338.0	12.4	331.8	11.5
339.7	12.9	324.0	13.5	319.5	13.1
318.0	15.3	315.4	14.7	308.9	14.7
306.3	16.9	305.4	16.0	298.2	16.35
298.2	17.64	298.2	17.24	282.7	19.00
283.8	19.5	285.6	18.8		

B. Electrical Measurements

The cell used embodied coaxial stainless steel electrodes and guard ring, and differed only in minor details of insulation and sealing from the previously described original construction.[3]

The other experimental arrangements were essentially the same as in previous measurements on the alcohols.

TABLE II. Parameters of dispersion in butyl alcohols.

A. *n*-Butyl alcohol					
T°K	ϵ_0	ϵ_1	ϵ_2	τ_1(μsec)	τ_2(μsec)
269.5	21.0	3.2	···	0.0018	···
246.6	25.1	3.5	···	0.0059	···
227.4	28.5	3.6	···	0.014	···
208.9	32.4	3.7	···	0.055	···
190.9	36.3	3.8	···	0.227	···
173.3	41.7	4.1	···	1.71	···
155.8	49.1	4.4	3.1	31.2	0.080
146.0	52.6	4.4	3.2	269	0.76
141.3	54.7	4.6	3.2	962	3.3
134.8	59	4.8	3.3	6320	23
B. *iso*-Butyl alcohol					
272.5	20.8	2.7	···	0.0024	···
245.2	25.2	2.9	···	0.0092	···
231.6	27.6	3.1	···	0.021	···
204.7	33.2	3.4	···	0.161	···
190.9	36.6	4.0	···	0.639	···
177.6	40.4	4.4	···	3.57	···
163.1	44.9	4.3	3.2	37.6	0.51
153.1	48.8	4.5	3.4	342	4.6
145.7	51.8	4.8	3.4	2280	38
136.2	56	5.5	3.5	44000	1130
C. *sec*-Butyl alcohol					
T°K		ϵ_0	ϵ_1	τ_1(μsec)	
269.7		21.4	···	0.0026	
245.8		26.0	···	0.030	
217.8		32.3	···	0.093	
200.0		37.2	4.0	0.057	
180.4		43.3	4.1	6.75	
165.9		48.6	4.2	76.8	
152.0		54.6	4.4	2000	

* Now at du Pont Film Department, Buffalo, New York. This work was supported in part by the Office of Naval Research and Office of Ordnance Research.

[1] F. X. Hassion and R. H. Cole, J. Chem. Phys. **23**, 1756 (1955); also F. X. Hassion and R. H. Cole, Nature **172**, 212 (1953).

[2] D. W. Davidson and R. H. Cole, J. Chem. Phys. **19**, 1484 (1951); **20**, 1389 (1952). For *iso*-propyl alcohol, see reference 1.

[3] R. H. Cole and P. M. Gross, Jr., Rev. Sci. Instr. **20**, 252 (1949).

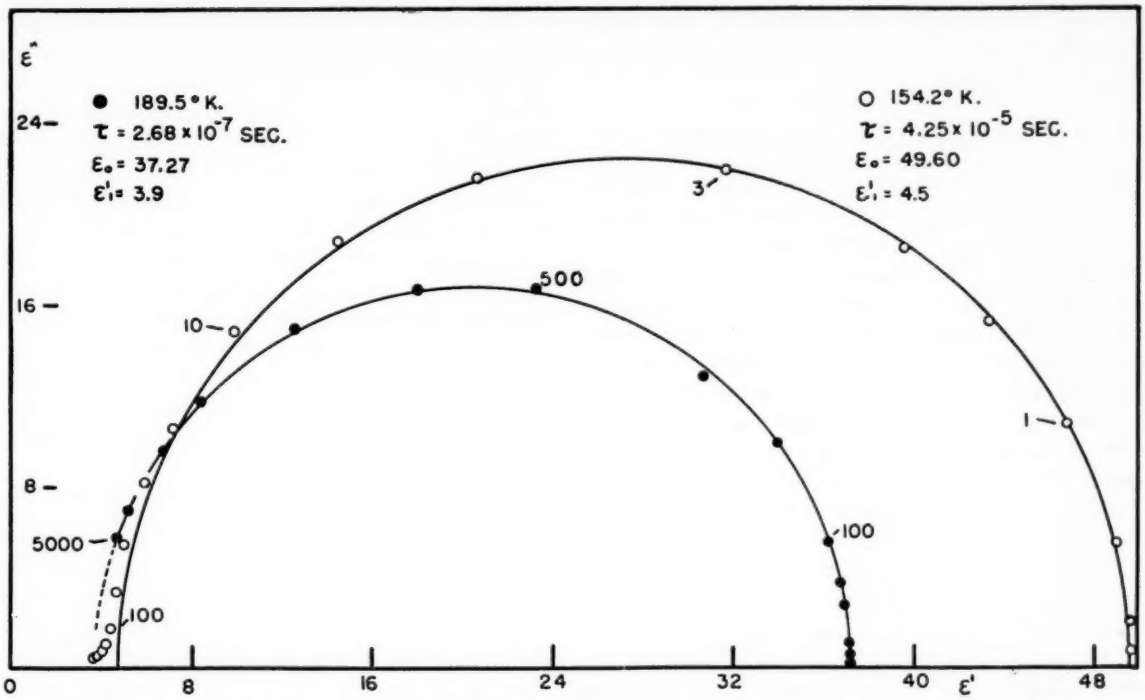

FIG. 1. Complex dielectric constant of *n*-butyl alcohol. The larger semicircle is for 154°K, the smaller for 189°K. Numbers by points are frequencies in kilocycles/sec.

III. RESULTS

A typical set of results for dispersion and absorption is shown in the complex dielectric constant loci for *n*-butyl alcohol at 190 and 154°K of Fig. 1. The high-frequency portion of the locus at 154°K is shown in Fig. 2, together with the residual circular arc locus found after subtracting the contributions of the low frequency Debye semicircular dispersion as in Fig. 1. The depression angles of the high-frequency loci were not determinable with high accuracy because of errors in the small differences by which they were determined, but were about 20° with no significant differences discernible for the three isomers.

The experimental results are summarized in Tables I and II. Values of static dielectric constants ϵ_0 for a number of temperatures above the measurable dispersion range are listed in Table I.

Particular efforts were taken with the precision of measurements at the standard temperature of 25°C; these values are believed accurate within 0.3%. The values at other temperatures were reproducible to one percent or better in different runs.

Representative results of dispersion measurements in Table II are expressed by values of ϵ_0, of the intermediate limit ϵ_1 between the principal and second dispersions, and of the high-frequency limit ϵ_2 of the second dispersion. The relaxation times τ_1 and τ_2 of the two dispersions, which together with the depression angle for the second define the two rate processes, are also given in Table II.

IV. DISCUSSION

The significance of the present results is conveniently considered in two parts: the first dealing with the mag-

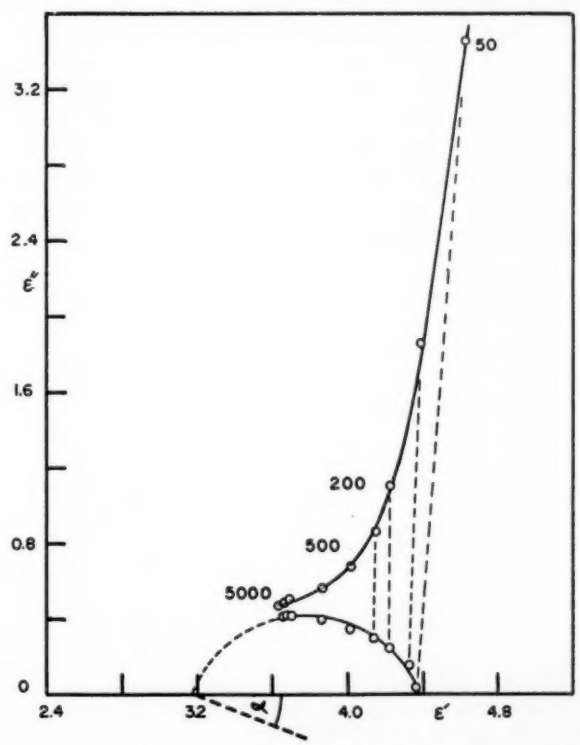

FIG. 2. High-frequency portion of dielectric constant locus for *n*-butyl alcohol at 154°K. The dashed lines indicate subtracted contributions of the principal dispersion.

nitude and temperature dependence of the static (equilibrium) dielectric constants, and the second with the dispersion behavior.

A. Static Dielectric Constants

As for other alcohols, values of ϵ_0 are significantly larger at all temperatures than for normal polar liquids or from calculations by Onsager's theory.[4]

The differences are in only qualitative agreement with calculations of Oster and Kirkwood[5] based on Kirkwood's general theory[6] and free rotation about hydrogen bonds of alcohol molecules as segments of infinite chains. The behavior is particularly interesting when examined as a function of temperature for the four isomers. It is convenient for this purpose to calculate the empirical values of Kirkwood's correlation factor g which are required for agreement with experiment of his dielectric constant equation

$$\epsilon_0=\epsilon_\infty+\frac{3\epsilon_0}{2\epsilon_0+\epsilon_\infty}\left(\frac{\epsilon_\infty+2}{3}\right)^2\frac{4\pi N\mu_0^2}{3kTV}g, \qquad (1)$$

where ϵ_∞ is the dielectric constant for induced polarization, V the molar volume, μ_0 the dipole moment of the free molecule (taken to be 1.68 debye), N is Avogadro's number, and kT is the thermal energy.

A proper choice of ϵ_∞ for the calculation is troublesome; we have somewhat arbitrarily taken $\epsilon_\infty=2.4$ at 0°C as a reasonable compromise between possible extremes (2.0 from n^2 and 3.2 from the value of ϵ_2 in the dispersion measurements). Correction for changes of density affecting V and ϵ_∞ was made by using an average temperature coefficient of 0.0008 per degree C for density and hence V. Correction of ϵ_∞ for density changes was made by the Clausius-Mosotti formula. The values used are evidently only approximate, but are adequate for the principal purpose of comparing effects of temperature and structure.

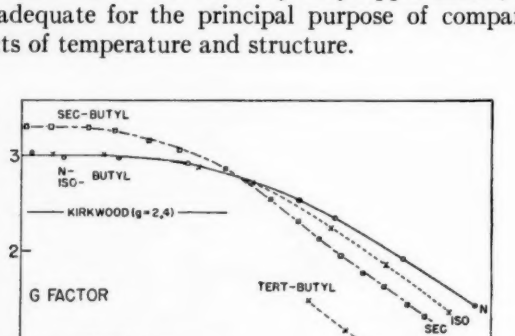

FIG. 3. Empirical correlation factors to account for observed dielectric constants plotted against absolute temperature. Values from the Onsager theory and Kirkwood theory for infinite chains with free rotation are indicated.

[4] L. Onsager, J. Am. Chem. Soc. **58**, 1486 (1936).
[5] G. Oster and J. G. Kirkwood, J. Chem. Phys. **11**, 175 (1943).
[6] J. G. Kirkwood, J. Chem. Phys. **7**, 911 (1939).

The values of g calculated from the dielectric constants for the three isomers measured in the present work are plotted in Fig. 3, together with values for *t*-butyl alcohol from measurements by Smyth and Dornte[7] at 30, 50, and 70°C. At temperatures below about −50°C, the calculated values of g are essentially constant, the figures for *sec*-butyl alcohol being significantly larger than for the primary alcohols. At higher temperatures, the decreases are more marked and set in sooner for less eccentric placement of the hydroxyl group in the molecule. These definite and considerable changes are indicative of less extensive and effective hydrogen bonding at the higher temperatures, and suggest an explanation in terms of a temperature-dependent distribution of lengths of hydrogen bonded chains.

B. Effect of Finite Extent of Chains

A rough model which gives a reasonable explanation of the decreased correlation factor and the isomeric differences can be based on an extension of Oster and Kirkwood's[7] calculation of g for infinite chains of doubly hydrogen-bonded molecules:

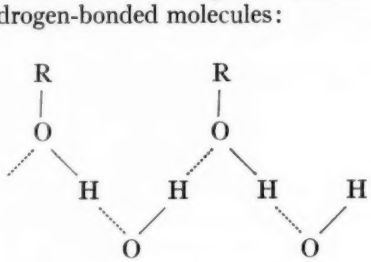

We assume that there exists a distribution of chains of varying lengths governed by the association equilibria

$$(\mathrm{ROH})_n+\mathrm{ROH}=(\mathrm{ROH})_{n+1},$$

with equilibrium concentrations governed by an equilibrium constant K:

$$K=C_{n+1}/C_nC_1=(1/C_0)\exp(\Delta F/RT), \qquad (2)$$

where C_n is the concentration of n-mer and C_0 the gross concentration as monomer. (The assumption that K is independent of n is a dubious one for small n especially, but a more elaborate treatment is neither practical nor warranted by the uses to which it will be put.) The results given by Kempter and Mecke[8] for their infrared alcohol solution measurements follow readily:

$$\alpha=C_1/C_0=(1-KC_0\alpha)^2,$$
$$C_n/C_0=\alpha^n(KC_0)^{n-1}. \qquad (3)$$

The correlation factor g for any molecule is evaluated from the product of its moment μ and the average moment $\bar{\mu}$ of its environment by the expression

[7] C. P. Smyth and R. W. Dornte, J. Am. Chem. Soc. **53**, 545 (1931).
[8] H. Kempter and R. Mecke, Z. physik. Chem. **B46**. 229 (1940).

$g=\mu\cdot\bar{\mu}/\mu^2$. For any molecule of an n-bonded chain, g is calculated in the same way as by Oster and Kirkwood for a molecule of an infinite chain with the assumption of random orientation of neighbors around the OH—O bond. The value of g is different for different members i of a finite chain, and it is convenient to define a mean value $\bar{g}_n$, where

$$n\bar{g}_n=\sum_i g_{in}.$$

For the single molecule, let μ_H and μ_R be the group moments and 2θ the bond angle, the latter being assumed equal to the angle between hydrogen bonds. One then obtains

$$n\bar{g}_n=n+2f(n-1)\cos^2\theta+2f(n-2)\cos^4\theta+\cdots+2f[n-(n-1)]\cos^{2(n-1)}\theta,$$

$$\bar{g}_n=1+2f\cot^2\theta-\frac{2f\cos^2\theta}{n}\frac{1-\cos^{2n}\theta}{\sin^4\theta},$$

where

$$f=(\mu_H+\mu_R)(\mu_H+\mu_R\cos2\theta)/(\mu_H^2+\mu_R^2+2\mu_H\mu_R\cos2\theta).$$

These expressions are inconvenient for subsequent summing, but for the values $\mu_H=1.55$, $\mu_R=1.2$, $2\theta=105°$, a fair approximation to the exact result is given by the simpler formulas

$$\bar{g}_n=2.40-2.00/n(n>1),\quad g_1=1. \tag{4}$$

The mean correlation factor is then readily obtained as

$$\bar{g}=(1/C_0)\sum_{n=1}^{\infty}n\bar{g}_nC_n=2.39-2.00\alpha^{\frac{1}{2}}+0.61\alpha, \tag{5}$$

on using Eq. (3) for C_n.

The value of g from the model depends on temperature implicitly through α which is determined by KC_0 and hence $\Delta F=\Delta H-T\Delta S$ in Eqs. (2) and (3). The plausibility of the model can then be tested by determining whether the observed temperature dependence is reproduced by otherwise acceptable values of ΔH and ΔS. The results of calculations for several choices are plotted in Fig. 4. Comparison with the empirical values in Fig. 3 shows that the values of ΔH of order 6–8 kcal/mole and $\Delta S=15$–25 cal/mole deg lead to variations of the observed type in the proper range of temperature.

The absolute agreement at lower temperatures is poor, because the value $g=2.39$ for the free rotation model is definitely too small to account for the measurements with any reasonable choice of ϵ_∞ in Eq. (1). This may be in part due to the crude assumptions of the model, but the distinctly larger values for *sec*-butyl alcohol indicate restrictions on relative configurations of neighbors about OH—O bonds.

An examination of atom models shows that steric hindrance by the alkyl group when the hydroxyl is on the second carbon as in *sec*-butyl alcohol prevents a variety of configurations for which the scalar product $\mu\cdot\bar{\mu}$, and hence g, is small. Thus the larger values of g and the decrease beginning at lower temperatures are both reasonable consequences, the latter as an entropy effect because the choice of configurations is more limited. The still smaller correlation and dielectric constants of *t*-butyl alcohol are readily understood as a result of still greater steric interference between neighbors which prevents extensive "polymerization."

Two other conclusions from the model of finite chains are significant for analysis of the relaxation processes. The first is that for any reasonable choice of association energy and entropy, the equilibrium fraction of single, unbonded molecules becomes rapidly insignificant at low temperatures, being of the order 10^{-3} at 220°K and 10^{-5} at 120°K from the calculations for the results of Fig. 4. These numbers are too small at all but the highest temperatures of the liquid for unbonded molecules to contribute significant polarizations. The second result is that the calculated concentration of singly bonded (chain end) molecules falls off at lower temperatures as $\exp(\Delta H/2RT)$. The concentration, though small, may be significant in the dispersion mechanism if it is a rate determining factor.

It should be recognized that the chain configurations considered are not to be envisaged as permanent polymer entities but rather as a time average representation of fluctuating local order and molecular coordination by hydrogen bonding.

C. Rate Laws of the Relaxation Processes

As in lower alcohols, the relaxation times do not give a linear plot of $\ln\tau_1$ *vs* $1/T$ for the entire range of temperatures. Hence they are not described by a simple rate law of the form

$$\ln\tau_1=-\ln k+\Delta H/RT, \tag{6}$$

unless temperature dependent values of k or ΔH are assumed. At the lower temperatures, linear plots are

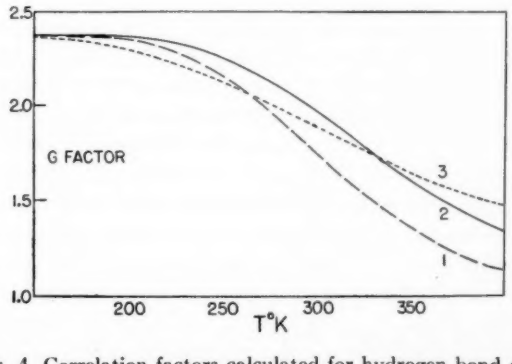

FIG. 4. Correlation factors calculated for hydrogen bond equilibria plotted against absolute temperature. Curve 1, $\Delta H=-7.7$ kcal/mole, $\Delta S=23$ cal/mole deg; Curve 2, $\Delta H=-7.7$ kcal/mole, $\Delta S=20.7$ cal/mole deg; Curve 3, $\Delta H=-4.6$ kcal/mole, $\Delta S=11.5$ cal/mole deg.

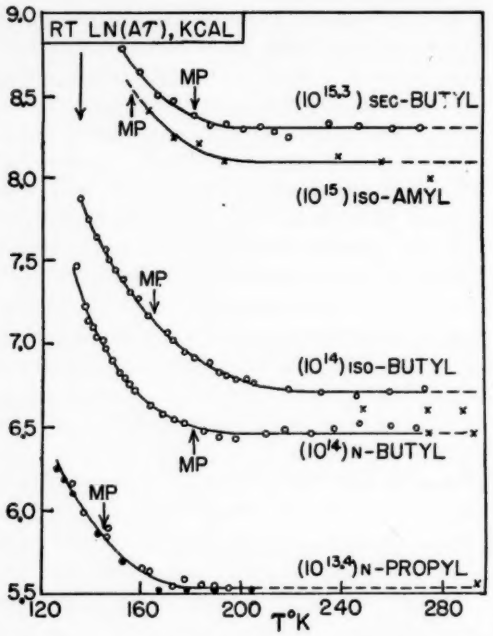

FIG. 5. Plots of $RT\ \ln(A\tau)$ against temperature for several alcohols, where τ is the relaxation time and the frequency factor A chosen is indicated in parentheses. $A \equiv k'$ used in text.

obtained for a relation of the form

$$\ln\tau = A + B/(T - T_\infty), \tag{7}$$

if the empirical constant T_∞ has a value of about 70° as for ethyl and propyl alcohols.[1,2] This relation fails, however, for the data at the higher temperatures of the present investigation, a conclusion which Magat and co-workers[9] reached for *n*-propyl alcohol by comparison of room temperature microwave results with the low temperature radio frequency data.[2]

Magat's conclusion that the deviations from the simple rate law (6) expressed by Eq. (7) set in only for the supercooled liquid is not supported by data now available for several alcohols. This can be shown by an analysis based on rewriting Eq. (6) in the form

$$RT\ \ln k'\tau = \Delta H + RT\ \ln(k'/k). \tag{8}$$

From this equation, a plot of $RT\ \ln k'\tau$ should for any values of k' be linear with intercept ΔH for $T=0$, and for a choice $k'=k$ the straight line will be horizontal. Plots of data for the three butyl alcohols are shown in Fig. 5, together with values for *n*-propyl alcohol,[2] and results of Mme. Reinisch[10] for *iso*-amyl alcohol. The horizontal lines at higher temperature result from the values of k' indicated by each curve and the departures at lower temperatures are obvious, as is the fact that their beginnings have no exact correspondence to the indicated melting points. It is thus reasonable to attribute the behavior at lower temperatures to onset of local structure which ultimately develops into the glassy state at temperatures in the range 70°–100°K, rather than to a change in character immediately and directly associated with the melting point.

TABLE III. Heats of activation and frequency factors for aliphatic alcohols at high temperatures.

Alcohol	ΔH (kcal/mole)	$-\log k$	Temp. range, °K
n-Propyl	5.54	13.4	>190
n-Butyl	6.29	14.2	200–270
iso-Butyl	6.72	14.0	220–270
sec-Butyl	8.26	15.3	220–270
iso-Amyl	8.08	15.0	200–270

The results also show that at temperatures sufficiently above the melting point one can deduce heats of activation and frequency factors from the measurements which have significance as a statement of the experimental results. The values obtained from the analysis are listed in Table III, together with the temperature intervals to which they apply (it is to be noted that the values from these fairly large intervals are in some cases appreciably different from those deduced by Magat[9] using less extensive data of several observers). Two general trends are indicated: both the heats and entropies are larger for the larger alkyl groups and for the less eccentric positions of the hydroxyl group. This dependence does not, however, in our opinion, mean that the primary origin of the dispersion is in the alkyl group. The effect appears rather to be a secondary influence involved in reorientation of hydrogen bonded hydroxyl groups, as discussed in the report of work on methyl-propyl alcohol solutions.[11]

The relaxation times τ_2 for the second dispersion could be obtained only below 155°K for *n*-butyl alcohol and 170°K for *iso*-butyl alcohol. Below these temperatures, the variations with temperature can be fitted by Eq. (7) with larger values of B and the same value $T_\infty = 72$°K as for the primary dispersion. The temperature range is thus one of major departures from simple rate law behavior, and so one in which it may again be surmised that structure effects are increasingly important. If this is so, it is probably best to await results at higher temperatures and frequencies before attempting detailed conclusions from these data, either by themselves or in comparison with results for other alcohols.

ACKNOWLEDGMENTS

One of us (W. D.) would like to acknowledge a fellowship from the E. I. du Pont de Nemours and Company.

[9] Magat, Brot, and Reinisch, Kolloid Z. **134**, 101 (1953).
[10] L. Reinisch, J. Chim. Phys. **51**, 113 (1954).
[11] D. J. Denney and R. H. Cole, J. Chem. Phys. **23**, 1767 (1955).

Dielectric Properties of Methanol and Methanol-1-Propanol Solutions

DONALD J. DENNEY* AND ROBERT H. COLE
Metcalf Chemical Laboratories, Brown University, Providence, Rhode Island
(Received January 5, 1955)

Measurements of dispersion in the solutions show that at all concentrations the principal dispersion is a simple relaxation process, while the higher frequency behavior gives evidence of overlapping dispersions. As in other alcohols, the temperature dependences of relaxation times differ markedly from simple rate laws, especially for temperatures below 200°K. The significance of the results in relation to reorientation of hydroxyl and alkyl groups and intermolecular hydrogen bonds is discussed. Difficulties in measurements on solid methanol are described and their possible origins examined.

I. INTRODUCTION

THE work reported here on methanol and methanol-1-propanol solutions was undertaken to extend previous investigations of aliphatic alcohols to the first member of the series.

The measurements of the liquid and solutions were made in order to study further the effect of the alkyl group on the several dispersion processes previously found for higher members. With the available range from 15 cy/sec to 2 Mc/sec, dispersion in the pure liquid could be measured only in a rather small interval of temperatures. The fact that solutions of alcohols supercool readily, and hence can be studied at lower temperatures and frequencies, led to measurements of methanol-1-propanol solutions. Originally intended as a means for extrapolation to properties of the pure liquid, this work gave illuminating information about the character of dispersion processes in alcohols as discussed later.

The measurements on solid methanol were prompted by several considerations. There are known to be two solid phases, the higher temperature one existing between the melting point (175.4°K) and a second-order transition at 158°K, below which a more ordered phase is stable. Tauer and Lipscomb[1] determined the high temperature x-ray structure to be orthorhombic with atomic positions indicative of chainwise hydrogen bonding in planes parallel to the *c*-axis. Large oxygen thermal amplitudes perpendicular to these planes appear to be lost in the lower temperature phase.

Smyth and McNeight[2] had in earlier work found evidence of dielectric dispersion in the high-temperature phase, but their limited frequency range gave only partial indications of the characteristics of the relaxation process. Further study of the behavior seemed worthwhile for further information on the polarization effects of the hydrogen bonding and the consequences of crystal anisotropy. Previous work in this laboratory on solid hydrogen bromide[3] had shown the existence of multiple dispersions in the orthorhombic ordered low-temperature phase, and an experimental means of preventing void formations with attendant gross errors in dielectric measurements had been developed. Similar procedures were used for the study of solid methanol, but the results were conflicting and rather inconclusive. Despite this, the observations are reported briefly, as they indicate difficulties to be overcome in a definitive investigation and by their nature suggest the underlying reasons for these difficulties.

II. EXPERIMENTAL METHODS

A. Preparation of Materials

Methanol was prepared by a modification of the procedure of Evers and Knox.[4] The synthetic starting material (Carbon and Carbide Chemicals Company) was dried by refluxing and distilling over magnesium. The condensate was refluxed over dried silver nitrate, and distilled in an atmosphere of dry nitrogen, and that portion of the distillate collected which had a specific conductance less than 5×10^{-8} mho/cm. The product was stored away from light in flasks previously treated with hot methanol vapor.

Tests for aldehydes and ketones using an alkaline solution of mercuric cyanide[5] were negative. Densities were $d_4^{25}=0.78665\pm0.0001$ (max), as compared with 0.78660 given in the International Critical Tables. Since the density increases by 0.003 per weight percent of water, less than 0.05% water content is indicated. The various tests and precautions were undertaken because of the hygroscopic nature of methanol and its tendency to undergo photochemical oxidation.

1-propanol (certified reagent from Fisher Scientific Company) was purified as in earlier work[6] and the product had a room temperature conductance in the range $6\text{–}20\times10^{-9}$ mho/cm. The solutions with methanol were prepared on a weight basis immediately before use. With the dielectric cells used, some rise of liquid conductance occurred on filling, which was minimized by

* Now at du Pont Photoproducts Department, Parlin, New Jersey. This work was supported in part by the Office of Ordnance Research.

[1] K. J. Tauer and W. N. Lipscomb, Acta Cryst. **5**, 606 (1952).
[2] C. P. Smyth and S. A. McNeight, J. Am. Chem. Soc. **58**, 1597 (1936).
[3] N. L. Brown and R. H. Cole, J. Chem. Phys. **21**, 1920 (1953).
[4] E. C. Evers and A. G. Knox, J. Am. Chem. Soc. **73**, 1739 (1951).
[5] H. Hartley and H. R. Raikes, J. Chem. Soc. **127**, 524 (1925).
[6] D. W. Davidson and R. H. Cole, J. Chem. Phys. **19**, 1484 (1951); R. H. Cole and D. W. Davidson, *ibid.* **20**, 1389 (1952).

several flushings and refillings. No effect of conductance differences on dielectric behavior was observed.

B. Dielectric Cells

The cell for solid methanol, described in detail elsewhere,[7] was a modification of the design used for work on solid hydrogen bromide.[3] Parallel plate nickel electrodes, one with a guard ring, were positioned by Teflon disks so attached as to produce expansion coefficients of the electrode spacings (2 and 1.2 mm) which were 4 and 7×10^{-4} per degree. These large coefficients acted to prevent void formations in the frozen samples between the electrodes, and the use of two spacings permitted tests for electrode polarization effects. The nominal capacitances were 1.0 and 1.6 $\mu\mu$f, exact values being obtained by calibration just above the freezing point of methanol.

The liquid cell is the one used in studies of ethanol[8] with minor modifications in the electrode connections to permit a different cooling system. These changes introduced a small residual direct capacitance between the high potential and guarded electrode leads, for which correction was made after calibration of the liquid capacitance to 0.5%. As a check, the dielectric constant of methanol was measured at 0°C with especial care. The value 37.92 obtained is in satisfactory agreement with the value 37.82 found by W. Dannhauser with another cell used for studies of butyl alcohols and the value 37.90 from the NBS tables.[9]

C. Electrical Measurements

The methods of dielectric and temperature measurement were similar to those for previous studies of alcohols.[6,8]

III. MEASUREMENTS ON SOLID METHANOL

A total of five runs were made on different samples. The results for the low-temperature phase stable below 157.8°K were quite reproducible, the values of dielectric constant at 152°K varying from 3.26 to 3.41 at 5 kc/sec with little dependence on frequency above 100 cy/sec. The temperature coefficient of these values and differences between samples were so small as to be indistinguishable from possible errors and uncertainties in the temperature dependent geometric capacitance of the cell.

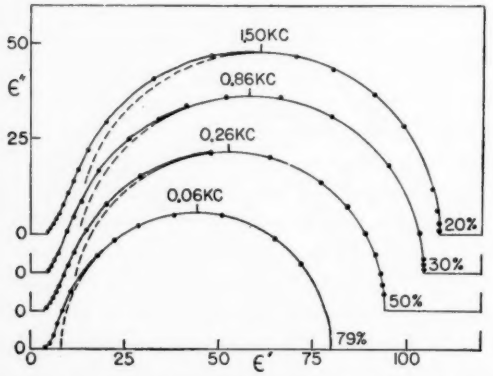

FIG. 1. Complex dielectric constants of four methanol-1-propanol solutions near 121°K.

The low values and slight temperature dependence are similar to the results of Smyth and McNeight,[2] and are typical of induced electronic and atomic polarization with no significant dipole polarization. It can therefore be concluded that a nonpolar configuration of dipoles is frozen in below the solid phase transition.

The behavior of the high-temperature phase stable from 157.8°K to the melting point at 175.4°K is more interesting from the point of view of dipole orientations, but, unfortunately, the present work does no more than indicate possible explanations of the highly variable results which were observed and suggest measures necessary to obtain values properly characterizing the volume properties of the solid.

The frequency dependence of dielectric constant was in all cases an increase at lower frequencies which showed no indications of leveling off at the lowest frequency of measurement (15 cy/sec). The values above 100 kc were independent of frequency and in the range 4.7 to 6.0 for temperatures more than three to five degrees below the melting point, then rose rapidly with increasing temperature to the value of ~75 characteristic of the liquid.

The increase of capacitance with decrease in frequency began at progressively higher frequencies as the melting point was approached, and values corresponding to dielectric constants of 10 to 15 or more were observed at 15 cy/sec several degrees below the melting point. This behavior was variable from one sample to another, and the following possible causes have been considered: (a) effects of voids in the sample which developed as it was frozen or subsequently cooled; (b) electrode or internal interfacial polarizations; (c) the anisotropic crystal structure.

The cell design employed was, as already described, patterned after ones found successful in other work on crystals where effects of voids were otherwise pronounced. We believe that there were no major errors of this kind sufficient to account for the discrepancies, and this conclusion is supported by the fact that dielectric constants for the low-temperature phase were reproducible from one sample to another or when obtained after a second cooling from the high-temperature phase. Further, measurements on a particular sample in the high-temperature phase could be repeated after a change of temperature and return to the original value, a procedure which almost invariably produces noticeable effects if cracks or voids are present.[3,10]

[7] D. J. Denney, Ph.D. thesis, Brown University, 1954.
[8] F. X. Hassion and R. H. Cole, J. Chem. Phys. **23**, 1756 (1955).
[9] Natl. Bur. Standards (U. S.) Circ. 514, Table of Dielectric Constants of Pure Liquids.
[10] R. W. Swenson and R. H. Cole, J. Chem. Phys. **22**, 284 (1954).

Electrode polarization errors are a similarly unlikely explanation, the evidence here being that there was no correlation of the varying values with change in the electrode separation from 2.0 to 1.2 mm, a change which should, other things being equal, have nearly doubled polarization errors. On the other hand, we have no grounds for ruling out the possibility of internal polarization effects at boundaries of microcrystals in the barely translucent solid samples. This explanation is similar to that surmised by Swenson and Cole[10] for low-frequency anomalies observed in the high-temperature phase of hydrogen chloride.

Probably the most important factor, however, is the fact that the high-temperature phase of methanol is now known from the x-ray work of Tauer and Lipscomb[1] to be significantly anisotropic with parallel linear chains of molecules. It is then to be expected that there will be large differences in polarizabilities parallel and perpendicular to the axis of these chains. With a polycrystalline sample, a highly variable net contribution to the average dielectric constant could result, depending on the conditions of growth in the freezing process. In this connection, it is significant to note that values obtained initially for a particular sample could not be reproduced after cooling to the low-temperature phase and rewarming.

Under the circumstances outlined, it is not possible to say whether the observed dispersion was a genuine volume effect, a consequence of internal surface effects, or both. Probably the whole question can be properly resolved only by measurements of single crystals. Growth of crystals large enough for the measurements would require considerable effort or ingenuity, but we doubt that reliable or meaningful dielectric data for solid methanol will otherwise be obtained.

IV. MEASUREMENTS ON METHANOL-1-PROPANOL SOLUTIONS

The dielectric behavior was determined by measurements of dielectric constant and loss for frequencies below 2 Mc/sec. At temperatures below about −140°C, variations in both real and imaginary parts, ϵ' and ϵ'', could be measured, while at higher temperatures only the variations of absorption conductance, and hence ϵ'', with frequency were measurable. The latter, in conjunction with the more complete results at lower temperatures, even so gave significant information about the relaxation behavior.

A. The Primary Dispersion

This dispersion, accounting for most of the dipole contribution to the static polarization, is for all concentrations accurately described by a Debye function. The low-frequency dispersion in solution is thus a single process with a rate which varies continuously between the extremes for the pure components, rather than being a concentration dependent sum of component contributions which preserve their identity in the solutions. As examples, data for four different concentrations at temperatures near 121°K are plotted as complex plane loci in Fig. 1. The semicircular loci show the agreement with the equations for a single relaxation time τ_1 and limiting low- and high-frequency dielectric constants ϵ_0 and ϵ_1. Representative values of these parameters, determined from the data by the analyses described in reference 8, are listed in Table I.

TABLE I. Parameters of dispersions in methanol and methanol-1-propanol solutions. (Values in parentheses are estimated or obtained by extrapolation.)

(a) Methanol T°K	ϵ_0	ϵ_1	ϵ_∞	τ_1(μsec)	τ_2(μsec)
273.2	37.92				
250.7	43.53				
232.6	49.00				
210.6	57.35				
196.5	63.26	(8.6)		0.0012	
187.2	67.91	(8.8)		0.0019	
176.5	73.76	(9.3)		0.0033	
170.0	77.70	(9.6)		0.0050	
163.3	82.17	(9.8)		0.0081	
(b) 20 wt percent 1-propanol					
271.6	35.12				
241.7	42.27				
202.9	55.19	(7.9)		0.0016	
181.6	64.67	(8.7)		0.0040	
169.2	71.46	(9.5)		0.0094	
158.3	77.56	(10.0)		0.0230	
125.2	102.7	11.3		22.1	1.6
120.5	104.8	12.6	4.3	159	21
115.7	(113.8)	13.6	4.0	2040	320
(c) 30 wt percent 1-propanol T°K	ϵ_0	ϵ_1	ϵ_∞	τ_1(μsec)	τ_2(μsec)
273.2	33.25				
234.9	42.36				
202.1	52.96	(7.8)		0.0018	
176.0	64.47	(8.7)		0.0077	
157.4	74.92	(9.7)		0.0380	
137.4	89.62	10.6		0.872	
126.9	98.68	11.4	4.4	17.5	1.1
123.0	102.5	12.5	4.2	81.4	7.9
119.0	107.0	12.4	3.8	527	65
116.1	(110.1)	12.5	3.7	2540	
(d) 50 wt percent 1-propanol					
273.2	30.43				
235.2	38.52				
200.4	48.78	(6.3)		0.0034	
176.9	58.07	(7.0)		0.0136	
160.0	66.55	(7.7)		0.0634	
138.6	79.88	8.8		2.02	
131.6	85.17	9.2	3.9	12.8	0.45
124.8	90.86	10.4	3.8	138	9.3
118.6	(96.6)	10.3	3.6	2020	200
(e) 79 wt percent 1-propanol T°K	ϵ_0	ϵ_1	ϵ_∞	τ_1(μsec)	τ_2(μsec)
273.2	26.41				
238.5	32.91	(4.3)		0.0016	
200.1	42.29	(5.0)		0.0107	
176.8	50.16	(5.5)		0.0557	
163.3	55.68	5.6		0.207	
149.3	62.49	6.6		1.53	
140.1	67.68	6.9		9.71	
136.5	69.81	6.7	3.2	22.8	0.27
130.5	73.52	7.2	3.2	127	2.0
121.7	(79.8)	8.2	3.2	2630	79

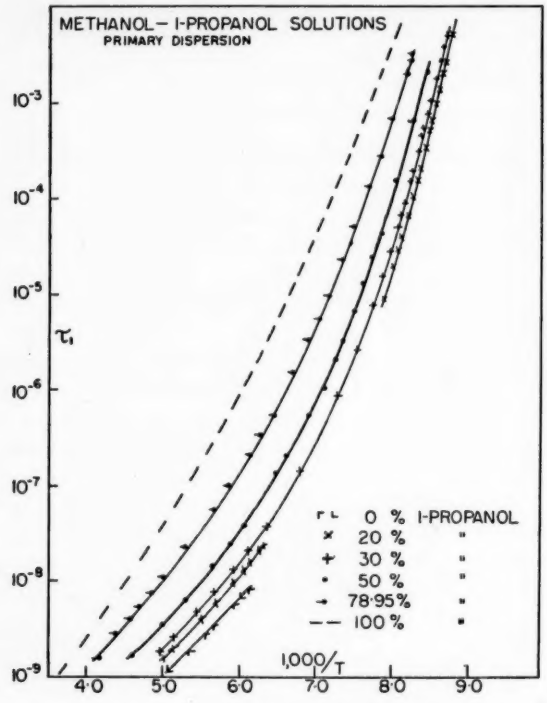

FIG. 2. Rate plots of relaxation times for the principal dispersion in methanol-1-propanol solutions.

The temperature dependences of relaxation times τ_1 are shown in the rate plot of $\log\tau_1$ *versus* $1/T$ in Fig. 2. These show marked curvature in all cases at temperatures between 140 and 160°K. Thus no temperature independent slopes or activation energies can be deduced from the data, and an onset of structural effects as for pure alcohols is indicated. The relaxation times for pure methanol were deduced from absorption conductance data together with known values of ϵ_0 and estimates of ϵ_1, and the linear rate plot corresponds to an activation energy of 3.8 kcal/mole in the range 163–197°K, a figure which is somewhat less than values of order 4.5 to 6 kcal/mole often cited for the energy of breaking hydrogen bonds in alcohols.

The equilibrium dielectric constants ϵ_0 can be fitted by empirical equations of the form $\epsilon_0=A+B/T$, with A varying from -16.8 for the 79% solution to -25.8 for the 20% solution. The negative values of A have, of course, no physical meaning, but rather indicate increasing correlation of molecular orientation at lower temperatures.

B. Secondary Dispersions

The simplicity of the lower frequency dispersion data is more striking when set in opposition to the fact that the data at higher frequencies show a complicated structure indicative of two overlapping contributions.

The further dispersion was analyzed by the additive assumption employed previously[6] to obtain values of dielectric constant and loss remaining after subtracting contributions of the principal low-frequency dispersion. The complex plane loci in Fig. 3 of values for four solutions at nearly the same temperature show a broad range of dispersion frequencies, and for the 79 weight percent solution in particular indicate a break at 700 cy/sec between two overlapping regions. That this overlapping is real is further indicated by the plots in Fig. 4 for this concentration at four temperatures, which show the same effect in every case. This effect was also evident in the 50 weight percent solution but could not be discerned with certainty at the lower concentrations of 1-propanol. The great breadth of the curves as compared to those for pure 1-propanol indicate, however, an overlapping of dispersions too broad and close in frequency to be resolved. On the basis of the evidence, the two compounds in solution act as distinct species in contributing to the secondary dispersion, each contribution, however, being modified by the presence of the other component.

The complicated structures of the curves in Figs. 3 and 4 are not conducive to representations by simple formulas, and quantitative reporting of the results is here limited to the listing in Table I of relaxation times τ_2 corresponding to the frequencies of maximum loss of such curves and the high-frequency limits ϵ_∞. One point of difficulty in the analysis to obtain the curves should be mentioned, namely, that the low-frequency intercepts of the derived high-frequency curves were noticeably larger than the limits ϵ_1 of the primary dispersion, rather than the same, as the analysis tacitly assumes. We venture the suggestion that this inconsistency is related to the closeness of the times τ_1 and τ_2 for the dispersions and consequent interaction of the underlying processes. It may be noted in this connection that the ratio τ_1/τ_2 varies from about 6 to 14 for the 20% solution in the range 115 to 125°K, while for the 79% solution the values vary from 33 at 122°K to 86 at 136°K.

One further result of significance is the fact that the relative amplitudes of the first and second dispersions do not depend significantly on temperature over the ranges studied and vary monotonically with concentration.

C. Discussion

In previous discussions[8] it has been proposed that the low-frequency dispersion process involves the partial breaking and reforming of intermolecular hydrogen bonds to permit reorientation of hydroxyl groups. In support of this explanation may be cited the evidence from a variety of equilibrium data, including the static dielectric constants, for extensive chainwise association by hydrogen bonding, together with the fact that the dispersion has simple Debye character rather than covering a broader frequency range as found in true polymers and predicted, for example, by the Kirkwood-Fuoss[11] theory of dilute polymer solutions. That the

[11] R. M. Fuoss and J. G. Kirkwood, J. Chem. Phys. **9**, 329 (1941).

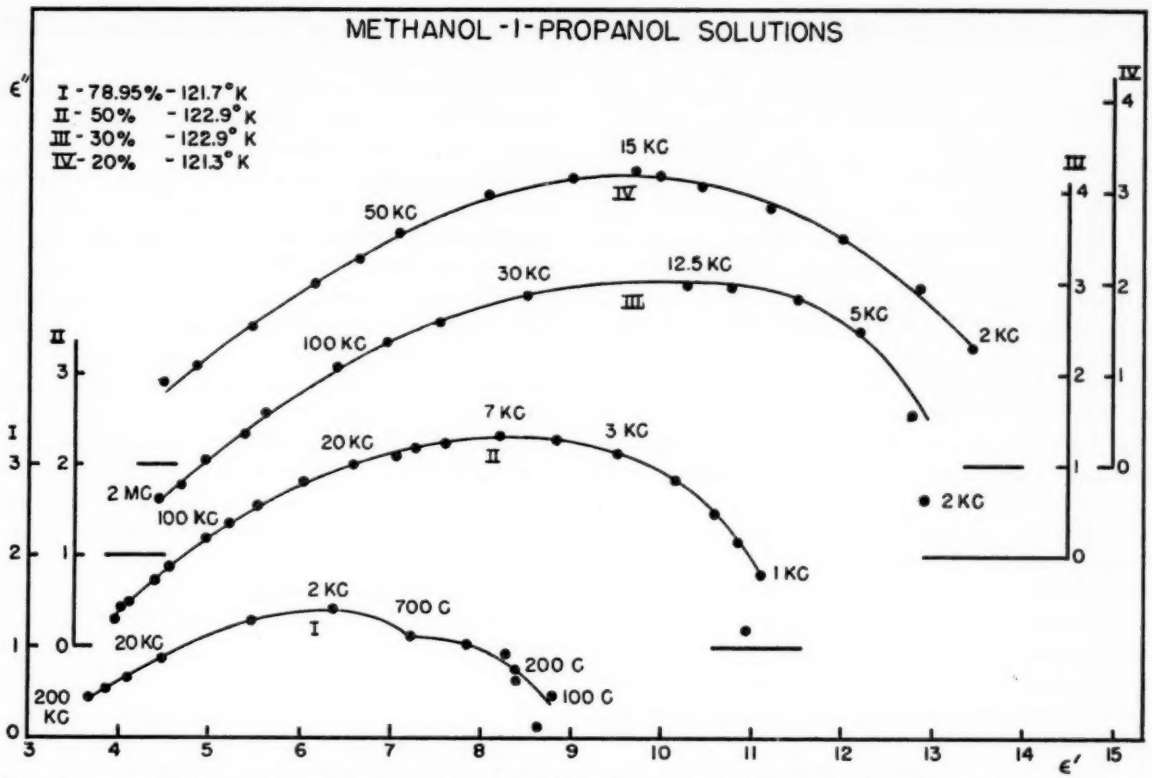

FIG. 3. Complex high-frequency dielectric constants, after subtraction of calculated principal dispersion contribution, for four solutions near 122°K. Ordinates for the curves have been displaced vertically to avoid overlap.

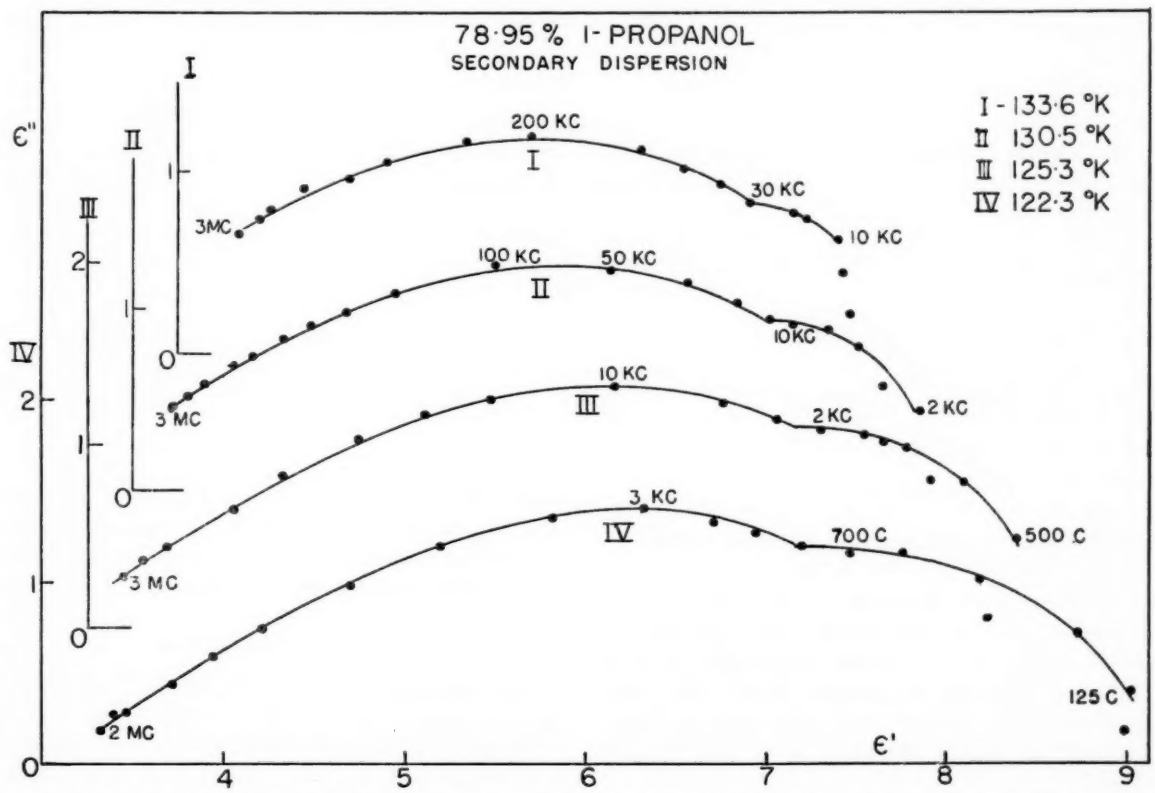

FIG. 4. Complex high-frequency dielectric constants, after subtraction of calculated principal dispersion contribution, for 79 wt percent 1-propanol solutions at four temperatures. Ordinates for the curves have been displaced vertically to avoid overlap.

simple frequency dependence is found also for solutions when the pure liquids have considerably different characteristic frequencies of dispersion suggests that the underlying process must involve rearrangements of large enough regions of the solution that the individuality of the two species of molecules is not significant. This conclusion is not inconsistent with the viewpoint that changes in hydrogen bonding are an essential element in the process, as the necessary energy and configurations must first be realized from interactions with the surroundings and then returned with a resultant net increase in thermal energy.

Similarly simple relaxation spectra have been reported by Schallamach[12] for solutions of 1-propanol with geraniol and glycerol. The temperature dependence of dielectric constant and loss at single frequencies led him to conclude that only a single dispersion region existed, whereas measurements on mixtures of one "associated" and one "nonassociated" liquid gave evidence of two superposed regions. On the basis of the evidence, one can reasonably discuss the dispersion in terms of single molecule processes only with due consideration of the interactions with neighboring molecules which are necessary for the realization of such processes.

The further dispersions at higher frequencies are significant by contrast. The proposition advanced by Magat and co-workers[13] that they result from unbonded or singly bonded molecules seems to us untenable in view of the fact that the concentration of such molecules, and, consequently, their contribution to the observed dispersions, would be strongly temperature dependent, contrary to the experimental evidence of no significant change in relative amplitudes of the principal and higher frequency dispersions with temperature. The explanation previously suggested for ethanol,[8] that higher frequency dispersion results from reorientations of C—O bond moments, is, however, compatible with the solution results if there is a specific influence of the molecular alkyl groups attached to the carbinol group (COH). This process must again, as for the principal dispersion, be considered in relation to the necessary interactions with neighbors for it to take place, and so apparent activation energies should not be discussed in terms of single molecule processes. The reasonably similar temperature dependences of the low- and high-frequency processes in fact suggests the importance of the interaction considerations.

ACKNOWLEDGMENTS

One of us (D. J. D.) would like to acknowledge a fellowship from the National Science Foundation.

[12] A. Schallamach, Trans. Faraday Soc. **42**, 180 (1946).

[13] Magat, Brot, and Reinisch, Kolloid Z. **134**, 101 (1953).

THE JOURNAL OF CHEMICAL PHYSICS VOLUME 23, NUMBER 10 OCTOBER, 1955

Excited Triplet States of Polyatomic Molecules. II. Flash-Lamp Studies on Aromatic Ketones*

DONALD S. MCCLURE AND PHILLIP L. HANST†
Department of Chemistry and Chemical Engineering, University of California, Berkeley, California
(Received December 8, 1954)

The apparatus for observing triplet-triplet transitions in polyatomic molecules is the same as in part I except that resonance lamps are here replaced by a flash lamp. Triplet-triplet spectra are reported for benzophenone, acetophenone, β-bromo and β-iodo naphthalene. No triplet-triplet absorption was found in benzene, biacetyl, acetone dibromo benzene, or diisopropyl ketone. Detailed studies of the energy levels of benzophenone and acetophenone are reported.

I. INTRODUCTION

THE high-intensity flash tube has been applied by Porter[1] and others to locate the absorption spectra of metastable molecules. It was desirable to apply this method to the search for triplet-triplet absorption bands, since it should be possible to work with substances having metastable triplet state half-lives as short as the half-life of the flash from the lamp. As expected, we had no difficulty in locating triplet-triplet absorption in a number of compounds. Detailed studies of the energy levels of benzophenone and acetophenone were made in order to correlate the new triplet levels found with the singlet levels.

II. EXPERIMENTAL

Our apparatus was essentially the same as in the previous report[2] except that the resonance lamps were replaced by a single flash tube (the photoflash) and the tungsten or hydrogen lamp used for continuous

* Supported in part by the Office of Naval Research.
† Now at the Franklin Institute, Philadelphia, Pennsylvania.
[1] G. Porter, Proc. Roy. Soc. (London) **A200**, 284 (1950).

[2] D. S. McClure, J. Chem. Phys. **19**, 670 (1951). Hereafter referred to as I.

background for the absorption spectrum was replaced by a second flash tube (the spectroflash). The arrangement for triggering the lamps and observing the absorption was very similar to Porter's.[1] The photoflash lamp excites the substance to its metastable triplet state, and 0.5 millisecond later, a rotating shutter between the sample cell and spectrograph slit opens. Simultaneously the spectroflash is triggered, and during a period of about 0.1 millisecond the absorption spectrum is photographed. Three repetitions of this process usually gave the most desirable plate blackening.

The spectroflash lamp had a one-mm bore quartz tube and was filled with argon at a pressure of 10 cm. A discharge of a 9 μf condenser at 10 000 volts through this tube produced partially continuous emission from 9000 A to 1900 A.

The photoflash was a one-cm diameter quartz tube with heavy sealed-in tungsten rods for electrodes, 36 cm apart. It contained argon at 10-cm pressure. The light emitted was not entirely continuous, but this was of no disadvantage to us. In order to achieve reliable triggering, both lamps were supplied with an internal third electrode 8 or 10 cm from the grounded main electrode.

The output of the lamp was measured by using the uranyl oxalate actinometer.[3] The uranyl ion concentration was 0.002 molar and the cylindrical absorption cell had an inside diameter of 12 mm. Under these conditions, the absorption would be greater than 90% at wavelengths shorter than 3200 A. Assuming an average quantum yield of 0.55 over the wavelength range below 3200 A the total number of moles of quanta absorbed in a 19 000 volt, 10 μf flash was 1.6×10^{-5}. Under the more usual conditions employed by us, 4400 volts and 80 μf, 4.2×10^{-6} moles of quanta in this wavelength region entered the cell. The actual number of quanta absorbed by a given sample would be difficult to determine, but these measurements give an order of magnitude value, since the range of high absorption by uranyl ion is close to the range of high absorption of many of the substances used.

The sample was contained in the rigid solvent[4] EPA at a low temperature as in I. A cell length of 19 cm was used in all experiments. We found that the heat generated in the solvent by the absorbed light from the flash caused the solvent to crack if liquid nitrogen was used as refrigerant. The solvent is evidently under stress, and the additional stress brought about by sudden thermal expansion causes the cracking. This problem was overcome by using liquid oxygen for refrigeration. Because of its higher boiling temperature, oxygen does not bring about the extra thermal contraction which nitrogen does, and the solvent is more strain free. The use of liquid oxygen in this apparatus is very hazardous, and we suggest that redesigning the cell or the use of a different solvent would be a better solution of the problem.

[3] M. Christie and G. Porter, Proc. Roy. Soc. (London) **A212**, 390 (1952).

[4] EPA is ethyl ether 5 parts, isopentane 5 parts, ethanol 2 parts, by volume.

TABLE I. Triplet-triplet absorption bands observed. Solvent, EPA; temperature 77°K.

Substance and molar concentration	Bands (A)
β-iodo napthalene, 0.000051	4240, 4000 (peak positions)
β-bromo napthalene, 0.000024	4230, 3980 (peak positions)
acetophenone 0.083 and 0.00083	Strong absorption beginning 4000
benzophenone 0.001, 0.00034, 0.000034	Strong band 5580 to 4900
	Strong absorption beginning 4050

III. RESULTS

With intense light over a broad region of wavelengths, the value of the concentration of the absorbing substance is not such a critical matter as it was in I, where mercury resonance lamps were used. It was observed in several cases that the triplet-triplet absorption simply became stronger as the concentration increased.

The triplet-triplet absorption of β-iodo-napthalene was expected to lie slightly to the red of the corresponding napthalene bands, and we therefore used this as a test substance. The bands found are given in Table I. The lifetime of the absorption was measured roughly by spacing the spectroflash 1, 5, and 10 milliseconds after the photoflash and observing the absorption intensity. The latter was strong, weak, and zero for the three times, respectively, in agreement with the 2.5 milliseconds mean lifetime of the metastable triplet state.[5] The expected triplet-triplet absorption was also easily found in β-bromo napthalene (lifetime of triplet state, 0.021 sec in EPA).[5] This was reported in I as a set of very faint bands, but it appeared strongly in these experiments.

Only two substances out of the seven investigated (not including the halogen naphthalenes) showed triplet-triplet absorption: benzophenone and acetophenone. The triplet state mean lifetimes in EPA of these substances are 0.006 and 0.008 second, respectively.[5] Figure 1 shows the triplet-triplet bands of these two compounds. This figure was made from microphotometer tracings of the photographs of (a) the spectrum obtained with only the spectroflash and (b) the spectrum obtained with both the spectroflash and the photoflash. The logarithm of the plate blackening in (a) was subtracted from that of (b). The resulting curve should be approximately proportional to the optical density of the absorbing substance. Optical density units are arbitrary as the plate gamma is not known. The extinction coefficient for the $T-T$ absorption could not be determined because the triplet

[5] D. S. McClure, J. Chem. Phys. **17**, 905 (1949).

concentration is not known. The largest error in the curves resulted from the attempt to correct for the emission spectra. The benzophenone curve is therefore uncertain in the region from 24 300 to 20 000 cm^{-1} and the acetophenone curve from 25 500 to 22 000 cm^{-1}. The slow rise in the benzophenone curve from 24 000 to 28 000 cm^{-1} seems to be real. This step-out could correspond to an electronic transition distinct from the one causing the sharp rise at 28 000 cm^{-1}, but more accurate photometric work would be necessary in order to verify this. The sharp peak at 18 700 cm^{-1} certainly represents another electronic transition. At high-benzophenone concentrations the entire spectral region from 15 000 to 32 000 cm^{-1} exhibits absorption. Only the one band beginning at about 25 500 cm^{-1} and extending to at least 32 000 cm^{-1} appears in the acetophenone spectrum. There is no general absorption at high concentrations as with benzophenone.

The violet bands of each substance fell in the region of the carbonyl absorption bands. The $T-T$ bands are so much stronger that very low concentrations could be used and the $S-S$ absorption did not interfere. In the case of benzophenone, we can say that if all the molecules were in the metastable triplet state in the experiments, the molar extinction coefficient, ϵ, for the observed $T-T$ bands would be 3000 at the peak, assuming an optical density of 2.0. Since only a small fraction were actually in the metastable state, ϵ must be greater than 3000.

We failed to find $T-T$ bands in the three aliphatic ketones, acetone, diisopropyl ketone, and biacetyl. In biacetyl at least, the triplet state should have been well populated under our experimental conditions, and we can only conclude that $T-T$ transitions in this region are very weak.

We searched the spectral region from 15 500 to 32 000 cm^{-1} for triplet-triplet absorption in benzene and *p*-dibromo benzene, but with no success.

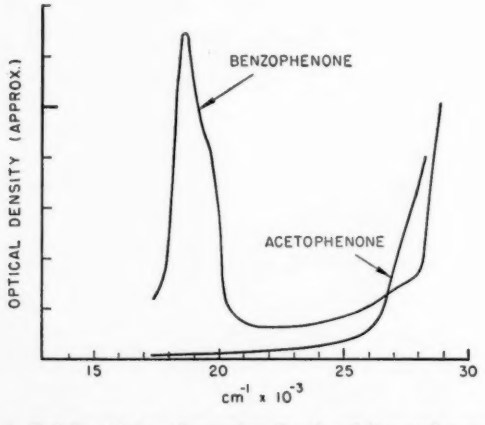

FIG. 1. Triplet-triplet absorption bands of benzophenone and acetophenone. The units of optical density are arbitrary, and the intensity scale is only to be interpreted qualitatively. The solvent is EPA, and the temperature, 77°K.

IV. THE ELECTRONIC ENERGY LEVELS OF BENZOPHENONE AND ACETOPHENONE

In order to learn more about the energy-level diagram of benzophenone, its ordinary absorption and emission spectra were studied. The polarized absorption and emission of single oriented crystals were photographed at 20°K. The benzophenone used was carefully purified by formation of the oxime and subsequent recrystallizations, decomposition of the oxime, recrystallization of the ketone, and a final sublimation *in vacuo*. The freshly prepared crystals gave a blue emission consisting of broad bands, very similar to the emission spectrum from a solid glassy solution of benzophenone.[6] These bands are shown in Fig. 2 and are recorded in Table II with those found by Gilmore *et al.* for comparison. The main peaks of the crystal emission spectrum are uniformly 500 cm^{-1} to the red of the broad peaks of the solution spectrum. This series of peaks undoubtedly represents a progression of the carbonyl stretching frequency. A shoulder appears on the red side of each peak of the crystal spectrum.

The emission spectrum of Fig. 2 is entirely different from that recently reported by Pesteil.[7] We were able to obtain a spectrum like his at 77°K in crystals of benzophenone which had stood in the room for a while. The spectrum of Fig. 2 is that of freshly purified, sublimed, and remelted material. The change in the spectrum may be the result of a polymorphic change in the crystal as it is known that there are four polymorphic crystal forms. We have not investigated this interesting

TABLE II. Emission and long wavelength absorption of benzophenone crystal. Peak positions and intensities are given.

(a) Emission of crystal, 20°K			(b) Emission from solid solution (EPA), 77°K	
$\nu(cm^{-1})$	Int.	Analysis	$\nu(cm^{-1})$	Int. (arbitrary units)
23 800	s	0–0	24 300	4.5
23 300	w (Shoulder)	0–500		
22 120	vs	0–1680 = ω_1+2x_{11}	22 700	7.0
21 700	m (Shoulder)	0–2100		
21 000	w	0–2800		
20 520	m	0–3280 = $2\omega_1+6x_{11}$	21 000	4.5
18 950	w	0–4850 = $3\omega_1+12x_{11}$	19 550	2.0
$\omega_1=1740\ cm^{-1}$, $x_{11}=-30\ cm^{-1}$			18 100	0.5

(c) Absorption of crystal, 20°K		
$\nu(cm^{-1})$	Int.	Analysis
26 580	s	0–1220 = ω_1+2x_{11}
27 800	vs	0–2380 = $2\omega_1+6x_{11}$
28 960	vs	0–3470 = $3\omega_1+12x_{11}$
30 050	s	0–4550 = $4\omega_1+20x_{11}$
31 130	m	0–5620 = $5\omega_1+30x_{11}$
32 200	w	
$\omega_1=1240\ cm^{-1}$, $x_{11}=-20\ cm^{-1}$		

[6] Gilmore, Gibson, and McClure, J. Chem. Phys. **20**, 829 (1952).

[7] P. Pesteil and M. Barbaron, Compt. rend. **238**, 1789 (1954).

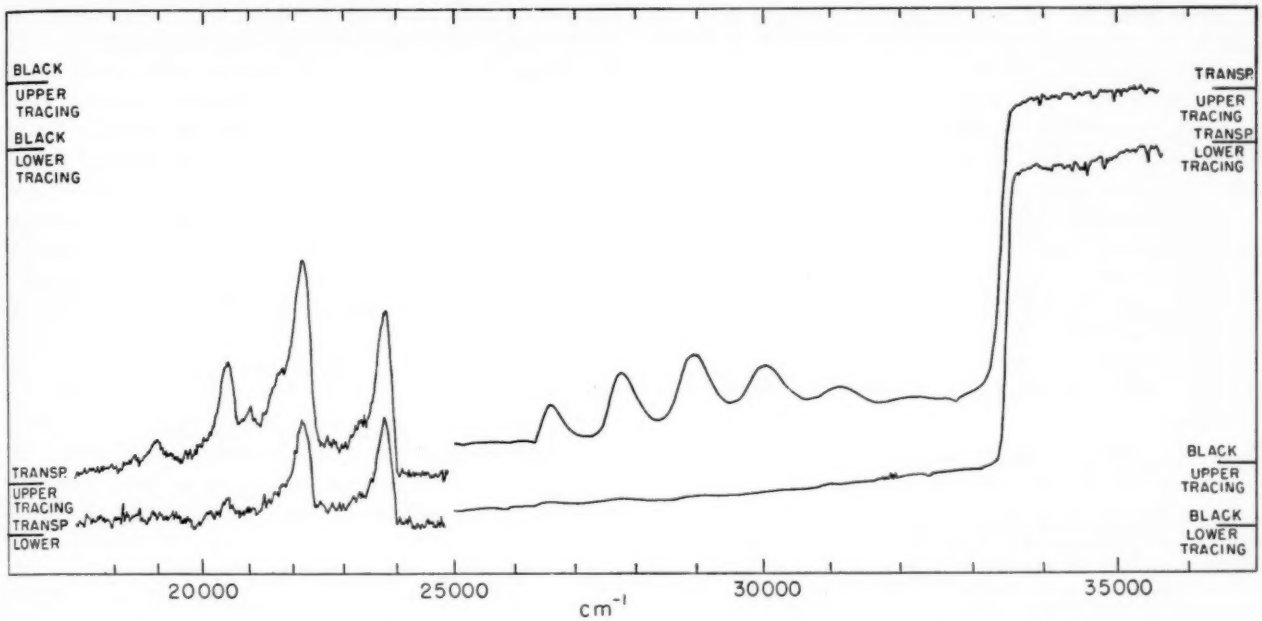

FIG. 2. Right: Polarized absorption of mono-oriented benzophenone crystals at 20°K. Top tracing perpendicular to needle axis, lower tracing along needle axis. Left: Polarized emission of the same crystals at 20°K.

possibility. The origin of the fluorescence reported by Pesteil is 24 000 cm^{-1}, while ours is at 23 800 cm^{-1}.

It is interesting to note the work of Ferguson and Tinson[8] in this connection. They discovered that the solid solutions of benzophenone in petroleum ether gave a blue-emission spectrum at low concentrations, and a green emission spectrum at higher concentrations. These spectral changes in solution and crystal do not seem to be completely understood.

The crystals formed by seeding a melt between quartz plates grow in groups of elongated crystallites with the long axes within a sector of about 5°. Extinction between crossed nicols occurs along this direction and by means of the quartz wedge, this is found to be the direction of minimum refractive index. The ultraviolet absorption of such mono-oriented crystals was entirely confined to the direction perpendicular to the needle axis. The absorption at 20°K is also shown in Fig. 1. The crystal thickness was about 10 microns. Crystals which appear the same were grown between NaCl plates and the polarized infrared spectrum in the carbonyl absorption region was determined.[9] The absorption was a maximum in the direction of ultraviolet absorption. (The uv absorption of the crystal between salt plates was in the same direction as in the other crystals.) Therefore the carbonyl groups must lie predominantly in a plane perpendicular to the needle axis. Corroborative evidence is furnished by the work of Banerjee and Haque.[10] They correlated the x-ray and diamagnetic anisotropy studies on the crystal modification obtained by precipitation of benzophenone from alcohol-water mixtures. This would be one of the modifications described by Groth.[11] The crystal is orthorhombic and the magnetic susceptibility along the c-axis is -149.3×10^{-6}, somewhat smaller than for the perpendicular direction in biphenyl. They assume therefore that the planes of the rings of the benzophenone molecule lie approximately but not exactly perpendicular to the c-axis. The carbonyl groups must therefore lie in a plane perpendicular to the c-axis. The c-axis must be the direction of minimum refractive index because of the way the rings are oriented with respect to it. This identifies the needle axis of our crystals as the c-axis. Even if the crystal modification is different in our experiments from that of Banerjee and Haque the molecular planes cannot be very far from perpendicular to the needle axis. Thus it seems quite certain that the ultraviolet carbonyl absorption band in benzophenone is polarized exclusively in the plane of the molecule. The emission spectrum is predominantly perpendicular to the needle axis also, but an appreciable portion is in the other polarization. We cannot say with certainty whether this is brought about by depolarizing influences of some sort, or if it means that the fluorescence polarization with respect to molecular axes is really different from the absorption.

We can say nothing about the polarization in the molecular plane from the crystal data. The planes parallel to the needle axis are probably 110 and 010, judging from Groth's diagram,[11] and both planes may grow prominent enough to make some contribution to absorption in the samples we used.

[8] J. Ferguson and Tinson, J. Chem. Soc. (London) 3083 (1952).
[9] We wish to thank Dr. George Pimentel for his help in this.
[10] K. Banerjee and A. Haque, Indian J. Phys. **12**, 87 (1938).
[11] P. Groth, *Elemente der Physikalischen und chemischen Krystallographie* (R. Oldenbourg, Munich and Berlin, 1921), p. 157.

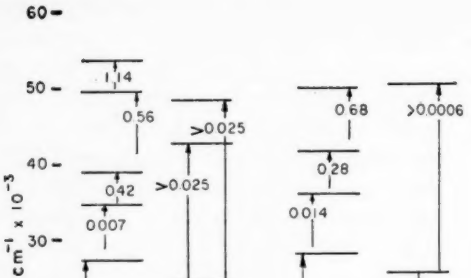

FIG. 3. Energy-level diagrams of benzophenone and acetophenone showing positions of the triplets relative to the singlets. Triplets are on the right of each diagram, singlets on the left. The *f*-numbers of the observed transitions are given. All the transitions in the singlet system originate at the ground state. The arrows on the diagram were not drawn to the ground state to avoid complications.

The polarization studies were not made in the region of strong absorption because thin enough crystals would be difficult to obtain and because intermolecular forces in the region of the allowed transitions would affect the spectrum in an unpredictable manner. Solution spectra at room temperature show that there are probably two regions of absorption[12] between 30 000 and 45 000 cm^{-1} and the spectra of the hindered benzophenones show two distinct peaks in this region (reference 12, spectrum No. 142). These bands are moderately well resolved in the spectrum at 77°K in a rigid glass, and we were able to obtain values for the *f*-numbers of the two transitions. The weak band has its peak at about 34 600 cm^{-1} with ϵ_{max} of 1900: the strong band has its peak at 39 000 cm^{-1} with ϵ_{max} of 18 500. Even stronger peaks appear in the spectrum at 49 000 cm^{-1} with ϵ_{max} of 31 000 and at 53 500 cm^{-1} with ϵ_{max} 56 000.[13] The origins of all these transitions are difficult to determine because of the overlapping and breadth of the bands. Figure 3 is an energy-level diagram showing the positions of singlets and triplets. The estimated energy of the vibrationless state is given except for the singlets above 30 000 cm^{-1}, for which the positions of the absorption maxima are given. The observed transitions are indicated on the diagram with an estimate of the *f*-number computed from the absorption intensity or, in the case of the triplet emission, from the lifetime of the excited state.

The spectrum of acetophenone is similar to that of benzophenone. The ordinary solution spectrum in hexane[14] shows the peak of the carbonyl transition to lie at 31 000 cm^{-1}, with $\log\epsilon_{max}=1.6$; the next peak is at 35 000 cm^{-1}, $\log\epsilon_{max}=2.9$, and the next is at 41 500 cm^{-1}, $\log\epsilon_{max}=4.1$. Since the spectrum of acetophenone should be very similar to that of benzaldehyde,[13] there should be a peak at 50 000 cm^{-1} with $\log\epsilon_{max}$ about equal to 4.3, and probably another high peak not far beyond 55 000 cm^{-1}. The emission spectrum[15] begins at 25 500 cm^{-1} in the low-temperature solid solution (EPA). The $T-T$ absorption found for this molecule must therefore have an upper state at about 50 500 cm^{-1} above the ground state. The energy-level diagram is shown in Fig. 2 for comparison with that of benzophenone.

The spectra of aldeheydes and ketones have been discussed by McMurry[16] and we will adopt his labeling of the symmetry elements and the other nomenclature used in these papers. The states of these molecules are approximately describable by using C_{2v} symmetry as far as transitions localized in the carbonyl group are concerned. The lowest frequency absorption and emission bands have the familiar properties of such transitions in the two molecules of interest here. According to theory, the upper states of these transitions are $^3A_2$ (emission bands) and $^1A_2$ (absorption bands). Our data lend some support to these assignments.

If the weak absorption at about 30 000 cm^{-1} is a $^1A_1 \rightarrow {}^1A_2$ transition, it is electronically forbidden and can only take place through destruction of the C_{2v} symmetry or by vibrational-electronic interaction. According to R. N. Jones[17] the rings of the benzophenone molecule must be tilted by about 30° to each other, so that there would seem to be ample distortion to permit the transition to occur. It is rather surprising that in the almost planar molecules of anthrone and fluorenone, the transitions corresponding to the benzophenone 30 000 cm^{-1} transition have the same, and greater strength, respectively. We therefore tested the possibility that a definite vibration makes the transition in benzophenone appear, and looked to the red of the first strong band of the 30 000 region for some trace of the 0—0 band which might be made to appear because of forces between molecules in the crystal. In crystals 0.1 and 2 mm thick, the absorption begins at 25 900 cm^{-1} (at 77°K), whereas in the 0.01 mm crystal of Fig. 2 it begins at 26 300 cm^{-1}. No other bands appear to the red of the peak at 26 580 cm^{-1}. This peak must therefore represent a O—O band of a certain kind; we suppose that its diffuseness means that it is composed of transitions to many low-frequency vibrations of the upper state and that the intensity distribution in the peak results from the combined effect of the Franck-

[12] Friedel and Orchin, *Ultraviolet Spectra of Aromatic Compounds*, John Wiley and Sons, Inc., New York, 1951. Spectrum No. 140.
[13] Platt and Klevens, A Survey of Vacuum Ultraviolet Spectra, Office of Naval Research Technical Report, 1954, Contract N6ori 20 IX, Fig. 42.
[14] Landolt-Bornstein Tabellen, Vol. I, part 3, sixth edition, 1951, p. 270, Fig. 132.
[15] R. Vanselow and A. Duncan, J. Am. Chem. Soc. **75**, 829 (1953).
[16] H. L. McMurry, J. Chem. Phys. **9**, 231, 241 (1941).
[17] R. N. Jones, J. Am. Chem. Soc. **67**, 2141 (1945).

Condon Principle and vibrational-electronic interaction. If the upper state is $^1A_2$, the only vibrations which can cause the observed in-plane polarization are out-of-plane vibrations. Some vibrations of this type in benzophenone must certainly be low enough in frequency to account for the diffuseness of the O—O peak. In-plane vibrations could have only a minor effect on the transition moment of a $^1A_1 \rightarrow {}^1A_2$ electronic transition. The polarization, band shape, and total intensity therefore support the $^1A_2$ assignment.

The symmetry allowed appearance of the emission spectrum of benzophenone can be explained from the types of singlet states mixed in by spin-orbit interaction. If the triplet upper state is $^3A_2$, then in-plane transitions are caused by mixing with $^1A_1$ and $^1B_2$ states, and an out-of-plane transition by $^1B_1$ states.[18] The fact that $^1B_1$ states cannot be as low in energy as the other types of states may be connected with the greater degree of in-plane polarization observed in the triplet emission. In any case, all the singlets mixed with the triplet under consideration can make allowed transitions to the ground state, so that vibrational-electronic interaction or out-of-plane distortion are not necessary to account for the transition.

The energy level schemes of acetophenone and benzophenone are very similar, as shown by Fig. 3. There is a one to one correspondence between levels having nearly the same energy and transition intensity, except that benzophenone has an extra level at 53 500 cm^{-1}. We have already discussed the lowest two of the excited levels. The next three singlets bear a close resemblance to the B_{2u}, B_{1u}, and E_{1u} levels of benzene when some allowance is made for the mixing that must occur among them.

The similarity between the energy level schemes of these two molecules is not so apparent in the triplet-triplet spectra. Unfortunately, only the upper portion of the energy level scheme is revealed by our experiments. The identification which seems most likely to us is as follows. The benzophenone triplet at 49 100 cm^{-1} and the acetophenone triplet at 50 500 cm^{-1} are analogous states. The acetophenone analogue of the benzophenone 41 400 cm^{-1} triplet must lie to the red of the region we investigated. This means it must lie below 41 500 cm^{-1}. These two triplet-triplet transitions seem to have about the same strength in benzophenone, and would be expected to be the same in acetophenone.

The possible $T-T$ transitions within the carbonyl group are, in McMurry's notation,[16] $^3E \rightarrow {}^3Z$ or $^3E \rightarrow {}^3V$, where in terms of molecular orbitals of the carbonyl group these transitions are $(y_0)(x_c\bar{x}_0)^3A_2 \rightarrow (y_0)(t_3\bar{z}_0)^3B_2$ and $(y_0)(x_c\bar{x}_0)^3A_2 \rightarrow (x_cx_0)(x_c\bar{x}_0)^3A_1$, respectively. The f-number of the first of these transitions was calculated approximately, and in the nonpolar approximation turned out to be 0.020. The second of these transitions is forbidden under C_{2v} selection rules, and should have about the same intensity as the ordinary singlet-singlet long wavelength carbonyl absorption band. The experiments show that the observed transitions are quite strong, so the $^3A_2 \rightarrow {}^3A_1$ transition is eliminated as a possibility. The first possibility seems very likely from the point of view of the intensity. If we assume that the $^1Z-{}^1E$ energy difference in acetone is the same as the $^3Z-{}^3E$ energy difference of benzophenone we should find a $T-T$ transition at about 18 000 cm^{-1}. This is close to the 5600 A $T-T$ transition in benzophenone, but there is enough uncertainty in the level positions for this transition to be assigned to either band.

The other $T-T$ transition cannot be assigned to a transition localized in the carbonyl group. Such a nonlocalized transition was observed in the singlet systems of aliphatic ketones by Holdsworth and Duncan.[19] The 60 000 cm^{-1} transition which they observed is very sensitive to substitution at the carbonyl group. In benzophenone and acetophenone, the π-electron orbitals of the rings must be mixed with the π orbitals of the carbonyl group in appreciable amounts, so that a delocalized transition is easily visualized as occurring partly in the benzene rings and partly in the carbonyl group. With enough such mixing the intensity of these transitions could approach that of the $A_g \rightarrow B_{1u}$ or $A_g \rightarrow E_{1u}$ transition in benzene. Further attempts to identify the $T-T$ transitions would have to be based on theoretical calculations of energy levels and intensities.

[18] D. S. McClure, J. Chem. Phys. **17**, 665 (1949).

[19] R. Holdsworth and A. Duncan, Chem. Revs. **41**, 311 (1947).

Pi-Electron Forces between Conjugated Double Bond Molecules*

EUGENE F. HAUGH† AND JOSEPH O. HIRSCHFELDER
Naval Research Laboratory, Department of Chemistry, University of Wisconsin, Madison, Wisconsin

(Received November 26, 1954)

The long-range forces between large conjugated double bond molecules are highly directional and anomalously strong. This is the result of pi electrons moving freely from one end of the conjugated double bond system to the other, making the molecule behave like an extended oscillator. All three types of dispersion forces: $\sigma\sigma$, $\sigma\pi$, and $\pi\pi$ are calculated for ethylene, acetylene, and the higher polyenes. In addition the $\pi\pi$ interaction energy is calculated for benzene. The free electron molecular orbitals are used for the π electrons and products of these orbitals are approximated by "transition monopoles." Our treatment of the σ electrons and the use of the transition monopoles were suggested by London. The resulting energies are easy to calculate and easy to interpret. The $\pi\pi$ energy is proportional to the square of the energy of interaction of two real transition dipoles (real in the sense of the monopoles being separated by a finite distance). Previously, Coulson and Davies calculated the $\pi\pi$ interaction energy using LCAO orbitals and evaluating all integrals accurately; however, because of the complicated nature of their calculations it was not possible for them to obtain a simple understanding of the variation of the energy with the orientations of the molecules. The values we obtain for the $\pi\pi$ energy agree with those of Coulson and Davies except for a scale factor, our results being uniformly $\frac{3}{5}$ smaller. Such a scale factor corresponds to an adjustable parameter in either the Coulson and Davies treatment or ours. The $\sigma\pi$ interaction energy has never previously been considered. For long polyenes, for which a simplified treatment is given, the $\pi\pi$ energy is larger than the $\sigma\pi$ which is larger than that of the $\sigma\sigma$. In the appendix, the free-electron model is used to calculate the pi-electron contribution to the polarizability and excellent agreement is obtained with the LCAO calculations of Davies.

1. INTRODUCTION

THE long-range dispersion forces between large conjugated double bond molecules are highly directional and very strong. This is due to pi electrons moving freely from one end of the conjugate double bond system to the other, making the molecule behave like an extended oscillator. These forces may help to explain some of the anomalous effects of steroids and other conjugated double bond molecules of biological importance. Also the pi-bond forces are important in the interaction between aromatic molecules and are partially responsible for the nonzero angles between the planes of neighboring molecules in an aromatic crystal. In this paper, a simple treatment is developed for calculating and explaining these forces.

In contrast to the pi electrons, molecules contain sigma electrons which are localized in specific chemical bonds or within the inner shells of the atoms. Corresponding to the two types of electrons, the dispersion energy can be divided into three terms:

$$E^{(\mathrm{dis})}=E_{\sigma\sigma}+E_{\sigma\pi}+E_{\pi\pi}. \tag{1.1}$$

Here $E_{\sigma\sigma}$ is that part which arises from the interaction between the σ electrons of the two molecules; $E_{\pi\pi}$ corresponds to the interaction between the π electrons of the two molecules; and $E_{\sigma\pi}$ gives the energy of interaction of the σ electrons of one molecule with the π electrons of the other molecule and vice versa. London[1] developed an excellent method for calculating the $E_{\sigma\sigma}$. It is the purpose of the present paper to describe a simple method for calculating $E_{\sigma\pi}$ and $E_{\pi\pi}$.

We use free electron molecular orbitals for the pi electrons and approximate products of these orbitals by "transition monopoles." The resulting values of $E_{\sigma\pi}$ and $E_{\pi\pi}$ are easy to calculate and easy to interpret. For example, to a good approximation in most cases, the values of $E_{\pi\pi}$ are proportional to the square of the energy of interaction of two real transition dipoles (real in the sense that the monopoles are separated by a finite distance). We are indebted to London[1] for the notion of transition monopoles and their use in connection with dispersion energy. Our results for $E_{\pi\pi}$ are to be compared with the calculations of Coulson and Davies[2] who used LCAO orbitals and evaluated all of the integrals accurately without using the monopole approximation. Because of the complications of their calculations it was not possible for them to obtain a simple understanding of the variation of the interaction energy with the orientations of the molecules. However, our values of $E_{\pi\pi}$ agree with those of Coulson and Davies except for a scale factor (our values being uniformly $\frac{3}{5}$ of the Coulson and Davies numbers). Such a scale factor corresponds to an adjustable parameter in either treatment. Prior to the present paper, there were no evaluations of $E_{\sigma\pi}$. For long polyenes $E_{\sigma\pi}$ is by no means negligible and, as a matter of fact, $E_{\pi\pi}>E_{\sigma\pi}>E_{\sigma\sigma}$. For ethylene, acetylene, and the lower polyenes, $E_{\sigma\sigma}>E_{\sigma\pi}>E_{\pi\pi}$. In the case of ethylene and acetylene where the complete dispersion energy is compared with experimental data, the agreement is satisfactory in the sense that it is quite comparable with the ratio of theoretical to observed values

* This work was supported in part by Contract N7onr-28511 with the Office of Naval Research.

† Present address: Research Division, Photo Products Department, E. I. du Pont de Nemours Company, Parlin, New Jersey.

[1] F. London, J. Chem. Phys. 46, 305 (1942).

[2] C. A. Coulson and P. L. Davies, Trans. Faraday Soc. 48, 777 (1952).

for simple molecules in which there are no complications due to pi electrons.

In the appendix, the free electron molecular orbitals are used to calculate the contributions of the pi-electrons to the polarizability of polyenes. Excellent agreement is obtained with the LCAO calculations of Davies[3] and the results seem to be consistent with experimental data. This agreement serves as a check on the accuracy of the free electron molecular orbitals as used in the present paper.

In retrospect, we feel that the simple free electron molecular orbitals, as used here, give roughly the right values for $E_{\sigma\pi}$ and $E_{\pi\pi}$. However, the fact that the orbitals have been taken as one-dimensional rather than as three-dimensional has its limitations. For example, consider the interaction of two ethylene molecules in which the C=C axes of the two molecules are parallel. With the present free electron orbitals, the value of $E_{\pi\pi}$ is independent of the orientation of the planes containing the hydrogen atoms. Such a result is obviously erroneous. An obvious improvement would result by replacing our present one-dimensional molecular orbital, $\phi_n(x)$, (see Eq. (2.29)) by three-dimensional free electron molecular orbitals such as

$$\Phi_n = y\phi_n(x)\exp[-\alpha(y^2+z^2)^{\frac{1}{2}}]. \tag{1.2}$$

Here x is the Cartesian coordinate along the axis of the conjugated double bond system and y and z are coordinates perpendicular to this axis. The parameter α, would of course be adjustable. The use of three-dimensional free-electron orbitals would not appreciably increase the amount of work required and at the same time it should improve the comparison of the dispersion energy for different orientations of the molecules.

2. METHOD

In dealing with dispersion forces, the molecules are sufficiently separated to make a perturbation calculation correct. Furthermore, it is not necessary to antisymmetrize the wave function for the two molecule system, since we may assume that there is no overlapping between the wave functions of different molecules. We may then employ a simple product of the electronic wave functions of the individual molecules as our zero order wave function for the system and treat the potential energy of interaction as the perturbation. Actually, the only part of the potential energy of interaction which affects the dispersion energy are the electron-electron interaction terms[4]

$$\varphi_e = \sum_{a=1}^{n_a}\sum_{b=1}^{n_b}\frac{e^2}{r_{ab}}. \tag{2.1}$$

Here the n_a electrons designated by the subscript a are in molecule A and the n_b electrons designated by the subscript b are in molecule B. Furthermore r_{ab} is the instantaneous separation between electrons a and b. If $\Psi_0{}^A$ and $\Psi_i{}^A$ are the electronic wave functions of molecule A in its ground state and ith excited state, respectively; if $\Psi_0{}^B$ and $\Psi_j{}^B$ are the wave functions of molecule B in its ground state and jth excited state, respectively; and if $E_0{}^A$, $E_i{}^A$, $E_0{}^B$, and $E_j{}^B$ are the energies of these molecular states, respectively, the usual second-order perturbation theory gives the energy of dispersion:

$$E^{(\mathrm{dis})} = -\sum_{l,k}{}' \frac{\left(\int \Psi_0{}^A\Psi_0{}^B\varphi_e\Psi_l{}^A\Psi_k{}^B d\tau^A d\tau^B\right)^2}{E_l{}^A+E_k{}^B-E_0{}^A-E_0{}^B}. \tag{2.2}$$

Here the prime over the summation sign indicates that those states with either l or k equal zero are excluded. The conjugate complex of the wave function does not appear in Eq. (2.2) since the wave functions in the following development are taken to be real. Furthermore, for present purposes it is convenient to suppose that the wave function for each of the molecules can be taken as a Slater determinant made up of molecular orbitals, ϕ^A and ϕ^B. The orbitals are numbered by a subscript according to their energy, ϵ. Thus ϕ_1 is the orbital of lowest energy, ϵ_1; ϕ_2 has the next higher energy, ϵ_2; etc. The molecules which we shall consider have an even number of electrons, $n=2N$, and their ground state is a singlet. To the approximation of the present treatment, there are no singlet-triplet transitions so that the only excited states which need be considered are themselves singlets. Thus the wave function for the ground state of a molecule is a Slater determinant with two electrons in each of the molecular orbitals: ϕ_1, ϕ_2, $\cdots$, ϕ_i, $\cdots$, ϕ_N. The wave functions of the excited states which we consider are the same as the wave function of the ground state except that one of the two electrons in the ith molecular orbital has been promoted to the jth molecular orbital. Such a transition is denoted by the symbol (i,j). In terms of these orbitals the ground state of the molecule A is the Slater determinant,

$$\Psi_0{}^A = \frac{1}{[(2N_A)!]^{\frac{1}{2}}}\begin{pmatrix} \phi_i{}^A\phi_i{}^A\phi_1{}^A\phi_1{}^A\cdots\phi_{i-1}{}^A\phi_{i-1}{}^A\phi_{i+1}{}^A\phi_{i+1}{}^A\cdots\phi_{N_A}{}^A\phi_{N_A}{}^A \\ \alpha\ \beta\ \alpha\ \beta\ \cdots\ \alpha\ \ \beta\ \ \alpha\ \ \beta\ \cdots\ \alpha\ \ \beta \end{pmatrix}. \tag{2.3}$$

[3] P. L. Davies, Doctor's Dissertation, King's College, University of London (1949).

[4] The matrix components which give the greatest contribution to the dispersion energy correspond to one electron in each of the two molecules making a transition. For such two electron transitions, only the electron-electron terms in the perturbation potential as given by Eq. (2.1) lead to nonvanishing matrix components. However, it should be pointed out that one-electron transitions do give small but finite contributions to the dispersion energy. For one-electron transition, it is the electron-other-nucleus terms in the perturbation potential which are important. In the present paper we ignore the small contributions from one-electron transitions. Matrix components involving the transition for more than one electron in a molecule vanish if molecular orbital wave functions are used.

Here the ith orbitals are moved from their normal positions in the determinant in order to facilitate the algebraic manipulations which follow. Similarly the excited state l of the molecule corresponding to the transition (i,j) has as its wave function the sum of two Slater determinants,

$$\Psi_l{}^A=\frac{1}{[2(2N_A)!]^{\frac{1}{2}}}\left[\begin{pmatrix}\phi_j{}^A\phi_i{}^A\phi_1{}^A\phi_1{}^A\cdots\phi_{i-1}{}^A\phi_{i-1}{}^A\phi_{i+1}{}^A\phi_{i+1}{}^A\cdots\phi_{N_A}{}^A\phi_{N_A}{}^A\\ \alpha\ \beta\ \alpha\ \beta\cdots\alpha\ \beta\ \alpha\ \beta\cdots\alpha\ \beta\end{pmatrix}\right.$$
$$\left.+\begin{pmatrix}\phi_i{}^A\phi_j{}^A\phi_1{}^A\phi_1{}^A\cdots\phi_{i-1}{}^A\phi_{i-1}{}^A\phi_{i+1}{}^A\phi_{i+1}{}^A\cdots\phi_{N_A}{}^A\phi_{N_A}{}^A\\ \alpha\ \beta\ \alpha\ \beta\ \ \alpha\ \beta\ \alpha\ \beta\cdots\alpha\ \beta\end{pmatrix}\right]. \tag{2.4}$$

Now integrating the product of $\Psi_0{}^A$ and $\Psi_l{}^A$ over all of the coordinate and spin space for electrons 1, 2, $\cdots(a-1)$, $(a+1)$, $\cdots 2N_A$ leads to the result,

$$\int\Psi_0{}^A\Psi_l{}^A d\tau_1 d\tau_2\cdots d\tau_{a-1}d\tau_{a+1}\cdots d\tau_{2NA}$$
$$=\frac{1}{2\sqrt{2}N_A}\phi_i{}^A(a)\phi_j{}^A(a)(\alpha(a)\alpha(a)+\beta(a)\beta(a)). \tag{2.5}$$

Since all of the electrons are equivalent, substitution of Eqs. (2.1) and (2.5) into Eq. (2.2) leads to the following expression for the dispersion energy in terms of the molecular orbitals.

$$E^{(\mathrm{dis})}=-\sum_{i=1}^{N_A}\sum_{j=N_A+1}^{\infty}\sum_{i'=1}^{N_B}\sum_{j'=N_B+1}^{\infty}$$
$$\times\frac{(ii'|2e^2/r_{ab}|jj')^2}{(\epsilon_j{}^A-\epsilon_i{}^A)+(\epsilon_{j'}{}^B-\epsilon_{i'}{}^B)}. \tag{2.6}$$

Here

$$\left(ii'\left|\frac{2e^2}{r_{ab}}\right|jj'\right)=\int\int\phi_i{}^A(a)\phi_j{}^A(a)$$
$$\times\frac{2e^2}{r_{ab}}\phi_{i'}{}^B(b)\phi_{j'}{}^B(b)dv_a dv_b, \tag{2.7}$$

where the integrations are taken over the coordinate space of electrons a and b. To avoid confusion, we let dv be an element of coordinate space as contrasted to $d\tau$ which includes spin as well as coordinate space.

In a molecule containing conjugated double bonds there are two kinds of molecular orbitals. First, there are the pi orbitals in which the electron is not localized in either a particular bond or in a particular atom but rather, the pi electron is free to roam over the length of the conjugated double bond system. The other electrons in the molecules, which we shall refer to as σ electrons, are localized in either individual atoms or chemical bonds. The usual treatment of dispersion energy applies to interactions between the sigma type electrons in one molecule and the sigma electrons of the second molecule, $E_{\sigma\sigma}$. In calculating $E_{\sigma\sigma}$, the terms e^2/r_{ab} are expanded in inverse powers of R, the separation between the molecules. This expansion converges rapidly provided that the linear dimensions of the electron orbitals are small compared to the separation between the molecules. For pi electrons, the size of the orbitals is comparable with the size of the molecules, so that this type of expansion would not converge rapidly when the molecules are separated by one or two molecular diameters. Thus a somewhat different treatment is required in the calculation of the energy of interaction of the pi electrons of one molecule with either the pi electrons of the other molecule, $E_{\pi\pi}$, or with the sigma electrons of the other molecule, $E_{\sigma\pi}$.

The London Approximation

F. London[1] suggested a method for approximating the matrix elements of Eq. (2.7) corresponding to either pi-pi or sigma-pi electron interactions in which cases the usual treatment (expansion of e^2/r_{ab} in inverse powers of R) does not apply for the values of the intermolecular separation which have the greatest physical interest. First, he considered the matrix element to be electrostatic energy of interaction between two electrical charge distributions:

$$\rho_{ij}{}^A(a)=\sqrt{2}e\phi_i{}^A(a)\phi_j{}^A(a),$$
$$\rho_{i'j'}{}^B(b)=\sqrt{2}e\phi_{i'}{}^B(b)\phi_{j'}{}^B(b). \tag{2.8}$$

The matrix component can then be written:

$$\left(ii'\left|\frac{2e^2}{r_{ab}}\right|jj'\right)=\int\int\rho_{ij}{}^A(a)\frac{1}{r_{ab}}\rho_{i'j'}{}^B(b)dv_a dv_b. \tag{2.9}$$

These charge distributions are negative in some regions of space and positive in others, depending upon the signs of the molecular orbitals. Thus the nodal surfaces of $\rho_{ij}{}^A$ divide all space into a number of cells or zones, k. Similarly the nodal surfaces of $\rho_{i'j'}{}^B$ divide space into a set of cells or zones labelled k'. The matrix component can then be written in the form:

$$\left(ii'\left|\frac{2e^2}{r_{ab}}\right|jj'\right)=\sum_k\sum_{k'}\int_{(k)}\int_{(k')}\rho_{ij}{}^A(a)$$
$$\times\frac{1}{r_{ab}}\rho_{i'j'}{}^B(b)dv_a dv_b. \tag{2.10}$$

Throughout each cell, the charge distribution maintains either a positive or negative sign. London now defines a

set of monopoles corresponding to the charge distributions. The charges on the monopoles are

$$g_{ij}^{A}(k)=\int_{(k)}\rho_{ij}^{A}(a)dv_a,$$
$$g_{i'j'}^{B}(k')=\int_{(k')}\rho_{i'j'}^{B}(b)dv_b. \tag{2.11}$$

The monopoles are considered to be located at the points $R_{ij}^{A}(k)$ and $R_{i'j'}^{B}(k')$ given by the first moments of the charge distributions within their respective zones,

$$\mathbf{R}_{ij}^{A}(k)=\int_{(k)}\mathbf{r}_a\rho_{ij}^{A}(a)dv_a/g_{ij}^{A}(k),$$
$$\mathbf{R}_{i'j'}^{B}(k')=\int_{(k')}\mathbf{r}_b\rho_{i'j'}^{B}(b)dv_b/g_{i'j'}^{B}(k'). \tag{2.12}$$

The London approximation then consists of replacing the individual integrals of Eq. (2.10) by the electrostatic interaction of the corresponding monopoles,

$$\left(ii'\left|\frac{2e^2}{r_{ab}}\right|jj'\right)=\sum_k\sum_{k'}g_{ij}^{A}(k)g_{i'j'}^{B}(k')\times\frac{1}{|\mathbf{R}_{ij}^{A}(k)-\mathbf{R}_{i'j'}^{B}(k')|}. \tag{2.13}$$

Since the London approximation forms the basis for the present calculations, it is important to examine its validity. Let us consider one of the integrals of Eq. (2.10).

Take $R_{ij}^{A}(k)$ to be the center of the coordinate system for electron a and $R_{i'j'}^{B}(k')$ the center of the coordinate system for electron b. Let the Z-axis for both coordinate systems point in the line from $R_{ij}^{A}(k)$ towards $R_{i'j'}^{B}(k')$. Let (r,θ,ϕ) be the spherical coordinates of electron a and (r',θ',ϕ') be the spherical coordinates of electron b in the two separate reference frames. Then we can expand $1/r_{ab}$ in a bipolar expansion[5]:

$$\frac{1}{r_{ab}}=\sum_{n=0}^{\infty}\sum_{n'=0}^{\infty}\sum_{m=-n_<}^{+n_<}B_{n,n'}^{|m|}(r,r';\mathfrak{R})\times P_n^{|m|}(\cos\theta)P_{n'}^{|m|}(\cos\theta')e^{im(\phi-\phi')}. \tag{2.14}$$

Here the $B_{n,n'}^{m}$ are the bipolar expansion coefficients, and $\mathfrak{R}=|\mathbf{R}_{ij}^{A}(k)-\mathbf{R}_{i'j'}^{B}(k')|$. If the kth zone of molecule A and the k'th zone of molecule B do not overlap or if $r+r'<\mathfrak{R}$, the bipolar expansion coefficients have the very simple form,

$$B_{n,n'}^{|m|}(r,r';\mathfrak{R})=\frac{(-1)^{n'+m}(n+n')!}{(n+|m|)!(n'+|m|)!}\frac{r^n r'^{n'}}{\mathfrak{R}^{n+n'+1}}. \tag{2.15}$$

In this case, the integral of Eq. (2.10) becomes:

$$\int_{(k)}\int_{(k')}\rho_{ij}^{A}(a)\frac{1}{r_{ab}}\rho_{i'j'}^{B}(b)d\tau_a d\tau_b=\sum_{l=0}^{\infty}\frac{l!}{\mathfrak{R}^{l+1}}K_l, \tag{2.16}$$

where the K_l are a set of constants given by

$$K_l=\sum_{n=0}^{l}S_nS'_{l-n}+\sum_{m=1}^{l/2\text{ or }(l-1)/2}2(-1)^m\times\sum_{n=m}^{l-m}[L_{nm}L'_{(l-n),m}+W_{nm}W'_{(l-n),m}]. \tag{2.17}$$

The summation going to $l/2$ or $(l-1)/2$ means to take whichever of the two is an integer. The constants in this equation are the integrals,

$$S_n=\frac{1}{n!}\int_{(k)}r^nP_n(\cos\theta)\rho_{ij}^{A}(k)dv_a, \tag{2.18}$$

$$S'_{l-n}=\frac{(-1)^{l-n}}{(l-n)!}\int_{(k')}r'^{(l-n)}P_{(l-n)}(\cos\theta')\times\rho_{i'j'}^{B}(k')dv_b, \tag{2.19}$$

$$L_n=\frac{1}{(n+m)!}\int_{(k)}r^nP_n^m(\cos\theta)\times\cos m\phi\rho_{ij}^{A}(k)dv_a, \tag{2.20}$$

$$L'_{l-n}=\frac{(-1)^{(l-n)}}{(l-n+m)!}\int_{(k')}r'^{(l-n)}P_{(l-n)}^{m}(\cos\theta')\times\cos m\phi'\rho_{i'j'}^{B}(k')dv_b, \tag{2.21}$$

$$W_{n,m}=\frac{1}{(n+m)!}\int_{(k)}r^nP_n^m(\cos\theta)\times\sin m\phi\rho_{ij}^{A}(k)dv_a, \tag{2.22}$$

$$W'_{l-n,m}=\frac{(-1)^{l-n}}{(l-n+m)!}\int_{(k')}r'^{(l-n)}P_{(l-n)}^{m}(\cos\theta')\times\sin m\phi'\rho_{i'j'}^{B}(k')dv_b. \tag{2.23}$$

Thus $S_0=g_{ij}^{A}(k)$, $S_0'=g_{i'j'}^{B}(k')$ and, because of the location of the origins of the two coordinate systems, $S_1=S_1'=L_{11}=L_{11}'=W_{11}=W_{11}'=0$. As a result the lead-

[5] See *Molecular Theory of Gases and Liquids* by Hirschfelder, Curtiss, and Bird (John Wiley and Sons, Inc., New York, 1954), p. 834, Eq. (12.1-28).

ing terms of Eq. (2.13) are

$$\int_{(k)}\int_{(k')}\rho_{ij}{}^{A}(a)\frac{1}{r_{ab}}\rho_{i'j'}{}^{B}(b)dv_a dv_b = \frac{g_{ij}{}^{A}(k)g_{i'j'}{}^{B}(k')}{\mathfrak{R}}+\frac{0}{\mathfrak{R}^2} + \frac{2[g_{ij}{}^{A}(k)S_2'+g_{i'j'}{}^{B}(k')S_2]}{\mathfrak{R}^3}+\cdots. \quad (2.24)$$

The London approximation therefore consists of taking the first term of this infinite series. The second term in the series vanishes because of the location of the monopoles. The third term, which gives the first corrections to the London approximation depends on the second moment of the charge distributions. The series converges rapidly and the London approximation is accurate provided that $\mathfrak{R}$ is large compared to the sum of the effective radii of the two charge distributions in the particular zones being considered.

The Coulson-Davies Method

Instead of using the London approximation, Coulson and Davies[4] expressed the molecular orbitals for pi electrons as linear combinations of the $2p$ atomic orbitals,

$$\chi_\alpha(a)=\left(\frac{c^5}{\pi}\right)^{\frac{1}{2}} Z_a \exp(-cr_{a\alpha}). \quad (2.25)$$

Here $r_{a\alpha}$ is the distance of the ath electron from the αth atom (carbon atoms in the problems considered here); the Z-axis is taken perpendicular to the axis of the molecule so that Z_a is the coordinate of the ath electron in this direction; and c is a constant which for carbon has the value $1.625/a_0$ where a_0 is the first Bohr radius. In a linear conjugated polyene with $2N$ carbon atoms, there are $2N$ molecular orbitals that can be formed by linear combinations of the above atomic orbitals:

$$\phi_j(a)=\sum_{\alpha=1}^{2N}\left(\frac{2}{2N+1}\right)^{\frac{1}{2}}\sin\left(\frac{j\alpha\pi}{2N+1}\right)\chi_\alpha(a), \quad j=1, 2, \cdots, 2N. \quad (2.26)$$

The one electron energies associated with these orbitals are

$$\epsilon_j=2\beta\cos\left(\frac{j\pi}{2N+1}\right), \quad j=1, 2, \cdots, 2N. \quad (2.27)$$

Here β is the "resonance integral" for which Coulson and Davies[6,7] employ the value -40 kcal/mole.

[6] C. A. Coulson (Proc. Roy. Soc. (London) **169A**, 413 (1939)) developed the molecular orbitals given in Eqs. (2.22) and (2.23) and C. A. Coulson and P. L. Davies (Trans. Faraday Soc. **48**, 777 1952)) applied them to problems involving pi-bond intermolecular forces.

[7] Mulliken, Rieke, and Brown, J. Am. Chem. Soc. **63**, 41 (1941).

Using the molecular orbitals of Eq. (2.26) the matrix elements of Eq. (2.7) which occur in the dispersion energy become linear combinations of integrals of the type,

$$\int\int\chi_\alpha{}^{A}(a)\chi_\beta{}^{B}(b)\frac{2e^2}{r_{ab}}\chi_{\alpha'}{}^{A}(a)\chi_{\beta'}{}^{B}(b)dv_a dv_b. \quad (2.28)$$

Because of the exponential decrease of the atomic orbitals with distance, the only integrals which have appreciable size correspond to α' and β' either coinciding with or being adjacent to α and β, respectively. Furthermore, since the size of the atomic orbitals is small compared to the separation, R, between the molecules, it is possible to evaluate integrals of the type of Eq. (2.11) in the same manner as is usually done for the matrix elements of Eq. (2.7) in the case of sigma-sigma electron interactions.

The FEM Orbitals

Recently a different type of molecular orbital has been introduced which is more satisfactory for the calculations that follow because of its greater simplicity.[8] Moreover, it is in no way inferior for predicting the energies of excited states and contains no constants which require empirical determination.

This approach is known as the free electron model (FEM) approximation. The delocalization of the pi electrons is taken literally and they are regarded as free to move in a one-dimensional box which extends along the skeleton of the conjugated carbon atoms. Thus the skeleton for a benzene molecule is essentially a circle around the benzene ring and for a linear polyene it is a line along the carbon network. Whenever there is a free endpoint such as the terminal carbon atom of a linear polyene, the "box" is extended an additional bond length, or the carbon-carbon distance.

For linear polyenes with N conjugated double bonds, the free electron model molecular orbitals are given by:

$$\phi_n=\left(\frac{2}{l}\right)^{\frac{1}{2}}\sin\frac{n\pi x}{l}, \quad n=1, 2, \cdots 2N, \quad (2.29)$$

with the energies

$$\epsilon_n=\frac{n^2h^2}{8ml^2}, \quad n=1, 2, \cdots, 2N. \quad (2.30)$$

Here l is the length of the one-dimensional box and is equal to $(2N+1)D$, where D is the carbon-carbon bond length, which we take to be 1.4 A, x is the distance along the electron path measured from one end, and m is the mass of the electron.

[8] H. Kuhn, Helv. Chim. Acta **31**, 1441 (1948), **31**, 1780 (1948); J. Chem. Phys. **16**, 840 (1948), **17**, 1198 (1949); N. S. Bayliss, J. Chem. Phys. **16**, 287 (1948); W. T. Simpson, J. Chem. Phys. **16**, 1124 (1948); Ruedenberg and Scherr, J. Chem. Phys. **21**, 1565 (1953); C. W. Scherr, J. Chem. Phys. **21**, 1582 (1953); J. R. Platt, J. Chem. Phys. **17**, 484 (1949); **21**, 1597 (1953).

Because of the simplicity of the free-electron orbitals it is possible to substitute them directly into the matrix components of Eq. (2.7) and evaluate the resulting integrals directly. However, these integrals can be expressed in a simple closed mathematical form only if the conjugate double bond molecules are parallel and collinear. For any other orientation, the resulting answers can only be expressed in numerical form. Thus, it is desirable to use the London approximation which leads to very simple results with very simple interpretations.

The total energy of dispersion is the sum of contributions from the sigma-sigma, pi-pi, and sigma-pi electron interactions:

$$E=E_{\sigma\sigma}+E_{\pi\pi}+E_{\sigma\pi}. \tag{2.31}$$

The treatment of these three types of interactions is quite distinct.

Determination of $E_{\sigma\sigma}$

A satisfactory treatment of $E_{\sigma\sigma}$ has been given independently by London and by de Boer[9] in terms of the polarizabilities of the chemical bonds, in the parallel and perpendicular directions, $\alpha_{\parallel}$ and $\alpha_{\perp}$, respectively. The mean bond polarizability is $\alpha=(\alpha_{\parallel}+2\alpha_{\perp})/3$ and $\delta=(\alpha_{\parallel}-\alpha_{\perp})/\alpha$ is a measure of the electrical asymmetry of the bond. In the London or de Boer treatment, the energy of the principal transition ($h\nu_{\parallel}$ or $h\nu_{\perp}$ depending whether the perturbation is parallel or perpendicular to the bond) plays an important role. We assume that this energy is equal to the bond ionization potential, I. Thus $I=h\nu_{\parallel}=h\nu_{\perp}$. For calculational purposes we assume that $I=100\,000\ \text{cm}^{-1}=12.4$ ev. With these assumptions, the London or de Boer treatment gives:

$$E_{\sigma\sigma}=-\frac{I}{8}\sum_{k_A,l_B}\frac{\alpha k_A\alpha l_B}{R_{AB}{}^6}\times\begin{Bmatrix}6\\+\delta k_A[3\cos^2\theta k_A-1]\\+\delta l_B[3\cos^2\theta l_B-1]\\+\delta k_A\delta l_B\left[\begin{pmatrix}\sin\theta k_A\sin\theta l_B\cos(\phi k_A-\phi l_B)\\-2\cos\theta k_A\cos\theta l_B\end{pmatrix}^2-\cos^2\theta k_A-\cos^2\theta l_B\right]\end{Bmatrix}. \tag{2.32}$$

This formula applies at large separations. At intermediate separations, R_{AB} is replaced by R_{k_A,l_B}. Here the k_A and l_B signify the chemical bonds in molecules A and B, respectively, and the summation is to be taken over all of the chemical bonds. The angles θ_{k_A} and θ_{l_B} are the angles which the bonds make with a radius vector joining the centers of the two molecules. The ϕ_{k_A} and ϕ_{l_B} are the angles which the projections of these bonds make with a plane passing through the radius vector. Values of the bond polarizabilities have been estimated by Denbigh.[10] For the aliphatic C−C bond and for the C−H bond:

	$\alpha\times10^{25}$ cm^3	δ
$(C-C)_{aliph}$	6.4	2.90
(C−H)	6.5	0.32

(2.33)

If the two molecules are held at a fixed separation between their centers and rotated through all orientations, we obtain for the averaged value of $E_{\sigma\sigma}$,

$$\bar{E}_{\sigma\sigma}=-\frac{3}{4}\frac{I}{R^6}\sum_{k_A,l_B}\alpha k_A\alpha l_B. \tag{2.34}$$

The values of the $E_{\sigma\sigma}$ as calculated by Eq. (2.12) are probably not accurate to within a factor of two but it is difficult to see how substantial improvements can be made in the formulation without making detailed calculations using accurate wave functions for each of the molecular species. This short summary of the treatment of the $E_{\sigma\sigma}$ is included here since we need to know values of the $E_{\sigma\sigma}$ in order to compare the calculated with the experimental values for the dispersion energy.

Determination of $E_{\pi\pi}$

In seeking the simplest determination of $E_{\pi\pi}$, we use the "free-electron" model for the molecular orbitals in Eq. (2.4). Then, we use the London method of approximating the resulting integrals. The combination of the two approximations leads to comparatively simple expressions for $E_{\pi\pi}$ which are easy to interpret. Our results are to be compared with the more accurate calculations of Coulson and Davies[4] who used LCAO molecular orbitals and accurately evaluated their integrals.

Determination of $E_{\sigma\pi}$

The sigma-pi electron interactions have not been considered by previous investigators as a source of intermolecular energy. It is therefore necessary to develop a new approach. Consider the interaction between the sigma electrons in molecule A and the pi electrons in molecule B. The sigma electrons are localized in chemical bonds. For the pi electrons we use the London notion of monopoles. The matrix components of Eq. (2.7) then become the sum of interaction integrals between the n_p sigma electrons in the pth chemical bond of molecule A with the kth monopole in molecule B. The

[9] F. London, J. Phys. Chem. **46**, 305 (1942); J. de Boer, Physica **9**, 363 (1942); also reference 5, p. 969.

[10] K. G. Denbigh, Trans. Faraday Soc. **36**, 936 (1940).

matrix components of Eq. (2.7) then become:

$$\left(ii'\left|\frac{2e^2}{r_{ab}}\right|jj'\right)=\sum_{\substack{p\\ \text{chemical bonds in } A}}\sum_{\substack{k\\ \text{monopoles in } B}}\sqrt{2}e\int[\phi_i{}^A(a)\phi_j{}^A(a)]_p \times\frac{g_{i'j'}{}^B(k)}{|\mathbf{r}_a-\mathbf{R}_{i'j'}{}^B(k)|}dv_a. \quad (2.35)$$

If the size of the chemical bond is small compared to the distance R_{pk} from the center of the pth chemical bond of molecule A to the kth monopole of molecule B, then $1/|\mathbf{r}_a-\mathbf{R}_{i'j'}{}^B(k)|$ can be expanded in inverse powers of R_{pk}. Let the Z-axis be the axis of the chemical bond and let the center of the bond be the origin. Then the spherical coordinates of the electron a are (r_a,θ_a,ϕ_a). Similarly the spherical coordinates of the monopole are $(R_{pk},\theta_{pk},\phi_{pk})$. Then[11]

$$\frac{1}{|\mathbf{r}_a-\mathbf{R}_{i'j'}{}^B(k)|}=\frac{1}{R_{pk}}\sum_{n=0}^{\infty}\sum_{m=-n}^{n}\frac{(n-|m|)!}{(n+|m|)!}\left(\frac{r_a}{R_{pk}}\right)^n \times P_n{}^{|m|}(\cos\theta_a)P_n{}^{|m|}(\cos\theta_{pk})e^{im(\phi_a-\phi_{pk})}. \quad (2.36)$$

The leading terms of this expansion are:

$$\frac{1}{|\mathbf{r}_a-\mathbf{R}_{i'j'}{}^B(k)|}=\frac{1}{R_{pk}}+\frac{r_a}{R_{pk}{}^2}\times\left[\begin{matrix}\cos\theta_a\cos\theta_{pk}+\sin\theta_a\sin\theta_{pk}\sin\phi_a\sin\phi_{pk}\\ +\sin\theta_a\sin\theta_{pk}\cos\phi_a\cos\phi_{pk}\end{matrix}\right]+\cdots=\frac{1}{R_{pk}}+\frac{x_aX_{pk}+y_aY_{pk}+z_aZ_{pk}}{R_{pk}{}^3}+\cdots. \quad (2.37)$$

Since $\phi_i{}^A(a)$ is orthogonal to $\phi_j{}^A(a)$ when we substitute this expansion, Eq. (2.37), into Eq. (2.35), the term $1/R_{pk}$ does not contribute. However, the next term does not lead to vanishing integrals and it plays the leading role in the sigma-pi dispersion forces. Thus to a good approximation,

$$\left(ii'\left|\frac{2e^2}{r_{ab}}\right|jj'\right)=\sum_{p,k}\frac{\sqrt{2}eg_{i'j'}{}^B(k)}{R_{pk}{}^3}\int\phi_i{}^A(a)\phi_j{}^A(a) \times[x_aX_{pk}+y_aY_{pk}+z_aZ_{pk}]dv_a. \quad (2.38)$$

Now the transition (i,j) is associated with a particular chemical bond p so that the x-component of the transition dipole moment of the chemical bond is given by

$$(\mu_x(p))_{ij}=e\int\Psi_0{}^A\Psi_l{}^A\left(\sum_{k=1}^{2N_A}x_k\right)d\tau_1\cdots d\tau_N. \quad (2.39)$$

Then making use of the equivalence of the electrons and Eq. (2.5) it follows that

$$(\mu_x(p))_{ij}=\sqrt{2}e\int\phi_i{}^A(a)\phi_j{}^A(a)x_adv_a. \quad (2.40)$$

The matrix components can therefore be written

$$\left(ii'\left|\frac{2e^2}{r_{ab}}\right|jj'\right)=\sum_{p,k}\frac{g_{i'j'}{}^B(k)}{R_{pk}{}^3}[X_{pk}(\mu_x(p))_{ij}+Y_{pk}(\mu_y(p))_{ij}+Z_{pk}(\mu_z(p))_{ij}]. \quad (2.41)$$

Now we must make use of the special properties of bond functions before substituting Eq. (2.41) back into Eq. (2.6). These properties are:

(1) Each transition $i\rightarrow j$ occurs in a particular chemical bond so that the summation over p in Eq. (2.41) is redundant.

(2) If a particular transition $i\rightarrow j$ has a transition dipole moment in the z-direction parallel to the bond, it cannot have a transition dipole moment in a direction perpendicular to the bond; and vice versa.

(3) The symbols i and j denote the sets of quantum numbers defining the state of the one electron bond orbital. These quantum numbers are quite analogous to the set of four (n,l,m,σ) defining the state of an electron in an atom. Here now the energy of the state depends on the quantum numbers corresponding to n, l, $|m|$.

Making use of these properties Eq. (2.6) becomes:

$$E_{\sigma_A\pi_B}=-\sum_{\substack{i,j\\ p}}\sum_{i',j'}\frac{\{\sum_k(g_{i'j'}{}^B(k)/R_{pk}{}^3)[(\mu_x(p))_{ij}X_{pk}+(\mu_y(p))_{ij}Y_{pk}]\}^2+(\mu_z(p))_{ij}{}^2[\sum_k(g_{i'j'}{}^B(k)Z_{pk}/R_{pk}{}^3)]^2}{(\epsilon_j{}^A-\epsilon_i{}^A)+(\epsilon_{j'}{}^B-\epsilon_{i'}{}^B)}. \quad (2.42)$$

To reduce this summation still further, we note that[12] the cross-term $(\mu_x(p))_{ij}(\mu_y(p))_{ij}$ is proportional to $[\delta_{m_i,m_j+1}-\delta_{m_i,m_j-1}]$. Furthermore the denominator of Eq. (2.40) depends only on the absolute value of m_i and of m_j and in the summation both m_i and $-m_i$ as well as m_j and $-m_j$ occur. On these accounts it follows that

[11] See reference 5, p. 842, Eq. (12.1–25).

[12] H. Margenau, Revs. Modern Phys. 11, 1 (1939), see discussion on p. 20.

the cross-terms vanish and so

$$E_{\sigma\pi}=-\sum_{p}\sum_{\substack{i,j\\ i',j'}}\frac{[\sum_k(g_{i'j'}{}^B(k)/R_{pk}{}^3)X_{pk}]^2(\mu_x(p))_{ij}{}^2+[\sum_k(g_{i'j'}{}^B(k)/R_{pk}{}^3)Y_{pk}]^2(\mu_y(p))_{ij}{}^2 +(\sum_k(g_{i'j'}{}^B(k)/R_{pk}{}^3)Z_{pk})^2(\mu_z(p))_{ij}{}^2}{(\epsilon_j{}^A-\epsilon_i{}^A)+(\epsilon_{j'}{}^B-\epsilon_{i'}{}^B)}. \quad (2.43)$$

Now let us assume that in molecule A there is only one principal transition in each chemical bond and that the energy of this transition is $\epsilon_j{}^A-\epsilon_i{}^A=I$, the ionization potential or roughly 100 000 cm^{-1} or 12.4 ev. Also the parallel and perpendicular bond polarizabilities are[13]

$$\alpha_\perp{}^A(p)=\frac{2(\mu_x(p))_{ij}{}^2}{I}=\frac{2(\mu_y(p))_{ij}{}^2}{I}, \qquad \alpha_\parallel{}^A(p)=\frac{2(\mu_z(p))_{ij}{}^2}{I}. \quad (2.44)$$

Then, the dispersion energy between the sigma electrons of molecule A and the pi electrons of molecule B can be written in the form,

$$E_{\sigma A\pi B}=-\sum_{p}\sum_{i'j'}\frac{[\alpha_\perp\{[\sum_k(g_{i'j'}{}^B(k)/R_{pk}{}^3)X_{pk}]^2+[\sum_k(g_{i'j'}{}^B(k)/R_{pk}{}^3)Y_{pk}]^2\} +\alpha_\parallel[\sum_k(g_{i'j'}{}^B(k)/R_{pk}{}^3)Z_{pk}]^2]}{2[1+(\epsilon_{j'}{}^B-\epsilon_{i'}{}^B)/I]}. \quad (2.45)$$

The total sigma-pi interaction energy between the two molecules is then the sum of $E_{\sigma A\pi B}$ and $E_{\sigma B\pi A}$.

Monopoles for Linear Polyenes

The calculation of the monopoles for linear polyenes is easily carried out using the FEM orbitals of Eq. (2.29), assuming that the polyenes are truly linear and that all carbon-carbon bonds have the same length, 1.4 A. For linear polyenes the charge density of the monopoles is given by Eq. (2.8)

$$\rho_{ij}=\frac{2^{\frac{1}{2}}e}{l}\sin\frac{i\pi x}{l}\sin\frac{j\pi x}{l}. \quad (2.46)$$

This has nodes whenever x is either a multiple of l/i or a multiple of l/j. Thus the first monopole lies between $x=0$ and $x=l/j$ and each of the other monopoles lie between successive nodes. If ξ_k is the x coordinate of the kth node, then the strength of the kth monopole is

$$g_{ij}(k)=\int_{\xi_{k-1}}^{\xi_k}\rho_{ij}dx =\frac{\sqrt{2}e}{\pi}\left[\begin{array}{l}\frac{1}{(j-i)}\left[\sin\left(\frac{(j-i)\pi\xi_k}{l}\right)-\sin\left(\frac{(j-i)\pi\xi_{k-1}}{l}\right)\right]\\ -\frac{1}{(j+i)}\left[\sin\left(\frac{(j+i)\pi\xi_k}{l}\right)-\sin\left(\frac{(j+i)\pi\xi_{k-1}}{l}\right)\right]\end{array}\right] \quad (2.47)$$

and the location of the centroid of the kth monopole $X_{ij}(k)$ is given by

$$X_{ij}(k)g_{ij}(k)=\frac{\sqrt{2}e}{\pi}\left[\begin{array}{l}\frac{l}{\pi(j-i)^2}\left[\cos\left(\frac{(j-i)\pi\xi_k}{l}\right)-\cos\left(\frac{(j-i)\pi\xi_{k-1}}{l}\right)\right]\\ -\frac{l}{\pi(j+i)^2}\left[\cos\left(\frac{(j+i)\pi\xi_k}{l}\right)-\cos\left(\frac{(j+i)\pi\xi_{k-1}}{l}\right)\right]\\ +\frac{1}{(j-i)}\left[\xi_k\sin\left(\frac{(j-i)\pi\xi_k}{l}\right)-\xi_{k-1}\sin\left(\frac{(j-i)\pi\xi_{k-1}}{l}\right)\right]\\ -\frac{1}{(j+i)}\left[\xi_k\left(\frac{(j+i)\pi\xi_k}{l}\right)-\xi_{k-1}\sin\left(\frac{(j+i)\pi\xi_{k-1}}{l}\right)\right]\end{array}\right]. \quad (2.48)$$

[13] See reference 5, p. 889, Eq. (12.6-16a).

TABLE I. Monopoles for linear polyenes. The numbers given above the lines are the strengths of the monopoles $g_{ij}(k)$ given in units of e. The numbers given below the lines are the distances in A between the monopoles. The transitions (i,j) are given on the left-hand side of this chart.

ETHYLENE

(1, 2)

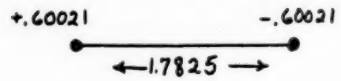

ACETYLENE

(1, 2)

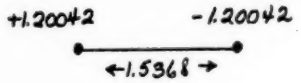

BUTADIENE

(1, 3)

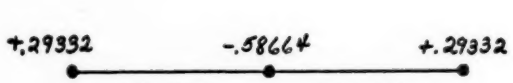

(1, 4)

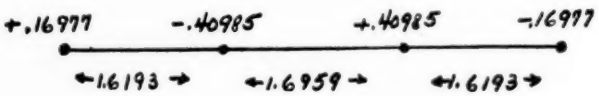

(2, 3)

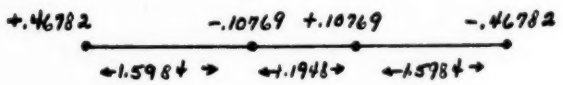

(2, 4)

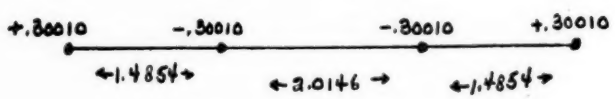

HEXATRIENE

(3, 4)

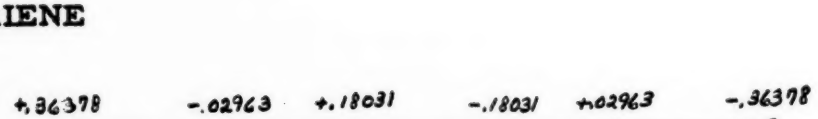

The results for a few polyenes are given in Table I. The notation (i,j) signifies that the monopoles are for the transition in which the excited state contains the jth FEM MO in place of the ith FEM MO in the ground state.

In each case the sum of the monopoles must be zero because of the orthogonality of the wave functions. The signs of the monopoles for a given transition may be changed simultaneously without affecting the result, since the quantity of significance is the square of the matrix element.

For a polyene with N double bonds, the transition $(N, N+1)$ represents the largest contribution and is the only one that is listed for hexatriene. These represent principal transitions. Principal transitions are those in which the molecular orbital of highest energy in the ground state is replaced by the molecular orbital of the next higher energy.

3. RESULTS

A. Ethylene

Ethylene is a simple example of a molecule containing pi electrons. We shall now discuss the calculation of the

dispersion energy for ethylene. We first consider the energy arising from the interaction of pi electrons in one molecule with the pi electrons in the other and shall compare the results with those obtained by Coulson and Davies who used the LCAO orbitals. Then we calculate the complete dispersion energy by taking account of the sigma electrons as well as the pi electrons, and we compare with the experimental data.

The qualitative behavior of the $E_{\pi\pi}$ interactions in ethylene is easy to understand in terms of Eqs. (2.6) and (2.13). According to Table I there is only one important transition in ethylene, (1,2) and there are only two monopoles associated with this transition. These monopoles are equal in magnitude and opposite in sign and correspond to a transition dipole having a dipole moment

$$\mu_{12}=g_{12}(1)[X_{12}(2)-X_{12}(1)]=5.14 \text{ debye}. \quad (3.1)$$

According to Eq. (2.30)

$$\epsilon_2-\epsilon_1=\frac{h^2}{8ml^2}(4-1)=1.0244\times10^{-11} \text{ erg}=6.39 \text{ ev}. \quad (3.2)$$

For separations R between the centers of the molecules large compared to the separation between the monopoles, Eq. (2.6) reduces to

$$E_{\pi\pi}=-\frac{G}{R^6}[-2\cos\theta_A\cos\theta_B+\sin\theta_A\sin\theta_B\cos(\phi_A-\phi_B)]^2, \quad (3.3)$$

where

$$G=\frac{\mu_{12}^4}{2(\epsilon_2-\epsilon_1)}=3.403\times10^{-11} \text{ (erg}-\text{A}^{-6}) =21.25 \text{ (ev}-\text{A}^{-6}), \quad (3.4)$$

and the angles θ_A and θ_B are the angles which the two molecules make with a radial vector joining their centers and ϕ_A and ϕ_B are the azimuthal angles which these molecules make with a plane passing through the radius vector.

At smaller separations Eq. (3.3) is not quite correct because the monopoles form a real dipole with a separation of 1.7825 A between the charge elements as contrasted to an ideal dipole with no separation between the charge elements. The lack of ideality of the dipole-dipole interaction can be taken into account by introducing a function $\gamma(R,\theta_A,\theta_B,\phi_A,\phi_B)$ into the equation for $E_{\pi\pi}$,

$$E_{\pi\pi}=-\gamma\frac{G}{R^6}[-2\cos\theta_A\cos\theta_B+\sin\theta_A\sin\theta_B\cos(\phi_B-\phi_A)]^2. \quad (3.5)$$

The values of $\gamma(R,\theta_A,\theta_B,\phi_A,\phi_B)$ are calculated using Eq. (2.13) to compute values of $E_{\pi\pi}$ for different configurations. In the case of ethylene where there is only one principal transition, (1,2) and only a single pair of monopoles Eq. (2.13) can be written in the simple form:

$$E_{\pi\pi}=-\frac{G}{R^4_{M_1M_2}}\left[\frac{1}{R_{M_1M_3}}+\frac{1}{R_{M_2M_4}}-\frac{1}{R_{M_1M_4}}-\frac{1}{R_{M_2M_3}}\right]^2, \quad (3.6)$$

where the $R_{M_iM_j}$ are the distances between the ith and jth monopoles as shown in Fig. 2; M_1 and M_2 being the monopoles of one molecule and M_3 and M_4 the monopoles of the other molecule. Thus the following results were obtained.

(*a*) *Parallel and Opposed*

C=C ↑
C=C d (A).
C=C ↓

The results for this case can be summarized by the equation:

$$E_{\pi\pi}=-(21.25/d \text{ (A)}^6)\gamma \text{ ev}. \quad (3.7)$$

Here γ is a slowly varying function of the separation d (A) which should approach a constant value at large separations. In Table II the present results (HH) are compared with those of Coulson and Davies (CD) who used LCAO orbitals. The values of $E_{\pi\pi}$ or of γ which

TABLE II. Ethylene parallel and opposed. Calculated values of the coefficient γ defined by Eq. (3.7).

d (A)	γ_{HH}	γ_{CD}	γ_{HH}/γ_{CD}
4	0.760	1.009	1.328
8	0.929	1.245	1.340
10	0.955	1.280	1.340
15	0.981	1.318	1.344
20	0.988	1.315	1.331
50	1.000	1.079	1.079

TABLE III. γ for ethylene parallel displaced [Eq. (3.8)].

y (A)	$d=3$ A	$d=8$ A
0	0.6312	0.9289
1	0.4722	0.9376
2	8.3913	1.1527
3	0.4918	1.0052
4	0.8514	1.0677
5	0.9819	1.3140
6	1.0305	0.4625
7	1.0451	0.8475
8	1.0471	0.9197
9	1.0458	0.9547
10	1.0420	0.9718
11	1.0363	
12	1.0340	0.9932
13	1.0255	
14	1.0267	1.0031
15	1.0237	
16		1.0071
18		1.0060
20		1.0071

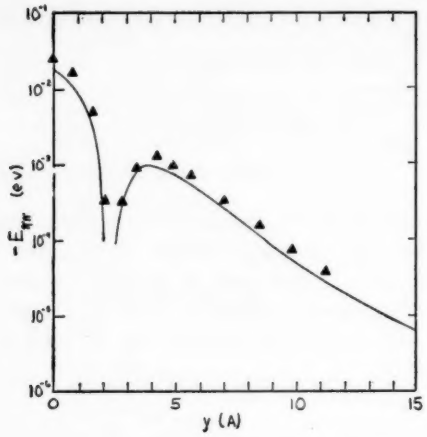

FIG. 1. E for ethylene in displaced parallel configuration for $d=3$ A. Triangles are results of Coulson and Davies.

Coulson and Davies calculate are uniformly 4/3 of our values (except for the calculations at 50 A separation).

(*b*) *Parallel and Displaced*

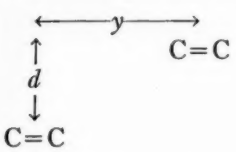

For this case, $R^2=y^2+d^2$; $\cos\theta_A=\cos\theta_B=y/R$; and $\phi_A=\phi_B=0$. Thus Eq. (3.5) can be written

$$E_{\pi\pi}=-\frac{21.25}{R^6(\text{A})}\left(2-3\frac{d^2}{R^2}\right)^2\gamma \text{ ev.} \qquad (3.8)$$

Comparing the values of $E_{\pi\pi}$ calculated from Eq. (2.13) and the expression for $E_{\pi\pi}$ of Eq. (3.8) we obtain the values of γ given in Table III. Figure 1 gives the values of $E_{\pi\pi}$ for $d=3$ A and shows the excellent agreement which is obtained with the more exact calculations of Coulson and Davies.

The most characteristic feature of the curve for $E_{\pi\pi}$ is the node which occurs between $y=2$ A and $y=3$ A for the case of $d=3$ A. If the monopoles behaved like an ideal dipole, then, according to Eq. (3.7), the node should occur when $y=d/\sqrt{2}$ or for $d=3$ A, the nodal y should be 2.12 A. Actually, since the monopoles lie a distance of 1.78 A apart, the corrections for lack of ideality are very large for this small separation. This is seen from the large value of γ in Table III for $y=2$ A and $d=3$ A. Actually we find that the node should occur for $y=2.43$ A. This is in almost perfect agreement with Coulson and Davies who find the node occurring for $y=2.45$ A. For $d=8$ A we obtain equally good agreement with Coulson and Davies for $E_{\pi\pi}$ as a function of y. In this case we find the node occurring at 5.58 A while Coulson and Davies calculations lead to 5.60 A. For $d=8$ A the node would occur at $y=5.66$ A if the monopoles were ideal. The larger the value of d, the more closely does the node occur at the ideal dipole value, $y=0.707$ d.

TABLE IV. γ for ethylene rotated in plane of other molecule and the radius vector (Eq. (3.9)). Here $R=7$ A.

χ Degrees	γ
0	1.101
15	1.080
30	1.042
45	0.980
60	1.006
75	0.882
90	1.000

(*c*) *One Molecule Rotated in Plane of Other Molecule and the Radius Vector*

Here $\theta_A=\pi/2$; $\theta_B=\pi/2-\chi$ and $\phi_A=\phi_B=0$.

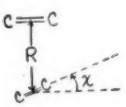

According to Eq. (3.3) for this case,

$$E_{\pi\pi}=-\frac{21.25\gamma}{R(\text{A})^6}\cos^2\chi \text{ ev.} \qquad (3.9)$$

For $R=7$ A, the values of γ which we calculate are given in Table IV. For this case the ideal-dipole approximation is very good. Coulson and Davies obtained the same qualitative behavior as our results except that here again their values are 4/3 of ours.

Complete Dispersion Energy for Ethylene

The formulas for $E_{\sigma\sigma}$ and for $E_{\sigma\pi}$ are given by Eqs. (2.32) and (2.44), respectively. Let us perform the calculation for 12 separate orientations of the two molecules when their centers are separated by 10 A. In the calculations of $E_{\sigma\pi}$ and of $E_{\sigma\sigma}$ we use the bond polarizabilities of $(\text{C}-\text{C})_{\text{aliph}}$ in place of C=C since we do not wish for the bond polarizabilities to include the contribution of the pi-electrons. For the C−H bonds we neglect the asymmetry of the polarizability tensor and use the average polarizability in place of $\alpha_{\parallel}$ and $\alpha_{\perp}$. This greatly simplifies the numerical calculations. It is convenient to number the monopoles (M) and centers of bonds (H) and (C) as shown in Fig. 2. For these calculations the C−H bond length is taken to be 1.07 A and the C=C distance is 1.34 A. The angle between adjacent C−H bonds is 100°. Let the distances between the centers of two C−H bonds be called $R_{H_iH_j}$; between the center of the first C=C bond and the center of C−H bond, $R_{C_1H_j}$; between the first monopole and the center of a C−H bond, $R_{M_1H_j}$; etc. The twelve cases considered are shown schematically in Fig. 3. For these cases the expression for $E_{\sigma\sigma}$ is (in ev when distances are

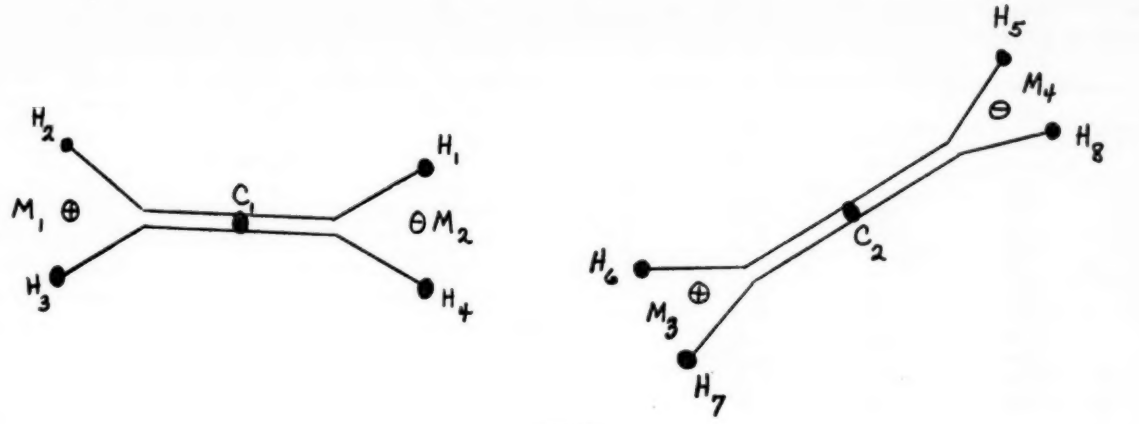

FIG. 2.

in A),

$$E_{\sigma\sigma}=-3.93\sum_{i=1}^{4}\sum_{j=5}^{8}\frac{1}{R^6_{H_iH_j}}$$
$$-0.645\sum_{j=5}^{8}\frac{1}{R^6_{C_1H_j}}[6+2.9(3\cos^2\theta_{C_1}-1)]$$
$$-0.645\sum_{i=1}^{4}\frac{1}{R^6_{C_2H_i}}[6+2.9(3\cos^2\theta_{C_1}-1)]$$
$$-\frac{0.635}{R^6_{C_1C_2}}\begin{bmatrix}0.2+0.29(\cos^2\theta_{C_1}+\cos^2\theta_{C_2})\\+8.41(2\cos\theta_{C_1}\cos\theta_{C_2}\\-\sin\theta_{C_1}\sin\theta_{C_2}\cos(\phi_{C_1}-\phi_{C_2}))^2\end{bmatrix}. \quad (3.10)$$

Here $(\theta_{C_1},\phi_{C_1})$ and $(\theta_{C_2},\phi_{C_2})$ are the angles that the C=C bonds make with the radius vector and a plane including the radius vector joining the center of the two bonds. Also, for the cases considered, the expression for $E_{\sigma\pi}$ is (in ev when distances are in A),

$$E_{\sigma\pi}=-1.113\sum_{i=1}^{4}\left[\frac{1}{R^4_{H_iM_3}}+\frac{1}{R^4_{H_iM_4}}-\frac{(R^2_{H_iM_3}+R^2_{H_iM_4}-R^2_{M_3M_4})}{R^3_{H_iM_3}R^3_{H_iM_4}}\right]$$
$$-1.113\sum_{j=5}^{8}\left[\frac{1}{R^4_{H_jM_1}}+\frac{1}{R^4_{H_jM_2}}-\frac{(R^2_{H_jM_1}+R^2_{H_jM_2}-R^2_{M_1M_2})}{R^3_{H_jM_1}R^3_{H_jM_2}}\right]$$
$$-(\text{only in cases } A_1 \text{ and } A_2)\ 3.218$$
$$\times\left[\left(\frac{1}{(Z_{M_3}-Z_{C_1})^2}-\frac{1}{(Z_{M_4}-Z_{C_1})^2}\right)^2+\left(\frac{1}{(Z_{M_1}-Z_{C_2})^2}-\frac{1}{(Z_{M_2}-Z_{C_2})}\right)^2\right]. \quad (3.11)$$

Here the Z_C and Z_M are the coordinates in the direction of the radius vector from C_1 to C_2; and $R_{M_1M_2}=R_{M_3M_4}=1.783$. For general orientations of the two molecules, the last term in Eq. (3.11) becomes somewhat more complicated but can easily be worked out from Eq. (2.44).

The results for the 12 different configurations of the ethylene molecules are given in Table V. In order to obtain mean values of the dispersion energy corresponding to spatially averaging over all orientations, first of all we must average with respect to rotations about the C−C bonds. This is accomplished by

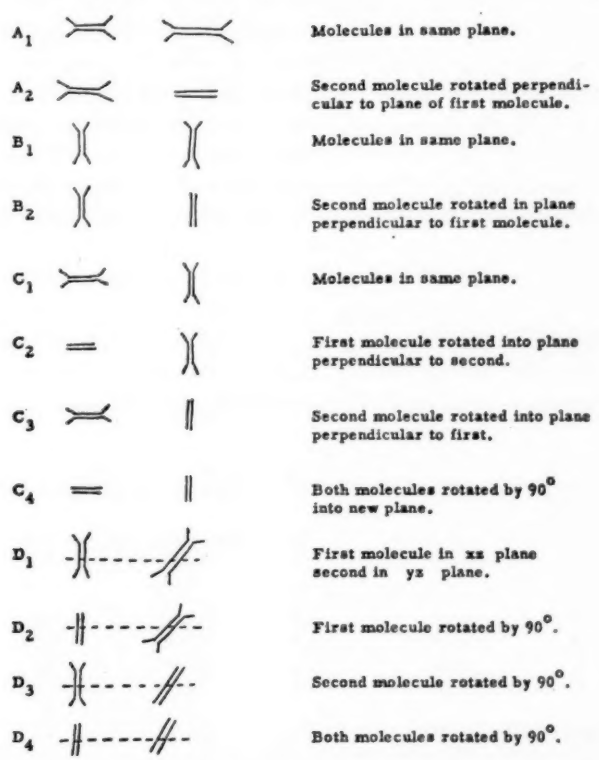
A1 Molecules in same plane.
A2 Second molecule rotated perpendicular to plane of first molecule.
B1 Molecules in same plane.
B2 Second molecule rotated in plane perpendicular to first molecule.
C1 Molecules in same plane.
C2 First molecule rotated into plane perpendicular to second.
C3 Second molecule rotated into plane perpendicular to first.
C4 Both molecules rotated by 90° into new plane.
D1 First molecule in xz plane second in yz plane.
D2 First molecule rotated by 90°.
D3 Second molecule rotated by 90°.
D4 Both molecules rotated by 90°.

FIG. 3. Twelve configurations of two ethylene molecules. The A_1, B_1, C_1, and D_1 represent four orientations of the carbon-carbon bonds. The other orientations differ from these by rotations of 90° about the C−C axes as indicated.

TABLE V. Energy of interaction between two ethylene molecules separated by a distance of 10 A. (All energies are given in units of 10^{-4} ev.)

Orientation	$-E_{\pi\pi}$	$-E_{\sigma\sigma}$	$-E_{\sigma\pi}$	$-E_{\text{total}}$
A_1	0.91	1.93	2.28	5.12
A_2	0.91	1.93	2.28	5.12
B_1	0.20	0.85	0.29	1.34
B_2	0.20	0.82	0.28	1.30
C_1	0.00	1.18	0.75	1.93
C_2	0.00	1.18	0.75	1.93
C_3	0.00	1.13	0.73	1.86
C_4	0.00	1.13	0.73	1.86
D_1	0.00	0.79	0.28	1.07
D_2	0.00	0.77	0.27	1.04
D_3	0.00	0.77	0.27	1.04
D_4	0.00	0.74	0.27	1.01
Mean values	0.13	1.04	0.64	1.81
Experimental dispersion energy from Lennard-Jones potential (6,12)				4.06

averaging the results for A_1 and A_2 to give an average A; average B_1 and B_2 to get an average B; average C_1, C_2, C_3, and C_4 to get an average C; average D_1, D_2, D_3, and D_4 to get an average D. In the above averaging each of the orientations is given equal weight. The resulting four orientations of the C−C axes correspond to the four configurations of the H−H axes in the interaction of two hydrogen molecules problem which Evett and Margenau[14] studied. They found that in this case, the most reliable mean values of the interaction energies is attained by assuming the weights 0.085, 0.25, 0.415, and 0.25 for the configurations A, B, C, and D. Using these weights we obtained the results indicated in Table V. First of all, it is surprising how little difference the orientation of the C−H bonds make in the $E_{\sigma\sigma}$ and $E_{\sigma\pi}$.

When one uses the Lennard-Jones (6,12) potential to fit the experimental data of viscosity of ethylene as a function of temperature, the force constants ϵ and σ are found to be 0.0177 ev and 4.232 A, respectively. If this Lennard-Jones potential were correct, the energy of dispersion would be equal to $4\epsilon\sigma^6/R^6$. This empirical potential energy curve therefore provides an experimental comparison of our average value of E_{total}. The fact that our theoretical value is smaller by a factor of $1.81/4.06=0.45$ is not surprising since most theoretical values of dispersion energies are smaller than the Lennard-Jones values by about this ratio.[15]

TABLE VI. Energy of interaction between two acetylene molecules separated by a distance of 10 A. (Energies are given in units of 10^{-4} ev).

Orientation	$-E_{\pi\pi}$	$-E_{\sigma\sigma}$	$-E_{\sigma\pi}$	$-E_{\text{total}}$
A	1.97	0.89	2.22	5.08
B	0.45	0.97	0.37	1.79
C	0.00	1.81	0.97	2.78
D	0.00	0.22	0.36	0.58
Mean values	0.28	1.12	0.77	2.17
Experimental dispersion energy from Lennard-Jones (6,12) potential				3.62

[14] A. Evett and H. Margenau, Phys. Rev. **90**, 1021 (1953).

Acetylene

The forces between two acetylene molecules are much the same as between two ethylenes. In acetylene the triple bond contains two pi bonds but these pi electrons can be treated in exactly the same manner as the pi electrons in ethylene. The carbon-carbon bond length in acetylene is 1.207 A and the carbon-hydrogen bond length is 1.060 A. Using the monopole strengths and separation given in Table I we obtain the skeletal structure of the acetylene molecule shown in Fig. 4. As in the case of ethylene, there is only one principal transition which needs to be considered, (1, 2) so that the formulas for the three different types of electron interaction are simple. For acetylene, the transition dipole moment is $\mu_{12}=8.86$ debye and the transition energy is $\epsilon_2-\epsilon_1=8.60$ ev. At large separations $E_{\pi\pi}$ is given by Eq. (3.3) where now $G=140$ ev−A^{-6}. At smaller separations $E_{\pi\pi}$ is given by Eq. (3.6) where $R_{M_1M_2}=1.537$ A. The formula for $E_{\sigma\sigma}$ is given by Eq. (3.10) where now the summation over "i" includes only 1 and 2 and the summation over "j" includes only 3 and 4. For the purposes of computation for the present paper, we consider only four basic orientations of the two acetylene molecules, namely the same orientations of the C−C bonds as were considered in the case of ethylene; A, B, C, D of Fig. 3. For acetylene, which is a linear molecule, it is not necessary to consider the subcases indicated by subscripts on the A, B, C, and D. For these cases, the sigma-pi interactions for acetylene are given by

$$E_{\sigma\pi}=-3.978\sum_{i=1}^{2}\left[\frac{1}{R^4_{H_iM_3}}+\frac{1}{R^4_{H_iM_4}}-\frac{(R^2_{H_iM_3}+R^2_{H_iM_4}-R^2_{M_1M_2})}{R^3_{H_iM_3}R^3_{H_iM_4}}\right]$$
$$-3.978\sum_{j=3}^{4}\left[\frac{1}{R^4_{H_jM_1}}+\frac{1}{R^4_{H_jM_2}}-\frac{(R^2_{H_jM_1}+R^2_{H_jM_2}-R^2_{M_1M_2})}{R^3_{H_jM_1}R^3_{H_jM_2}}\right]$$
$$-(\text{only in case } A)\ 11.51\times\left[\left(\frac{1}{(Z_{M_1}-Z_{C_2})^2}-\frac{1}{(Z_{M_2}-Z_{C_2})^2}\right)^2+\left(\frac{1}{(Z_{M_3}-Z_{C_1})^2}-\frac{1}{(Z_{M_4}-Z_{C_1})^2}\right)^2\right]. \quad (3.12)$$

[15] See reference 5, p. 966, Table 13.3-1.

TABLE VII. Contributions to $-E_{\pi\pi}$ (ev) for butadienes in parallel opposed configuration.

Term	$d=4$ (A)	8	15	20	30	50
1(11,44)	5.98×10^{-6}	...	...	...	...	...
2(21,34)	8.08×10^{-6}	1.20×10^{-6}	1.08×10^{-7}	2.40×10^{-8}	2.46×10^{-9}	1.25×10^{-10}
1(22,33)	2.51×10^{-2}	9.29×10^{-4}	2.86×10^{-5}	5.39×10^{-6}	4.93×10^{-7}	2.35×10^{-8}
1(11,33)	7.42×10^{-4}	2.35×10^{-6}	6.35×10^{-9}	3.70×10^{-10}	...	...
2(21,43)	1.07×10^{-3}	4.45×10^{-6}	1.33×10^{-8}	8.18×10^{-10}	...	...
1(22,44)	2.76×10^{-4}	2.22×10^{-6}	7.25×10^{-9}	4.56×10^{-10}	...	...
Total value $-E_{\pi\pi}$ (ev)						
Present calculations	2.72×10^{-2}	9.39×10^{-4}	2.87×10^{-5}	5.41×10^{-6}	4.94×10^{-7}	2.36×10^{-8}
Coulson and Davies	4.06×10^{-2}	1.48×10^{-3}	4.59×10^{-5}	8.62×10^{-6}	7.99×10^{-7}	3.47×10^{-8}

Here again the Z's are coordinates in the direction of the radius vector going from C_1 to C_2, and again the formula for a general orientation would have a last term which is somewhat more complicated. The results of these calculations are given in Table VI. The mean values are obtained, as in the case of ethylene, by assigning the weights: 0.085, 0.25, 0.415, and 0.25 to the configurations A, B, C, and D. Using the Lennard-Jones parameters $\epsilon=0.016$ ev and $\sigma=4.221$ A determined from fitting experimental viscosity of gas data, we obtain an empirical check on our theoretical calculations. In this case our theoretical dispersion energy is smaller than the empirical value by the factor $2.17/3.62=0.60$ which is almost the same as for the case of ethylene.

Butadiene

Now let us consider the pi-pi dispersion energy for butadiene. This example is much more complicated than either the ethylene or the acetylene cases. There are four transitions which must be considered. They are, in the order of their importance: (2,3), (2,4), (1,3), and (1,4). At large separations, the (2,3) and the (1,4) charge distributions could be approximated by a dipole but the (2,4) and (1,3) are essentially quadrupole charge distributions. Naturally, the positions of the nodes and maxima in the energy of interaction are difficult to describe in terms of simple equations. Nevertheless, the "long-polyene approximation" which is considered presently gives a surprisingly good representation at large separations. In this approximation only the principal transition, (2,3), is considered. However, at small separations there is no satisfactory way of avoiding the detailed calculations. Let us use the symbol (ii',jj') to indicate the transition (i,j) in molecule A and the transition (i',j') in the molecule B. The numbers preceding each term indicates its degeneracy. Let us consider two configurations.

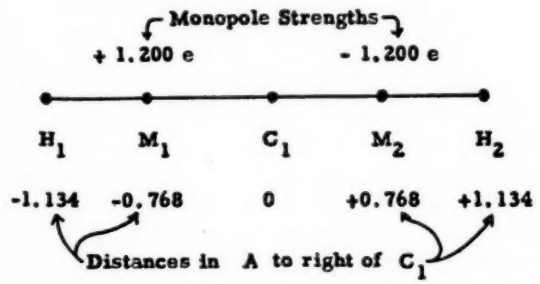

FIG. 4. Skeletal structure of acetylene. Here C_1 is the center of the C—C bond and H_1 and H_2 are the centers of the C—H bonds. The M_1 and M_2 are the two monopoles for the principal transition.

(a) *Parallel and Opposed*

The results for this case are given in Table VII. From symmetry considerations it is easy to see that the transitions (11,34), (21,33), (21,44), and (22,34) do not contribute to the energy of dispersion. It is seen that the principal transition (22,33) is always the largest contributor, followed by (21,34) and (22,44). However, at large separations only the (22,33) is important.

(b) *Displaced Parallel Configuration*

Here the symbols y and d have the same significance as in the case of ethylene. The contributions of the various transitions and the values of $E_{\pi\pi}$ are given in Table VIII for various values of y when $d=8$ A. The variation of $E_{\pi\pi}$ with y is shown in Fig. 5. Because the dispersion energy is the sum of a number of terms each having different nodal points, $E_{\pi\pi}$ has a minimum value different from zero.

Hexatriene

For hexatriene, we consider only the principal transition, (33,44) whereas Coulson and Davies consider a

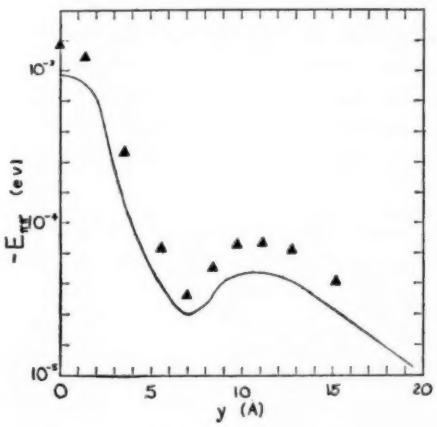

FIG. 5.

TABLE VIII. Contributions to $-E_{\pi\pi}$ (ev) for butadienes in displaced parallel configuration for $d=8$ A.

y (A)	$-(22,33)$	$-(22,44)$	$-(11,33)$	$-2(21,43)$	$-2(22,34)$	$-2(2,33)$	$-$Total $E_{\pi\pi}$
0	9.29×10^{-4}	2.22×10^{-6}	2.35×10^{-6}	4.46×10^{-6}	0	0	9.38×10^{-4}
1	8.41×10^{-4}	1.68×10^{-6}	1.72×10^{-6}	3.32×10^{-6}	7.44×10^{-6}	8.12×10^{-6}	8.63×10^{-4}
2	6.20×10^{-4}	6.44×10^{-7}	5.65×10^{-7}	1.10×10^{-6}	2.32×10^{-5}	2.48×10^{-5}	6.81×10^{-4}
3	3.63×10^{-4}	4.31×10^{-8}	1.33×10^{-8}	5.26×10^{-8}	3.46×10^{-5}	3.62×10^{-5}	4.35×10^{-4}
4	1.58×10^{-4}	8.24×10^{-8}	1.36×10^{-7}	2.10×10^{-7}	2.10×10^{-7}	3.46×10^{-5}	2.28×10^{-4}
5	4.15×10^{-5}	3.27×10^{-7}	3.68×10^{-7}	6.82×10^{-7}	2.60×10^{-5}	2.56×10^{-5}	9.45×10^{-5}
6	1.84×10^{-6}	4.10×10^{-7}	4.01×10^{-7}	8.08×10^{-7}	1.51×10^{-5}	1.44×10^{-5}	3.30×10^{-5}
7	5.75×10^{-6}	3.38×10^{-7}	2.89×10^{-7}	6.18×10^{-7}	7.02×10^{-6}	6.42×10^{-6}	2.04×10^{-5}
8	2.36×10^{-5}	2.05×10^{-7}	1.61×10^{-7}	3.58×10^{-7}	2.50×10^{-6}	2.18×10^{-6}	2.90×10^{-5}
9	3.91×10^{-5}	1.01×10^{-7}	7.37×10^{-8}	1.70×10^{-7}	5.96×10^{-7}	4.84×10^{-7}	4.05×10^{-5}
10	4.71×10^{-5}	4.17×10^{-8}	2.86×10^{-8}	6.80×10^{-8}	4.80×10^{-8}	2.86×10^{-8}	4.73×10^{-5}
12	4.50×10^{-5}	3.95×10^{-9}	2.31×10^{-9}	5.94×10^{-9}	1.06×10^{-7}	1.15×10^{-7}	4.52×10^{-5}
14	3.37×10^{-5}	1.60×10^{-11}	5.44×10^{-16}	6.78×10^{-12}	2.10×10^{-7}	2.08×10^{-7}	3.41×10^{-5}
16	2.29×10^{-5}	2.25×10^{-10}	2.17×10^{-10}	4.34×10^{-10}	1.89×10^{-7}	1.81×10^{-7}	2.33×10^{-5}
18	1.50×10^{-5}	3.35×10^{-10}	2.81×10^{-10}	6.02×10^{-10}	1.33×10^{-7}	1.26×10^{-7}	1.53×10^{-5}
20	9.77×10^{-6}	2.70×10^{-10}	2.18×10^{-10}	4.76×10^{-10}	8.52×10^{-8}	8.10×10^{-8}	9.94×10^{-6}

large number of transitions. Table IX compares our results with those of Coulson and Davies for the parallel opposed configuration. Uniformly, the Coulson and Davies values are 5/3 of ours.

It is interesting to compare the results of the present calculations using the FEM orbitals with the calculations of Coulson and Davies using the LCAO orbitals. The first difference to note is that the degeneracy of the terms is not always the same for the LCAO and the FEM treatments. For example in the parallel opposed configuration, in the LCAO treatment the (22,44) is 4-fold degenerate, whereas in the FEM treatment the (22,44) is singly degenerate. However, in the FEM treatment the singly degenerate (11,33) and the doubly degenerate (21,43) have very nearly the same values for the matrix elements. There is therefore very little physical effect of this difference in the degeneracies. Rather uniformly, the Coulson and Davies results give values of $-E_{\pi\pi}$ larger than ours by a factor of 5/3. Such a difference could arise through the particular empirical value of the resonance integral which Coulson and Davies used or in honest differences between the LCAO and the FEM approximations.

Approximate Treatment of Long Polyenes

Let us develop an approximate method for treating the dispersion energy between linear polyenes for the case that the number of double bonds, N, is large and the separation between the two molecules is large compared to the length of the molecule. We consider the energy arising from the interaction of pi electrons with pi electrons, $E_{\pi\pi}$, the energy arising from the interaction of sigma electrons with sigma electrons, $E_{\sigma\sigma}$, and the energy arising from the interaction of sigma electrons with pi electrons, $E_{\sigma\pi}$.

TABLE IX. $-E_{\pi\pi}$ (ev) for hexatriene in the parallel opposed configuration.

d (A)	Our results	Coulson and Davies
4	6.04×10^{-2}	11.35×10^{-2}
8	3.57×10^{-3}	6.07×10^{-3}
15	1.43×10^{-4}	2.42×10^{-4}
20	2.86×10^{-5}	4.85×10^{-5}
30	2.75×10^{-6}	4.70×10^{-6}
50	1.35×10^{-7}	4.01×10^{-7}

We include only the principal transition for the pi electrons so that the transition charge density is given by:

$$\rho=\frac{2^{\frac{1}{2}}e}{l}\sin\frac{N\pi x}{l}\sin\frac{(N+1)\pi x}{l}. \tag{3.13}$$

Using a familiar trigonometric identity this may be rewritten:

$$\rho=\frac{\sqrt{2}e}{l}\left[\cos\frac{\pi x}{l}-\cos\frac{(2N+1)\pi x}{l}\right]. \tag{3.14}$$

For large N the second term in the brackets is a rapidly oscillating function so we make the approximation that it may be neglected. Our approximate charge density is then given by:

$$\rho=\frac{\sqrt{2}e}{l}\cos\frac{\pi x}{l}. \tag{3.15}$$

In using the London approximation we then obtain a "dipole" and it may easily be seen to consist of a positive and negative charge of magnitude $g_{N,N+1}{}^{B}(+)=-g_{N,N+1}{}^{B}(-)=(\sqrt{2}/\pi)e$ separated by a distance of $2l/\pi$. The dipole moment is then $(2\sqrt{2}el)/\pi^2$. In Table X we compare this dipole moment with the dipole moments for the principal transitions for ethylene, butadiene, and hexatriene. It is seen that even for ethylene the deviation is not great and that the asymptotic value is rapidly approached, which suggests that the approximation is a good one. We now make a further approximation that the interaction of two such dipoles may be given by the interaction of two ideal dipoles as in Eq. (3.3). Finally, making use of the fact that the length of the molecule is $(2N+1)\times1.4$ A we obtain the

following result for the dispersion energy arising from pi-pi interaction:

$$E_{\pi\pi}=-0.14003(2N+1)^5 \times\frac{[-2\cos\theta_a\cos\theta_b+\sin\theta_a\sin\theta_b\cos(\phi_b-\phi_a)]^2}{R^6}, \quad (3.16)$$

where R, the separation, is measured in A. Averaging over angles introduces a factor of $\frac{2}{3}$ and gives the result:

$$\bar{E}_{\pi\pi}=-0.09335\frac{(2N+1)^5}{R^6}. \quad (3.17)$$

It is seen that $E_{\pi\pi}$ is proportional to the fifth power of the length of the polyene, a result also reported by Coulson and Davies. However, their coefficient is somewhat larger. Thus, for $\theta_a=\theta_b=\pi/2$, $\phi_a=\phi_b$, their coefficient is 0.246 compared to the foregoing value of 0.14003.

In treating $\bar{E}_{\sigma\sigma}$ we use Eq. (2.32) (which treats all bonds as if they were at the center of the molecule) and average over all orientations of the molecules. The averaging over all orientations has the effect of making all of the terms with δ's vanish so that

$$\bar{E}_{\sigma\sigma}=-\tfrac{3}{4}I(\sum_{k_A}\alpha_{k_A})(\sum_{l_B}\alpha_{l_B})/R^6. \quad (3.18)$$

Here the sums are to be taken over all of the chemical bonds in the two molecules. Since a polyene with N double bonds has $(2N-1)$ C−C bonds and $(2N+2)$ C−H bonds which have nearly the same average polarizability, it follows that

$$\bar{E}_{\sigma\sigma}=-\frac{3.91(4N+1)^2}{R^6}\ (\text{ev}-\text{A}^{-6}). \quad (3.19)$$

We have, of course, regarded all double bonds as single bonds in this calculation inasmuch as we do not wish to include the pi electrons in this expression. It is seen that $E_{\sigma\sigma}$ varies approximately as the square of the length of the molecule so that for sufficiently long molecules it is negligible compared with $E_{\pi\pi}$.

In order to obtain a simple form for the average value of $E_{\sigma\pi}$ for long polyenes at large separations, let us assume: (1) that each of the chemical bonds has a mean polarizability $\alpha=0.645\times10^{-24}$ cm^3 and we ignore the difference between the perpendicular and parallel polarizabilities as well as the difference between the polarizabilities of the C−C and of the C−H bonds. (2) We assume that the centers of each of the chemical bonds coincides with the center of the molecule. Let S=distance between the monopoles of molecule B, and R_+ and R_- be the distances from the center of molecule A to the plus and minus monopoles, respectively. The geometry

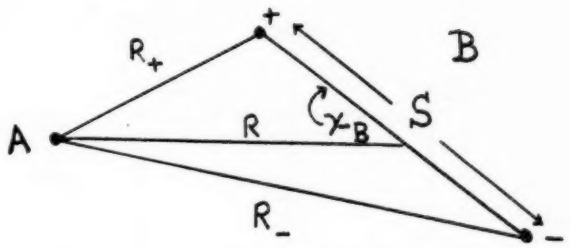

FIG. 6.

is then as shown in Fig. 6. Then:

$$E_{\sigma_A\pi_B}=-\frac{[4N+1]\alpha g^2}{2\left[1+\frac{\epsilon_{N+1}-\epsilon_N}{I}\right]} \times\left[\frac{1}{R_+^4}+\frac{1}{R_-^4}-\frac{R_+^2+R_-^2-S^2}{R_+^3R_-^3}\right]. \quad (3.20)$$

From the geometry of Fig. 6 it follows that:

$$R_+^2=R^2+\frac{S^2}{4}-RS\cos\chi_B, \qquad R_-^2=R^2+\frac{S^2}{4}+RS\cos\chi_B. \quad (3.21)$$

Substituting these expressions into Eq. (3.20) and expanding the resulting equation in powers of S/R, it follows that the term in $1/R^6$ is the leading term and it is given by

$$E_{\sigma_A\pi_B}=-\frac{\alpha g^2[4N+1]}{2\left[1+\frac{\epsilon_{N+1}-\epsilon_N}{I}\right]}\frac{S^2}{R^6}(1+3\cos^2\chi_B). \quad (3.22)$$

Now remembering that $(\epsilon_{N+1}-\epsilon_N)=19.17/(2N+1)$ ev; $I=12.4$ ev; $S=2.8(2N+1)\times10^{-8}/\pi$; and $g=\sqrt{2}e/\pi$, it follows that

$$E_{\sigma_A\pi_B}=-\frac{0.747(4N+1)(2N+1)^3}{2(N+1.27)R^6}(1+3\cos^2\chi_B). \quad (3.23)$$

Now $E_{\sigma\pi}=E_{\sigma_A\pi_B}+E_{\sigma_B\pi_A}$ and so

$$E_{\sigma\pi}=-\frac{0.747(4N+1)(2N+1)^3}{(N+1.27)R^6} \times[1+\tfrac{3}{2}\cos^2\chi_A+\tfrac{3}{2}\cos^2\chi_B]. \quad (3.24)$$

TABLE X. Comparison of principal transition dipole moments with asymptotic value.

Molecule	$\mu_{N,N+1}$ Transition dipole moment
Ethylene	0.25473el
Butadiene	0.27512el
Hexatriene	0.28073el
Asymptotic value	0.28658el

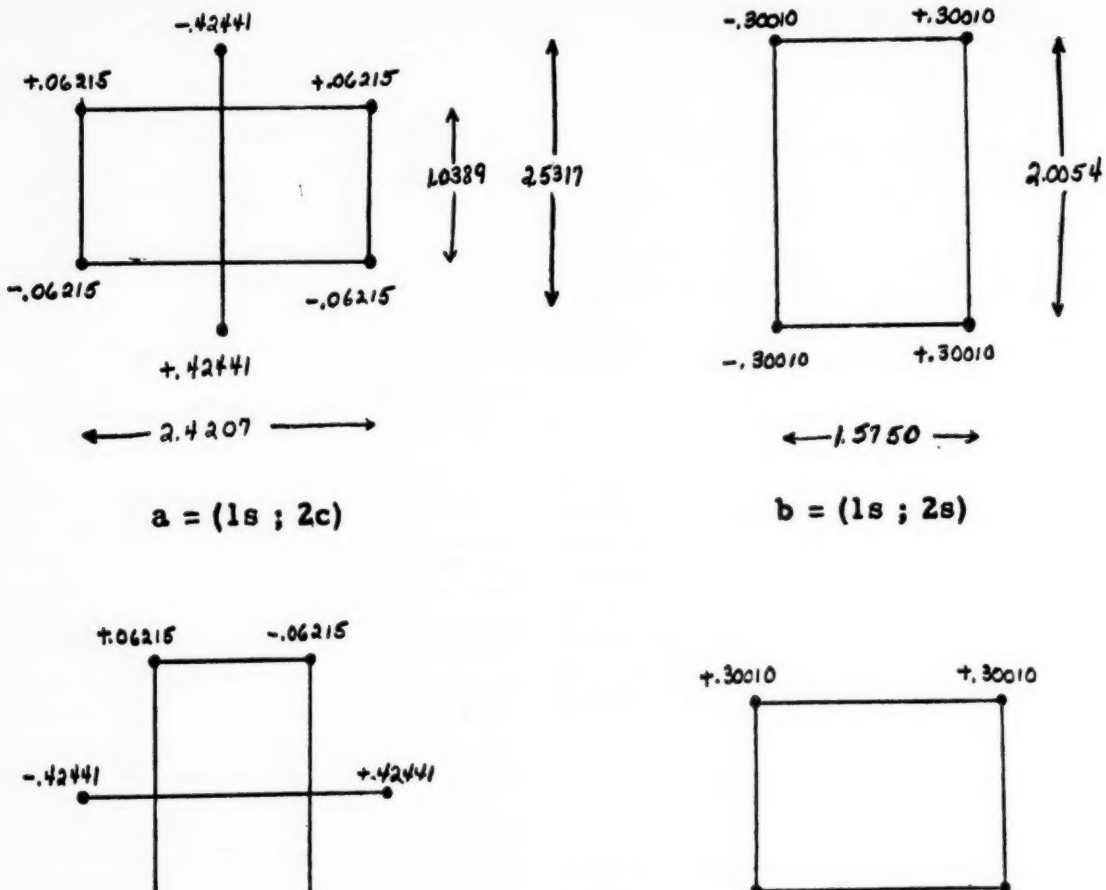

FIG. 7. Monopoles for principal transitions for benzene (units are Angstroms and electronic charge e).

Averaging $E_{\sigma\pi}$ over all orientations of the two molecules corresponds to averaging $\cos^2\chi$. Since the spatially averaged value of $\cos^2\chi=\frac{1}{3}$, it follows that

$$\bar{E}_{\sigma\pi}=-\frac{1.49(4N+1)(2N+1)^3}{(N+1.27)R^6}.$$

TABLE XI. Coefficients of $1/R^6$ for different polyenes using "long polyene approximation." The coefficients are given in units of ev$-$A^{-6}.

N	$-E_{\sigma\sigma}R^6$	$-E_{\sigma\pi}R^6$	$-E_{\pi\pi}R^6$	$-E_{\text{total}}R^6$
1	98	89	23	210
2	317	512	292	1120
3	661	1560	1570	3790
4	1139	3520	5510	10 160
6	2440	8800	34 700	45 900
8	4260	26 200	133 000	163 500
10	6570	50 400	381 000	438 000

We see that $E_{\sigma\pi}$ varies approximately as the cube of the length of the molecule so that its significance for large molecules is greater than $E_{\sigma\sigma}$ but less than $E_{\pi\pi}$.

In Table XI we present the coefficients of $1/R^6$ for the three dispersion energy terms for various values of N. It is interesting to compare the results for N equals one with our previous results for ethylene which are given in Table XII. It may be concluded that the long polyene approximation is fairly satisfactory even in the case of ethylene, the smallest polyene.

TABLE XII. Comparison of "long polyene approximation" with accurate FEM calculations for ethylene. The coefficients are given in units of ev$-$A^{-6}, and have the values approached when the molecules are separated by large distances.

	$-E_{\sigma\sigma}R^6$	$-E_{\sigma\pi}R^6$	$-E_{\pi\pi}R^6$	$-E_{\text{total}}R^6$
Accurate FEM	104	64	13	181
"Long polyene approx."	98	89	23	210

Benzene

The FEM MO's for benzene[7] which we shall regard as having a circular free electron path, are given by:

$$\phi_0=\frac{1}{(2\pi)^{\frac{1}{2}}},$$

$$\left.\begin{aligned}\phi_{nc}&=\frac{1}{\pi^{\frac{1}{2}}}\cos n\theta\\ \phi_{ns}&=\frac{1}{\pi^{\frac{1}{2}}}\sin n\theta\end{aligned}\right\}n=1,\,2,\,3. \tag{3.25}$$

Their energy is given by

$$\epsilon_n=\frac{n^2h^2}{2mC^2},\quad n=0,\,1,\,2,\,3. \tag{3.26}$$

Here θ is the angular coordinate of the electron and C is the circumference of the ring. We assume that all the carbon-carbon separations are 1.4 A so that, roughly speaking, $C=6\times1.4$ A. Note that for n greater than zero the molecular orbitals are doubly degenerate.

In the ground state of benzene, the six π electrons are located in the three orbitals ϕ_0, ϕ_{1c}, and ϕ_{1s}.

In treating benzene we shall consider only the principal transitions which result from transitions of π electrons from either the $1c$ or the $1s$ orbitals to either the $2c$ or the $2s$ orbitals.

Substituting the FEM MO's as given by (3.25) into Eq. (2.8) we have the following expressions for the transition charge densities:

$$\begin{aligned}\rho_a&=\rho_{1s;\,2c}=\frac{\sqrt{2}e}{\pi}\sin\theta\cos2\theta,\\ \rho_b&=\rho_{1s;\,2s}=\frac{\sqrt{2}e}{\pi}\sin\theta\sin2\theta,\\ \rho_c&=\rho_{1c;\,2c}=\frac{\sqrt{2}e}{\pi}\cos\theta\cos2\theta,\\ \rho_d&=\rho_{1c;\,2s}=\frac{\sqrt{2}e}{\pi}\cos\theta\sin2\theta.\end{aligned} \tag{3.27}$$

The energy associated with these transitions may be deduced from Eq. (3.26) and has the value:

$$\epsilon_2-\epsilon_1=3h^2/2mC^2. \tag{3.28}$$

In calculating the monopoles it is helpful to note that

$$\begin{aligned}\rho_c&=(\text{rotation by }90°)\times\rho_a,\\ \rho_d&=(\text{rotation by }90°)\times\rho_b,\end{aligned} \tag{3.29}$$

so that we need carry out calculations only for ρ_a and ρ_b. In each charge density region we locate the effective charge by calculating the first moment, i.e., we obtain the mean values of x and y. In general the monopoles are not located on the ring but are inside it, and are illustrated in Fig. 7. The position of the atoms relative to the monopoles is of no importance in the FEM model.

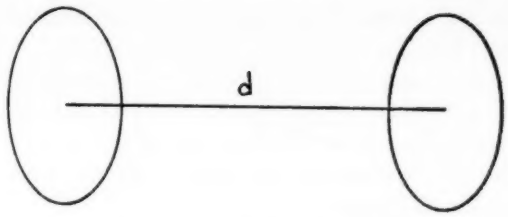

FIG. 8. Parallel opposed configuration for benzene.

Let us calculate the dispersion energy between two benzene molecules arising from pi-pi interaction for the orientation in which the two benzene rings are parallel and facing each other and are separated by a distance, d (see Fig. 8).

Let us denote the energy arising from the interaction of monopole distribution $(1s;\,2c)=a$ with monopole distribution $(1s;\,2s)=b$ by the symbol (a,b), and so forth. From symmetry considerations we see that the terms (a,b), (a,c), (b,d), and (c,d) are zero. The terms which contribute are $(a,a)=(c,c)$, $(b,b)=(d,d)$, and $(a,d)=(b,c)$, the last two being each twofold degenerate. It is then a straightforward matter to calculate the different energy terms and the results are presented in Table XIII. In Table XIII the term values are multiplied by their degeneracy to give their contribution to the total dispersion energy. To a good approximation, $E_{\pi\pi}$ varies inversely as the sixth power of the separation so that it is convenient to write it in the form:

$$E_{\pi\pi}=-\frac{145\gamma}{d^6}\ (\text{ev}-\text{A}^{-6}), \tag{3.30}$$

where γ is a slowly varying function with values given in Table XIII.

Davies[3] has made a rather extensive study of the $\pi-\pi$ interactions of two benzene molecules using the LCAO method. His results agree well with the values given in Table XIII except that they are larger in the ratio $228/145=1.57$. Davies also considered the variation of

TABLE XIII. $-E_{\pi\pi}$ dispersion energy for benzene for parallel opposed configuration (in ev).

d (A)	$-2(a,a)$	$-2(b,b)$	$-4(a,d)$	$-E_{\pi\pi}$	γ
5	3.07×10^{-3}	1.17×10^{-3}	2.31×10^{-3}	6.55×10^{-3}	0.705
10	6.19×10^{-5}	2.36×10^{-5}	4.71×10^{-5}	1.33×10^{-4}	0.916
15	5.72×10^{-6}	2.18×10^{-6}	4.36×10^{-6}	1.23×10^{-5}	0.965
25	2.74×10^{-7}	1.04×10^{-7}	2.09×10^{-7}	5.87×10^{-7}	0.987
50	4.34×10^{-9}	1.65×10^{-9}	3.30×10^{-9}	9.29×10^{-9}	1.000

the $\pi-\pi$ dispersion forces with angles and with various types of displacements. He concludes that the $\sigma-\pi$ and $\sigma-\sigma$ forces must be much larger than the $\pi-\pi$ forces in order to account for the properties of crystalline benzene. As matter of fact de Boer[16] succeeded in explaining the heat of sublimation of benzene without ever considering π electrons.

APPENDIX. POLARIZABILITY OF THE POLYENES

The longitudinal polarizability of the polyenes arising from the π electrons may be calculated using Eqs. (2.44) and (2.40). For this calculation we shall not assume the polyene to be linear. Rather let us consider all C—C bonds to be 120° and that the polyene is in the configuration (see Fig. 9). Because of the angle of 120°, Eq. (2.40) must be written

$$\mu_{ij}=\sqrt{2}e\int\phi_i(x)\frac{\sqrt{3}}{2}x\phi_j(x)dx. \tag{A.1}$$

Inserting the free-electron functions (2.29) for the transition $N\rightarrow N+1$ for an N-polyene gives the result:

$$(\mu)_{N,N+1}=\frac{\sqrt{6}el}{\pi^2}\left[\frac{1}{(2N+1)^2}-1\right]. \tag{A.2}$$

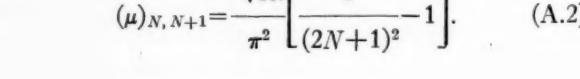

FIG. 9. *Trans*-polyene for $N=3$. The extra bonds correspond to the free electron path and the dashed line represents the axis at the polyene.

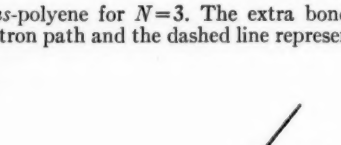

FIG. 10. Ethylene.

[16] J. de Boer, Trans. Faraday Soc. **32**, 10 (1936).

TABLE XIV. Polarizabilities of the N-polyenes.

N	$H-H$	Davies
1	38×10^{-25} cm³	35×10^{-25} cm³
2	209	204
3	596	596
4	1290	
5	2370	2400

It then follows from (2.44) that the polarizability is:

$$\alpha_N=1.81\times10^{-25}\frac{[(2N+1)^2-1]^2}{2N+1}\text{ cm}^3. \tag{A.3}$$

Results using this equation are compared in Table XIV with values obtained by Davies[17] who used LCAO molecular orbitals.

For large polyenes (A.3) becomes:

$$\alpha_N=1.81\times10^{-25}(2N+1)^3\text{ cm}^3 \tag{A.4}$$

so that the polarizability is proportional to the cube of the length of the molecule. Davies obtains nearly the same result:

$$(\alpha_N)_{\text{Davies}}=1.82\times10^{-25}(2N+1)^3\text{ cm}^3. \tag{A.5}$$

In the case of ethylene it is more significant to calculate the polarizability along the axis of the double bond. From Fig. 10 we see that the dipole moment integral (2.40) must be written:

$$\mu_{12}=\sqrt{2}e\left[\int_0^{l/3}\phi_1\left(\frac{\sqrt{3}}{2}x\right)\phi_2dx+\int_{l/3}^{2l/3}\phi_1x\phi_2dx+\int_{2l/3}^{l}\phi_1\left(\frac{\sqrt{3}}{2}x\right)\phi_2dx\right]. \tag{A.6}$$

It is then found that $\alpha_{11}=9.1\times10^{-25}$ cm³. This compares well with the bond polarizabilities of Denbigh (Trans. Faraday Soc. **36**, 936 (1940)), who found that α_{11} for a double bond is 28.6×10^{-25} cm³ and for a single bond is 18.8×10^{-25} cm³. The difference, which is presumably the contribution of the pi electrons, is 9.8×10^{-25} cm³, which agrees well with our value of 9.1×10^{-25} cm³.

[17] P. L. Davies, Trans. Faraday Soc. **48**, 789 (1952).

Oxygen-18 Isotope Effect in the Reaction of Oxygen with Copper

RICHARD B. BERNSTEIN
Department of Chemistry, University of Michigan, Ann Arbor, Michigan
(Received December 13, 1954)

The fractionation of oxygen-18 in the reaction of copper with oxygen of natural isotopic composition has been measured over the temperature range 68–256°C. The oxide films (estimated thicknesses varying from 150–2500 A) were removed for O^{18} assay by treatment with hydrogen at 350°C. Using the CO_2 equilibration technique, the O^{18}/O^{16} ratios for the resulting water samples were determined mass spectrometrically and compared with the ratio for a reference sample of water prepared from the original oxygen gas.

The direction of the fractionation indicated that O_2^{16} reacts preferentially compared to $O^{16}O^{18}$. The isotope effect appeared to be independent of the oxygen pressure over the limited range studied (2–25 cm Hg). The magnitude of the fractionation factor was 2.0% at 150°C, with a small negative temperature coefficient. From this it was possible to estimate a value of $\Delta E_{act}=17$ cal/mole, which may be compared with the calculated isotopic zero-point energy difference of 64 cal/mole. The theoretical implications of the experimental results are discussed.

INTRODUCTION

A GREAT deal of experimental work on the kinetics of the reaction of oxygen with metals has appeared in the literature. A review of the experimental and theoretical aspects of this subject appears in the recent book by Kubaschewski and Hopkins.[1] Tylecote[2] has summarized the voluminous literature on the reaction of oxygen with copper.

Depending upon the extent of oxide film formation and the temperature, it appears that at least three oxidation mechanisms and rate laws apply to the oxidation of copper. In the case of low temperatures and very thin films (less than about 25 A) the logarithmic law is obeyed[3] as predicted from the Mott-Cabrera theory.[4,5] At higher temperatures and for films of intermediate thickness (up to about 10^4 A) the cubic law is observed,[3,6] as discussed by Cabrera.[7] For thicker films the familiar parabolic law describes the kinetics, as explained by the Wagner theory.[8]

It was thought that new and independent information bearing on the mechanism of the reaction of oxygen with metals could be obtained by a study of the oxygen isotope effect. For example, in the thick film region it is generally agreed that the rate-determining step is the diffusion of cuprous ions through the cuprous oxide lattice. At moderate pressures the reaction rate depends only very slightly upon the pressure[9] so that the surface may be considered to be saturated with an adsorbed layer of oxygen. Any O^{18} fractionation which might be observed in the course of the oxidation would then be associated with an isotope exchange equilibrium between gaseous oxygen and adsorbed atomic or molecular oxygen. In the case of adsorbed atoms this exchange would favor the concentration of the light isotope in the adsorbed layer; for adsorbed molecular oxygen the reverse would be expected. A possible rate-limiting step under certain conditions might involve an irreversible process such as the rupture of the O—O bond; for example, the reaction $4e^-+O_2\rightarrow 2O^=$. Here the effect would be such that O^{16} would tend to be concentrated in the oxide.

Dole and Lane[10] have reported some preliminary results on the fractionation of O^{18} during the chemisorption of oxygen on copper and steel at room temperature. The residual oxygen remaining unreacted after chemisorption was analyzed and found to be depleted in O^{16}, corresponding to a fractionation factor of about 1.05 for copper and 1.025 for steel.

The present report deals with a study of the O^{18} fractionation in the reaction of oxygen with copper for the case of oxide films of intermediate thickness. The method involves removal of the oxide film, measurement of its O^{18}/O^{16} ratio and comparison with the isotope ratio for the gaseous oxygen.

EXPERIMENTAL

Materials

The copper samples were prepared by hydrogen reduction of short lengths of CuO wire, Reagent Grade (General Chemical Company), stated to contain less than 0.01% of impurities. Samples ranging from 1–12 g were used. They were normally contained in small Pyrex boats which were perforated to allow gas circulation.

The oxygen used for most of the experiments was commercial tank oxygen (Bird Gas Division, Liquid Carbonic Corporation) purified by passage through silica gel, ascarite, P_2O_5, and a cold trap at −78°C. Mass spectral analysis showed it to contain only nitro-

[1] O. Kubaschewski and B. E. Hopkins, *Oxidation of Metals and Alloys* (Academic Press, Inc., New York, 1953).
[2] R. F. Tylecote, J. Inst. Metals **78**, 259 (1950).
[3] T. N. Rhodin, J. Am. Chem. Soc. **72**, 5102 (1950).
[4] N. F. Mott, Trans. Faraday Soc. **43**, 429 (1947).
[5] N. Cabrera and N. F. Mott, Repts. Progr. Phys. **12**, 163 (1948–1949).
[6] W. E. Campbell and U. B. Thomas, Trans. Electrochem. Soc. **91**, 623 (1947).
[7] N. Cabrera, Phil. Mag. **40**, 175 (1949).
[8] C. Wagner, Z. physik. Chem. **B21**, 25 (1933).
[9] C. Wagner and K. Grunewald, Z. physik. Chem. **B40**, 455 (1938).
[10] M. Dole and G. A. Lane, J. Chem. Phys. **22**, 949 (1954).

gen and argon (totalling approximately 0.5%). A reference sample of some twenty grams of water was prepared from this oxygen by a nearly stoichiometric reaction with oxygen-free hydrogen at about 1000°C over a platinum gauze catalyst.[11] For certain check experiments oxygen was prepared by the electrolysis of a 40% NaOH solution using nickel electrodes. The electrolytic oxygen was purified by passage through a bubbler tube of 95% H_2SO_4 followed by ascarite, silica gel, and anhydrous $CaSO_4$. Mass spectrometric analysis showed it to be of greater than 99.9% purity.

Hydrogen from a commercial cylinder was purified by passage through a "De-Oxo" catalyst tube (J. T. Baker Chemical Company) followed by ascarite, silica gel, P_2O_5, and a cold trap at −195°C.

Carbon dioxide was obtained from two sources: either dry ice or a commercial tank (Matheson "Bone-Dry" grade). After passing through a train containing silica gel and P_2O_5, the gas was subjected to a trap-to-trap distillation from −78° to −195°C. The mass spectrum of the resulting CO_2 revealed no significant impurities.

Apparatus, Procedure, and Analytical Method

The experiments were carried out in a conventional high vacuum apparatus. The Pyrex reaction vessel was enclosed in a specially constructed electric furnace provided with transparent Vycor walls, which permitted visual observation of the surface of the copper during the course of its oxidation. The extent of oxidation was monitored by means of a differential oil manometer as well as a mercury manometer. The decrease in oxygen pressure at constant temperature and at essentially constant volume could be related to the oxygen uptake by the copper. In certain experiments the weight increase of the metal sample was measured as a check.

In a typical experiment the copper sample was evacuated to 10^{-4} mm Hg, then heated (while continuously pumping) to the desired temperature, controlled to ±1°C. A calibrated Chromel-Alumel thermocouple was located directly on the outer wall of the reaction vessel to indicate the temperature of the sample. Oxygen was admitted and the rate of oxygen consumption followed manometrically. After reaction for a definite time the excess oxygen was pumped away. Hydrogen was then admitted and the sample was heated to 350°C for approximately 10 minutes (which was found to be sufficient to reduce the oxide quantitatively). The water was distilled (*in vacuo*) into a special weighing ampoule provided with a stopcock and $ joint. It was thus possible to measure the quantity of water formed in each run. In most of the experiments the water samples ranged from 5–25 mg, which were determined to ±0.1 mg.

The water sample was then distilled into an equilibration[12] tube of about 10 cc volume. A small quantity of CO_2 was metered out from a standard volume and distilled into the equilibration tube. In order to minimize the correction for isotopic dilution the molar ratio of CO_2 to H_2O was usually kept less than 0.1.

After allowing the CO_2-H_2O equilibration to proceed at room temperature for 2–5 days, the CO_2 was distilled from the equilibration tube at −78°C into a sampling tube at −195°C.* In the case of the reference water, large samples (*ca* 250 mg) were used; since the CO_2/H_2O ratio was of the order of 0.005 no dilution correction was required.

An isotope-ratio mass spectrometer (Nier design) was used to determine the $C^{12}O^{16}O^{18}/C^{12}O_2^{16}$ ratio (m/e 46/44) for CO_2 from the reference water, CO_2 from the "unknown" water sample, and CO_2 from the storage bulb. From these ratios and the known value of the CO_2/H_2O molar ratio the isotopic enrichment may be calculated.

The exact expression for the dilution correction given by Dostrovsky and Klein[13] may be considerably simplified for the "tracer" case to give the following very good approximation:

$$N_0=\frac{r_e}{K}+\frac{b}{a}(r_e-r_0), \tag{1}$$

where N_0=atom fraction of O^{18} in "unknown" H_2O before equilibration; r_0=46/44 ratio for initial CO_2 (storage bulb), r_e=46/44 ratio for equilibrated CO_2; b/a is the molar ratio, $(CO_2)/(H_2O)$; K is the isotope exchange equilibrium constant=2.08 at room temperature.[12]

To establish confidence in the O^{18} analytical technique several samples of O^{18}—enriched water (Stuart Oxygen Company, stated to contain 1.4% O^{18}) were assayed and compared with distilled tap water. Normalizing these values, assuming 0.200% O^{18} in distilled H_2O, three independent determinations gave 1.42, 1.44, and 1.42% O^{18} for the enriched water.

The separation factor in the reaction of oxygen with copper is defined:

$$S=\frac{[(O^{18})/(O^{16})]_{\text{oxide film}}}{[(O^{18})/(O^{16})]_{\text{oxygen gas}}}. \tag{2}$$

Because of the negligible dilution correction for the reference water, Eq. (2) becomes:

$$S=\frac{\frac{r_m}{K}+\frac{b}{a}(r_m-r_0)}{\frac{r_0}{K}}, \tag{3}$$

[11] Anderson, Halford, and Bates, J. Chem. Phys. **2**, 342 (1934).
[12] M. Cohn and H. C. Urey, J. Am. Chem. Soc. **60**, 679 (1938); J. P. Hunt and H. Taube, J. Chem. Phys. **19**, 602 (1951).

* At the suggestion of a referee, certain check experiments were performed which indicated that when tank CO_2 was equilibrated with distilled tap water and separated using the procedure described, the O^{18}/O^{16} ratio of the CO_2 showed an increase of about 1%. This effect introduces only a very slight error in the calculated fractionation factors, which involve essentially the *ratio* of the O^{18}/O^{16} ratios for CO_2 equilibrated with the unknown water sample compared to CO_2 equilibrated with the reference water sample.

[13] I. Dostrovsky and F. S. Klein, Anal. Chem. **24**, 414 (1952).

where $r_m = 46/44$ ratio for CO_2 after equilibration with "unknown" water from the metal oxide, and $r_0 = 46/44$ ratio for CO_2 after equilibration with reference water prepared from oxygen gas. Defining the O^{16} enrichment

$$\epsilon \equiv 1 - S, \tag{4}$$

one obtains the expression:

$$\epsilon = \frac{r_0 - r_m}{r_0} - 2.08\frac{b}{a}\frac{(r_m - r_0)}{r_0}. \tag{5}$$

Equation (5) was used in all cases to calculate the enrichment factor from the four measured quantities r_0, r_m, r_0, and b/a.

In the course of this work a large number of intercomparisons of various isotope ratios were obtained; some of these results are summarized here. All values are normalized to the reference oxygen as standard.

A. Percentage difference, based on 46/44 ratios, corrected for CO_2 dilution effect.

1. Reference H_2O from standard O_2	0.00 (assumed)
2. Distilled tap water	-2.2 ± 0.2

B. Percentage difference, based on 34/32 ratios.

1. Reference O_2 (purified; tank No. 1)	0.00 (assumed)
2. O_2 (tank No. 2, Matheson)	0.00 ± 0.05
3. O_2 (purified; tank No. 3, Bird)	0.00 ± 0.05
4. O_2, electrolytic (av of 4 analyses for 4 different batches)	-3.9 ± 0.15

From the results of B 1, 2, and 3 it appears that there is no appreciable isotopic difference among the different tanks of oxygen. Experiments have also shown that the 34/32 ratios for tank oxygen and atmospheric oxygen differ by less than 0.2%. Thus the result A 2 is a measure of the so-called Dole effect,[14] i.e., the anomalous difference of 2.5% in the O^{18} ratio for atmospheric oxygen compared with oxygen from lake water.†

The O^{18} depletion of the electrolytic oxygen (B 4) was somewhat greater than anticipated. On the basis of the electrolytic fractionation, about 1%,[15] and the Dole effect, above, one would estimate a maximum depletion of about 3.5%, compared with the observed value of 3.9 ± 0.15%. This difference may not be serious, however, in view of the large range of values reported for the electrolytic fractionation factor, from 1.008 to 1.035,[16] and its corresponding uncertainty.

The electrolytic oxygen served an important function in checking the direction and magnitude of the isotope effect in the oxygen-copper reaction, as it was initially depleted in O^{18} far below the level of either atmospheric oxygen, water, or ordinary carbon dioxide. Thus any leak or contamination would tend to *increase* the O^{18}/O^{16} ratio. Since in the reaction with copper the O^{16} was found to concentrate in the oxide, the water obtained from the oxide should be further depleted in O^{18}. Experiments with the electrolytic oxygen therefore constituted a severe test of the validity of the experimental procedures.

The enrichments calculated according to Eq. (5) require small corrections to bring all data to the common basis of infinitesimal extent of reaction. The fraction of substrate (oxygen) consumed, represented by $f = \Delta P_t / P_0$, (where P_0 = initial oxygen pressure and ΔP_t = total pressure decrement in the course of the reaction) was usually less than 0.1. The standard logarithmic correction formula was employed.[17] For $f < 0.1$ it was convenient to use the simplified formula:

$$\epsilon_0 = \epsilon(1 + f/2). \tag{6}$$

The corrected fractionation factor, α, is then defined:

$$\alpha \equiv 1 + \epsilon_0. \tag{7}$$

RESULTS

Certain preliminary experiments were carried out at 337° and 377°C using copper foil of known geometrical area. The total amount of oxygen reacted was, however, insufficient for isotopic analysis (for which a minimum of 3 mg of water is desirable), due to the small area of the sample. The oxidation followed the parabolic law after the first few minutes and the rate constants agreed (within a factor of 2) with the values calculated using the constants of the Arrhenius equation given in reference 1, p. 163. Other experiments with the high surface area copper wire over the temperature range 303–387°C also followed the parabolic equation. From these data it was possible to estimate the extent of available surface and thus the specific surface area, which was found to be about 500 cm^2/g. Due to the difficulty in reproducibly reducing and annealing the specimens it was not possible to replicate the rate constants to better than a factor of 2. This difficulty was first pointed out by Dunn[18] in connection with his studies with active copper prepared by reduction of the oxide. It is possible therefore that the specific surface area varied from run to run by as much as a factor of two. However, assuming a constant value of 500 cm^2/g, the estimated oxide film thickness corresponding to a given weight of oxygen reacted was calculated, using the method of Vernon.[19] Clearly these values are only indicative of the order of magnitude of the film thickness for any given run. Table I summarizes the reaction conditions and gross observations for all the experiments for which valid isotopic assays were carried out.

[14] M. Dole, J. Am. Chem. Soc. **57**, 2731 (1935); Chem. Revs. **51**, 263 (1952).

† *Note added in proof.*—2.2 ± 0.2% is outside the range of values commonly reported for the Dole effect (2.5–2.8%), suggesting that fractionation might have occurred in the preparation of the reference water. If so, all fractionation factors, α, would be low by 0.3–0.6%. Experiments to check this point are now in progress.

[15] H. L. Johnston, J. Am. Chem. Soc. **57**, 484 (1935); Selwood. Taylor, Hipple, and Bleakney, *ibid.* **57**, 642 (1935); M. Dole, J, Chem. Phys. **4**, 268 (1936).

[16] I. Kirshenbaum, *Physical Properties and Analysis of Heavy Water* (McGraw-Hill Company, Inc., New York, 1951), p. 243.

[17] W. G. Henderson, Jr., and R. B. Bernstein, J. Am. Chem. Soc. **76**, 5344 (1954); Friedman, Bernstein, and Gunning, J. Chem. Phys. **23**, 111 (1955).

[18] J. S. Dunn, Proc. Roy. Soc. (London) **A111**, 210 (1926).

[19] W. H. Vernon, J. Chem. Soc. **1926**, 2273.

TABLE I. Summary of reaction data.

Run no.	Temp. (°C)	Oxygen pressure P_0 (cm Hg)	Wt. Cu (g)	Wt.[a] of O_2 reacted (mg)	Time (min)	Est.[b] oxide thickness (A)	Final appearance of oxide surface
11	203	18.0	2.185	13.0	55	1400	Black
12	201	1.9	2.185	11.4	110	1200	Black
13	155	16.3	2.185	3.4	355	360	Brown-black
14	155	4.6	2.185	3.35	400	360	Dark brown
15	256	2.9	2.185	7.0	12	750	Black
16	254	12.7	2.185	8.45	12	900	Black
17	183	9.8	2.185	6.6	240	700	Brown-black
18	133	21.5	11.485	15.2	69	400	Brown
19	100	20.5	11.485	12.8	80	330	Dark red-brown
20	100	23.2	11.485	12.7	35	330	Dark red-brown
21	99	10.3	11.485	9.8	40	260	Red-brown
22	77	18.7	11.485	9.2	175	240	Orange-red
23	135	16.2	11.485	23.8	90	620	Black
24	68	19.2	11.485	9.6	830	250	Red-brown
25	70	14.4	11.485	5.7	1300	150	Orange
26	120	12.8	11.485	9.7	25	250	Red-brown
27[c]	112	12.6	11.485	8.8	75	230	Brown-black
28[c]	128	10.5	11.485	8.8	60	230	Brown-black
30	229	8.3	1.671	13.8	7.5	2500	Black

[a] Weight of O_2 calculated from weight of H_2O recovered upon hydrogenation.
[b] Assuming a constant specific surface area of 500 cm²/g for the copper.
[c] Electrolytic oxygen used.

The appearance of the specimen may possibly give some indication of the extent of cupric oxide formation. It is of interest to note that Dighton and Miley[20] were able to measure the effective contribution of each of the oxides, Cu_2O and CuO, to the total film thickness. For one particular film formed at 180°C the ratio Cu_2O to CuO was 770 A/48 A = 16.0; for one produced at 221°C the same ratio was 2000/122 = 16.4. Even in the worst case of a film produced at 277°C the ratio was 5983/1016 = 5.9; it is believed therefore that in the present work the films consisted primarily of cuprous oxide even though the dark appearance of cupric oxide was observed for several of the thicker films.

For most of the experiments, carried out at temperatures below 250°C, the oxidation curves were not parabolic. Log-log plots showed that many of the curves followed the cubic law approximately. It appeared that the condition of the sample, affected by the treatment during a given run, seriously influenced the course of the oxidation in the subsequent run. Evans[21] has discussed the influence of physical factors upon the rate laws; such behavior for the irregular porous samples used is not unexpected.

The procedure for the measurement of the isotopic fractionation has been outlined in the previous section. Table II summarizes the O^{18} fractionation data. Examination of the data revealed no systematic dependence of α upon the pressure over the range of pressures investigated. All points were therefore plotted on the same graph in Fig. 1, which shows the dependence of α upon the reciprocal of the absolute temperature. The solid line represents the least-squares fit to the data. The fractionation factors for experiments performed with the electrolytic oxygen, of low O^{18} content, are seen to agree quite well with the rest of the results.

The average deviation of all the points from the line is ± 0.0020, which is slightly greater than that anticipated on the basis of the analytical imprecision. The dotted line in Fig. 1 has been drawn through the data to extrapolate to an α of unity at $1/T = 0$. The slope is 8.5 deg^{-1}, corresponding to an apparent activation energy of 17 cal/mole. The average deviation of the points with respect to this line is ± 0.0022. Both lines pass through the point $\alpha = 1.020$ at 150°C.

Four additional experiments were carried out at considerably higher temperatures (300–400°C), where quite thick films were formed in very short times (<2 min). Because of the extremely high rate of oxygen consumption and the inadequacy of mixing in the reaction chamber the local oxygen isotopic composition in the region of the metal was probably not maintained that of the bulk of the oxygen supply. These results are therefore of very doubtful validity. The enrichment values obtained under these conditions were less than the experimental uncertainty of $\pm 0.2\%$. It is planned to do further work in the high temperature region with a modified apparatus.

Several auxiliary isotope exchange experiments were performed, in which it was found that there was negligible O^{18} exchange between gaseous oxygen and bulk cupr*ic* oxide (wire) at 400°C (in agreement with the results of Allen and Lauder.[22]) Winter and coworkers[23] also showed, for a variety of metal oxides, that after the exchange of the first few surface layers of oxide the rate becomes extremely slow. Winter[24] also investigated the exchange of oxygen-18 with the growing

TABLE II. Summary of O^{18} fractionation data.

Run No.	T(°C)	f	ϵ	α
24	68	0.042	0.0197	1.0201
25	70	0.036	0.0231	1.0235
22	77	0.036	0.0198	1.0202
21	99	0.061	0.0237	1.0244
19	100	0.046	0.0215	1.0220
20	100	0.034	0.0220	1.0224
27*	112	0.055	0.0188	1.0193
26	120	0.059	0.0185	1.0190
28*	128	0.063	0.0179	1.0185
18	133	0.048	0.0190	1.0195
23	135	0.129	0.0208	1.0221
13	155	0.040	0.0249	1.0254
14	155	0.054	0.0174	1.0179
17	183	0.063	0.0225	1.0232
12	201	0.40	0.0169	1.0217
11	203	0.066	0.0185	1.0191
30	229	0.11	0.0155	1.0163
16	254	0.061	0.0152	1.0157
15	256	0.24	0.0154	1.0176

* Electrolytic oxygen used.

[20] A. L. Dighton and H. A. Miley, Trans. Electrochem. Soc. **81**, 321 (1942).
[21] U. R. Evans, Trans. Electrochem. Soc. **91**, 547 (1947).
[22] J. A. Allen and I. Lauder, Nature **164**, 142 (1949).
[23] G. Houghton and E. R. Winter, Nature **164**, 1130 (1949); E. R. Winter, J. Chem. Soc. **1950**, 1170.
[24] E. R. Winter, J. Chem. Soc. **1954**, 3342.

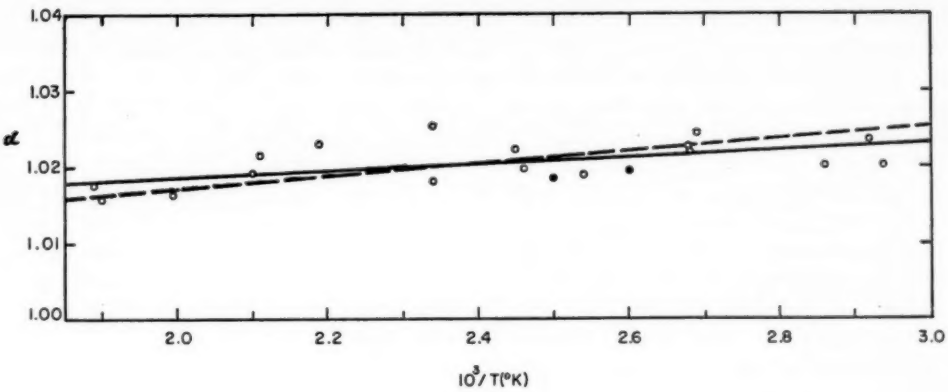

FIG. 1. Temperature dependence of the O^{18} fractionation factor in the reaction of oxygen with copper. ○ Purified tank oxygen. ● Electrolytic oxygen. ——— Least-squares line through data. — — — — Line extrapolating to $\alpha=1$ at $1/T=0$.

cuprous oxide film on copper at 50–110°C and pressures of 3 cm and found negligible exchange.

DISCUSSION

It is of interest to compare the fractionation factors obtained in the present investigation with the results of Dole and Lane[10] for the chemisorption of oxygen on copper at room temperature. Extrapolation of the dotted line of Fig. 1 to 25°C gives as an upper limit the value $\alpha=1.029$, which is significantly lower than the fractionation factor of 1.05 found by these authors.[25] The mechanism of the low temperature, very thin film chemisorption reaction is, of course, thought to be quite different than that associated with the formation of the films of intermediate thickness at elevated temperatures. Rhodin[3] was able to demonstrate for copper the transition at 80°C from the thin film (low temperature), logarithmic law to the intermediate thickness, cubic law of oxidation.

Any satisfactory explanation of the O^{18} fractionation data should therefore account for the following qualitative observations:

(1) The direction of the fractionation is such that O^{16} tends to concentrate in the oxide film.

(2) The fractionation factor appears to be essentially independent of pressure (for pressures exceeding a few cm Hg).

(3) The fractionation factor appears to be independent of the extent of oxide film formation in the intermediate thickness range (150–2500 A).

(4) The isotope effect for the chemisorption reaction is apparently larger than that associated with the formation of films of intermediate thickness.

Cuprous oxide is known to be a metal-deficit semiconductor. The oxidation theory of Cabrera and Mott[5] applied to the intermediate film thickness region makes use of the assumption that the cation transport (and thus the oxidation rate) is proportional to the number of cation vacancies/cm³, n_i, and the strength of the electrostatic field, F, established by the oxygen ions located at the oxide-oxygen interface. The field strength is, of course, V/X, where X is the oxide film thickness and V is the electrostatic potential set up across the oxide film; V is assumed independent of X. It is further hypothesized that the density of cation vacancies is proportional to the surface density of oxygen ions, N, which in turn is proportional to the field strength. Thus the oxidation rate, dX/dt, is found to be proportional to F^2 and is thus inversely proportional to X^2, in accord with the cubic law of oxidation. Here the rate should be independent of the oxygen pressure provided the surface is saturated with adsorbed oxygen.

According to this picture the isotopic composition of the oxide film would be identical with that of the surface layer of oxide ions. Any observed fractionation of O^{18} in the oxide would therefore reflect the fractionation associated with one of the possible steps in the establishment of the $O^=$ layer:

$$(1)\quad O_2(g)\rightleftharpoons O_2(\text{ads})$$
$$(2)\quad O_2(\text{ads})\rightleftharpoons 2O(\text{ads})$$
$$(3)\quad O_2(\text{ads})+4e^-\rightarrow 2O^=$$
$$(4)\quad O(\text{ads})+2e^-\rightarrow O^=.$$

Since little or no isotopic fractionation would be associated with steps (1)‡ and (4) (the O—O bond is not ruptured), attention will be primarily centered on (2) and (3).

Winter's[24] results, which indicated no exchange between $O_2(g)$ and the growing film of cuprous oxide, suggest strongly that steps 3 and/or 4 are essentially irreversible (as indicated). His additional observation that the exchange reaction $O_2^{16}+O_2^{18}\rightleftharpoons 2O^{16}O^{18}$ does not occur in the course of the oxidation implies that the dissociative adsorption of oxygen on cuprous oxide under the conditions of his experiments is an irreversible process. Winter concurs with the mechanism of Garner *et al.*[26] and writes the slow step:

$$O_2(g)+2Cu^+\rightarrow 2O^-(\text{ads})+2Cu^{++}, \qquad (8)$$

[25] M. Dole, private communication, in which a more recent corrected value of α is given for the reaction of oxygen with copper at room temperature.

‡ For the equilibrium between gaseous and adsorbed O_2 molecules one anticipates a slight (<0.3%) O^{18} enrichment in the adsorbed layer (based on the analogy with isotopic vapor pressure ratios).

[26] Garner, Stone, and Tiley, Proc. Roy Soc. (London) **A211**, 472 (1952).

followed by rapid changes including the gain of an electron by O^-, etc. Unfortunately this appears to be incompatible with the Cabrera-Mott concept of a quasi-equilibrium involving adsorbed atomic oxygen and oxygen ions, which is essential to the derivation of the cubic law of oxidation. Actually, this may be explained if one notes that the actual rate law observed by Winter (using very finely divided copper powder) was of the exponential type, $p/po=\exp(-kt)$, rather than cubic. This kinetic behavior was first noted by Wilkins and Rideal,[27] at pressures below about 1 cm. Experiments of Garner *et al.*[26,28] with finely divided cuprous oxide powder showed that the rate of adsorption of oxygen (at low pressures) was proportional to the oxygen pressure. Thus the mechanism of Winter is self-consistent, but may not be relevant for the case of the usual cubic law oxidations carried out at moderate pressures.

Considering first the situation corresponding to the mechanism of Winter it is of interest to estimate the magnitude of the isotope effect for reaction of Eq. (8). Using the theory of Bigeleisen[29] the ratio of the isotopic rate constants for O_2^{16} and $O^{16}O^{18}$ would be

$$\alpha=\frac{k}{k^*}=\left(\frac{m^*}{m}\right)^{\frac{1}{2}}(1+\delta),$$

where

$$\delta=\sum G(u)\Delta u-\sum G(u^\ddagger)\Delta u^\ddagger,$$

m^*/m is the Slater[30] reduced mass ratio and the other quantities have their usual significance. The lower limit of α (corresponding to $T\rightarrow\infty$) is thus the Slater factor, calculated to be 1.029. The upper limit, calculated in the usual way for the case of the free atom activated complex is $\alpha=1.080$ at 150°C. Since the observed fractionation at 150° lies well below the lower limit, this mechanism would seem to be eliminated. It should be noted however, that the high value of α obtained by Dole[25] may well be associated with this type of mechanism.

Next consider the fractionation associated with the isotopic exchange equilibrium between gaseous oxygen molecules and adsorbed oxygen atoms. The upper limit for the fractionation factor may be readily calculated from an examination of the case of equilibrium between gaseous oxygen molecules and free atoms:

$$O_2^{16}(g)+O^{18}(g)\rightleftarrows O^{16}O^{18}(g)+O^{16}(g).$$

The method of calculation is given by Bigeleisen and Mayer[31] and Urey.[32] Assuming $\nu(O^{16}-O^{16})=1580$ cm^{-1} and $\Delta\nu=45$ cm^{-1} one obtains the value $\alpha=1.050$ at 150°C. This result is consistent with the value of the appropriate partition function ratio (Q_2/Q_1) listed in Table X of reference 32. It may be of interest to compare the apparent activation energy for the fractionation factor, 17 cal/mole, with the theoretical upper limit as given by the isotopic zero point energy difference (for O_2^{16} and $O^{16}O^{18}$) of 64 cal/mole.

For the adsorption-exchange reaction:

$$O_2^{16}(g)+O^{18}-S\rightleftarrows O^{16}O^{18}(g)+O^{16}-S,$$

(where S represents an adsorption site), it is not possible to calculate the fractionation factor without some assumption as to the $O^{16}-S$ force constant or vibration frequency. However, by inverting the procedure, it is possible to estimate the frequency which would be required to account for the observed value of $\alpha=1.020\pm0.002$ at 150°C. This was done, first, by assuming the ratio $\Delta\nu/\nu=0.029$ (equivalent to an effective mass $m_s=16$ awu). This gives a value for $\nu(O^{16}-S)$ of 1150 ± 50 cm^{-1}. The other extreme case, assuming $\Delta\nu/\nu=0.061$ (equivalent to an effective mass $m_s=\infty$) gives the result $\nu(O^{16}-S)=780\pm25$ cm^{-1}. The actual frequency would then be expected to lie within the range 780–1150 cm^{-1}, which does not seem implausible.

It is therefore suggested on the basis of the present results that the mechanism of the O^{18} fractionation observed in the oxidation of copper (under the conditions of these experiments) involves the isotopic exchange equilibrium between gaseous oxygen molecules and chemisorbed oxygen atoms§ which favors the concentration of O^{16} in the adsorbed layer. Then, in accord with the assumptions inherent in the Cabrera-Mott theory, it is expected that the isotopic composition of the oxide will be the same as that of the adsorbed layer. This interpretation appears to be consistent with the present observations.

ACKNOWLEDGMENTS

The author is grateful for financial assistance received from the following sources: (a) Michigan Memorial—Phoenix Project No. 78, (b) DuPont Grant for Fundamental Research in Chemistry, and (c) U. S. Atomic Energy Commission, Contract AT(11-1)-321.

[27] F. J. Wilkins and E. K. Rideal, Proc. Roy. Soc. (London) **A128**, 394 (1930).
[28] Garner, Gray, Stone, Savage, and Tiley, Disc. Faraday Soc. **8**, 246 (1950).
[29] J. Bigeleisen, J. Chem. Phys. **17**, 675 (1949).
[30] N. B. Slater, Proc. Roy. Soc. (London) **A194**, 112 (1948).
[31] J. Bigeleisen and M. G. Mayer, J. Chem. Phys. **15**, 261 (1947).
[32] H. C. Urey, J. Chem. Soc. **1947**, 562.
§ It should be pointed out that this exchange mechanism is not supported by the (low-pressure) experiments of Winter,[24] as previously discussed.

Heat Capacity and Entropy of FeF_2 and CoF_2 from 11 to 300°K. Thermal Anomalies Associated with Antiferromagnetic Ordering

EDWARD CATALANO* AND J. W. STOUT
Institute for the Study of Metals and Department of Chemistry, University of Chicago, Chicago, Illinois
(Received December 10, 1954)

The heat capacities of FeF_2 and CoF_2 have been measured between 11 and 300°K. Both salts show anomalies in heat capacity associated with the antiferromagnetic ordering of the magnetic ions. The heat capacity of FeF_2 exhibits a sharp maximum of 17.8 cal deg^{-1} mole^{-1} at 78.35°K and that of CoF_2 has a maximum of 5.64 cal deg^{-1} mole^{-1} at 37.70°K. Values of the heat capacity, entropy, enthalpy, and free energy are tabulated at selected temperatures. The values of the entropy and enthalpy at 298.16°K are: FeF_2, $S^0=20.79\pm0.04$ cal deg^{-1} mole^{-1}, $H^0-H_0^0=3049\pm6$ cal mole^{-1}; CoF_2, $S^0=19.59\pm0.04$ cal deg^{-1} mole^{-1}, $H^0-H_0^0=2978\pm6$ cal mole^{-1}.

THIS paper is the third in a series presenting the results of low-temperature heat-capacity measurements on the anhydrous difluorides of manganese, iron, cobalt, nickel, and zinc. These compounds are isomorphous,[1] of the rutile structure, and differ from one another principally in the number of 3*d*-electrons in the positive ion. MnF_2, FeF_2, CoF_2, and NiF_2 are paramagnetic and measurements of the magnetic structure by neutron diffraction[2] and of the magnetic anisotropy[3] show that at low temperatures the atomic magnetic moments are arranged in an ordered antiferromagnetic array. The entropy change in passing from the high-temperature disordered state to the low-temperature ordered one is reflected by an anomaly in the heat capacity and the heat-capacity data are valuable in determining the details of the cooperative ordering process.

The results of low-temperature heat-capacity measurements on MnF_2[4] and NiF_2[5] have been presented previously. In this paper the data on FeF_2 and CoF_2 will be given. The results of measurements on the diamagnetic compound ZnF_2, and a discussion of the separation of the contributions of the lattice and of the magnetic system to the entropy and heat capacity of the paramagnetic compounds will be given in a future paper.

The calorimeter and the method of experimental measurements used for FeF_2 and CoF_2 were the same as those described previously.[5] The principal change was the refilling of the resistance thermometer with pure helium so as to improve the thermal contact between thermometer and sample.

PREPARATION OF SAMPLES

Ferrous Fluoride

Hydrated ferrous chloride was crystallized from a solution made by dissolving carbonyl iron in aqueous HCl. After partial drying at room temperature under vacuum the ferrous chloride was placed in a graphite boat in a graphite-lined nickel tube and heated in anhydrous HF in order to convert it to FeF_2. The temperature of the furnace was kept at 400°C with a slow stream of HF passing through it for about twelve hours. Two such treatments removed all water and reduced the chloride content to less than 0.01%. The FeF_2, mixed with a little iron, was then transferred to a graphite crucible which was heated in a HF atmosphere to a temperature of 1050°C. The nickel furnace tube was lined with Armco iron in order to maintain a reducing atmosphere and to minimize the introduction of other metallic impurities. The FeF_2 melted, and upon slow cooling formed large crystals which could be easily separated from the metallic iron also present in the crucible. The crystals were transparent and light tan in color. The sample used for the heat-capacity measurements was made by crushing this clear material to about 1 mm particle size.

The only impurities detected in a spectrochemical analysis were, in weight percent: Mn, 0.001; Mg, 0.001; Al, 0.004; V, 0.005, Ni 0.001. No Co, Cu, Si, Na, or K was found. An analysis for total iron in the sample, by titration against standardized potassium permanganate solution, was made. The results of four determinations were 59.47, 59.45, 59.46, and 59.50 weight percent iron as compared to 59.51% calculated from the formula FeF_2. A colorimetric analysis, using potassium thiocyanate, gave 0.1% by weight of ferric ion in the sample.

Cobaltous Fluoride

In order to have a starting material without excessive nickel impurity, we began with commercial sodium cobaltinitrite whose nickel content was considerably lower than other available cobalt salts. This was converted to an aqueous solution of $CoCl_2$ from which

* Eastman Kodak Company Fellow 1951–1952; Allied Chemical Dye Corporation Fellow 1952–1953.

[1] See J. W. Stout and S. A. Reed [J. Am. Chem. Soc. **76**, 5279 (1954)] for precise lattice parameters and discussion of the structure.

[2] R. A. Erickson, Phys. Rev. **90**, 779 (1953).

[3] (a) M. Griffel and J. W. Stout, J. Chem. Phys. **18**, 1455 (1950); (b) J. W. Stout and L. M. Matarrese, Revs. Modern Phys. **25**, 338 (1953); (c) L. M. Matarrese and J. W. Stout, Phys. Rev. **94**, 1792 (1954).

[4] J. W. Stout and H. E. Adams, J. Am. Chem. Soc. **64**, 1535 (1942).

[5] E. Catalano and J. W. Stout, J. Chem. Phys. **23**, 1284 (1955).

TABLE I. The heat capacity of FeF_2. 0°C=273.16°K. Molecular weight 93.85.

T_{Av} °K	Approx ΔT	$\Delta H/\Delta T$ cal deg^{-1} mole^{-1}
	Series I	
51.83	2.36	5.149
54.60	4.74	5.675
59.34	4.76	6.629
64.51	5.59	7.778
70.15	5.69	9.251
75.62	5.23	11.78
81.71	6.94	7.595
88.44	6.54	7.288
94.63	5.84	7.627
100.46	5.77	8.024
106.20	5.68	8.426
111.83	5.59	8.818
116.90	5.55	9.172
122.40	5.44	9.540
128.14	6.03	9.927
134.15	6.03	10.32
140.19	6.00	10.68
146.29	6.16	11.03
	Series II	
11.33	0.88	0.049
12.28	0.98	0.067
13.25	1.14	0.092
14.47	1.37	0.136
15.80	1.21	0.195
16.95	1.13	0.257
18.34	1.64	0.351
19.94	1.60	0.475
22.17	2.06	0.675
24.29	2.13	0.893
26.44	2.23	1.145
28.88	2.76	1.450
31.73	2.94	1.836
34.77	3.13	2.278
37.96	3.30	2.768
41.35	3.45	3.310
44.74	3.31	3.881
48.22	3.65	4.491
51.91	3.72	5.159
55.95	4.37	5.941
	Series III	
57.15	4.09	6.174
60.89	3.38	6.954
64.03	2.90	7.657
66.76	2.55	8.315
69.17	2.28	8.945
71.34	2.06	9.588
73.30	1.86	10.29
75.08	1.69	11.12
76.67	1.50	12.28
78.12	1.40	12.90
79.89	2.12	7.562
82.01	2.12	7.182
84.08	2.05	7.143
86.29	2.35	7.189
88.78	2.60	.302
	Series IV	
76.392	0.273	11.98
	Series V	
76.566	0.591	12.16
77.143	0.572	12.78
77.599	0.353	13.53
77.897	0.240	14.28
78.062	0.089	15.08
78.151	0.086	15.65
78.235	0.082	16.46
78.315	0.078	17.61
78.411	0.114	11.35
78.536	0.137	9.12
78.677	0.145	8.57
78.823	0.150	8.26
78.973	0.153	8.05
79.252	0.409	7.794
79.754	0.595	7.549
80.362	0.611	7.377
	Series VI	
78.202	0.083	16.21
78.279	0.079	17.14
78.358	0.090	14.95
	Series VII	
149.26	6.49	11.20
155.58	6.07	11.55
161.81	6.32	11.86
168.27	6.54	12.19
174.68	6.18	12.48
180.99	6.39	12.75
187.47	6.49	13.04
194.19	6.78	13.31
200.91	7.05	13.56
207.79	6.72	13.81
214.50	6.69	14.04
221.48	7.04	14.28
228.50	6.75	14.51
235.52	7.07	14.71
242.49	6.79	14.92
249.11	6.55	15.12
255.27	6.45	15.26
261.88	6.86	15.42
268.58	6.63	15.59
275.22	6.41	15.78
282.22	6.76	15.92
289.24	6.56	16.07
295.91	6.37	16.21
307.30	5.07	16.52

$CoCO_3$ was precipitated by the addition of an ammonium bicarbonate solution. The $CoF_2 \cdot 4H_2O$, prepared by adding the carbonate to a 40% HF solution, was dried at 120°C and then heated in a graphite boat in a stream of anhydrous HF at 950°C. The sintered crystallites of CoF_2 were from 0.05 to 0.1 mm in diameter.

A spectrochemical analysis of the sample used for the heat-capacity measurements showed the presence, in weight percent, of: Mn, 0.002; Si, 0.005; Ni, 0.003; Fe, 0.04; Al, 0.001; Cu, 0.001; Mg, 0.004. Not detected were V, Na, and K. The sample was analyzed for cobalt gravimetrically by precipitating the cobalt salt of *o*-aminobenzoic acid.[6] The results of four determinations were, in weight percent: 60.76, 60.78, 60.83, 60.85; that calculated for CoF_2 is 60.80.

EXPERIMENTAL RESULTS

In the calculation of the heat capacities, the defined calorie equal to 4.1840 absolute joules is used. The ice point temperature was taken as 273.16°K. The temperatures listed in Tables I and II are the arithmetic mean of the initial and final temperatures. The approximate temperature rise of each measurement is also listed. The "heat capacities" in these tables are the ratios of the increase in enthalpy, ΔH, to the rise in temperature, ΔT, and are equal to the differential heat capacity C_p only when the correction for curvature is negligible. In the neighborhood of the heat capacity maxima very short runs with a temperature rise less than 0.1°K were taken. Because of the small temperature rise these runs are less accurate than usual. We estimate that they are reliable to about 0.5%. Although the error in the absolute value of the temperature may be several hundredths of a degree, the relative values of temperatures close to one another can be measured with the resistance thermometer to better than one thousandth of a degree, and, in order to show the variation of heat capacity with temperature, the mean temperatures of the very short runs are listed in Tables I and II to the nearest 0.001°K.

[6] R. Duval and C. Duval, Anal. Chim. Acta **5**, 84 (1951).

Ferrous Fluoride

The sample of FeF_2 weighed 229.57 g *in vacuo* (2.4461 moles). The experimental heat-capacity measurements are listed, in chronological order, in Table I. After the first measurement, at 51.83°, the calorimeter was warmed to room temperature and then cooled again to 52°K after which the remaining measurements of Series I were taken. At the end of Series II, which began at 10.9°K, the calorimeter was warmed to 77°K. The next day it was cooled to 55°K and the measurements of Series III taken. At the conclusion of Series III the calorimeter was cooled to 76.26°K and the single point of Series IV obtained. SeriesV and VI comprise measurements with small temperature rise designed to determine the detailed shape of the heat-capacity curve in

TABLE II. The heat capacity of CoF_2. 0°C=273.16°K. Molecular weight 96.94.

T_{Av} °K	Approx ΔT	$\Delta H/\Delta T$ cal deg^{-1} mole^{-1}
	Series I	
51.92	2.43	3.177
56.38	6.34	3.654
61.78	4.89	4.240
66.41	4.41	4.743
	Series II	
52.71	2.79	3.261
57.34	6.04	3.753
62.80	4.67	4.352
67.09	3.91	4.818
71.24	4.34	5.252
75.69	4.56	5.718
80.50	5.05	6.207
85.19	4.87	6.677
90.19	5.07	7.149
95.61	5.74	7.625
101.57	6.11	8.137
107.97	6.68	8.657
114.61	6.59	9.169
128.45	6.77	10.16
135.88	7.41	10.63
143.27	7.36	11.09
150.40	6.92	11.50
157.44	7.10	11.88
164.66	7.23	12.25
171.34	7.25	12.56
178.75	7.50	12.90
186.40	7.71	13.23
194.09	7.54	13.53
201.52	7.16	13.82
211.02	8.06	14.15
218.92	7.76	14.41
226.57	7.41	14.65
235.08	7.06	14.90
242.70	7.45	15.10
250.90	7.79	15.33
258.63	7.48	15.53
265.97	7.21	15.73
	Series III	
10.73	0.40	0.076
11.41	0.91	0.102
12.58	1.61	0.154
14.82	1.62	0.290
16.64	2.02	0.441
18.65	1.98	0.638
20.71	2.06	0.868
22.97	2.21	1.160
25.36	2.42	1.511
27.92	2.65	1.930
30.73	2.88	2.460
33.99	3.61	3.265
37.01	3.88	3.864
42.27	6.57	2.360
47.48	3.76	2.740
51.32	3.89	3.119
55.28	3.98	3.534
	Series IV	
14.06	1.55	0.240
15.54	1.38	0.347
16.98	1.30	0.468
18.33	1.28	0.603
19.61	1.29	0.741
	Series V	
34.19	1.54	3.295
35.42	0.90	3.720
36.19	0.61	4.059
36.79	0.59	4.440
37.35	0.55	5.055
37.99	0.74	3.768
38.88	1.16	2.363
40.10	1.29	2.258
41.72	1.99	2.298
43.77	2.11	2.425
45.92	2.19	2.600
	Series VI	
37.442	0.076	5.19
37.517	0.074	5.36
37.590	0.072	5.55
37.661	0.071	5.65
37.730	0.072	5.61
37.802	0.074	5.52
37.869	0.094	4.22
37.969	0.119	3.26
38.086	0.135	2.84
38.217	0.145	2.64
38.373	0.152	2.52
38.534	0.157	2.43
38.697	0.162	2.38
38.863	0.165	2.35
39.029	0.169	2.32
39.257	0.307	2.291
	Series VII	
37.694	0.071	5.63
37.768	0.071	5.57
37.850	0.088	4.50
	Series VIII	
275.45	6.90	15.92
283.33	8.85	16.10
291.79	8.53	16.27
299.89	8.21	16.50
122.34	7.29	9.732
273.64	6.92	15.93
301.64	8.17	16.52

the neighborhood of the anomaly. Before the start of Series V, the calorimeter was cooled to 51°K and then warmed rapidly to 76.27°K. After the completion of Series V the calorimeter was cooled to 78.16°K and the measurements of Series VI obtained. There is no evidence of dependence of heat capacity on the thermal history of the sample. In the region of high heat capacity preceding the maximum a slight increase in the time for thermal equilibrium in the calorimeter was noted. This is probably an increase in the thermal time constant of the calorimetric system because of the large heat capacity without a corresponding rise in thermal conductivity of the system as a whole, and does not indicate any unusual slowness in exchange of thermal energy between the magnetic system and the lattice.

Cobaltous Fluoride

The sample of CoF_2 weighed 242.83 g *in vacuo* (2.5049 moles). The experimental heat-capacity measurements are listed, in chronological order, in Table II. After the preliminary measurements of Series I, the calorimeter was warmed to room temperature and then cooled to 51°K before beginning Series II. A point in this series near 121°K has been discarded because of timing uncertainty. Series III, beginning at 10.5°K, disclosed the existence of a thermal anomaly in the nighborhood of 40°K. After the completion of this series, the calorimeter was cooled to 13.3°K and the measurements of Series IV, extending to 20.3°K, were taken. The calorimeter stood overnight at 20°K, was then heated to 33.4°K, and the data of Series V obtained. Series VI and VII are very short runs in the neighborhood of the anomaly in heat capacity. Before starting Series VI the calorimeter was cooled from 47° to 34.9°K, and then warmed to 37.4°K. After the last measurement of Series VI, ending at 39.1°K, the calorimeter was cooled, over a period of about twenty minutes, to 37.66°K and the measurements of Series VII begun immediately. There is no indication of dependence of heat capacity on thermal history or of slowness in attaining thermal equilibrium in any of the measurements.

THE ANOMALIES IN HEAT CAPACITY

Both FeF_2 and CoF_2 show lambda-shaped anomalies in heat capacity. The heat-capacity data in the vicinity of the anomaly are shown for FeF_2 in Fig. 1 and for CoF_2 in Fig. 2. Points have been omitted in the figures where the temperature rise was so large that the mean heat capacity, $\Delta H/\Delta T$, is appreciably different from the differential heat capacity. The heat-capacity peak in FeF_2 is much sharper than that in CoF_2 or those previously observed in MnF_2[4] and NiF_2.[5] The heat capacity rises to the very high value of 17.8 cal deg^{-1} mole^{-1} at 78.35±0.02°K.

Even with measurements having a temperature rise of 0.08°K the resolution is insufficient to decide whether the heat-capacity-temperature curve near the maxi-

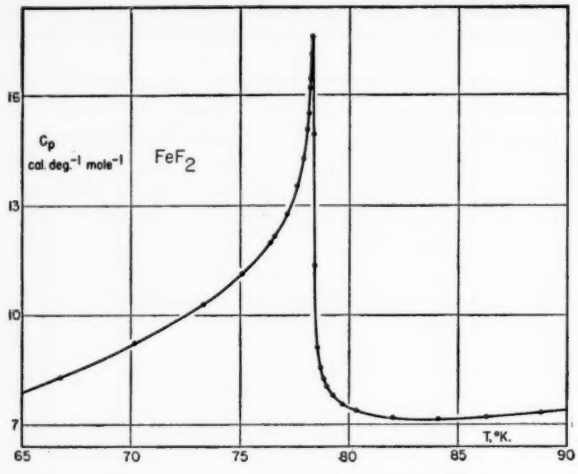

FIG. 1. Heat capacity of FeF_2 in the anomalous region.

mum is smooth, although changing very rapidly in slope, or whether there is a discontinuity in heat capacity or the slope of heat capacity *versus* temperature. In choosing the values of the maximum heat capacity, we have assumed a smooth curve. The drop in heat capacity on the high-temperature side of the maximum is extremely rapid. In a range of only 0.2°K above the temperature of the maximum, the heat capacity decreases by a factor of two. The anomaly in the heat capacity is clearly connected with the antiferromagnetic ordering of the atomic magnetic moments of the ferrous ions. Below 78°K there is a rapid change in the magnetic anisotropy[3b] of FeF_2 and long-range order of the spins is observed in the neutron diffraction pattern.[2] By extrapolating a curve calculated from the Van Vleck theory,[7] Erikson[2] obtained a temperature of 90°K at which the long-range order disappears. It is evident from the shape of the heat capacity curve that near 78°K the ordering is changing with temperature much more rapidly than predicted by molecular field theories of the Van Vleck type and Erickson's actual data are not inconsistent with the disappearance of long-range order between 78°K and 79°K. At room temperature, the magnetic anisotropy[3b] of FeF_2 is larger in magnitude than that of MnF_2, CoF_2, or NiF_2. This anisotropy arises from the influence, through the spin-orbit interaction, of the electrostatic crystalline fields on the energy states corresponding to different orientations of the spin moment with respect to the crystallographic directions. It is probable that the sharpness of the heat-capacity maximum in FeF_2 is connected with the large paramagnetic anisotropy in this compound.

The heat-capacity curve of CoF_2 is clearly rounded at the top. The maximum heat capacity is 5.64 cal deg^{-1} mole^{-1} at a temperature of 37.70±0.05°K. The curve drops slowly to 5.52 cal deg^{-1} mole^{-1} at 37.80°K. Above this temperature there is a rapid decrease in heat capacity. The anomaly in CoF_2 arises from the antiferromagnetic ordering of the magnetic moments of the cobaltous ions. Erickson[2] found a long-range antiferromagnetic order in the moments which, by extrapolation, disappeared at a temperature between 45 and 50°K. Stout and Matarrese,[3b] in measurements of the magnetic anisotropy of single crystals of CoF_2, found that a rapid drop in the magnetic anisotropy occurred below 100°K. At the time of the preliminary report[3b] of these measurements, calculations of the data between 20°K and 60°K had not been completed. The final calculation shows that although the major variation of magnetic anisotropy occurs between 40°K and 100°K there is a definite maximum and minimum in the magnetic anisotropy *versus* temperature curve between 35°K and 40°K and a pronounced difference in the slope of the curve below 35°K and above 40°K. The spin quantum number in Co^{++} is $S=\frac{3}{2}$ and, if the orbital moment is "frozen" by the crystalline fields, one might expect a magnetic contribution of $R\ln 4 = 2.75$ cal deg^{-1} mole^{-1} arising from disordering of the spin moments. Actually, the total entropy of CoF_2, including that of the lattice, is only 1.72 cal deg^{-1} mole^{-1} at 40°K. As will be shown in a later paper where the lattice contribution to the entropy will be estimated, the entropy change associated with the antiferromagnetic ordering of CoF_2 is about $R\ln 2$. This indicates that the ground state is doubly degenerate and that at 40°K there is no appreciable population of higher states. Such a pattern of energy levels is consistent with magnetic measurements on dilute cobalt salts[8] and might be anticipated from the crystalline field calculations of Schlapp and Penney.[9]

THERMODYNAMIC PROPERTIES OF FeF_2 and CoF_2

Values of the heat capacity, entropy, and the enthalpy and free energy functions are listed in Table III for

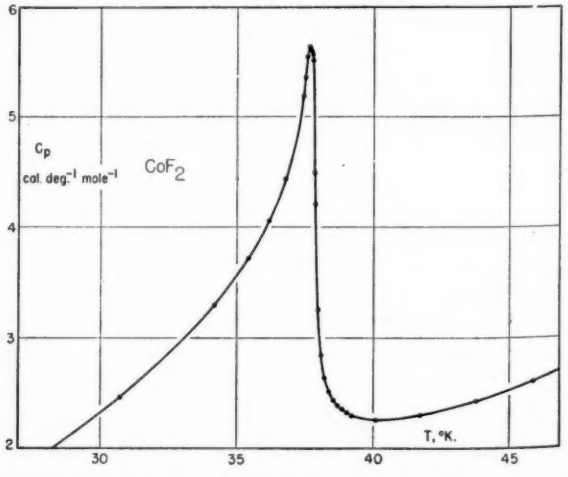

FIG. 2. Heat capacity of CoF_2 in the anomalous region.

[7] J. H. Van Vleck, J. Chem. Phys. **9**, 85 (1941).

[8] C. G. B. Garrett, *Magnetic Cooling* (Harvard University Press, Cambridge, 1954), p. 64.

[9] R. Schlapp and W. G. Penny, Phys. Rev. **42**, 666 (1932).

FeF_2 and in Table IV for CoF_2. The C_p listed is the differential heat capacity and in drawing the smooth curves the experimental points were corrected for curvature where necessary. In order to make the extrapolation to the absolute zero of temperature, plots were made of C_P/T^3 *versus* temperature in the range 10 to 20°K. Unlike NiF_2,[5] where C_P/T^3 decreased with increasing temperature in this range, both FeF_2 and CoF_2 gave curves of C_P/T^3 *versus* T increasing considerably with temperature. From the data on ZnF_2, to be presented in a later paper, it was estimated that the lattice contribution to C_P/T^3 would be 2.1×10^{-5} cal deg^{-4} mole^{-1} for FeF_2 and 2.3×10^{-5} cal deg^{-4} mole^{-1}, for CoF_2. According to the spin-wave theory of antiferromagnetism[10] the magnetic contribution to the heat capacity contains an exponential factor which vanishes at sufficiently low temperatures. It is presumably this magnetic contribution which accounts for the observed rise in C_P/T^3 between 10°K and 20°K. On the plot of C_P/T^3 *versus* T, smooth curves were drawn through the experimental data and approaching asymptotically at $T=0$ the estimated lattice contribution. The extrapolated contribution to the entropy below 10°K is 0.009 cal deg^{-1} mole^{-1} for FeF_2 and 0.013 cal deg^{-1} mole^{-1} for CoF_2.

TABLE III. Thermodynamic properties of FeF_2.

T °K	C_p^0 cal deg^{-1} mole^{-1}	S^0 cal deg^{-1} mole^{-1}	$H^0-H_0^0$ cal mole^{-1}	$-\frac{F^0-H_0^0}{T}$ cal deg^{-1} mole^{-1}
15	0.155	0.039	0.46	0.009
20	0.479	0.124	1.97	0.025
25	0.972	0.281	5.52	0.060
30	1.597	0.512	11.91	0.115
35	2.314	0.811	21.65	0.192
40	3.092	1.170	35.15	0.291
45	3.925	1.582	52.67	0.411
50	4.811	2.041	74.49	0.551
55	5.750	2.543	100.9	0.709
60	6.764	3.086	132.1	0.884
65	7.884	3.671	168.7	1.076
70	9.179	4.301	211.2	1.283
75	11.06	4.992	261.3	1.507
78.35	17.8	5.546	303.9	1.667
80	7.447	5.717	317.4	1.749
90	7.364	6.568	389.6	2.238
100	7.994	7.374	466.2	2.712
110	8.690	8.168	549.7	3.172
120	9.381	8.954	640.0	3.621
130	10.05	9.732	737.2	4.061
140	10.67	10.499	840.8	4.493
150	11.25	11.255	950.4	4.919
160	11.79	11.998	1065.6	5.338
170	12.27	12.728	1185.9	5.752
180	12.71	13.442	1310.9	6.159
190	13.14	14.141	1440.1	6.561
200	13.53	14.824	1573.5	6.957
210	13.89	15.493	1710.6	7.348
220	14.23	16.147	1851.2	7.733
230	14.55	16.787	1995.1	8.113
240	14.84	17.412	2142.0	8.487
250	15.14	18.024	2292.0	8.856
260	15.41	18.624	2444.7	9.221
270	15.65	19.210	2600.1	9.580
280	15.87	19.783	2757.6	9.934
290	16.09	20.343	2917.4	10.283
300	16.32	20.893	3079.5	10.628
273.16	15.72	19.39	2650	9.69
298.16	16.28	20.79±0.04	3049±6	10.57±0.02

TABLE IV. Thermodynamic properties of CoF_2.

T °K	C_p^0 cal deg^{-1} mole^{-1}	S^0 cal deg^{-1} mole^{-1}	$H^0-H_0^0$ cal mole^{-1}	$-\frac{F^0-H_0^0}{T}$ cal deg^{-1} mole^{-1}
15	0.302	0.074	0.90	0.014
20	0.784	0.222	3.53	0.046
25	1.456	0.466	9.05	0.104
30	2.316	0.804	18.37	0.191
35	3.557	1.244	32.75	0.309
37.70	5.64	1.562	44.31	0.387
40	2.255	1.720	50.45	0.459
45	2.520	1.997	62.21	0.615
50	2.984	2.286	75.94	0.767
55	3.504	2.594	92.14	0.919
60	4.043	2.922	111.0	1.072
65	4.593	3.268	132.6	1.228
70	5.123	3.628	156.9	1.387
75	5.647	3.999	183.8	1.549
80	6.162	4.380	213.3	1.714
90	7.131	5.163	279.9	2.053
100	8.004	5.960	355.6	2.404
110	8.816	6.762	439.8	2.764
120	9.565	7.561	531.7	3.130
130	10.26	8.355	630.9	3.502
140	10.90	9.138	736.7	3.876
150	11.48	9.911	848.7	4.253
160	12.02	10.669	966.2	4.630
170	12.50	11.413	1088.8	5.008
180	12.96	12.140	1216.1	5.384
190	13.38	12.852	1347.8	5.758
200	13.76	13.548	1483.5	6.130
210	14.11	14.228	1622.9	6.500
220	14.44	14.892	1765.7	6.866
230	14.75	15.541	1911.7	7.229
240	15.04	16.175	2060.6	7.589
250	15.31	16.794	2212.4	7.945
260	15.57	17.399	2366.7	8.297
270	15.81	17.992	2523.6	8.645
280	16.04	18.571	2682.9	8.989
290	16.26	19.137	2844.4	9.329
300	16.48	19.692	3008.1	9.666
273.16	15.89	18.18	2574	8.75
298.16	16.44	19.59	2978	9.60
		±0.04	±6	±0.02

The accuracy of the smoothed heat-capacity data is estimated as 3% at 15°K, 1% at 20°K, and 0.2% between 40°K and 200°K except in the neighborhood of the anomalies where, because of the short runs, the accuracy is about 0.5%. Above 200°K, because of the increased heat leak, the uncertainty rises slowly reaching about 0.5% at 300°K. The accuracy of the functions S^0, $H^0-H_0^0$, and $-(F^0-H_0^0)/T$ is about 0.2% above 60°K but the entries in Tables III and IV are given to a higher precision than this for internal consistency.

The values of entropy and free energy in Tables III and IV do not include the contributions arising from nuclear spin randomness or isotope mixing. It is clear from the magnetic anisotropy[3b] and neutron diffraction[2] data that the magnetic systems of FeF_2 and CoF_2 have reached an ordered state at the lowest temperatures of the heat-capacity measurements and that there remains at these temperatures no appreciable electronic contribution to the entropy. The values of the thermodynamic quantities listed in Tables III

[10] R. Kubo, Phys. Rev. **87**, 568 (1952).

and IV are therefore the correct ones to be used in chemical calculations.

ACKNOWLEDGMENTS

We thank Miss Myrtle Bachelder for the chemical analysis, Mrs. Althea Tompkins for the spectrochemical analysis, Dr. L. M. Matarrese for the determination of the ferric iron content of the FeF_2 sample, and Mr. Stanley Reed for assistance with the calculations. The preparation of the material in this paper for publication was supported in part by the Office of Naval Research (Contract N6ori-02051).

THE JOURNAL OF CHEMICAL PHYSICS VOLUME 23, NUMBER 10 OCTOBER, 1955

Interaction Energy among Three Helium Atoms*

ARNOLD SHOSTAK
The Catholic University of America, Washington, D. C.
(Received January 5, 1955)

Molecular orbitals made up of linear combinations of atomic orbitals, as well as orbital, total, and interaction energies, have been calculated for the linear configuration of three He $1-s$ atoms, with equal separation between the center and each outer atom. Roothaan's self-consistent field matrix method was applied to this case. All electronic interactions were considered, their contributions appearing in the Hamiltonian used in solving for total energy. The assumption of additivity of the energies of all pairs of atoms in determining interaction energy is shown not to be valid for internuclear separations approaching collision diameter of the $1-s$ He atom, about 1 A. Deviation from additivity, as determined using the results of Wehner's MO calculation for the system He_2 is about 30% for the smallest internuclear separation considered, around 0.93 A.

INTRODUCTION

THE free energy, entropy and specific heat of many of the simpler gases have been calculated from the partition function of the systems of these gases by assuming that the potential energy of the whole system can be expressed as the sum of the potential energy among all possible pairs of atoms or molecules of the system.[1] In particular, the potential energy contribution U to the total energy, in the partition function of a system $Q=\sum e^{-\epsilon_{\text{total}}/kT}$, is taken to be the scalarly additive sum of all pair interaction energies of the system, i.e., $u(r_1,r_2,r_3\cdots r_n)$ is taken as equal to $V_1(r_1r_2)+V_2(r_1,r_3)+\cdots V(r_1,r_n)\cdots$ rather than as in some other form $V(r_1,r_2,r_3,r_4\cdots)$.

Löwdin,[2] investigating cohesive energies of certain of the alkali-halide types of ionic crystals, and using the device of reducing three-center integrals to two-center ones by expanding the electronic wave function of the third atom in terms of the coordinates of the second atom, has shown that in the case of ionic crystals, the cohesive energy of an ionic crystal is nonadditive in the sense that it cannot be expressed as a simple sum of interaction energies related to the various ion pairs constituting the lattice.

Rosen,[3] using the valence-bond method to test validity of the additivity assumption in the case of chemically saturated structures, has investigated the case of three helium atoms in a linear configuration. Rosen concludes that where the overlap integral is small compared to unity, nonadditivity effects are negligible; and that for distances involved in most physical situations, the effect of nonadditivity in the repulsive forces of helium is negligible.

The present investigation was undertaken to determine, by use of the method of molecular orbitals, for what internuclear separations nonadditivity is important; and what the magnitudes of the nonadditivity effects are for a system of three helium atoms, all in the $1-s$ state, in linear configuration, with the same internuclear separations R between atoms "a" and "b" as between atoms "b" and "c."

ROOTHAAN'S LCAO SCF METHOD

Much impetus has been given to the use of that molecular orbital method which employs linear combinations of atomic orbitals (LCAO), since the development by Roothaan[4] of an LCAO, self-consistent field theory, in which the Hamiltonian includes, from the very beginning, terms representing electronic interactions, as contrasted with the alternative procedure of making energy calculations leaving these terms out of the Hamiltonian, and subsequently treating the interactions as perturbations. Roothaan's method is effective also, in that the bookkeeping of the many integrals which arise in computing the energy is systematized. Recently, this method has been used extensively by a

* This article was composed for the fulfillment of the publication requirement for the degree of Doctor of Philosophy in the Graduate School of Arts and Sciences of the Catholic University of America, Washington, D. C.

[1] J. Mayer and M. G. Mayer, *Statistical Mechanics* (John Wiley & Sons, Inc., New York, 1940).

[2] P. O. Löwdin, thesis, University of Uppsala, Uppsala, Sweden, 1948.

[3] P. Rosen, J. Chem. Phys. **21**, 1007 (1953).

[4] C. C. J. Roothaan, Revs. Modern Phys. **23**, 69 (1951).

group of Catholic University of America, headed by Dr. Virginia Griffing. Mulligan,[5] of this group, conducted an investigation of the ground state of CO_2. Vanderslice and Griffing[6] applied the method to molecular systems H_3, linear H_4, and BeH_2; Macek[7] has considered quadratic H_4; and more recently, Wehner[8] has studied He_2. Wehner's calculations for this case give interaction energy results which do not differ sensibly from those derived by Slater.[9] Since so many investigators have used Roothaan's method, only a very brief outline will be given here. It will be found that Roothaan's[4] and Mulligan's[5] theses are lucid expositions of this LCAO method.

Each electron in the molecule is represented by LCAO MO's $\phi_i=\sum_p a_{ip}\chi_p$, in which i represents the MO's, p the atomic orbitals, and the a's are undetermined coefficients. A total N-electron normalized wave function, Φ, for the closed-shell ground state, is then written as the antisymmetrized product of the LCAO MO's.

The electronic energy of the normalized antisymmetric total wave function is, then, $E=\int\bar{\Phi}\mathfrak{H}\Phi d\tau$, where $\mathfrak{H}$ is the total Hamiltonian operator. A variational method minimizes this energy and leads to the following expression which the MO's have to satisfy, i.e., $(H+G)a_i=\epsilon_i S a_i$ where H has elements $H_{pq}=\int\bar{\chi}_p H\chi_q d\tau$ and G is the electronic interaction matrix whose elements are given as a linear combination of Coulombic and resonance-exchange terms, i.e., $G_{pq}=\sum_i(2J_{ipq}-K_{ipq})$.

The equation $(H+G)a_i=\epsilon_i S a_i$ is then solved for the ϵ_i's and a_i's, in a self-consistency procedure, until originally assumed and finally calculated ϵ_i's agree in value. Total and interaction energies of the system are then able to be computed.

APPLICATION TO He_3 LINEAR CONFIGURATION

Application of the Roothaan matrix method to the case of three linear He atoms, each in $1-s$ state, with equal separations between the outer and center atoms, is now considered.

First, three MO's, of increasing numbers of nodes, are written:

$$\phi_1=a_{1a}\chi_a+a_{1b}\chi_b+a_{1c}\chi_c \qquad (\sigma_g)$$

$$\phi_2=a_{2a}\chi_a-a_{2c}\chi_c \qquad (\sigma_u)$$

$$\phi_3=a_{3a}\chi_a-a_{3b}\chi_b+a_{3c}\chi_c \qquad (\sigma_g)$$

where $\chi_a=(Z^3/\pi)^{\frac{1}{2}}e^{-Zr_a}$, is a Slater-hydrogen type orbital, with r_a the distance, in Bohr radii, measured from the nucleus of atom "a." The coefficients a_{1a}, a_{2a}, etc., are all assumed to be positive constants.

The use of simple Slater-type eigenfunctions as atomic orbitals in this calculation involves introduction of an effective nuclear charge, Z, (in a.u.), to take into account screening of the nucleus by all electrons but that under consideration. (For the He atom, there is only one screening electron.) In the case of He, Kellner[10] has found, by minimizing energy as a function of the screening, that $Z=27/16=1.6875$, here rounded off to 1.7. The parameter $ZR=\rho$ is used hereafter in discussing internuclear separations.

Owing to the symmetrical arrangement of the linear He_3 system, $a_{1a}=a_{1c}$, $a_{2a}=a_{2c}$ and $a_{3a}=a_{3c}$.

The MO's above form bases of representations for the symmetry group $D_{\infty h}$, and appear pictorially as in Fig. 1.

Each of these one-electron MO's is filled by two electrons, of opposite spin, to form three molecular spin orbitals (MSO's). Since there are six electrons in the closed shell, three-helium configuration, these three MO's are then completely filled to form three MSO's. The antisymmetrized product which is the determinantal wave function made up of these MSO's, is that function which appears in expression (1) when calculating total energy.

The total energy of the molecular system under consideration is then given by

$$E=2\sum_i H_i+\sum_{i,j}(2J_{ij}-K_{ij}), \qquad (16)$$

which is equivalent in matrix procedure, to computing, for each value of ρ,

$$E=\begin{bmatrix}a_{1a}\\a_{1b}\\a_{1c}\end{bmatrix}(2H+G)(a_{1a}\ a_{1b}\ a_{1c})+\begin{bmatrix}a_{2a}\\a_{2b}\\a_{2c}\end{bmatrix}(2H+G)(a_{2a}\ a_{2b}\ a_{2c})+\begin{bmatrix}a_{3a}\\a_{3b}\\a_{3c}\end{bmatrix}(2H+G)(a_{3a}\ a_{3b}\ a_{3c}). \qquad (17)$$

Coefficients used are those resulting from the self-consistency procedure for various ρ's, and are given in Table I.

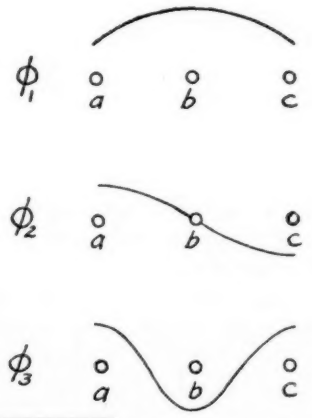

FIG. 1. Wave functions for He_3 system.

[5] J. F. Mulligan, J. Chem. Phys. **19**, 347 (1951).
[6] J. Vanderslice and V. Griffing, J. Chem. Phys. **23**, 1035 (1955).
[7] A. Macek, Ph.D. thesis, Catholic University of America, 1954.
[8] F. Wehner, Ph.D. thesis, Catholic University of America, 1954.
[9] J. C. Slater, Phys. Rev. **32**, 349 (1928).
[10] G. W. Kellner, Z. Physik **44**, 91 (1927).

The G matrix used is also that which results from the self-consistency procedure. Values of elements of this matrix, for various internuclear separations, are given in Table VI.

Total He_3 system energy is then determined from (17) by adding the nuclear repulsion energy, namely,

$$\frac{2(Z_{\text{real}})^2}{R_{ab}}+\frac{(Z_{\text{real}})^2}{R_{ac}}=\frac{10}{R}.$$

Interaction energy follows as the difference between total energy for $\rho=30$ (where interaction can be assumed to be negligible), and the total energies for various ρ's, as computed in this fashion. Results are shown in Table III.

CONSTRUCTING THE G MATRIX

Each element G_{pq} of the G matrix depends on the values of the undetermined coefficients used in making up the LCAO's. These coefficients will, in general (although, as will appear, some are completely determined by ortho-normality conditions), vary with each cycle of the self-consistent field procedure. Thus, the initial step in construction of the G matrix is to consider the relationships among the undetermined coefficients.

(a) Estimating the Coefficients

The coefficients of ϕ_2, of one node, $(\phi=a_{2a}\chi_a-a_{2c}\chi_c)$, are determined by the condition $\int\phi_2^2d\tau=\delta_{22}=1$. Whereupon, there results $a_{2a}^2-2a_{2a}^2S_{ac}+a_{2a}^2=1$, (since $a_{2a}=a_{2c}$), and

$$a_{2a}=\frac{1}{(2-2S_{ac})^{\frac{1}{2}}}=a_{2c}. \tag{18}$$

The condition that $\int\phi_1^2d\tau=1$ reduces to

$$2a_{1a}^2+a_{1b}^2+2S_{ab}a_{1a}a_{1b}+2a_{1a}^2S_{ac}+2a_{1b}a_{1a}S_{bc}=1, \tag{19}$$

when $a_{1a}=a_{1c}$.

$\int\phi_3^2d\tau$ leads to

$$2a_{3a}^2+a_{3b}^2-4S_{ab}a_{3a}a_{3b}+2S_{ac}a_{3a}^2=1, \tag{20}$$

since $S_{ab}=S_{bc}$ and $a_{3a}=a_{3c}$.

Finally, $\int\phi_1\phi_3d\tau=0$ yields

$$[(2+2S_{ac})a_{3a}-2S_{ab}a_{3b}]a_{1a}=[a_{3b}-2S_{ab}a_{3a}]a_{1b}, \tag{21}$$

if $a_{1a}=a_{1c}$ and $a_{3a}=a_{3c}$. a_{2a} and a_{2c} are completely determined, as in (18). a_{2b} is taken as zero. Values for the overlap integrals are found in the Appendix.

An assumption of some ratio of a_{3b} to a_{3a}, in (20) is now tantamount to an assumption of values for all of the coefficients in the three MO's. Accordingly, the self-consistency procedure is simplified in that but one parameter relating to the undetermined coefficients (i.e., a_{3b}/a_{3a}) is required.

(b) Elements of G Matrix

The G matrix was constructed by computing elements $G_{pq}=\sum_i(2J_{ipq}-K_{ipq})$ in the manner indicated in Eqs. (6), (7), (8), and (9). It was found effective to make up the (9×9) array $(2J_{prqs}-J_{prsq})$, multiply all elements of the rows of this array by the appropriate coefficient-determined multiplier (which for each row is the same for all elements) to create a new array of the products of the multiplication. In this way, all G_{pq} were established to form a (3×3) matrix

$$\begin{pmatrix}G_{aa} & G_{ab} & G_{ac}\\ G_{ba} & G_{bb} & G_{bc}\\ G_{ca} & G_{cb} & G_{cc}\end{pmatrix}.$$

Owing to the symmetry of the He_3 configuration, it was found that $G_{aa}=G_{cc}$, $G_{ab}=G_{ba}=G_{bc}=G_{cb}$, and $G_{ac}=G_{ca}$.

This symmetry is found in the H matrix, hence also in the L matrix. Accordingly, the labor entailed in formulating these matrices was much reduced.

A discussion of the actual evaluation of all integrals appearing in the G matrix is found in the Appendix.

CONSTRUCTION OF THE H MATRIX

Each element, H_{pq}, of the H-matrix, is made up of an orbital kinetic-energy part, and a nonkinetic bare-nuclear-field part. Consider, for instance, the element

$$H_{ab}=\int\bar{\chi}_a\left(-\frac{\nabla^2}{2}\right)\chi_bd\tau^1+\int\bar{\chi}_a\frac{1}{r_a}\chi_bd\tau^1$$
$$+\int\bar{\chi}_a\frac{1}{r_b}\chi_bd\tau^1+\int\bar{\chi}_a\frac{1}{r_c}\chi_bd\tau^1.$$

The integrals which make up the first term on the right-hand side, corresponding to the kinetic energy, have been tabulated for Slater-type $1-s$ orbitals by Roothaan.[11] These are discussed in the Appendix. The two-center, bare-nuclear-field potential energy integrals, which are the second and third terms, have also been evaluated for many values of the internuclear separation R (Bohr radii). Integrals which are of the form of the third term on the right-hand side are three-center in character. These have been calculated for H_3 by Hirschfelder and Weygandt[12] and are also discussed, with method of application to He_3, in the Appendix.

The resultant (3×3) H matrix,

$$\begin{pmatrix}H_{aa} & H_{ab} & H_{ac}\\ H_{ba} & H_{bb} & H_{bc}\\ H_{ca} & H_{cb} & H_{cc}\end{pmatrix},$$

has symmetry of the same form as that of the G matrix, i.e., $H_{aa}=H_{cc}$, $H_{ab}=H_{ba}=H_{bc}=H_{cb}$, and $H_{ac}=H_{ca}$.

[11] C. C. J. Roothaan, J. Chem. Phys. **19**, 1445 (1951).

[12] J. O. Hirschfelder and C. N. Weygandt, J. Chem. Phys. **6**, 795 (1938).

SELF-CONSISTENCY PROCEDURE

Once having estimated a set of a's, the G matrix (function of the a's) is made up in the foregoing manner, and added to the H matrix. The S matrix for the ρ involved is already available, having been used in determining the a's. The secular equation for each MO, $La_i=\epsilon_i Sa_i$, is then solved using the linear equation solver of Filler, Cowan, and Roothaan,[13] which is available at Catholic University. This instrument is essentially an analog computer giving eigenvectors and eigenvalues of the secular equation simultaneously. The L and S matrices are inserted into the machine, and balance is attempted using the assumed a's. Balance is usually found only by modifying these a's. This means that new a's (some compromise between assumed and those given by the equation solver) must be used in reconstructing the G, hence the L matrix, and balance sought again. In the case of this system, the usual number of cycles for this process was four or five and, in fact, made up much of the work of the calculation.

The process of assuming a's, then adjusting them as indicated by the equation solver is, in effect, the scheme for attaining self-consistency.

TABLE I. Variation of the LCAO coefficients.

MO / ρ	ϕ_1			ϕ_2			ϕ_3		
	a_{1a}	a_{1b}	a_{1c}	a_{2a}	a_{2b}	$-a_{2c}$	a_{3a}	$-a_{3b}$	a_{3c}
30	0.408	0.816	0.408	0.707	0	0.707	0.577	0.577	0.577
10	0.413	0.811	0.413	0.707	0	0.707	0.574	0.585	0.574
8	0.426	0.788	0.426	0.706	0	0.706	0.565	0.610	0.565
5	0.454	0.684	0.454	0.706	0	0.706	0.558	0.726	0.558
4	0.505	0.533	0.505	0.711	0	0.711	0.525	0.893	0.525
3	0.543	0.348	0.543	0.724	0	0.724	0.572	1.087*	0.572

* Ratio a_{3b}/a_{3a} equals 1.526.

After having attained this condition, the eigenvalues ϵ_i's, measured in the equation solver, gave the LCAO orbital energies. The orbital energies, then, come into the calculation most directly in connection with determining the correct a's for the system.

RESULTS

(i) The three LCAO MO's for linear configuration of He_3, as obtained by the self-consistent field procedure, are given in Table I for various values of the internuclear separation. At wide separation ($\rho=10-30$), the central coefficient, a_{32}, has magnitude approximately equal to that of the outer coefficients, but as the He atoms are made to approach each other, the charge distribution contribution corresponding to a_{32} is considerably increased, whereas that of a_{31} and a_{33} are relatively lessened. The values of the coefficients of ϕ_2 are but slightly increased as the atoms approach each other, owing to the absence of overlap with any charge distributions of the center atom, whose coefficient in this configuration is zero. The charge distributions corresponding to ϕ_1 are in inverse relation to those of ϕ_3, the central coefficient dropping perceptibly as ρ goes down to 3.

[13] Filler, Cowan, and Roothaan, Office of Naval Research Report, University of Chicago, Part II, 1949.

TABLE II. Orbital energies (Hartree units).

MO / ρ	ϕ_1	ϕ_2	ϕ_3
30	−0.892	−0.892	−0.892
10	−0.894	−0.894	−0.894
8	−0.910	−0.892	−0.890
5	−0.975	−0.872	−0.860
4	−1.095	−0.774	−0.765
3	−1.396	−0.668	−0.668

(ii) The orbital energies which are eigenvalues of the equation $(H+G)a_i=\epsilon_i Sa_i$, are listed for each of the LCAO MO's, as functions of the internuclear separation, in Table II. Also, the ϵ_i's are plotted in Fig. 2. These energies have been shown by Koopmans[14] to approximately represent the "vertical ionization" energies; that is, the energies of the electron shells of the molecule. As the He atoms approach each other, the energy of ϕ_1 decreases, in something of an exponential manner, indicating that this lowest energy configuration becomes more binding with decrease in internuclear separation. On the other hand, the orbital energies of ϕ_2 and ϕ_3, of one and two nodes respectively, increase as ρ decreases, indicating that these configurations become increasingly antibonding. There are no minima in the vertical ionization energies of any of the three MO's, all curves varying monotonically.

(iii) The interatomic potential energy, or complete interaction energy (Table III), calculated as indicated previously, is seen to be positive at all distances, giving rise to repulsion. This energy increases abruptly in the

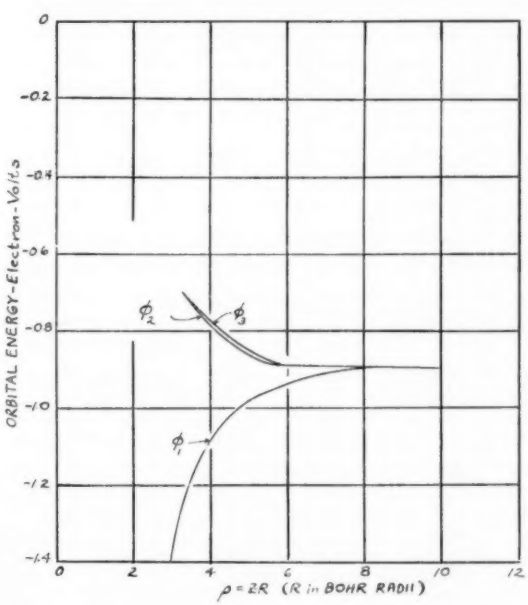

FIG. 2. Orbital energies for three MO's of He_3 system.

[14] T. Koopmans, Physica **1**, 104 (1933).

region where separation is approximately equal to the collision diameter (9) for the helium atom, i.e., 1 A. Plotted along with the computed interaction energy of this method, in Fig. 3, is interaction energy computed by adding twice the energy for the case of two He $1-s$ atoms for various values of ρ, as calculated by Wehner,[8] using Roothaan's method, plus the energy corresponding to separation of 2ρ. Wehner has indicated close agreement of his MO method (for small separations calculation) with results given by Slater.[9] It appears that nonadditivity of simple pair potentials in this case becomes important at about $\rho=4.7$, the difference, indicated by $(2B+C)-(A)$ in Table III, running up to approximately 30% at $\rho=3$. Figure 3 also gives curves of nonadditivity as established in this calculation, as well as that estimated by Rosen.[3] It appears that the valence-bond method underestimates the effects of nonadditivity in this configuration of the He_3 system.

DISCUSSION

Mulligan[5] has enumerated the inherent sources of errors in the LCAO SCF method of calculation. Approximations are employed in most of the integrals which were used in making up the L matrix. The two- and three-center integrals become quite large at small internuclear separations, and have important bearing on the energy values.

At large separations ($\rho=10$), interaction energy calculations are not very accurate. The equation solver as used, gave the LCAO coefficients to but three significant figures. Accordingly, the total energy was accurate only in the same way, and in calculating interaction energy as the difference between two large total energies of almost the same magnitude, small percentage errors in total energy were found to result in large percentage errors in interaction energies. By computing for very large ρ, ($=30$), with an LCAO SCF method, a value for the total energy, using the same means for evaluating integrals throughout, was developed, to give a basis for calculation of interaction energy. (Total energy at $\rho=30$ as computed in this way is 232.3794 ev.) It is possible to compute the eigenvalues ϵ_i's, hence total and interaction energies for large separations, by actually expanding the secular determinant into a cubic, using machine-derived eigenvalues as a starting point in some method of successive approximations, to get

TABLE III. Interaction energy—electron-volts.

Case / ρ	(A) 3 He $1-s$ atoms	(B) 2 He $1-s$ atoms, separation R	(C) 2 He $1-s$ atoms, separation $2R$	$(2B+C)$ Sum of pairs interaction	$(2B+C)-(A)$ Non-additivity deviation
30	0.0000	0.0000	0.0000	0.0000	0.0000
10	0.0049	0.0004	0.0000	0.0008	−0.0041
8	0.0100	0.0050	0.0000	0.0100	0.0000
5	0.7250	0.3630	0.0003	0.7263	0.0013
4	2.2500	1.4000	0.0050	2.8050	0.5050
3	9.3900	6.3000	0.1000	12.7000	3.3100

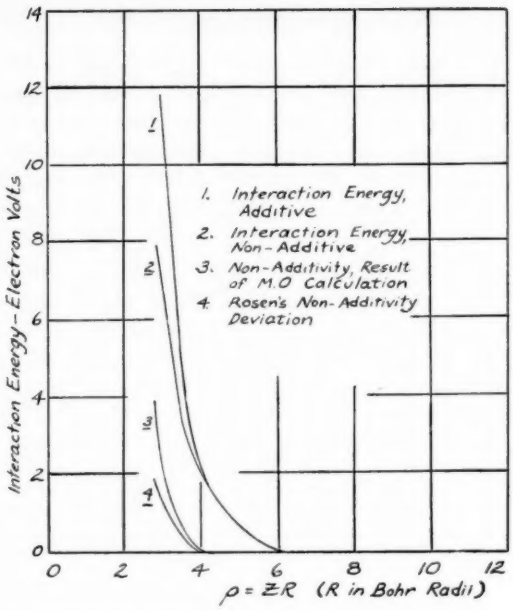
Interaction Energy - Electron Volts
ρ = ZR (R in Bohr Radii)
1. Interaction Energy, Additive
2. Interaction Energy, Non-Additive
3. Non-Additivity Result of M.O Calculation
4. Rosen's Non-Additivity Deviation

FIG. 3. Interaction energy, Mo method, for 3 He $1-s$ atoms in linear array, equally spaced.

the ϵ_i's to better than three significant figures. This procedure would not greatly improve interaction calculations, however, since interaction energies at $\rho=10$ for the He_2 system are shown by Wehner[8] to be in the order of 0.00005 ev.

ACKNOWLEDGMENTS

The author wishes to express his appreciation to Dr. K. F. Herzfeld for suggesting the problem, and to him and Dr. Virginia Griffing for their continued help and guidance. He is also grateful to Dr. J. T. Vanderslice and to Dr. Andrej Macek for their suggestions.

APPENDIX. EVALUATION OF INTEGRALS

Atomic orbitals used in this calculation are Slater-type $1-s$ orbitals, of form

$$\chi_a=\left(\frac{Z^3}{\pi}\right)^{\frac{1}{2}}e^{-Zr_a},\quad \chi_b=\left(\frac{Z^3}{\pi}\right)^{\frac{1}{2}}e^{-Zr_b},\quad \chi_c=\left(\frac{Z^3}{\pi}\right)^{\frac{1}{2}}e^{-Zr_c}.$$

Here, Z is effective nuclear charge (1.7 atomic units), and r_a is distance measured from the center of atom a, in atomic units, or Bohr radii (one a.u.$=0.5293$ A).

Energy contributions to the Hamiltonian, as well as nuclear repulsion and total energies, are calculated in Hartree units (27.204 ev). Integrals which involve these energies, therefore, are also given in Hartree units. Interaction energies appearing in Results, however, have been converted to electron-volts.

(a) Overlap Integrals

$S_{aa}=S_{bb}=S_{cc}=\int\bar{\chi}_a\chi_a d\tau=1$, $S_{ab}=S_{bc}=S_{ba}=S_{cb}=\int\bar{\chi}_a\chi_b d\tau$ and $S_{ac}=S_{ca}=\int\bar{\chi}_a\chi_c d\tau$, are given by

Hirschfelder and Linnett,[15] as well as by Mulliken and others.[16] These integrals are given as functions of ρ in Table IV.

(b) Integrals of the H Matrix

(i) *Kinetic Energy Integrals*

These are of form $\int \bar{\chi}_p{}^\mu(-\nabla^2/2)\chi_q{}^\mu d\tau^\mu$, and for $1-s$ functions are easily in closed form. The two-center type (i.e., $\int \bar{\chi}_a'(-\nabla^2/2)\chi_b' d\tau'$) are given by Roothaan[11] in the form of linear combinations of two-center overlap and one-electron bare-nuclear-field integrals.

(ii) *Bare Nuclear-Field Integrals*

The nuclear field integrals are of the form $\int \bar{\chi}_p{}^\mu(2/r)\chi_q{}^\mu d\tau^\mu$ (2 is real nuclear charge), where p and q take on the values a, b, and c, and where r is r_a, r_b, or r_c. One-center integrals of this form (i.e., $\int \bar{\chi}_a{}^\mu(2/r_a)\chi_a{}^\mu d\tau^\mu = 2Z$)

TABLE IV. Elements of S matrix.

ρ \ S_{pq}	$S_{aa}=S_{bb}=S_{cc}$	$S_{ab}=S_{bc}=S_{cb}=S_{ba}$	$S_{ac}=S_{ca}$
30	1	0.0000000	0.0000000
10	1	0.0020127	0.0000003
8	1	0.0101757	0.0000112
5	1	0.0965772	0.0020127
4	1	0.1892620	0.0101756
3	1	0.3485090	0.0470963

have been directly integrated in spherical coordinates.[17] Two-center, one-electron integrals of form

$$\int \bar{\chi}_a{}^\mu \frac{2}{r_a}\chi_b{}^\mu d\tau^\mu = \int \bar{\chi}_a{}^\mu \frac{2}{r_b}\chi_b{}^\mu d\tau^\mu,$$

have been integrated in elliptical coordinates, and are given for H_2 by Hirschfelder and Linnett.[14]

Three-center, one-electron integrals of form

$$\int \frac{\bar{\chi}_a{}^\mu \chi_b{}^\mu d\tau^\mu}{r_c} = \int \frac{\bar{\chi}_b{}^\mu \chi_c{}^\mu d\tau^\mu}{r_a}$$

are given by Hirschfelder and Weygandt[12] for hydrogen $1-s$ functions. Conversion to $Z=1.7$ is as in the two-center type.

H matrices, made up from these integrals as indicated previously, are given in Table V for various values of ρ.

TABLE V. Elements of H matrix.

ρ \ H_{pq}	$H_{aa}=H_{cc}$	$H_{ab}=H_{ba}=H_{bc}=H_{cb}$	$H_{ac}=H_{ca}$	H_{bb}
30	−2.1249999	0.0000000	0.0000000	−2.1816666
10	−2.4649999	−0.0107085	−0.0007722	−2.6349999
8	−2.5924994	−0.0167553	−0.0030307	−2.8049900
5	−2.9748026	−0.3433418	−0.0898789	−3.3146294
4	−3.2285750	−0.7412728	−0.1388679	−3.6521500
3	−3.6437374	−1.5512030	−0.4112641	−4.1991904

TABLE VI. Elements of G matrix.

ρ \ G_{pq}	$G_{aa}=G_{cc}$	$G_{ab}=G_{ba}=G_{bc}=G_{cb}$	$G_{ac}=G_{ca}$	G_{bb}
30	1.2324999	0.0000000	0.0000000	1.2891666
10	1.5724798	0.0024250	−0.0000029	1.7425427
8	1.6889600	0.0121570	0.0013247	1.9364213
5	2.0791764	0.2001588	0.0018533	2.4163010
4	2.3229034	0.4565956	0.0158915	2.7286148
3	2.6796110	0.9978442	0.1007468	3.1745575

(c) Integrals of the G Matrix

Integrals of the G matrix are also of one-two- and three-center varieties, of form

$$\int \frac{\bar{\chi}_p{}^\mu \bar{\chi}_r{}^\nu \chi_q{}^\mu \chi_t{}^\nu d\tau^{\mu\nu}}{r^{\mu\nu}}.$$

When $p=r=q=t$, there results the one-center type. When two pairs of subscripts are identical, a two-center integral results, and when only one pair is identical, the integral is of three-center form. The one-center integral has been evaluated in spherical coordinates for Slater-type functions. For $z=1.7$, its value is 1.0625.

Two-center integrals have been evaluated for H_2, and are given by Hirschfelder and Linnett.[14]

Three-center integrals were derived by use of Mulliken's approximation[18]:

$$J_{ab|cd} = \tfrac{1}{4}(S_{ab}S_{cd})[J_{aa|cc}+J_{aa|dd}+J_{bb|cc}+J_{bb|dd}].$$

Here,

$$J_{ab|cd} = \int \frac{\bar{\chi}_a{}^1 \bar{\chi}_c{}^2 \chi_b{}^1 \chi_d{}^2}{r_{12}} d\tau^{12}$$

and S_{ab} is the usual overlap integral, $\int \bar{\chi}_a \chi_b d\tau$.

G matrices using the one-, two-, and three-center integrals here described, and computed in the manner outlined previously, after self-consistency had been attained, are given as functions of ρ, in Table VI.

[15] J. O. Hirschfelder and J. W. Linnett, J. Chem. Phys. **18**, 130 (1950).

[16] Mulliken, Rieke, Orloff, and Orloff, J. Chem. Phys. **17**, 1248 (1949).

[17] Eyring, Walter, and Kimball, *Quantum Chemistry* (John Wiley & Sons, Inc., New York, 1944).

[18] R. S. Mulliken, J. Chem. Phys. **46**, 675 (1949).

Thermodynamic Properties of Ideal Gaseous Methanol

E. V. IVASH, *Department of Physics, University of Texas, Austin, Texas*
AND
JAMES C. M. LI AND KENNETH S. PITZER, *Department of Chemistry and Chemical Engineering, University of California, Berkeley, California**

(Received December 13, 1954)

New calculations are presented for the thermodynamic properties of methanol which are based upon the most recent spectroscopic data. The molecular constants related to the internal rotation are now well established. The vibrational assignment is discussed and additional arguments are presented for the correctness of the selections of Herzberg and Plyler. The method of statistical calculation is essentially that of Halford, but avoids an approximation. Complete thermodynamic functions are tabulated for the range 100 to 1000°K. Agreement with experimental thermodynamic data is satisfactory.

I. INTRODUCTION

THE problem of internal rotation in methyl alcohol has been solved by Dennison and his co-workers[1–3] to such an extent that the theory is now consistent with almost all of the observed microwave and infrared spectra. The molecular constants thus determined may be used to calculate the thermodynamic functions for the hypothetical ideal gaseous state, and the results compared with the experimental values.

The corrections of Weltner and Pitzer[4] for the abnormal gas imperfection of methanol appear to bring experimental thermodynamic data into agreement with values calculated from spectroscopic parameters, but a more precise comparison of best values is desirable.

Unfortunately, the thermodynamic functions cannot be obtained by the relatively simple method of Pitzer and Gwinn,[5] since at low temperatures this molecule falls outside the limits of validity of the calculations. The general situation has been discussed by Halford[6] who has devised a special method for methyl alcohol which takes advantage of an approximate sine square relation involving the quantum number K for the partition function of internal rotation. This results not only in a great simplification in calculation but also makes possible the separation of the partition function for internal rotation from that for over-all rotation. While Halford's approximation is empirically successful over the important range of temperature, his derivation does not readily allow the computation of additional terms which would yield still higher accuracy. We have developed a more general formulation which does allow computation to virtually any desired accuracy and which is given in the Appendix. It is found that Halford's method is excellent at all temperatures of practical importance.

II. INTERNAL ROTATION

In these calculations, the molecular parameters of Ivash and Dennison[3] have been adopted, together with fundamental physical constants recommended by Rossini *et al.*[7] The internal rotational energy, as defined in Eqs. (4) and (5) of the Appendix, has been calculated by the continued fraction method for the lowest four torsional levels. The second-order perturbation-theory expression, Eq. (19), is found to yield high accuracy for the $n=3$ levels and practically perfect results for the $n=4$ levels and therefore all higher levels. Table I gives a comparison of the energies computed from the perturbation theory with the exact values from continued fractions and with crude values based on the formula for free rotation. Table II gives the exact values for the $n=0-3$ levels for various values of the parameter $x=4C_1K/C$. These energies were used for the calculation of the partition function and the thermodynamic functions associated with internal rotation which are given in Table III.

Since our general method of calculation neglects any effect of nuclear spin, a calculation was made to estimate the low-temperature limit of applicability. The partition function was calculated for each spin species at 50 and

TABLE I. Comparison of internal rotational energies of methanol given by various methods.

		Internal rotational energy in cm^{-1}		
n	$\tau+K(C_1/C)-1$	Continued fraction	Second-order perturbation	Free rotation
2	0.0	483.616	460.381	436.920
	1.5	754.598	757.606	748.808
3	1.0	887.551	887.455	880.494
	0.0	1190.030	1190.143	1185.451
4	0.5	1362.694	1362.681	1358.722
	1.0	1549.250	1549.242	1545.855
	1.5	1749.785	1749.783	1746.850

* The work at the University of California received support from the American Petroleum Institute through Research Project 50.

[1] J. S. Koehler and D. M. Dennison, Phy. Rev. **57**, 1006 (1940).
[2] D. G. Burkhard and D. M. Dennison, Phys. Rev. **84**, 408 (1951).
[3] E. V. Ivash and D. M. Dennison, J. Chem. Phys. **21**, 1804 (1953).
[4] W. Weltner and K. S. Pitzer, J. Am. Chem. Soc. **73**, 2606 (1951).
[5] K. S. Pitzer and W. D. Gwinn, J. Chem. Phys. **10**, 428 (1942).
[6] J. O. Halford, J. Chem. Phys. **18**, 444, 1051 (1950).
[7] Rossini, Gucker, Johnston, Pauling, and Vinal, J. Am. Chem. Soc. **74**, 2699 (1952).

100°K by direct numerical summation. At 100°K there was no difference between the spin species; further, Halford's approximation was found to be excellent. Even at 50°K, a temperature of no practical interest, the error in the specific heat calculated by the method described in the Appendix was no more than 0.01 cal/mole degree.

III. THERMODYNAMIC PROPERTIES AND VIBRATION FREQUENCIES

A complete vibrational assignment is necessary in order to calculate thermodynamic functions for comparison with experimental values. Various authors have offered assignments which agree in most respects. Herzberg[8] summarizes earlier work and offers an assignment which seems reliable with the possible exception of the two methyl rocking frequencies. More recently Plyler[9] has studied the infrared spectrum again and offers improved numerical values for some of the frequencies. Plyler's assignment is substantially the same as Herzberg's.

In the case of methanol the shift in frequency values from the gas to liquid phase is particularly large because

TABLE II. Internal rotational energies of methanol (continued fraction values).

x \ n	Internal rotational energy in cm^{-1} 0	1	2	3
0	128.825	425.303	483.616	1190.030
1	129.565	408.586	504.715	1109.183
2	131.656	381.801	544.773	1031.740
3	134.685	357.620	591.522	957.853
4	137.948	338.777	642.908	887.551
5	140.513	326.743	698.346	820.885
6	141.493	322.589	754.598	760.906

of the strong hydrogen bonding effects in the liquid. There may be enough interaction with the O—H group to give an appreciable shift even for vibrations which are primarily methyl rocking motions.

The particular methyl rocking motion which is perpendicular to the plane of the C—O—H nuclei should be relatively free from interaction with the O—H bending motions since the only interacting mode is the very low frequency torsional oscillation. Since the O (or OH) mass is a little less than that of a fluorine atom, we should expect a frequency slightly higher than that of methyl fluoride where the methyl rocking mode[10] is at 1195 cm^{-1}. Noether[11] reports a weak band in CH_3OD at 1232 cm^{-1} and there is an absorption with very confused structure in CH_3OH between 1200 and 1280 cm^{-1}. We adopt a rounded value near the middle of this region, 1230 cm^{-1}, for this frequency in CH_3OH with full

[8] G. Herzberg, *Infrared and Raman Spectra of Polyatomic Molecules* (D. Van Nostrand Company, Inc., New York, 1945), p. 335.
[9] E. K. Plyler, J. Research Natl. Bur. Standards **48**, 281 (1952).
[10] Reference 8, p. 315.
[11] H. D. Noether, J. Chem. Phys. **10**, 693 (1942).

TABLE III. Internal rotational thermodynamic properties of methanol.

T °K	$-F/T$ cal/mole °K	H cal/mole	S cal/mole °K	C_p cal/mole °K
100	−0.086	43.3	0.347	0.878
150	0.133	98.5	0.789	1.263
200	0.346	164.9	1.171	1.362
250	0.542	232.8	1.473	1.354
273.16	0.626	264.0	1.593	1.338
298.16	0.712	297.2	1.709	1.317
300	0.718	299.6	1.717	1.316
350	0.876	364.3	1.917	1.273
400	1.017	427.0	2.084	1.234
500	1.258	547.2	2.352	1.173
600	1.459	662.2	2.562	1.131
700	1.629	773.7	2.734	1.101
800	1.776	882.6	2.880	1.080
1000	2.021	1095.8	3.117	1.052

realization that it is not very precise. The corresponding Raman line in the liquid is at 1171 cm^{-1}. As is shown in Table IV this frequency selection yields good agreement with the product rule for the A'' frequencies for CH_3OH, CH_3OD, and CD_3OH.

For the A' mode of methyl rocking there will be much greater interaction with the OH bending mode which in this case comes at 1346 cm^{-1}. This interaction causes the OH bending frequency to decrease by more than a factor of $\sqrt{2}$ on deuterium substitution. If we take Noether's values shown in Table IV for CD_3OH and CH_3OD which are themselves consistent with the product rule, then we may use the product rule to calculate a 1075 cm^{-1} value for the A' rocking mode in CH_3OH. This frequency, like that for the A'' mode, is a little larger than the corresponding value for the Raman spectrum of the liquid which was located by Herzberg at 1056 cm^{-1}. In the infrared spectrum of the vapor a weak band at 1075 cm^{-1} would be buried under the

TABLE IV. Vibration frequencies of methanol and product rule ratios.

		CH_3OH	CD_3OH	CH_3OD
A'	OH stretching	3682	3680	2720
	CH stretching	2976	2232	2965
	CH stretching	2846	2094	2850
	HCH bending	1479	1080	1480
	HCH bending	1427	1055	1427
	OH bending	1346	1289	869
	CO stretching	1033	990	1040
	CH_3 rocking	(1075)	856	1205
A''	CH stretching	2976	2232	2965
	HCH bending	1455	1123	1459
	CH_3 rocking	1230	879	1232
	Molecular weight	32.03	35.05	33.03
	I_xI_y 10^{79}	22.39	50.29	27.21
	I_z 10^{40}	35.31	43.51	38.03
	$I_{\text{internal rotation}}10^{41}$	10.09	11.15	16.23
A'	Ratio observed	···	0.218	0.537
	Theoretical	···	0.215	0.536
A''	Ratio observed	···	0.414	1.00
	Theoretical	···	0.412	1.00

TABLE V. Complete thermodynamic functions for methanol.

	$(F^0-F^0)/T$ cal/mole °K	$H^0-H_0^0$ cal/mole	S^0 cal/mole °K	C_p^0 cal/mole °K
100	38.61	838	46.99	8.83
150	42.05	1291	50.66	9.23
200	44.55	1759	53.35	9.48
250	46.54	2242	55.50	9.88
273.16	47.33	2473	56.39	10.15
298.16	48.13	2731	57.29	10.49
300	48.19	2751	57.36	10.52
350	49.62	3297	59.04	11.35
400	50.90	3887	60.61	12.29
500	53.14	5213	63.56	14.22
600	55.11	6727	66.32	16.02
700	56.90	8411	68.91	17.62
800	58.55	10 245	71.36	19.04
900	60.11	12 210	73.67	20.29
1000	61.58	14 295	75.87	21.38

R-branch of the very strong CO stretching band centered at 1033 cm^{-1}.

We adopt for our calculations the frequency assignments shown in Table IV, which may be regarded essentially as those of Herzberg and Plyler. Our discussion has merely yielded gas phase frequencies for the two methyl rocking motions (in place of the liquid phase values given by Herzberg and Plyler) and additional arguments have been presented for the correctness of the assignments.

The application of standard statistical methods to the data of Tables III and IV yields the complete thermodynamic functions for methanol given in Table V, and based on the harmonic oscillator approximation. Experimental thermodynamic data available for comparison include the entropy value of Kelley[12] and the heat capacity data of Eucken and Franck[13] and of Weltner and Pitzer.[4] The unusual gas imperfection corrections of the latter authors were applied also to the entropy value. Eucken and Franck's measurements were made at extremely low pressures where the ideal gas law may be assumed. These data are compared in Table VI with the calculated values of the present paper. The agreement is very good, particularly when one remembers that the vibrational anharmonicity corrections will raise slightly the heat capacity values at the higher temperatures.

IV. ACKNOWLEDGMENTS

One of us (EVI) wishes to thank Professor D. M. Dennison for suggesting this problem, and for the many interesting and valuable discussions he has had with him.

TABLE VI. Comparison with experimental thermodynamic data.

T	Function	Calculated	Experimental	References
200°K	C_v^0	7.49	7.45±0.11	13
280	C_v^0	8.26	8.38±0.08	13
403.2	C_p^0	12.35	12.43±0.1	4
464	C_p^0	13.53	13.67±0.1	4
340	S^0	58.71	58.57±0.3	12, 4

[12] K. K. Kelley, J. Am. Chem. Soc. **51**, 181 (1929).
[13] A. Eucken and E. U. Franck, Z. Elektrochem. **52**, 195 (1948).

APPENDIX

The symbols of Dennison and his co-workers[1-3] will be used in this section, some of which differ from the symbols employed by Pitzer and Gwinn. Care must also be taken not to confuse certain symbols in this section with those used to denote thermodynamic properties in the earlier sections.

The rotational partition function Q for an asymmetric hindered rotator of the methanol type may be written

$$Q=\frac{1}{S}\sum_{n=0}^{\infty}\sum_{K=-\infty}^{\infty}\sum_{\tau=1}^{S}\sum_{J=|K|}^{\infty}(2J+1)\times\exp[-(E_{JK\tau n}-E_0)/kT]. \quad (1)$$

The rotational energy levels $E_{JK\tau n}$ are given by

$$E_{JK\tau n}=\frac{\hbar^2}{2}\frac{C_1(A+B)-D^2}{2A(BC_1-D^2)}(J^2+J-K^2)+\frac{\hbar^2}{2}\frac{K^2}{C}+E_{K\tau n}{}^i, \quad (2)$$

where $E_{K\tau n}{}^i$ are the internal rotational energy levels, $E_0=E_{0010}$, and S is the symmetry number for internal rotation. For methanol $S=3$.

Formula (1) for Q does not take into account the effect of nuclear spin which, as is well known, is usually negligible for ordinary calculations. Moreover, the energy-level expression (2) neglects the off-diagonal elements of the Hamiltonian given by Burkhard and Dennison. For molecules such as methanol for which D and $A-B$ are relatively small, the effect of this approximation on the thermodynamic functions is slight.

To determine Q more explicitly one must sum over the four quantum numbers involved, J, K, τ, and n. Summing first over J in the usual manner, one obtains

$$Q=\frac{1}{S\alpha}\sum_{K,\tau,n}\exp(-\delta K^2-F_{K\tau n}{}^i), \quad (3)$$

where $\delta=\hbar^2/2kTC$, $F_{K\tau n}{}^i=(E_{K\tau n}{}^i-E_{010}{}^i)/kT$, and

$$\alpha=\frac{\hbar^2}{2kT}\frac{C_1(A+B)-D^2}{2A(BC_1-D^2)}.$$

For a simple threefold cosine potential barrier, the internal energies $E_{K\tau n}{}^i$ are the roots of the continued fraction relation

$$(1)-\frac{1}{(-2)-}\frac{1}{(-5)-}\frac{1}{(-8)-}\cdots=\frac{1}{(4)-}\frac{1}{(7)-}\frac{1}{(10)-}\cdots, \quad (4)$$

where

$$(\eta)=\frac{2\hbar^2C}{C_1C_2H}(\eta-\tau-KC_1/C)^2-\frac{4}{H}(E_{K\tau n}{}^i-H/2), \quad (5)$$

and thus is a function of the internal rotational energy, the molecular parameters C_1, C_2, and H, and the quantum numbers K and τ.

As shown by Koehler and Dennison[1] the internal rotational energy for given values of n and τ is periodic in K with a period of $3C/C_1$ for a molecule with $S=3$. Moreover, the energies of types 1, 2, and 3 are connected by the relations

$$E_{K1n}{}^i=E^i{}_{K+C/C_1,3,n}=E^i{}_{K+2C/C_1,2,n}. \quad (6)$$

Thus, if $E_{K\tau n}{}^i$ is plotted as a function of K the resulting curves for the different τ's will be identical in shape, but translated a distance C/C_1 with respect to each other. These conclusions hold also for any general value of the symmetry number S, except that the period of the internal energy then becomes SC/C_1.

The sum over τ may now be obtained in the following manner. Let

$$Q_\tau=\sum_{\tau=1}^{S}\exp(-F_{K\tau n}{}^i). \quad (7)$$

Then, utilizing the properties of the internal energies discussed,

$$Q_\tau=\sum_{l=0}^{S-1}\exp(-F^i{}_{K+lC/C_1,1,n}). \quad (8)$$

Since the internal energies are periodic in K with a period SC/C_1, one can expand $\exp(F_{K1n}{}^i)$ in the Fourier series

$$\exp(-F_{K1n}{}^i)=\sum_{p=0}^{\infty}b_p\cos pz,$$

where $z=2\pi C_1K/SC$, and b_p are the Fourier coefficients. Substituting in Eq. (8), one obtains

$$Q_\tau=\sum_{l=0}^{S-1}\sum_{p=0}^{\infty}b_p\cos p(z+2\pi l/S). \quad (9)$$

Now

$$\sum_{l=0}^{S-1}\cos p(z+2\pi l/S)=\cos pz\sum_{l=0}^{S-1}\cos(2\pi pl/S)-\sin pz\sum_{l=0}^{S-1}\sin(2\pi pl/S).$$

The sums on the right-hand side are both zero unless $p=$integer $\times S$. Thus, only those terms will remain in Eq. (9) for which p is an integral multiple of S. Consequently, Q can be expanded in a Fourier series in z with a period of $2\pi/S$. Thus,

$$Q_\tau=\sum_{p=0}^{\infty}a_p\cos pSz, \quad (10)$$

where the coefficients a_p are given by

$$a_0=\frac{S}{2\pi}\int_0^{2\pi}\exp(-F_{K1n}{}^i)dz, \quad (11)$$

$$a_p=\frac{S}{\pi}\int_0^{2\pi}\exp(-F_{K1n}{}^i)\cos pSzdz, \quad p=1,2,3,\cdots. \quad (12)$$

Making use of relation (10), Eq. (3) becomes

$$Q=\frac{1}{S\alpha}\sum_{K,n,p}a_p\exp(-\delta K^2)\cos(2\pi pC_1KC). \quad (13)$$

Replacing the sum over K by an integral and making use of the relation

$$\int_{-\infty}^{\infty}\exp(-\delta K^2)\cos pS\gamma KdK=\left(\frac{\pi}{\delta}\right)^{\frac{1}{2}}\exp(-p^2S^2\gamma^2/4\delta), \quad (14)$$

where $\gamma=2\pi C_1/SC$, one obtains

$$Q=\frac{1}{S\alpha}\left(\frac{\pi}{\delta}\right)^{\frac{1}{2}}\sum_{n,p}a_p(n)\exp(-p^2S^2\gamma^2/4\delta). \quad (15)$$

The factor $S^2\gamma^2/4\delta=\pi^2C_1{}^2/\delta C^2$ occurring in the exponential is roughly 12 for methyl alcohol at 200°K, and increases linearly with the absolute temperature. Most other molecules of similar type should have as large or larger values. For temperatures which are not too low, therefore, the $p=1, 2, \cdots$ terms in Eq. (15) are quite negligible in comparison with the $p=0$ term, and may be ignored. Combining Eqs. (11) and (15) one then obtains

$$Q=\frac{1}{2\pi\alpha}\left(\frac{\pi}{\delta}\right)^{\frac{1}{2}}\int_0^{2\pi}dz\sum_{n=0}^{\infty}\varphi_n(z), \quad (16)$$

where

$$\varphi_n(z)=\exp(-F_{K1n}{}^i).$$

The maximum error ΔQ caused by neglecting the $p=1, 2, \cdots$ terms in Eq. (15) may be readily estimated from Eqs. (12), (15), and (16) to be

$$\Delta Q\leq\frac{1}{\pi\alpha}\left(\frac{\pi}{\delta}\right)^{\frac{1}{2}}\int_0^{2\pi}dz\exp(-S^2\gamma^2/4\delta)\sum_{n=0}^{\infty}\varphi_n(z)=2Q\exp(-S^2\gamma^2/4\delta). \quad (17)$$

For methyl alcohol the maximum error ΔQ so deter-

mined is about 2×10^{-5} at 200°K. The actual error, because of the oscillatory character of the integrand is several orders of magnitude smaller. Indeed, numerical calculations show that the error is still minute even at 50°K.

It is convenient for calculations to make a change of variable and let $x=6z/\pi$. Then for the case of methyl alcohol for which $S=3$, Eq. (16) becomes

$$Q=\frac{1}{6\alpha}\left(\frac{\pi}{\delta}\right)^{\frac{1}{2}}\sum_{n=0}^{\infty}\int_0^6\varphi_n(x)dx. \tag{18}$$

It is to be noted that the internal and external rotational contributions to Q have been separated from each other, even though there is actually a coupling between the two corresponding motions.

In the actual calculation it is convenient to divide Q into two parts. The first is obtained by solving exactly for the internal rotational energies for $n=0$ to $n=n'$, and then applying Eq. (18), summing, however, only over these particular values of n. The integrals involved can be evaluated by Simpson's rule without any loss in accuracy, since the spacing of x is of the same order of magnitude as that of K. This gives the contribution to Q of levels with values of n from 0 to n'. The remaining portion of Q corresponding to n from $n'+1$ to infinlty can be determined for a suitably high n' by making use of an approximate expression for the internal energy levels. This relation is found by carrying out a second order perturbation calculation for free internal rotation with $H/2$ as the zero-point energy. The result is

$$E_{Km}=\frac{H}{2}+\frac{\hbar^2C}{2C_1C_2}(m-KC_1/C)^2 + \frac{H^2C_1C_2}{16\hbar^2C}\left[(m-KC_1/C)^2-\frac{9}{4}\right]^{-1}, \tag{19}$$

where m is the quantum number for free rotation as defined by Koehler and Dennison. For methyl alcohol the perturbation calculation is found to be entirely adequate for values of $n=4$ or higher.

The partition function Q can then be written as the sum of two terms, Q_a and Q_b, where

$$Q_a=\frac{1}{6\alpha}\left(\frac{\pi}{\delta}\right)^{\frac{1}{2}}\sum_{n=0}^{n'}\int_0^6\varphi_n(x)dx, \tag{20}$$

and

$$Q_b=\frac{1}{3\alpha}\sum_{K,m}\exp[-\delta K^2-(E_{Km}-E_0)/kT]. \tag{21}$$

To evaluate Q_b the summation is first replaced by a double integral. The limits of K corresponding to that of n from $n'+1$ to infinity and for all values of τ are from $-\infty$ to $|m-3(n'+1)/2|\,(C/C_1)$ and from $|m+3(n'+1)/2|\,(C/C_1)$ to $+\infty$, all integers inclusive, while $|m|$ takes on all integral values. The double integral can then be reduced to a single one by a change in variable and an integration, yielding

$$Q_b=\frac{2}{3\alpha}\left(\frac{\pi}{\delta}\right)^{\frac{1}{2}}\int_{3(n'+1)/2}^{\infty}\times\exp\{-[E_0-E_{Km}(y)]/kT\}dy, \tag{22}$$

where $y=m-KC_1/C$. Using Eq. (19) and carrying out the integration in Eq. (22), one obtains

$$Q_b=\frac{1}{3\alpha}\left(\frac{2\pi^2C_1C_2kT}{\hbar^2C\delta}\right)^{\frac{1}{2}}\exp[-(E_0-H/2)/kT] \times\left\{2\pi^{-\frac{1}{2}}\left[1+\frac{1}{16}\left(\frac{H}{kT}\right)^2\right] \times\int_\xi^\infty\exp(-t^2)dt-\frac{1}{16\pi^{\frac{1}{2}}}\left(\frac{H}{kT}\right)^2\frac{\exp(-\xi^2)}{\xi}\right\}, \tag{23}$$

where

$$\xi=\frac{3(n'+1)}{2}\left(\frac{\hbar^2C}{2C_1C_2kT}\right)^{\frac{1}{2}}.$$

The partition function Q having been obtained, its temperature derivatives and the thermodynamic functions can be calculated in the usual manner.

Electronic Structures of Transition-Metal Complexes*

L. E. ORGEL†
Gates and Crellin Laboratories of Chemistry, California Institute of Technology, Pasadena, California
(Received December 28, 1954)

The empirically determined values of the parameter Dq, which in transition-metal complexes, measure the influence of the ligands on the metal d-orbitals are interpreted theoretically. A quantitative treatment of "the magnetic criterion of the bond type," is given. Values of Slater-Condon parameters for transition metal ions are tabulated.

IN a previous paper[1] we have attempted to interpret in detail the electronic spectra of a number of transition metal complexes. In the course of this work we estimated the value of the parameter Dq, which is one-tenth of the separation between the t_{2g} and e_g $3d$-orbitals in octahedral complexes or the t_1 and e $3d$-orbitals in tetrahedral complexes. In this paper we shall first discuss the theoretical significance of the separation $10Dq$ and then draw some conclusions of chemical interest from the observed Dq values. Finally we shall show quantitatively how the covalent or ionic character of the complexes, as determined by the magnetic criterion of bond type,[2] depends on the electronic structure of the metal ion and the Dq value characteristic of the ligand.

The theoretical analysis of the meaning of the observed Dq values is necessarily tentative, but it is probable that the accumulation of data for a wider variety of ligands will make it possible to draw more definite conclusions. The treatment of the magnetic criterion of bond types is largely independent of the uncertainties of the preceding discussion.

INTERPRETATION OF Dq

(a) Molecular-Orbital Method - Empirical LCAO Method[3]

The orbitals of the central metal atom which are likely to be used in complex formation by elements of the first transition series belong to the $3d$, $4s$, $4p$, and $4d$-subshells. In this discussion we shall neglect the $4d$-orbitals although in a more quantitative treatment they would have to be taken into account. The transformation properties of the relevant orbitals in the point group O_h of a regular octahedral complex are given in Table I. We will use the symbols ϕ_{4p_x} etc. to designate metal orbitals and $\chi_{\pi 2}$ etc. for ligand orbitals. The detailed forms of the latter are readily obtained by inspection or by means of group theory.[4] The molecular-orbitals for the complex will be linear combinations of ligand and metal orbitals which transform as the same representation of the symmetry group.

If the ligands have π orbitals available for bonding then each metal orbital of A_{1g}, E_g, and T_{2g} symmetry forms a bonding and an antibonding combination with a ligand orbital, e.g., for the A_{1g} symmetry we have bonding and antibonding combinations $C_1\phi_{4s}+C_2\chi_{\sigma 1}$ and $C_3\phi_{4s}-C_4\chi_{\sigma 1}$, where

$$C_1^2+C_2^2+2C_1C_2S_{4s,\sigma 1}=C_3^2+C_4^2-2C_3C_4S_{4s,\sigma 1}=1$$

$$C_1C_3-C_2C_4+(C_2C_3-C_1C_4)S_{4s,\sigma 1}=0$$

and

$$S_{4s,\sigma 1}=\int \phi_{4s}\chi_{\sigma 1}d\tau.$$

The T_{1u} orbitals will be more complicated since both σ and π orbitals on the ligand will be involved. If the ligands do not have any π orbitals then the T_{1u} orbital takes on the same simple form as the other σ orbitals while the metal T_{2g} orbitals remain uncombined.

Since the ground states of all the divalent and trivalent transition metal ions belong to $3d^n\ 4s^0\ 4p^0$ configurations we may safely assume that the bonding σ orbitals of A_{1g} and T_{1u} symmetry each contain two electrons which come from the ligands, while the corresponding antibonding orbitals are empty. The e_{2g} bonding orbitals will also be filled by four electrons from the ligands. However the e_{2g} antibonding orbitals are not necessarily empty but, together with the t_{2g} orbitals, must accommodate the metal $3d$-electrons. In general there is not a single way of distributing the $3d$-electrons among these orbitals which will adequately describe the ground state of the ion, but a number of configurations have to be mixed. In a few special cases however a single configuration does suffice.[1] The bonding orbitals

TABLE I. Symmetry classification of orbitals in octahedral complexes.

	Metal ion	Ligand
A_{1g}	$4s$	σ_1
E_g	$3d_{z^2}$, $3d_{x^2-y^2}$	σ_2, σ_3
T_{1u}	$4p_x$, $4p_y$, $4p_z$	σ_4, σ_5, σ_6, π_1, π_2, π_3
T_{1g}	...	π_4, π_5, π_6
T_{2u}	...	π_7, π_8, π_9
T_{2g}	$3d_{xy}$, $3d_{xz}$, $3d_{yz}$	π_{10}, π_{11}, π_{12}

* Contribution No. 1948 from the Gates and Crellin Laboratories.
† Arthur A. Noyes Fellow, 1954.
[1] L. E. Orgel, J. Chem. Phys. **23**, 1004 (1955).
[2] L. Pauling, J. Am. Chem. Soc. **53**, 167 (1931).
[3] J. H. Van Vleck, J. Chem. Phys. **3**, 807 (1935).
[4] Eyring, Walter, and Kimball, *Quantum Chemistry* (John Wiley and Sons, Inc., New York, 1944).

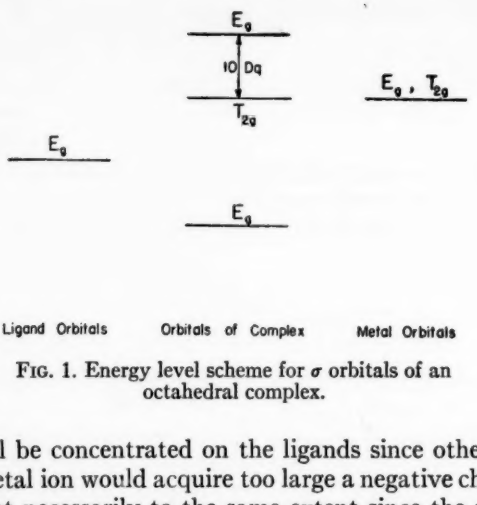

FIG. 1. Energy level scheme for σ orbitals of an octahedral complex.

will all be concentrated on the ligands since otherwise the metal ion would acquire too large a negative charge, but not necessarily to the same extent since the metal orbitals differ both in their electronegativity and their overlap properties.

We may illustrate the various cases which occur by taking some simple examples. In $[Cr(NH_3)_6]^{+++}$, after filling the six bonding σ orbitals, there are three d-electrons which must be accommodated in the t_{2g} and antibonding e_g orbitals. It can be shown[1] that the ground state is described by the single configuration $(t_{2g})^3$. In $[V(NH_3)_6]^{+++}$ on the other hand the ground state is found to be a mixture of the configurations $(t_{2g})^2$ and $(t_{2g})(e_g)$. In $[Ni(NH_3)_6]^{++}$ the ground state may be described accurately in terms of the single configuration $(t_{2g})^6(e_g)^2$ while in the "covalent" cobalt complex $[Co(NH_3)_6]^{+++}$ a number of configurations must be mixed, the most important of which is $(t_{2g})^6$.

In all of these examples the energy level diagram for the orbitals involving $3d$-electrons is of the type shown in Fig. 1. The t_{2g} level is unaffected by complex formation since no π bonding is possible (except by hyperconjugation, which we neglect). The e_g orbitals are pushed apart by the bonding interaction in a symmetric fashion as shown. Clearly, in this theory, we must identify $10Dq$ with the bonding or antibonding energy of a single-$3d$-electron in an e_g orbital. In $[Cr(NH_3)_6]^{+++}$ there are just four electrons in the bonding e_g orbital, so the bonding energy is just $40Dq$. In $[Ni(NH_3)_6]^{++}$ there are four bonding and two antibonding e_g electrons, so that the bonding due to e_g orbitals is $20Dq$. In other cases such as the V^{+++} and Co^{+++} complexes already discussed the exact bonding energy depends on the extent of mixing of configurations. It will be between $30Dq$ and $40Dq$ in the V^{+++} complex and rather less than $40Dq$ for the cobalt complex. In the latter case, however, the extra bonding energy is partly offset by the atomic promotion energy required to produce the singlet state of Co^{+++}.

In complexes such as $[Fe(CN)_6]^{4-}$ the interaction between the t_{2g} d-orbitals and the π orbitals of the ligands depresses the former and so increases the separation $10Dq$. Unfortunately it is not possible at present to separate the π bonding contribution to Dq from the other contributions. A detailed study of the spectra of phosphine, arsine, and related complexes might make this possible.

(b) The Crystal-Field Method

The extensive literature on this subject has been reviewed recently by Bleaney and Stevens.[5] The splitting between the t_{2g} and e_g orbitals is attributed to the electrostatic field of the ligands.

(c) Valence-Bond Theory

Certain aspects of the valence bond theory of the spectra of complexes were discussed in a previous paper.[6] Here we need only add that the use of $3d$-orbitals in bonding in complexes such as $[Ni(NH_3)_6]^{++}$ which was indicated in the molecular orbital theory is equivalent in valence-bond theory to the participation of resonance structures involving three-electron bonds. In the nickel complexes six of the eight d-electrons are put into the nonbonding t_{2g} orbitals. The remaining two go into the e_g orbital which then forms two three-electron bonds with the ligands. These two bonds, together with four sp^3 bonds, then resonate among the six bond directions.

None of these simple theories is entirely adequate, while more detailed calculations, such as a molecular orbital treatment including all of the electron repulsion integrals, which would automatically incorporate the electrostatic theory, are not at present feasible. The success of calculations based purely on electrostatics depends on the introduction of relatively large polarizations of the ligands. We have shown that the cause of the separation between the d-orbitals does not affect the magnetic or optical properties of the complexes, at least in a first approximation.[1] We could, therefore, equally well ascribe part of splitting to chemical bond formation. We shall not emphasize this difference, since descriptions in terms of polarized ligands or coordinate bonds are to some extent equivalent, differing in particular in that the former neglects the Pauli principle. We shall interpret the experimental data in terms of simple molecular-orbital theory, but we must remember that this is only a rather bad approximation and probably seriously underestimates electrostatic effects. Our bond energies will be consistenly high, perhaps by a large amount, but they will be useful as indicating upper limits for the contributions of the d-orbitals to chemical bonding.

TABLE II. Dq values for hydrates in cm^{-1}.

	Ti	V	Cr	Mn	Fe	Co	Ni	Cu
Divalent ion	...	1220	1260	...	1050	970	850	(1250)
Trivalent ion	2040	1900	1770	2100	2100	...	...	...

[5] D. Bleaney and W. K. Stevens, Repts. Progr. in Phys. **16**, 108 (1953).
[6] L. E. Orgel, J. Chem. Soc. 4756 (1952).

The Dq values for the hydrates[1] are given in Table II. In divalent salts Dq is about 1000 cm^{-1} corresponding to a bond energy of 60 kcal for a two electron bond. In trivalent salts Dq is about 2000 cm^{-1} so that the energy of a bond is about 120 kcal. These values are quite low compared with the heats of hydration of divalent and trivalent transition metal ions which are about 85 kcal and 170 kcal per bond respectively.[7] Since our estimates of d-orbital bonding are themselves too high it is clear that both in "ionic" and "covalent" complexes the d-orbitals are less effective than the s and p in bonding. This point is illustrated by the case of Cr^{+++} for which the hydration energy is 182 kcal per bond while the upper limit of the d-electron bond energy is 102 kcal.

The heats of hydration of the divalent ions increase as we progress along the first transition series[7] while the bonding per electron in the e_g bonding orbital decreases. This implies that the relative importance of the d-electrons is greatest in V^{++} and Cr^{++} and least in Co^{++} and Ni^{++}.

The results of a previous discussion of transition metal hydrates[6] are valid in the present treatment but must be interpreted in a slightly different way. The estimated heats of hydration in the absence of any crystal field splitting refer to states in which not only the crystal-field energy but also the d-orbital bonding energy is averaged over all the states into which the ground state of the free ion is split. This quantity should increase steadily across the series provided that the energy of the s- and p-bonds increases more rapidly than the energy of the d-orbital bonding decreases through the occupation of the e_{2g} antibonding orbital.

The experimental data for ligands other than water is very incomplete. The available evidence suggests that the Dq values will vary in much the same way from element to element as do those for water. If this is true we would expect the heats of formation of these complexes to parallel those of the hydrates. The sequence of ligands which are derived on the basis of spectroscopic data[1] agrees quite well with the sequence which we would expect on grounds of the stability of the complexes or the "covalent" bond forming tendency of the ligands. The only serious anomalies are those of the fluoride ion, which is notable for the frequency with which it forms "ionic" complexes, but which seems to require a rather high Dq value in the $[Co(NH_3)_5F]^{++}$ ion; and of the other halogens which require small Dq's.

The very low values of Dq found for tetrahedral complexes may be understood if we assume that the σ bonding is mainly sp^3 in character, with a smaller contribution from d-orbital bonds. This is not unlikely in tetrahedral complexes, in contrast to octahedral complexes. In the latter two of the bonds can be formed only by the e_{2g} d-orbitals.

[7] L. L. Quill, *The Chemistry and Metallurgy of Miscellaneous Materials: Thermodynamics* (McGraw-Hill Book Company, Inc., New York, 1950).

The Magnetic Criterion of Bond Type

The energies of the atomic states arising from a given d^n configuration are altered to different extents by any perturbation which removes the degeneracy of the $3d$-orbitals. It may happen that the order of levels is changed in such a way that the ground state in the presence of a perturbation is of different spin multiplicity from that of the ground state of the free ion. Hund's rule requires that any such change is a decrease. According to the magnetic criterion of bond type we classify compounds in which a decrease in spin multiplicity occurs as covalent.[6] We shall discuss this phenomenon in terms of the electronic structure of the ion and the Dq value for the complex and later consider how far the terms "ionic" and "covalent" are justified in the description of transition-metal complexes.

A complete treatment of this problem would require the calculation of energy level diagrams such as that given for Ni^{++} for all the different ions and stereochemical arrangements in which we are interested. Calculations on the d^4, d^5, and d^6 configurations of the important octahedral complexes would be very lengthy while square planar complexes could not be treated in this way at all. Instead we shall use the strong field approximation which gives less exact information.

We suppose that in octahedral complexes the t_{2g} orbital is so much more stable than the e_g orbital that the ground states of the d^n configurations may be taken to belong to the $(t_{2g})^n$ configuration, provided that $n \leq 6$. We then calculate the electrostatic repulsion energy between the d-electrons in the ground states of the $(t_{2g})^n$ configurations in terms of Slater-Condon parameters and compare them with the corresponding values for the free ions.[8] In this way we obtain the promotion energy to the valence-states corresponding to "covalent-bond" formation.

We make use of the easily verified results:

$$J(xy, xy) = J(xz, xz) = J(yz, yz) = F_0 + 4F_2 + 36F_4 = J_1$$
$$J(xy, yz) = J(xy, xz) = J(xz, yz) = F_0 - 2F_2 - 4F_4 = J_2$$
$$K(xy, yz) = K(xy, xz) = K(xz, yz) = 3F_2 + 20F_4 = K$$

where J's and K's are Coulomb and exchange integrals respectively and the F_i's are Slater-Condon parameters.

The symmetries and repulsion energies of the ground states of the $(t_{2g})^n$ configurations are given in columns 1 and 2 of Table III. The energies of the lowest states of the free ions having the maximum possible multiplicity and the promotion energies to "covalent" states are given in columns 3 and 4. For the d^2 state the free ion energy is given for complete mixing of the $^3T_{1g}$ states by the field (see next paragraph).

In our calculations of the extra stabilization of the covalent ion in the complex we follow the convention of Schlapp and Penney[9] and fix the zero of our energy

[8] E. U. Condon and G. H. Shortley, *The Theory of Atomic Spectra* (Cambridge University Press, London, 1935).

[9] R. Schlapp and W. G. Penney, Phys. Rev. **42**, 666 (1932).

TABLE III.

	Symmetry of ground state in strong field	Energy of ground state in strong field	Energy of ground state of free ions	Promotion energy	Crystal field energy in strong field	Normal crystal field energy	Extra stabilization energy
d^1	$^2T_{2g}$	0	0	0	4 Dq	4 Dq	0
d^2	$^3T_{1g}$	$-5F_2-24F_4$	$-5F_2-24F_4$	0	8Dq	8 Dq	0
d^3	$^4A_{2g}$	$-15F_2-72F_4$	$-15F_2-72F_4$	0	12 Dq	12 Dq	0
d^4	$^3T_{1g}$	$-15F_2-44F_4$	$-21F_2-189F_4$	$6F_2+145F_4$	16 Dq	6 Dq	10 Dq
d^5	$^2T_{2g}$	$-20F_2-40F_4$	$-35F_2-315F_4$	$15F_2+275F_4$	20 Dq	0	20 Dq
d^6	$^1A_{1g}$	$-30F_2-60F_4$	$-35F_2-315F_4$	$5F_2+255F_4$	24 Dq	4 Dq	20 Dq

scale so that the t_{2g} level lies at -4 Dq and the e_g level at 6 Dq. In the strong field case the stabilization of the configuration d^n is then $4n$ Dq provided $n\leq 6$. The stabilizations of the lowest of the levels into which the ground state of the free ions are split have laready been calculated. In all cases except that of the d^2 configuration the energy of the lowest level depends linearly on Dq so that no ambiguity arises. In the d^2 configuration we must, for consistency, take the splitting as 8 Dq to correspond to the lowest triplet state in a *strong* field. The stabilizations of the $(t_{2g})^n$ configurations and of the free ions are given in columns 5 and 6 of Table III, and the extra stabilization energy on going over to the covalent complexes in column 7.

The configurations d^1-d^3 are of no interest in the present content since no change of spin multiplicity is possible and so there is a continuous transition from weak to strong field case as the separation 10 Dq increases. The most interesting configurations are d^5 and d^6. Making use of the fact that, for most transition-metal ions, the ratio F_4/F_2 is quite close to 0.072,[10] the value for hydrogen-like orbitals, we see that the promotion energies for the d^5 and d^6 configurations are about 34.8 F_2 and 23.4 F_2, respectively. The extra cubic-field stabilization of the covalent states is the same for the two configurations so that we will require a larger Dq value to obtain "covalent" complexes of d^5 ions than of d^6 ions. Since Dq for any given ligand does not vary much for metal ions of the same valency this implies that the d^5 ions should form "ionic" complexes with ligands whose complexes with corresponding d^6 ions are covalent. This is found to be so e.g., in the pair $[Fe(NH_3)_6]^{+++}$ and $[Co(NH_3)_6]^{+++}$.[11] The ions with four d-electrons, with promotion energy 16.44 F_2 and only half the crystal field stabilization of the d^5 and d^6 ions should be intermediate between the latter in their ease of "covalent" complex formation.

We may place upper limits on the value of Dq required to produce "covalent" complexes by equating the promotion energy to the crystal field stabilization. The values obtained in this way are a little too high since the true energy levels for the states of low multiplicity lie somewhat below those given by strong field theory, approaching the latter asymptotically as the field increases. For Fe^{+++} we estimate that $F_2=1600$ cm^{-1} and $F_4=130$ cm^{-1} and for Co^{+++} that $F_2=1800$ cm^{-1} and $F_4=150$ cm^{-1}.[10] This gives upper limits of about 3000 cm^{-1} and 2350 cm^{-1}, respectively, for the critical Dq values. The behavior of the hexamine is quite reasonable if we recall that in $[Cr(NH_3)_6]^{+++}$ $Dq=2150$ cm^{-1}. The $[Co(H_2O)_6]^{+++}$ ion is particularly interesting for there is evidence that while the ground state is a singlet, there is a state of higher multiplicity nearby.[12] This places the critical value of Dq close to 2000 cm^{-1}.

For Mn^{++} we have $F_2=1435$ cm^{-1} and $F_4=95$ cm^{-1} and for Fe^{++} $F_2=1540$ cm^{-1} and $F_4=120$ cm^{-1} giving critical Dq values of 2400 cm^{-1} and 1900 cm^{-1}, respectively. This suggests strongly that only the cyanide ion of the ligands which we discussed in the previous paper should form covalent complexes. While the cyanides are certainly covalent there is one other ion [Fe(*o*-phenanthroline)$_3$]$^{++}$ which should be paramagnetic according to our theory but which is in fact diamagnetic. Other physical properties of this ion e.g., its formation constant, are also anomalous.[13] It appears that double bonding must be particularly important in this case, since this seems the only way in which *o*-phenanthroline should differ from say ammonia which gives normal complexes. We would expect [Mn(*o*-phenanthroline)$_3$]$^{++}$ to be a normal "ionic" complex.

In square planar complexes the effect of the crystal field cannot be described in terms of a single parameter so that the methods available in octahedral complexes are not applicable. We can easily calculate the promotion energies to postulated valence states but, unfortunately, only in the case of the d^8 configuration is it possible to choose a unique valence state, namely $(3d_{xy})^2(3d_{xz})^2(3d_{yz})^2(3d_{z^2})^2$, if we take the z-axis perpendicular to the molecular plane and the x- and y axes in the directions of the ligands. The valence state energy, ground state energy and promotion energy are found to be $-38F_2-342F_2$, $-50F_2-387F_4$, and $12F_2+45F_4$, respectively. In nickel the promotion energy amounts to about 24 000 cm^{-1} or 70 kcal, so that the factors stabilising the planar structure, in particular the more efficient use of the d-orbitals, must account for almost this amount of energy.

In the second and third transition series the tendency

[10] Slater-Condon parameters for transition-metal ions are given in the appendix.

[11] Magnetic susceptibilities are taken from Landolt-Bërnstein, *Atom und Molekularphysik* (Springer-Verlag, Berlin, Germany, 1951), sixth edition.

[12] H. Taube, Chem. Revs. **50**, 69 (1952).

[13] H. Irving and R. J. P. Williams, J. Chem. Soc. 3192 (1953).

to "covalent bond" formation is much greater. A study of atomic and solution spectra data shows that two important factors are involved. Firstly, the spread of the d^n configurations decrease from the first to the second transition series, showing that F_2 and F_4 are smaller and hence the promotion energy required to produce covalent complexes is smaller. Secondly, the little spectroscopic evidence available shows that Dq increases markedly on going from a given complex of a metal of the first transition series to the analogous complex of a metal of the second or third transition series, e.g., the longest wavelength absorption maxima in $[Rh(Ethylenediamine)_3]^{+++}$ and $[Ir(Ethylenediamine)_3]^{+++}$ are at 3200 A while that of $[Co(Ethylenediamine)_3]^{+++}$ is at about 4000 A.[14] Similarly we find that while the common complexes of Cu^{++} are blue or violet in color the corresponding complexes of Ag^{++} are orange or yellow.[15]

This discussion of bond type enables us to amplify the conclusions of a previous paper. The bonding in "covalent" complexes is not essentially different from that in "ionic" ones in the way which the term suggests. If the terms are to be retained a complex such as $[Co(NH_3)_6]^{+++}$ is to be regarded as covalent because two d-orbitals are available for bond formation in the valence state of the Co^{+++} ion. On the other hand the isoelectronic complex $[Fe(NH_3)_6]^{++}$ is ionic because the $3d$-orbitals are used in forming three electron bonds. This would provide a good reason for regarding Cr^{+++} complexes as covalent, although the magnetic criterion of bond type is not applicable, since two $3d$-orbitals are available for bond formation.

If we restrict our attention to a single metal ion it is usually true that the bonding in complexes with low spin multiplicity is more covalent, in the conventional sense, than that in complexes with high spin multiplicity. This is not necessarily the case since double bonding has the same effect as increased covalent bonding and so may confuse the picture, e.g., in the complexes formed by heterocyclic amines such as o-phenanthroline.

APPENDIX

In the course of this work a set of values for the Slater-Condon parameters for various transition-metal atoms and ions was prepared. As they are of considerable interest both in calculations of the type given in this paper and in other calculations on the valence-states of transition-metals[16] they are presented in Table IV.

TABLE IV. Values of Slater-Condon parameters F_2 and F_4. The number of $4s$ electrons is not indicated.

	Sc I	Sc II	Ti I	Ti II	Ti III	V I	V II	V III	V IV
d^2F_2	660	740	900	(1000)	1100				1440
F_4	45	55	65	(75)	80				100
d^3F_2			(760)	(845)		1055	1100	1170	
F_4			(55)	(55)		80	80	85	
d^4F_2						900	880		
F_4									

	Cr I	Cr II	Cr III	Cr IV	Mn I	Mn II	Mn III	Mn IV
d^3F_2			1290	(1580)				
F_4			110	(110)				
d^4F_2	1300	1350	1350					1665
F_4	80	85	85					105
d^5F_2	1000	1075			1340	1390	1435	
F_4	65	70			90	90	95	
d^6F_2						(980)		
F_4						(95)		

	Fe I	Fe II	Fe III	Co I	Co III	Ni I	Ni II	Ni III
d^5F_2			1700					
F_4			110					
d^6F_2	1430	1480	1540		1760			
F_4	105	115	120		140			
d^7F_2	1250	1270		1440	1 600			
F_4	105	105		120	120			
d^8F_2				1230		1500	1600	(1560)
F_4				100		110	110	(110)

	Cu II	Cu III
d^8F_2	1800	1800
F_4	120	120

The empirical data[17] were fitted by trial and error. Considerable use was made of the energy level diagrams given by Laporte and Platt.[18] The present values agree quite well with those obtained in more detailed studies,[19,20] where such a check is possible.

[14] W. Kuhn and K. Bein, Z. anorg. Chem. **216**, 321 (1936).
[15] N. V. Sidgewick, *The Chemical Elements and their Compounds* (Oxford University Press, London, 1911).
[16] J. Dunitz and L. E. Orgel, J. Chem. Phys. **23**, 954 (1955).
[17] *Atomic Energy Levels* (National Bureau of Standards, Washington, D. C., 1949, 1952), p. 467.
[18] O. Laporte and J. Platt, Phys. Rev. **61**, 305 (1942).
[19] A. Many, Phys. Rev. **70**, 511 (1946).
[20] A. A. Schweizer, Phys. Rev. **80**, 1080 (1950).

Band Widths in the Spectra of Manganous and Other Transition-Metal Complexes

L. E. ORGEL*
Gates and Crellin Laboratories of Chemistry, California Institute of Technology, Pasadena, California
(Received January 24, 1955)

The spectrum of the hydrated manganous ion is interpreted in detail and the factors influencing the widths of the bands are deduced. The band widths in other transition-metal spectra are shown to be explicable in the same way.

IN a previous paper we have calculated the energy level diagram for the manganous ion as a function of the cubic field parameter Dq.[1] Very recently a detailed study of the weak visible and ultraviolet absorption bands of the hydrated manganous ion has been reported by Jorgensen, who shows that six bands are present below 30 000 cm^{-1}.[2] The calculated energy level scheme enables us to identify these bands with some certainty and hence to discern the factors influencing their widths. These factors are found to account also for the widths of the absorption bands of many other transition metal complexes.

SPECTRUM OF HYDRATED MANGANOUS IONS

The weak absorption bands of the hydrated manganous ion may be correlated with the energy levels of the ion in a cubic field in the following way:

ν in cm^{-1}	Level classification
18 800	$^4G(T_{1g})$
23 000	$^4G(T_{2g})$
24 900	$^4G(A_{1g})$
25 150	$^4G(E_g)$
28 000	$^4D(T_{2g})$
29 700	$^4D(E_g)$

where e.g., $^4D(E_g)$ stands for the level of E_g symmetry which goes over, adiabatically, to the ^4D state of the free ion when the cubic field is decreased to zero. This identification is based on the following facts. The $^4G(A_{1g})$ and $^4G(E_g)$ states were calculated to be accidentally degenerate and to occur at a distance above the ground state equal to the $^6S-{}^4G$ separation of the free ion, i.e., at about 26 800 cm^{-1}.[3] There is only one pair of bands which are very close together, namely those at 24 900 cm^{-1} and 25 150 cm^{-1}. If we identify these as the A_{1g} and E_g states or vice versa, then we must make a corresponding correction by subtracting 1800 cm^{-1} from all other ^4G levels measured on Fig. 6 of reference 1. Further maxima are then predicted at 18 800 cm^{-1} and 23 200 cm^{-1}, if we take $Dq=790$ cm^{-1}. By a similar argument if we assume that the band at 29 700 cm^{-1} is the $^4D(E_g)$ level, which is not affected by the cubic field, we predict a second transition at 28 000 cm^{-1}, using the same value of Dq as for the ^4G levels. The ^4D level of the free ion is at 32 300 cm^{-1} so we have had to apply a correction of 2600 cm^{-1} in this case. If for the ^4P level, which lies between the ^4D and ^4G states in the free ion, we interpolate a correction of 2200 cm^{-1} we then predict that the $^4P(T_{1g})$ level is at 32 600 cm^{-1}.

Confirmation of this analysis is based on the crystal spectra measured by Gielesen.[4] The bands of $MnCl_2$, $4H_2O$ at 27 350 cm^{-1} and 29 115 cm^{-1} clearly correspond to the bands in solution at 28 000 cm^{-1} and 29 700 cm^{-1}. It seems then that the band at 31 550 cm^{-1} in the solid would correspond to one at 32 150 cm^{-1} in solution, which is in good agreement with the predicted band at 32 600 cm^{-1}.

The calculated energy level diagram then shows a large gap before a series of three levels, beginning at 44 000 cm^{-1}. In the crystal there is such a gap, but it terminates at 39 500 cm^{-1}, so that even if we allow 1000 cm^{-1} for the blue shift which occurs in going from $MnCl_2\cdot 4H_2O$ to the aqueous solution there is still a discrepancy of 3500 cm^{-1} between the position of the $^4F(A_{2g})$ level, which is unaffected by the crystal field, and the corresponding level of the free ion.

Despite the discrepancies noted above we feel sufficiently confident of the qualitative correctness of our assignments to draw certain conclusions from the quantitative disagreements. The ^4G, ^4D, and ^4F levels of the manganous ion in aqueous solution are apparently 25 000 cm^{-1}, 29 700 cm^{-1}, and 40 500 cm^{-1}, respectively, above the ^6S state, compared with corresponding values of 26 800 cm^{-1}, 32 300 cm^{-1}, and 43 600 cm^{-1} in the free ion. This, we believe, provides definite evidence on "the equivalent state of ionization," of the manganous ion, for, as we have shown,[1] the separations between the states of the d^5 configuration should decrease slightly as the $4s$ and $4p$ orbitals and to a lesser extent the $3d$ orbitals[5] become filled with electrons from the ligands. The observed separations are a little less than those for the $3d^54s^2$ configuration of the free atom, which suggests that two, or perhaps slightly more, electrons are in fourth quantum shell orbitals. This is in accordance with our interpretation of certain less definite evidence from other transition-metal spectra e.g., that of

* Arthur A. Noyes Fellow, 1954.
[1] L. E. Orgel, J. Chem. Phys. **23**, 1819 (1955), preceding paper.
[2] C. K. Jorgensen, Acta Chem. Scand. **8**, 1502 (1954).
[3] *Atomic Energy Levels* (National Bureau of Standards, Washington, D. C., 1949, 1952), p. 467.
[4] G. Gielesen, Ann. Physik, Series 5, **22**, 537 (1935).
[5] L. E. Orgel, J. Chem. Phys. **23**, 1058(L) (1955).

$[V(H_2O)_6]^{+++}$, and with Pauling's conclusions which are based on considerations of a quite different kind.[6] A second factor that may be important is the reduction in the size of the repulsions between the d-electrons due to their being spread out over the ligands, through σ or even π bonding.

BAND WIDTHS IN SOLUTIONS OF TRANSITION-METAL COMPLEXES

The order of increasing band width in the spectrum of the hydrated manganous ion is[2]:

$$^4G(A_{1g}) \approx {}^4G(E_g) < {}^4D(E_g) < {}^4D(T_{2g}) < {}^4G(T_{2g}) < {}^4G(T_{1g}).$$

This is also the order of increasing slope of the plots of the energies of these levels against the cubic field parameter at the appropriate Dq value of 780 cm^{-1}. There are two, closely connected, qualitative factors which account for this correlation.

The radius of a transition metal ion is dependent on the distribution of its electrons between the t_{2g} and e_g d-orbitals.[7] It is not difficult to see that, for any state, the numbers of electrons in the two orbitals are related to the slope of the energy level curve at the appropriate Dq value as follows

$$dE/d(Dq) = 4n_1 - 6n_2,$$

where n_1 and n_2 are the numbers of electrons in the t_{2g} and e_g orbitals, respectively.[2] It follows that in transitions between states with different slopes the distribution of electrons is changed and so, therefore, is the equilibrium metal-ligand distance. The ground-state is usually close to its equilibrium configuration, so that, in accordance with the Franck-Condon principle, transitions take place to a variety of vibrational levels of the excited state. If these are sufficient in number, and if the change of configuration is great, the spectrum may appear as a broad continuum, otherwise a broad band with some fine structure may be observed.

In solution, and to a lesser extent in crystals at high temperatures, there will be small fluctuations in the configuration of the complex due to thermal excitation. The measured spectrum is in fact an average taken over the spectra of the different thermally accessible configurations, each weighted according to the Boltzmann distribution. Any band will be broadened to the extent that the energy $h\nu$ of the transition is sensitive to small changes of configuration and, to a first approximation, this may be equated to $d(h\nu)/d(Dq)$. A similar qualitative relationship has been suggested by Bjerrum *et al.*[8]

We have seen that each of these factors leads to a monotonic increase in the widths of the different bands of a given complex with $d(h\nu)/d(Dq)$. The ground state of the manganous ion is not affected by the cubic field and so the widths of the bands are proportional to the slopes of the excited state levels. This conclusion is confirmed by the spectra of a number of such complexes with configurations other than d^5, and to a lesser extent by that of the ferric ion.[2]

The strong field approximation may be used to identify the two strongest transitions of the chromic ion as quartet-quartet transitions between the $(t_{2g})^3$ and $(t_{2g})^2(e_g)$ configurations.[9] For both of these transitions $d(h\nu)/d(Dq) = 10$ and so we expect two bands with similar, quite large widths. Accurate calculations show that for $Dq = 1770$ cm^{-1} the correct values are 10 and 11.8. The lowest quartet-doublet transitions, identified by Finkelstein and Van Vleck,[10] are essentially with the $(t_{2g})^3$ configuration and so that we would expect narrow bands. The visible bands of $[Cr(H_2O)_6]^{+++}$ at 5800 A and 4100 A have half-widths of 1625 cm^{-1} and 2150 cm^{-1} respectively, and are not resolved in the crystal.[11] The weak forbidden bands are very narrow, and are comparable to those of rare-earth complexes.[2,12]

The spin-allowed bands of trivalent cobalt complexes resemble closely those of chromium, but this similarity does not extent to the spin-forbidden bands. In cobaltic complexes all of the four lowest transitions are between the $(t_{2g})^6$ and $(t_{2g})^5(e_g)$ configurations and so have $d(h\nu)/d(Dq) = 10$. In agreement with this the spin-allowed transitions have half-widths of 1750 cm^{-1} and 1950 cm^{-1}, while the observed spin-forbidden transition is of comparable width.[2]

The d^1 and d^9 configurations give rise to only one transition in octahedral complexes, for which $d(h\nu)/d(Dq) = 10$. No example of fine structure has been reported in the spectra of these complexes. The greater than usual width of the bands in the hydrated cupric ion supports the proposed distorted octahedral structure,[8,9] since the two loosely held water molecules are important in determining the level of the *excited* state. Also the equilibrium configuration of at least one of the excited states is quite different from that of the ground state, for a different pair of water molecules must be loosely held.

The energy level diagram for the nickelous ion leads us to expect that all of the triplet-triplet transitions will be broad, the ratio of the half-widths depending a little on the Dq value. The triplet-singlet transitions should include two sharp ones to the $^1D(^1E_{1g})$ and $^1G(^1A_{1g})$ states and a variety of others with different band widths. In qualitative agreement with this the triplet-triplet transitions are without fine structure both in the crystal and in solution, while there are many

[6] L. Pauling, *The Nature of the Chemical Bond* (Cornell University Press, Ithaca, New York, 1948).
[7] J. H. Van Santen and J. S. van Wieringen, Rec. trav. chim. **71**, 420 (1952).
[8] Bjerrum, Ballhausen, and Jorgensen, Acta Chem. Scand. **8**, 1275 (1954).
[9] L. E. Orgel, J. Chem. Soc. 4756 (1952).
[10] R. Finkelstein and J. H. Van Vleck, J. Chem. Phys. **8**, 790 (1940).
[11] C. K. Jorgensen, Acta Chem. Scand. **8**, 1495 (1954).
[12] O. Deutschbein, Ann. Physik [5] **14**, 712 (1932).

very weak sharp lines in the crystal. The best quantitative comparison is for $[Ni(Ethylenediamine)_3]^{++}$ for which the allowed bands, in order of increasing frequency, have half-widths of 1500 cm^{-1}, 1650 cm^{-1}, and 1800 cm^{-1}.[2] The calculated values of $d(h\nu)/d(Dq)$ are 10, 14.38, and 15.62, respectively, for $Dq=1120$ cm^{-1} in reasonable agreement with experiment. The weak bands of the hydrated nickel ion have not been identified with certainty, but they are not incompatible with the theory. By choosing complexes in which the weak bands fall clear of the stronger continuous bands it may be possible to check the prediction more rigorously.

For the other transition-metal ions the experimental data, and for the d^6 configuration the theory, are less complete. Weak sharp bands are expected for all complexes with between two and eight d-electrons and having maximum spin multiplicity. Of the covalent complexes with four, five, and six d-electrons only the first should have such transitions. Similarly planar complexes with eight d-electrons should have only broad bands. The spin-allowed transitions should all be more or less broad as may be seen from the energy level diagrams.[1] The experimental evidence does not contradict these findings, but the comparison is not very extensive in most cases.

DISCUSSION

We have shown that the band width for transition-metal complexes is determined by $d(h\nu)/d(Dq)$ and not by the behavior of individual energy levels. The paradox of the occurrence of very sharp and very broad bands in the same spectrum is thus resolved. The usual statement that the d-electrons of transition metals are less shielded than, say, the $4f$-electrons of the rare earths is justified by the fact that $dE/d(Dq)$ for an individual level may be so large that the thermal motion of the ligands can appreciably affect the d-electron energies.

A similar discussion should apply to solutions of rare-earth complexes, but here the band widths would, of course, be an order of magnitude smaller. This possibility is being investigated.

It is possible that the study of band widths in solution will provide useful information about the deformability of complexes and may also help in making spectroscopic assignments.

ACKNOWLEDGMENTS

The author is particularly grateful to Professor J. Bjerrum and to Dr. C. Jorgensen and Dr. C. J. Ballhausen for communicating manuscripts on related topics prior to their publication.

THE JOURNAL OF CHEMICAL PHYSICS VOLUME 23, NUMBER 10 OCTOBER, 1955

Prediction of Madelung Constants

DAVID H. TEMPLETON
Department of Chemistry, and Radiation Laboratory, University of California, Berkeley, California, and Institute of Chemistry, University of Uppsala, Uppsala, Sweden

(Received January 4, 1955)

Madelung constants of both simple and complex salts can be reduced to a common scale by taking the nearest-neighbor distance as the unit distance and then dividing by half the sum of the squares of the charges of all the atoms in the stoichiometric unit. These "reduced Madelung constants," α, can be predicted within a few percent by the relation $\alpha=1.89-1/m$, where m is the harmonic mean coordination number. Madelung constants have been calculated for LaOCl, YOF, ReO_3, and several perovskite structures for comparison with the predictions.

IN a previous note[1] it was shown that for binary salts one can predict the Madelung constant with some success from an empirical correlation with the coordination numbers. This treatment has now been generalized so that it applies to structures containing more than two kinds of ions.

The "reduced Madelung constant" α was defined[2] as

$$\alpha=-2A(R_0)/z_a z_c n, \tag{1}$$

where $A(R_0)$ is the Madelung constant with the nearest-neighbor distance R_0 taken as the unit distance, z_a and z_c are anion and cation charge numbers, and n is the number of atoms in the stoichiometric unit or "molecule." To permit application to more complex structures, the reduced Madelung constant is now defined as

$$\alpha=2A(R_0)/\Sigma z^2. \tag{2}$$

The summation in Eq. (2) includes the n atoms. It can be shown from charge neutrality that for binary salts $-z_a z_c n=\Sigma z^2$, so that in this case definitions (1) and (2) are equivalent.

It was shown previously that α can be represented by the empirical equation

$$\alpha=1.89-1.00/m, \tag{3}$$

where m is the weighted harmonic mean of the co-

[1] D. H. Templeton, J. Chem. Phys. **21**, 2097 (1953).
[2] A negative sign has been introduced because now z_a is taken as negative.

ordination numbers, with an average accuracy of better than 1% for a dozen cases of binary structures. The predictions of the more general formulation are now compared with calculations for 19 ternary structures.

TERNARY SALTS WITH EQUAL DISTANCES

When the nearest neighbors of the various ions are at the same distance, the predictions of Eq. (3) are in reasonably good agreement with calculated values of the reduced Madelung constants. For seven cases listed in Table I, the discrepancy averages less than two percent. The sources of the data are as follows.

Spinels:—Madelung constants have been reported for various spinel-type structures by Verway, de Boer, and van Santen[3,4] as a function of the anion parameter u. In this structure, when $u=0.3875$, the nearest-neighbor distances are $0.23816a$ for both the tetrahedral and the octahedral cation sites. The values listed for the inverse structures are for the ordered arrangement.[4] The value of m is 4.42.

Oxyfluorides:—Yttrium oxyfluoride and several similar compounds have the fluorite-type structure with oxygen and fluorine distributed among the anion positions in certain ways. Zachariasen[5] describes the atomic positions for a rhombohedral form and a tetragonal form. Each structure is distorted slightly from the ideal fluorite type, and the nearest-neighbor distances are not quite equal for oxygen and fluorine. However, the constants listed in Table I are calculated for the undistorted structures. The calculations were made by Bertaut's method[6] with correction for series termination.[7] By calculation of the difference between A for YOF and 9/4 A for CaF_2, it was possible to obtain accuracy of one part in 10 000 with $\beta=1.5\pi$.

In the rhombohedral and tetragonal oxyfluorides the anions of one kind occur in layers, so that each has three or four, respectively, nearest anion neighbors of the same kind. It is obvious that the Madelung constant would be greater if the anions were distributed according to the NaCl structure among the anion sites so that oxygen and fluorine atoms alternate. This cubic arrangement (space group $T_d^2-F\bar{4}3m$)

4Y in: 0,0,0; 0,1/2,1/2; 1/2,0,1/2; 1/2,1/2,0

4O in: 1/4,1/4,1/4; 1/4,3/4,3/4; 3/4,1/4,3/4; 3/4,3/4,1/4

4F in: 3/4,3/4,3/4; 3/4,1/4,1/4; 1/4,3/4,1/4; 1/4,1/4,3/4

probably has the largest Madelung constant possible for structures of this type. Because of the symmetry, no distortion is to be expected. The Madelung constant is easily evaluated by the equation:

$$4A\,(\mathrm{YOF})=9A\,(\mathrm{ZnS})-8A\,(\mathrm{NaCl}), \qquad (4)$$

where the Madelung constants of YOF, cubic ZnS, and NaCl all have the cell edge as scale factor. This relation was found by comparison of the terms entering the Madelung sum, and checked by showing that the squares of the respective structure factor equations fit the same relation. It has been pointed out by Bertaut[8] that the latter condition, together with his expression for the computation of the Madelung constant,[6] is sufficient to prove such expressions. This "NaCl" structure has not been observed to occur, but it should be pointed out that its diffraction intensities would be so similar to those for a structure with random anion distribution that in practice it is imposible to distinguish them. The distortions and relative crystal energies of these various oxyfluoride structures will be discussed in a paper now in preparation. For these crystals, $m=4.80$.

TABLE I. Madelung constants for ternary compounds with equal nearest-neighbor distances.

Structure	A	alpha calculated	alpha predicted
Spinel[a]			
4–2 normal	132.6[b]	1.579	1.66
4–2 inverse	139.2	1.652	1.66
2–3 normal	135.2	1.695	1.66
2–3 inverse	132.3	1.658	1.66
YOF			
tetragonal[c]	11.504[d]	1.6435	1.68
rhombohedral[c]	11.526	1.6466	1.68
cubic[c]	11.7156	1.6737	1.68

[a] $u=0.3875$.
[b] Unit length $=a$.
[c] Undistorted "ideal" structure.
[d] Unit length $=(\sqrt{3}/4)a$.
[e] Hypothetical structure described in text.

TABLE II. Madelung constants for salts with two nearest neighbor distances.

Structure	A[a]	α	α_m	α(predicted)
Spinel				
4–2 normal	138.1	1.495	1.63	1.66
4–2 inverse	132.6	1.435	1.59	1.66
2–3 normal	128.6	1.465	1.64	1.66
2–3 inverse	131.7	1.501	1.72	1.66
LaOCl	18.75	1.560	1.72	1.70
Perovskite				
1–5 normal	58.53535	1.540	1.68	1.74
1–2 normal	12.37744	1.547	1.81	1.74
3–3 normal	44.55489	1.485	1.85	1.74
1–2 inverse	10.91768	1.365	1.79	1.74
1–5 inverse	46.85727	1.233	1.68	1.74
K_2PtCl_6	63.49026	1.323	1.55	1.72
$(NH_4)_3AlF_6$	53.00488	1.472	1.73	1.74

[a] Unit length $=a$.

[3] Verway, de Boer, and van Santen, J. Chem. Phys. **16**, 1091 (1948).
[4] de Boer, van Santen, and Verway, J. Chem. Phys. **18**, 1032 (1950).
[5] W. H. Zachariasen, Acta Cryst. **4**, 231 (1951).
[6] F. Bertaut, J. phys. radium **13**, 499 (1952).
[7] D. H. Templeton, J. Chem. Phys. **23**, 1629 (1955).
[8] F. Bertaut, Compt. rend. **239**, 234 (1954).

SALTS WITH TWO DISTANCES

When the nearest neighbors of different atoms are at different distances, one can expect α to be less than the value predicted by Eq. (3). The prediction will correspond more closely to α_m, defined as

$$\alpha_m=\alpha R_m/R_0, \tag{5}$$

where R_m is some kind of average nearest-neighbor distance. Inspection of the leading terms in the Madelung series suggests that one take the harmonic mean of the distances, weighted according to their frequency in the structure and according to the product of the charges of the ions involved. This is equivalent to defining R_m in terms of an average leading term in the series. The results of this procedure for a few cases are presented in Table II. The accuracy of the predictions leaves something to be desired, but no other averaging scheme has been found to be any better. In twelve cases the average accuracy of the predictions is 3.5%, and the worst case is off by 10%. The sources of data are as follows:

Spinels:—The calculations of Verway, de Boer, and van Santen[3,4] for spinels extend down to a parameter value of 0.375 at which the anions are in perfect close packing. The octahedral and tetrahedral distances are, respectively, $a/4$ and $\sqrt{3}a/8$, with ratio 1.155.

Lanthanum oxychloride:—The Madelung constant of LaOCl has been calculated independently by Mrs. Carol Dauben, and by the author, using Bertaut's method[6] corrected[7] for $\beta=3\pi$. The unit cell dimensions and atomic parameters used were:[9]

$$a=4.119\text{ A}$$
$$c=6.883\text{ A}$$
$$u=0.179$$
$$v=0.639.$$

For these parameters the La—O distance is 2.400 A and the La—Cl distances, which are very nearly equal, average 3.170 A. The distance ratio is 1.321, and m is 5.35.

Perovskites:—The cubic perovskite structure can be described as ABX_3 with the following atomic positions:

A at: 0,0,0

B at: 1/2,1/2,1/2

$3X$ at: 0,1/2,1/2; 1/2,0,1/2; 1/2,1/2,0.

Sherman,[10] in his review, lists the Madelung constant for the case with charge numbers +1, +2, and −1, respectively, for A, B, and X. This type will be referred to as the 1–2 type. If the cation charges are interchanged, it is called the 2–1 type. In an analogous way one can define 1–5, 5–1, and 3–3 types (in which X has charge −2). It is easy to show, by Bertaut's method, that the following identities are true:

$$A(1\text{–}5)=4A(1\text{–}2)+A(\text{CsCl})+2A(\text{NaCl}) \tag{6}$$
$$A(5\text{–}1)=4A(1\text{–}2)+9A(\text{CsCl})-6A(\text{NaCl}) \tag{7}$$
$$A(2\text{–}1)=A(1\text{–}2)+A(\text{CsCl})-A(\text{NaCl}) \tag{8}$$
$$A(3\text{–}3)=4A(1\text{–}2)+A(\text{CsCl})-2A(\text{NaCl}). \tag{9}$$

Here each Madelung constant must have the same scale factor, for example the edge of the unit cell. The nearest neighbors of the A and B atoms are at distances $\sqrt{2}a/2$ and $a/2$, respectively, with ratio 1.414, and m is 6.67.

The ReO_3 structure can be considered as a 0–6 type perovskite, and its Madelung constant is given by the identity:

$$A(\text{ReO}_3)=4A(1\text{–}2)+4A(\text{CsCl})+4A(\text{NaCl}). \tag{10}$$

The resulting reduced Madelung constant $\alpha=1.49233$ is in good agreement with 1.47 predicted by Eq. (3) for $m=2.40$.

Potassium chloroplatinate and ammonium fluoroaluminate:—Sherman[10] has reported Madelung constants for K_2PtCl_6 and $(NH_4)_3AlF_6$ for structures with the anion parameters equal to 0.25. These were checked to six or seven figures by the identities:

$$A(\text{K}_2\text{PtCl}_6)=4A(1\text{–}2)+4A(\text{NaCl}) \tag{11}$$
$$A((\text{NH}_4)_3\text{AlF}_6)=4A(1\text{–}2)+A(\text{NaCl}) \tag{12}$$

where (1–2) again represents the $KMgF_3$ type perovskite. These can be derived by Bertaut's method if one considers a perovskite with cell dimension half as large as those of the other crystals. In these structures the distance ratio is 1.414 like the perovskites, to which they are closely related, and m is 5.87 and 6.67 respectively.

THEORETICAL JUSTIFICATION

The recipe contained in Eq. (2) was first derived quite empirically and on the basis of considerably less data than are presented here. I am indebted to Dr. Bertaut for suggesting that his theory might give it a theoretical basis.

In the notation of a previous paper[7] one can write, if $R=R_0/2$ and if s is substituted for α to avoid confusion,

$$A(R_0)=\frac{6}{5Z}\Sigma z^2-\frac{36\pi R^3}{ZV}\Sigma|F|^2\frac{(\sin s-s\cos s)^2}{s^8}. \tag{13}$$

Since the average value of $|F|^2$ is Σz^2, $A(R_0)$ can be approximated:[7]

$$A(R_0)=\frac{6}{5Z}\Sigma z^2-\frac{18\Sigma z^2}{\pi Z}\int_\gamma^\infty\frac{(\sin s-s\cos s)^2}{s^6}ds, \tag{14}$$

if a proper value of γ can be determined. The integra-

[9] L. G. Sillén and A. L. Nylander, Svensk Kem. Tidskr. **53**, 367 (1941); W. H. Zachariasen, Acta Cryst. **2**, 388 (1949); D. H. Templeton and C. H. Dauben, J. Am. Chem. Soc. **75**, 6069 (1953).

[10] J. Sherman, Chem. Revs. **11**, 93 (1932).

tion limit γ is roughly the value of $2\pi hR$ at which the first large values of $|F|^2$ appear in the series in Eq. (13). A large value of $|F|^2$ is possible only if the positive and negative ions are in positions separated by about half an interplanar spacing, so that they contribute to the structure factor with a phase difference of π. This can be true only if $1/h$ is less than or of the order of $2R_0$ or $4R$. Thus γ is of the order of $\pi/2$, and Eq. (14) can be written:

$$2A(R_0)(\Sigma z^2/Z)^{-1}=2.4-\frac{36}{\pi}\int_{\pi/2}^{\infty}\frac{(\sin s-s\cos s)^2}{s^6}ds. \quad (15)$$

The left member of Eq. (15) is identical with the reduced Madelung constant as defined in Eq. (2), since the sum in Eq. (15) is taken over Z times as many atoms as the sum in Eq. (2). The integral in Eq. (15) has been evaluated elsewhere.[7] Thus,

$$\alpha=2.4-4(0.1727)=1.71. \quad (16)$$

The form of Eq. (15) justifies Σz^2 as the correct normalization factor for removing the dependence of the Madelung constant on the charge numbers and formula type of the crystal, and it lends plausibility to the similarity in values for α for very diverse structures. The numerical result of Eq. (16) is to be compared with actual values which lie mostly between 1.48 and 1.76.

DISCUSSION

It cannot be expected that Eq. (3) will yield accurate predictions for any structure whatever. Rather it represents approximately the largest value which is possible for a given coordination number. If a substance is a salt, it can be stable only in structures with Madelung constants not too far below the largest one possible, since the crystal energy is determined principally by the electrostatic potentials. Metallic alloys give examples of structures which are not stable for salts. An extreme case is that of NaTl, for which Hoppe[11] has derived the Madelung constant, which is the same as that of NaCl when the scale distance in each case is the unit cell edge. However, α is 13% less than for NaCl because of the shorter nearest-neighbor distance. For NaTl, $\alpha=1.51$, compared with 1.64 predicted for coordination four, or 1.76 for coordination eight. In this structure each atom has four nearest neighbors of the same kind as well as four nearest neighbors of the other kind, all at the same distance. Thus, the leading terms in the Madelung series cancel. It is obvious that such a structure will be very unstable for a salt with respect to such structures as the NaCl, CsCl, and ZnS types. To exclude such cases the predictions should be restricted to true salts.

The examples cited in Tables I and II are all the ternary structures for which data could be found.[12] There is serious doubt that platinum or its analog actually has a charge of +4 in K_2PtCl_6 or any of its isomorphs, and several of the spinel and perovskite structures listed in the tables may not exist in actual crystals. Thus, the record of the predictions is not quite as bad as Tables I and II might indicate.

However, Table I brings attention to one factor which has not been considered. In two structures which differ by the interchange of cations between sites of different coordination number but equal neighbor distance, such as the normal and inverted spinels, the structure with high charge in the high coordination has the greater Madelung constant. A more complicated formulation which took this effect into account presumably would be more successful, but it does not seem justified with the present data. Moreover, the chief value of the prediction method lies in its simplicity as a quick rule of thumb for rough estimates and for detection of errors.

This research was made possible by a John Simon Guggenheim Memorial Fellowship which permitted my stay in Sweden and my very helpful conversations with Dr. Bertaut in Paris. I thank Professor G. Hägg for his hospitality in providing me with the facilities of the Institute of Chemistry at the University of Uppsala. I am indebted to Mrs. Carol Dauben for checking many of the calculations and for assistance with the manuscript. The completion of this work was supported by the U. S. Atomic Energy Commission.

[11] R. Hoppe, Angew. Chem. **65**, 324 (1953).

[12] Note added February 15, 1955: From the data of C. Delorme and F. Bertaut (J. phys. radium **14**, 129 (1953)) one can derive $\alpha_m=1.66$ compared with α(predicted)$=1.60$ for $Fe^{+++}Cu^{+}O_2^{---}$.

Absorption Spectra of Luminescent Thallous Chloride Solutions*

ALLEN B. SCOTT AND KUO-HAO HU
Department of Chemistry, Oregon State College, Corvallis, Oregon

(Received January 19, 1955)

The absorption spectra of solutions of KCl, made luminescent by the addition of TlCl, have been analyzed with the assistance of dissociation constants for TlCl and $TlCl_2^-$ obtained from solubility measurements. Absorptivities for each of the absorbing species have been found at several wavelengths. Spectra of solutions having a wide variety of KCl and TlCl concentrations were calculated from the absorptivities and dissociation constants; these agree quite well with the observed spectra except at high Cl^- concentration, where the disagreement is ascribed to the formation of more highly coordinated complexes. Decrease of dielectric constant of the solvent shifts the absorption band in the direction to be expected from an increase in the stability of molecular TlCl and the complex ions.

INTRODUCTION

THE ultraviolet absorption spectra of solutions of alkali halides, made luminescent by the addition of a small amount of a heavy metal halide, have been found to be remarkably similar to the spectra of the corresponding solid phosphors. Fromherz and Lih,[1] for example, found that a solution 3.9 M with respect to KCl and 0.00053 M with respect to TlCl had a distinct absorption band with a maximum at 240.2 mμ, while solid KCl containing a small amount of TlCl has an absorption maximum at 247.5 mμ.[2] The solid has an additional band with a maximum at 195 mμ which cannot be observed in the solutions. The variation in the absorption spectrum of the solution with concentration was explained in a qualitative way by Fromherz and Lih as being due to a variation in the relative concentrations of simple Tl^+ ions, uncharged TlCl molecules, and complex ions such as $TlCl_3^-$. Unfortunately the data were insufficient to allow a calculation of the formulas of complexes or of their dissociation constants.

Pringsheim and Vogels[3] confirmed their results and also observed the variation of luminescent intensity with added Cl^- concentration in TlCl solutions, which indicated that the luminescence as well as the absorption is due to complexion formation. Hilsch[4] reviewed the evidence that luminescence and absorption in the solid phosphors are also due to "complex centers."

Recently the formulas and dissociation constants of thallous complexes in chloride solutions have been obtained from solubility data.[5] This information greatly simplifies the interpretation of the absorption spectra of solutions. From the dissociation constants, the concentrations of each of the absorbing species can be calculated in a given solution; from the observed spectra of solutions of several concentrations, the molar absorptivity for each species can be obtained at suitable wavelengths. As a test not only of the correctness of the absorptivities, but also of the validity of the formulas and dissociation constants provided by the solubility experiments, the absorption spectrum may then be computed for a solution of any desired concentration of alkali chloride and thallous chloride and compared with the observed spectrum.

This report describes the systematic study of KCl solutions containing small amounts of TlCl. The effect of variation of solvent composition upon the absorption spectrum is also reported. The results presented here should be of considerable use in the analysis of the fluorescence of such solutions, now being undertaken in this laboratory, which should in turn have an important bearing upon the problem of the solid phosphor.

EXPERIMENTAL RESULTS

Measurements of absorption were made by means of a Beckmann Model DU Spectrophotometer, using a hydrogen-lamp source, at room temperature. Salts were analytical grade, purified by recrystallization. Nonaqueous solvents were cp grade. Distilled water, in a cell matching that used for the solutions, was used as a reference standard for all measurements, so that blank corrections were not required.

In Table I are listed the molal concentrations of KCl and TlCl in each of the aqueous solutions studied.

TABLE I. Concentration of aqueous solutions.

Series	Conc KCl, moles/kgH_2O	Conc TlCl, moles/kg$H_2O \times 10^4$
I	0.0	5.0, 10.0, 35.0, 71.0, 100
II	1.0	0.45, 2.5, 3.8, 5.0, 7.5, 10.0, 11.6, 24.0, 36.7, 47.6
III	2.0	0.50, 2.5, 5.0, 7.5, 10.0, 12.5, 25.0
IV	3.0	2.5, 5.0, 7.5, 10.0, 12.5
V	0.25, 0.50, 0.75, 1.0, 1.25, 1.50, 2.0, 2.5, 3.0, 4.0	5.0
V	0.1, 0.5, 1.0, 1.5, 2.0, 3.0, 4.0	0.0

* Supported by the Office of Ordnance Research, Published with the approval of the Oregon State College Monographs Committee, Research Paper No. 277. Department of Chemistry, School of Science.

[1] H. Fromherz and K. H. Lih, Z. physik Chem. **A153**, 321 (1931).
[2] R. Hilsch and R. Pohl, Z. physik **48**, 384 (1928).
[3] P. Pringsheim and H. Vogels, Physica **7**, 225 (1940).
[4] R. Hilsch, Proc. Phys. Soc. (London) **49** (extra part), 40 (1937).
[5] K. H. Hu and A. B. Scott, J. Am. Chem. Soc. (to be published).

Absorption spectra for a few examples of Series IV and V are shown by the unbroken curves of Fig. 1. The results are in general agreement with those of Fromherz and Lih,[1] although no attempt was made to duplicate exactly the solution compositions previously used.

ANALYSIS OF SPECTRA

Thallium may be present in the form of Tl^+, TlCl, or $TlCl_2^-$. Only in KCl solutions of concentration greater than 3.0 M are there indications of the presence of complex ions containing more than two chloride ions.[5] The dissociation constants are:

$$TlCl = Tl^+ + Cl^- \quad K_D = 0.26$$
$$TlCl_2^- = TlCl + Cl^- \quad K_2 = 1.7.$$

If the concentrations (in moles/liter) of $TlCl_2^-$, Tl^+, TlCl, and Cl^- are represented by w, x, y, and z, respectively, and the total concentration of thallium is represented by t, the concentrations of the species present are given by

$$w = \frac{zf_\pm^2 t}{zf_\pm^2\left(\frac{K_2}{z}+1\right)+\frac{K_D K_2}{z}}. \qquad (1)$$
$$y = \frac{K_2 w}{z}, \text{ and } x = t-w-y,$$

where $f_\pm$ is the mean ionic activity coefficient. For all solutions except Series I, $f_\pm$ was taken as that due to the KCl. Values of $f_\pm$ given by Harned[6] were used, interpolated where necessary, and corrected for use with volume concentrations.

The absorbance[7] per cm, A/b, for one of the solutions at any wavelength, λ, is given by

$$A/b = w\epsilon_w + x\epsilon_x + y\epsilon_y + z\epsilon_z. \qquad (2)$$

ϵ_z is the molar absorptivity for KCl, and the other ϵ's are respectively for $TlCl_2^-$, Tl^+, and TlCl. The equation is valid only when z may be taken to be the same as the KCl concentration, which is very nearly true in all the solutions except those of Series I.

TABLE II. Molar absorptivity.

	liter mole^{-1} cm^{-1}			
λ, mμ	$TlCl_2^-$ $\epsilon_w \times 10^3$	Tl^+ $\epsilon_x \times 10^3$	TlCl $\epsilon_y \times 10^3$	KCl ϵ_z
220	1.4	3.1	3.4	0.015
225	1.9	2.3	4.1	0.007
230	3.6	1.2	3.8	0.007
235	4.3	0.43	3.1	0.013
240	4.3	0.12	2.0	0.017
245	4.5	0.00	0.50	0.017
250	3.4	0.00	0.00	0.013
260	1.0	0.00	0.00	0.005
270	0.22	0.00	0.00	0.001

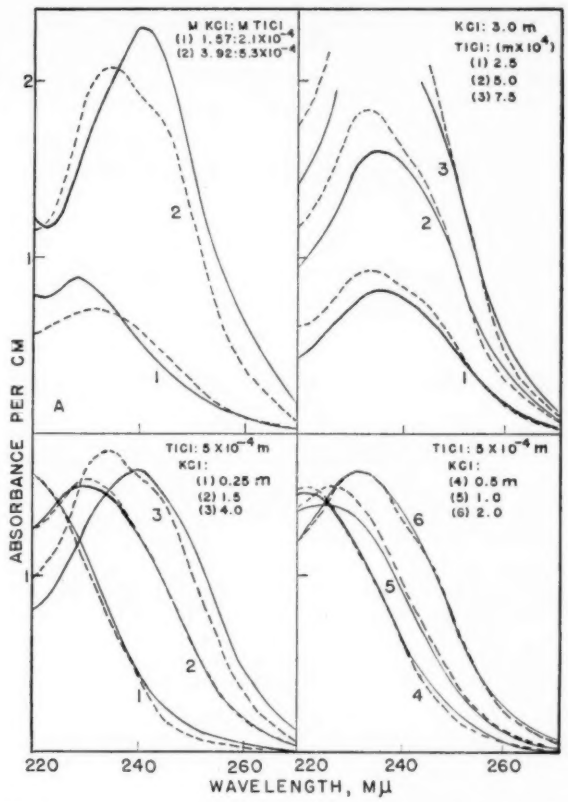

FIG. 1. Absorption spectra of KCl solutions containing KCl. Broken curves calculated. A: Observed data of Fromherz and Lih.

The above equations may be combined and rearranged to give

$$A/b + [w(1+K_2/z)-t]\epsilon_x - z\epsilon_z = w\left(\epsilon_w + \frac{K_2}{z}\epsilon_y\right). \qquad (3)$$

ϵ_x may be obtained from spectra of dilute solutions of TlCl, in which association is negligible. ϵ_z is very small in the spectral region of interest, but because z may be large, it is important to have a fairly reliable value. Since impurities in the KCl may contribute to its absorption, ϵ_z was computed from the absorption spectra of Series VI solutions, which were made up from the same stock of KCl as the others.

From Table II it may be seen that the KCl solutions exhibited a very low, broad absorption band, having a maximum absorbance at about 242 mμ, which may be due to impurities such as heavy metals or iron. The original KCl, before recrystallization, contained not more than 5×10^{-4}% heavy metals, estimated as Pb, and 3×10^{-4}% Fe: the combined concentration of these imputities in 1.0 M KCl was then less than 6×10^{-6} M. At the lowest TlCl concentration, 45×10^{-6} M, these impurities may have a significant effect upon the TlCl

[6] H. S. Harned, J. Am. Chem. Soc. **51**, 416 (1929).
[7] Definitions and symbols are those recommended by the Joint Committee on Nomenclature in Applied Spectroscopy, Anal. Chem. **24**, 1349 (1952).

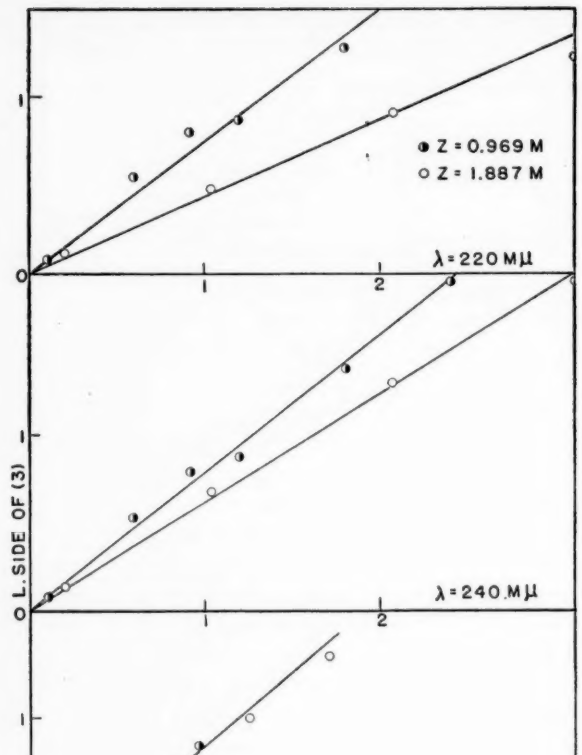

FIG. 2. Plot of left side of Eq. (3) against $TlCl_2^-$ concentration, moles liter^{-1}.

absorption curve; however the slopes of the curves of Fig. 2 were established principally by the data obtained at much higher TlCl concentration where the effect of impurities upon the absorbance of the TlCl should be negligible. The absorbance of the KCl, including impurities, given by the term $z\epsilon_z$, was not greater than 10% of the total absorbance even in the most dilute TlCl solutions at all wavelengths listed in Table II.

The left side of the equation was plotted against w for a series of solutions of constant z (e.g. Series II) using the experimentally determined A/b at a chosen λ. The slope, equal to $\epsilon_w+(K_2\epsilon_y/z)$ should be constant if the molar absorptivities do not vary with concentration. A new set of points, and new slope, may be obtained by choosing a different value of z (as in Series III). The two slopes determine two linear equations in ϵ_w and ϵ_y, each of which may then be found.

The advantage of this graphical method is that the data for several solutions may be averaged before solving the simultaneous equations, and further the linearity of the plots provides a good test of the constancy of the ϵ's and K's. Figure 2 shows a plot of the left side of Eq. (3) against $TlCl_2^-$ concentration for $z=0.969$ M (Series II) and $z=1.887$ M (Series III), at wavelengths of 220, 240, and 250 mμ. Similar plots were prepared for 225, 230, 235, 245, 260, and 270 mμ and the molar absorptivities, obtained as outlined above, are given in Table II.

Further evidence for the validity of Eq. (3) is provided by the fact that all the curves such as those of Fig. 2 passed through the origin.

The absorptivities were tested by calculating w, x, and y for solutions of Series IV and V from (1) and A/b at each of the λ's in Table II from (2). Examples of the absorption spectra so obtained are shown by the broken curves of Fig. 1; these are to be compared with the unbroken curves representing the observed spectra. Also shown are spectra calculated for two solutions studied by Fromherz and Lih, with their observed values.

In general, the deviation of the calculated from the observed absorbance is no greater than that to be expected from the error in estimating the slopes such as those of Fig. 2. At high Cl^- concentrations, however, the calculated absorptivities were always too large in the region 220–235 mμ and too small at higher wavelengths. This result substantiates the evidence, provided by solubility measurements,[5] that complex ions containing three or more chloride ions are present in concentrated KCl solutions, as it may reasonably be expected that the absorption maximum of $TlCl_3^-$, for instance, would lie at a longer wavelength than that of $TlCl_2^-$. The concentration of such complexes cannot be large, however, even in the most concentrated solutions studied here.

EFFECT OF SOLVENT

Any change of the solvent may be expected to affect the absorbance of the above solutions by at least three causes: (a) a change of number or type of solvent molecules coordinated with the absorbing species, (b) a change of dielectric constant in the vicinity of the absorbing species resulting in a shift of excited and ground states, and (c) a change in the concentrations of the various species occasioned by a change of dielectric constant. If the effect due to (c) predominates, we would expect a shift of the absorption band to higher wavelength with decreasing dielectric constant, as the stability of TlCl and $TlCl_2^-$ would be increased.

Absorption spectra for 1 M solutions of KCl, also

TABLE III. Effect of change in solvent on band maximum in 1 m KCl containing 0.0005 M TlCl.

Vol. % alcohol in aqueous solution	Wavelength of maximum absorption, mμ		
	CH_3OH	C_2H_5OH	C_3H_7OH
0	226	226	226
10	228	228	229
20	230	230	230
30	232	232	231
40	236	236	
50	237	238	

0.0005 M with respect to TlCl, but in which the solvent was water mixed with various proportions of methanol, ethanol, or propanol, were measured. In all cases the maximum of the absorption band was moved toward higher wavelength by increasing alcohol content of the solvent, as illustrated by Table III.

The dielectric constants of 50% CH_3OH solution and 50% C_2H_5OH solution are 60 and 53 respectively,[8] so that it is to be expected that the equilibrium concentrations of the ions and complexes in the two solutions would be about the same. This is borne out by the data of the table.

[8] Calculated from data given by International Critical Tables VI, 100.

THE JOURNAL OF CHEMICAL PHYSICS VOLUME 23, NUMBER 10 OCTOBER, 1955

Electronic Population Analysis on LCAO-MO Molecular Wave Functions.* I

R. S. MULLIKEN
Laboratory of Molecular Structure and Spectra, Department of Physics, The University of Chicago, Chicago 37, Illinois
(Received January 6, 1955)

With increasing availability of good all-electron LCAO MO (LCAO molecular orbital) wave functions for molecules, a systematic procedure for obtaining maximum insight from such data has become desirable. An analysis in quantitative form is given here in terms of breakdowns of the electronic population into partial and total "gross atomic populations," or into partial and total "net atomic populations" together with "overlap populations." "Gross atomic populations" distribute the electrons almost perfectly among the various AOs (atomic orbitals) of the various atoms in the molecule. From these numbers, a definite figure is obtained for the amount of promotion (e.g., from $2s$ to $2p$) in each atom; and also for the gross charge Q on each atom if the bonds are polar. The total overlap population for any pair of atoms in a molecule is in general made up of positive and negative contributions. If the total overlap population between two atoms is positive, they are bonded; if negative, they are antibonded.

Tables of gross atomic populations and overlap populations, also gross atomic charges Q, computed from SCF (self-consistent field) LCAO-MO data on CO and H_2O, are given. The amount of s-p promotion is found to be nearly the same for the O atom in CO and in H_2O (0.14 electron in CO and $0.15e$ in H_2O). For the C atom in CO it is $0.50e$. For the N atom in N_2 it is $0.26e$ according to calculations by Scherr. In spite of very strong polarity in the π bonds in CO, the σ and π overlap populations are very similar to those in N_2. In CO the total overlap population for the π electrons is about twice that for the σ electrons. The most easily ionized electrons of CO are in an MO such that its gross atomic population is 94% localized on the carbon atom; these electrons account for the (weak) electron donor properties of CO. A comparison between changes of bond lengths observed on removal of an electron from one or another MO of CO and H_2, and corresponding changes in computed overlap populations, shows good correlation. Several other points of interest are discussed.

1. INTRODUCTION

RECENT progress in the accurate determination of molecular electronic wave functions in the approximation of Roothaan's SCF LCAO-MO method[1] and related methods makes it desirable to examine the types of information which can be obtained from such wave functions. The values of various physical properties of molecules (e.g., dipole moments, quadrupole moments) can be computed fairly readily and with some degree of reliability once SCF-LCAO-MO wave functions are available, and a few such calculations are on hand. Rather accurate molecular ionization potentials are obtained concomitantly with SCF-LCAO-MO wave functions. Significant though less accurate calculations of certain molecular excitation energies can also be made. Refinement of the SCF-LCAO-MO method will make possible increasingly accurate calculations.

The reliable computation of dissociation energies will probably remain for some time a hard nut to crack, mainly because of the difficulty in knowing how much the errors differ in the two large quantities (atomic and molecular energies) whose computed values must be subtracted in order to obtain dissociation energies. Nevertheless, much new insight into the bonding and antibonding characteristics and the polarities of the MOs of the electrons in a molecule can be obtained from inspection of SCF-LCAO-MO wave functions.

The study of *overlap populations*, computed from the LCAO coefficients, shows more, since these give quantitative figures which may be taken as measures of bonding and antibonding strengths. Further, again by computation from the LCAO coefficients, statistics concerning the distribution of electronic population among the atoms in a molecule, and among the different orbitals in each atom, can be obtained. From these statistics, values of gross charges on atoms, and of amounts of promotion, can be obtained. It seems probable that all these results may be fairly reliable even without great refinement in the SCF-LCAO calculations. The present paper deals mainly with the determination of atomic and overlap populations, illustrated by two examples taken from among a few mole-

* This work was assisted in part by the Office of Scientific Research, Air Research and Development Command, under Project R-351-40-4 Contract AF 18(600)-471 with The University of Chicago, Chicago 37, Illinois.
[1] C. C. J. Roothaan, Revs. Modern Phys. 23, 69 (1951).

cules for which fairly complete SCF-LCAO-MO wave functions have recently become available.

2. POPULATION BREAKDOWNS

First consider any normalized MO ϕ of a diatomic molecule, written in approximate form as a linear combination of normalized AOs χ_r and χ_s of the two respective atoms k and l:

$$\phi = c_r\chi_r + c_s\chi_s. \tag{1}$$

Each AO may be either a pure or a hybrid one. If the MO ϕ is occupied by N electrons (usually $N=2$), this population may be considered as divided into three subpopulations whose detailed distributions in space are given by the three terms in the following expression:

$$N\phi^2 = Nc_r^2(\chi_r)^2 + 2Nc_rc_sS_{rs}(\chi_r\chi_s/S_{rs}) + Nc_s^2(\chi_s)^2, \tag{2}$$

where S_{rs} is the overlap integral $\int_\infty \chi_r\chi_s dv$. The function ϕ, and likewise each of the three functions χ_r^2, $\chi_r\chi_s/S_{rs}$, and χ_s^2, is a *normalized* distribution. Hence, on integration of each term in Eq. (2) over all space, one obtains the following breakdown of N into three parts[2]:

$$N = Nc_r^2 + 2Nc_rc_sS_{rs} + Nc_s^2. \tag{3}$$

The sub-populations Nc_r^2 and Nc_s^2 will be called the *net atomic populations* on atoms k and l, and $2Nc_rc_sS_{rs}$ will be called the *overlap population*.

The three sub-populations may be likened to those of two cities (k and l) and of a (joint) suburb which lies between them. However, it should be noticed that the three distributions χ_r^2, $\chi_r\chi_s/S_{rs}$, and χ_s^2 are not entirely mutually nonoverlapping like those of the cities and their suburb. This peculiarity of the present population breakdown, although it hinders giving a simple physical meaning to the three sub-populations, does not impair the real usefulness of the breakdown.

In general, any molecule contains electrons in several MOs, to each of which Eqs. (1)–(3) are applicable. Let the several MOs be called ϕ_i. Further, if either or both of χ_r and χ_s in Eq. (1) are *hybrid* AOs, they may (*if* desired) each be replaced by linear combinations of (two or sometimes more) pure AOs. Finally, the molecule may be polyatomic. In the general case, Eqs. (1) and (3) are replaced by the following:

$$\phi_i = \sum_{r_k} c_{ir_k}\chi_{r_k}, \tag{1'}$$

$$N(i) = N(i)\sum_{r_k} c_{ir_k}^2 + 2N(i)\sum_{l>k} c_{ir_k}c_{is_l}S_{r_ks_l}. \tag{3'}$$

In Eq. (3'), $N(i)$ is most often 2.

In the subsequent application of Eqs. (1') and (3'), the following symbolism will be used:

$$\left.\begin{aligned}
n(i;r_ks_l) &= 2N(i)c_{ir_k}c_{is_l}S_{r_ks_l};\\
n(i;k,l) &= \sum_r\sum_s n(i;r_k,s_l);\\
n(r_k,s_l) &= \sum_i n(i;r_k,s_l);\\
n(k,l) &= \sum_r\sum_s n(r_k,s_l);\\
n(i) &= \sum_{r_k,s_l} n(i;r_k,s_l);\\
n &= \sum_i n(i) = \sum_{k,l} n(k,l) = \sum_{r_k,s_l} n(r_k,s_l).
\end{aligned}\right\} \tag{4}$$

The quantities $n(i;r_k,s_l)$, $n(r_k,s_l)$, and so on, are partial and subtotal *overlap* populations[3] corresponding to various degrees and kinds of breakdown of a total overlap population n. In general any of the n's may have negative values. Positive and negative n's for a given pair of atoms correspond respectively to net bonding or antibonding between them (see paper II of this series for a detailed discussion).

Further quantities

$$n(i;r_k) = N(i)c_{ir_k}^2;$$

$$n(r_k) = \sum_i n(i;r_k); \quad n(k) = \sum_r n(r_k) \tag{5}$$

can also be defined for partial and sub-total *net atomic populations; $n(k)$* is the *total* net atomic population on atom k. However, these quantities will not be used in the applications below.[4]

The foregoing equations are applicable only when the molecular wave function is one that corresponds to a single LCAO-MO electron configuration. Their extension to wave functions which include configuration interaction should be fairly straightforward, but will not be considered here.

Equations for a similar breakdown of the electronic population into AO and overlap populations would also be of interest for wave functions of the Heitler-London type. In addition, breakdowns into two-electron distribution functions [Eq. (3') is based on one-electron functions only] would be of interest. But these further types of electronic population analysis, which have been considered by McWeeny in unpublished work, will not be developed here.

The net atomic and the overlap populations defined in the foregoing for single-configuration LCAO-MO wave functions, and the gross atomic populations de-

[2] Breakdowns of the total charge into overlap and "net" atomic populations have been in use for some time, e.g., R. S. Mulliken, Phys. Rev. **41**, 66 (1932); J. Chem. Phys. **3**, 573 (1935), Eqs. (38), (39), (42).

[3] The first of Eqs. (4) in general form was given by R. McWeeny, J. Chem. Phys. **19**, 1614*L* (1951) and **20**, 920 (1952); what is here called "overlap population" he called "bond charge." The former term is preferred here because it is more accurately, or at least more unambiguously, descriptive.

[4] The first of Eqs. (5) is given in reference 3, where $n(i;r_k)$ is called the "atom charge."

fined in Sec. 3, have a property of invariance without which their usefulness would be questionable—namely, those populations which represent sums over all MOs [e.g., $n(r_k)$, $n(k)$, $n(r_k,s_l)$, $n(k,l)$, n, but *not* $n(i;r_k)$, $n(i;r_k,s_l)$, etc.] are invariant quantities (like the energy and other molecular properties[1]) with respect to any orthogonal transformation among the *occupied* LCAO MOs (in particular, among those of any one group-theoretical species) in the given configuration. Proofs are given by Scherr in an accompanying paper,[5] and an example is discussed in paper III of this series.

3. GROSS ATOMIC POPULATIONS AND CHARGES; AMOUNTS OF PROMOTION

A particularly useful type of breakdown is one which allocates the whole population among the atomic centers only. Here it may first be noted [see Eq. (3) or (3′)] that the total population is a sum of net atomic populations and (positive or negative) overlap populations. Referring back to the simplest two-center case [see Eq. (3)], it is seen that the overlap term is related completely symmetrically to the two centers, even if these are unlike and the coefficients c_r and c_s therefore unequal. Hence it appears necessary to assign exactly half of the overlap population, plus, of course, the appropriate net atomic population, to each center. The same reasoning holds in the general case of Eq. (3′).

Applying the indicated procedure to Eq. (3), one obtains for the *gross atomic populations* $N(k)$ and $N(l)$ on atoms k and l the expressions:

$$N(k)=N(c_r^2+c_rc_sS_{rs}); \quad N(l)=N(c_rc_sS_{rs}+c_s^2). \tag{6}$$

The sum of $N(k)$ and $N(l)$ is just N [see Eq. (3)].

In the general case one has[6,7]:

$$N(i;r_k)=N(i)c_{ir_k}(c_{ir_k}+\sum_{l\neq k} c_{is_l}S_{r_ks_l}), \tag{6′}$$

$$\left.\begin{aligned} N(i;k)&=\sum_r N(i;r_k);\\ N(k)&=\sum_i N(i;k)=\sum_r N(r_k);\\ N(i)&=\sum_{r_k} N(i;r_k)=\sum_k N(i;k);\\ N(r_k)&=\sum_i N(i;r_k);\\ N&=\sum_i N(i)=\sum_{r_k} N(r_k). \end{aligned}\right\} \tag{7}$$

$N(i;r_k)$ is the partial gross population in MO ϕ_i and AO χ_{r_k}; $N(i;k)$ is the subtotal in MO ϕ_i on atom k. $N(k)$ is the total gross population on atom k. $N(i)$ is the total population (necessarily an integer) in MO ϕ_i. $N(r_k)$ is the total gross population in AO χ_{r_k}. N is the over-all total population (necessarily an integer) of electrons in the molecule. $N(r_k)$, $N(k)$, and N are invariant with respect to orthogonal transformations of the occupied LCAO MOs.[5]

Ideally, the definition of $N(i;r_k)$ by Eq. (6′) would be such that no $N(i;r_k)$ would ever be less than zero. Actually, very small negative values[8] occasionally occur (see Table V, first row and column, and footnote). Likewise, if $N(r_k)$ corresponded ideally to the population of the AO χ_{r_k} in atom k, its value for a non-degenerate or a single individual AO (e.g., $1s$, $2s$, or $2p\sigma$) should never exceed the number 2.00 of electrons in a closed atomic sub-shell. Actually, $N(r_k)$ in some instances does very slightly exceed 2.00 (again see Table V and its footnote). The reason why these slight but only slight imperfections exist is obscure. But since they *are* only slight, it appears that the gross atomic populations calculated using Eq. (6′) may be taken as representing rather accurately the "true" populations in various AOs for an atom in a molecule. It should be realized, of course, that fundamentally there is no such thing as an atom *in* a molecule except in an approximate sense.

If definitions (6′) and (7) are accepted, one can at once define[9] the "gross charge," $Q(r_k)$, in any AO, or that, $Q(k)$, on any atom:

$$Q(r_k)=N_O(r_k)-N(r_k); \quad Q(k)=N_O(k)-N(k), \tag{8}$$

where $N_O(r_k)$ is the number of electrons in the AO χ_r and $N_O(k)$ the total number of electrons in the ground state of the free neutral atom k. The Q's in Eqs. (8) are in units of $+e$. Some examples of the application of Eq. (8) are given in Tables IV and V.

If the quantities $N(r_k)$ are known for the atoms in a molecule, a population summary or effective electron configuration for any atom can be written down. Comparison between this and the configuration of the free atom in its ground state shows, in general, differences, namely the quantities $Q(r_k)$. In the event that there is no gross charge $Q(k)$ on the atom, these differences can be expressed in terms of *amounts of promotion*. In case the promotion involves no increase in valence (isovalent promotion[10]), its amount may be identified with amount of *gross hybridization*. The same quantities can still be defined if there is a gross charge on the atom, although only at the cost of some arbitrariness. An example will make these matters clearer.

According to SCF-LCAO-MO calculations (see Table IV), the effective electron configurations for the two atoms in CO are as follows:

$$1s_C^{2.00}2s_C^{1.49}2p\sigma_C^{1.40}2p\pi_C^{1.02}; \; 1s_O^{2.00}2s_O^{1.86}2p\sigma_O^{1.25}2p\pi_O^{2.98},$$

[5] C. W. Scherr, J. Chem. Phys. **23**, 569 (1955). See Appendix II for invariance theorems. Scherr has used the methods and notation of the present paper, which was prepared some time ago in preliminary form, in discussing his results on N_2.

[6] R. S. Mulliken, J. chim. phys. **46**, 675 (1949), Sec. 21. The present $N(i;r_k)$ is there called F_{ri}: see Eq. (139) there.

[7] B. H. Chirgwin and C. A. Coulson, Proc. Roy. Soc. (London) **201A**, 196 (1950), who speak of "formal charges" for what are here called "gross populations." Also reference 3.

[8] Reference 6, footnote 73.

[9] Reference 2, Eq. (39).

[10] R. S. Mulliken, J. Phys. Chem. **56**, 295 (1952).

TABLE I. Computed SCF-LCAO MOs for CO (by R. C. Sahni, reference 12).

ϕ_i \ χ_r	$2s_O$	$2p\sigma_O$	$2s_C$	$2p\sigma_C$	$2p\pi_O$	$2p\pi_C$	calc $-\epsilon_i$(ev)	obs I_i(v)
2σ	0.675	0.231	0.270	0.227			43.37	
4σ	0.718	−0.607	−0.493	−0.168			20.01	19.70
1π					0.8145	0.4162	15.97	16.58
5σ	0.187	−0.189	0.615	−0.763			13.37	14.01

or briefly,

$$1s_C^{2.00}2s_C^{1.49}2p_C^{2.42};\quad 1s_O^{2.00}2s_O^{1.86}2p_O^{4.23},$$

as compared with

$$1s_C^{2.00}2s_C^{2.00}2p_C^{2.00};\quad 1s_O^{2.00}2s_O^{2.00}2p_O^{4.00}$$

in the ground states of the two atoms. It is evident that in CO there has been promotion out of $2s$ for both atoms, but also there has been a charge transfer of $-0.09e$ from C to O. One might ask, how much of this transfer has been out of $2s_C$ and how much out of $2p_C$, and how much has been into $2s_O$ and how much into $2p_O$? These questions appear to have no definite answer, if indeed they have any real meaning. One may, however, reason that most of the charge transfer has been out of $2p_C$ and into $2p_O$, because the net $2s$ promotions which exist in CO, both out of $2s_C$ into $2p\sigma_C$ and out of $2s_O$ into $2p\sigma_O$, must have arisen mainly as a response to the possibility of gains in stability by hybridization; and if so, the extent of these promotions should be relatively independent of loss or gain of charge in, say, the $2p$ AOs.

In any event, one may arbitrarily *define* the amounts of promotion in the atoms in CO on the basis that charge transfer involves only the $2p$ AOs. One can then say that, in units of $-e$, the amount of $2s\rightarrow 2p\sigma$ promotion is 0.51 in the C and 0.14 in the O atom.

4. EXAMPLES AND APPLICATIONS: SURVEY

The first successful computations by the LCAO-SCF method considered π electrons only, in an assumed Goeppert-Mayer-Sklar field representing the remaining electrons. Next Mulligan[11] (CO_2) and recently Sahni[12] (CO) have published results of LCAO-SCF calculations including all but the $1s$ electrons explicitly in the calculations, although the values of many of the integrals were approximated instead of computed. Meantime Fischer[13] carried out an approximately SCF LCAO treatment on LiH and BeH^+ in which all integrals were evaluated exactly. Higuchi[14] gave an SCF-LCAO treatment of several electronic states of CH, but did not include the carbon $1s$ electrons in the calculations. Duncan treated SF_6 including valence electrons only, and has recently treated HF with all electrons included.[15] Ellison and Shull[16] have published an LCAO-SCF treatment of H_2O with some of the integrals approximated, but with *all* electrons included. Sahni[17] has carried out a complete treatment of BH, and Scherr[5] a complete treatment of N_2, in which all electrons were included and all integrals computed exactly. A preliminary report of a similar complete treatment of NH_3 has also appeared.[18] The work of Ellison and Shull, and of Scherr, show that the explicit inclusion of inner-shell (here $1s$) electrons in the SCF procedure is very important. All calculations thus far made, except some of those of Fischer and of Higuchi have been based exclusively on Slater-type AOs with essentially Slater's values of the effective nuclear charges, and have been made only for the equilibrium internuclear distances. However, Ellison and Shull made calculations for several values of the bond angle in H_2O. Configuration interaction has not been taken into account in most of the papers mentioned except for $2s-2p$ hybridization. Higuchi considered configuration interaction rather extensively for CH.

The use of the methods of population analysis described in preceding sections of this paper will now be illustrated by applylng them to the approximate LCAO-SCF wave functions obtained by Sahni for CO and by Ellison and Shull for H_2O. Although these wave functions are subject to some revision, they are doubtless sufficiently accurate for the present illustrative purpose. In another paper, Scherr[5] has applied the present methods to his exact LCAO-SCF N_2 wave functions.

The electron configuration of CO (equilibrium interatomic distance 1.128 A) is

$$(1\sigma)^2(2\sigma)^2(3\sigma)^2(4\sigma)^2(1\pi)^4(5\sigma)^2.$$

The MOs 1σ and 2σ were approximated by Sahni as $1s_O$ and $1s_C$ respectively. The LCAO coefficients (see Eq. (1′)) as determined by Sahni for the remaining MOs, all normalized and orthogonal, are reproduced in Table I. The $2p\sigma$ AOs are here defined in such a way that the positive lobe of each points toward the other atom. The computed orbital energies ϵ are also given in Table I, and compared with the observed ionization

[11] J. F. Mulligan, J. Chem. Phys. **19**, 347 (1951).
[12] R. C. Sahni, Trans. Faraday Soc. **49**, 1 (1953).
[13] I. Fischer, Arkiv Fysik **5**, 349 (1952).
[14] J. Higuchi, J. Chem. Phys. **22**, 1339 (1954).
[15] A. B. F. Duncan, J. Chem. Phys. **20**, 951 (1952); J. Am. Chem. Soc. **77**, 2107 (1955).
[16] F. O. Ellison and H. Shull, J. Chem. Phys. **21**, 1420(L) (1953) and later full paper.
[17] R. C. Sahni (to be published).
[18] H. Kaplan, on p. 30 of Quarterly Progress Report for October 15, 1954 of the Solid-State and Molecular Theory Group at the Massachusetts Institute of Technology, Cambridge, Massachusetts.

TABLE II. Computed SCF-LCAO MOs for H_2O (by Ellison and Shull, reference 16).

ϕ_i \ χ_r	$1s_O$	$2s_O$	$2p\pi_O$	$a_1(H_2)$	$2py_O$	$b_2(H_2)$	$2px_O$	calc $-\epsilon_i(ev)$	obs $I_i(v)$
$1a_1$	1.0002	0.0163	0.0024	−0.0039				557.3	
$2a_1$	−0.029	0.845	0.133	0.208				36.2	
$1b_2$					0.543	0.613		18.6	16.2
$3a_1$	−0.026	−0.461	0.827	0.393				13.2	14.5
$1b_1$							1.000	11.8	12.56

potentials, with which[19] they should approximately agree.

The electron configuration of H_2O (symmetry C_{2v}, apex angle 105°, O-H equilibrium distance 0.958 A; z axis bisecting apex angle, x axis taken perpendicular to the molecule plane) is

$$(1a_1)^2(2a_1)^2(1b_2)^2(3a_1)^2(1b_1)^2.$$

The LCAO MOs are here best expressed as linear combinations of O atom AOs and the following two normalized GOs (group orbitals) of the H_2 group:

$$\begin{aligned} a_1(H_2) &= (1s_a+1s_b)/[2(1+S)]^{\frac{1}{2}}, \\ b_2(H_2) &= (1s_a-1s_b)/[2(1-S)]^{\frac{1}{2}}, \end{aligned} \tag{9}$$

where $1s_a$ and $1s_b$ refer to $1s$ AOs on the two H atoms, and $S=\int 1s_a 1s_b dv$. The coefficients of the AOs and GOs as determined by Ellison and Shull for the various normalized MOs are reproduced in Table II, together with the corresponding computed ϵ_i's and observed I_i's.

For convenience of reference, values of various overlap integrals $S_{rs}=\int \chi_r \chi_s dv$ used in the population analysis are listed in Table III. In the case of H_2O, S's for the overlap of O atom AOs with normalized H_2 GOs $a_1(H_2)$ or $b_2(H_2)$ are also included.

Leaving aside the inner-shell MOs, which are nearly but not quite $1s$, inspection of the coefficients shows at once that the lowest σ MO in CO (3σ), and the lowest a_1 MO in H_2O ($2a_1$), have large consistently positive overlaps and so must be very strongly bonding. The higher σ MOs in CO, and the higher a_1 MOs, show both positive and negative overlaps, indicating little net bonding. The 1π MO in CO and the $1b_2$ MO in H_2O are evidently strongly bonding. The result, shown by the LCAO-SCF calculations, that most of the bonding power of the σ electrons in CO, and of the a_1 electrons in H_2O, resides in the lowest-energy outer-shell MO of the species, is especially notable.

5. EXAMPLES AND APPLICATIONS: GROSS ATOMIC POPULATIONS AND CHARGES; AMOUNTS OF PROMOTION

In Tables IV and V, a survey is made of the atomic populations in the AOs and atoms of CO and H_2O; the AO and atomic charges are also given. These results have been computed, using Eqs. (6′), (7), and (8), from the coefficients and S's in Table I-III. Tables IV and V show many interesting details which largely speak for themselves. There are nevertheless several points about which comment may be helpful.

Referring to Table IV, it is notable that the individual MOs of CO are all strongly polar, although the molecule as a whole is almost nonpolar, i.e., $Q(O)$ and $Q(C)$ are small. It is also notable that the π MO, and the totality of the σ MOs, each separately show almost the same charge distributions as in two normal atoms:

$$\sum_{\sigma\ \mathrm{MOs}} (i)\, N(i;O)=3.108, \qquad \sum_{\sigma\ \mathrm{MOs}} (i)\, N(i;C)=2.892;$$

$$N_\pi(O)=2.980, \qquad N_\pi(C)=1.020,$$

as compared with

$$\sum_{\sigma\ \mathrm{AOs}} (r)\, N(r;O)=3.000, \qquad \sum_{\sigma\ \mathrm{AOs}} (r)\, N(r;C)=3.000;$$

$$N_\pi(O)=3.000, \qquad N_\pi(C)=1.000$$

for neutral O and C atoms both in $^3\Pi$ phases of their ground states; that is to say, for $2s^2 2p\sigma 2p\pi^3$, $^3P\Pi$ combined with $2s^2 2p\sigma 2p\pi$, $^3P\Pi$. The slight charge transfer from O to C in the 1π MO relative to this combination corresponds to (the presence of) a small amount of $2s^2 2p\sigma^2 2p\pi^2$, $^3P\Sigma^-$ combined with $2s^2 2p\pi^2$, $^3P\Sigma^-$. No other combination derived from two normal atoms exists which could be involved in the normal electron configuration of CO. It is very striking that just *because* of strong C^+O^- polarlty in the 1π MO, together

TABLE III. Values of overlap integrals $S_{rs}=\int \chi_r \chi_s dv$.

χ_r \ χ_s	$2s_O$	$2p\sigma_O$	$2p\pi_O$
$2s_C$	0.4063	0.3147	0
$2p\sigma_C$	0.4807	0.3018	0
$2p\pi_C$	0	0	0.2409

χ_r \ χ_s	$1s_O$	$2s_O$	$2p\pi_O$	$2py_O$	$1s_b(H)$
$1s_a(H)$	0.0610	0.4946	0.2118	0.2760	0.3479
$a_1(H_2)$	0.0736	0.5965	0.2554	0	
$b_2(H_2)$	0	0	0	0.4935	

[19] See Sec. 6 of reference 6.

TABLE IV. Gross atomic populations and charges in CO (see Eqs. (6′), (7), (8).

ϕ_i \ χ_{r_k}	Partial populations $N(i;r_k)$								
	$2s_O$	$2p\sigma_O$	$2p\pi_O$	$2s_C$	$2p\sigma_C$	$2p\pi_C$	$N(i;O)$	$N(i;C)$	$N(i)$
3σ	1.207	0.178		0.333	0.282		1.385	0.615	2.000
4σ	0.627	0.985		0.386	0.002		1.612	0.388	2.000
1π			2.980			1.020	2.980	1.020	4.000
5σ	0.026	0.085		0.776	1.113		0.111	1.889	2.000
$N(r_k)$	1.860	1.248	2.980	1.495	1.397	1.020	$N(O)=$ 6.088	$N(C)=$ 3.912	$N=$ 10.000
$Q(r_k)$ in e units	+0.140	−0.248	+0.020	+0.505	−0.397	−0.020	$Q(O)=$ −0.088	$Q(C)=$ +0.088	0.000

with lack of marked polarity in the totality of the σ MOs, an atomic population distribution very close to that of two normal atoms is reproduced. It is also notable that the CO molecule nevertheless (see discussion following Tables VI and VIII) achieves almost as strong π and σ bonding as in the isoelectronic molecule N_2. This close similarity in character of bonding, combined with lack of over-all polarity, seems to account well for the close similarity in physical properties between CO and N_2.

Like N_2, CO has one strongly bonding σ MO (3σ) and two more or less nearly nonbonding σ MOs (4σ and 5σ). However, whereas in N_2 the two nearly nonbonding σ MOs are of course nonpolar, in CO they are both very strongly polar, the deeper of the two (4σ) having strong C^+O^- polarity, the less deeply bound (5σ) having such strong C^-O^+ polarity that it approximates to a pure (but very strongly $2s-2p\sigma$ hybridized) carbon σ AO. This last fact and the fact that 5σ is the most easily ionized MO of CO (see Table I) make understandable the moderate ability of CO to act as an electron donor[20] (as e.g., in $2B_2H_6+CO \rightleftharpoons 2H_3BCO$, and perhaps in the initial stages of the reaction of CO with metals to form carbonyls), as contrasted with the much greater inertness of N_2.

Work of recent years[21] has shown that one cannot expect molecular dipole moments in general to be simply related to a sum of products $\Sigma Q r_e$ of atomic charges times interatomic distances. However, if one has accurate molecular wave functions, one can compute dipole moments. In this connection Table VI is of interest (the μ_{calc} values are from references 12 and 16, the Q values from Tables IV and V).

From Tables IV and V, an effective electron configuration for each atom in the molecule CO or H_2O can be written down, and from this the amount of $2s-2p\sigma$ promotion can be read off. For CO, reference may be made to the end of Sec. 3. For H_2O, the effective atomic electron configurations found are

$$1s_O^{2.00}2s_O^{1.85}2p_O^{4.50};\ 1s_{H_a}^{0.82};\ 1s_{H_b}^{0.82}.$$

It is especially notable that, in spite of the considerable total of electron transfer from the two H atoms onto the O atom, there is a deficit of $0.15e$ in the $2s_O$ AO as compared with a free oxygen atom in its ground state. This deficit, which represents promotion, is explained by the ensuing gains from $2s_O-2pz_O$ hybridization, and is, interestingly enough, approximately the same as the corresponding figure ($0.14e$) for the $2s_O$ AO in CO. This suggests that about this amount of promotion is likely

TABLE V. Gross atomic populations and charges in H_2O (see Eqs. (6′), (7), (8)).[a]

ϕ_i \ χ_{r_k}	Partial populations $N(i;r_k)$									
	$1s_O$	$2s_O$	$2pz_O$	$2py_O$	$2px_O$	$a_1(H_2)$	$b_2(H_2)$	$N(i;O)$	$N(i;H_2)$	$N(i)$
$1a_1$	2.0002	0.0005	0.0000			−0.0005		2.0007	−0.0005	2.000
$2a_1$	0.0008	1.638	0.049			0.309		1.688	0.309	1.997
$1b_2$				0.918			1.080	0.918	1.080	1.998
$3a_1$	−0.0001	0.209	1.534			0.257		1.743	0.257	2.000
$1b_1$					2.000			2.000		2.000
$N(r_k)$	2.0009	1.847	1.583	0.918	2.000	0.565	1.080	$N(O)=$ 8.349	$N(H_2)=$ 1.645	$N=$ 9.995
$Q(r_k)$ in e units	0.00	+0.15	−0.58	+0.08	0.00	+0.43	−0.08	$Q(O)=$ −0.35	$Q(H_2)=$ +0.35	0.00

[a] The slight deviations recorded of some of the $N(i)$'s from 2.000 are attributable to the fact that the coefficients in Table II (with a few exceptions) have been rounded off to three figures after the decimal point, as given in Ellison and Shull's first publication. The small *negative* partial populations listed and the excess of the values of $N(1a_1;O)$ and $N(1s_O)$ over 2.000, are, however, not due to rounding, but to the imperfections of the definitions of Eqs. (6′), (7).

[20] R. S. Mulliken, J. Am. Chem. Soc. **74**, 811 (1952), p. 822–823.
[21] C. A. Coulson, Proc. Roy. Soc. (London) 207A, **63** (1951).

to be found characteristic of the oxygen atom in its stable covalent compounds. It appears very likely that rather reliable information on promotion in atoms in molecules can be obtained by SCF-LCAO calculations.[22]

6. EXAMPLES AND APPLICATIONS: OVERLAP POPULATIONS

In Tables VII and VIII are given details of overlap populations in CO and H_2O, computed from the coefficients and S's ln Table I–III, using Eqs. (4). The break-downs are in terms of pairs of overlapping nonhybrid AOs. An alternative breakdown for each molecule based on a *smaller* number of pairs of overlapping $2s-2pz$ *hybrid* AOs (C and O atom AOs in CO, O atom AOs in H_2O) would be of considerable interest, but is omitted here; the reader may find it instructive to work these out. The last two columns of Table VII will be explained.

The bond structure of CO has already been discussed in connection with Tables I and IV. Each of these tables displays well some aspects of the complete picture, but a study of Table VII (overlap populations) adds further insight. In so far as overlap population is a good measure of covalent bonding, the individual $n(i)$'s in Table VII give measures of the bonding powers of the electrons in the various MOs ϕ_i, and their total, n, gives a measure of the total covalent strength. It is of interest that n for CO (1.018) is somewhat, but not greatly, less than n for N_2 (1.276).[5] It is further of interest that using the $n(i)$'s as measures, the total bonding power of the (six) electrons in the σ MOs ($\sum_{\sigma\ \mathrm{MOs}} n(i)=0.364$) is about one third, and that of the four electrons in the 1π MO ($n(1\pi)=0.654$) is almost two thirds of the total n. The corresponding figures for N_2 are 0.395 and 0.880.[5] These figures, for CO as for N_2, correspond rather well to the idea of the presence of a triple bond (one σ and two π bonds) in both these molecules, provided one admits,[10] contrary to some early ideas in quantum-mechanical valence theory, that π bonds can be as strong as σ bonds.

TABLE VI. Dipole moments (in D).

	μ_{calc}	Qr_e	μ_{obs}
CO	1.00 (C^+O^-)	0.48 (C^+O^-)	0.12
H_2O	1.51 ($H_2^+O^-$)	0.98 ($H_2^+O^-$)	1.84

In diatomic spectroscopy, a long familiar empirical criterion of the bonding power of an electron in any MO has been the change Δr_e in the equilibrium interatomic distance r_e in a molecule upon removal of an electron from that MO. In the last two columns of Table VII, data on $\Delta r_e/r_e$ from the CO^+ spectrum, using r_e as known (1.128 A) for CO, are compared with values of $-\Delta n/n$ using the calculated $n(i)$ values from the earlier columns of Table VII (note that since only *one* electron is removed on ionization, $-\Delta n(i)$ has been taken as one-half or one-fourth of $n(i)$ in the cases of σ and π MOs respectively). The correlation is good for the 1π (bonding) and the 5σ (slightly antibonding) MOs, but is poor for 4σ (observed, mildly bonding; computed,

TABLE VII. Computed overlap populations for CO (see Eqs. (4)).

χ_{r_k}, χ_{s_l} / ϕ_i	Partial populations $n(i; r_k, s_l)$						Change on Ionzn.	
	$2s_O, 2s_C$	$2s_O, 2p\sigma_C$	$2p\sigma_O, 2s_C$	$2p\sigma_O, 2p\sigma_C$	$2p\pi_O, 2p\pi_C$	$n(i)$	calc $-\Delta n/n$	obsd $2\Delta r_e/r_e$
3σ	0.296	0.294	0.078	0.064		0.732		
4σ	−0.574	−0.232	0.376	0.124		−0.308	−0.151	+0.072
1π					0.654	0.654	+0.161	+0.206
5σ	0.186	−0.274	−0.146	0.174		−0.060	−0.029	−0.022
$n(r_k,s_l)$	−0.092	−0.212	0.308	0.362	0.654	$n=$ 1.018		

TABLE VIII. Computed overlap populations for H_2O (see Eqs. (4)).

χ_{r_k}, χ_{s_l} / ϕ_i	Partial populations $n(i; r_k, s_l)$						
	$1s_O, a_1(H_2)$	$2s_O, a_1(H_2)$	$2pz_O, a_1(H_2)$	$2py_O, b_2(H_2)$	$1s_a(H), 1s_b(H)$	$n(i)$	
$1a_1$	−0.0012	0.000	0.000		0.000	−0.001	
$2a_1$	−0.0018	0.419	0.028		0.024	+0.469	
$1b_2$				0.658	−0.450	+0.208	
$3a_1$	−0.0030	−0.432	0.332		0.084	−0.019	
$1b_1$						0.000	
$n(r_k,s_l)$	−0.0060	−0.013	0.360	0.658	−0.342	$n=$ 0.657	

[22] Similar results as to amounts of promotion in first-row atoms have been obtained in reference 10 by use of the magic formula method, and (see survey in Sec. XII of reference 10) by other methods.

TABLE IX. Overlap population for H_2.

ϕ_i \ χ_r, χ_s	$n=n(i;r,s)$ $1s_a(H), 1s_b(H)$	Change on Ionzn. calc $-\Delta n/n$	obs $2\Delta r_e/r_e$
$1\sigma_g$	0.858	+0.500	+0.429

antibonding). The writer thinks it likely that more refined and accurate computations would show better agreements and feels that moderate disagreements such as that noted are only what might be expected at the present stage of progress.

For comparison with Table VII, Table IX of corresponding data on the H_2 molecule is of interest.

Table VIII for H_2O indicates that the bonding is almost entirely confined to the deeply buried (see Table II) $2a_1$ MO and the $1b_2$ MO. It also indicates that the bonding in the $2a_1$ MO, in spite of an appreciable amount of $2s-2pz$ hybridization (see Table II) is almost exclusively between the $2s_O$ MO and the hydrogens.

The $1s_a(H)$, $1s_b(H)$ overlap populations are also of especial interest. In AO-VB theory, one would expect a considerable nonbonded repulsion between the H atoms. This would correspond in LCAO-MO theory to a net excess of antibonding (i.e., negative) H—H overlap population in the $1b_2$ MO over bonding (i.e., positive) H—H overlap population in the a_1 MOs. This expectation is realized, but the negative excess is surprisingly large $[n(1s_a,1s_b)=-0.342]$, due to a combination of a surprisingly large $H_2{}^+O^-$ polarlty in the a_1 MOs (see Table V), combined with a surprising $H_2{}^-O^+$ polarity in the $1b_2$ MO. Ellison and Shull noted also that their computations lead to the prediction of a bond angle somewhat exceedlng 120°. All these effects are so surprising that it seems likely that the values of some of the integrals (in particular the three-center integrals) which were only estimated were insufficiently exact. Indeed, Ellison and Shull consider this to be among the possible explanations of the too-large predicted angles.

Another factor which must contribute somewhat to reducing the H-H nonbonded repulsions is $1s-2p\sigma$ hybridization in the H atom AOs. A rough consideration indicates that a stabilization of about 0.3 ev, but more or less independent of bond angle, might be obtained in this way.

Attention should be called here to the fact that Linnett and Heath, Simanouti, and others have brought forward rather convincing evidence from infrared force constant data, to the effect that the theoretically expected nonbonded repulsions between H atoms in molecules of the type AH_n are unimportant, if not nonexistent.[23] Theoretically such a situation seems difficult to understand. If the evidence is valid, it will apparently be necessary to call on rather extensive configuration interaction to explain it.

An interesting feature of Table VIII is the occurrence of small negative overlap populations between $1s_O$ and the H atom AOs. These correspond to "forced hybridization" in LCAO-MO theory and to "nonbonded repulsions" between the $1s_O$ and the $1s_H$ electrons in AO-VB theory (see paper III).

7. FUTURE APPLICATIONS

To mention a few out of many possibilities, it will be intensely interesting to learn how the amount of gross charge Q on, and of $s-p$ promotion in, the central atom varies within such series as HF, H_2O, H_3N, H_4C; HF, HO, HN, HC, HB; CH, CH_2, CH_3, CH_4; CH_4, C_2H_6, C_2H_4, and C_2H_2. In contemplating the results for such series, the concept of promotion will probably emerge as more fundamental than that of hybridization or of valency. It will be very interesting to see how the amount of $s-p$ promotion in CH_4 and other "tetravalent" carbon compounds lags behind that required (1.0e) for full formal tetravalence. There may even prove to be not much less promotion in the "bivalent" carbon atom of CH_2 than in "tetravalent" carbon atoms.

ACKNOWLEDGMENTS

The writer is indebted to Mr. W. Jaunzemis for calculations whose results are embodied in the tables, and to Dr. C. W. Scherr for valuable criticism and suggestions on the papers of this series.

[23] D. F. Heath and J. W. Linnett, Trans. Faraday Soc. **44**, 556 (1947) on H_2O; Heath, Linnett, and Wheatley, *ibid.* **46**, 137 (1950), on H_2O, H_2S, H_2Se, NH_3, AsH_3, CH_4, etc.; T. Simanouti, J. Chem. Phys. **17**, 245, 734 (1949); Heath and Linnett, J. Chem. Phys. **18**, 147 (1950).

THE JOURNAL OF CHEMICAL PHYSICS VOLUME 23, NUMBER 10 OCTOBER, 1955

Electronic Population Analysis on LCAO-MO Molecular Wave Functions. II. Overlap Populations, Bond Orders, and Covalent Bond Energies*

R. S. MULLIKEN
Laboratory of Molecular Structure and Spectra, Department of Physics, The University of Chicago, Chicago 37, Illinois

(Received January 6, 1955)

LCAO molecular orbital overlap populations give in general much more flexible and widely useful measures of the non-Coulombic parts of covalent bond energies than do LCAO bond orders. They are immediately applicable to both π and σ bonds, including bonds involving hybrid AOs of all kinds, and they take account directly of the effects of variations in bond length on bond strength. In the last section of this paper, a number of ways of defining LCAO bond orders are reviewed, and their advantages and disadvantages discussed.

If all LCAO parameters β are assumed proportional to corresponding overlap integrals S times suitable mean atomic ionization energies $\bar{I}$, a simple general approximate formula for covalent resonance energies is obtained in terms of partial overlap populations and $\bar{I}$'s, including one or two empirical coefficients. This formula indicates that forced hybridization (see III of this series) due to inner shells should make important negative contributions to bond energies. The application of the formula to H_2, CO, and H_2O is discussed.

The assumption of proportionality of β values to $S\bar{I}$ values may be useful also in estimating unknown β values.

1. GENERAL CONSIDERATIONS

IN the preceding paper,[1] hereafter referred to as I, definitions and formulas, applicable for LCAO–MO wave functions, have been given for overlap populations. In general, the total overlap population $n(k,l)$ between two atoms k and l is the sum of a number of terms (see Eqs. (4) of I), some positive, some negative. The atoms can usually be considered as bonded or as antibonded according as $n(k,l)$ is positive or negative. Further, one may hope to use the partial and total overlap populations between k and l as more or less quantitative measures of the strength of covalent bonding or antibonding between those atoms.

To investigate this possibility, it will be useful to examine first the simple case of H_2^+. In its stable ground state and its unstable first excited state, respectively, H_2^+ has one electron in the MO $1\sigma_g$ or $1\sigma_u$, of the forms $(1s_a \pm 1s_b)/[2(1\pm S)]^{\frac{1}{2}}$ in LCAO–MO approximation, where S is the overlap integral between $1s_a$ and $1s_b$. Equations (2) and (3) of I then become

$$[\phi(1\sigma_g \text{ or } 1\sigma_u)]^2=[\tfrac{1}{2}/(1\pm S)](1s_a)^2 \pm[S/(1\pm S)](1s_a 1s_b/S)+[\tfrac{1}{2}/(1\pm S)]1s_b^2; \quad (1)$$

$$1=\tfrac{1}{2}/(1\pm S) \pm S/(1\pm S) +\tfrac{1}{2}/(1\pm S). \quad (2)$$

The first of these equations can also be written as

$$[\phi(1\sigma_g \text{ or } 1\sigma_u)]^2=[1/(1\pm S)][\tfrac{1}{2}(1s_a)^2+\tfrac{1}{2}(1s_b)^2] \pm[S/(1\pm S)][1s_a 1s_b/S], \quad (3)$$

and may be instructively compared with the "atomic-mean" distribution

$$\tfrac{1}{2}(1s_a)^2+\tfrac{1}{2}(1s_b)^2 \quad (4)$$

which would exist if the electrons were distributed with equal probability between $1s$ AOs on the two nuclei. Relative to the latter, the actual distribution in the $1\sigma_g$ MO corresponds to a shift of a quantity $\frac{1}{2}S/(1+S)$ of the electronic population from each of the two centers into the overlap region.

Similarly the $1\sigma_u$ distribution represents a shift of population *out of* the overlap *onto* the two centers. The overlap population is then $-S/(1-S)$, and the corresponding population on the two centers ("net atomic population") exceeds the total population $(+1)$ by $S/(1-S)$. In rare extreme cases where S approaches 1 (as for example with the $\gamma>0$ hybrids for $(n\sigma_u)^2$ in Fig. 3 of the following paper III), even the (negative) overlap population may greatly exceed the total population. This illustrates the fact that the concept of overlap population is in general a somewhat formal rather than physical one.

Figure 1 shows contour maps of cross sections, through the nuclei, of the atomic-mean distribution, the overlap distribution, and their superpositions with appropriate coefficients to give the actual LCAO–MO $1\sigma_g$ and $1\sigma_u$ distributions. Referring to Fig. 1(b), it will be noted that the overlap function has a distribution which is concentrated to a large extent in what Berlin[2] calls the binding region. This is, roughly, the region between the nuclei; more accurately, it includes all points where an electron would exert electrostatic forces on the two nuclei tending to decrease their distance apart. Nevertheless an appreciable part of the overlap distribution falls in the antibinding region (roughly, the region behind the nuclei; more accurately, all points where the presence of an electron would tend to increase the distance between the nuclei). On the whole, accession to, or withdrawal from, the overlap region evidently results in transfer of charge respec-

* This work was assisted in part by the Office of Scientific Research, Air Research and Development Command, under Project R–351–40–4 of Contract AF 18(600)–471 with The University of Chicago.

[1] R. S. Mulliken, J. Chem. Phys. **23**, 1833 (1955).

[2] T. H. Berlin, J. Chem. Phys. **19**, 208 (1951).

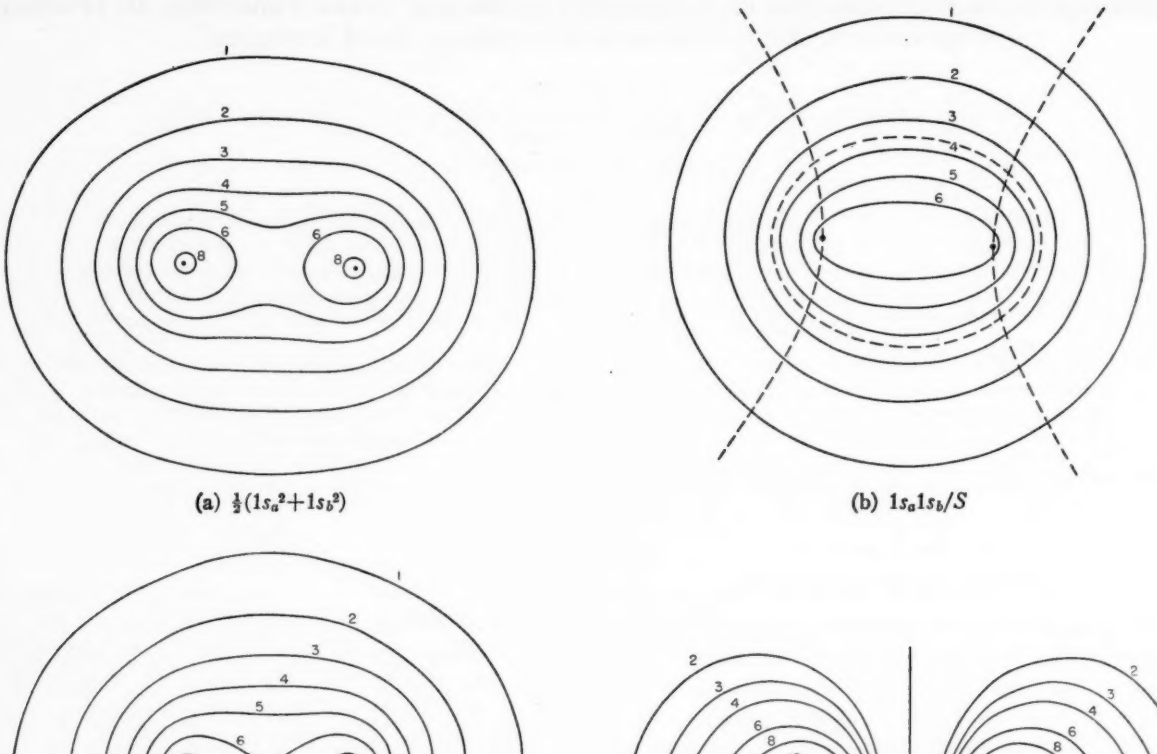

FIG. 1. Normalized population distribution functions for the electron in H_2^+: (a) mean of free-atom distributions; (b) overlap function distribution; (c) distribution in ground-state MO; (d) distribution in first excited MO. See also C. A. Coulson, *Valence* (Clarendon Press, Oxford, 1952), pp. 80–81. In Fig. 1(b), the dashed-line ellipse is so drawn that one-half of the total overlap distribution is inside and one half outside it. The quasi-hyperbolic dashed lines divide the overlap distribution between an inner "binding" region and two outer "antibinding" regions, in the terminology of Berlin.[2]

tively more into the binding region or into the antibinding region. Hence it is clear, at least so far as potential energy contributions are concerned, that positive and negative overlap populations must be closely associated with covalent bonding and covalent antibonding respectively.

2. COVALENT BOND ENERGIES

The orbital energies ϵ for the MOs $1\sigma_g$ and $1\sigma_u$ of H_2^+ according to LCAO theory may be written as follows:

$$1\sigma_g\colon\ \epsilon=\alpha-\beta/(1+S);\quad 1\sigma_u\colon\ \epsilon=\alpha+\beta/(1-S).$$

The quantities α and β, which are both negative, are given by

$$\beta=\int\chi_r H\chi_s dv-S\alpha;\quad \alpha=\int\chi_r H\chi_r dv, \tag{5}$$

where χ_r and χ_s here are $1s$ AOs of the two atoms, and H is the Hamiltonian operator; α and β may be called Coulomb-energy and overlap-energy parameters.

There are reasons[3] for supposing that, approximately, but rather generally,

$$-\beta=aIS, \tag{6}$$

where a is a constant, and I is an atomic ionization potential, here that of $1s_H$. If so, then

$$\epsilon(1\sigma_g)=\alpha-aIS/(1+S);\quad \epsilon(1\sigma_u)=\alpha+aIS/(1-S) \tag{7}$$

so that the overlap energies $\mp\beta/(1\pm S)$ are directly proportional to the overlap populations $S/(1+S)$ and $-S/(1-S)$ for $1\sigma_g$ and $1\sigma_u$, respectively. This result is readily understandable, and would have been directly

[3] R. S. Mulliken, J. Phys. Chem. **56**, 295 (1952).

plausible, on the basis of the discussion of Fig. 1 given above.

In general,[4] the orbital energy ϵ_i of any LCAO MO ϕ_i is given by a sum of Coulomb-energy and overlap-energy terms:

$$N(i)\epsilon_i=\sum_{r_k} N(i;r_k)\alpha(r_k)+2\sum_{l>k} N(i)c_{ir_k}c_{is_l}\beta(r_k,s_l). \quad (8)$$

In terms of partial overlap populations (see Eqs. (4) of I), Eq. (8) becomes[5]

$$N(i)\epsilon_i=\sum_{r_k} N(i;r_k)\alpha(r_k) +\sum_{l>k} n(i;r_k,s_l)[\beta(r_k,s_l)/S(r_k,s_l)]. \quad (9)$$

In Eq. (8), the overlap energy, denoted from here on by Ω, is expressed in terms of quantities $[N(i)c_{ir_k}c_{is_l}]$ which are essentially Coulson bond orders,[6,7] each times a corresponding β. In Eq. (9), Ω is expressed in terms of overlap populations, each times a corresponding quantity β/S. Since there is reason to believe[3] that $\beta(r_k,s_l)/S(r_k,s_l)$ is more nearly a constant than $\beta(r_k,s_l)$ with respect both to variations in interatomic distance and in the AO and atom pairs r_k, s_l involved, it would seem that overlap populations should in general be better measures than bond orders for covalent bond energies. This is especially true where hybrid σ AOs must be considered, where β's and S's may vary strongly and summations of several kinds of overlap energy terms with different β's may be needed. In limited fields, in particular for π-electron systems where r_k and s_l are $2p\pi$ AOs only, usually of carbon and usually with no great variations in interatomic distances, overlap populations have less advantage over bond orders. A more detailed comparison, combined with a discussion of bond orders of various types, is given below in Sec. 4.

In a previous paper, reasons were given for supposing that, roughly,

$$-\beta_{rs}/S_{rs}=A_\tau\bar{I}_{rs} \quad (10)$$

where A_τ is a constant (to be determined empirically) for any particular type (e.g., σ or π) of AOs χ_r and χ_s, and $\bar{I}_{rs}$ is the mean valence-state ionization energy for ionization from the valence and/or inner shells (e.g., the L or K shell) of the atoms to which χ_r and χ_s belong.[8] Equation (10) is a generalization of Eq. (6).

One then obtains for the overlap energy $\Omega(k,l)$ for any pair of atoms k and l in a molecule the following expressions [see Eqs. (4) of I for the n's]:

$$\left.\begin{aligned}\Omega_i(r_k,s_l)&=A_\tau\bar{I}_{rs}n(i;r_k,s_l);\\ \Omega(r_k,s_l)&=A_\tau\bar{I}_{rs}n(r_k,s_l);\\ \Omega(k,l)&=A_\sigma\sum_{\sigma\text{ pairs}}\Omega(r_k,s_l)+A_\pi\sum_{\pi\text{ pairs}}\Omega(r_k,s_l).\end{aligned}\right\} \quad (11)$$

There is empirical evidence[8] that A_π is considerably larger than A_σ. It may also be that more than one A_σ may be needed, e.g., A_σ is probably different for molecules where χ_r and χ_s are both s AOs (in particular, for H_2) than in other cases.[8] Equations (11) are, more or less, a pure LCAO–MO theory counterpart of the "magic formula" for energies of atomization, based on AO–VB theory with some admixture of LCAO theory, which was given, for molecules not containing strongly polar bonds, in a previous paper.[3] Equations (11) would be used, and the A_τ's determined, primarily for molecules in their equilibrium configurations.

If Eq. (10) is roughly correct, it should be very helpful in estimating β values for bonds between various atom-pairs, for use in applications of the semiempirical LCAO MO theory. However, this important possibility will not be pursued further here.

The total energy of a molecule in LCAO theory is a sum of ϵ's (see Eq. (9)) over all electrons, plus a sum of internuclear and interelectronic repulsion terms. In the energy of atomization, contributions should in general be present not only from the overlap-energy (β) terms, but also from various Coulomb (including polar), promotion energy, and configuration-interaction terms. In the cases of H_2 and H_2^+, the overlap energy alone gives by itself a close approximation to the negative of the dissociation energy,[3] but there is no assurance that such a simple relation will be true in general, even for homopolar molecules. A careful analysis of the question of whether or how the energy of atomization of a molecule can be divided into a sum of overlap-energy terms proportional to overlap populations (Eqs. (11)), plus *other* terms, seems to be badly needed. There are indications that in many cases (unlike that of H_2), the major contributions even for homopolar bond energies may come from Coulomb-energy terms. A semiempirical formulation worked out along these lines should be valuable, particularly since it may be a long time before energies of atomization can be accurately calculated purely quantum-mechanically. Although some exploratory studies aimed toward such a formulation have been made in this laboratory, the matter will not be further discussed here.

The notable empirical success of the bond order concept in application to π-electron systems does, however, indicate that the overlap-energy (β) terms in Eq. (8) or (9), even though they may not be the only terms contributing to covalent bond energies, do play a major role, at least for first-row π-electron bonds. Consequently, it is reasonable to expect that the quantities $\Omega(k,l)$ of

[4] R. S. Mulliken, J. chim. phys. **46**, 675 (1949), Section 21.

[5] The fact that the overlap populations $n(i;r_k,s_l)$ appear explicitly in the overlap terms in Eq. (9), as well as (implicitly) in the Coulomb terms [since the $N(i;r_k)$'s *include* the overlap populations, See Eq. (6') of I], is a consequence of the way in which the β's are defined [see Eq. (5); in general, $\beta_{rs}=\int\chi_r H\chi_s dv -\frac{1}{2}S_{rs}(\alpha_r+\alpha_s)$].

[6] C. A. Coulson, Proc. Roy. Soc. (London) **169A**, 419 (1939).

[7] Except that they are normalized as if, in Eq. (3) of *I*, S_{rs} were zero so that $c_r^2+c_s^2=1$.

[8] See reference 3, p. 296, footnotes 39 and 40, and Table VIII.

Eqs. (11), defined on a similar foundation but more flexibly and generally than bond orders, should be even more significant than the latter.

The relation of overlap populations to covalent bonding will be further considered in papers III and IV of this series.

3. APPLICATIONS OF SEMIEMPIRICAL BOND ENERGY FORMULA

It is of interest to see whether sensible values of covalent bond energies can be obtained using Eq. (11) in connection with the overlap populations computed for H_2, CO, and H_2O in Secs. 4–6 of I. For purposes of calibration, A_σ may tentatively be determined from data for H_2, setting

$$\Omega = A_\sigma I_H n,$$

using n from Table IX of I and $I_H = 13.60$ ev. Putting Ω equal to the empirical dissociation energy $D_0 = 4.476$ ev for H_2, which is close to the overlap energy (4.07 ev) computed by LCAO MO theory (see Sec. 2) using $1s$ AOs with $Z = 1$,[9] one gets $A_\sigma = 0.384$. If now it is assumed that this A_σ can be used for (all) the MOs of H_2O one gets for the latter

$$\begin{aligned}\Omega(H_2O) &= A_\sigma(\bar{I}'n' + \bar{I}''n'') \\ &= (0.384)[(17.41 \times 0.663) - (271.8)(0.006)] \\ &= (4.43) - (0.63) = 3.80 \text{ ev},\end{aligned}$$

using data from a previous paper for the $\bar{I}$'s.[10] Here n'' refers to the overlap population involving $1s_O$, n' to the remaining overlaps, while $\bar{I}''$ and $\bar{I}'$ are the corresponding mean I's. Notable is the relatively large negative energy contribution corresponding to the negative $1s_O - 1s_H$ overlap populations. (In N_2, the corresponding negative contributions to the energy of covalent bonding arising from negative overlap populations between the $1s_N$ and other AOs are much larger still.[11])

The Ω of 3.80 ev just calculated is much smaller than the empirical atomization energy D of H_2O (9.54 ev). However, in the first place, part of the observed D of H_2O must be credited to ionic forces. One approach to an estimation of the ionic contribution to D is to compute $-2e^2Q_OQ_H/r_{OH}$ (see Eq. (8) of I), using $-Q_O = 2Q_H = 0.35$ from Table V of I. The result is 1.84 ev; however, this should be increased by a contribution representing ionic-covalent resonance. Another approach depends on Pauling's electronegativity scale, according to which the energy difference between a pure covalent single bond and a partially ionic single bond is given, in ev, by the square of the difference in electronegativity on his scale. For H and O, the latter is 1.40; for two bonds as in H_2O, the result is $2(1.40)^2 = 3.92$ ev. On this basis, the corrected empirical D for purely covalent H_2O would be 5.6 ev. This is sufficiently near to the value 3.8 ev calculated above to encourage the idea that Eq. (11), but with a somewhat larger A_σ for other molecules than for H_2, may prove to be useful and significant.

As applied to CO, Eq. (11) takes the form

$$\Omega(CO) = A_\sigma\bar{I}'n_\sigma' + A_\sigma\bar{I}''n'' + A_\pi\bar{I}'n_\pi'.$$

Unfortunately, n'' is not known, but it may be assumed to have about the same value (-0.0374)[11] as for N_2. Then with $\bar{I}' = 18$, $\bar{I}'' = 214$, and n_σ' and n_π' from Table VII of I, the foregoing equation becomes

$$\Omega(CO) = 6.55A_\sigma - 8.00A_\sigma + 11.78A_\pi.$$

This would say that the covalent bond energy is roughly equal to that of the π electrons alone. If A_π is considerably larger than A_σ,[3] an agreement between the calculated Ω and the observed D (probably 11.1 ev) is obtained which is about as good as that found above for H_2O corrected to a pure covalent basis.

4. LCAO BOND ORDERS AND OVERLAP POPULATIONS

The concept of (covalent) bond order, introduced into LCAO–MO theory by Coulson,[6] has been used mainly as a measure of extent of π character in the bonds of conjugated or mesomeric organic molecules. It has been used largely in connection with bond-order bond-length relations. As has been pointed out briefly after Eq. (9), overlap populations are rather similar to bond orders in furnishing measures of covalent bond energies, but apparently should be *better* measures, as well as being much more capable of generalization for bonds of varying type and length. However, it seemed worth while to review here several ways in which LCAO bond orders have been or can be defined, making also a few comparisons with overlap populations.

Coulson's original definition of bond order was based on the simplifying assumption that overlap integrals may be neglected in computing the coefficients in LCAO MOs. Letting d_i refer to the coefficients obtained if S_{rs} is neglected, Eq. (3) of I for the simple case of N electrons in a single 2-center MO becomes

$$N(d_r^2 + d_s^2) = N. \tag{12}$$

The corresponding Coulson bond order is

$$p(r,s) = Nd_rd_s, \tag{13}$$

which for a homopolar-bond MO ($d_r = d_s = 2^{-\frac{1}{2}}$) occupied by two electrons ($N = 2$) gives $p(r,s) = 1$. Hence, the *unit* of Coulson bond order is *one homopolar bond.*

For a pair of electrons in a partially polar MO, Coulson's covalent bond order falls somewhat below 1 and in the limiting case of a pure ionic bond ($d_r = 1$, $d_s = 0$), it is zero. Even for a strongly polar bond, however, $p(r,s)$ remains large; e.g. even in the very extreme case $d_r^2 = 0.99$, $d_s^2 = 0.01$, $p(r,s)$ is still 0.2.[12] It is of

[9] See reference 4, Sec. 28, and reference 3, p. 296.
[10] Reference 3, Table VIII.
[11] C. W. Scherr, J. Chem. Phys. **23**, 569 (1955).
[12] See R. S. Mulliken, pp. 67–68 of Shelter Island Conference on Quantum Mechanical Methods in Valence Theory, published 1952 by the Office of Naval Research, Washington, D. C.

interest that *overlap populations* show a similar kind of behavior in polar bonds.

In partially polar bonds, the loss of covalent bond energy is more or less made up by the incidence of ionic bond energy (plus, according to AO–VB theory, energy of ionic-covalent resonance). One might perhaps roughly define an *ionic bond order* as

$$p_{\text{ionic}}(k,l) = -Q(k)Q(l)(a_0/R), \tag{14}$$

with $Q(k)$ and $Q(l)$ obtained using Eq. (8) of I. This p_{ionic} would be the mutual energy of attraction of the gross charges on atoms k and l in atomic units (i.e., units e^2/a_0, or 27.2 ev).

For a polyatomic molecule containing one AO per atom, with LCAO MOs

$$\phi_i = \sum_r d_{ir}\chi_i,$$

Coulson's general definitions of partial and total covalent bond order for a pair of bonded atoms are

$$p_i(r,s) = N(i) \sum_{s>r} d_{ir}d_{is}; \quad p = \sum_i p_i(r,s). \tag{15}$$

For non-neighbor atoms, Coulson set $p(r,s)$ equal to zero. For the most general case with hybrid AOs, hence more than one nonhybrid AO per atom (see Eq. (1′ of I)), Eqs. (15) might perhaps be generalized to

$$\left.\begin{aligned} p_i(r_k,s_l) &= N(i)d_{ir_k}d_{is_l}; \quad p_i(k,l) = \sum_{l>k} p_i(r_k,s_l); \\ p(k,l) &= \sum_i p_i(k,l). \end{aligned}\right\} \tag{16}$$

The present writer,[4] and Chirgwin and Coulson,[13] have discussed the redefinition of covalent bond orders when overlap integrals are no longer neglected. Again considering first the simple case of a single 2-center MO, Eq. (3) of I reads

$$N(c_r^2 + 2c_rc_sS_{rs} + c_s^2) = N.$$

One might now define the bond order as

$$p'(r,s) = Nc_rc_s. \tag{17}$$

However, for a homopolar bond, where $c_r = c_s = [2(1+S)]^{-\frac{1}{2}}$, $p'(r,s) = 1/(1+S)$ for $N=2$, instead of $p(r,s)=1$.

In order to preserve the original unit of bond order, c_r and c_s may be multiplied by a common factor ν such that, if the resulting quantities are called d_r'' and d_s'', $d_r''^2 + d_s''^2 = 1$. Then

$$\begin{gathered} d_r'' = \nu c_r; \; \nu^2 = 1/(c_r^2+c_s^2) = 1/(1-2c_rc_sS_{rs}); \\ p''(r,s) = Nd_r''d_s'' = Nc_rc_s/(c_r^2+c_s^2). \end{gathered}$$

For a homopolar bond, $p''(r,s)$ is now 1, as required. In the polyatomic case, for one MO per atom in each MO ϕ_i,

$$\left.\begin{aligned} &d_{ir}'' = \nu_i c_r; \quad \nu_i^2 = 1/(\sum_r c_r^2); \\ &p_i''(r,s) = N(i)d_{ir}''d_{is}''; \quad p''(r,s) = \sum_i p_i''(r,s). \end{aligned}\right\} \tag{18}$$

The d_{ir}'''s are in many cases the same as the d_{ir}'s, but in general are somewhat different.[13,14]

Still another way of defining bond orders taking overlap into account has been given by Chirgwin and Coulson.[13]

Another way[15] to preserve the original unit of bond order, yet at the same time to gain certain other advantages not possessed by the bond orders p'' of Eqs. (18), is to define

$$p'''(r,s) = N(1+S_{rs})c_rc_s,$$

or, for the general case

$$\left.\begin{aligned} p_i'''(r_k,s_l) &= N(i)(1+S_{r_ks_l})c_{ir_k}c_{is_l}; \\ p_i'''(k,l) &= \sum_{l>k} p_i'''(r_k,s_l); \\ p'''(k,l) &= \sum_i p_i'''(k,l). \end{aligned}\right\} \tag{19}$$

The values of $p'''(k,l)$ are now in general nearly the same as those of $p(k,l)$ or $p''(k,l)$ as given by Eqs. (16) or (17); and for the case of a single homopolar bond, $p'''(k,l)=1$, as required.

As Coulson,[6] and Coulson and Longuet-Higgins,[16] have pointed out, Coulson bond orders are intimately connected with bond energies. Here it is best[4] not to neglect overlap. The orbital energy ϵ_i of any LCAO MO ϕ_i is then given in general by Eq. (8), which may be rewritten in terms of (partial) bond orders of the special type defined in Eq. (17) as

$$N(i)\epsilon_i = \sum_{r_k} N(i;r_k)\alpha(r_k) + 2\sum_{l>k} p_i'(r_k,s_l)\beta(r_k,s_l). \tag{20}$$

The corresponding equation in terms of overlap populations has been given above as Eq. (9).

For bond orders of types p, p'', or p''', the *unit* of resonance energy is "one homopolar bond" with energy β. This is satisfactory so long as there is only one β for each bond and so long as this β does not vary much from one bond to another, as for example for the π electrons in a conjugated system; though even here, β varies more or less with bond length. In hybrid σ bonds, and in general, one has to deal with more than

[13] Chirgwin and Coulson, Proc. Roy. Soc. (London) **20A**, 196 (1950).

[14] The writer stated very stupidly in reference 4 following Eq. (141a) that the d_{ri}'s "are of course proportional to" the c_{ri}'s. While a corresponding statement is true (by definition) for the d''_{ir}'s, it is *not* in general justified for the d_{ri}'s.

[15] See reference 4, Eqs. (145b). See B. and A. Pullman, *Les Theories Electroniques de la Chimie Organique* (Masson and Company, Paris, 1952), p. 340, for some calculated values of $p''(k,l)$ for conjugated systems.

[16] C. A. Coulson and H. C. Longuet-Higgins, Proc. Roy. Soc. (London) **191A**, 39 (1947).

one β, and if the quantities β/S (see Eq. (9)) are fairly constant, the advantages of overlap populations over bond orders as measures of resonance energy are obvious.

Overlap populations have a further superiority over the bond orders p or p'' in that they take proper account of the effects of overlap in antibonding MOs and in all MOs where antibonding effects occur. For example, if one asks for the total bond order for two pairs of electrons one in a bonding and the other in a corresponding antibonding MO, one obtains by either Eqs. (16) or (18) a bond order $+1$ for the bonding MO and -1 for the antibonding MO, or a total of zero. Yet it is known that the net effect of two such pairs is a strongly antibonding one (a nonbonded repulsion in AO–VB theory), a fact which is correctly represented by adding the overlap populations $2S/(1+S)$ and $-2S/(1-S)$ in the two MOs, giving a total of $-4S^2/(1-S^2)$. Similar considerations apply to excited states of molecules, where antibonding MOs are more prevalent than in ground states.

The difficulties discussed in the last paragraph can be overcome by using the modified bond orders p''' defined by Eqs. (19), which although like p and p'' they give for instance a bond order $+1$ for the bonding electrons in He_2, give $-(1+S)/(1-S)$ for the antibonding electrons, and thus a net antibonding effect for the four electrons.[15] Another possibility would be to use bond orders p' defined in the manner of Eq. (17). These would reproduce correctly the net antibonding effect for cases like that of two He atoms, but would sacrifice the advantages of Coulson's original definition which makes the bond order 1.00 for a homopolar single bond. In view of the considerations advanced in the second preceding paragraph, it seems preferable in general to use overlap populations. Nevertheless ordinary bond orders p remain fairly satisfactory if their application is restricted to the π electrons in the ground states of conjugated systems not containing very polar bonds.

ACKNOWLEDGMENT

The writer is indebted to Mr. N. S. Ham for drawing the figure and for related calculations.

THE JOURNAL OF CHEMICAL PHYSICS VOLUME 23, NUMBER 10 OCTOBER, 1955

Transformation of Adsorbed Water on Solid Surfaces and its Dielectric Losses and Conductivities

SHIGEHIKO KUROSAKI, SHŌGO SAITŌ,* AND GENJU SATŌ
Department of Applied Physics, Hitachi, Central Research Laboratory, Kokubunji, Tokyo, Japan
(Received January 4, 1955)

The adsorption isotherm of water vapor on nonalkali glass cloth was obtained at 25°C, and its dielectric power factor was measured also in the frequency range of 80 kc/sec~11 mc/sec.

The power factor of glass cloth and surface dc conductivities of nonalkali glass, soda glass, fused silica, Teflon, and polymethylmethacrylate plates increased rapidly to maximum peaks, when they were exposed to water vapor, and then gradually decreased to certain constant values.

These phenomena may be interpreted as physical picture of phase changes in the adsorbed water phase from the amorphous state to the crystalline state, as well as the deposit films of evaporated metals on solid surfaces. But the surface conductivity of polycapramide increases as the moisture content increases with time, suggesting a rapid absorption of water molecules into the solid. An analysis of this process of phase change of adsorbed water is outlined.

INTRODUCTION

THE results of some dielectric properties of adsorbed water upon porous silica gel has been presented in the previous paper,[1] and it has been assumed from the data that there are three different states in the adsorbed water films depending upon moisture content.

The variation of physical properties of the adsorbed phase with the adsorbed amount has been supported by several other investigators also.[2–4]

On the other hand, little information has been obtained on the phase change of adsorbed substances with time.

During the course of an investigation of the dielectric properties of adsorbed water on glass, it was observed that the dielectric power factor and the surface dc conductivity of glass, which was adsorbing water vapor at a constant humidity decreased unexpectedly with time, in spite of an increase in moisture content of the glass. This result is contrary to the common-sense view that the power factor or electric conductivity of moist solids increases as moisture content is progressively increased, and is not explicable by the physical picture of adsorption of water molecules having an invariable configuration.

It is well known that the deposit of evaporated metal

* Graduate Student, Department of Chemistry, Tokyo College of Science. Present address, Electrotechnical Laboratory, Nagatachō, Tokyo.

[1] S. Kurosaki, J. Phys. Chem. **58**, 320 (1954).

[2] I. Higuti, Science Rep. Tôhoku Univ. **33**, 99 (1949).

[3] I. Higuti and M. Shimizu, J. Phys. Chem. **56**, 198 (1952).

[4] Snelgrove, Greenspan, and McIntosh, Can. J. Chem. **31**, 72 (1953)

on solids at lower temperatures is in an amorphous or a microcrystalline state in the early stages of deposition, and then gradually transforms to a crystalline state.[5,6] In the case of adsorbed water vapor on glass, this fact will not greatly differ from the case of a deposit film of evaporated metal on glass. That is, a transformation of adsorbed water upon the glass surface should be considered.

Outlined in the present article is the experimental evidence of the transformation in the water vapor adsorbed on glasses and several organic high polymers, and general explanation of the variation in the dieletric power factor or the electric conductivity of solids which adsorb water vapor.

EXPERIMENTAL

Adsorption isotherms of water on nonalkali glass cloth were obtained at 25°C for two cases: (1) the case of adsorption on perfectly outgassed glass cloth, (2) on that that has already adsorbed water vapor to some extent.

In the case of (1), the specimen was outgassed at 250°C 10^{-4} mm Hg for 2 hours over phosphorus pentoxide, and (2) at 25°C for 24 hours over 95% sulfuric acid.

The apparatus was essentially the same as that of Higuti[7]: the adsorption vessel and a supply system of water vapor were immersed in a thermostat as well as a calibrated gas buret and connecting capillary tubes were coiled with a copper wire (0.4 mm diameter), which was of use as an electric heater to prevent condensation of water vapor. Using this apparatus the volume of adsorbed water vapor could be accurately estimated.

The nonalkali glass cloth was taken from Nittō Bōseki Company, and the mean diameter of its fibers was about 7μ, having the density of 2.54. Analysis in our laboratory gave the following composition; SiO_2 51.20, Al_2O_3 17.00, CaO 17.89, B_2O_3 11.40, MgO 1.57, BaO 0.67, Na_2O 0.155, K_2O 0.045 wt. %.

For the purpose of dielectric measurements, the nonalkali glass cloth was held between poles of a capacitor of the parallel plate type, which was suspended in a glass vessel connected to a vacuum system, a supply system of water vapor, and an oil manometer. The measurements of dielectric losses were carried out using the Q-meter described previously,[1] over the frequency range of 80 kc/sec to 11 mc/sec.

The capacitor consisted of two brass disks separated by three tiny glass spacers, its capacity being 58.4 $\mu\mu$f when empty. The specimen was held to a certain volume fraction in the space of the pole gap.

The variation of dielectric losses with time was observed at 250 kc/sec under various humidities and temperatures by putting various amounts of water vapor into the vessel. After putting in the water vapor, the pressure of the water vapor in the vessel was nearly constant but decreased continuously, showing definitely that the moisture content was increasing.

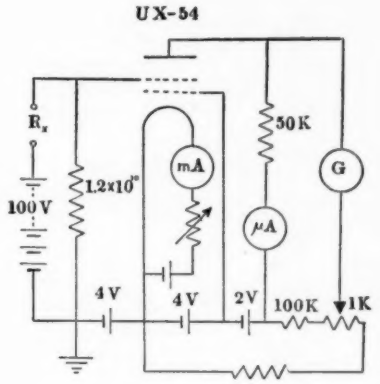

FIG. 1. Circuit diagram for measurement of surface conductivity.

Surface dc conductivities of a nonalkali glass plate were measured under several humidities with the circuit shown in Fig. 1, which is a bridge circuit using a UX-54 (FP-54) tube as one of the resistance arms of the bridge.

The measuring cell, in which the glass plate was suspended, was a large glass desiccator type vessel connected to a vacuum pump, a manometer, and a supply system of water vapor; and before taking measurements, it was evacuated sufficiently to dry the surface of the specimen, and then water vapor was put, as rapidly as possible, into the vessel through a vacuum cock. The dc conductivity of glass surfaces could be obtained at specified time intervals with the balanced circuit shown in Fig. 1.

The variation of surface conductivities of soda glass, fused silica, Teflon, polymethylmethacrylate, and polycapramide plates was also measured by exposing to water vapor for comparison to nonalkali glass.

RESULTS AND DISCUSSION

(A) Adsorption Isotherm of Water Vapor on Glass Cloth

The adsoprtion isotherm of water vapor on nonalkali glass cloth was shown in Fig. 2. This result agrees

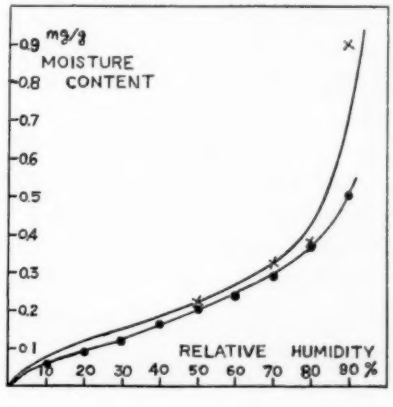

FIG. 2. Adsorption isotherms of water vapor on nonalkali glass cloth. (● perfectly dried, × imperfectly dried.)

[5] H. Koenig, Reichsber. Physik 1, 4 (1944).
[6] T. Sakurai and S. Munesue, Science Rep. Research Inst. Tôhoku Univ. 4, 96 (1952).
[7] I. Higuti, Bull. Inst. Phys. Chem. Research, Tokyo 14, 853 (1935).

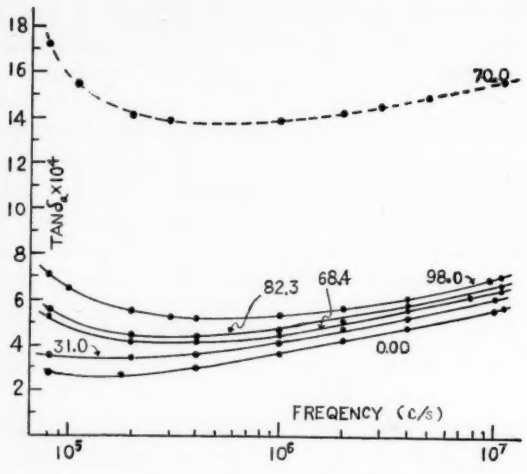

FIG. 3. The apparent dielectric power factor of nonalkali glass cloth at the inscribed humidities. Broken line represents the real values of nonalkali glass itself.

roughly with that of Razouk and Salem[8] for adsorption of water vapor on glass wool washed with water before drying.

The adsorption isotherms of water vapor on perfectly and imperfectly dried glasses were nearly the same, but the moisture content of the latter seems a little greater than that of the former, apparently at the same humidity.

Trouton pointed out that the perfectly dried glass adsorbed water vapor with greater difficulty than the imperfectly dried glass,[9] owing to the lack of water nuclei or active sites on the surface of the former; that is, the rate of adsorption of the former was lower than that of the latter. This observation is analogous to the behavior of silica gel, which adsorbs water vapor with more difficulty when it is thoroughly dried in higher temperatures than 600°C.

The slight difference between two curves in Fig. 2 may be attributed to the difference of adsorption velocities of water vapor on perfectly and imperfectly dried glass clothes, because it may take more time for the former to attain adsoprtion equilibrium, and, therefore, its moisture content may be underestimated.

From the *BET* plot of the obtained results, the effective surface area of this glass cloth may be estimated at 2550 cm^2/g, or about 1.5 times the geometric surface area.

(B) Spectra of Dielectric Adsorption

The apparent dielectric power factors of the dried and moist nonalkali glass cloth were plotted against frequency as shown in Fig. 3, where the volume fraction of glass itself in the gap of the capacitor was 0.392.

It increased linearly with the increasing moisture content, and the curve of the graphs were steeper when measured in lower frequencies.

The dielectric adsorption spectra of glass have been investigated by Stevels[10] over a wide frequency range, and it has been considered that the total spectra consisted of four kinds of losses, that is, conduction loss, relaxation loss, vibration loss, and deformation loss. The second loss has its peak at about 10 cps at 27°C, and its foot reaches to the megacycle region. The observed higher values of power factors in lower frequencies shown in Fig. 3 seem to be the foot of the relaxation loss, overlapping with the conduction loss of adsorbed water.

(C) The Dependence of the Power Factor and Surface Conductivity on Time

The most significant feature of the present results is the variation of dielectric losses or surface conductivities with time for glasses and several other solids which are adsorbing water vapor in a constant humidity.

Typical results of the dependence of the dielectric power factor on time were shown in Fig. 4 for dried glass cloth, and in Fig. 5 for glass cloth which had already adsorbed water vapor under 3.2% relative humidities.

As was stated in the last section, the lower the measuring frequency, the more remarkable the variation of power factor per unit moisture content. This leads to the assumption that there is appreciable contribution of dc conductance to the observed loss at 250 kc/sec shown in Figs. 4 and 5.

This assumption is ascertained by measuring the surface conductivity of nonalkali glass plate. Figure 6 shows the dependence of surface dc conductivities of nonalkali glass, soda glass, and fused silica plates on time, and Fig. 7 shows that of three polymer plates.

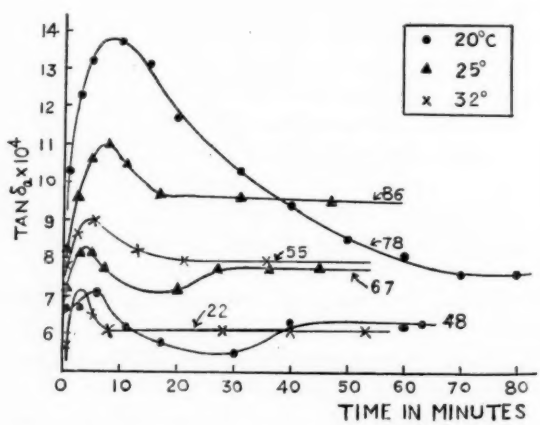

FIG. 4. Tanδ changes of perfectly dried glass cloth during moisture adsorption at the inscribed relative humidities.

[8] R. I. Razouk and A. S. Salem, J. Phys. & Colloid Chem. **52**, 1208 (1948).

[9] F. T. Trouton, Proc. Roy. Soc. (London) **A79**, 383 (1907).

[10] J. M. Stevels, Philips Research Repts. **7**, 161 (1952); Glastech. Ber. **227**, 30 (1953).

Obviously, the height of the peak of dc conductivity in the early stage of adsorption on glass surfaces seems independent of the alkali content of glass. This signifies that the surface conductance of moist glass does not originate from the alkali ion in glass, but mainly from the water adsorbed upon glass surfaces, suggesting the ionization of adsorbed water.

On the basis of the data described above, it seems reasonable to assume that there is a transformation with time in the water adsorbed upon glass or several hydrophobic solids, that is, immediately after adsorption, the state of adsorbed water may be likened to an unstable form of fair ion-conductance, but may be set to a more stable state of less conductance after leaving it as is for a long period.

This process is nothing but an aging of the water adsorbed on solid surfaces. It seems reasonable to regard the former state as an amorphous state, and the latter as a crystalline one, forming a more rigid structure than the former.

This hypothesis corresponds to the behavior of the deposit of evaporated metal on glass surface.

Numerous investigations have been made on the rate of adsorption of gases upon solid surfaces,[11] the simplest expression of the moisture content as a function of time may be described as

$$N \equiv N(t) = N_\infty(1-e^{-\kappa t}), \qquad (1)$$

where N_∞ represents the moisture content per unit mass of the dried adsorbent when $t=\infty$, and κ is a constant.

As is well known, the Eq. (1) may be derived from Langmuir's theory,[12] ascertained by Berl and Weingaertner[13] experimentally. Equation (1) shows that the "*amorphous*" water molecules adsorbed on solids are piled up with the velocity in proportion to $N_\infty e^{-\kappa t}$.

On the other hand, the rate of crystallization of these piled molecules should be treated similarly to that of the crystal growth in the supercooled liquid.

The theory of the kinetics of crystal growth was developed by Avrami[14] with the assumptions that the crystal phase is nucleated by tiny germ nuclei existing in the old phase beforehand, some of these germ nuclei of subcritical size are activated to growth nuclei exceeding a definite critical size, residual germs are swallowed by crystal grains grown from growth nuclei, and in the last step of crystal growing, crystal grains impinge upon each other bringing the cessation of growth. In the initial stage of the generation of nuclei, the amount of subcritical nuclei is not yet sufficient to reach the steady state of growth, accordingly generation of growth nuclei is not observed in a period of incubation time τ.

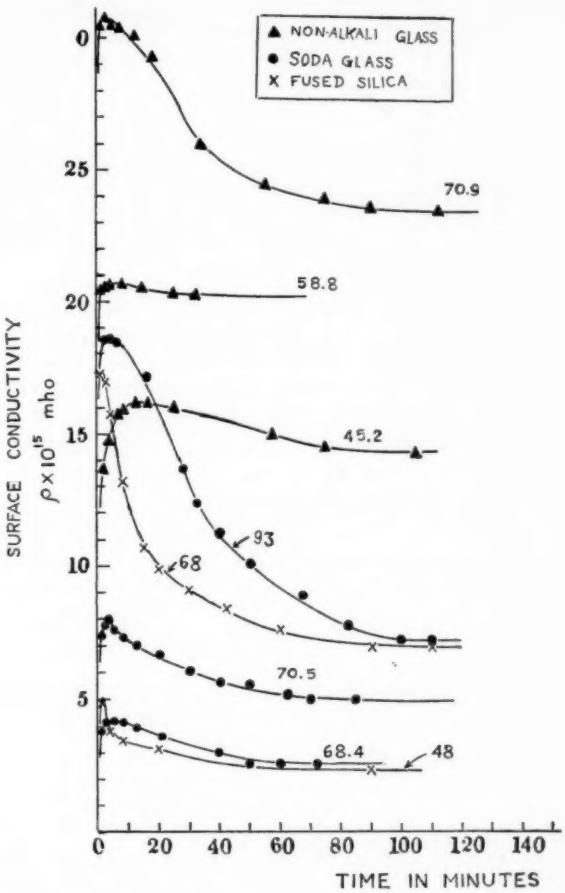

FIG. 6. Surface conductivity changes during moisture adsorption on glass and fused silica at the inscribed humidities.

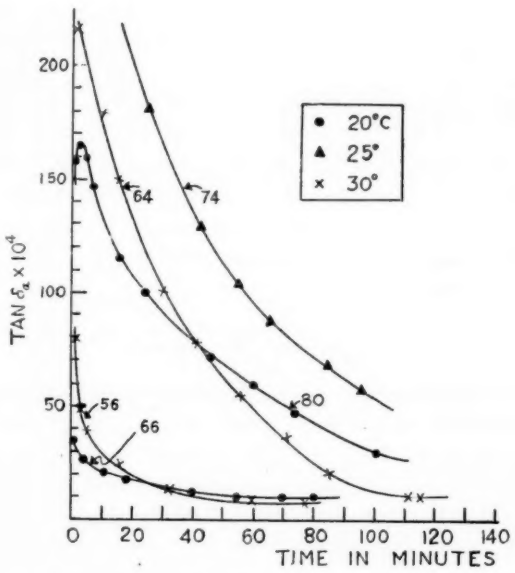

FIG. 5. Tanδ changes of the imperfectly dried glass cloth during moisture adsorption at the inscribed relative humidities.

[11] S. Brunauer *The Adsorption of Gases and Vapors, I* (Oxford University Press, New York, 1945), p. 455.
[12] I. Langmuir, J. Am. Chem. Soc. **40**, 1361 (1918).
[13] E. Berl and E. Weingaertner, Z. physik Chem. **A173**, 35 (1953).
[14] M. Avrami, J. Chem. Phys. **7**, 1103 (1939); **8**, 212 (1940); **9**, 177 (1941).

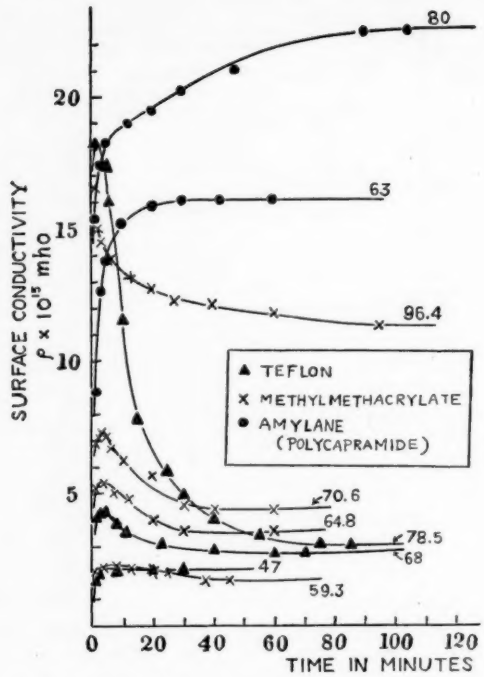

FIG. 7. Surface conductivity changes during moisture adsorption on high polymers at the inscribed relative humidities.

In the crystallization of the *amorphous adsorbed water*, it may be treated similarly to the above. It is natural to assume that the crystallization begins in the lowest layer of adsorbed water film, but for simplicity, let us take the nuclei of the *crystalline adsorbed water* as being distributed randomly, then the amount of crystalline adsorbed water at the time t, $n \equiv n(t)$ may be represented with the Avrami's theory

$$n = n_\infty \{1 - e^{-\lambda(t-\tau)^m}\}, \tag{2}$$

where n_∞ is the ultimate amount of crystal, λ is the rate coefficient of crystallization, τ is the incubation or induction period of crystallization, and $\lambda = 0$ when $t \leq \tau$, and m takes the numbers between 1 to 4 according to the types of crystal growth.

Letting n' represent the amount of *crystalline adsorbed water* per unit mass of the dried adsorbent, we are led to the following relation by considering the variation of the total amount of amorphous bed in relation to time.

$$n' = n_\infty (1 - e^{-\kappa t})\{1 - e^{-\lambda(t-\tau)^m}\}. \tag{3}$$

By the first assumption, the power factor of adsorbed water is assumed to depend mainly upon the amount of *amorphous adsorbed water*, so that

$$\tan\delta \equiv \tan\delta(t) = C_1(N - n') + C_2 n', \tag{4}$$

where both C_1 and C_2 are constants, and $C_1 \gg C_2$.

Substituting (1) and (3) into (4), we obtain

$$\begin{aligned}\tan\delta &= C_1 N_\infty (1 - e^{-\kappa t}) \\ &\quad \times [1 - (C_1 - C_2) n_\infty \{1 - e^{-\lambda(t-\tau)^m}\}/C_1 N_\infty] \\ &= K_1 (1 - e^{-\kappa t})[1 - K_2\{1 - e^{-\lambda(t-\tau)^m}\}],\end{aligned} \tag{5}$$

where $K_1 = C_1 N_\infty$, and $K_2 = n_\infty (C_1 - C_2)/C_1 N_\infty < 1$.

Unfortunately, so many unknown coefficients are present in Eq. (5), that it is difficult to analyze the experimental results quantitatively by applying this equation. But it would be possible to lead curve having similar characteristics to them in the Figs. 4–7 by taking suitable values of K_1, K_2, κ, λ, τ, and m in Eq. (5).

It would be possible, however, to obtain the values of K_1 and κ experimentally, if the rate of moisture adsorption and N_∞ were measured, then K_2 would be obtained also from the ultimate value of power factor at $t = \infty$.

As shown in Figs. 4 and 5, when the glass cloth which had already adsorbed a little water vapor was exposed to moisture, its apparent power factor increased steeper and higher than that of perfectly dried glass cloth did. This seems to show that the former having many active sites of moisture adsorption on its surfaces, adsorbs moisture more rapidly than the latter, and much more *amorphous adsorbed water* molecules are piled up before crystallization begins; of course, retardation time is smaller also in the former and the time necessary to reach $\tan\delta_{max}$ is shorter as clarified in Fig. 5.

The variation of dc conductivities on moist glass and fused silica surfaces shown in Fig. 6 may be treated also as described above.

In the case of organic high polymers, the shape of dc conductivity-time curves on Teflon and polymethylmethacrylate resembles that of glass or fused silica, suggesting the piling and setting process of adsorbed water molecules, but the latter process may be caused not by crystallization of adsorbed water, but mainly by its diffusion into these adsorbents. In the case of hydrophilic polycapramide, water molecules are not piled up on the surface of the adsorbent, but dissolve in it at once, bringing normal increase of conductivity proportional to moisture content.

ACKNOWLEDGMENTS

The authors wish to express their thanks to Dr. R. Kawai, Dr. K. Yumoto, and Dr. J. Ohkubo, and to Professor Y. Toriyama for their encouragement and valuable advice. Grateful acknowledgment is made also to Mr. Y. Maeda, and Mr. T. Mitsuishi and to the staff of the Metal Department for their guidance and discussion.

Self-Diffusion of Liquid Sodium*

R. E. MEYER† AND N. H. NACHTRIEB
Institute for the Study of Metals, University of Chicago, Chicago, Illinois
(Received January 18, 1955)

The self-diffusion of liquid sodium in the temperature range, 98° to 226°, has been studied by the capillary reservoir technique. The data fit the empirical equation, $D=1.10\times10^{-3}\exp(-2430/RT)$. The Stokes-Einstein equation gives a good correlation of the self-diffusion and viscosity data. The difference in the self-diffusion coefficients of the solid and liquid sodium is explained in terms of the "relaxation" theory of diffusion proposed by Nachtrieb and Handler.

INTRODUCTION

IN recent years considerable attention has been centered upon self-diffusion studies in solids and liquids. Such studies provide useful information which may be used in the development and testing of theories of the liquid and solid states. However, relatively little work has been done with liquid metals, particularly with metals whose self-diffusion coefficients have already been measured in the solid state. Since the self-diffusion of solid sodium had already been studied as a function of both temperature and pressure,[1] liquid sodium was selected for these determinations. The relative simplicity of liquid and solid sodium metal recommends it as a profitable metal to study.

THEORY

Equations have been derived which relate the coefficients of self-diffusion and viscosity. A comparison of the measured diffusion and viscosity coefficients provides a way of testing these equations and therefore also the assumptions with which the equations have been derived.

The derivation of the Stokes-Einstein equation[2] assumes that the diffusing particles move through a continuous medium and that Stokes' law may therefore be applied to the motion of the particles through the fluid. The equation so derived is

$$D=kT/6\pi\eta r, \tag{1}$$

where D is the diffusion coefficient, k is Boltzmann's constant, T the absolute temperature, η the viscosity coefficient, and r is the radius of the diffusing particle. It would be expected that this equation would hold only approximately, since Stokes' law would hold only for the case where the diffusing particle is considerably larger than the solvent molecules. Recently, however, Hoffman has shown that it does hold well for liquid mercury if one uses the ionic radius for r in the equation.[3] This use of the ionic radius is not without justification since Eyring has given empirical evidence which suggests that the ion rather than the atom is the unit of flow in liquid metals.[4]

A second equation was derived by Eyring on the basis of his reaction rate theory and his hole theory of the liquid state[5]:

$$D=\lambda_1 kT/\lambda_2\lambda_3\eta, \tag{2}$$

where λ_3 is the interatomic distance in the direction of diffusion, and λ_1 and λ_2 are the interatomic distances perpendicular to λ_3. For spherical molecules in a liquid having a high degree of local order λ_1, λ_2, and λ_3 may be taken as approximately equal. The mean jump distance, λ, of a molecule into an adjacent hole is not necessarily the same as the interatomic distances, although it is probably approximately so. Within the limits of our knowledge of the structure of liquids we may assume that the four distances are equal, and approximate Eq. (2) by:

$$D=kT/\eta\lambda. \tag{3}$$

The temperature dependence of D in these equations can be derived if we use the empirical relation $\eta=\eta_0\exp(E/RT)$ where E is the experimental activation energy and η_0 is a constant independent of temperature. Both the Stokes-Einstein and Eyring equations‡ give equations of the form:

$$D=(\text{constant})T\exp(-E/RT), \tag{4}$$

where E is the activation energy for viscous flow. If $\log D$ is differentiated with respect to the reciprocal of

* Based upon the dissertation submitted by Robert E. Meyer in partial fulfillment for the Ph.D degree in chemistry at the University of Chicago. Work supported in part by the U. S. Air Force under Contract, the sponsoring agency being the Aeronautical Research Laboratory of the Wright Air Development Center, Air Research and Development Command.

† National Science Foundation Fellow.

[1] Nachtrieb, Catalano, and Weil, J. Chem. Phys. **20**, 1185 (1952); Nachtrieb, Catalano, Weil, and Lawson, J. Chem. Phys. **20**, 1189 (1952).

[2] A. E. Einstein, Ann. Physik **17**, 549 (1905); **19**, 371 (1906); Z. Elektrochem. **14**, 235 (1908).

[3] R. E. Hoffman, J. Chem. Phys. **20**, 1567 (1952).

[4] Glasstone, Laidler, and Eyring, *The Theory of Rate Processes* (McGraw-Hill Book Company, Inc., New York, 1941), p. 496.

[5] See reference 4, p. 519.

‡ Strictly speaking, the pre-exponential of Eq. (4) is not temperature-independent, because of thermal expansion. In Eyring's notation, $D=\lambda^2(kT/h)\exp-\Delta F/RT$ or, to the same approximation noted above, $D=\text{const}\ V^{\frac{1}{3}}\cdot T e^{\Delta S/R}e^{-\Delta H/RT}$. Differentiation gives $d\ \ln D/d(1/T)=(-2/3)T^2\cdot(1/V)(dV/dT)-T-\Delta H/R$. Since the coefficient of expansion of liquid sodium is 2.20×10^{-4}, the first term contributes only 26 calories and is smaller by more than an order of magnitude than the experimental uncertainty in $\Delta H/R$. The difference between the energy and enthalpy of activation is likewise wholly negligible at atmospheric pressure.

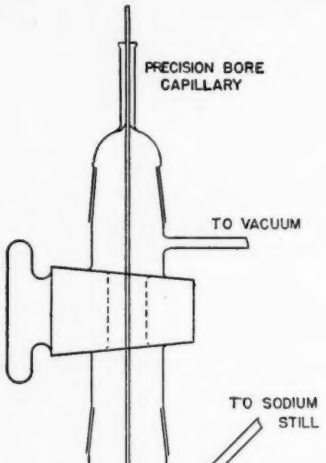

FIG. 1. Diagram of diffusion apparatus.

the temperature the following expression is obtained:

$$-R(d\ln D/d(1/T))=RT+E. \quad (5)$$

The quantity $-R[d\ln D/d(1/T)]$ is the activation energy of diffusion found by plotting $\ln D$ against $1/T$. Therefore, the difference between the activation energies of diffusion and viscous flow should be, at any temperature, equal to RT. This is approximately true for liquid mercury since the activation energies of self-diffusion and viscosity are respectively 1160 and 650 calories per mole and RT is about 640 calories per mole for the average temperature of the runs.[3] Alternatively, one could plot $\ln(D/T)$ *versus* $1/T$ and obtain E directly, but the conventional plot is made in this paper.

EXPERIMENTAL

The experimental method used is the capillary-reservoir technique first described by Anderson and Saddington.[6] About fifty grams of nonradioactive sodium is kept thermostated in a Pyrex container. A capillary, closed at one end and open at the other is filled with radioactive sodium. The capillary is then lowered into the bath of nonradioactive sodium until the open end is just above the surface of the liquid and left there until thermal equilibrium is reached. The diffusion run is then begun with the complete immersion of the capillary. After a measured length of time, the capillary is removed from the bath and the average concentration of radioactive sodium in the capillary is determined. The diffusion coefficient may then be calculated from the length of the capillary, the elapsed time of the run, and the ratio of the average concentration of radioactivity in the capillary after the run to the original concentration of radioactivity in the capillary.

For this experiment, the boundary conditions for the solution of the diffusion equation, $dC/dt=D(d^2C/dx^2)$, are

$$\begin{aligned} &\text{for} \quad 0<x<L, \quad \text{at} \quad t=0, \quad C=C_0, \\ &\text{for} \quad x>L, \quad \text{at all } t, \quad C=0, \end{aligned}$$

where C is the concentration of the isotope, L is the length of the capillary, and t is the time. The positive direction of x is out of the capillary and x has its zero at the closed end of the capillary.

The solution of the diffusion equation gives an infinite series for the ratio of the average concentration of isotope after diffusion to the original concentration, C_{av}/C_0. For the conditions of this experiment all but the first term may be neglected, giving the expression:

$$\ln\pi^2C_{av}/8C_0=-\pi^2Dt/4L^2. \quad (6)$$

In order to reduce the formation of sodium oxide in the bath the apparatus shown in Fig. 1 was devised. It uses a 20 mm bore stopcock which served as a vacuum lock to prevent air from reaching the sodium. The sodium was distilled directly into the diffusion chamber so that at no time during the course of the experiment was the sodium ever in contact with the atmosphere. The procedure was to introduce the capillaries into the top portion of the apparatus with the stopcock closed. The top portion was then evacuated. Vacuum grease and rubber rings in grooves in the drill rod insured a vacuum tight fit of the drillrod in the precision bore tubing. The stopcock was then opened and the capillary lowered into the sodium bath by pushing the drill rod downward. Dry nitrogen was then admitted as a precaution against vacuum failure during the run. The drill rod and capillary were slowly rotated by a synchronous motor in order to insure that the concentration fell off rapidly to zero at the open end of the capillary, as required by the boundary conditions. At the end of the run the capillaries were removed by the reverse process.

The capillaries were filled by forcing solid sodium into the capillary with an hydraulic press. A dry box on the bed plate of the press minimized the oxidation of the sodium during the filling process.

RESULTS AND DISCUSSION

The results of the experiment are shown in Table I. Duplicate runs give an idea of the errors involved in this experiment. The results are shown plotted in Fig. 2, in which $\ln D$ is plotted against the reciprocal of the absolute temperature. The equation of the straight line, which was calculated by the method of least squares, is $D=1.10\times10^{-3}\exp(-2430/RT)$. The probable errors, also calculated by least squares, are $\pm0.37\times10^{-3}$ cm^2/sec in the pre-exponential and ±200 calories per mole

[6] J. S. Anderson and K. Saddington, J. Chem. Soc. (London) S381, (1949).

in the activation energy. The average deviation of the experimentally determined points from the line is 3.6%.

The activation energy for viscous flow in the temperature range of these experiments is about 1500 calories per mole.[7] Since the average temperature of the runs is about 440°K, RT is about 880 calories per mole, in close agreement with the difference in the activation energies for diffusion and viscous flow. This evidence suggests that for liquid sodium the form of the diffusion equation is $D=$ (constant) $T\exp(-E/RT)$ where E is the activation energy for viscous flow. We should expect, therefore, that plots of $\ln(D/T)$ against $1/T$ would give straight lines and that the conventional plots of $\ln D$ against $1/T$ would not be straight. Unfortunately the data available at present are not sufficiently accurate and extensive to test this conclusion.

The Stokes-Einstein and Eyring equations may be tested quantitatively by using the published viscosity data for liquid sodium.[7] Substitution of the viscosity data into the Stokes-Einstein equation yields values ranging from 0.91 A° to 0.95 A° for the ionic radius, with an average value of 0.93 A°. This value is in excellent agreement with the published estimates of the ionic radius (0.98 A° for the Goldschmidt value[8] and 0.95 A° for the Pauling value[9]). Because of the assumptions involved in the derivation of the Stokes-Einstein equation, this agreement is regarded as fortuitous.

Combination of the viscosity and diffusion data in the Eyring equation gives a value of 17.3 A° for the interatomic distance. X-ray studies of liquid sodium give 3.83 A° for the average distance between nearest neighbors.[10] The Eyring equation therefore gives a value which is correct to order of magnitude only.

The data of the previous work on self-diffusion in solid sodium can be represented by the equation

TABLE I. Experimental results.

Temp. deg C	Time, sec $\times 10^{-4}$	D, cm²/sec $\times 10^{5}$
98.0	5.02	4.19
98.0	5.66	4.35
98.6	6.28	4.14
98.6	6.20	3.87
101.7	5.68	3.94
101.7	5.68	4.28
134.3	5.88	5.39
134.8	5.79	5.67
175.3	2.32	7.12
175.5	5.81	7.47
217.5	2.11	9.59
226.5	2.51	8.97

[7] Y. S. Chiong, Proc. Roy. Soc. (London) **A157**, 264 (1936).
[8] Goldschmidt, Ber. deut. chem. Ges. **60**, 1263 (1927).
[9] Pauling, J. Am. Chem. Soc. **49**, 765 (1927).
[10] F. H. Trimble and N. S. Gingrich, Phys. Rev. **53**, 278 (1938).

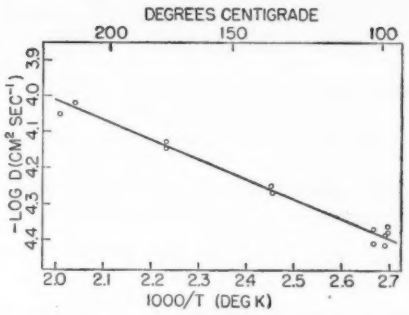

FIG. 2. Temperature dependence of the self-diffusion coefficients of liquid sodium.

$D=0.242\exp(-10\,450/RT)$, and may be compared with the equation for the liquid, $D=1.10\times10^{-3}\exp(-2430/RT)$. The "relaxion" theory of diffusion in solids as proposed by Nachtrieb and Handler,[11] provides a possible explanation for the difference in pre-exponentials and activation energies. This theory proposes that diffusion in solids takes place in disordered liquid-like regions which form about vacancies. The measured activation energy for diffusion in solids is considered to be made up of the activation energy of liquid diffusion plus the additional energy necessary to form the disordered region. This additional energy, which corresponds to 8000 calories per mole in sodium, consists of the energy necessary to "melt" the number of atoms in the disordered region. This number is estimated to be about fourteen, and when multiplied by the latent heat of melting of sodium, 636 calories per mole, gives about 8900 calories per mole.

The difference in the pre-exponentials may be explained by a large entropy of activation in the solid and a relatively small activation entropy in the liquid. Both Zener[12] and Eyring[5] present theories of the pre-exponential in which an $\exp(\Delta S/R)$ term appears in the pre-exponential. If the difference in the two terms, 0.242 and 1.10×10^{-3} cm²/sec, is attributed entirely to this entropy term, then the difference in activation entropies of solid and liquid diffusion would be about 10.7 entropy units. This is not an unreasonable value since one would expect considerable disordering in the "melting" process of the "relaxion" theory. The total entropy of activation in the solid is composed of the 10.7 entropy units plus the entropy of activation of the liquid. The latter entropy may be estimated by using the random walk expression for diffusion,

$$D=(1/6)\sum_i \Gamma_i\delta_i^2 \qquad (7)$$

where Γ_i is the mean jump frequency, δ_i is the associated elementary jump distance, and the summation extends over all jump modes i. If the assumption is made that all jump modes are the same, then the equation will

[11] N. H. Nachtrieb and G. Handler, Acta Metallurgica (to be published).
[12] C. Zener, J. Appl. Phys. **22**, 372 (1950).

read:

$$D=(1/6)\Gamma\delta^2. \tag{8}$$

As Zener has done, Γ may be written as

$$\Gamma=\nu \exp^{(\Delta S/R)} \exp(-\Delta H/RT) \tag{9}$$

where ν is the characteristic lattice vibration frequency. One then obtains for D_0 the expression

$$D_0=(1/6)\delta^2\nu \exp(\Delta S/R). \tag{10}$$

If the jump distance is assumed to be the mean distance of closest approach, 3.83 A, and the vibration frequency in the liquid is taken to be about the same§ as the Debye frequency for the solid ($\theta_D=159°$ K), we obtain 0.7 eu as the entropy of activation for diffusion in liquid sodium. In view of the uncertainties in jump distance (essentially an admission of our lack of detailed knowledge of the liquid structure) and of the vibration frequency in the liquid, it is possible to say only that the entropy of activation for diffusion in liquid sodium is quite small . . . perhaps zero.[11]

§ Andrade [E. N. da C. Andrade, Proc. Roy. Soc. (London) **215A**, 36 (1952)] has, for example, made similar assumptions in discussing the viscosity of liquids. Evidence that the vibration frequency of many normal metals changes only slightly on fusion is deduced by Kleppa [G. Careri and A. Paoletti, Nuovo cimento **11**, 399 (1954)] from measurements of ultrasonic velocities. According to the latter the Grüneisen constant changes from 1.25 for solid sodium to 1.18 for the liquid.

[11] In this connection it is interesting to note that the activation entropies for self-diffusion in mercury[3] and in indium[14] calculated in the same manner are somewhat less than zero if the jump distance is approximated by the interatomic distance. Smaller "jump distances" and positive or zero activation entropies would be possible if diffusion in the liquid were to involve cooperative movements of neighboring atoms.

THE JOURNAL OF CHEMICAL PHYSICS VOLUME 23, NUMBER 10 OCTOBER, 1955

Refined Procedure for Analysis of Electron Diffraction Data and Its Application to CCl_4

L. S. Bartell,* L. O. Brockway, and R. H. Schwendeman
Department of Chemistry, University of Michigan, Ann Arbor, Michigan

(Received July 19, 1954)

A refined procedure for obtaining the structure of free molecules from electron diffraction data is described which compensates for the interference arising from non-nuclear scattering. The procedure is applied to CCl_4 using somewhat more extensive rotating sector data than has hitherto been published for this molecule. Estimates are made for the first time in electron diffraction results of the effect of anharmonicity of vibration on the measurement of internuclear distance and of the effect of the failure of the Born approximation on the measurement of amplitudes of vibration. A method of estimating the reliability of the results is described.

RECENT advances in the experimental technique of electron diffraction by gases have made it possible to obtain diffraction data of considerably greater accuracy than that previously available. It is no longer true that the approximations involved in the procedures of analysis in general use are freer from uncertainty than the best experimental data. The availability of punched-card methods for the calculations, however, has now made it practicable to carry out analyses almost entirely free of uncertainties of interpretation. In addition to yielding more accurate results a more rigorous analysis permits the assignment of uncertainty in a straightforward way from considerations of experimental accuracy.

In electron diffraction it is the scattering of the incident beam by the well-localized nuclei that provides information about the structure of the molecules. The scattering by the diffusely distributed planetary electrons interferes with the measurement of the nuclear scattering at small-to-moderate scattering angles and, unless corrections are made, uncertainties are introduced into the determination of the internal motion and the precise location of some of the atoms. A widely used method to compensate partially for electronic scattering is the division of the total scattered intensity curve by the smooth background of atomic scattering. This method, however, fails to take into account the incoherent scattering and the differences between electronic structures of different atoms. A practical procedure for treating this source of error is described in the next section.

If the numerical results are to be significant to within a few thousandths of an angstrom unit, the anharmonicity of the intramolecular vibrations must also be considered. This factor, which has heretofore been ignored in diffraction studies of bonded distances, is responsible for shifting the apparent internuclear distances obtained by conventional procedures of analysis to values of the order of 0.01 A greater than the true equilibrium internuclear distances.[1] Another factor neglected in the past is that electrons scattered by atoms undergo a shift in phase which is dependent upon both the atomic number of the atoms and the angle of scatter-

* Present address: Department of Chemistry, Iowa State College, Ames, Iowa.

[1] L. Bartell, J. Chem. Phys. **23**, 1219 (1955).

ing. For atoms only moderately different in atomic number the influence upon the scattering pattern of molecules is not unlike that of thermal motion, and accordingly, corrections must be made in the determination of amplitudes of vibration between pairs of atoms of different atomic number.[2] If the difference in atomic number is large the measurement of internuclear distance also will be affected. Compensations are made for the above factors in the results to be presented.

Carbon tetrachloride was selected for this investigation in part because it has been used so frequently in earlier modifications of the electron diffraction method and also because we needed the best possible parameter values in this molecule for comparison with the results in a new study of several substituted chloromethanes. Carbon tetrachloride as a reference molecule has the advantage of a known configuration and of providing a strong interference pattern, but it is not as amenable to independent standardization of its scale factor by spectroscopic means as some other molecules. The refined results are of interest nonetheless because of the many previous investigations and of the convenient opportunity it affords for a full description of the diffraction techniques used in this laboratory.

EFFECT OF NON-NUCLEAR SCATTERING

In electron diffraction investigations of the structure of free molecules it is customary to work with the ratio, $M(s)$, of the molecular scattering, I_M, to the atomic scattering, I_A. If appropriate experimental conditions are satisfied (e.g., single scattering, good localization of the specimen, absence of extraneous scattering, etc.), $M(s)$ assumes a form that can be readily interpreted in terms of molecular structure. In the procedure to follow it is assumed that the ideal experimental conditions have been met or that suitable corrections have been made in the intensity data. An experimental measure of $M(s)$ is obtained from the curve of the total scattered intensity, I_T, by drawing a smooth background, I_B, through the molecular oscillations with the aid of criteria[3,4] to make I_B approximate I_A closely, so that

$$M(s)=(I_T/I_B)-1. \tag{1}$$

The theoretical relationship between $M(s)$ and molecular structure is given by[5]

$$M(s)=\sum_i \sum_j{}' C_{ij}\mu_{ij}(s) \int_0^\infty P_{ij}(r)(\sin sr)/sr\,dr, \tag{2}$$

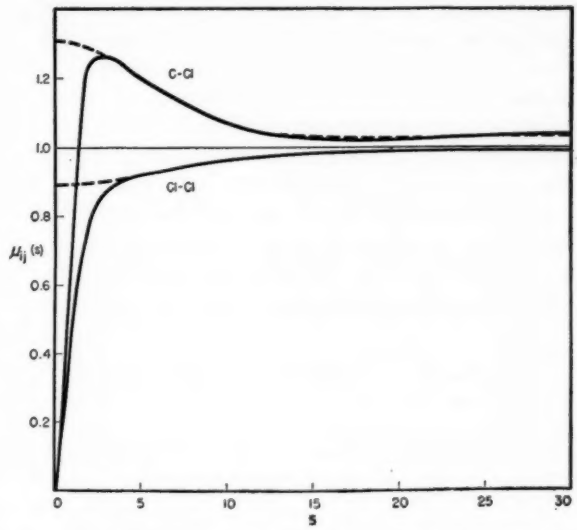

FIG. 1. The functions $\mu_{ij}(s)$ for CCl_4. Solid line = theoretical; dashed line = curve-fit representation using Gaussian functions.

where $C_{ij}=Z_iZ_j/\sum_i (Z_i^2+Z_i)$, Z_i is the atomic number of the ith atom in the molecule, s is the variable $(4\pi \sin\frac{1}{2}\theta)/\lambda$, θ is the scattering angle, λ is the wavelength of the electron beam, and $P_{ij}(r)$ is the probability distribution describing the separation, r, between nuclei i and j. The functions μ_{ij} are related to the electronic structure of the atoms in the molecule by the following expression:

$$\mu_{ij}=\frac{\{Z_i-F_i(s)\}\{Z_j-F_j(s)\}\sum_i (Z_i^2+Z_j)}{Z_iZ_j\sum_i \{[Z_1-F_i(s)]^2+Z_iS_i(s)\}} \tag{3}$$

in which $F_i(s)$ is the x-ray atomic scattering factor and $S_i(s)$ is the x-ray incoherent scattering function of atom i. If all the internuclear distances are considered to be undergoing harmonic variations, Eq. (2) reduces to

$$M(s)=\sum_i \sum_j{}' C_{ij}\mu_{ij} \exp(-\ell_{ij}^2s^2/2)(\sin sr_{ij})/sr_{ij}, \tag{4}$$

where r_{ij} is the equilibrium separation between nuclei i and j and ℓ_{ij} is the root mean square of the amplitude of displacement $(r-r_{ij})$.

It is evident from the form of Eq. (2) that information about internuclear spacings in the form of distribution curves, $P_{ij}(r)$, could be derived directly from a knowledge of $M(s)$ by Fourier inversion if the functions μ_{ij} were constant with respect to s. An examination of Eq. (3) shows that the μ_{ij} do approach constancy (unity) at moderate to large s but may deviate by a large amount at small s. In general the deviations from unity are larger, the larger the differences that exist between atomic numbers in the molecule. Figure 1 shows the functions for CCl_4.

The Norwegian school takes into account the variability of μ_{ij} with s but in a way that makes the interpretation of the distance between the weaker scattering centers in molecules with several similar distances

[2] V. Schomaker and R. Glauber, Nature **170**, 291 (1952); Phys. Rev. **89**, 667 (1953). L. Bartell and L. Brockway, Nature **171**, 978 (1953).

[3] J. Karle and I. L. Karle, J. Chem. Phys. **18**, 957 (1950).

[4] Bauer, Keidel, Harvey, Coffin, and Bregman, Final Report on project covered by contract N6ori-213, Task Order NR052-040, Cornell University (1950); K. P. Coffin, Doctoral thesis, Cornell University, 1951; S. H. Bauer, ASXRED meeting, Pennsylvania State College, June 1949; S. H. Bauer, Second International Congress of Crystallography, Stockholm, 1951.

[5] P. Debye, J. Chem. Phys. **9**, 55 (1941).

rather tedious.[6] Most of the other investigators have neglected the variability of μ_{ij} except at very small s and have reduced diffraction data to molecular structure by two methods[7]: (a) the correlation method in which experimental $M(s)$ curves are compared to constant coefficient theoretical curves, $M_c(s)$, calculated for proposed molecular models by means of Eq. (2) or Eq. (4) with the assumption that $\mu_{ij}=1$, and (b) the radial distribution method in which an approximate Fourier analysis is performed upon the experimental intensity function to obtain a radial distribution curve, $f(r)$, where

$$f(r)=\int_0^{s(\max)} sM(s)\exp(-bs^2)\sin sr\,ds. \qquad (5)$$

In the correlation method the great disparity between $M(s)$ and $M_c(s)$ at very small s is not serious because the selection of the most likely model can be based on comparison outside that range. In the radial distribution method, however, the value of the integrand of Eq. (5) from $s=0$ to some small value is important in determining the form (but not the position of the essential features) of the radial distribution curve $f(r)$. Consequently, the interpretation of the radial distribution curve is facilitated by substituting for the experimental $M(s)$ a calculated constant coefficient curve in the range from $s=0$ to $s\sim 3$. The resulting $f(r)$ curve is closely related to the $P_{ij}(r)$ functions and can be used to obtain a measure of both the internuclear distances, r_{ij}, and the amplitudes of vibration, ℓ_{ij}.[8]

The deviation of the μ_{ij} from constancy in the range from $s=3$ to $s=20$ is less pronounced than the deviation at smaller s, but it is nevertheless sufficient that its neglect reduces the applicability of the criteria used to establish the background line, I_B, and makes uncertain the measurements of the "index of resolution" of the pattern $\{M_{\text{exp}}(s)/M_{\text{theor}}(s)\}$, the amplitudes of vibration, the distances between the weaker scatterers in a molecule, and the actual resolution of approximately equal internuclear distances. The most serious obstacle to the more exact treatment has heretofore been the excessive labor involved in the computation. It is shown below how the corrections can be carried out by a simple extension of the punched-card computational procedure described by Karle and Karle.[3]

The compensation for variable μ_{ij} is applied here by converting the experimental $M(s)$ function to a function with constant coefficients, $M_c(s)$, which is then used in computing the distribution function and in correlation with the theoretical $M(s)$ functions calculated from Eq. (4) with $\mu_{ij}=1$. This conversion uses a difference function, ΔM, given by

$$\Delta M=M(s)-M_c(s)$$
$$=\sum_i \sum_j{}' c_{ij}(\mu_{ij}-1)\times\exp(-\ell_{ij}^2s^2/2)(\sin sr_{ij})/sr_{ij}, \qquad (6)$$

in which the μ_{ij} can be computed from tabulated values of $F_i(s)$ and $S_i(s)$. The correction, ΔM, is not usually very sensitive to assumptions about the structure of the molecule because $(\mu_{ij}-1)$ damps out rapidly unless large differences exist between atomic numbers. In any case, it is possible to arrive at ΔM by successive approximations, starting with values of r_{ij} and ℓ_{ij} obtained from an uncorrected radial distribution curve. If $(\mu_{ij}-1)$ can be expressed in terms of a series of Gaussian functions such that

$$(\mu_{ij}-1)=\{\sum_n G_n\exp(-g_ns^2)\}_{ij}, \qquad (7)$$

then the function ΔM can be computed by exactly the procedure prescribed for the theoretical $M(s)$ in Eq. (4) with $\mu_{ij}=1$. The utility of this method lies in the fact that ΔM can be calculated readily by punched-card methods and that a good curve fit of $(\mu_{ij}-1)$ can be obtained with a small number of terms. It has been our experience that, for molecules containing atoms no heavier than Cl, the $(\mu_{ij}-1)$ function can often be fitted in the range from $s=3$ to $s_{\max}$ by a small constant, G_0, and one term with $g_n\neq 0$. It is seldom necessary to use more than two terms with $g_n\neq 0$ for light molecules.

The range of intensity data from $s=0$ to $s=3$, which cannot be treated satisfactorily in this manner, is insensitive to molecular structure parameters and hence can be ignored completely in the correlation method. Compensation for this range in the radial distribution method can be made as already described. The corrected experimental curve, $M_c(s)=M(s)-\Delta M$, can then be analyzed in terms of the spatial distribution of nuclei in the molecule, the corrections to be described for the failure of the Born approximation and anharmonicity of intramolecular vibrations being most conveniently made after the correlation or radial distribution treatment has been performed.

The primary advantage of the foregoing treatment over previous treatments designed to take into account the effect of non-nuclear scattering is that the radial distribution function can be interpreted as the sum of a number of simple bell-shaped peaks.[9] Each internuclear distance gives rise to just one such peak instead of several regions of positive and of negative amplitudes as is the case in the Norwegian treatment. Further, the area of each component peak as measured directly from the base line of $f(r)$ is simply related to the scattering powers of the atoms involved, and the breadth of each

[6] H. Viervoll, Acta Chem. Scand. **1**, 120 (1947).

[7] S. H. Bauer *et al.* have proposed a method for partially compensating for the variability; see K. P. Coffin (Doctoral thesis, Cornell University, 1951). Schomaker has often pointed out the effect of the μ_{ij} on the radial distribution curve. Other investigators have occasionally made compensations in the correlation method.

[8] I. L. Karle and J. Karle, J. Chem. Phys. **17**, 1052 (1949).

[9] It should be noted that the treatment described here has been developed for molecules whose distances show harmonic variations [see Eqs. (2) and (4)], but the application to molecules having nonharmonic motions, such as internal rotations, is readily made. In either case the base line to which the resolved peaks are properly referred is flat and should lead to more precise peak areas.

component is readily interpreted in terms of amplitude of vibration without further consideration of effects of the μ_{ij}. The greater ease of resolving a complex peak into its components by means of this scheme is apparent. It is only fair to note that the rapidity with which the scheme converges, if very heavy atoms are present, has not been tested quantitatively.

EXPERIMENTAL PROCEDURE

The electron diffraction apparatus used in this research and the technique used to obtain the diffraction patterns are described in detail elsewhere.[10] Patterns were taken of CCl_4 vapor at 20 mm pressure with an R^3 sector, using specimen-to-plate distances of 25 and 10 cm to record the inner and outer portion of the patterns. The diffraction data, which included the first fifteen interference maxima, extended to $s=34$ at which point the internal motion of the molecule had reduced the amplitude of the sinusoidal molecular interference terms to about 7% of the amplitude calculated for a rigid molecule. Microphotometer traces were obtained by the method described by Karle, Hoober, and Karle[11] in which patterns are spun about their centers while being scanned in order to average out irregularities in the photographic emulsion. Optical densities were obtained by reading the amplified microphotometer records under 10 power magnification with a device for accurate interpolation, and these readings were converted to relative intensities.[12]

A background line which agreed well with the theoretical atomic intensity curve was drawn through the experimental intensity curve with the aid of suitable criteria[3,4] in order to separate the contributions of the atomic and molecular scattering. The experimental $M(s)$ curve was computed according to Eq. (1) and corrected to a constant coefficient curve according to Eq. (6), using for the μ_{ij} the approximations

$$\mu_{CCl}-1=0.030+0.278\exp(-0.0189s^2),$$
$$\mu_{ClCl}-1=-0.009-0.0951\exp(-0.0124s^2),$$

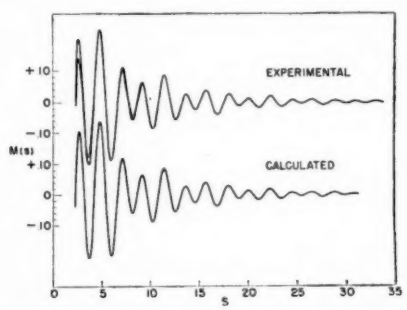

FIG. 2. Comparison of experimental and calculated $M(s)$ curves for CCl_4. In the experimental curve the dashed line represents the uncorrected $M(s)$, and the solid line represents the corrected constant coefficient $M_e(s)$. The lower curve is the theoretical constant coefficient $M_e(s)$ using in the exponential factor the experimental ℓ's (Table I).

[10] L. Brockway and L. Bartell, Rev. Sci. Instr. **25**, 569 (1954).
[11] Karle, Hoober, and Karle, J. Chem. Phys. **15**, 765 (1947).
[12] L. Bartell and L. Brockway, J. Appl. Phys. **24**, 656 (1953).

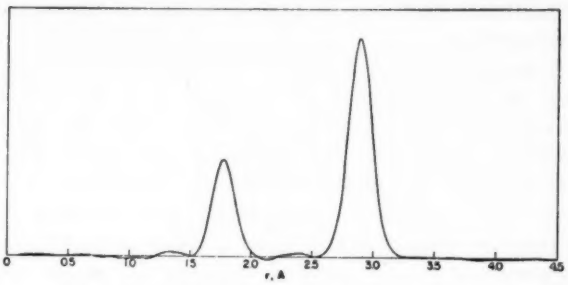

FIG. 3. Experimental radial distribution curve for CCl_4.

which can be compared with the theoretical μ_{ij} in Fig. 1. Figure 2 compares the uncorrected and corrected experimental $M(s)$ curves with the theoretical constant coefficient curve.

The radial distribution function for CCl_4 shown in Fig. 3 was calculated with the corrected data according to Eq. (5) by the punched-card method described by Shaffer, Schomaker, and Pauling,[13] using a value of 0.0023 for the constant b. A calculation showed that this value of b was adequate to reduce to a negligible amount the extraneous ripple arising from the cutoff of the integral at s_{max}, since the intramolecular motion of the molecule itself contributed strongly to damping the integrand. At the same time, b is not so large that the effective weight function, $s\exp(-bs^2)$, imposed upon the diffraction data places an unduly small emphasis on the outer portion of the data.

UNCERTAINTIES

The limits of error usually assigned to electron diffraction results in the past were relatively large compared to the apparent internal consistency of the experimental data. This largeness was dictated by experience with many determinations instead of by straightforward analysis in any given case. It seems reasonable to ascribe a large part of the need for this empirical factor of caution to failures in the approximations used in the analysis and interpretation of data. Since more rigorous methods were used in this investigation, the estimation of the reliability of the results presented here was based upon an examination of the uncertainty in the experimental data and the uncertainty in the corrections for anharmonicity.

Experimental uncertainties were separated into three categories, the first of which included errors in the settings and calibration of the diffraction apparatus and systematic errors in the measurement of the scattering angle. Such errors primarily affect the determination of the scale factor of internuclear distances rather than molecular shape. Checks of the apparatus, the uniformity in thickness and in flatness of the photographic plates, and the tracing by the microphotometer indicated that the uncertainty due to this category

[13] Shaffer, Schomaker, and Pauling, J. Chem. Phys. **14**, 659 (1946).

amounts to about one part per thousand in the present investigation.

A second category included random errors associated with the measurement of intensity as a function of scattering angle. These errors, which affect the determination of the shape of molecules and amplitude of vibrations as well as the size, reveal themselves in the correlation method as a scattering of the s/s_0 values and in the radial distribution curve as random fluctuations appearing in the background between the peaks. This latter evidence was used to estimate uncertainties of the second category in r_{ij} and l_{ij} by determining the extent to which fluctuations in the distribution curve of the observed amplitude and breadth were capable of altering the positions and breadths of the peaks. The average breadth of the fluctuations observed in curves obtained by the present method is comparable to the breadths of the internuclear peaks. It can be shown that if the amplitude of the fluctuations is y in the vicinity of a peak of height A, then the uncertainty in l_{ij} and r_{ij} is given very roughly by

$$\delta r_{ij} \sim \delta l_{ij} \sim y(2b+l_{ij}^2)^{\frac{1}{2}}/A. \quad (8)$$

A more precise evaluation of the uncertainty requires a closer examination of the form of the disturbance. The value of y observed in our current investigations has generally been one or two percent of the height of the strongest peaks.

The third group of uncertainties included the systematic errors in intensity measurement, such as in the determination of the slope of the calibration curve relating optical density to intensity and in the failure to meet ideal diffraction conditions. The absence of serious extraneous scattering was inferred from the agreement of the theoretical and experimental background curves, the high index of resolution of the pattern at small $s(\sim 93\%)$ and tests of the distribution of the gas sample in the diffraction chamber.[10] These errors, which mainly affect the extent of damping of $M(s)$, are not adequately represented by the random fluctuations in the distribution function because they influence the shape of the peaks more than the base line between the peaks. The distortion, being more or less symmetrical about each peak, has a significant effect only on the measurement of the l_{ij} unless the systematic errors are quite large. The associated uncertainty in l_{ij} in the present investigation was estimated to be 0.002 A by considering the envelope of the damping of the molecular terms of $M(s)$ in relation to the estimated uncertainties of 3% [of the amplitude of $M(s)$] in the index of resolution at small values of s and of 1.5% of $M(s)$ in the emulsion calibration curve. In addition the uncertainity owing to the measured spread of the specimen was estimated and found to be less important than the preceding factors.

TABLE I. Distances and amplitudes in CCl_4.

	Internuclear distance (A)	l_{ij}'(elec. diff.)	l_{ij}'(spect.)
C−Cl	$r_{RD}=1.769\pm0.005$[a] $r_{RD}^0=1.766\pm0.003$[b] $r_e=1.760\pm0.004$[c]	0.060 ± 0.005	0.054
Cl−Cl	$r_{RD}=2.887\pm0.004$[a]	0.068 ± 0.003	0.067

[a] r_{RD} = position of maximum of symmetrical curve best fitting upper part of experimental RD curve.
[b] r_{RD}^0 = position of maximum of $P_{ij}(r)/r$ curve.
[c] r_e = equilibrium separation.

RESULTS

Amplitudes of Vibration

It was shown by Karle and Karle[8] that the amplitudes of intramolecular motion, the l_{ij} of Eq. (4), can be studied by refined electron diffraction methods. It has recently been pointed out,[2] however, that the apparent amplitudes, l_{ij}, obtained by the application of Eq. (4) or Eq. (5), must be corrected for the failure of the Born approximation upon which Eqs. (4) and (5) are based. The correction for 40 kv electrons is given approximately by

$$l_{ij}' = \{l_{ij}^2 - 3.2\times10^{-6}(Z_i-Z_j)^2\}^{\frac{1}{2}}. \quad (9)$$

The difference between l_{CCl}' and l_{CCl} is 0.003 A for $l_{CCl}=0.060$ A and is 0.004 A for $l_{CCl}=0.040$ A. The small asymmetry of the peaks does not interfere with the measurement of their breadth.

The experimental results, obtained from the radial distribution curve, are listed in Table I and are in satisfactory agreement with the spectroscopic results as calculated by Morino[14] *et al.* but higher than the only other electron diffraction values[8] ($l_{CCl}=0.041\pm0.005$ A; $l_{ClCl}=0.054\pm0.005$ A).

Internuclear Distances

It is of interest to report the values of the internuclear distances in CCl_4 obtained from the diffraction data with the assumption that the radial distribution peaks are symmetrical with respect to the equilibrium distances, for it is these values which should be compared to previous published results of electron diffraction investigations. Fitting the upper two-thirds of the radial distribution peaks with symmetrical Gaussian functions gave values, r_{RD}, of 1.769 ± 0.005 A for the C−Cl peak and 2.887 ± 0.004 A for the Cl−Cl peak, the uncertainties representing all of the known sources of experimental error without any consideration of errors of interpretation. Since the C−Cl peak is less precisely determinable from the diffraction data than the stronger Cl−Cl peak a somewhat more precise value of the equilibrium C−Cl distance can be found from the latter peak, assuming tetrahedral symmetry, than from the C−Cl peak directly. It should be noted, however, that intramolecular vibrations complicate the computation, and, in general, it is not to be expected that the positions

[14] Morino, Kuchitsu, Takahashi, and Maeda, J. Chem. Phys. 21, 1927 (1953).

of the peak maxima will be exactly in the ratio calculated for a rigid tetrahedral molecule. Application of the correlation procedure leads to the same internuclear distance as the radial distribution method to within 0.001 A. These results are in agreement with all but the oldest values in the literature to within the reported uncertainties.

The foregoing results are not to be interpreted as true equilibrium distances (in the spectroscopic sense) because of the distortions introduced by the anharmonicities of the intramolecular vibrations. In order to estimate the effect of anharmonicity it was assumed that the interaction between the bonded atoms could be represented by a Morse function

$$V(r)=D\{e^{-2a(r-r_e)}-2e^{-a(r-r_e)}\},$$

where r_e is the equilibrium distance, D is a constant equal to the dissociation energy, and $a=(k/2D)^{\frac{1}{2}}$ in which k is the force constant. The probability distribution, and hence, the radial distribution peak, of the C—Cl distance is then characterized by three molecular parameters, r_e, ℓ_{ij}, and a, all of which could be determined, in principle, from accurate data. In practice the data are not sufficiently precise to fix the anharmonicity parameter a but a reasonable value for a can be easily estimated from spectroscopic or thermal measurements involving C—Cl bonds. The values for r_e, ℓ_{ij}, and a new parameter r_{RD}^0, the position of the maximum of the nuclear radial distribution curve $P_{ij}(r)/r$, (usually $r_{RD}>r_{RD}^0>r_e$) are readily found by fitting the experimental peaks with Morse-type distribution functions once a value for a is assumed.[1] It was assumed that $a=2.0$ A^{-1} for the C—Cl bond. The theoretical treatment of the asymmetry of the Cl—Cl peak is an exceedingly difficult problem and is beyond the scope of the present investigation. It seems reasonable, however, to assume that the distribution describing the Cl—Cl separation can be represented approximately by a Morse-type distribution function with a value of a between 2 and 4. Fortunately, the result for the weighted C—Cl distance is not unduly sensitive to the assumptions made about the Cl—Cl distribution. The different distance parameters listed in Table I for the C—Cl bond were arrived at on the above basis.

It would be expected that r_{RD} would converge to r_{RD}^0 with decreasing b and sufficiently large $s_{\max}$. For the C—Cl bond in CCl_4, r_{RD}^0 is very nearly the same at 0° as at 300°K because of the cancellation of the small effects of vibration and rotation. Perhaps more significant parameters for describing the internuclear distance are the position of the maximum of the best fit $P_{C-Cl}(r)$ which is at 1.768 A, or the center of gravity which is at about 1.771 A.

It is reasonable to inquire whether the experimental intensity curve itself showed any evidence of anharmonicity or need for the foregoing corrections. The answer is that the effects sought are so small that they

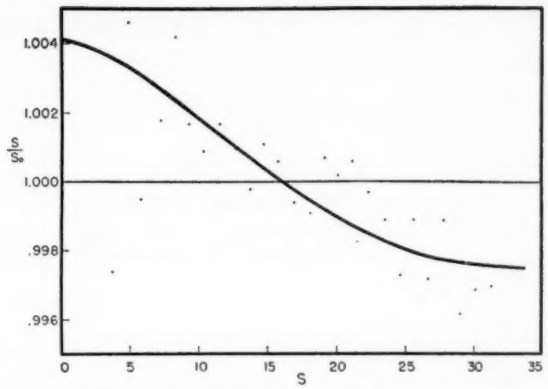

FIG. 4. Curve = the dependence of the s/s_0 values upon s that is estimated to hold for CCl_4 at 300°K; the deviation of this curve from constancy is a measure of the anharmonicity of intramolecular vibrations. Points = experimental s/s_0 correlation values for CCl_4.

approach in magnitude the experimental uncertainties but that the diffraction data are somewhat better represented by the anharmonic model than the harmonic model. Anharmonicity manifests itself in the radial distribution method by introducing slight asymmetry into the peaks and in the correlation method by imparting a more or less smooth frequency modulation into the $M_{\exp}(s)$ curve. It has been noted in most of the radial distribution curves obtained in this laboratory by the careful application of the rotating sector method that the peaks do show slight asymmetry of the expected magnitude and direction. The peaks for CCl_4 shown in Fig. 3 possess this characteristic although it is apparent that the random fluctuations in the base line interfere with the evaluation of the effect. Figure 4 compares the experimental s/s_0 values with the values estimated to occur for CCl_4 vibrating asymmetrically at 300°K. For the outer 22 s/s_0 values the mean deviation from the anharmonic curve is about 8 parts per 10 000, while the mean deviation from constancy (harmonic vibrations) is about 15 parts per 10 000.

The above distinctions between the equilibrium internuclear distance and other naturally derived distance parameters were made in the present investigation because it was believed that such distinctions were necessary to keep the error in interpretation as small as the experimental error.

ACKNOWLEDGMENTS

We appreciate the support of the Horace H. Rackham School of Graduate Studies in providing a Rackham Post-Doctoral Fellowship for L. S. Bartell and the Henry Earle Riggs Fellowship for R. H. Schwendeman. We are very grateful to Dr. J. Karle and the Naval Research Laboratory for a deck of cards punched with exponential functions and to Dr. V. Schomaker and the California Institute of Technology for cards punched with sine functions.

Structures of CF_3Cl and CH_3Cl

L. S. BARTELL* AND L. O. BROCKWAY
Department of Chemistry, University of Michigan, Ann Arbor, Michigan

(Received December 29, 1955)

The molecular structures of CF_3Cl and CH_3Cl were determined by refined procedures of electron diffraction. For CF_3Cl, the most probable C−F and C−Cl distances are 1.328 A and 1.751 A respectively and $\angle FCF = 108.6°$. Results for CH_3Cl agree with the complete microwave determination. Vibrational amplitudes are in agreement with approximate calculations by Morino.

IT is well known that the introduction of fluorine atoms into organic molecules may have a marked stablizing influence on the molecules, especially when two or more fluorine atoms are attached to the same carbon atom.[1] Early investigations of the molecular structures of organic fluorides indicated that the C−F bonds and also bonds to other elements attached to the carbon decreased in length as the number of fluorines on the carbon was increased. In particular, a value of 1.72 ± 0.03 A was reported[2] for the C−Cl bond in CF_3Cl as contrasted with the distance 1.77 A accepted then for C−Cl in CH_3Cl.

More recent improvements in both the diffraction and spectroscopic techniques for determining molecular structures have made it possible to obtain greater precision in the values for internuclear distances, and more precise values are of special interest among organic fluorides where attempts have been made to obtain a quantitative correlation between changes in internuclear distances and in chemical reactivity due to increasing the number of fluorine atoms. For this reason the examination of CF_3Cl and its comparison with CH_3Cl by the rotating sector method of electron diffraction is part of a systematic study of the effect of fluorine substitution in molecules of the CH_3X type. In addition, the availability of the results of microwave studies of these two molecules provides an excellent opportunity for comparing the results of the two methods of structure determination.

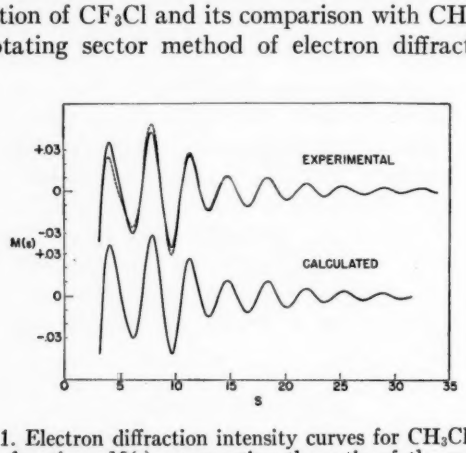

FIG. 1. Electron diffraction intensity curves for CH_3Cl. These are the functions $M(s)$ representing the ratio of the molecular scattering to the background of atomic scattering. The experimental curves include one corrected for non-nuclear scattering (solid line) and the uncorrected curve (dashed line).

PROCEDURE

Diffraction patterns of 40 kv electrons were obtained on Kodak Contrast Lantern Slides using the rotating sector apparatus described in detail elsewhere.[3] Camera distances of 25 cm and 9 cm were used with an r^3 sector to record the patterns from $s=3$ to $s=34$. The pressure of the sample at the gas nozzle was 50 mm for CF_3Cl and 75 mm for CH_3Cl. Intensities, obtained by densitometry,[3,4] proved to be sensitive to detail in the pattern to a few parts per ten thousand.

The detailed procedure for the interpretation of the data and the assignment of uncertainties has been described.[5] It includes converting the experimental intensities to the function $M(s)$ representing the ratio of the "molecular" intensity (i.e., dependent on the interatomic distances) to the atomic or background intensity, correcting $M(s)$ for non-nuclear scattering, and computing a radial distribution function $f(r)$ using the expression:

$$f(r) = \int_0^{s(\max)} sM(s) \exp(-bs^2) \sin sr \, ds.$$

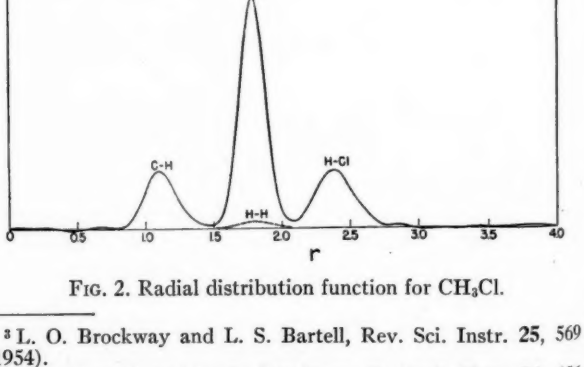

FIG. 2. Radial distribution function for CH_3Cl.

* Present address: Department of Chemistry, Iowa State College, Ames, Iowa.

[1] A. L. Henne and T. Midgley, Jr., Am. Chem. Soc. **58**, 882 (1936); A. L. Henne, "Aliphatic Fluorides," in H. Gilman, *Organic Chemistry* (John Wiley and Sons, Inc., New York, 1943), Vol. I., Chap. II.

[2] L. O. Brockway and R. L. Livingston, Report to Naval Research Laboratory, Contract No. N1735-7912, June 30, 1944.

[3] L. O. Brockway and L. S. Bartell, Rev. Sci. Instr. **25**, 569 (1954).

[4] L. S. Bartell and L. O. Brockway, J. Appl. Phys. **24**, 656 (1953).

[5] Bartell, Brockway, and Schwendeman, J. Chem. Phys. **23**, 1854 (1955); L. S. Bartell, J. Chem. Phys. **23**, 1219 (1955).

TABLE I. Distances and amplitudes determined from the radial distribution curves for CH_3Cl and CF_3Cl.

r_{RD}		l_{ij}(e.d.)	l_{ij}(calc)[a]
CH_3Cl			
C−H	1.11 ±0.01 A	0.089±0.010 A	0.078 A
C−Cl	1.784±0.003	0.060±0.004	0.050
H−Cl	2.38 ±0.01	0.119±0.010	0.114
CF_3Cl			
C−F	1.328±0.002	0.049±0.002	0.045
C−Cl	1.751±0.004	0.054±0.005	0.050
F−F	2.158±0.003	0.058±0.003	0.056
F−Cl	2.539±0.003	0.066±0.003	···

[a] Approximate calculations by Morino, reference 7.

Table II. Comparison of electron diffraction and microwave results for CH_3Cl and CF_3Cl.

	Electron diffraction	Microwave
CH_3Cl		
C−H	r_v=1.11 ±0.01 A	1.113 A
C−Cl	r_v=1.783±0.003 A	1.7810 A
<HCH	110±2°	110°31′
CF_3Cl		
C−F	r_v=1.328±0.002 A	1.328±0.002 A[a]
C−Cl	r_v=1.751±0.004 A	1.748±0.009 A[a]
<FCF	108.6±0.4°	(108.6±0.4°)

[a] Values computed from the spectroscopic moments of inertia and the diffraction value of the angle. The uncertainties include only the effect of uncertainty in the bond angle and ignore experimental and interpretational errors.

For direct comparison with the experimental $M(s)$ curve a theoretical $M(s)$ curve based on assumed equilibrium internuclear distances and vibrational amplitudes is computed using the function:

$$M(s)=\sum_i \sum_j' c_{ij} \exp(-l_{ij}^2 s^2/2)(\sin sr_{ij})/sr_{ij}.$$

CH_3Cl

Figure 1 compares the experimental $M(s)$ functions for CH_3Cl, including the uncorrected curve and the curve corrected for non-nuclear scattering, with the theoretical function for the model determined by the radial distribution curve. The ratios of the s and s_0 values read from the maxima and minima of the theoretical and experimental curves show an average deviation of 0.0025. The radial distribution function was calculated with the damping function $\exp(-0.0023\, s^2)$ and is shown in Fig. 2. The distinctness with which the weak hydrogen distances appear is an illustration of the effectiveness of the rotating sectormicrophotometer method. The relative areas of the peaks agree with the theoretical areas to within one percent. The experimental amplitudes of vibration, l_{ij}, obtained from the distribution curve and corrected for the small error due to the failure of the Born approximation,[6] are listed in Table I. The results are in fairly good agreement with the approximate calculations of Morino[7] for amplitudes of atomic pairs in given groups without regard to the molecules in which they occur.

The positions, r_{RD}, of the maxima of the radial distribution peaks listed in Table I are averages of the centers of the peaks at different ordinates corrected for the expected asymmetry.[5] In this case where the exceptionally complete microwave determination[8] enjoys a distinct advantage in accuracy over the electron diffraction result it is gratifying to see that the structure deduced by diffraction (Table II) is completely confirmed. Here the diffraction value for the C−Cl bond to be compared with the spectroscopic value, r_v, is very slightly less than r_{RD}. It should be pointed out that the beautifully precise microwave result is neither the equilibrium internuclear separation nor the most probable separation, due to the asymmetry of $P(r)$. The equilibrium separation is about 0.008 A less than r_v for the C−Cl bond.

CF_3Cl

The experimental and theoretical intensity curves for CF_3Cl are compared in Fig. 3. In the earlier electron diffraction investigation the discrepancy between the uncorrected $M(s)$ and the nuclear $M(s)$ in the vicinity of the third maximum contributed to the selection of a somewhat erroneous model. The average deviation of the s/s_0 ratios is 0.0012, and if allowance is made for the effect of anharmonicity,[5] the agreement is even somewhat better.

The radial distribution function shown in Fig. 4 resolves each of the internuclear distances so well that there is no ambiguity in locating the positions of the component peaks. The relative areas of the resolved peaks agree with the theoretical areas to within the uncertainty (near the foot of the peaks) of separating the asymmetric components. Measurements of the amplitudes and distances in the molecule are listed in Tables I and II.

A distribution function, $P(r)$, computed on the basis of a Morse type potential function[5] has maximum positions, r_m, which are very nearly the same as the maxima, r_{RD}, for both C−F and C−Cl in the experimental distribution function $f(r)$, which is related to $P(r)/r$. The effect of the damping factor $\exp(-0.0023\, s^2)$ in $f(r)$ is almost precisely compensated in this case by the effect of dividing $P(r)$ by r. Although the centers of gravity of the distributions are approximately 0.003 A greater than the positions of the maxima, the spectroscopically determined r_v should be nearly identical to r_m (and r_{RD}).

The microwave study[9] of CF_3Cl was not sufficiently complete to permit the determination of the molecular structure but yielded moments of inertia in agreement

[6] L. S. Bartell and L. O. Brockway, Nature **171**, 978 (1953).
[7] Morino, Kuchitsu, Takahashi, and Maeda, J. Chem. Phys. **21**, 1927 (1953).
[8] Miller, Aamodt, Dousmanis, Townes, and Kraitchman, J. Chem. Phys. **20**, 1112 (1952).
[9] D. K. Coles and R. H. Hughes, Phys. Rev. **76**, 858 (1949).

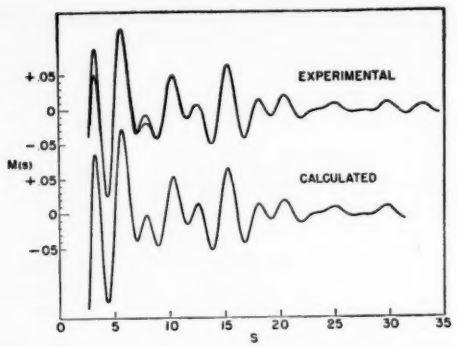

FIG. 3. Electron diffraction intensity curves for CF_3Cl.

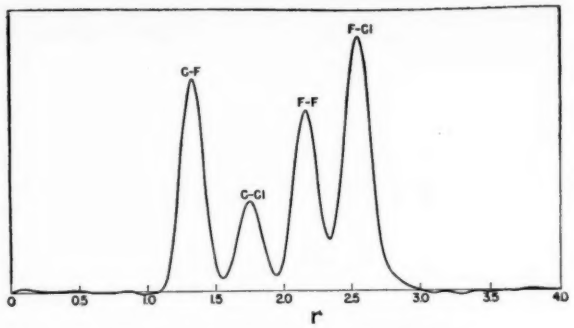

FIG. 4. Radial distribution function for CF_3Cl.

with the diffraction results to within interpretational error. In the original estimates of the internuclear distances from the microwave data it was assumed that the FCF angle was tetrahedral. The diffraction data show that the angle is certainly less than the tetrahedral value, in agreement with recent determinations of the FCF angle in other compounds. Accordingly, as already pointed out by Sheridan and Gordy,[10] the original estimates of the distances were in error, particularly in the case of the C—Cl distance. The microwave results listed in Table II were recalculated from the spectroscopic data using the FCF angle determined by diffraction, with the listed uncertainties indicating the sensitivity of the parameters to the 0.4° uncertainty in the FCF angle without regard to the additional appreciable error involved in the conventional reduction of spectroscopic data.

The angle reported for the diffraction determination was calculated from the estimated most probable positions of the nuclei. The uncertainty in the interpretation of the data in terms of the angle which arises from the nonlocalization of the nuclei was judged to be about as great as the uncertainty due to experimental error and both sources are included in the reported uncertainty.

[10] J. Sheridan and W. Gordy, J. Chem. Phys. **20**, 591 (1952).

The diffraction and recalculated microwave results agree exactly for the C—F bond and very closely for the C—Cl bond.

The decrease in the length of the C—Cl bond on substitution of three fluorine atoms in methyl chloride is 0.032 A, with an uncertainity of 0.006 A. This may be compared with the previous estimate of 0.05 A with an uncertainty nearly as large. Of special interest is the fact that the C—Cl bond in methyl chloride is shortened by 0.015 A on substitution of three chlorines for the hydrogens and by an additional 0.017 A on fluorine substitution. The substitution of three fluorines into either CH_3Cl or CCl_4 is accompanied by a tremendous decrease in the ease of removing chlorine from the moelcule by a hydrolysis or other substitution reactions, but this increase in chemical stability is accompanied by the rather small changes in bond distance amounting to 0.03 A or less.

ACKNOWLEDGMENTS

We acknowledge gratefully the support of the Horace H. Rackham School of Graduate Studies in providing funds for some of the equipment and for a Rackham Post-Doctoral Fellowship for L. S. Bartell.

Use of the Lattice Model for Entropy Calculations

F. BUECHE, *Department of Physics, University of Wyoming, Laramie, Wyoming*

AND

W. R. KRIGBAUM, *Department of Chemistry, Duke University, Durham, North Carolina*

(Received January 5, 1955)

The influence of choice of cell size upon the calculated entropy of mixing of solutions is discussed. It is shown that the lattice type calculation, when properly applied, leads to the same result for all possible choices of cell size. A new method is presented for calculating the entropy of mixing which does not assume a lattice. This method confirms the result of the lattice calculation.

THE lattice model effectively divides the solution into cells of equal size. One limitation associated with the use of such a model is the difficulty in specifying a cell size compatible with the geometry and molecular volume of both the solvent and solute molecules. A further disturbing feature is the fact that the calculated entropy of mixing appears to depend upon the choice of cell size. This note will point out that the aforementioned limitation is not as serious as might be supposed, and that the choice of cell size has no effect on the result if the configurations are properly counted.

We consider a mixture of N_1 solvent molecules and N_2 polymer molecules, having respective molecular volumes V_1 and V_2, and represent the ratio V_2/V_1 by x. The entropy of mixing will be calculated using the three possible choices of cell sizes.

In the first of these, one solvent molecule occupies a site, so that the lattice consists of $N_0=(N_1+N_2x)$ sites. The number ν_{i+1} of configurations available to polymer molecule $(i+1)$ is:

$$\nu_{i+1}=(N_0-ix)[(z-1)(1-f_i)]^{(x-1)}. \tag{1}$$

Employing the Flory approximation,[1] $f_i=ix/N_0$, there is obtained for the ratio of the number of configurations for molecule $(i+1)$ in the solution and in amorphous polymer:

$$\frac{\nu_{i+1}}{\nu_{i+1}^*}=\left(\frac{N_0/x-i}{N_2-i}\right)^z\left(\frac{N_2x}{N_0}\right)^{x-1}. \tag{2}$$

Since the corresponding factor for the solvent is unity, ΔW is given by:

$$\Delta W_I=\prod_{i=1}^{N_2}\left(\frac{\nu_i}{\nu i^*}\right)=\left[\frac{(N_0/x)\,!}{(N_0/x-N_2)\,!N_2\,!}\right]^x\left(\frac{N_2x}{N_0}\right)^{N_2(x-1)}. \tag{3}$$

Setting $\Delta S_M=kl n\Delta W$, and using Stirling's approximation for the factorials, leads to Flory's result[1] for the entropy of mixing:

$$\Delta S_M=-k[N_1\ln(N_1/N_0)+N_2\ln(N_2x/N_0)]. \tag{4}$$

[1] P. J. Flory, J. Chem. Phys. **10**, 51 (1942).

For the second model we select a smaller cell size. If a solvent molecule occupies β sites, the lattice will consist of βN_0 sites. Corresponding to Eqs. (1) and (2) we have:

$$\nu_{i+1}=\beta(N_0-ix)[(z-1)(1-f_i)]^{\beta x-1}, \tag{5}$$

$$\frac{\nu_{i+1}}{\nu_{i+1}^*}=\left(\frac{N_0/x-i}{N_2-i}\right)^{\beta x}\left(\frac{N_2x}{N_0}\right)^{\beta x-1}. \tag{6}$$

Since the ratio of the number of configurations available to a solvent molecule in the solution and in pure solvent is $(N_1/N_0)^{\beta-1}$, there is obtained for ΔW:

$$\Delta W_{II}=\left\{\frac{\left(\frac{N_0}{x}\right)\,!}{\left(\frac{N_0}{x}-N_2\right)\,!N_2\,!}\right\}^{\beta x}\times\left(\frac{N_2x}{N_0}\right)^{N_2(\beta x-1)}\left(\frac{N_1}{N_0}\right)^{N_1(\beta-1)}. \tag{7}$$

The expression for the entropy of mixing obtained through use of Eq. (7) is identical with Eq. (4). Thus the cell size may be made arbitrarily small, which offers a convenient means of treating those systems for which the molar volume ratio x is not an integer.

The third case, treatment of which has sometimes led to error, involves the choice of a cell volume *larger* than the molecular volume of the smaller component. If β solvent molecules occupy a single site, then the lattice will consist of N_0/β sites. It would appear that the first segment of molecule $(i+1)$ could enter the lattice in $(N_0-ix)/\beta$ ways, that the second would find $z(1-f_1)$ sites available, and that each of the remaining $(x/\beta-2)$ segments would find $(z-1)(1-f_i)$ sites available. Thus,

$$\nu_{i+1}=(1/\beta)(N_0-ix)[(z-1)(1-f_i)]^{x/\beta-1}. \tag{8}$$

Equation (8) yields for the entropy of mixing:

$$\Delta S_M=-k[(N_1/\beta)\ln(N_1/N_0)+N_2\ln(N_2x/N_0)]. \tag{9}$$

Comparison of Eqs. (4) and (9) reveals that the selection of a cell volume which is larger than the molecular volume of the smaller component apparently leads to a different answer for the same configurational problem.

Equation (9) has been employed[1,2] to introduce through the parameter β a dependence of the entropy of mixing on the flexibility of the polymer chain.

In order to gain some insight into the error in Eqs. (8) and (9), we derive the Flory equation by a method somewhat analogous to that proposed by Hildebrand.[3] This is based upon the fact that the entropy is inversely proportional to the probability of a given configuration of the components. Considering the same system as before, we first focus our attention on the N_1 molecules of pure solvent. The probability that the center of one of these molecules will be found in a volume element δ_1 is $N_1\delta_1/N_1V_1$; the probability of successfully locating a second molecule within a volume element δ_1 is $(N_1-1)\delta_1/(N_1V_1-\delta_1)$, etc. The probability of finding a specified configuration for the pure solvent is therefore:

$$P_1=\prod_{i=1}^{N_1}\left[\frac{N_1\delta_1-(i-1)\delta_1}{N_1V_1-(i-1_1)\delta}\right]$$

$$=\frac{N_1![N_1(V_1/\delta_1)-N_1]!}{[N_1(V_1/\delta_1)]!}. \quad (10)$$

Similarly, for component 2:

$$P_2=\frac{N_2![N_2(V_2/\delta_2)-N_2]!}{[N_2(V_2/\delta_2)]!}. \quad (11)$$

Bearing in mind that one must keep the relative concentrations of the two components equal in the volume elements sampled and in those remaining untested, one obtains for the mixture:

$$P_{12}=\prod_{i=1}^{N_1}\left[\frac{N_1\delta_1-(i-1)\delta_1}{V_T-(i-1)\delta_1(1+N_2V_2/N_1V_1)}\right]$$

$$\times\prod_{j=1}^{N_2}\left[\frac{N_2\delta_2-(j-1)\delta_2}{V_T-(j-1)\delta_2(1+N_1V_1/N_2V_2)}\right],$$

where V_T is the total volume of the mixture. Introduction of the factors $(1+N_2V_2/N_1V_1)$ and $(1+N_1V_1/N_2V_2)$ ensures that the sample and solution concentrations remain identical or, in other words, that we sample the solution randomly. This expression may be rewritten:

$$P_{12}=\frac{N_1!\left[\dfrac{V_T}{\delta_1(1+N_2V_2/N_1V_1)}-N_1\right]!}{\left(1+\dfrac{N_2V_2}{N_1V_1}\right)^{N_1}\left[\dfrac{V_T}{\delta_1(1+N_2V_2/N_1V_1)}\right]!}$$

$$\times\frac{N_2!\left[\dfrac{V_T}{\delta_2(1+N_1V_1/N_2V_2)}-N_2\right]!}{\left(1+\dfrac{N_1V_1}{N_2V_2}\right)^{N_2}\left[\dfrac{V_T}{\delta_2(1+N_1V_1/N_2V_2)}\right]!}. \quad (12)$$

[2] T. Kawai, Bull. Chem. Soc. Japan **25**, 452 (1952).
[3] J. H. Hildebrand, J. Chem. Phys. **15**, 225 (1947).

If $(N_1V_1+N_2V_2)=V_T$, we have at once:

$$P_1P_2/P_{12}=(V_T/N_1V_1)^{N_1}(V_T/N_2V_2)^{N_2}. \quad (13)$$

Recalling that $\Delta S_M=k\ln(P_1P_2/P_{12})$, the entropy of mixing expression obtained from Eq. (13) is seen to be identical with Eq. (4). It is worthwhile to notice that this approach makes no reference to molecular flexibility; the entropy change is completely the result of the increased volume of the mixture in which the molecules may be found.

We will make use of this approach to expose the error which resulted in the anomalous entropy expression obtained using a large cell volume. In deriving Eq. (8) we assumed that the first segment could enter the lattice in $(N_0-ix)/\beta$ ways, and each of the $(x/\beta-1)$ remaining segments in $(z-1)(1-f_i)$ ways. This counting process is actually in error. Suppose we have already located a portion of the chain, starting from one end. We know that the next segment can project in $(z-1)(1-f_i)$ ways from the last segment located, and that it occupies a contiguous volume equal to βV_1. However, when we come to sample the possible β regions of solvent size which make up the segment volume, we find that each sample volume can be located in $(z-1)(1-f_i)$ nonequivalent positions. The probability that we will choose the proper sequence of sample volumes is $[(z-1)(1-f_i)]^{-\beta}$. Thus, we find that altogether there are $[(z-1)(1-f_i)]^{\beta}$ independent recognizable configurations available to this new chain segment. It differs from the factor obtained previously because the gross counting procedure used there ignores the fact that the solution is actually composed of entities smaller than the cell size. In doing so, possible small scale modifications in the configurations are not counted.

If we follow the correct procedure and attribute $[(z-1)(1-f_i)]^{\beta}$ new configurations to each new segment, we then have in place of Eq. (8)

$$\nu_{i+1}=(N_0-ix)[(z-1)(1-f_i)]^{\beta-1}$$

$$\times[(z-1)(1-f_i)]^{\beta(x/\beta-1)}, \quad (14)$$

which is seen to be identical with Eq. (1).

With the above facts in mind, it is evident that the lattice type calculation is essentially equivalent to the nonlattice type of calculation. When all configurations are taken into account, the result obtained from a lattice treatment is independent of the choice of β. Thus, one is not restricted in the choice of the lattice, and realistic polymer segments may be employed in the calculation provided that one takes proper care of the actual segment size as indicated above. We see that objections to a lattice treatment based on the artificial division of the solution into cells of equal size are largely unfounded. A more valid objection is that the lattice treatment corresponds to a hard sphere approximation, as shown by the Hildebrand type calculation. Finally, we note that the entropy of mixing is quite insensitive

to molecular flexibility. The parameter z might serve as a measure of molecular flexibility; however, the principle terms involving z cancel as indicated in Eqs. (1) and (2), since the flexibility of the polymer molecule is assumed to be the same in the solution and in the amorphous polymer. One sees, therefore, that ν_i can be dependent upon chain flexibility only through the factor f_1.

THE JOURNAL OF CHEMICAL PHYSICS VOLUME 23, NUMBER 10 OCTOBER, 1955

Some Applications in Physics of the *P* Function

JOSEPH I. MASTERS
Technical Operations, Incorporated, Arlington, Massachusetts
(Received November 22, 1954)

The mathematical background and typical applications in physics are presented for a recently tabulated function. Because of its properties, the P function should prove to be a useful aid in the solution of certain problems in applied mathematics involving surface integrations in cylindrical coordinates. A tabulation of the function in its normalized form is appended. Particular attention is paid to the application of the P function to multiple scattering problems involving circular symmetry.

INTRODUCTION

THE function $P(Z/\sigma, R/\sigma)$, previously referred to as the off-set circular probability function, or the circular coverage function, has been developed and tabulated by H. H. Germond for his use in the solution of certain military coverage problems.[1] Actually, this function, because of its flexibility and integral properties, has application in several areas where it has yet to be introduced. It is the purpose of this discussion to review the basic mathematics familiar to those who have worked with the P function, and to present some typical regions of application.

FORMULATION OF THE *P* FUNCTION

1. Definitions

The off-set circular probability function, which will be abbreviated the P function, is the integral of the normalized circular Gaussian function

$$\exp(-x^2/2\sigma^2)/2\pi\sigma^2$$

over a circular area of radius Z centered at a point $x=R$. Choosing an origin at the center of the off-set circle, the integral may be written:

$$P\left(\frac{Z}{\sigma},\frac{R}{\sigma}\right)=\int_0^{2\pi}\int_0^{Z}\frac{\exp(-x^2/2\sigma^2)}{2\pi\sigma^2}rdrd\theta, \quad (1)$$

wherein

$$x^2=R^2+r^2-2rR\cos\theta. \quad (2)$$

Equation (1) may be reduced to a single integral by recognizing

$$\int_0^{2\pi}\exp(rR\cos\theta/\sigma^2)d\theta$$

as a special case of Bessel's integral[2] equal to $2\pi I_0(rR/\sigma^2)$. Thus a more useful form of the P function is

$$P\left(\frac{Z}{\sigma},\frac{R}{\sigma}\right)=\frac{\exp(-R^2/2\sigma^2)}{\sigma^2}\int_0^{Z}\times\exp(-r^2/2\sigma^2)I_0\left(\frac{rR}{\sigma^2}\right)rdr. \quad (3)$$

In discussing the flexibility of the two parameter P function it is convenient to perform a normalization such that the function always has the value unity when $R=0$. The normalized version, abbreviated P^*, is the P function divided by its value at $R=0$ and is written here as:

$$P^*\left(\frac{Z}{\sigma},\frac{R}{\sigma}\right)=\frac{P\left(\frac{Z}{\sigma},\frac{R}{\sigma}\right)}{P\left(\frac{Z}{\sigma},\frac{0}{\sigma}\right)}=\frac{\exp(-R^2/2\sigma^2)\int_0^{Z}\exp(-r^2/2\sigma^2)I_0\left(\frac{rR}{\sigma^2}\right)rdr}{\int_0^{Z}\exp(-r^2/2\sigma^2)rdr}, \quad (4)$$

where

$$\int_0^{Z}\exp(-r^2/2\sigma^2)rdr=\sigma^2[1-\exp(-Z^2/2\sigma^2)].$$

Equation (4) may be expanded in series form for the purpose of tabulation.[1] Tables of the P^* function and its normalization factor sufficiently accurate for most work are included (see Appendix I).

[1] H. H. Germond, "The circular coverage function," RM-330, January 26, 1950. Copies of this report may be obtained from The Rand Corporation, Santa Monica, California.

[2] G. N. Watson, *A Treatise on the Theory of Bessel Functions* (Cambridge University Press, Cambridge, England, 1952).

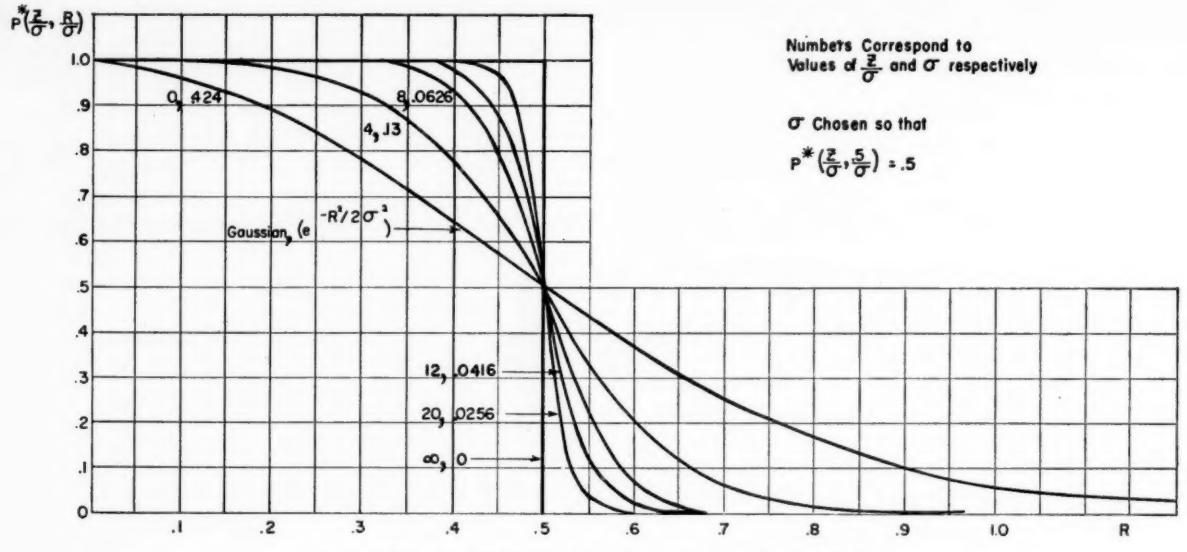

FIG. 1. Function $P^*(Z/\sigma, R/\sigma)$ *vs* R for a few values of Z/σ.

The range of the P^* function for variations of the parameter Z/σ is illustrated in Fig. 1. Although each curve represents a different value of Z/σ, the value of σ in each case is adjusted so that the curve will pass through the common point (0.5, 0.5). Therefore, *a* Z/σ curve represents a family of curves associated with a variation of the parameter σ. The two extremes of the P^* function may be evaluated by investigating Eq. (4) for small Z/σ and large Z/σ.

If Z approaches zero, the integrands of Eq. (4) become constant, producing as one limit of the P^* function:

$$\lim_{Z/\sigma\to 0} P^*\left(\frac{Z}{\sigma},\frac{R}{\sigma}\right) = \lim_{Z/\sigma\to 0} \frac{\exp(-R^2/2\sigma^2)\exp(-Z^2/2\sigma^2)I_0(ZR/\sigma^2)Z}{\exp(-Z^2/2\sigma^2)Z} = \exp(-R^2/2\sigma^2)$$

the unnormalized Gaussian.

If Z/σ becomes large, $(Z/\sigma>3)$, the normalization factor $p(Z/\sigma, 0)$ rapidly becomes unity and may be omitted. Furthermore, as R is varied, the off-set circle of radius Z may be approximated by a line when it crosses the point $x=0$ $(Z=R)$ for small σ. In this case, Eq. (1) is rewritten in terms of Cartesian coordinates, s and y.

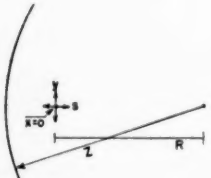

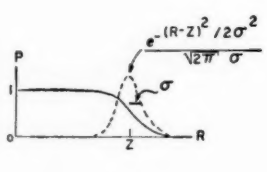

$$P^*\left(\frac{Z}{\sigma}\gg 1,\frac{R}{\sigma}\right) \sim \int_{(R-Z)}^{\infty}\int_{-\infty}^{\infty}\frac{\exp(-s^2/2\sigma^2)\exp(-y^2/2\sigma^2)dsdy}{(2\pi)^{\frac{1}{2}}\sigma(2\pi)^{\frac{1}{2}}\sigma} = 1-\int_{-\infty}^{(R-Z)}\frac{\exp(-s^2/2\sigma^2)}{(2\pi)^{\frac{1}{2}}\sigma}ds = 1-\int_{-\infty}^{R}\frac{\exp[-(R'-Z)^2/2\sigma^2]}{(2\pi)^{\frac{1}{2}}\sigma}dR'.$$

The second term is the integral of a normal error curve which is centered at $R=Z$. As $\sigma\to 0$, it is apparent that the effect of this term is localized at $R=Z$ and that the width at half-height of the P^* function occurs at $R=Z$. Therefore, the other limit of the P^* function is a unit step function of width Z.

2. Integral Property

A very important property of the P function is that the product

$$\frac{\exp(-y^2/2\gamma^2)}{2\pi\gamma^2}\cdot P(Z/\sigma, R/\sigma)$$

can be integrated over an infinite surface, and that this integral is a P function.*

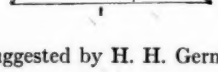

* This step was suggested by H. H. Germond in private communication.

FIG. 2.

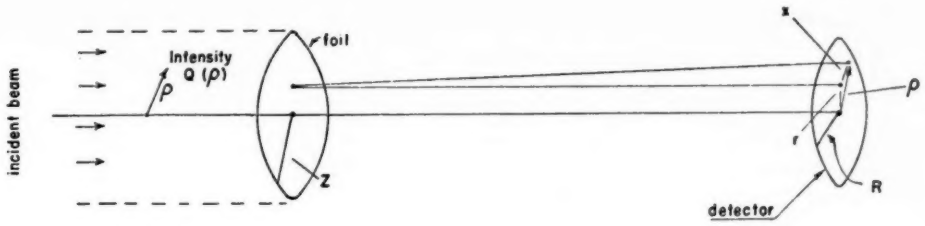

$$P\left(\frac{Z}{\tau},\frac{t}{\tau}\right)$$

$$=\int_0^{2\pi}\int_0^{\infty}\frac{\exp(-y^2/2\gamma^2)}{2\pi\gamma^2}P\left(\frac{Z}{\sigma},\frac{R}{\sigma}\right)RdRd\theta, \quad (5)\dagger$$

where

$$\tau^2=\sigma^2+\gamma^2 \quad \text{and} \quad y^2=R^2+t^2-2Rt\cos\theta. \quad (6)$$

To prove the identity of Eq. (5) substitute Eq. (6) and (3) and apply Bessel's integral to the resulting cosine term, whereupon Eq. (5) becomes:‡

$$\frac{\exp(-t^2/2\gamma^2)}{\sigma^2\gamma^2}\int_{r=0}^{r=Z}\exp(-r^2/2\sigma^2)rdr$$

$$\times\int_{R=0}^{R=\infty}\exp[-(R^2/2)(\tau^2/\sigma^2\gamma^2)]$$

$$\times I_0\left(\frac{tR}{\gamma^2}\right)I_0\left(\frac{rR}{\sigma^2}\right)RdR.$$

The infinite integral is of the form of Weber's 2nd exponential integral[2] and may be written:

$$\frac{\sigma^2\gamma^2}{\tau^2}\exp\left[\frac{\sigma^2\gamma^2}{2\tau^2}\left(\frac{r^2}{\sigma^4}+\frac{t^2}{\gamma^4}\right)\right]I_0\left(\frac{tr}{\tau^2}\right),$$

so that the expression reduces finally to:

$$\frac{\exp(-t^2/2\tau^2)}{\tau^2}\int_{r=0}^{r=Z}\exp(-r^2/2\tau^2)I_0\left(\frac{tr}{\tau^2}\right)rdr.$$

By analogy with Eq. (3) this is $P(Z/\tau, t/\tau)$.

3. Coverage

The fractional coverage by a circular area of radius b centered at $R=0$ of an infinite plane, weighted radially as a P function, is

$$C_p=\frac{\int_0^b P(Z/\gamma, R/\gamma)2\pi RdR}{\int_0^{\infty}P(Z/\gamma, R/\gamma)2\pi RdR}. \quad (7)$$

By expanding $P(Z/\gamma, R/\gamma)$ using Eq. (3) it is easily shown that the denominator is πZ^2. Using a notation due to Germond[1] the numerator is expressed as

$$\gamma^2 S(Z/\gamma, b/\gamma)$$

and Eq. (7) becomes:

$$C_p=S(Z/\gamma, b/\gamma)/\pi(Z/\gamma)^2. \quad (7a)$$

C_p is plotted in Appendix II as a function of its parameters.§

It can be shown by symmetry that $S(Z/\gamma, b/\gamma)=S(b/\gamma, Z/\gamma)$ so that the fractional coverage by the P function $P(Z/\gamma, R/\gamma)$ of a circular area of radius b centered at $R=0$ is

$$C_a=\frac{\gamma^2 S(Z/\gamma, b/\gamma)}{\pi b^2}=\frac{S(b/\gamma, Z/\gamma)}{\pi(b/\gamma)^2} \quad (7b)$$

obtainable from Appendix II.

APPLICATIONS

1. Multiple Scattering

Dickinson and Dodder[3] have developed a graphical technique for determination of particle loss from a uniform beam received by a circular detector when a cen-

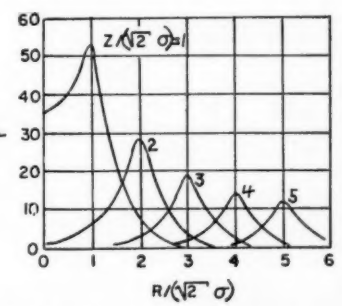

FIG. 3. Fraction of particles lost by scattering for a uniform incident beam and the scattering geometry of Fig. 2.

† It can be shown that

$$\int_0^{2\pi}\frac{\exp(-y^2/2\gamma^2)}{2\pi\gamma^2}Rd\theta=\frac{\partial}{\partial R}\left[P\left(\frac{R}{\gamma},\frac{t}{\gamma}\right)\right]$$

by differentiating the double integral form of the P function (see Eq. (1)) with respect to the second upper limit. Therefore Eq. (5) may be written:

$$P\left(\frac{Z}{\tau},\frac{t}{\tau}\right)=\int_0^{\infty}P\left(\frac{Z}{\sigma},\frac{R}{\sigma}\right)\frac{\partial}{\partial R}\left[P\left(\frac{R}{\gamma},\frac{t}{\gamma}\right)\right]dR, \quad \tau^2=\sigma^2+\gamma^2.$$

‡ A procedure to prove Eq. (5) from Eq. (1) without the use of Bessel function (series) identities has not been found by the author.

§ A more accurate evaluation of this fraction is found in tabular form in reference 1.

[3] W. C. Dickinson and D. C. Dodder, Rev. Sci. Instr. **24**, 428 (1953).

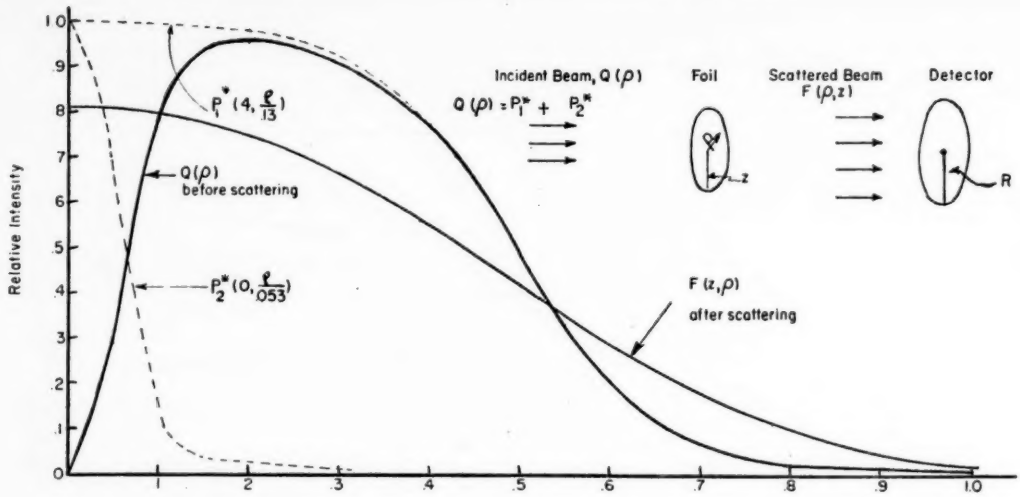

FIG. 4. Alteration of incident beam by scattering. (Note: In the equation $Q(\rho) = P_1^* + P_2^*$, change the plus sign to minus.)

tered circular foil is introduced perpendicular to the beam. This problem (see Fig. 2) is an application of the P function.

Dickinson and Dodder have assumed that multiple scattering will cause any particle striking the foil to hit a circle x units from its intended terminus in the plane of the detector with probability density given by the Gaussian function.

The P function technique below is somewhat less restrictive, in that the probability distribution for a single particle may be any function that can be approximated by some linear combination of Gaussian functions

$$\sum_i \frac{a_i \exp(-x^2/2\sigma_i^2)}{2\pi\sigma_i^2}.$$

The portion of the uniform beam, $Q(\rho)$ constant, intercepted by the foil reappears as a new distribution $F(Z,\rho)$ in the plane of the detector. This distribution may be found by summing over each particle the probability density that any particle passing through the foil will terminate at ρ in the plane of the detector. For a continuum of particles this sum is exactly the integral of the function

$$\sum_i \frac{a_i \exp(-x^2/2\sigma_i^2)}{2\pi\sigma_i^2}$$

centered at ρ over the circle of radius Z.

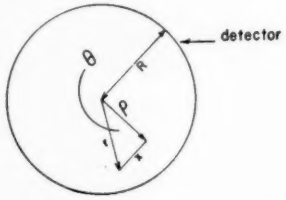

$$F(Z,\rho) = \int_0^{2\pi} \int_0^{Z} \sum_i \frac{a_i \exp(-x^2/2\sigma_i^2)}{2\pi\sigma_i^2} r\,dr\,d\theta,$$

where r is a radial variable of integration.

By comparison with Eqs. (1) and (3), $F(Z,\rho)$ is a sum of P functions

$$\sum_i a_i P(Z/\sigma_i, \rho/\sigma_i).$$

Therefore from Eqs. (7a) and (7b) it follows that the fraction of particles lost by scattering is given by

$$f = 1 - \int_0^R \sum_i a_i P\left(\frac{Z}{\sigma_i}, \frac{\rho}{\sigma_i}\right) 2\pi\rho\,d\rho \Big/ \pi R^2$$

$$= 1 - \sum_i a_i S\left(\frac{R}{\sigma_i}, \frac{Z}{\sigma_i}\right) \Big/ \pi\left(\frac{R}{\sigma_i}\right)^2 \quad R \leq Z,$$

and (8)

$$f = 1 - \int_0^R \sum_i a_i P\left(\frac{Z}{\sigma_i}, \frac{\rho}{\sigma^i}\right) 2\pi\rho\,d\rho \Big/ \pi Z^2$$

$$= 1 - \sum_i a_i S\left(\frac{Z}{\sigma_i}, \frac{R}{\sigma_i}\right) \Big/ \pi\left(\frac{Z}{\sigma_i}\right)^2 \quad R \geq Z.$$

For the case $a_{i=1} = 1$, $a_{i>1} = 0$ a plot of f *vs* R/σ for various Z/σ such as that produced by the graphical method of Dickinson and Dodder[3] is easily constructed from Eq. (8) and Appendix II. Their plot is reproduced in Fig. 3.

The scattering problem of Dickinson and Dodder may be extended to the case of a normally incident, centered, nonuniform beam of radial symmetry whose relative intensity, $Q(\rho)$, becomes negligible as ρ approaches Z, the foil radius. Then the distribution in the plane of the detector after scattering by the foil becomes

$$F(Z,\rho) = \int_0^{2\pi} \int_0^{Z} \sum_i \frac{a_i \exp(-x^2/2\sigma_i^2)}{2\pi\sigma_i^2} Q(r) r\,dr\,d\theta$$

$$= \int_0^{2\pi} \int_0^{\infty} \sum_i \frac{a_i \exp(-x^2/2\sigma_i^2)}{2\pi\sigma_i^2} Q(r) r\,dr\,d\theta \quad (9)$$

where r is a radial variable of integration.

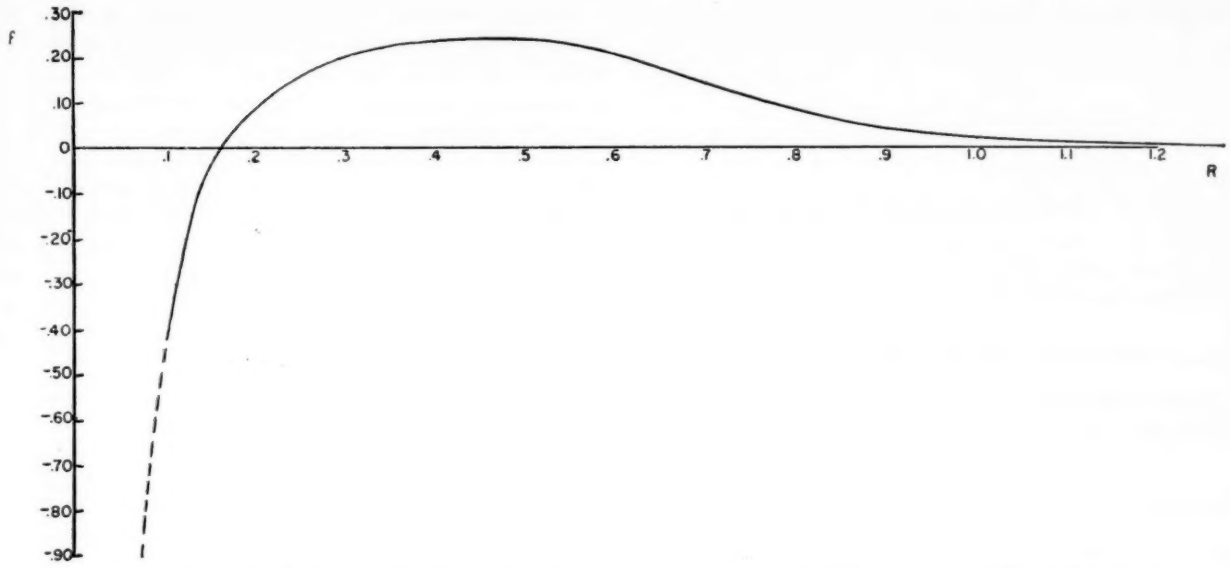

FIG. 5. The fraction, f, of particles lost by scattering *vs* detector radius, for the scattering geometry of Fig. 4.

In order to conveniently evaluate Eq. (9), it is sufficient that the function $Q(\rho)$ be one of a large class of functions approximated with sufficient accuracy by an appropriate linear combination of P functions.|| The distribution $F(Z,\rho)$ after scattering may then be found from Eq. (9) following Eq. (5).

As an example let $a_i=1$, $a_{i>1}=0$, $Z=1$ and consider the distribution approximated by the simple combination of P^* functions (see Figs. 1 and 4)

$$Q(\rho)\cong P_1^*(4,\rho/0.13)-P_2^*(0,\rho/0.053)$$
$$Q(\rho>Z)\cong 0.$$

Figure 4 compares $F(Z,\rho)$ obtained by using Eqs. (9) and (5) with the unscattered distribution $Q(\rho)$.

The fraction, f, of normally incident particles distributed as $Q(\rho)$ which are scattered out of a detector of radius R, due to the presence of a foil of unit radius and scattering coefficient σ, is then obtained by the procedure of Eq. (8). The fraction f is graphed in Fig. 5 as a function of R for $\sigma=2.2$, both in units of Z. If the beam were undisturbed, the detector would receive no particles at $\rho=0$; therefore, it is reasonable that the scattering produces a net gain (a negative f) in particles for R less than 0.16.

2. Classical Diffusion Theory

The P function simplifies the integration of solutions of certain diffusion problems in cylindrical coordinates. As a typical example consider a cylindrical coordinate system contained in an infinite medium of diffusivity, h, whose temperature distribution is initially $f(r)$. The temperature at later times, t, is given by the distribution[4]

$$T(r,t)=\frac{\exp(-r^2/2\sigma^2)}{\sigma^2}\int_0^\infty \exp(-r'^2/2\sigma^2)I_0\times\left(\frac{rr'}{\sigma^2}\right)f(r')r'dr', \quad (10)$$

where $\sigma^2=2ht$. Here again it is only necessary to approximate $f(r')$ by a linear combination of P functions of the form:

$$\sum_i a_i P\left(\frac{Z_i}{\gamma_i},\frac{r'}{\gamma_i}\right).$$

When the expression for

$$\sum_i a_i P\left(\frac{Z_i}{\gamma_i},\frac{r'}{\gamma_i}\right)$$

stated in Eq. (3) replaces $f(r')$ in Eq. (10), $T(r,t)$ becomes:

$$T(r,t)=\frac{\exp(-r^2/2\sigma^2)}{\sigma^2}\int_{r'=0}^{r'=\infty}\exp(-r'^2/2\sigma^2)\times I_0\left(\frac{rr'}{\sigma^2}\right)r'dr'\sum_i\frac{a_i\exp(-r'^2/2\gamma_i^2)}{\gamma_i^2}\times\int_{y=0}^{y=Z_i}\exp(-y^2/2\gamma_i^2)I_0\left(\frac{r'y}{\gamma_i^2}\right)ydy. \quad (11)$$

Equation (11) is identical with the expansion appearing in the proof of Eq. (5) after the order of inte-

|| This is not to imply that $Q(r)$ may be rigorously expanded by a series of P functions such as a Fourier expansion of trigonometric functions, as the former do not form a complete orthogonal set.

[4] H. S. Carslaw and J. C. Jaeger, *Conduction of Heat in Solids* (Oxford University Press, London, 1947).

gration is altered. Therefore,

$$T(r,t)=\sum_i a_i P\left(\frac{Z_i}{\tau_i},\frac{r}{\tau_i}\right), \tag{12}$$

where $\tau_i^2=(2ht)+\gamma_i^2$.

All of the solutions contained in paragraphs 103 V and VI of Carslaw and Jaeger[4] may be evaluated for prescribed initial temperature distributions by similar operations involving the P function.

APPENDIX I. TABLES OF P^* FUNCTIONS

Table II gives values of the P^* function: $P(Z/\gamma, R/\gamma)/P(Z/\gamma, 0/\gamma)$ for various Z/γ and R/γ. The values of Z/γ determine the column and the values of R/γ determine the row where the numerical values of the function are given. For values of Z/γ greater than 3.0 it was found convenient to represent rows by the difference $R/\gamma-Z/\gamma$.

In order to facilitate determination of the P function $P(Z/\gamma, R/\gamma)$, values of the normalization factor of the P^* function: $P(Z/\gamma, 0/\gamma)=1-\exp(-Z^2/2\gamma^2)$ are tabulated for various Z/γ greater than 0.30 in Table I. If Z/γ is less than 0.30, values of $P(Z/\gamma, 0/\gamma)$ may be obtained with accuracy consistent with Table I from the formula

$$P(Z/\gamma, 0/\gamma)=\frac{Z^2}{2\gamma^2}\left(1-\frac{Z^2}{4\gamma^2}\right).$$

TABLE I.

Z/γ	$P(Z/\gamma, 0/\gamma)$	Z/γ	$P(Z/\gamma, 0/\gamma)$	Z/γ	$P(Z/\gamma, 0/\gamma)$	Z/γ	$P(Z/\gamma, 0/\gamma)$
0.30	0.044	0.82	0.285	1.34	0.592	1.86	0.823
0.31	0.047	0.83	0.291	1.35	0.598	1.87	0.826
0.32	0.050	0.84	0.297	1.36	0.603	1.88	0.829
0.33	0.053	0.85	0.303	1.37	0.609	1.89	0.832
0.34	0.056	0.86	0.309	1.38	0.614	1.90	0.836
0.35	0.059	0.87	0.315	1.39	0.619	1.91	0.839
0.36	0.063	0.88	0.321	1.40	0.624	1.92	0.842
0.37	0.066	0.89	0.327	1.41	0.630	1.93	0.845
0.38	0.069	0.90	0.333	1.42	0.635	1.94	0.848
0.39	0.073	0.91	0.339	1.43	0.640	1.95	0.851
0.40	0.077	0.92	0.345	1.44	0.645	1.96	0.854
0.41	0.081	0.93	0.351	1.45	0.651	1.97	0.856
0.42	0.085	0.94	0.357	1.46	0.656	1.98	0.859
0.43	0.088	0.95	0.363	1.47	0.661	1.99	0.862
0.44	0.092	0.96	0.369	1.48	0.666	2.00	0.865
0.45	0.096	0.97	0.375	1.49	0.670	2.05	0.878
0.46	0.100	0.98	0.381	1.50	0.675	2.10	0.890
0.47	0.104	0.99	0.387	1.51	0.680	2.15	0.901
0.48	0.109	1.00	0.393	1.52	0.685	2.20	0.911
0.49	0.113	1.01	0.399	1.53	0.690	2.25	0.921
0.50	0.117	1.02	0.406	1.54	0.695	2.30	0.929
0.51	0.122	1.03	0.412	1.55	0.699	2.35	0.937
0.52	0.126	1.04	0.418	1.56	0.704	2.40	0.944
0.53	0.131	1.05	0.424	1.57	0.708	2.45	0.950
0.54	0.136	1.06	0.430	1.58	0.713	2.50	0.956
0.55	0.140	1.07	0.436	1.59	0.717	2.55	0.961
0.56	0.145	1.08	0.442	1.60	0.722	2.60	0.966
0.57	0.150	1.09	0.448	1.61	0.726	2.65	0.970
0.58	0.155	1.10	0.454	1.62	0.731	2.70	0.974
0.59	0.160	1.11	0.460	1.63	0.735	2.75	0.977
0.60	0.165	1.12	0.466	1.64	0.739	2.80	0.980
0.61	0.170	1.13	0.472	1.65	0.744	2.85	0.983
0.62	0.175	1.14	0.478	1.66	0.748	2.90	0.985
0.63	0.180	1.15	0.484	1.67	0.752	2.95	0.987
0.64	0.185	1.16	0.490	1.68	0.756	3.00	0.989
0.65	0.190	1.17	0.496	1.69	0.760	3.05	0.991
0.66	0.196	1.18	0.502	1.70	0.764	3.10	0.992
0.67	0.201	1.19	0.508	1.71	0.768	3.15	0.993
0.68	0.206	1.20	0.513	1.72	0.772	3.20	0.994
0.69	0.212	1.21	0.519	1.73	0.776	3.25	0.995
0.70	0.217	1.22	0.525	1.74	0.780	3.30	0.996
0.71	0.223	1.23	0.531	1.75	0.784	3.35	0.996
0.72	0.228	1.24	0.536	1.76	0.787	3.40	0.997
0.73	0.234	1.25	0.542	1.77	0.791	3.45	0.997
0.74	0.239	1.26	0.548	1.78	0.795	3.50	0.998
0.75	0.245	1.27	0.554	1.79	0.798	3.55	0.998
0.76	0.251	1.28	0.559	1.80	0.802	3.60	0.998
0.77	0.256	1.29	0.565	1.81	0.806	3.65	0.999
0.78	0.262	1.30	0.570	1.82	0.809	3.70	0.999
0.79	0.268	1.31	0.576	1.83	0.812	3.75	0.999
0.80	0.274	1.32	0.582	1.84	0.816	3.80	0.999
0.81	0.279	1.33	0.587	1.85	0.819	3.85	1.000

For Z/γ greater than 3.85 it is assumed that the function equals unity. Therefore, the P function for any Z/γ, R/γ may be found by finding the P^* function for this argument from Table II and multiplying the value thus found by the value of the normalization factor for the given Z/γ obtained directly from Table I.

For example, if Z/γ is 2.35 and R/γ is 4.2, interpolation in Table II gives a value of 0.024 for the P^* function. In Table I a value of 0.937 corresponds to Z/γ of 2.35. Therefore, the P function $P(2.35, 4.2)$ is $(0.937) \cdot (0.024) = 0.022$.

It is to be noted that the parameters Z/γ and γ are dummy variables in the determination of functional values. Therefore, $P(Z/\eta, R/\eta)$, $P(Z/\tau, R/\tau)$, etc. may be found directly from the tables by merely replacing γ by η, τ, etc.

TABLE II.

R/γ \ Z/γ	0	0.4	0.6	0.8	0.9	1.0
0	1.000	1.000	1.000	1.000	1.000	1.000
0.1	0.995	0.995	0.995	0.996	0.996	0.996
0.2	0.980	0.980	0.982	0.983	0.984	0.985
0.3	0.956	0.957	0.960	0.963	0.965	0.966
0.4	0.923	0.926	0.929	0.935	0.938	0.940
0.5	0.883	0.887	0.892	0.900	0.905	0.908
0.6	0.835	0.841	0.850	0.860	0.866	0.870
0.7	0.783	0.790	0.799	0.814	0.822	0.828
0.8	0.726	0.735	0.747	0.764	0.774	0.781
0.9	0.667	0.677	0.692	0.712	0.723	0.731
1.0	0.607	0.618	0.633	0.657	0.670	0.679
1.1	0.546	0.559	0.575	0.601	0.616	0.625
1.2	0.487	0.501	0.518	0.546	0.561	0.572
1.3	0.430	0.444	0.462	0.490	0.507	0.518
1.4	0.375	0.390	0.409	0.438	0.455	0.467
1.5	0.325	0.338	0.358	0.388	0.404	0.416
1.6	0.278	0.293	0.310	0.340	0.357	0.368
1.7	0.236	0.247	0.267	0.296	0.312	0.323
1.8	0.198	0.211	0.227	0.255	0.271	0.282
1.9	0.164	0.177	0.192	0.218	0.233	0.243
2.0	0.135	0.146	0.160	0.185	0.199	0.208
2.1	0.110	0.117	0.134	0.155	0.168	0.177
2.2	0.089	0.098	0.109	0.130	0.141	0.149
2.3	0.071	0.078	0.089	0.107	0.117	0.124
2.4	0.056	0.063	0.072	0.087	0.096	0.103
2.5	0.044	0.049	0.057	0.071	0.079	0.084
2.6	0.034	0.039	0.045	0.057	0.064	0.069
2.7	0.026	0.030	0.035	0.045	0.051	0.055
2.8	0.020	0.023	0.027	0.036	0.041	0.044
2.9	0.015	0.018	0.021	0.026	0.031	0.035
3.0	0.011	0.013	0.016	0.022	0.025	0.027
3.1	0.008	0.010	0.012	0.017	0.020	0.021
3.2	0.006	0.007	0.009	0.013	0.015	0.017
3.3	0.004	0.005	0.007	0.010	0.011	0.013
3.4	0.003	0.004	0.005	0.008	0.009	0.010
3.5	0.002	0.003	0.004	0.006	0.007	0.007
3.6	0.002	0.002	0.003	0.004	0.005	0.005
3.7	0.001	0.001	0.002	0.003	0.004	0.004
3.8	0.001	0.001	0.001	0.002	0.003	0.003
3.9	0.001	0.001	0.001	0.001	0.002	0.002
4.0	0.000	0.000	0.001	0.001	0.001	0.002
4.1			0.000	0.001	0.001	0.001
4.2				0.001	0.001	0.001
4.3				0.000	0.000	0.001
4.4						0.000

TABLE II—*Continued.*

R/γ \ Z/γ	1.0	1.1	1.2	1.3	1.4	1.5	1.6	1.7	1.8	1.9	2.0
0.0	1.000	1.000	1.000	1.000	1.000	1.000	1.000	1.000	1.000	1.000	1.000
0.1	0.996	0.996	0.997	0.997	0.997	0.997	0.997	0.998	0.998	0.998	0.998
0.2	0.985	0.986	0.987	0.987	0.988	0.989	0.990	0.991	0.992	0.993	0.994
0.3	0.966	0.968	0.970	0.972	0.974	0.976	0.978	0.980	0.982	0.984	0.986
0.4	0.940	0.943	0.947	0.950	0.953	0.957	0.961	0.965	0.969	0.972	0.975
0.5	0.908	0.913	0.918	0.923	0.928	0.934	0.940	0.945	0.951	0.956	0.961
0.6	0.870	0.877	0.884	0.891	0.898	0.906	0.914	0.922	0.930	0.937	0.944
0.7	0.828	0.836	0.845	0.855	0.864	0.875	0.884	0.895	0.905	0.914	0.924
0.8	0.781	0.791	0.803	0.814	0.826	0.839	0.851	0.864	0.877	0.889	0.900
0.9	0.731	0.743	0.757	0.771	0.785	0.800	0.815	0.830	0.845	0.864	0.874

TABLE II—*Continued.*

R/γ \ Z/γ	1.0	1.1	1.2	1.3	1.4	1.5	1.6	1.7	1.8	1.9	2.0
1.0	0.678	0.693	0.708	0.724	0.740	0.758	0.775	0.793	0.811	0.828	0.845
1.1	0.625	0.641	0.658	0.676	0.694	0.714	0.734	0.754	0.774	0.794	0.814
1.2	0.572	0.589	0.607	0.627	0.647	0.669	0.690	0.712	0.735	0.758	0.780
1.3	0.518	0.537	0.556	0.577	0.599	0.622	0.646	0.670	0.695	0.719	0.744
1.4	0.467	0.485	0.506	0.527	0.550	0.575	0.600	0.626	0.653	0.679	0.706
1.5	0.416	0.435	0.456	0.479	0.502	0.528	0.554	0.581	0.609	0.638	0.666
1.6	0.369	0.388	0.408	0.431	0.455	0.481	0.508	0.536	0.566	0.596	0.626
1.7	0.323	0.342	0.363	0.385	0.409	0.436	0.463	0.492	0.522	0.553	0.584
1.8	0.282	0.300	0.320	0.342	0.366	0.392	0.419	0.448	0.478	0.510	0.542
1.9	0.243	0.261	0.280	0.301	0.324	0.350	0.377	0.405	0.436	0.467	0.500
2.0	0.206	0.224	0.243	0.263	0.285	0.310	0.336	0.364	0.394	0.426	0.459
2.1	0.177	0.192	0.209	0.228	0.249	0.272	0.298	0.325	0.354	0.385	0.418
2.2	0.149	0.163	0.179	0.196	0.216	0.238	0.262	0.288	0.316	0.346	0.378
2.3	0.124	0.137	0.151	0.168	0.186	0.206	0.229	0.253	0.280	0.309	0.340
2.4	0.103	0.114	0.127	0.142	0.158	0.177	0.198	0.221	0.246	0.274	0.303
2.5	0.084	0.094	0.106	0.119	0.134	0.151	0.170	0.191	0.215	0.241	0.268
2.6	0.069	0.077	0.087	0.099	0.112	0.128	0.145	0.164	0.186	0.210	0.236
2.7	0.055	0.063	0.072	0.082	0.094	0.107	0.123	0.140	0.160	0.182	0.206
2.8	0.044	0.051	0.058	0.067	0.077	0.089	0.103	0.119	0.136	0.156	0.179
2.9	0.035	0.041	0.047	0.055	0.063	0.074	0.086	0.100	0.115	0.133	0.154
3.0	0.027	0.032	0.037	0.044	0.051	0.060	0.071	0.083	0.097	0.113	0.131
3.1	0.021	0.025	0.030	0.035	0.041	0.049	0.058	0.068	0.081	0.095	0.111
3.2	0.017	0.020	0.023	0.028	0.033	0.040	0.047	0.056	0.067	0.079	0.093
3.3	0.013	0.015	0.018	0.022	0.026	0.032	0.038	0.046	0.054	0.065	0.077
3.4	0.010	0.011	0.014	0.017	0.020	0.025	0.030	0.037	0.044	0.053	0.064
3.5	0.007	0.009	0.011	0.013	0.016	0.020	0.024	0.029	0.036	0.043	0.053
3.6	0.006	0.007	0.008	0.010	0.012	0.015	0.019	0.023	0.028	0.035	0.043
3.7	0.004	0.005	0.006	0.008	0.009	0.012	0.015	0.018	0.023	0.028	0.034
3.8	0.003	0.004	0.004	0.006	0.007	0.009	0.011	0.014	0.018	0.022	0.027
3.9	0.002	0.003	0.003	0.004	0.005	0.007	0.009	0.012	0.014	0.017	0.022
4.0	0.002	0.002	0.002	0.003	0.004	0.005	0.007	0.008	0.011	0.014	0.017
4.1	0.001	0.002	0.002	0.002	0.003	0.004	0.005	0.007	0.008	0.011	0.013
4.2	0.001	0.001	0.001	0.002	0.002	0.003	0.004	0.005	0.006	0.008	0.010
4.3	0.001	0.001	0.001	0.001	0.002	0.002	0.003	0.004	0.005	0.006	0.006
4.4	0.000	0.001	0.001	0.001	0.001	0.001	0.002	0.003	0.004	0.005	0.006
4.5		0.000	0.000	0.001	0.001	0.001	0.002	0.002	0.003	0.004	0.004
4.6				0.000	0.001	0.001	0.001	0.001	0.002	0.003	0.003
4.7					0.000	0.001	0.001	0.001	0.001	0.002	0.002
4.8						0.000	0.001	0.001	0.001	0.001	0.002
4.9							0.000	0.001	0.001	0.001	0.001
5.0								0.000	0.001	0.001	0.001
5.1									0.000	0.001	0.001
5.2										0.000	0.000

TABLE II—*Continued.*

R/γ \ Z/γ	2.0	2.1	2.2	2.3	2.4	2.5	2.6	2.7	2.8	2.9	3.0
0.0	1.000	1.000	1.000	1.000	1.000	1.000	1.000	1.000	1.000	1.000	1.000
0.1	0.998	0.999	0.999	0.999	0.999	0.999	0.999	0.999	0.999	1.000	1.000
0.2	0.994	0.995	0.995	0.996	0.997	0.997	0.997	0.998	0.998	0.999	0.999
0.3	0.986	0.988	0.989	0.991	0.992	0.993	0.994	0.995	0.996	0.997	0.998
0.4	0.975	0.978	0.981	0.984	0.986	0.988	0.990	0.992	0.993	0.995	0.996
0.5	0.961	0.966	0.970	0.974	0.978	0.981	0.984	0.987	0.989	0.991	0.993
0.6	0.944	0.951	0.957	0.963	0.968	0.973	0.977	0.981	0.984	0.987	0.990
0.7	0.924	0.933	0.941	0.949	0.956	0.962	0.968	0.974	0.978	0.982	0.986
0.8	0.900	0.912	0.922	0.932	0.942	0.950	0.958	0.965	0.971	0.976	0.981
0.9	0.874	0.888	0.901	0.914	0.926	0.936	0.945	0.954	0.962	0.969	0.974
1.0	0.845	0.862	0.878	0.893	0.907	0.919	0.931	0.942	0.951	0.960	0.967
1.1	0.814	0.833	0.852	0.869	0.886	0.901	0.915	0.928	0.939	0.949	0.958
1.2	0.780	0.802	0.823	0.843	0.863	0.880	0.896	0.911	0.925	0.937	0.948
1.3	0.744	0.768	0.792	0.815	0.837	0.857	0.875	0.893	0.909	0.923	0.936
1.4	0.706	0.733	0.759	0.784	0.808	0.831	0.852	0.872	0.891	0.907	0.922
1.5	0.666	0.695	0.723	0.751	0.778	0.803	0.827	0.850	0.870	0.889	0.906
1.6	0.626	0.656	0.687	0.716	0.746	0.773	0.799	0.825	0.848	0.869	0.888
1.7	0.584	0.616	0.648	0.680	0.711	0.741	0.770	0.797	0.823	0.846	0.868
1.8	0.542	0.575	0.609	0.642	0.675	0.707	0.738	0.767	0.795	0.822	0.846
1.9	0.500	0.534	0.568	0.603	0.637	0.671	0.704	0.736	0.766	0.795	0.821
2.0	0.459	0.493	0.528	0.563	0.599	0.634	0.668	0.702	0.735	0.765	0.794
2.1	0.418	0.452	0.487	0.523	0.559	0.595	0.631	0.667	0.701	0.734	0.765
2.2	0.378	0.411	0.446	0.482	0.519	0.556	0.593	0.630	0.666	0.701	0.734

TABLE II—*Continued.*

R/γ \ Z/γ	2.0	2.1	2.2	2.3	2.4	2.5	2.6	2.7	2.8	2.9	3.0
2.3	0.340	0.372	0.407	0.442	0.479	0.517	0.554	0.592	0.629	0.666	0.701
2.4	0.303	0.335	0.368	0.403	0.440	0.477	0.515	0.554	0.592	0.630	0.666
2.5	0.268	0.299	0.331	0.365	0.401	0.436	0.476	0.514	0.553	0.592	0.631
2.6	0.236	0.265	0.295	0.328	0.363	0.399	0.436	0.475	0.514	0.554	0.592
2.7	0.206	0.233	0.262	0.293	0.326	0.361	0.398	0.436	0.475	0.515	0.554
2.8	0.179	0.203	0.230	0.260	0.291	0.325	0.360	0.398	0.436	0.475	0.515
2.9	0.154	0.176	0.201	0.229	0.258	0.290	0.324	0.360	0.398	0.437	0.476
3.0	0.131	0.152	0.174	0.200	0.227	0.257	0.290	0.324	0.360	0.398	0.437
3.1	0.111	0.129	0.150	0.173	0.199	0.227	0.257	0.290	0.324	0.361	0.399
3.2	0.093	0.109	0.128	0.149	0.172	0.198	0.226	0.257	0.290	0.325	0.362
3.3	0.077	0.092	0.108	0.127	0.148	0.172	0.198	0.226	0.257	0.291	0.326
3.4	0.064	0.077	0.091	0.108	0.127	0.148	0.171	0.198	0.227	0.258	0.291
3.5	0.053	0.063	0.076	0.090	0.107	0.126	0.148	0.172	0.198	0.227	0.259
3.6	0.043	0.052	0.063	0.075	0.090	0.107	0.126	0.148	0.172	0.199	0.228
3.7	0.034	0.042	0.051	0.062	0.075	0.090	0.107	0.126	0.148	0.172	0.199
3.8	0.027	0.034	0.042	0.061	0.062	0.075	0.090	0.107	0.126	0.149	0.173
3.9	0.022	0.027	0.034	0.041	0.051	0.062	0.075	0.090	0.107	0.127	0.149
4.0	0.017	0.021	0.027	0.033	0.041	0.051	0.062	0.075	0.090	0.107	0.127
4.1	0.013	0.017	0.021	0.027	0.033	0.041	0.051	0.062	0.075	0.090	0.108
4.2	0.010	0.013	0.017	0.021	0.027	0.033	0.041	0.051	0.062	0.075	0.091
4.3	0.008	0.010	0.013	0.017	0.021	0.027	0.033	0.041	0.051	0.062	0.076
4.4	0.006	0.008	0.010	0.013	0.017	0.021	0.027	0.033	0.041	0.061	0.063
4.5	0.004	0.006	0.008	0.010	0.013	0.017	0.021	0.027	0.033	0.042	0.051
4.6	0.003	0.004	0.006	0.008	0.010	0.013	0.017	0.021	0.027	0.034	0.042
4.7	0.002	0.003	0.004	0.006	0.008	0.010	0.013	0.017	0.021	0.027	0.034
4.8	0.002	0.002	0.003	0.004	0.006	0.008	0.010	0.013	0.017	0.021	0.027
4.9	0.001	0.002	0.002	0.003	0.004	0.006	0.008	0.010	0.013	0.017	0.021
5.0	0.001	0.001	0.002	0.002	0.003	0.004	0.006	0.008	0.010	0.013	0.017
5.1	0.001	0.001	0.001	0.002	0.002	0.003	0.004	0.006	0.008	0.010	0.013
5.2	0.000	0.001	0.001	0.001	0.002	0.002	0.003	0.004	0.006	0.008	0.010
5.3		0.001	0.001	0.001	0.001	0.002	0.002	0.003	0.004	0.006	0.008
5.4		0.000	0.000	0.001	0.001	0.001	0.002	0.002	0.003	0.004	0.006
5.5				0.000	0.001	0.001	0.001	0.002	0.002	0.003	0.004
5.6					0.000	0.001	0.001	0.001	0.002	0.002	0.003
5.7						0.000	0.001	0.001	0.001	0.002	0.002
5.8							0.000	0.001	0.001	0.001	0.002
5.9								0.001	0.001	0.001	0.001
6.0								0.000	0.001	0.001	0.001

TABLE II—*Continued.*

$R/\gamma - Z/\gamma$ \ Z/γ	3.0	4.0	6.0	10.0	20.0	∞
−4.0		1.000	1.000	1.000	1.000	
−3.8		1.000	1.000	1.000	1.000	
−3.6		1.000	1.000	1.000	1.000	
−3.4		0.999	0.999	1.000	1.000	
−3.2		0.999	0.999	0.999	0.999	
−3.0	1.000	0.997	0.998	0.998	0.999	0.999
−2.9	1.000	0.996	0.997	0.998	0.998	0.998
−2.8	0.999	0.995	0.996	0.997	0.997	0.997
−2.7	0.998	0.994	0.995	0.996	0.996	0.997
−2.6	0.996	0.992	0.994	0.995	0.995	0.995
−2.5	0.993	0.989	0.992	0.993	0.993	0.994
−2.4	0.990	0.987	0.989	0.990	0.991	0.992
−2.3	0.986	0.983	0.986	0.988	0.989	0.989
−2.2	0.981	0.978	0.982	0.984	0.985	0.986
−2.1	0.974	0.973	0.977	0.980	0.981	0.982
−2.0	0.967	0.966	0.971	0.974	0.976	0.977
−1.9	0.958	0.958	0.964	0.967	0.970	0.971
−1.8	0.948	0.949	0.956	0.960	0.962	0.964
−1.7	0.936	0.938	0.945	0.950	0.953	0.955
−1.6	0.922	0.925	0.934	0.939	0.942	0.945
−1.5	0.906	0.910	0.920	0.926	0.930	0.933
−1.4	0.888	0.893	0.904	0.911	0.915	0.919
−1.3	0.868	0.874	0.886	0.894	0.899	0.903
−1.2	0.846	0.853	0.866	0.874	0.880	0.885
−1.1	0.821	0.830	0.843	0.852	0.859	0.864
−1.0	0.794	0.804	0.818	0.828	0.835	0.841
−0.9	0.765	0.776	0.791	0.803	0.809	0.816
−0.8	0.734	0.745	0.761	0.773	0.781	0.788

TABLE II—*Continued.*

$R/\gamma - Z/\gamma$ \ Z/γ	3.0	4.0	6.0	10.0	20.0	∞
−0.7	0.701	0.713	0.730	0.742	0.750	0.756
−0.6	0.666	0.679	0.696	0.708	0.717	0.726
−0.5	0.631	0.643	0.660	0.673	0.683	0.692
−0.4	0.592	0.605	0.623	0.636	0.646	0.655
−0.3	0.554	0.567	0.585	0.598	0.608	0.618
−0.2	0.515	0.528	0.546	0.559	0.569	0.579
−0.1	0.476	0.489	0.506	0.520	0.530	0.540
0.0	0.437	0.450	0.467	0.480	0.490	0.500
0.1	0.399	0.411	0.428	0.440	0.450	0.460
0.2	0.362	0.373	0.389	0.402	0.411	0.421
0.3	0.326	0.337	0.351	0.363	0.372	0.382
0.4	0.291	0.301	0.315	0.327	0.336	0.345
0.5	0.259	0.268	0.281	0.292	0.300	0.309
0.6	0.228	0.237	0.248	0.253	0.266	0.274
0.7	0.199	0.207	0.218	0.227	0.234	0.242
0.8	0.173	0.180	0.190	0.198	0.205	0.212
0.9	0.149	0.155	0.164	0.172	0.178	0.184
1.0	0.127	0.133	0.141	0.147	0.153	0.159
1.1	0.106	0.113	0.120	0.126	0.130	0.136
1.2	0.091	0.095	0.101	0.106	0.110	0.115
1.3	0.076	0.079	0.085	0.089	0.093	0.097
1.4	0.063	0.066	0.070	0.074	0.077	0.081
1.5	0.051	0.054	0.061	0.061	0.064	0.067
1.6	0.042	0.044	0.047	0.050	0.053	0.055
1.7	0.034	0.036	0.038	0.040	0.042	0.045
1.8	0.027	0.029	0.031	0.032	0.034	0.036
1.9	0.021	0.023	0.024	0.026	0.027	0.029
2.0	0.017	0.018	0.019	0.020	0.022	0.023
2.1	0.013	0.014	0.015	0.016	0.017	0.018
2.2	0.010	0.011	0.012	0.013	0.013	0.014
2.3	0.008	0.008	0.009	0.010	0.010	0.011
2.4	0.006	0.006	0.007	0.007	0.008	0.008
2.5	0.004	0.006	0.006	0.006	0.006	0.006
2.6	0.003	0.004	0.004	0.004	0.004	0.005
2.7	0.002	0.003	0.003	0.003	0.003	0.004
2.8	0.002	0.002	0.002	0.002	0.002	0.003
2.9	0.001	0.001	0.001	0.002	0.002	0.002
3.0	0.001	0.001	0.001	0.001	0.001	0.001
3.2	0.000	0.000	0.001	0.001	0.001	
3.4			0.000	0.000	0.000	

APPENDIX II

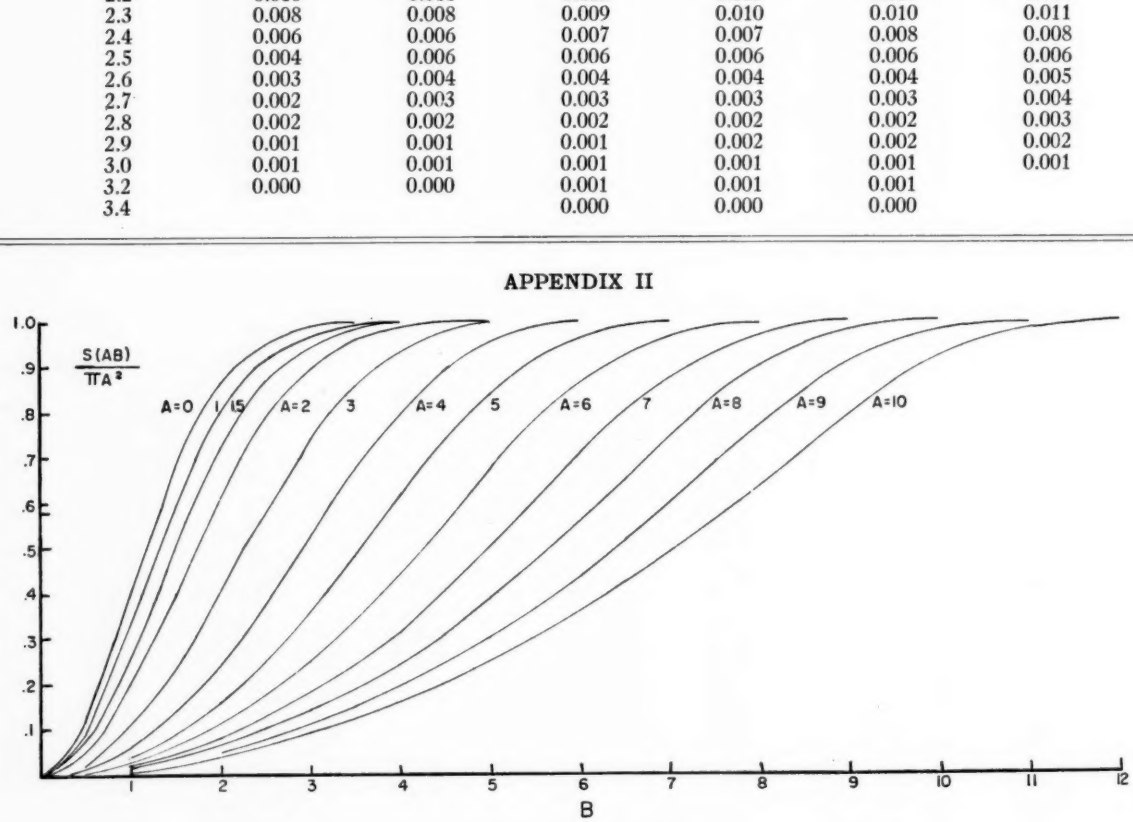

ACKNOWLEDGMENTS

The author is indebted to Dr. Clarke, Dr. Henriques, and Dr. Schorr of the Technical Operations staff for valuable suggestions regarding the preparation and presentation of this paper.

THE JOURNAL OF CHEMICAL PHYSICS VOLUME 23, NUMBER 10 OCTOBER, 1955

Flame Structure Studies. III. Gas Sampling in a Low-Pressure Propane-Air Flame

RAYMOND FRIEDMAN AND JOSEPH A. CYPHERS
Westinghouse Electric Corporation, Research Laboratories, East Pittsburgh, Pennsylvania

(Received January 24, 1955)

A previous investigation of this series showed that the temperature in a very lean, low-pressure propane-air flame continues rising for more than a centimeter downstream from the zone of blue luminosity. This suggested a two-stage combustion process: (I) the hydrocarbon oxidizes rapidly and luminously to carbon monoxide; (II) the carbon monoxide oxidizes more slowly to carbon dioxide. The current gas-sampling study has provided support for this hypothesis. Both water-cooled and uncooled probes have been used to obtain gas samples from the region of the flame just beyond the luminous zone. Tests were made to insure that reaction-quenching in the probe was effective and that flame disturbance was minimized. Gas analyses were performed both mass-spectrometrically and by a vacuum-freezing technique. Most of the samples were taken from a flame burning at 46 mm Hg abs pressure, with a mass air-propane ratio of 30. Substantial proportions of CO, and about $\frac{1}{3}$ as much H_2, were found as much as a centimeter downstream from the luminous zone, with probes of much less than a millimeter diam. The CO concentration decayed exponentially with distance; a kinetic analysis yielded a decay constant of 231 reciprocal seconds. (The flame temperature was 1605°K.) The H_2/CO ratio was considerably less than that corresponding to water-gas equilibrium in the flame. No traces of hydrocarbons were found beyond the luminous zone.

I. INTRODUCTION

THE object of this series of studies is to reveal the mechanism by which thermal energy is released in a uniformly propagating flame. Previous papers of the series[1,2] have dealt with measurement of temperature distribution in very lean propane-air flames. It may be recalled that Friedman and Burke[2] found the temperature in a low-pressure flame to continue rising for more than a centimeter downstream from the zone of blue luminosity. They pointed out that this suggested a two-stage combustion process, the hydrocarbon oxidizing to carbon monoxide in a rapid, luminous first stage, and the carbon monoxide oxidizing to carbon dioxide in a much slower second stage, with far less luminosity. The current investigation was undertaken in an effort to verify this hypothesis by withdrawing and analyzing gas samples from the portion of the flame beyond the luminous zone.

In order to determine the variation of gas composition in a nearly one-dimensional flame by the technique of sample-withdrawal, a number of requirements must be satisfied. Firstly, the presence of the sampling probe must not appreciably disturb the flow streamlines in the flame. Secondly, chemical reactions in the gas must be quenched immediately upon entry into the probe. Thirdly, an adequate method of gas analysis must be available. To a certain extent, these requirements are mutually contradictory; flow disturbances would be minimized by an extremely small probe with very slow sample-withdrawal, while quenching would be facilitated by a completely water-cooled, and hence relatively large, probe. Furthermore, for extremely slow sample-withdrawal, the choice of methods for gas analysis becomes restricted to those applicable to very small samples.

Clearly, compromises must be made. It turns out that, for the relatively thick low-pressure flat flames we are dealing with, apparently satisfactory results can be obtained in the region just downstream of the luminous zone, when carefully designed probes are used. However, it was not possible to sample in the luminous zone itself, or upstream thereof, because of local distortion of the flame by the probe.

This paper will describe the probing techniques which were used, and the experiments which were performed to evaluate their quenching effectiveness. Also, results of gas-sampling studies in a very lean, low-pressure propane-air flame are presented, and the significance of these results is discussed.

II. FLAME-SAMPLING TECHNIQUES

For obvious reasons, most of the gas-sampling studies were made in the same flame as that employed in the earlier temperature-traverse study[2]; this was a flat flame, with a mass air-propane ratio of about 30, burning at about 0.06 atmos, upon a burner of 25-cm diameter. Inasmuch as the apparatus is described at length in the previous publication, only the special features relating to gas-sampling will be discussed here.

Figure 1 shows the relative positions of the probe and the flame. The gas-sampling tube, passing through the side of the tank with a flexible bellows seal, could be moved vertically by a traversing mechanism involving a lead-screw and pivots. The position of the probe tip relative to the flame could be observed through either of two windows ninety degrees apart, and could be measured with a cathetometer.

The probe approached the flame from above (downstream), rather than from below (upstream), since this minimized flow disturbance in the flame. The probe itself, about 7 cm long, to be described in detail below, was joined to a larger, approximately horizontal, rigid tube, of 0.6-cm i.d. This tube, with its annular water

[1] R. Friedman, *Fourth Symposium on Combustion* (Williams and Wilkins, Baltimore, 1953), pp. 259–263.
[2] R. Friedman and E. Burke, J. Chem. Phys. **22**, 824 (1954).

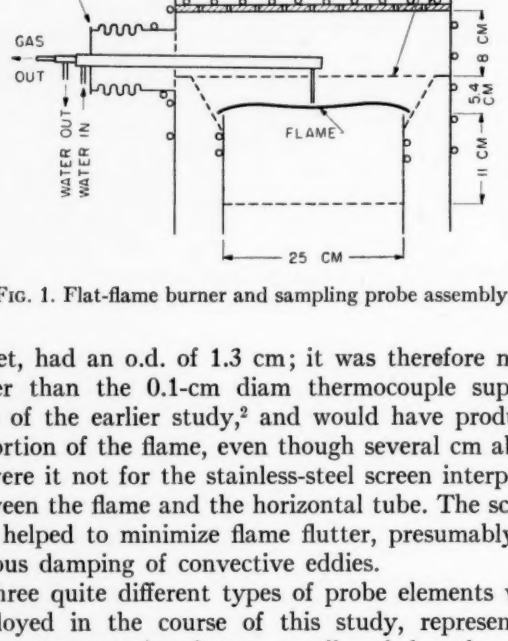

FIG. 1. Flat-flame burner and sampling probe assembly.

jacket, had an o.d. of 1.3 cm; it was therefore much larger than the 0.1-cm diam thermocouple support tube of the earlier study,[2] and would have produced distortion of the flame, even though several cm above it, were it not for the stainless-steel screen interposed between the flame and the horizontal tube. The screen also helped to minimize flame flutter, presumably by viscous damping of convective eddies.

Three quite different types of probe elements were employed in the course of this study, representing various compromises between well-cooled probes and extremely small probes. These will be described.

A probe designated as Type A is shown schematically in Fig. 2. This was the smallest completely-cooled probe which we were able to construct. The tip of the probe was made of silver, because of the high thermal conductivity of this metal. Circulating water was brought within 0.3 cm of the end of the probe; heat transfer calculations showed that, under flame conditions, the temperature difference between the tip and the water was less than 5°C. The 0.0038-cm diam sampling orifice was formed by passing a tungsten wire through the silver tube, fusing the end of the tube with a small, hot flame, and, after resolidification, withdrawing the wire, thus leaving a hole of the same size as the wire. The three concentric Monel tubes were assembled by a judicious combination of silver-soldering and soft-soldering. The silver tip containing the orifice could be unsoldered and replaced whenever the orifice became clogged; this occurred occasionally. Distilled water was used as the coolant, to avoid formation of deposits in the narrow annular passages. With a pressure drop of 70 psi, a water flow of one ml per sec was obtained. Under flame conditions, the temperature rise of this water was less than 10°C.

The gas pressure inside the probe was generally less than 2 mm Hg, while the flame gases were usually at 46 mm Hg, so that critical flow (sonic velocity at throat) would be expected to occur through the orifice. The molecular mean free path of the gas inside the probe was roughly one-fifth the i.d. of the probe; one would therefore expect that quenching of reaction by the cold walls would be extremely rapid.

Let us now consider the gas flow into the probe from the viewpoint of possible disturbances to the flame. Flow measurements under typical flame-sampling conditions show that about 0.1 cu cm (at flame temperature and pressure) of flame gas per sec is drawn into the probe. Since the unperturbed flow velocity of the hot flame gas is about 100 cm per sec, one may calculate that the gas withdrawn for sampling corresponds to the flow across a flame area of $0.1/100=0.001$ sq cm. When this is compared with the flow cross section blocked by the probe tip $[\pi(0.09)^2/4=0.0064$ sq cm$]$, one sees that flow disturbance due to sample withdrawal is small compared with disturbance due to finite size of the probe.

It was found that when the tip of this probe was more than about 0.7 cm above the beginning of the luminous zone, the flame surface below the probe appeared undisturbed, but when the probe was brought closer than this, the portion of the flame immediately below the probe would pucker up and appear to attach itself to the probe. Clearly, no significant measurements could be taken when this occurred. (The intensely luminous zone was about 0.3 cm thick, so the flame-distortion occurred when the probe was about 0.4 cm beyond the *end* of the luminous zone. Measurements in this paper, however, are referred to the *beginning* of the luminous zone, since this could be observed more precisely with the cathetometer.)

One may conclude that this Type A probe, while possessing excellent reaction-quenching efficiency, is too large, and probably too strong a heat sink, to explore any part of the flame but the region substantially downstream from the luminous zone. To anticipate the results, we found that measurable concentrations of

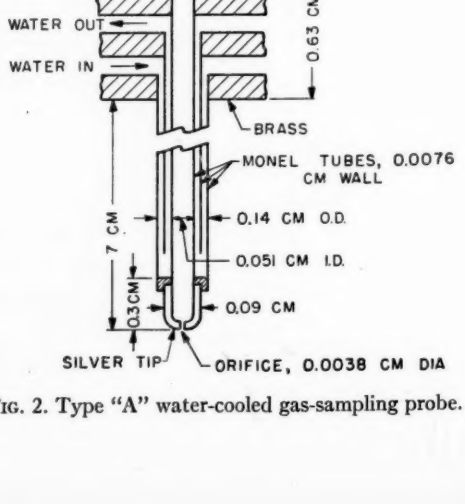

FIG. 2. Type "A" water-cooled gas-sampling probe.

carbon monoxide and hydrogen existed even in this region. Therefore, the reaction-quenching efficiencies of other types of probes could be evaluated by comparison of sampling results in this region with those obtained with a Type A probe.

The Type B probes consisted of small but heavy-walled silver tubes, 7 cm long, water-cooled only at the upper extremity. In this design, one relies on the high thermal conductivity of the silver to keep the tip from getting extremely hot. The probe may be made up of several various-sized tubes, the diameters decreasing from top to bottom. A number of such probes were built, and the tip temperatures measured both with thermocouples and with temperature-indicating paints. None of these probes were found to have tip temperatures below 300–400°C, and, in view of the satisfactory results with the Type A probe and the Type C probes (below), no flame traverses were made with these probes.

The Type C probes were simply fused quartz tubes, originally 2-mm o.d. and 1-mm i.d., the end of each probe being drawn down to a capillary tip. Similar probes have been used by Prescott *et al.*[3] The base of each probe was sealed to the water-cooled brass support tube by a Teflon gasket. Two of these probes are shown in Fig. 3. Probe No. 2–C is seen to neck down abruptly, while 1–C tapers much more gradually. In each case, the constriction was drawn down to such a size that, for comparable pressure drop, the sampling rate was about the same as for the Type A probe described above.

With these probes, it was possible to approach from above to within about 0.3 cm of the beginning of the luminous zone (i.e., to the end of the luminous zone) before visible flame distortion occurred. Hence, samples could be taken over a larger portion of the flame than with the Type A probe. However, these probes ran only a little cooler than the flame gas (because of radiative heat loss); one could not be sure *a priori* whether this slight cooling plus the pressure drop (from 46 to 1 or 2 mm Hg) would be adequate to quench the reaction. Therefore, a series of tests was made to determine the quenching efficiency of Type C probes. These tests are now described.

First, the fact that the gas samples contained at least some unreacted CO and H_2, in the presence of a large excess of O_2, showed these probes to have a certain degree of quenching effectiveness. If this quenching were imperfect, it would be expected to depend on (a) the flow pattern just inside the probe, and (b) the pressure inside the probe. Sampling experiments performed with the two probes of Fig. 3, which differ substantially from one another in internal geometry, gave essentially the same results. Further, tests made with a mean pressure of 4 mm Hg inside the probe gave results similar to those obtained with a mean internal probe pressure

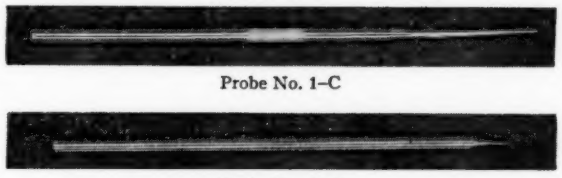

FIG. 3. Two type-C sampling probes.

of 1 mm Hg. Finally, a comparison between quartz probe 2–C and the Type A probe gave good agreement. (Some of these various test results will be seen in Figs. 4 and 5, to be discussed later.)

Therefore, we may conclude that Type C probes have satisfactory quenching effectiveness for reactions involving the species CO, in very lean propane-air flames burning at 46 mm Hg. One should not extrapolate this conclusion to other flame conditions or other reactive species, particularly free radicals, without further tests.

The water-cooled sampling line leaving the burner, shown in Fig. 1, leads to a manifold to which are connected, by short lengths of heavy rubber hose, a series of glass sampling bottles, each with a stopcock. Each bottle has a volume of 260 ml. Prior to each run, this system was evacuated to less than five microns, a leak-test was performed, and the stopcocks were then closed. To take a sample, the probe was moved to the desired position relative to the flame, the manifold line being open to a cold-trap, followed by a vacuum pump. At time zero, a stopcock in this line was closed and one of the sampling bottles on the manifold was opened. After a predetermined time interval, usually about 500 sec, the sampling bottle was closed again. During this time, the pressure in the sampling bottle and sampling line would be rising uniformly from a few microns to a few mm (usually 2 mm). Continual small adjustments of the position of the probe relative to the flame would be made during the period of sample-withdrawal, in order to compensate for slight shifts in the flame position.

III. GAS-ANALYSIS TECHNIQUES

The contents of the sampling bottles would always be analyzed within 24 hours. Tests were made which showed that air leakage into the bottles during the period before analysis was negligible.

Some of the samples were analyzed with a 180° mass spectrometer (Consolidated Engineering Corporation, Type 21–101). These results were useful in that they demonstrated the absence of all hydrocarbons and the presence of small amounts of hydrogen in the sampled region, but the precision of the important carbon monoxide analyses was not as high as was desired. This is because most of the mixtures consisted of one percent or less of CO in the presence of a very high percentage of N_2; thus the mass-28 peak was useless, and the CO analyses had to be based on the mass-12 peak alone.

Therefore, the CO and CO_2 content of many of the

[3] Prescott, Hudson, Foner, and Avery, J. Chem. Phys. **22**, 145 (1954).

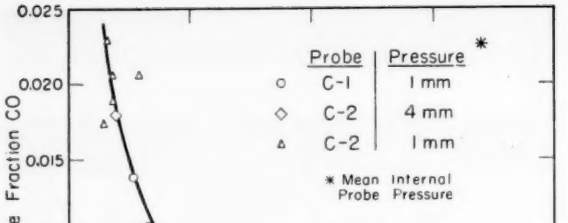
Mole Fraction CO
Distance Beyond Beginning of Luminous Zone (cm)
Probe | Pressure *
C-1 | 1 mm
C-2 | 4 mm
C-2 | 1 mm
* Mean Internal Probe Pressure

FIG. 4. Linear plot of [CO] *vs* x. (Mass air-propane ratio=30, pressure=46 mm Hg.)

samples was determined by a more precise method, involving vacuum freezing and distillation. This technique was first developed in these laboratories by McGeary *et al.*,[4] and resembles the method described by Minkoff and Parthasathi.[5] An all-glass system with Hg cutoffs is used. First, H_2O is removed from the sample by freezing at $-80°C$. Then, CO_2 is isolated by freezing at $-196°C$ and distilled into a one-cc gas burette, where it is measured. Finally, CO is oxidized to CO_2 by passage over copper oxide, and is measured as CO_2 after any newly formed H_2O is removed by freezing. The validity of this system of analysis was demonstrated by analyzing blended gas mixtures of known composition.

Of course, the presence of hydrocarbons in the flame samples would interfere with this method. However, as mentioned above, the mass-spectrometric results demonstrated the absence of hydrocarbons.

Both methods of analysis gave very erratic results when attempts were made to measure water vapor, apparently because of the high absorptivity of water vapor on glass. No results for H_2O are reported.

IV. RESULTS

The distribution of carbon monoxide in the lean propane-air flame under investigation is shown in Fig. 4 (linear plot) and Fig. 5 (semilog plot). The points are labeled so that sampling conditions may be distinguished. The scatter in the points, while larger than one would prefer, is still sufficiently small so that valid conclusions may be drawn from the results. However, the existence of this scatter limits the possibility of determining the effect of any parameter such as flame pressure or air-propane ratio upon the results, unless the parameter in question were to be varied over wide limits. (For practical reasons, this is difficult.) The two main factors contributing to the scatter are: (a) the lack of high precision in the available methods of gas analysis, and (b) the difficulty of maintaining the distance between probe and luminous zone absolutely constant during the requisite 500-sec period.

Figure 4 shows that, sufficiently far downstream, all the CO has been consumed. Consideration of the chemical equilibrium of the hot gases indicates that the CO concentration should eventually drop to 0.0016%. Such a small amount would not be detectable, of course.

Table I shows results of mass-spectrometric analyses. The main conclusion to be drawn from this table is that a little hydrogen is definitely present; the H_2 to CO ratio is about one to five. It may be noted that no hydrocarbons are indicated in the analyses. If any trace-quantities of hydrocarbons are present, one would expect that they would be cracking products such as C_2H_4, C_2H_2, and CH_4. The sensitivity of the mass spectrometer was believed to be such that as little as 0.02% of any of these compounds could have been detected.

The precision of measurement of the very small percentages of hydrogen present was not believed to be sufficiently good to justify detailed study of the influence of the various parameters on the hydrogen distribution. However, it is of interest to compare the observed CO/H_2 ratio with the calculated value of this ratio if the water-gas reaction $CO+H_2O=CO_2+H_2$ were to be in equilibrium in the sampled region. Upon

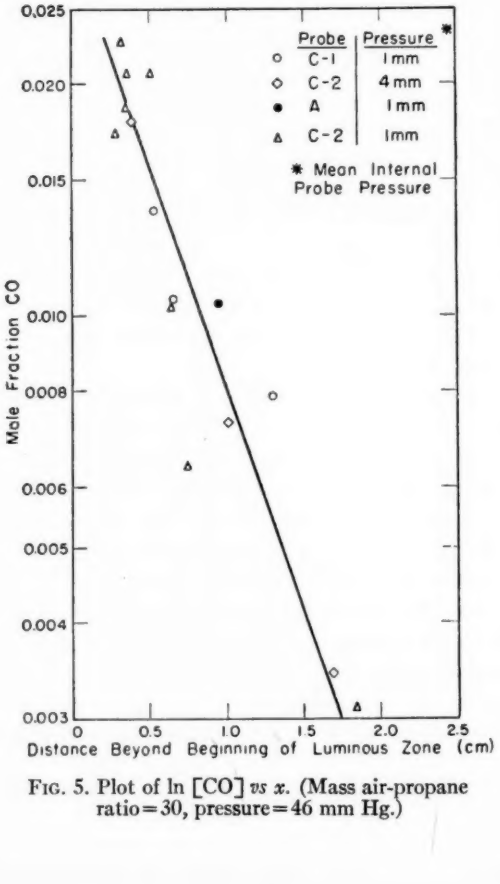
Mole Fraction CO
Distance Beyond Beginning of Luminous Zone (cm)
Probe | Pressure *
C-1 | 1 mm
C-2 | 4 mm
A | 1 mm
C-2 | 1 mm
* Mean Internal Probe Pressure

FIG. 5. Plot of ln [CO] *vs* x. (Mass air-propane ratio=30, pressure=46 mm Hg.)

[4] McGeary, Stanley, and Yensen, Trans. Am. Soc. Metals **42**, 900 (1950).

[5] G. J. Minkoff and N. V. V. Parthasathi, Analyst **79**, 379 (1954).

making standard thermodynamic computations, using the earlier flame temperature measurements (2) and equilibrium data given by Wagman *et al.*,[6] one obtains CO/H_2 ratios near 2, as shown in Fig. 6. Upon comparison with the observed value of 5 for the CO/H_2 ratio, one must conclude that the water-gas reaction is not fast enough to maintain equilibrium when in competition with the oxidizing reactions of this flame.

A few samples were taken from a flame at a mass air-propane ratio of 26.5 instead of 30. This represented the most extreme variation of air-propane ratio that gave satisfactory flame shape with this burner, at 46 mm Hg. Results with the Type A probe showed 1% of CO and roughly 0.3% of H_2 to be present in the gases one cm downstream from the beginning of luminosity. No hydrocarbons were detected with the mass spectrometer. These results are essentially the same as those obtained with the leaner flames. Variation of air-propane ratio, on the lean side, would be expected to have two opposing effects on the distance required for the CO concentration to decay: on the one hand, decreasing the ratio increases burning velocity, thus decreasing residence time in a zone of given width; on the other hand, the flame temperature, and therefore the reaction rate, would increase. Evidently, these effects partially compensated, in our experiment, and the net effect was too small to be measurable.

V. DISCUSSION

The temperature explorations of the earlier study[2] suggested a two-stage combustion process; the gas analyses reported herein tend to confirm this hypothesis. It remains to make a quantitative comparison of the two studies in the sampled portion of the flame; i.e., to compare the $Q(x)$ curve (heat-release rate *vs* distance) determined by differential analysis of the temperature distribution with a $Q(x)$ curve calculated from the measured concentrations of incompletely-burned constituents, chiefly CO.

TABLE I. Mass-spectrometric analyses of samples taken from a propane-air flame (mass air-propane ratio = 30, pressure = 46 mm Hg).

Probe type	C	A	A
Sample no.	B–3–H	B–2–G	B–6–G
Distance[a] (cm)	0.36	0.89	1.27
Mole-fraction[b] of:			
CO	1.9	1.3	0.9
H_2	0.4	0.2	0.2
CO_2	3.2	5.2	5.6
O_2	16.3	13.6	13.6
N_2	77.2	78.7	78.6
A	1.0	1.0	1.1
	100.0	100.0	100.0

[a] Distance of probe-tip downstream from beginning of luminous zone.
[b] Analyses on water-free basis. Data in curves of Fig. 4 and Fig. 5, however, are on total basis.

[6] Wagman, Kilpatrick, Taylor, Pitzer, and Rossini, J. Research Natl. Bur. Standards **34**, 143 (1945).

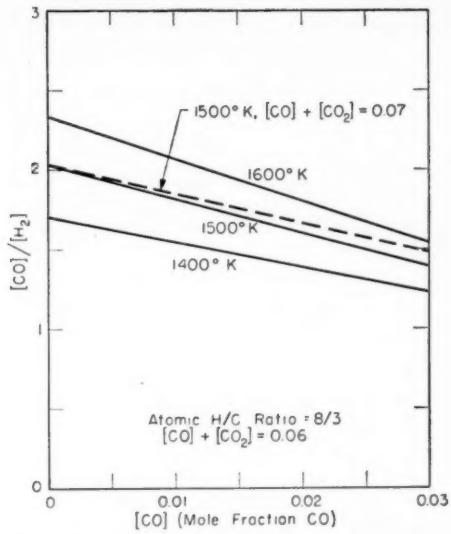

FIG. 6. Theoretical $[CO]/[H_2]$ ratio corresponding to water-gas equilibrium in flame gases.

Figure 5 gives the rate of decrease of CO concentration as the gas flows downstream. Two factors contribute to $d[CO]/dx$, the consumption by chemical reaction and the downstream diffusion. The following differential equation may be written:

$$\frac{d}{dx}\left(D\rho\frac{d[CO]}{dx}\right)-v\rho\frac{d[CO]}{dx}-k\rho[CO]=0. \qquad (1)$$

Here, [CO] denotes mole-fraction of CO; we are ignoring the very slight difference between the molecular weight of CO and the molecular weight of the mixture, which is mostly N_2. D is molecular diffusion coefficient, ρ is density, v is flow velocity, x is distance, and k is a rate constant. We are assuming here that the reaction by which CO disappears is first-order with respect to [CO]; it may of course also depend on $[O_2]$ or $[H_2O]$ (see Barskii and Zeldovich[7]), but the concentrations of these species are known to be nearly constant throughout the region of the flame of present interest. Therefore, if such terms are present, they may be considered to be lumped in with k. It would follow that k would vary with total pressure; however, in this investigation, all sampling has been done at a single flame pressure.

We note that $k\rho$ and, to a lesser extent, $D\rho$ are temperature-dependent. However, the temperature does not change a great deal in the portion of the flame of interest, so that we may obtain a first approximation by ignoring this temperature variation. Then, integration with the boundary conditions $[CO]=0$ at $x=$ infinity and $[CO]=[CO]_0$ at $x=x_0$ yields:

$$\ln[CO]_0-\ln[CO]=\left[\left(1+\frac{4kD}{v^2}\right)^{\frac{1}{2}}-1\right]\frac{v(x-x_0)}{2D}. \qquad (2)$$

[7] G. A. Barskii and Y. B. Zeldovich, Zhur. Fiz. Khim. **25**, 523 (1951). See Chem. Abstracts **46**, 6921.

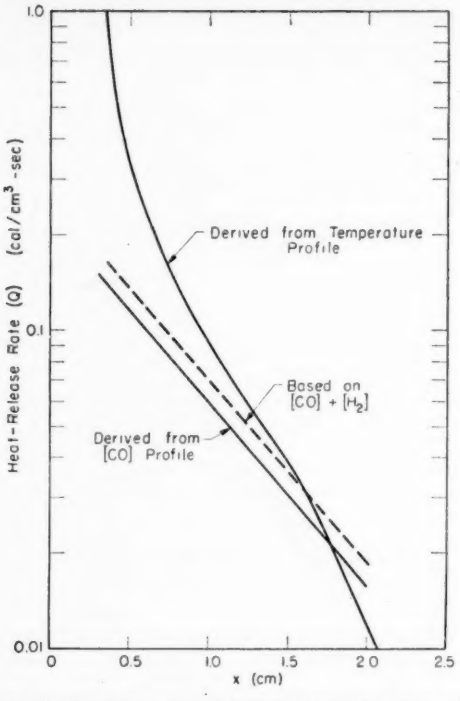

FIG. 7. Heat-release rate beyond luminous part of flame as calculated from two kinds of data.

It follows from Eq. (2) that a plot of $\ln[CO]$ *vs* x should be linear; this is in agreement with Fig. 5.

(It is possible to demonstrate from Eq. (2), by series expansion of the radical, that the effect of diffusion may be ignored in an analysis of this type whenever D is small enough so that

$$4kD/v^2 \ll 1. \tag{3}$$

For the case under investigation, the above critical parameter has a magnitude of about 5; hence, diffusion is not negligible.)

We may compute a value for D at flame conditions from Eq. (8.2–44) and Table 8.4–12 of Hirschfelder *et al.*,[8] by treating the gas as a binary mixture of CO and N_2. We obtain $D=55$ cm²/sec. For v, the flow velocity of the hot gases, we use 101 cm/sec (see previous study[2]). Then, from Eq. (2) and the slope of the curve of Fig. 5, we obtain $k=231$ sec^{-1}. For the reaction $CO+\frac{1}{2}O_2 \rightarrow CO_2$, Wagman *et al.*[6] give $\Delta H_{1500°K} = -67.0$ kcal/mole. From these data we may compute a $Q(x)$ curve showing the heat-release to be expected from the measured rate of disappearance of CO.

Such a curve is shown in Fig. 7, where it may be compared with the $Q(x)$ curve of the earlier study (2). The order-of-magnitude agreement obtained is gratifying. Except for the vicinity of $x=2$ cm, where neither curve is very accurate, the $Q(x)$ based on temperature distribution is seen to be somewhat higher than the $Q(x)$ based on [CO] distribution. It may be recalled that roughly $\frac{1}{5}$ as much H_2 as CO was found to be present in this portion of the flame. The heat of combustion (per mole) of H_2 is about $\frac{7}{8}$ that of CO. Therefore, as a very rough approximation, one might increase $Q(x)$ based on [CO] by the factor $(1+\frac{1}{5}\cdot\frac{7}{8})$, in order to take account of the heat of combusiton of the H_2 as well as the CO. The result of such an approximation is shown as a dotted curve in Fig. 7. (This approximation is rather poor because the diffusion characteristics of H_2 have not been taken into account. However, the $[H_2](x)$ data are not sufficiently precise to justify more refined analysis.)

The two-stage nature of the combustion of a lean propane-air flame revealed by this study fits in nicely with some recent results of Longwell and Weiss,[9] who sampled gases burning incompletely under highly turbulent conditions in a "homogeneous reactor," and found that, for lean mixtures, the unburned portion of the gas consisted mainly of CO, with a little H_2, but no hydrocarbons.

VI. ACKNOWLEDGMENTS

The authors wish to acknowledge the contributions of a number of people to various phases of this study. Mrs. F. H. Hickman assembled and operated the vacuum-freezing gas-analysis apparatus. Mr. A. G. Sharkey, Jr., of the United States Bureau of Mines, Bruceton, Pennsylvania, was responsible for the mass-spectrometric analyses. Mr. G. Hunter fabricated the probes.

[8] Hirschfelder, Curtiss, and Bird, *Molecular Theory of Gases and Liquids* (John Wiley and Sons, Inc., New York, 1954).

[9] J. P. Longwell and M. A. Weiss, Ind. Eng. Chem. **47**, 1634 (1955).

Phenomenological Relations of Electro-Osmosis in Paper Electrochromatography*

SCOTT E. WOOD
Department of Chemistry, Illinois Institute of Technology, Chicago 16, Illinois
(Received January 7, 1955)

Phenomenological equations, based on the thermodynamics of irreversible processes have been developed for the electro-osmosis as observed in paper electrochromatography when the electrodes are placed directly on or in the paper.

WOOD and Strain[1] have studied the electro-osmosis in moist filter paper with electrodes on the paper, a system which is used many times in electrochromotography. The electro osmotic flow was very small in this case and a steady state seemed to be approached. As the potential which causes the electro osmosis is applied continuously during the experiment, forces opposing the osmotic flow must develop with time within the system. Such forces were merely suggested in the original paper and the final phenomenological relations given. It seems of interest to publish the development of these equations at this time since no further work in this field is planned by the author for the present. It must be emphasized that this is only an initial attempt in the study of a very complex system.

The system is considered to be a horizontal sheet of filter paper, moistened with a supporting electrolytic solution. The electrodes are placed along opposite edges of the paper. In the experimental work, a dilute solution of lactic acid was used and the electroösmotic flow was assumed to be positive toward the cathode. At the start of the experiment, the supporting solution is assumed to be uniformly distributed throughout the paper. When the voltage is applied, the solution will begin to move uniformly toward one of the electrodes. This movement results in a decrease in the quantity of solution adjacent to one electrode and in an increase in the quantity of solution adjacent to the other. As the migration proceeds, that part of the solution which is still uniformly distributed in the paper will continue to move causing the regions of unequal distribution to increase in size. In time the solution will become unequally distributed across the entire length of the paper.

The effects of the electrode reactions are not considered. If water is formed or consumed in these reactions, there will obviously be a flow, but the actual quantity of water thus formed or consumed in most experiments will usually be small. The formation of new ions and of a concentration gradient will effect the osmotic flow near the electrodes. This effect cannot be treated mathematically at the present time. However it should not affect the over-all flow to any great extent provided that the regions having a concentration gradient do not extend too far into the paper.

In order to treat this problem mathematically, the paper is referred to a set of coordinate axes so that the flow of electricity and solution is parallel to the x axis. The positive direction is taken toward the cathode. The mass of solution per unit volume of paper, ρ, will be a function of x and the time, t. This quantity is called the density of solution in the paper. The velocity of the solution, v, the velocity of the individual species, v_k, and the potential gradient, $d\phi/dx$, will also depend upon x and t.

A volume element of the paper is defined as that volume lying between two planes perpendicular to the x axis, one at x and the other at $x+dx$. It is necessary to assume that the cross section of the paper, q, is uniform throughout the paper. The forces acting on the solution in this volume element are those resulting from the potential gradient and from the density gradient. That resulting from the potential gradient is $qdx\sum_k e_k\rho_k(\partial\phi/\partial x)_t$, where e_k is the charge per unit mass of the kth substance and ρ_k is the density of the kth substance in the paper. The density gradient causes two forces, one a "pressure" force and the other a "surface" force. Except at the electrodes, the pressure must, of necessity, be uniform throughout the paper. However, unless the paper is saturated with solution, only a fraction of any cross section will be occupied by the solution. This fraction is also a function of x and t. If a is the fraction of the total cross section covered by the solution, the net force acting in the x direction on the solution in the volume element is $-qP(\partial a/\partial x)_t dx$, where P is the pressure. Similarly the ratio of surface area[2] to unit mass of solution, r, in the volume element will depend upon x and t. If γ is the surface energy per unit area, the surface energy per unit volume of paper is $r\rho\gamma$ and the force per unit volume of solution is

* This work is based on experiments done while the author was at Argonne National Laboratory on leave of absence from Illinois Institute of Technology.

[1] S. E. Wood and H. H. Strain, Anal. Chem. **26**, 1869–72 (1954).

[2] It is difficult to define exactly the surface area and the associated surface energy in this case. The area may include both the area of a surface between the fibers of the paper and the solution as well as the area between air and the solution. The total surface energy would then include the energies of both types of surface. The definition of a surface between the fibers and solution would appear to be impossible. On the other hand, it might be assumed that such an area and its associated energy are constant and that the variation of the total area and surface energy is due solely to the air-liquid interface. The discussion here is considered to be more phenomenological than rigid.

$-\gamma(\partial r\rho/\partial x)_t$. The force equation may then be written as

$$\rho\left(\frac{\partial v}{\partial t}\right)_x = -P\left(\frac{\partial a}{\partial x}\right)_t - \gamma\left(\frac{\partial r\rho}{\partial x}\right)_t + \sum_k e_k\rho_k\left(\frac{\partial \phi}{\partial x}\right)_t. \quad (1)$$

Further insight into the phenomena of electro-osmosis can be obtained through the use of the thermodynamics of irreversible processes. The volume shall be that determined by the dimensions of the paper and shall be constant. The temperature and pressure are also assumed to be constant. The air enclosed in the volume is ignored because the presence of air does not effect the results in any way. Furthermore, viscous forces are not considered. The equations of continuity applicable to the volume element previously defined are

$$(\partial\rho/\partial t)_x = -(\partial v\rho/\partial x)_t, \quad (2)$$

and

$$(\partial\rho_k/\partial t)_x = -(\partial v_k\rho_k/\partial x)_t. \quad (3)$$

The energy per unit volume of paper excluding the kinetic energy of the solution at constant x is a function of t and ρ and, therefore,

$$\left(\frac{\partial E}{\partial t}\right)_x = \left(\frac{\partial E}{\partial t}\right)_{x,\rho} + \left(\frac{\partial E}{\partial \rho}\right)_{t,x}\left(\frac{\partial \rho}{\partial t}\right)_x. \quad (4)$$

Then according to the first law,

$$\left[\frac{\partial(E+1/2v^2\rho)}{\partial t}\right]_x = -\mathrm{div}Q - P\left(\frac{\partial av}{\partial x}\right)_t + \sum_k e_k\rho_k v_k\left(\frac{\partial \phi}{\partial x}\right)_t + \gamma\left(\frac{\partial r\rho}{\partial t}\right)_x + 1/2v^2\left(\frac{\partial \rho}{\partial t}\right)_x + \left(\frac{\partial E}{\partial \rho}\right)_{t,x}\left(\frac{\partial \rho}{\partial t}\right)_x \quad (5)$$

where Q is the heat flow per unit time per unit area of the volume element. The term $\frac{1}{2}v^2(\partial\rho/\partial t)_x$ represents the increase in the kinetic energy per unit volume of paper resulting from the increase in density of the solution in the paper. According to the second law,

$$dE = TdS + \sum_k e_k\rho_k d\phi + \gamma d(r\rho) + \left(\frac{\partial E}{\partial \rho}\right)_{S,\phi,r\rho} d\rho, \quad (6)$$

from which

$$\left(\frac{\partial E}{\partial t}\right)_x = T\left(\frac{\partial S}{\partial t}\right)_x + \sum_k e_k\rho_k\left(\frac{\partial \phi}{\partial t}\right)_x + \gamma\left(\frac{\partial r\rho}{\partial t}\right)_x + \left(\frac{\partial E}{\partial \rho}\right)_{S,\phi,r\rho}\left(\frac{\partial \rho}{\partial t}\right)_x, \quad (7)$$

and also

$$\left(\frac{\partial E}{\partial \rho}\right)_{t,x} = T\left(\frac{\partial S}{\partial \rho}\right)_{t,x} + \left(\frac{\partial E}{\partial \rho}\right)_{S,\phi,r\rho}. \quad (8)$$

By combining (1), (2), (5), (7), and (8), the equation

$$T\left(\frac{\partial S}{\partial t}\right)_x = -\mathrm{div}Q - Pa\left(\frac{\partial v}{\partial x}\right)_t + \gamma v\left(\frac{\partial r\rho}{\partial x}\right)_t + \sum_k e_k\rho_k v_k\left(\frac{\partial \phi}{\partial x}\right)_t - \left[\left(\frac{\partial \phi}{\partial t}\right)_x + v\left(\frac{\partial \phi}{\partial x}\right)_t\right]\sum_k e_k\rho_k + T\left(\frac{\partial S}{\partial \rho}\right)_{t,x}\left(\frac{\partial v\rho}{\partial x}\right)_t \quad (9)$$

is obtained which gives the increase of the entropy per unit volume of paper in respect to time at constant x; but

$$(\partial\phi/\partial t)_x + v(\partial\phi/\partial x)_t = d\phi/dt,$$

which equals zero. Then, since there is no temperature gradient and also since

$$Pa(\partial v/\partial x)_t = (\partial Pav/\partial x)_t - v(\partial Pa/\partial x)_t,$$

Eq. (9) may be written as:

$$\left(\frac{\partial S}{\partial t}\right)_x = -\mathrm{div}(Q/T) - \left[\frac{\partial(Pav/T)}{\partial x}\right]_t + \left(\frac{\partial S}{\partial \rho}\right)_{t,x}\left(\frac{\partial v\rho}{\partial x}\right)_t + \frac{v}{T}\left[\gamma\left(\frac{\partial r\rho}{\partial x}\right)_t + P\left(\frac{\partial a}{\partial x}\right)_t\right] + \frac{\sum_k e_k\rho_k v_k}{T}\left(\frac{\partial \phi}{\partial x}\right)_t. \quad (10)$$

The first three terms on the right-hand side of this equation represent the increase in entropy per unit volume due to the flow of entropy into the volume while the last two terms represent the entropy production due to the irreversible processes. These last terms are both products of a "flux" and a corresponding force. Then the phenomenological equations may be written as

$$I = L_{11}(\partial\phi/\partial x)_t + L_{12}F, \quad (11)$$

and

$$v = L_{21}(\partial\phi/\partial x)_t + L_{22}F, \quad (12)$$

where I is the current equal to $\sum e_k\rho_k v_k$ and

$$F = \gamma(\partial r\rho/\partial x)_t + P(\partial a/\partial x)_t.$$

As with all the other variables, the phenomenological coefficients, L_{11}, L_{12}, L_{21}, and L_{22}, will be functions of x and t. Experiments designed in terms of these last equations might be very useful in the study of the electro-osmosis under these conditions, particularly in the steady state and the rate of approach to the steady state. But, because the effects are small, the measurements would have to be very accurate.

dc Resistivity in the Nickel and Nickel Zinc Ferrite System

L. G. VAN UITERT
Bell Telephone Laboratories, Inc., Murray Hill Laboratory, Murray Hill, New Jersey
(Received January 10, 1955)

The dependence of the resistivities of nickel and nickel zinc ferrites prepared from high purity reagents upon composition and firing temperature has been studied.

It has been determined that iron deficient nickel zinc ferrites are of much higher resistivity than iron deficient nickel or zinc ferrites.

The iron deficient ferrites prepared, which were fired in oxygen below 1300°C and have Ni:Zn ratios greater than 3:7, show a positive thermoelectric voltage. Other compositions or materials fired above 1300°C have a negative thermoelectric voltage.

The effect of excess iron upon resistivity is dependent upon the presence or absence of zinc at temperatures below 1300°C.

THE nickel zinc ferrites have been found to be one of the most versatile of the ferrite systems for general use. They present a wide choice in permeability, coercive force and magnetic and electrical losses. They have relatively high resistivity at carrier frequencies and sufficiently low losses for microwave applications.

It is important in many applications to control the resistivity of the ferrite. There are two general approaches to this problem. The first is by controlling the firing temperature and atmosphere, and the second is by the addition of minor constituents to increase or decrease the conductivity. The present study is limited to the former approach for nickel and nickel zinc ferrites prepared from high purity reagents.

PREPARATION OF SAMPLES

The ferrite samples were prepared in the solid state from mixtures of the oxides. The starting materials were wet mixed, calcined at 900°C, ball milled in an iron mill in carbon tetrachloride with a Halowax binder and dried. The materials were analyzed for their metal contents at this stage. They were then pressed into disks that were approximately one inch in diameter and one-tenth of an inch thick. These disks were then fired in oxygen for ten hours at the designated temperatures and subsequently surface ground to have flat parallel faces.

MEASUREMENT OF SAMPLES

It was determined that the desired data could be obtained quickly and with accuracy by measuring the voltage drop across and the current through the sample, using indium-amalgam contacts. The contacts are applied by rubbing a stick of indium which has been slightly wetted with mercury onto a clean ground ferrite surface.

The indium-amalgam was shown to make a low resistance contact to the ferrite samples by three methods. First, samples were measured, using the contact at a given sample thickness and again after grinding the samples to one-half of this thickness. The resistivities calculated from these two sets of measurements were found to be in good agreement. Second, the resistivity of a bar of ferrite was measured between indium-amalgam contacts and by the four contact potential drop method. Again, excellent agreement was obtained. Third, the measured resistivities between contacts for several ferrites were plotted as a function of the applied voltage employing the indium-amalgam contact and found to be constant. This, in conjunction with the previous tests, shows that the contact resistance of the indium-amalgam is negligible over a wide range of voltages.

The samples which contained zinc were measured as prepared and, due to the surface loss of zinc, again after grinding the edges of the disks to where a constant resistivity was obtained. It was not found necessary to do this to obtain constant resistivities in the nickel ferrite samples. All resistivity measurements were made at approximately 25°C.

The signs for the thermoelectric voltages for the ferrites were determined using a galvanometer, a hot silver plate and a cold silver probe cut from the same bar, and the disks faced with the indium-amalgam contacts on each side. Definite results were obtained even on the high resistivity materials, due to the high thermal gradient and excellent contacting properties of the amalgam. Materials listed as *p*-type showed the same direction of deflection as *p*-type germanium and those listed as *n*-type the same direction of deflection as *n*-type germanium.

THE RESISTIVITY VALUES

It should be pointed out that in the following discussion the effects are those obtained for changing the firing temperature of fixed starting compositions. The data are plotted on the basis of the analyzed metal ratios of the materials before the final firing. Some of the observed effects resulting from firing conditions can be traced to alteration of the metal ratios during firing, such as the surface loss of zinc in the nickel zinc ferrites. Others can be attributed to the gain or loss of oxygen from the $M^{2+}:M^{3+}$ spinel stoichiometry during the firing cycle.

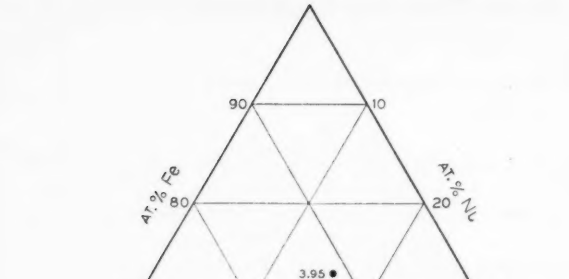

FIG. 1. The logarithms of the resistivity values for samples fired at 1250°C.

RESISTIVITY AND THE TERNARY METAL DIAGRAM AT ONE TEMPERATURE

Figure 1 presents a composition plot of the compounds fired at 1250°C and their body resistivities measured after grinding their edges. Several interesting trends are to be noted.

1. Abrupt changes in resistivity occur as the stoichiometry varies from an iron deficiency to an iron excess.

(a) For the 3:7 nickel zinc ferrites, resistivity drops from about 10^{10} to 10^{2} ohm centimeters upon going from an iron deficiency to an iron excess over the M^{2+}:$2M^{3+}$ stoichiometry (also see Fig. 2).

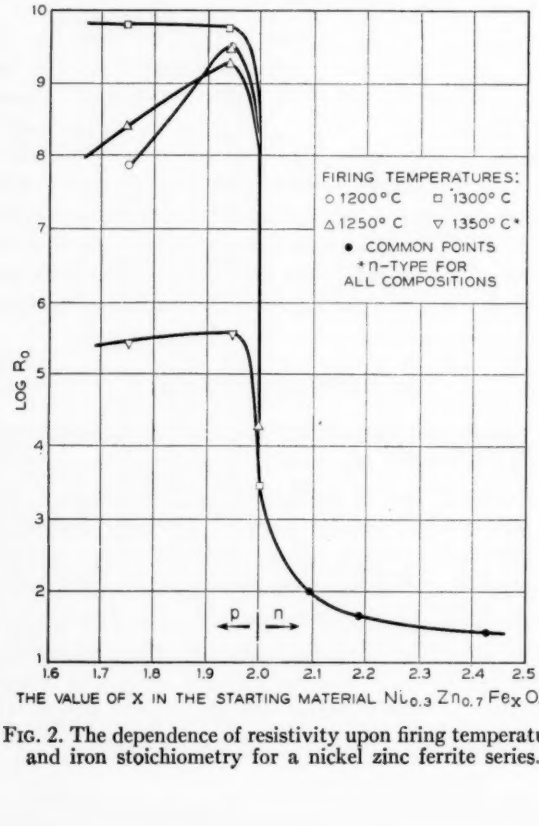
FIRING TEMPERATURES:
○ 1200° C □ 1300° C
△ 1250° C ▽ 1350° C*
● COMMON POINTS
*n-TYPE FOR ALL COMPOSITIONS
LOG R0
p
n
THE VALUE OF X IN THE STARTING MATERIAL Ni0.3 Zn0.7 FeX O4±

FIG. 2. The dependence of resistivity upon firing temperature and iron stoichiometry for a nickel zinc ferrite series.

(b) For the nickel ferrites, resistivity increases from $10^{4.5}$ to $10^{6.4}$ ohm centimeters at 1250°C, rather than dropping for the same variation in iron content (also see Fig. 3).

2. For a constant iron deficiency resistivity is high for zinc-nickel ratios between 7:3 and 3:7 but falls on the order of four log units upon altering the zinc concentration above or below these ratios to zinc or nickel ferrite (also see Fig. 4).

3. For a small excess of iron, reistivity remains low for zinc-nickel ratios above 2:8 and increases by three log units upon eliminating the zinc.

4. The iron excess, nickel and nickel zinc ferrites have negative thermoelectric voltages, while the iron deficient ones are positive as long as the nickel to zinc ratio is about 5:14 or higher. As zinc ferrite is approached, the iron deficient ferrites also become *n*-type. This is coincident with the large decrease in resistivity for the high zinc ferrites, as shown in Fig. 4.

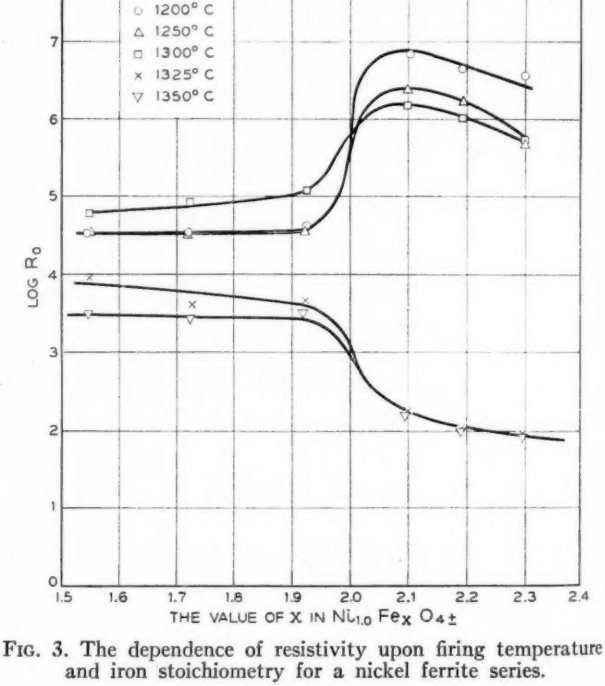

FIG. 3. The dependence of resistivity upon firing temperature and iron stoichiometry for a nickel ferrite series.

The fired samples for critical members of this series were analyzed chemically to ascertain that the indicated metal ratios did not change appreciably during the firing process.

The effect of losing zinc from the surfaces of the disks during firing can be seen in Fig. 4. Comparisons are given between the resistivities of a series of ferrite disks, which have the starting compositions corresponding to $Ni_{1-x}Zn_xFe_{1.9}$, before grinding their edges and after grinding to constant values of resistivity. It is to be noted that the resistivities measured before sur-

face grinding the sample edges were much lower than those found after. The differences in these values increase with the zinc content and temperature of firing samples.

RESISTIVITY VARIATIONS WITH FIRING TEMPERATURE

It is well to examine the resistivity variations of the nickel ferrites, which are less complex, with firing temperature before examining the nickel zinc ferrites. This can most simply be done with reference to the possible phase relationships depicted in Formula I.

The main horizontal line represents the phases that are theoretically present in nickel ferrites that are stoichiometric or off-stoichiometry at the oxygen pressures required to preserve the M^{2+}:$2M^{3+}$ spinel structure. Arrows pointing up indicate reduced states

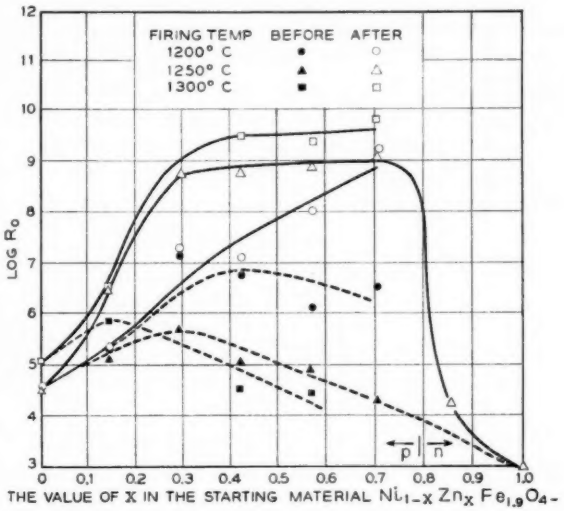

FIG. 4. The resistivities for the prepared disks of the indicated series before and after surface grinding the sample edges.

that may evolve at higher oxygen dissociation pressures, and arrows pointing down indicate oxidized states that can be developed at lower oxygen dissociation pressures or may be present because of incomplete reaction at the firing temperature employed. The phases indicated by stars represent hole structures, such as are common to subtractional type solid solutions.

Figure 3 shows the resistivities of several nickel ferrites which vary systematically from an iron deficiency to an iron excess for several firing temperatures. The ferrites having an iron deficiency do not vary extremely in resistivity. Resistivity increases up to a firing temperature of 1300°C and then drops. The dominant conductivity mechanism in the iron deficient ferrites is *p*-type up to a firing temperature of 1300°C and *n*-type at higher firing temperatures. The iron excess ferrites are *n*-type at all firing temperatures. Figure 5 shows that these trends are also true for the nickel zinc ferrites but that variations in resistivity are more pronounced as the zinc content is increased.

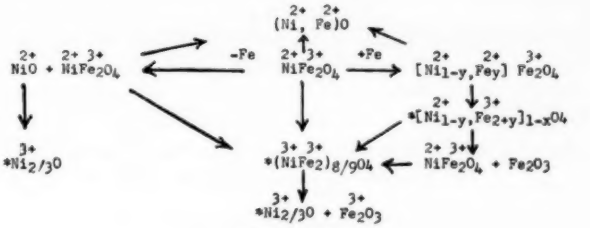

Formula I

The nickel ferrites which have excess iron present have a fairly high resistivity which decreases gradually with temperature until 1300°C is reached, above which temperature there is an abrupt drop in resistivity to a quite low level. The observed drop is in the same temperature range as the demonstrated conversion of Fe_2O_3 to Fe_3O_4[2] in air and probably represents the transition:

$$NiFe_2O_4 + Fe_2O_3 \text{ and/or } [Ni^{2+}_{1-y}, Fe^{3+}_{2+y}]_{1-x}O_4$$
$$\text{to } [Ni_{1-y}{}^{2+}, Fe_y{}^{2+}]Fe_2O_4 \text{ and } (Ni^{2+}, Fe^{2+})0.$$

Chemical analysis, after firing, of the materials involved do not lead to a clear-cut interpretation of their structure. However, some information can be obtained as indicated by the analysis of Table I.

It is evident that in all cases, more oxygen was present than the amount required to account for the

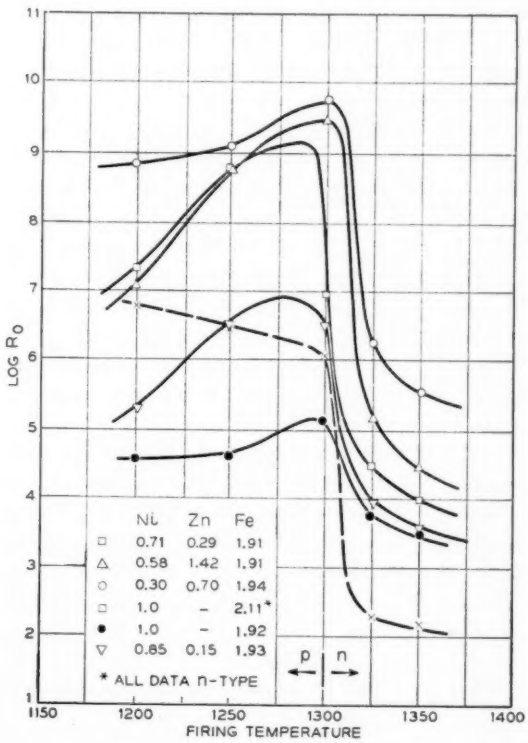

FIG. 5. The dependence of resistivity upon firing temperature in °C for the indicated starting compositions.

[2] J. C. Hostetter and H. S. Roberts, J. Am. Ceram. Soc. 4 [11], 932 (1921).

TABLE I.

Sample	Firing temperature	Composition Ni	Fe	O	Density
A	1250°C	1.0	2.18	4.36	4.65
A	1350°C	1.0	2.17	4.29	5.15
B	1250°C	1.0	1.74	3.65	4.86
B	1350°C	1.0	1.74	3.62	5.20

presence of the metal ions in equivalents of NiO and Fe_2O_3. It is apparent, therefore, that some oxidized phases are present, such as indicated above. The oxygen required to form the oxidized phases may have been obtained from the firing atmosphere (O_2) or absorbed on grain surfaces during the cooling cycle in the furnace leading to a complex phase structure in the finished ferrite sample. Oxygen picked up beyond the $M^{2+}:2M^{3+}$ spinel stoichiometry would make it impossible to conclude what the valence states may be for the metal ions inside the crystallites, which may have been influenced by surface oxygen absorption on cooling. The matter is further complicated by the greater densities and oxygen dissociation pressures during firing of the materials which were fired at 1350°C.

The excess nickel compositions show a tendency to increase resistivity with firing temperature up to 1300°C and to decrease above this temperature. This behavior suggests that the best approximation to $M^{2+}:2M^{3+}$ spinel stoichiometry in these materials is realized around 1300°C. Below 1300°C the principal conductivity mechanism would be via the $Ni^{2+}-Ni^{3+}$ mechanism[3] associated with the presence of excess oxygen. Above 1300°C the principal conductivity mechanism would be via the $Fe^{2+}-Fe^{3+}$ mechanism associated with the partial reduction of the $M^{2+}:2M^{3+}$ spinel.

Figure 5 shows the resistivity dependence upon firing temperature for $Ni_{1.0}Fe_{2.1}O_{4+}$, $Ni_{1.0}Fe_{1.9}O_{4+}$ and a series of nickel zinc ferrites which had the starting composition $Ni_{1-x}Zn_xFe_{1.9}O_{4-}$. It is apparent that the dominant mechanisms affecting resistivity above1300°C are based on the development of divalent iron in the ferrite at these temperatures.

It has been noted previously that replacing part of the nickel with zinc in the iron deficient ferrites result in a marked improvement in resistivity. Figure 5 indicates that this improvement is present to either side of the resistivity drop around 1300°C and increases with the zinc content up to Ni:Zn=3:7. The higher the zinc content of the ferrite the lower the firing temperature required to get a good reactivity of the materials in firing. The tendency to increase resistivity with zinc content in some cases may be due to the decrease in oxygen pickup during cooling as a consequence of the increased reactivity, and hence the higher density and greater structural perfection of the material at a given temperature (refer to the 1200°C firing in Fig. 4). However, when the firing temperature is sufficiently high so that all the compositions of a series such as are shown in Fig. 4 sinter well, it is still found that the high resistivity values occur for the mixed nickel zinc compositions. This is demonstrated by the high resistivity plateau in Fig. 4.

TABLE II.

	Ni	Zn	Fe
Calcined	0.298	0.689	2.00
Fired	0.298	0.559	2.00

[3] Verewey, Haaijman, Romeijn, and Van Oosterhout, Philips Research Repts. 5, 173–187 (1950).

THE VOLATILIZATION OF ZINC AT ELEVATED TEMPERATURES

A metal analysis of a nickel zinc sample was carried out after calcining at 900°C and again after firing as the powder at 1350°C. The results are shown in Table II. Approximately 18.8% of the zinc was distilled out of the powder in ten hours at the elevated temperature. The oxygen stoichiometry at the elevated temperature shows that the excess iron was present in the stoichiometric ratio of M_3O_4.

TABLE III.

	Ni	Zn	Fe
Calcined	0.299	0.702	2.00
Fired	0.298	0.648	2.00

Although the loss of zinc occurs principally at the surface of the compressed parts, chemical analysis shows that there can be a loss of zinc throughout the body of the material also. A known starting composition was compacted and fired as a disk at 1300°C and then surface ground to a constant value of resistivity before analyses. The metal ratios found are reported in Table III. This shows a 7.7% loss in zinc. Analyses of materials fired at 1250°C show zinc loss is relatively negligible at this temperature.

CONCLUSIONS

The general inferences that can be drawn from the above observations are as follows:

a. Nickel zinc ferrites that do not contain divalent iron are inherently of high resistivity.

b. Because of improvement in homogeneity and structural perfection, the resistivities of the nickel and nickel zinc ferrites prepared in the described manner which do not contain excess iron increase with firing temperature up to 1300°C.

c. Above 1300°C the development of divalent iron in the ferrite bodies causes a sharp drop in the resistivities of all nickel and nickel zinc ferrites. The loss of zinc in the high zinc materials increases the proba-

bility of the formation of divalent iron in these materials also.

d. Small amounts of excess iron are incorporated into the nickel zinc ferrites in the stoichiometry of M_3O_4 creating divalent iron in the system which leads to low resistivity values at much lower firing temperatures than in the nickel ferrites.

e. Excess iron in the less reactive and hence more porous nickel ferrites may be incorporated as an oxidized phase in the material fired below 1300°C and furnace cooled in oxygen, leading to relatively high resistivities.

f. For these materials, the dominant conductivity mechanisms in the iron deficient nickel and nickel zinc ferrites, where Ni:Zn=3:7 or higher, are *p*-type for firing temperatures up to 1300°C in oxygen. For higher firing temperatures, lower nickel concentrations and for iron excesses they are *n*-type.

ACKNOWLEDGMENTS

The author wishes to thank S. S. Flaschen, for suggesting the indium amalgam contact, and A. Goss, J. E. Kunzler, and F. Schnettler, of this laboratory, for helpful discussion.

THE JOURNAL OF CHEMICAL PHYSICS VOLUME 23, NUMBER 10 OCTOBER, 1955

Absorption Bands of N_2O Near 4.5μ*

K. LAKSHMI† AND J. H. SHAW
Department of Physics and Astronomy, The Ohio State University, Columbus, Ohio
(Received January 24, 1955)

The absorption bands of N_2O near 4.5μ have been remeasured. In addition to the intense lines of the ν_3 and $\nu_3+\nu_2-\nu_2$ bands, many new weak lines have also been observed and their frequencies determined. Although no band assignments could be made for these weaker lines, the molecular constants obtained from the other two bands agree well with the values reported by Thompson and Williams.

A DETAILED laboratory study of the N_2O band structure near 4.5μ has been made to enable lines of this molecule which appear in the solar spectrum to be identified. The spectra were obtained using an original grating having 7200 lines per inch, ruled by John Strong, and a lead telluride detector. An absorption cell 15 cm long, containing from 5 to 10 mm Hg of N_2O, was used for most of the spectra. However, N_2O pressures of up to 500 mm Hg were required to give measurable absorption at the edges of the bands and, under these conditions, pressure broadening effects gave some loss of resolution. Nevertheless, in many places, lines as close as 0.1 cm^{-1} could be resolved and the map in Fig. 1 shows more structure than the spectrum recently published by Thompson and Williams.[1]

The frequencies of the lines were calculated with a grating constant obtained by measuring the second order spectrum of the 2.3μ CO overtone band and using the frequencies of the CO lines given by Plyler, Benedict, and Silverman.[2] There is excellent agreement between the frequency values of the present work and those given by Thompson and Williams. In most cases the agreement is to within $\pm$0.05 cm^{-1}.

Most of the lines have been identified as belonging to either the ν_3 or $\nu_3+\nu_2-\nu_2$ band systems of the $N^{14}N^{14}O^{16}$ molecule, but many additional weak lines are also present in Fig. 1. Some of these lines were observed and measured by Thompson and Williams who tentatively

TABLE I. Frequencies of N_2O lines below 2160 cm^{-1}.

Line No.	Freq. cm^{-1}	Line No.	Freq. cm^{-1}
1	2128.57	28	2146.31
2	29.68	29	46.89
3	30.67	30	47.19
4	30.93	31	47.86
5	31.76	32	48.39
6	32.02	33	49.46
7	32.83	34	49.78
8	33.26	35	50.44
9	33.99	36	50.73
10	34.34	37	51.52
11	35.03	38	51.94
12	35.43	39	52.54
13	35.89	40	53.19
14	36.59	41	53.64
15	37.04	42	54.23
16	37.68	43	54.47
17	37.86	44	54.96
18	38.88	45	55.64
19	39.08	46	56.20
20	39.89	47	56.50
21	40.98	48	56.94
22	42.01	49	57.58
23	43.06	50	58.08
24	43.93	51	58.63
25	44.15	52	58.88
26	45.23	53	59.22
27	45.91	54	59.55

* Supported in part by a contract between the Geophysics Research Division of the Air Force Cambridge Research Center and the Ohio State University Research Foundation.
† Aurelia Henry Reinhardt International Fellow of the American Association of University Women for the year 1953–1954.
[1] H. W. Thompson and R. L. Williams, Proc. Roy. Soc. (London) A220, 435 (1953).
[2] Plyler, Benedict, and Silverman, J. Chem. Phys. **20**, 175 (1952).

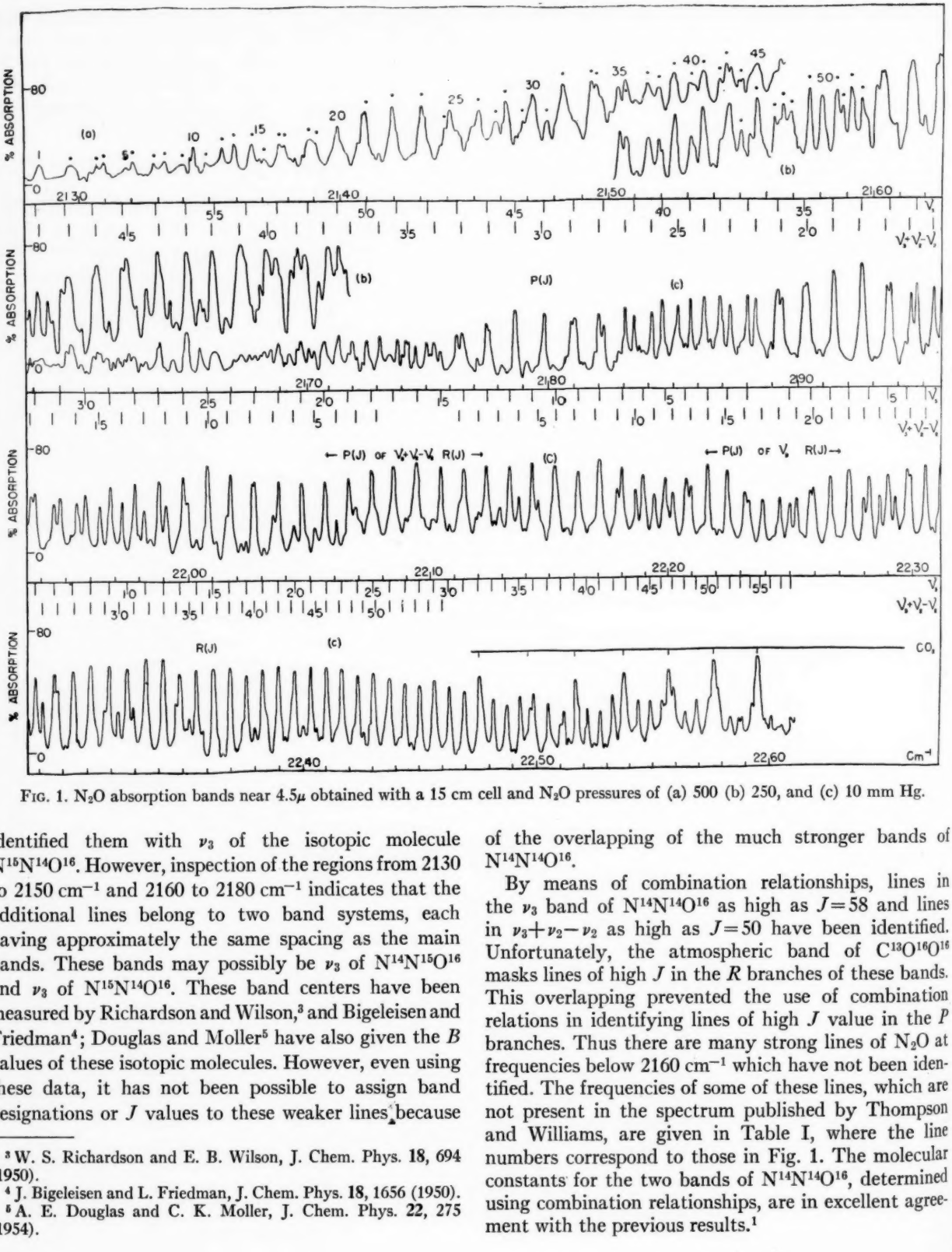

FIG. 1. N_2O absorption bands near 4.5μ obtained with a 15 cm cell and N_2O pressures of (a) 500 (b) 250, and (c) 10 mm Hg.

identified them with ν_3 of the isotopic molecule $N^{15}N^{14}O^{16}$. However, inspection of the regions from 2130 to 2150 cm^{-1} and 2160 to 2180 cm^{-1} indicates that the additional lines belong to two band systems, each having approximately the same spacing as the main bands. These bands may possibly be ν_3 of $N^{14}N^{15}O^{16}$ and ν_3 of $N^{15}N^{14}O^{16}$. These band centers have been measured by Richardson and Wilson,[3] and Bigeleisen and Friedman[4]; Douglas and Moller[5] have also given the B values of these isotopic molecules. However, even using these data, it has not been possible to assign band designations or J values to these weaker lines because of the overlapping of the much stronger bands of $N^{14}N^{14}O^{16}$.

By means of combination relationships, lines in the ν_3 band of $N^{14}N^{14}O^{16}$ as high as $J=58$ and lines in $\nu_3+\nu_2-\nu_2$ as high as $J=50$ have been identified. Unfortunately, the atmospheric band of $C^{13}O^{16}O^{16}$ masks lines of high J in the R branches of these bands. This overlapping prevented the use of combination relations in identifying lines of high J value in the P branches. Thus there are many strong lines of N_2O at frequencies below 2160 cm^{-1} which have not been identified. The frequencies of some of these lines, which are not present in the spectrum published by Thompson and Williams, are given in Table I, where the line numbers correspond to those in Fig. 1. The molecular constants for the two bands of $N^{14}N^{14}O^{16}$, determined using combination relationships, are in excellent agreement with the previous results.[1]

[3] W. S. Richardson and E. B. Wilson, J. Chem. Phys. **18**, 694 (1950).
[4] J. Bigeleisen and L. Friedman, J. Chem. Phys. **18**, 1656 (1950).
[5] A. E. Douglas and C. K. Moller, J. Chem. Phys. **22**, 275 (1954).

Gaseous Detonations. VII. A Study of Thermodynamic Equilibration in Acetylene-Oxygen Waves*

G. B. KISTIAKOWSKY AND WALTER G. ZINMAN
Gibbs Chemical Laboratory, Harvard University, Cambridge, Massachusetts

(Received January 7, 1955)

The observed detonation velocities in acetylene-oxygen mixtures containing from 5 to 50% acetylene and thermo-hydrodynamic calculations which assume complete equilibrium to be attained in the Chapman-Jouguet plane agree within 0.5%. This is of special interest because in successive parts of this composition range each of the several reactions, *viz.* dissociation of excess oxygen, carbon dioxide, water, and hydrogen becomes the main endothermic process. Temperatures may be calculated from the detonation velocities which agree with the theoretical equilibrium values to better than 1% over the range from 3000 to 4500°K.

In acetylene-oxygen mixtures containing 53 and 55% of the former, the observed detonation velocities agree with equilibrium calculations only when it is assumed that undersaturated carbon vapor, taken to be in equilibrium with unburned acetylene, has 170 Kcal as its heat of sublimation.

The velocities in mixtures containing from 60 to 70% acetylene agree quite well with calculations assuming homogeneous equilibrium. However, supersaturation of carbon vapor with respect to the solid must be assumed.

In mixtures containing 71% acetylene a sudden rise in detonation velocity is observed partway down the tube. The final velocity, as well as the constant velocities in still richer mixtures, are consistent with calculations assuming complete equilibrium, including solid carbon.

The discontinuity observed with 71% mixtures is interpreted as the overtaking of the Chapman-Jouguet plane of the primary detonation wave by a secondary shock wave developed by the delayed precipitation of carbon. It is suggested that because of the dependence of the delays of nucleation on the degree of supersaturation of a vapor, high velocities corresponding to complete equilibrium could be observed with leaner mixtures also, if detonation velocities were measured far enough from the point of initiation.

THE propagation velocity of a steady, plane, detonation wave has been the subject of numerous theoretical investigations[1] starting in 1889. Zeldowitch,[2] Doering,[3] and von Neumann[4] all concluded that such a wave consists of a shock front followed by a steady-state region of exothermic chemical reactions, and then by the nonsteady regime of the rarefaction wave. Separating the latter regions is the imaginary Chapman-Jouguet (C–J) plane for which the relation holds:

$$D=c_0+u, \tag{1}$$

D being the detonation velocity, c_0 the sound velocity, and u the mass velocity of the medium in the state characterizing the C–J plane. Rigorous hydrodynamic relations lead to the detonation velocity if c_0 is known; but the latter follows if the nature of the thermodynamic state of the medium in the C–J plane and its thermodynamic functions as well as the initial state of the reactants are known.

With the introduction into the detonation theory by the above authors of the concept of finite chemical rates, the C–J plane became identified with the state of thermodynamic equilibrium among the reaction products, although they all noted that special circumstances may lead to nonequilibration. The recent paper by Kirkwood and Wood[5] completes the formal theory, the C–J plane being associated with the condition:

$$\sum_{j=1}^{n} \sigma^j r^j = 0, \tag{2}$$

where j identifies one of the n reactions assumed to occur in the steady-state region, r^j is the net rate of this reaction, and σ^j measures, loosely speaking, the effect of this reaction, due to mole number and enthalpy changes, on the pressure of the system. The authors point out that Eq. (2) is satisfied firstly when all r^j vanish because equilibrium has been established. The second case arises when some r^j with positive σ^j balance those with negative σ^j, while still finite; in this case equilibrium is not established. Finally, Kirkwood and Wood note that when the summation in (2) has two or more zeros, the theory provides no information as to which of the states so defined corresponds to the C–J plane and therefore satisfies Eq. (1).

From the kinetic point of view the most plausible reason for case 2 to occur is for some reactions with negative σ to last longer than those with positive σ because of slower rates. The likely examples are the strongly endothermic dissociations and the transfer of kinetic energy to internal degrees of freedom in inert addenda. In these cases the detonation velocity would be higher than that calculated on the assumption of equilibrium. The opposite effect may be kinetically expected in case 3 if one of the reactions with positive σ has such a long induction period that the summation in (2) decreases to zero (for instance because partial equilibrium has been attained) before this reaction

* The research reported in this document was made possible by funds extended Harvard University under ONR Contract N5ori-076 T.O. XIX NR-053-094.

[1] See for detailed bibliography: J. G. Kirkwood and W. W. Wood, J. Chem. Phys. **22**, 1915 (1954).

[2] Y. B. Zeldowitch, Theory of Combustion and Detonation of Gases (Translated from Russian in Technical Report F-TS-1226-IA Air Materiel Command, Dayton, Ohio).

[3] W. Doering, Ann. Physik **43**, 421 (1943).

[4] J. von Neumann, OSRD Report 549 (1952).

[5] J. G. Kirkwood and W. W. Wood, J. Chem. Phys. **22**, 1915 (1954).

TABLE I. Tests for overdrive. Run A: A steady wave obtained with 7.5% acetylene+92.5% oxygen at one-atmosphere pressure in the 5-cm tube. Run B: An overdriven wave obtained with 6.0% acetylene+94.0% oxygen at an initial pressure of one atmosphere in the same tube.

Distance from diaphragm (cm) to start of interval	Gauge to gauge velocity (m/sec) Run A	Run B
68.6	1764	1714
80.1	1763	1693
91.5	1755	1713
102.9	1760	1679
114.3	1761	1679
125.8	1758	1671
137.2	1769	1683
	Mean: 1762	

sets in. This might happen with the condensation of a supersaturated vapor. If the first zero of the summation defines the C–J plane, the detonation velocity may now be less than predicted on the basis of complete equilibrium calculation.

Experimental work has on the whole strongly supported the hypothesis of equilibration in the C–J plane, the agreement obtained being the better the more refined the calculations and the experiments. Much of the earlier work is of only qualitative significance because no allowance was made for the tube diameter effect[6,7] which decreases the detonation velocity below that of the plane wave; almost without exception the velocities reported in earlier work are below the equilibrium values. Zeldowitch[2] maintains that in hydrogen-chlorine mixtures the velocity is higher than the equilibrium value and attributes this to a slow dissociation equilibration of the reaction products. The experimental evidence which he cites is open, however, to serious doubts. It was reported from this laboratory[8] that in certain hydrogen-oxygen mixtures the observed velocities were *ca* 1% higher than calculated, but in the light of subsequent unpublished work this conclusion cannot be maintained. Faster than calculated velocities were also observed in rich cyanogen-oxygen mixtures,[6] but the calculations are open to doubt because of uncertainties in the chemical potential of unreacted cyanogen at the very high temperatures involved. In lean acetylene-oxygen mixtures the observed velocities are also higher than calculated.[9] The calculations in this case are quite reliable and the slow excitation of the vibrational heat capacity of excess oxygen, as well as its slow dissociation, could explain the occurrence of case (2). In mixtures containing from *ca* 60 to 70% acetylene, the observed velocities are much lower than calcuated.[9] The decomposition of unreacted acetylene into solid carbon and hydrogen is a reaction with positive σ. Because of delays in the nucleation of solid carbon this reaction could have an induction period[9] and so lead to case (3) of Kirkwood and Wood. The present experiments deal with these two possible deviations from equilibration in the C–J plane.

EXPERIMENTAL DETAILS

The equipment and experimental procedures were similar to those previously described,[6] except as noted below.

In addition to the piezoelectric gauges, described previously, also the ionization "gap" gauges[10] were used occasionally for velocity measurements. They functioned at least as well as the others and, as they are far easier to construct, their advantage is obvious. Our analysis of previous work suggested that stability and constancy of detonation velocities were perhaps not sufficiently demonstrated. Therefore seven to eight gauges were mounted equidistantly in each of the experimental tubes, and only those runs in which at least six gauges gave signals on the raster sweep of the scope were used for velocity calculations.

During the period of these experiments, the apparatus for mixing and storing explosive gas mixtures underwent several reconstructions and was finally converted by Mr. P. H. Kydd to an all-metal system in which a special "O" ring sealed piston pump provided for the mixing and transfer of mixtures from stainless steel storage tanks to the explosion tubes.

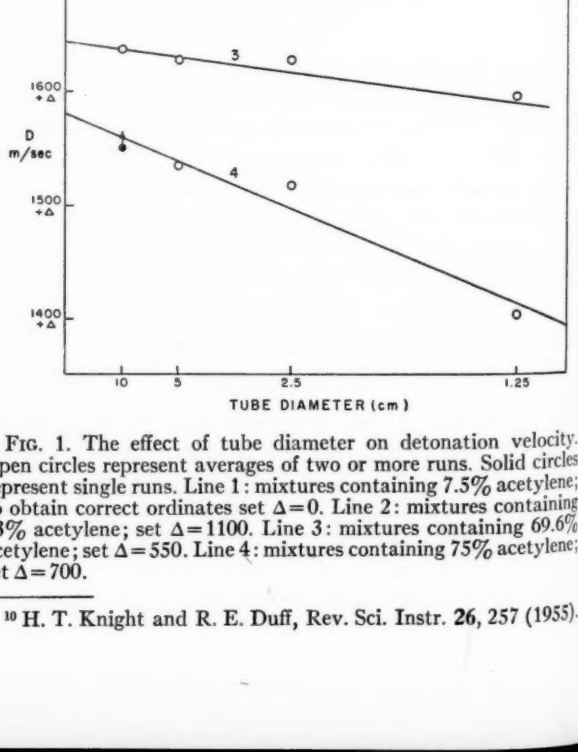

FIG. 1. The effect of tube diameter on detonation velocity. Open circles represent averages of two or more runs. Solid circles represent single runs. Line 1: mixtures containing 7.5% acetylene; to obtain correct ordinates set $\Delta=0$. Line 2: mixtures containing 53% acetylene; set $\Delta=1100$. Line 3: mixtures containing 69.6% acetylene; set $\Delta=550$. Line 4: mixtures containing 75% acetylene; set $\Delta=700$.

[6] Kistiakowsky, Knight, and Malin, J. Chem. Phys. **20**, 876 (1952).
[7] H. Guenoche and N. Manson, Rev. inst. franç. pétrole **9**, 214 (1954).
[8] Berets, Greene, and Kistiakowsky, J. Am. Chem. Soc. **72**, 1080 (1950).
[9] Kistiakowsky, Knight, and Malin, J. Chem. Phys. **20**, 994 (1952).
[10] H. T. Knight and R. E. Duff, Rev. Sci. Instr. **26**, 257 (1955).

Airco oxygen, containing 0.5% argon and less than 0.1% nitrogen, as well as Linde argon, containing 0.4% nitrogen, were used without purification.

Acetylene from Prestolite tanks was passed through Dry Ice traps and was found mass spectrometrically to be 99.8% pure, the rest being largely methane.

All compositions given below are formal, not allowing for stated impurities in the main ingredients. A correction for argon in oxygen has been applied in all calculations.

In earlier phases of this work much difficulty was experienced in obtaining reproducible velocities with rich mixtures, a difficulty noted also by other workers. This was overcome by removing from the tubes, prior to each run, all loose carbon which settles out after each explosion. Some of this carbon gets stirred up on admission of a fresh charge and slows down the wave because of its inertia.

RESULTS AND CONCLUSIONS

The detonations were initiated in equimolar acetylene-oxygen mixtures, separated from the experimental mixtures by thin plastic diaphragms. With this initiation technique no steady waves could be obtained in the 150-cm long experimental sections when the mixtures in the latter contained less than 5% acetylene. With slightly richer mixtures the main difficulty was the overdrive from the initiator compartment. Interval velocities between adjacent gauges were therefore analyzed by the usual statistical procedures for significant trends, and only those runs accepted in which these were not observed. Table I shows examples of acceptable and overdriven waves. Additional tests of overdrive were made by using initiator mixtures at different pressures, so as to vary the pressure of the wave striking the experimental mixture. Table II shows that a wide range of initiator strengths exists within which the same detonation velocity is observed in the experimental mixture. Such tests, made with mixtures containing from 5 to 12% acetylene, insured that the results given below represent true stationary velocities of unsupported waves.

Other errors involved in the present measurements may be estimated from the following data. Each velocity was calculated by the method of least squares from gauge-to-gauge interval velocities. The standard deviation of the means so calculated ranged from 3 to 8 m/sec, except in runs rejected because of significant trends. The velocity in each mixture, at a given pressure, in a given tube, was measured at least twice. The standard deviation of velocities within each of 44 pairs of identical runs was 4 m/sec. In seven other pairs separately prepared gas mixtures were used for each of the twin runs. Here the standard deviation was 7 m/sec. The compositions included in this analysis range from the leanest to the richest used. The systematic errors due to the time standard used, gauge location errors, gas impurities, their deviations from ideality, etc. add up to certainly less than 0.2% in the velocities. Thus it appears that a probable error of 0.4% in each value given, representing a mean of at least two separate measurements, is a conservative estimate.

TABLE II. Tests for overdrive. Detonation velocity of a mixture of 8.2% acetylene+91.8% oxygen at 1 atmos pressure in the 5-cm tube.

Pressure of the initiator mixture (atmospheres)	Observed mean velocity (m/sec)
3/8	1795±6
1/2	1793±3
5/8	1792±5
3/3	1790±5
7/8	1791±3
1	1792±2

Earlier work from this Laboratory[6] showed that a small but significant increment must be added to the velocities measured in the widest tube used (10 cm) to extrapolate to the infinite plane wave. In Fig. 1 are shown the plots of measured velocities against inverse tube diameter obtained with diverse acetylene-oxygen mixtures. The three mixtures containing 70% acetylene and less show experimentally identical slopes, resulting in an increment of 6 m/sec for the extrapolation from 10-cm diameter to the plane wave. This figure agrees well with an extrapolation of 9 m/sec determined previously[9] for the equimolar mixture. It is also consistent with current measurements on compositions containing 8.27, 25, 55, 60, and 65% acetylene, in each of which only two tubes of different diameters were used. Over this wide composition range, therefore, there appears to be no dependence of the magnitude of the diameter effect on composition. On the other hand, the 75% mixture shows a much steeper slope, and the measurements in two tubes on the 80% mixture confirm this value. The sudden change in slope may be related to the different nature of the detonation wave in these rich mixtures, which is discussed on the following pages.

The correction[6] for gas nonideality in the C–J plane amounts to *ca* -0.15%[11] at 1 atmos initial pressure, and thus effectively cancels the increment obtained by the extrapolation to infinite diameter from the velocities in the 10-cm tube. The latter, therefore, may be directly compared with theoretical velocities.

The hydrodynamic velocity calculations on lean mixtures were kindly performed by Dr. R. E. Duff, using IBM computing machines. Aside from the uncertainties in the thermodynamic functions, all taken from the NBS tables,[12] the calculations should be accurate to better than 0.1% in the composition, pressure and temperature of the C–J state. The

[11] In reference 6 this correction was given as -0.4% due to an arithmetical error called to our attention by Dr. R. E. Duff of the Los Alamos Laboratory.

[12] Natl. Bur. Standards, Selected Values of Thermodynamic Functions (1945, 1947, 1949).

TABLE III. A comparison of experimental and calculated detonation velocities at 1 atmos total pressure.

% C_2H_2	4	5	7.5	8	8.27	10	12	15	25
D obs m/sec		1609	1775	1793	1800		1952		2332
D calc equil.	1491	1598	1765	1792[a]	1802[a]	1874	1950[a]	2042	2326
D calc nonequil.	1623	1708	1842	1867[a]	1877[a]	1936	2002[a]	2088	2349

[a] Interpolated.

molecular species allowed for were: CO_2, CO, H_2O, OH, O_2, H_2, H. The concentrations of carbon vapor, hydrogen peroxide, and ozone were not allowed for but are too small to affect the results; the chemical potential of the radical HO_2 is not known but, by analogy with ozone, it may also be safely assumed to be unimportant. The major error in these calculated velocities arises from uncertainties in the thermodynamic functions used. Only a guess can be offered that the total error is of the order of $\frac{1}{4}$% in velocities.

The problem of nonequilibrium velocities has no single solution because so many alternative assumptions may be made. At our request, Dr. Duff calculated velocities in several mixtures assuming that the vibrational heat capacity of unreacted oxygen was not excited but that its dissociation into the atoms was normal; all the other equilibria remain thus unaffected except through changed temperature.

In Table III are shown the experimentally observed and the calculated velocities. The excellent agreement with equilibrium calculations is well within combined errors. The disagreement with the nonequilibrium calculation is far outside the limits of error. Starting from Dr. Duff's values we have estimated the effect of an additional assumption that no unreacted oxygen is dissociated into atoms but that other equilibria are altered only through changed temperature. This approximately doubles the deviation from experimental values as compared with Dr. Duff's nonequilibrium calculations.

The present measurements on lean mixtures differ from those of Malin and Knight[9] by less than 2%. In view of our experience with overdrive by strong initiation, the reason for the discrepancy is clear; in richer mixtures, where overdrive is not important, the present measurements join smoothly the earlier data. The excellent agreement of the latter with calculated velocities was stated[9] to be subject to review because of the then unknown diameter effect. This has now been shown to be insignificant. Thus, over the entire composition range, from 5 to 50% acetylene, the measurements agree with calculations to better than 0.5%. Kinetically this agreement is significant because in very lean mixtures it is the dissociation and excitation of the excess oxygen which are the main reactions with negative σ; in the middle of the composition range this role is taken over by the dissociations of water and carbon dioxide; finally, near the equimolar composition, the dissociation of hydrogen is the dominant endothermic reaction. Notwithstanding the variety of these reactions and the wide range of temperatures involved, the equilibrium is fully attained. In fact, the measurements of detonation velocities emerge as an exceptionally precise technique for the study of gaseous equilibria, considering that temperatures involved are very high. Thus, if the entire discrepancy between the measured and calculated velocities is treated as an error in experimental temperature estimation, this error averages considerably less than 1% over the range from 3000 to 4500°K.

TABLE IV. Calculations of detonation velocity in a mixture containing 53% C_2H_2 and 47% O_2.

	λ_C=170 Kcal	λ_C=141 Kcal
D m/sec	2816	2750
T°K	4275°	4039
P atmos	40.6	38.8
Partial Pressures:		
CO	23.42	22.20
H_2	8.16	9.13
H	7.30	5.20
C_2H_2	1.49	0.71
C	0.13	1.32
CH	0.03	0.20
A	0.06	0.06

The success of the equilibrium calculations for mixtures containing 50% and less acetylene has a bearing on the interpretation of our measurements with mixtures containing 53 and 55% acetylene. Because of the high temperatures involved, the excess acetylene, at equilibrium, should dissociate significantly into hydrogen and gaseous monatomic carbon, particularly if the heat of sublimation of the latter is only 141 Kcal. Since the high heat of sublimation, 170 Kcal, is not as yet universally accepted,[13] it is of interest to compare our measurements in this composition range with calculations. The experimental values are 2826 and 2745 m/sec for 53 and 55% acetylene at 1 atmos intitial pressure in the 10-cm tube and these, as noted before, may be regarded as the velocities of plane waves in ideal gases. The calculations were carried out by the methods previously described,[6] allowing for CO, H_2, H, C_2H_2, CH, C_g, and the results are shown in Table IV. As the carbon vapor is undersaturated, no allowance was made for C_2, C_3, etc. By the substitution into the appropriate equilibrium equations of the calculated concentrations of the above specie, it was *post factum*

[13] Langer, Hipple, and Stevenson. J. Chem. Phys. **22**, 1836 (1954).

determined that O_2, CO_2, H_2O, CH_4, C_2H_4 should be present in such small concentrations as not to affect the results of the calculation. Using 170 Kcal for the heat of sublimation of carbon, the calculated velocities are found to be 2816 and 2741 m/sec, in perfect agreement with observations. For the 53% mixture, 2750 m/sec is obtained when 141 Kcal is taken to be the heat of sublimation; for 55% this calculation was not performed since the outcome was obvious. The results on leaner mixtures establish that hydrogen attains dissociation equilibrium; if it is assumed arbitrarily that unoxidized acetylene is neither dissociated nor vibrationally excited, the velocity for 53% acetylene is calculated to be in excess of 2900 m/sec. Only the assumption of a finite but incomplete transfer of energy to the vibrational degrees of freedom of unoxidized acetylene in the *C–J* plane, combined with 141 Kcal for the heat of sublimation, can lead to agreement with experiment. For instance, if no dissociation occurs but vibrational heat capacity is fully excited, the calculated value is 2830 m/sec. This notwithstanding, the evidence appears to be heavily in favor of 170 Kcal and equilibration, by analogy with leaner mixtures.

The accompanying Fig. 2 shows observed velocities in still richer mixtures at 1 atmos pressure, as well as previously calculated[9] velocities. The agreement of current measurements with earlier[9] data on pure acetylene is excellent. In mixtures containing from 60 to 70% acetylene, the experimental values fall close to curve (1) calculated under the assumption that no solid carbon is formed in the *C–J* plane but that homogeneous equilibrium is established. Actually the assumption that acetylene is in equilibrium with CH and C_g is of no importance here because of low temperatures, but either carbon vapor or acetylene must be assumed to be supersaturated with respect to solid carbon to obtain the lower curve. The calculation allows only for the molecular specie listed for the calculation with the 53% acetylene mixture. An allowance for several minor side reactions (C_2, C_2H_4, CH_4, etc.) would lower the calculated values slightly and thus probably bring them into still better agreement with experiment than shown by Fig. 2.

Figure 2 shows a discontinuous change in detonation velocity for the 71:29% mixture. What is actually observed with this and only this composition is a steady velocity which rises rather suddenly in the middle of the experimental section of the tube, as shown in Fig. 3. The same observation was made with the 2.5-cm tube, but the transition occurred further away from initiation. Experiments were made with argon added to acetylene-oxygen mixtures kept at 1 atmos pressure. Similar velocity transitions were observed with mixtures having 69:31 to 71:29 acetylene:oxygen ratios. The occurrence of transitions became sensitive to the strength of initiation, so that no definite correlation between the partial pressure of argon and the acetylene:oxygen ratio exhibiting the transition could be established.

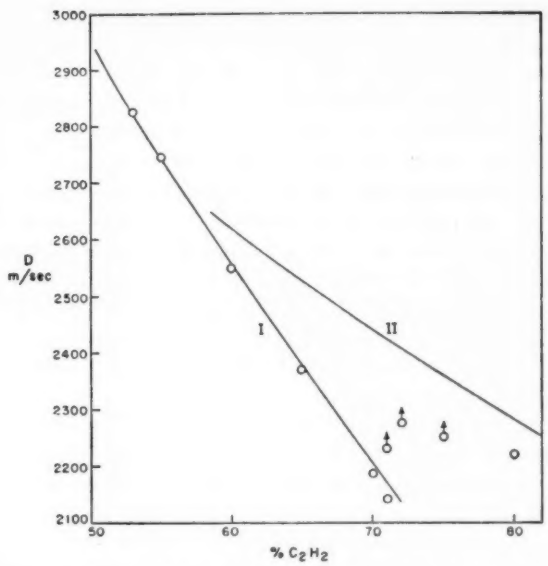

FIG. 2. Observed (circles) and calculated (lines) detonation velocities in rich acetylene-oxygen mixtures.

The velocities in acetylene:oxygen mixtures containing more than 71% of the former lie below the upper calculated curve, for which complete equilibrium, including solid carbon, has been assumed. The discrepancy is of the order of 70 m/sec since according to Fig. 3 the ultimate velocities attained after the transition should be somewhat higher than represented by points in Fig. 2, showing velocities for 71, 72, and 75% acetylene compositions. Such discrepancy is to be expected, since the carbon recovered after the explosions is extremely fine, having an ultimate graphitic platelet diameter of the order of 100 A. The particles might be even finer in the *C–J* plane, prior to the heat treatment they receive in the rarefaction wave. It does not take very many Kcal of assumed excess chemical potential

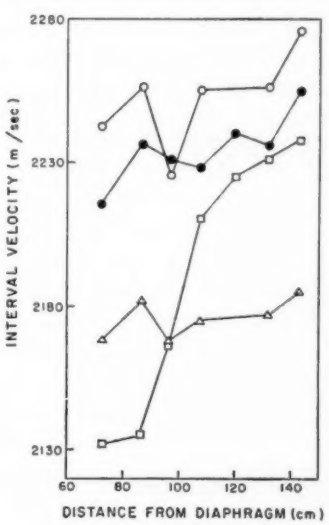

FIG. 3. Gauge to gauge interval detonation velocities. Triangles: 70% C_2H_2 +30% O_2; squares: 71% C_2H_2+29% O_2; open circles: 72% C_2H_2+28% O_2; solid circles: 75% C_2H_2+25% O_2. 5 cm diameter tube.

of solid carbon to decrease the calculated velocities by 70 m/sec and so bring them close to experimental values. Additionally, the calculations make no allowance for various side reactions, including the retention of some hydrogen by the solid. Detonations in pure acetylene, where the precipitation of solid carbon (or carbon-like materials) is the only reaction exothermic enough to support a detonation, have been recently demonstrated.[14] All this put together is convincing evidence that the existence of two discrete segments in the velocity-composition curve is due to the sudden change in the thermodynamic state of the *C–J* plane, from one involving only homogeneous equilibria to that of total equilibrium.

The mechanism of the sudden transition is not entirely clear and only a hypothesis can be offered. It is related to the mechanism by which Doering[3] describes a gradual development of a detonation wave in which the chemical processes consist of a fast and a slow reaction. The precipitation of solid carbon in the 71:29 mixtures must start behind the *C–J* plane at a distance which is small compared to the length of the experimental section of the tubes used. Because of the exothermic character of this process, a pressure decrease develops across the new reaction zone as it moves with the detonation front through the medium. Thus, the second reaction zone may develop its own shock front. Meanwhile the progress of the primary detonation front down the tube levels out the rarefaction wave.[15] The second shock front, since it moves with supersonic velocity with respect to the medium ahead of it, should therefore eventually catch up with the original *C–J* plane. This is tantamount to saying that at this instant the energy released in the second reaction zone begins to contribute to the propagation of the detonation front and so the velocity rises. When the steady state has reestablished itself, it extends from the primary shock front to the end of the second reaction zone. In the language of Kirkwood and Wood, while the parameters of the initial detonation wave were determined by the first zero of summation in Eq. (2), those of the final wave are determined by the second. The nature of the processes which cause the summation in (2) to be negative between these two states of the system is not clear, but the delayed appearance of the velocity discontinuity in narrower tube suggests that they may involve energy losses to the walls of the tube. The proposed mechanism of the velocity transition implies that the distance from this shock front to the *C–J* plane should be much greater in waves in which solid carbon appears in the *C–J* plane. A consequence of this is the increased energy loss to the walls of the containing tube, and hence a larger diameter effect. This is just what Fig. 1 indicates. Also, the observation on detonation waves in pure acetylene,[14] where the first reaction zone (oxidation) is necessarily absent, indicates that the distance between the shock front and the "second" reaction zone is quite large.

The hypothesis offered here implies that velocity transitions should occur over the entire range of acetylene-oxygen mixtures in which one of the products is solid carbon. However, the distance of travel of the detonation wave at which the discontinuity occurs must depend on the induction period of the nucleation of solid carbon, and that is extremely sensitive to the degree of supersaturation. The strong upward velocity trend in the 72:28 and 75:25 mixtures (Fig. 3) suggests, in fact, that here the discontinuity may have occurred closer to the front end of the tube than could be observed with our measuring system. It was hoped that on cooling the mixtures by the addition of argon the degree of supersaturation would be increased and so the discontinuity would occur in much leaner mixtures. The results only partially support this proposition, and a further investigation of this interesting phenomenon must be undertaken with other techniques than the velocity gauges.

In conclusion, we note that the only observed failure of complete equilibrium to be established in the *C–J* plane is that due to a reaction with a true induction period; even this failure is only apparent, in the sense that had tubes long enough been available, high detonation velocities corresponding to complete equilibrium would have been observed over the entire composition range.

It is a pleasure to thank Dr. R. E. Duff for several calculations of detonation velocities and Dr. H. T. Knight for acquainting us with the construction of gap gauges.

[14] Duff, Knight, and Wright, J. Chem. Phys. **22**, 1618 (1954).
[15] G. I. Taylor, Proc. Roy. Soc. (London) **A200**, 235 (1950).

Far Ultraviolet Absorption Spectra of Ethylene and Ethylene-d_4†

P. G. WILKINSON AND R. S. MULLIKEN
Laboratory of Molecular Structure and Spectra, Department of Physics, The University of Chicago, Chicago 37, Illinois

(Received December 29, 1954)

The absorption spectra of ethylene and ethylene-d_4 have been reinvestigated in the 1500 A to 2050 A region, using the first order of the Harrison 21-foot vacuum spectrograph. Vibrational constants of the C=C stretching vibration in the R (first Rydberg) state were determined to be: C_2H_4, $\omega_2^0=1381.5$ cm^{-1}; $x_{22}^0=-11.2$ cm^{-1}; C_2D_4, $\omega_2^0=1306.8$ cm^{-1}; $x_{22}^0=-8.2$ cm^{-1}; and (tentatively) in the V state: C_2H_4, $\omega_2^0=852$ cm^{-1}; $x_{22}^0=-1.9$ cm^{-1}; C_2D_4, $\omega_2^0=797$ cm^{-1}; $x_{22}^0=-1.8$ cm^{-1}. Newly observed fine structure in the $v'-0$ stretching vibration progression in the long wavelength part of the $V\leftarrow N$ transition of C_2D_4 is tentatively attributed to a torsional oscillation. The 0—0 bands of the $V\leftarrow N$ transition, though too weak to be seen, were estimated to lie near 2500 A. The probable dissociation of ethylene into CH_2 radicals in the $V\leftarrow N$ continuum is discussed.

The torsional frequency in the R state was redetermined as 141 cm^{-1} (C_2D_4) and 236 cm^{-1} (C_2H_4), decreasing somewhat with increasing stretching quantum number. An attempt has been made to fit the corresponding vibrational levels, for both isotopes, to those calculated for a torsional oscillator-rotator using a potential function of the form $V=\frac{1}{2}V_0(1+\cos 2\theta)$. Rough agreement is obtained for a reasonable barrier height of about 790 cm^{-1}. (Values of 650 cm^{-1} for C_2D_4 and 920 cm^{-1} for C_2H_4 are obtained when the two isotopes are treated separately.) The anomalous isotope effect and intensities in the $R\leftarrow N$ twisting bands are tentatively attributed to perturbation of the R state levels by V state levels and/or the departure of the twisting potential from the simple cosine form. These views are encouraged by the fact that a higher Rydberg state shows similar twisting bands but with much less anomalous isotope effect and intensities.

I. INTRODUCTION

THE vacuum ultraviolet absorption spectrum of C_2H_4 was first studied by Stark and Lipp[1] who found two broad bands at 1910 A and 1940 A. Four additional bands to longer wavelengths were found by Snow and Alsopp,[2] and many more were reported by Scheibe and Grieneisen[3] in the 1700 A to 1980 A region. Finally both C_2H_4 and C_2D_4 were photographed from 1000 A to 1750 A by Price and by Price and Tutte.[4] Later, Platt, Klevens, and Price,[5] and Wilkinson and Johnston[6] made photographic absorption coefficient measurements on C_2H_4 over the range 2000 A to 1450 A. Very recently, Zelikoff and Watanabe,[7] and Jones and Taylor[8] made more precise photoelectric measurements on the absorption coefficient of C_2H_4 from 1950 A to 1050 A. Although the absolute absorption coefficients in the previous work[5,6] disagree somewhat from each other and from Zelikoff and Watanabe[7] and Jones and Taylor,[8] the latter must be regarded as being essentially correct owing to the much higher accuracies possible with the photoelectric method.

The absorption spectra of C_2H_4 (Fig. 1(a)) and C_2D_4 (Fig. 1(b)) in the region 1500 A to 1750 A appear to consist of a broad continuum with a maximum at about 1620 A on which are superimposed several pairs of sharp strong bands. Rising out of the apparent continuum as it weakens towards longer wavelengths beyond the first strong peaks is a progression of broad weak absorption bands which extend in C_2H_4 from 1752 A to at least 2069 A and may be seen in Fig. 2. The C_2D_4 bands in this region are much sharper and more numerous (Fig. 2).

This paper reports a high resolution study of the absorption spectra of C_2H_4 and C_2D_4 from 1500–2050 A. Both the ν_2 stretching and the ν_4 twisting vibration may be identified in the sharp peaks of the $R\leftarrow N$ transition from 1500 A to 1750 A.

A study of the isotope effect on the twisting vibration reveals that this cannot be predicted accurately by assumption of harmonic oscillation about the double bond. Treatment of the R state as a torsional oscillator-rotator using a cosine potential function proves to be satisfactory qualitatively but does not predict accurately the experimentally observed levels. It is probable that the R state is strongly perturbed by the neighboring V state and that a very peculiar potential curve results.

Price and Tutte,[4] and Mulliken[9] have suggested that the strong continuum together with the long wavelength progression should be identified as belonging to the $V(^1B_{1u})\leftarrow N(^1A_{1g})$ transition. The V states of C_2H_4 and oxygen should be closely analogous in electronic structure, and this suggests that the weak long wavelength ethylene bands are an upper state progression of the ν_2 C=C stretching vibration, analogous to the

† This work assisted in part by the Office of Ordnance Research under Project TB2-0001, of Contract DA-11-022-ORD-1002 with The University of Chicago.

[1] J. Stark and P. Lipp, Z. physik. Chem. **86**, 36 (1913).
[2] C. P. Snow and C. B. Alsopp, Trans. Faraday Soc. **30**, 93 (1934).
[3] G. Scheibe and H. Grieneisen, Z. physik. Chem. **25B**, 52 (1934).
[4] W. C. Price, Phys. Rev. **47**, 444 (1935); W. C. Price and W. T. Tutte, Proc. Roy. Soc. (London) **A174**, 207 (1940).
[5] Platt, Klevens, and Price, J. Chem. Phys. **17**, 466 (1949).
[6] P. G. Wilkinson, and H. L. Johnston, J. Chem. Phys. **18**, 190 (1950).
[7] M. Zelikoff and K. Watanabe, J. Opt. Soc. Am. **43**, 756 (1953).
[8] L. C. Jones and L. W. Taylor, Anal. Chem. **27**, 228 (1955).
[9] R. S. Mulliken, J. Chem. Phys. **7**, 29 (1939); Revs. Modern Phys. **14**, 265 (1942).

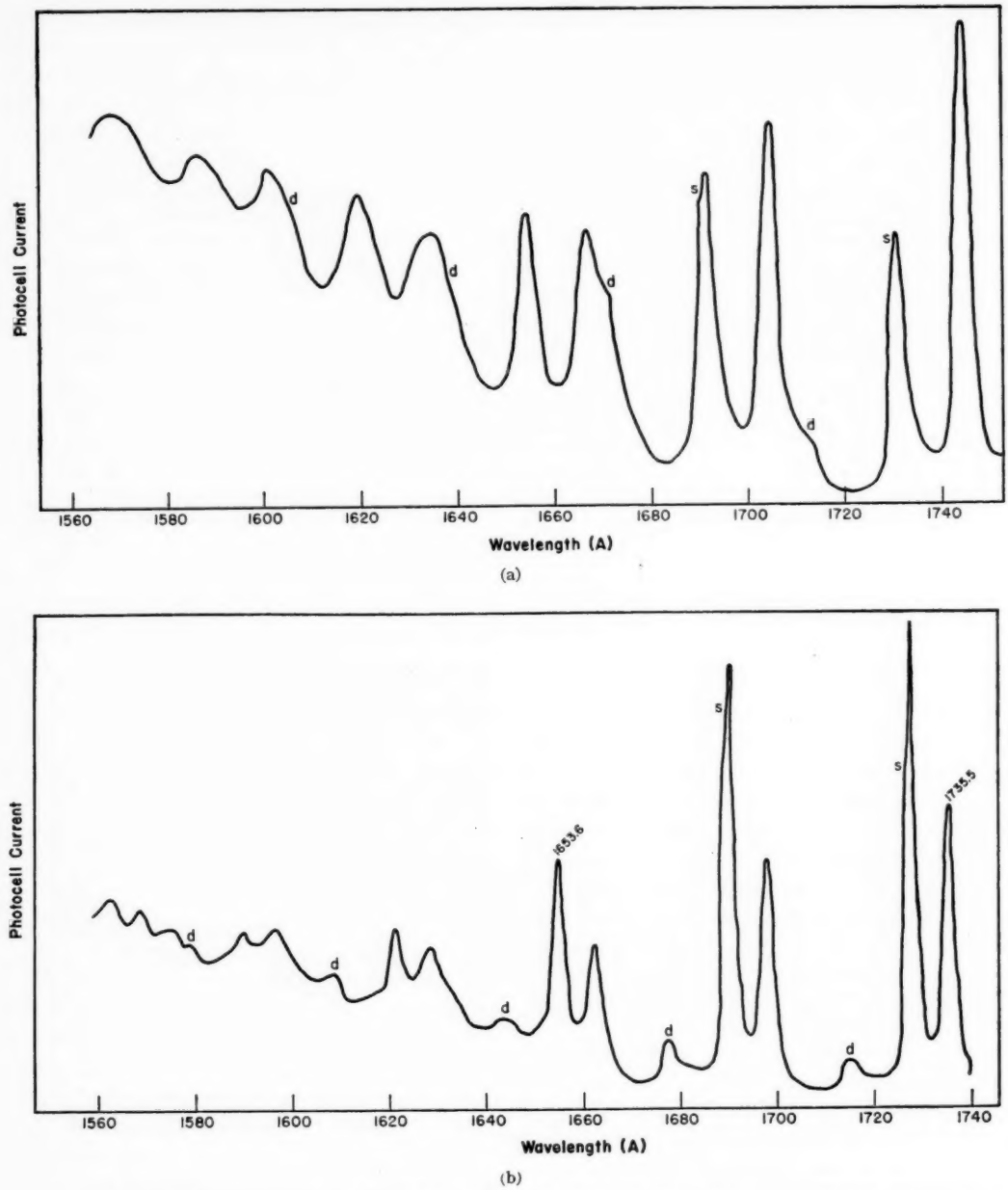

FIG. 1. Microphotometer tracing of C_2H_4(a) and C_2D_4(b) from photograph taken on 21-foot vacuum spectrograph using xenon continuum as background. Points marked *s* show splitting of member. Points marked *d* are *d* bands discussed in text.

Schumann-Runge bands of oxygen, with structure due to torsional oscillation more or less resolved in the case of C_2D_4 but unresolved in C_2H_4. This conclusion is strongly supported by the observed intensity distribution and by a suggested vibrational analysis.

II. EXPERIMENTAL

The Spectrograph

The Harrison 21-foot vacuum grating spectrograph[10] has been modified in the following respects since being installed in this Laboratory: (1) a new 30 000 line per inch Bausch and Lomb concave diffraction grating with a 45×150 mm ruled aluminum surface has been mounted; (2) reproducible grating tilt and movement controls have been added which make possible rapid and accurate shifting of spectral regions; (3) a new rapid pumping system has been installed which greatly increases the convenience of operating the instrument; and (4) a new bilateral slit has been designed and installed.

The jaws of the new vacuum slit are of carefully machined and lapped hardened stainless steel and are

[10] G. R. Harrison, Rev. Sci. Instr. **2**, 600 (1931); **4**, 651 (1933); A. B. F. Duncan and G. R. Harrison, Phys. Rev. **49**, 211 (1936).

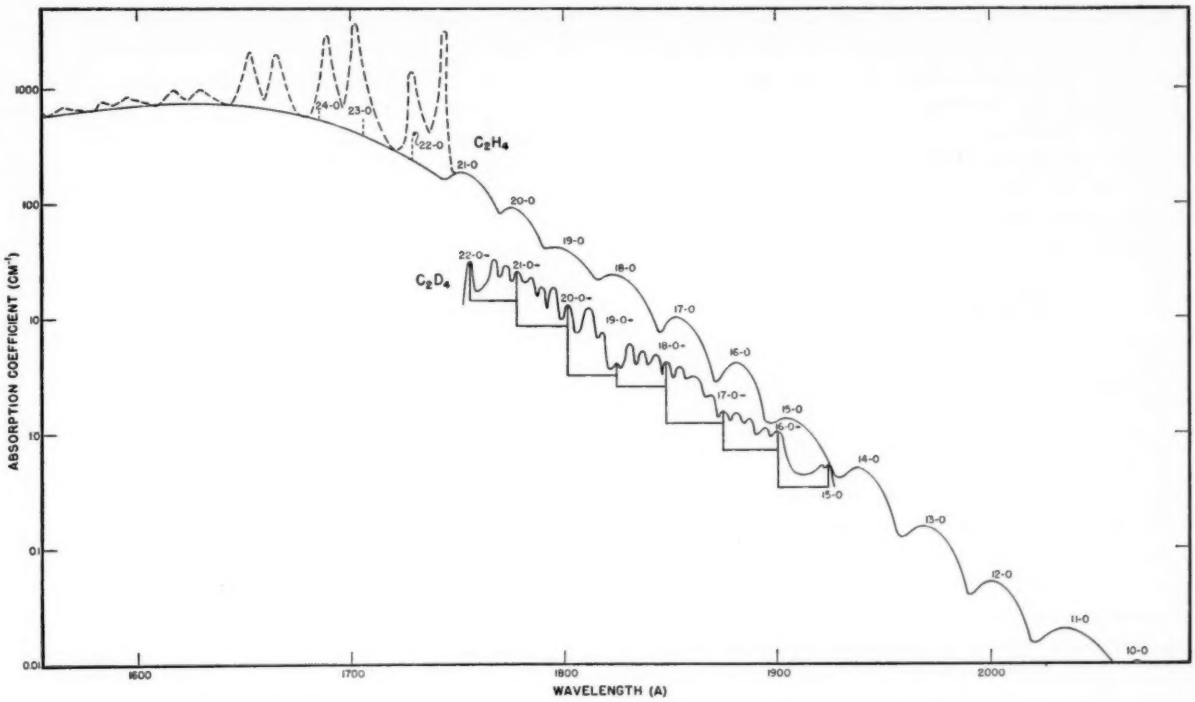

FIG. 2. Absorption coefficients of C_2H_4 and C_2D_4 from 1550 A to 2050 A. The dashed and solid curves correspond to the $R \leftarrow N$ and $V \leftarrow N$ transitions, respectively.

actuated by a precision drive tool steel conical wedge against a spring tension. Adjustment of the slit width, rotation of the slit with respect to the grating, and movement of a special diaphragm across the slit are possible without breaking the vacuum.

Careful tests of the resolving power of the spectrograph in the first order were carried out using the carbon monoxide fourth positive bands as a source and the fine grained Ilford Q1 vacuum ultraviolet plates. It proved possible to resolve emission lines 0.015 A apart in the 1700 A region. This corresponds to a resolving power of about 100 000 at slit widths between 2μ and 10μ.

Light Source

The C_2H_4 spectrum was photographed in absorption from 1720 A to 2050 A using the hydrogen continuum as a background. Later, after a new xenon source powered by microwave energy was developed,[11] this was used for C_2H_4 in the region 1500 A to 1750 A and for C_2D_4 from 1500 A to 1850 A.

Absorption Cell

Both C_2H_4 and C_2D_4 were photographed in path lengths of 13 meters, 15 cm, and 22 cm, the longest path length being obtained by flowing the gas through the body of the 21-foot spectrograph and the shorter path lengths by flowing through two different absorption cells with synthetic fluorite windows.[12]

Low pressures were measured by three Pirani gauges at various locations on the spectrograph and could be checked by a calibrated McLeod gauge also in the system. High pressures were recorded on a mercury manometer.

Gas Preparation and Purification

Since there has been some question concerning the purity of the C_2H_4 used in previous work, great care was taken to prepare a gas of highest quality. Four different preparations and vacuum distillations of ethylene were made. In two preparations tank C_2H_4[13] was the starting material; in two other preparations, the C_2H_4 was prepared by the phosphoric acid dehydration of ethyl alcohol. In all cases, the equivalent of at least twelve simple vacuum distillations was carried out, and the gas was then stored in five-liter flasks. In one sample, the inside of the five-liter flask was coated with evaporated sodium to remove any traces of residual oxygen. Careful tests on the melting point were made using a calibrated copper-constantan thermocouple. The melting point in all cases indicated a total dissolved impurity level of less than 0.05%, which was the limit of detection. No differences between the spectra of the four samples were noticed.

[11] P. G. Wilkinson and Y. Tanaka, J. Opt. Soc. Am. **45**, 344 (1955).

[12] Obtained from The Optovac Company, Boston, Massachusetts.

[13] Obtained from the Mathieson Chemical Company, Joliet, Illinois.

The purity of the C_2D_4 was less certain, since only about 700 cc of gas at normal temperature and pressure was available for purification. This was obtained originally, through the kindness of Professor M. de Hemptinne of the University of Louvain, as CD_2Br-CD_2Br, converted to C_2D_4 in this laboratory, and carefully put through six vacuum distillations just prior to use. Although this sample had to be used repeatedly, it was redistilled several times before each run.

Photographic Methods

Ilford Q1 photographic plates and a slit width of 10μ were employed when resolving powers of 100 000 were required. The somewhat faster but grainier Eastman SWR plates were employed when slightly lower resolving powers were acceptable.[14] Exposure times varied between fifteen and ninety minutes depending on conditions. The plates were scanned with a Leeds and Northrup microphotometer at slow speeds and at the highest sensitivity adjustment possible to show up weak and diffuse absorption bands to the best advantage. It proved to be possible to estimate positions of sharp spectra absorption lines to within 0.01 A by this method. The accuracy in location of diffuse band centers was somewhat less than this but did not exceed 0.2 A in the most unfavorable case. The mercury lines, 1942.276 A, 1849.520 A, 1820.339 A, the carbon lines 1930.905 A, 1658.120 A, 1657.902 A, 1657.247 A, 1657.005 A, 1561.436 A, 1560.690 A, 1560.304 A, and the nitrogen lines 1742.727 A and 1745.249 A were used as standards. A linear dispersion was used over short wavelength ranges and deviation corrections from linearity were applied when necessary.

III. THE $R \leftarrow N$ BAND SYSTEM

Survey

Microphotometer tracings of the absorption spectra of C_2H_4 and C_2D_4 are shown in Fig. 1. The pressure in each case was 0.05 mm in a path length of 22 cm with a slit width of 10μ and effective resolving power approaching 100 000.

Price and Tutte[4] have shown that the strong sharp bands (Fig. 1) belong to a Rydberg transition, $R \leftarrow N$, in which R is the lowest lying Rydberg state of the molecule. Since there are other Rydberg states belonging to this series, and there are at least two other Rydberg series, it is convenient to adopt a more specific nomenclature. In general, a Rydberg state will be designated $R_{v_1v_2v_3}\cdots$, $R'_{v_1v_2v_3}\cdots$, or $R''_{v_1v_2v_3}\cdots$, where v_1, v_2, v_3, etc. are vibrational quantum numbers of the various normal vibrations listed in order numerically according to the usual ground state notation.[15] In the present discussion only the C=C stretching (ν_2) and the twisting (ν_4) vibrations are identified with certainty in the Rydberg transitions. The designation R_{mn} is used for the vibrational level $v_2=m$, $v_4=n$, $v_1=v_3=v_5=\cdots=0$, for the lowest-lying electronically excited Rydberg state. The $R_{00} \leftarrow N$ transition consists of one sharp peak at 1744.10 A for C_2H_4 and 1735.48 A for C_2D_4, while the transition $R_{02} \leftarrow N$ occurs at 1729.88 A in C_2H_4 and at 1727.02 A in C_2D_4 (Fig. 1). The $R_{00}' \leftarrow N$ transition is observed at 1520 A and the $R_{00}'' \leftarrow N$ transition at 1440 A.

The ground state, $N(^1A_{1g})$, is well known to be planar,[16] and all the R states are believed also to be planar,[16] whereas the equilibrium configuration of the $V(^1B_{1u})$ state is believed to be 90° twisted[16] and perhaps also even bent or staggered.[17]

The interesting features of the $R \leftarrow N$ system are as follows: (1) The identification of the $R_{v_2,0} \leftarrow N$ bands as a progression of the upper state ν_2 or C=C stretching vibration seems rather certain from the isotope effect (see below). These bands together with corresponding members of the $R_{v_2,2} \leftarrow N$ progression form obvious doublets (Fig. 1), which will be referred to as "Rydberg doublets" or simply "doublets." The doublet spacing has been identified[9] as corresponding to two quanta of twisting of the CH_2 groups relative to each other and about the figure axis. Since the twisting frequency, ν_4, is nontotally symmetric, it should be excited during an electronic transition only with 0, 2, 4, $\cdots$ quanta if both R and N states are planar.[18] This frequency should show a larger isotope effect than any of the other normal frequencies of ethylene. However, the ratio of the doublet spacing in C_2H_4 to that in C_2D_4 is considerably *larger* than for a pure harmonic torsional oscillation. (2) Certain "red shoulders" in C_2H_4 (d in Fig. 1(a)) appear to have analogs in the d bands of C_2D_4 (Fig. 1(b)). These d bands are tentatively ascribed for both isotopes to excitation of the fourth torsional level but possibly may be due to excitation of a different vibration. (3) There is a small splitting (24–65 cm^{-1}) which certainly occurs in the second member in each Rydberg doublet for both molecules, and very probably also in the first member. (4) The intensity of the transition $R_{00} \leftarrow N$ is stronger than that of the $R_{02} \leftarrow N$ transition in C_2H_4, while the reverse is true in C_2D_4. This anomaly, first pointed out by Price and Tutte,[4] is repeated in the next pairs, $R_{10} \leftarrow N$ and $R_{12} \leftarrow N$, while, finally, in the higher stretching vibrational states, the two members of each doublet become about equal in intensity.

The Stretching Vibration

The frequencies of all the observed bands of the $R \leftarrow N$ transition of C_2H_4 and C_2D_4 are listed in Table I.

[14] The normal graininess of the Eastman SWR emulsion was reduced by development with one third strength Eastman D19 developer.

[15] G. Herzberg, *Infrared and Raman Spectra* (D. Van Nostrand Company, Inc., New York, 1945), p. 107.

[16] See R. S. Mulliken, Phys. Rev. **41**, 751 (1932); **43**, 301 (1933); J. Chem. Phys. **3**, 517 (1935).

[17] A. D. Walsh, J. Chem. Soc. 2325 (1935).

[18] H. Sponer and E. Teller, Revs. Modern Phys. **13**, 89 (1941).

TABLE I. $R \leftarrow N$ absorption bands in C_2H_4 and C_2D_4.[a] S-splitting in a band.

Upper state	C_2H_4 ν (cm^{-1})[b]	C_2H_4 ν (cm^{-1})[c]	C_2H_4 ν (cm^{-1}) this work	C_2H_4 λ(A) this work	C_2H_4 $\Delta_1G(\nu_2)$ cm^{-1}	C_2D_4 ν (cm^{-1})[b]	C_2D_4 ν (cm^{-1}) this work	C_2D_4 λ(A) this work	C_2D_4 $\Delta_1G(\nu_2)$ cm^{-1}
R_{00}	57 340	57 340	57 336.0	1744.10	1370.3	57 620	57 620.8	1735.48	1294.7
R_{02}	57 815	57 800	57 807.6S	1729.88		57 910	57 903.0S	1727.02	
R_{02}			57 858.0S	1728.37			57 927.0S	1726.30	
R_{04}			58 420d	1711.73		58 340	58 333.4d	1714.28	
R_{10}	58 715	58 720	58 706.3	1703.40	1349.1	58 910	58 915.5	1697.35	1283.8
R_{12}	59 185	59 180	59 167.2S	1690.18		59 200	59 190.7S	1689.46	
R_{12}			59 231.0S	1688.32			59 218.0S	1688.69	
R_{14}			59 904.7d	1669.32		59 650	59 637.3d	1676.80	
R_{20}	60 070	60 070	60 055.4	1665.13	1323.7	60 190	60 199.3	1661.15	1266.9
R_{22}	60 530	60 530	60 513.2	1652.53		60 480	60 473.6	1653.62	
R_{24}			61 226d	1633.30		60 930	60 918d	1640.89	
R_{30}			61 379.1	1629.22	1310.4	61 460	61 466.2	1626.92	1239.5
R_{32}		61 860	61 838.6	1617.11		61 750	61 739.0	1619.72	
R_{34}			62 547d	1598.81		62 195	62 212d	1607.41	
R_{40}		62 540	62 689.5	1595.16			62 705.7	1594.75	
R_{42}		63 070	63 151.8	1583.49			62 976.6	1587.89	
R_{44}			63 879d	1565.46			63 455d	1575.92	

[a] The estimated errors in the spectroscopic data are ±15 cm^{-1}, ±60 cm^{-1}, and ±2 cm^{-1} (C_2H_4) or ±1 cm^{-1} (C_2D_4) for the data of Price and Tutte,[b] Zelikoff and Watanabe,[c] and the present work, respectively. The d bands are probably transitions to the 4th torsional level. See text for discussion.
[b] W. C. Price and W. T. Tutte, Proc. Roy. Soc. (London) **A174**, 207 (1940).
[c] M. Zelikoff and K. Watanabe, J. Opt. Soc. Am. **43**, 756 (1953).

In general, the vibrational term, or energy in cm^{-1} for a molecule without degenerate vibrations, like ethylene, is of the form[19]

$$G(v_1,v_2\cdots)=G(0,0\cdots)+\sum_i \omega_i{}^0 v_i+\sum_i\sum_{k\geq i} x_{ik}{}^0 v_i v_k+\cdots.$$

From the observed positions of successive bands which differ only in the value of a single v_i, experimental values of term differences such as

$$\Delta_1G(v_i)=G(v_1\cdots v_{i+1}\cdots v_n)-G(v_1\cdots v_i\cdots v_n),$$

and

$$\Delta_2G(v_i)=G(v_1\cdots v_{i+2}\cdots v_n)-G(v_1\cdots v_i\cdots v_n)$$

can be obtained. From the data in Table I, differences of the type $\Delta_1G(v_2)$ for $v_1=v_3=\cdots=0$, and $\Delta_2G(v_4)$ for $v_1=v_3=v_5=\cdots=0$, can be obtained. $\Delta_1G(v_2)$ values so found for $v_4=0$, are given in columns six and ten. From these ΔG's, values of the coefficients $\omega_2{}^0$ and $x_{22}{}^0$ can be determined. The results are: for C_2H_4, $\omega_2{}^0=1381.5$ cm^{-1}, $x_{22}{}^0=-11.2$ cm^{-1}; for C_2D_4, $\omega_2{}^0=1306.8$ cm^{-1}, $x_{22}{}^0=-8.2$ cm^{-1}. To the extent that ν_2 can be approximated by a vibration of two rigid CH_2 or CD_2 groups against each other, one expects the ω_2 values[20] for C_2H_4 and C_2D_4 to be in the ratio $(16/14)^{\frac{1}{2}}=1.069$ and the x_{22} values[20] in the ratio $16/14=1.14$. The agreement of these ratios with the observed values 1.059 and 1.36 is sufficiently good to establish pretty well that we are in fact dealing with a C=C stretching vibration—a conclusion already reached by Price and Tutte.[4]

The C=C distance in the ground state is 1.353 A[21] and the infrared fundamental corresponding to the C=C stretching frequency is 1623 cm^{-1}.[21] By using these data, our new stretching frequency, and the empirical relation, $r_0{}^n\omega=$constant,[22] where r_0 is the C=C distance, and $n=2.88$, one may estimate that in the R state $r_0=1.45$ A. The two larger moments of inertia should then both be increased on excitation to the R state. This is in agreement with the observation (Fig. 3) that the $R \leftarrow N$ bands show a slight red shading.

In Table I, the letter S following a frequency signifies that this band is split. This splitting may be seen clearly in Fig. 3 and very probably should be interpreted as partial resolution of P and R rotational branches. The appearance of the second member of each Rydberg doublet (Fig. 3) closely resembles the rotational envelope observed in the infrared rotation-vibration absorption bands.[21] The frequency difference between P and R branch peak intensities in the infrared rotation-vibration bands is about 30 cm^{-1} for C_2D_4 and 50 cm^{-1} for C_2H_4 which is in approximate agreement with the splitting observed here. This frequency separation should depend primarily on the thermal distribution of rotational levels in the ground, N^1B_{1u}, state and

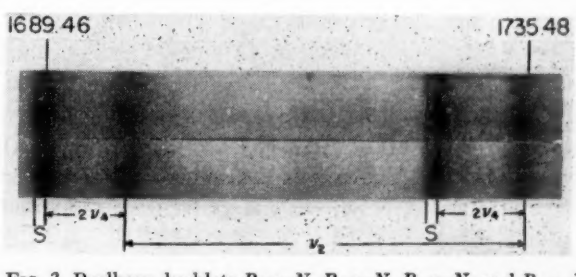

FIG. 3. Rydberg doublets $R_{00} \leftarrow N$, $R_{02} \leftarrow N$, $R_{10} \leftarrow N$, and $R_{12} \leftarrow N$ in C_2D_4. ν_2 is the C=C stretching frequency and ν_4 is the torsional frequency. S marks a splitting in a member.

[19] See reference 15, p. 206.
[20] The isotope effect should be nearly but not quite the same for both ω_2 and x_{22} as for $\omega_2{}^0$ and $x_{22}{}^0$.
[21] W. S. Gallaway and E. F. Barker, J. Chem. Phys. **10**, 88 (1942).
[22] G. Herzberg, *Spectra of Diatomic Molecules* (D. Van Nostrand Company, Inc., New York, 1950), p. 456.

TABLE II. Observed twisting levels of C_2H_4 and C_2D_4 in the R state.[a]

v_2'	v_4'	$\Delta_2G(v_4)$ and $\Delta_4G(v_4)$ C_2H_4	C_2D_4	Ratio, C_2H_4 to C_2D_4 $\Delta_2G(v_4)$	$\Delta_4G(v_4)$
0	2	471.6	282.2	1.671	
	4	1084	713		1.52
1	2	458.9	275.2	1.668	
	4	1198	729		1.64
2	2	457.8	274.3	1.669	
	4	1171	743		1.58
3	2	459.5	272.8	1.684	
	4	1167	729		1.57
4	2	462.3	270.9	1.706	
	4	1189	749.0		1.59

[a] The interpretation of the observed splitting in the Rydberg doublets as partial resolution of P and R branches and the difficulty in the location of the band origin introduces a possible uncertainty in $(2v_4)_D$ and $(2v_4)_H$ which may raise the isotope ratio by a small amount (about 2%). The actual values used in this table were frequency differences in the strongest peak intensities.

only partly on the differences in moments of inertia in the R and N states.

It is not clear why the first member of the Rydberg doublet does not show the splitting as prominently as the second. The rotation-vibration band envelopes should actually consist of P, R, and Q branches. The differences between the smallest and the intermediate moments of inertia in the two states largely determine whether the Q branch lies near the band origin or is strongly shaded to one side. As already mentioned, the two larger moments of inertia should both be increased on excitation to the R state, while on valence-theoretical grounds it seems probable that the smallest moment of inertia is little changed for a planar R state. However, an appreciable change in the effective value of the intermediate moment of inertia in going from the planar to a twisting form of the R state may quite possibly account for the difference in band appearance between the two members of each Rydberg doublet. An extremely high resolving power would be necessary to resolve the rotational structure.

The Twisting Vibration

In Table II, values of $\Delta_2G(v_4)$, for v_2 values from 0 to 4, are listed; these are based on data of Table I. Quantities which may be identified as $\Delta_4G(v_4)$ (if it is assumed that the upper levels of the d bands are the states $R_{v_2.4}$) are also listed in Table II. For a parabolic twisting potential, $\Delta_2G(v_4)$ and $\Delta_4G(v_4)$ would be equal to $2\omega_4^0$ and $4\omega_4^0$, respectively, and x_{44}^0 would be zero. Actually, the tentative $\Delta_4G(v_4)$ are much larger than twice the $\Delta_2G(v_4)$ values, indicating a very large positive anharmonicity, i.e., very large positive x_{44}^0 values.

For a parabolic potential, the ratio of the ω_4 values for C_2H_4 to that for C_2D_4 would be $2^{\frac{1}{2}}$. The observed ratios are very considerably larger especially for $\Delta_2G(v_4)$, as can be seen from Table II. This again suggests a large positive anharmonicity and it seems likely further that the twisting potential for the R state is of an unusual shape (see further discussion at the end of this section).

When, in an electronic transition of a polyatomic molecule, a nontotally symmetrical vibration is excited by n quanta, the relative intensities for various values of n are easily computed in the harmonic oscillator approximation. It is easily seen that they should be proportional to the squares of the quantities $\int\psi'(v')\psi''(v'')dv$,[23] where the ψ's are harmonic oscillator wave functions (Hermite orthogonal functions), with the ψ' and ψ'' sets based on force constants or ω values appropriate to the upper and lower electronic states respectively. In the present case, v' and v'' refer to v_4' and v_4'', with $v_4''=0$ and $v_4'=0$, 2, or 4.

If I_{00}, I_{02}, and I_{04} refer to the intensities of the $R_{00}-N$, $R_{02}-N$, and $R_{04}-N$ bands respectively, the theoretical relative intensities for the case of harmonic torsional oscillations in the R state are then:

$$I_{02}/I_{00}=[(\omega_4'-\omega_4'')/(\omega_4'+\omega_4'')]^2/2;$$
$$I_{04}/I_{00}=3[(\omega_4'-\omega_4'')/(\omega_4'+\omega_4'')]^4/8.$$

Assuming that values of $\Delta_2G(v_4)$ from Table II are to a sufficient approximation equal to $2\omega_4'$, and using the established value $\omega_4''=1027$ cm^{-1} for C_2H_4 and 727 cm^{-1} for C_2D_4,[24] the foregoing equations predict relative intensities in the ratios 1:0.19:0.06 and 1:0.23:0.08 for the transitions to $v_4'=0$, 2, and 4 in C_2H_4 and C_2D_4, respectively.

Based on photometric peak heights in Fig. 1, the corresponding experimental intensities for the bands with $v_2'=0$ are in the ratios 1:0.6:0.2 for C_2H_4 and 1:2:0.1 for C_2D_4 (see Fig. 1), in considerable disagreement with the predicted values. In the twisting bands with higher v_2' values the relative intensities are in similar but somewhat more disagreement with the predicted values. In interpreting the experimental intensities, however, one must of course bear in mind (1) that photometric peak intensities for incompletely resolved bands composed of discrete lines are poor measures of true integrated absorption coefficients, and (2), that if there is predissociation in the upper state (as is definitely a possibility here) and if the extent of such predissociation increases with twisting or stretching, it may well increase the apparent experimental intensity of higher v_4' and v_2' bands markedly.

It is relevant here to report briefly the result of a preliminary examination of the $R''\leftarrow N$ system at 1430 A–1450 A. The R'' state is the lowest state in a second Rydberg series converging to the same ionization potential as the R series. In the $R''-N$ system the estimated experimental relative intensities for the transitions with $v_4'=0$, 2, and 4 and $v_2'=0$, are 1:0.33:0, for both C_2H_4 and C_2D_4, in fairly satisfactory agreement with the calculated values. Further, the isotopic ratio

[23] Neglecting a slight correction for the change in over-all spectroscopic frequency from one band to another.

[24] R. L. Arnett and B. L. Crawford, J. Chem. Phys. 18, 118 (1950).

for the quantities, $\Delta_2G(v_4)$ is much lower (1.50) than the R state value (1.68), and agrees much better with the harmonic oscillator prediction (1.414).

These considerations indicate that the interpretation of the $R\leftarrow N$ Rydberg doublets and very likely also of the d bands as due to excitation of the twisting vibration are probably justified in spite of the marked abnormalities in spacings, isotope effect, and intensities noted above. In view of the evident fact that the higher vibrational levels, and perhaps part of the dissociation continuum, of the $V(^1B_{1u})$ state overlap the vibrational levels of the R state, it seems extremely likely that the abnormalities noted in the $R\leftarrow N$ twisting bands are due in large measure to strong perturbations, and perhaps some predissociation, by the V state levels.

IV. THE R STATE AS A TORSIONAL OSCILLATOR-ROTATOR

Introduction

Approximate theoretical calculations (including the effect of hyperconjugation) on the twisting frequency of ethylene and on the corresponding potential functions for the ground state and the ionized state have been made by Mulliken and Roothaan.[25] In the ground state, $N(^1A_g)$, the potential barrier hindering internal rotation is 2.66 electron volts (21 500 cm^{-1})[26] whereas in the ionized and Rydberg states it should be much less than this, in fact so low that the possibility of free internal rotation must be considered.[27]

Theory

The general problem of the torsional oscillator has been discussed in detail by Nielsen[28] and a special application to rotation in diatomic crystals was discussed earlier by Pauling.[29] The treatment given below follows fairly closely that given by these authors. We assume that the twisting motion in the R state can be treated as that of a quantum-mechanical torsional oscillator-rotator, with a hindering potential of the form

$$V=\tfrac{1}{2}V_0(1-\cos 2\theta). \qquad (1)$$

The top of the barrier (V_0) corresponds to the molecule in the "twisted" condition ($\theta=\pi/2$), and the bottom to the planar condition ($\theta=0$): see Fig. 4.

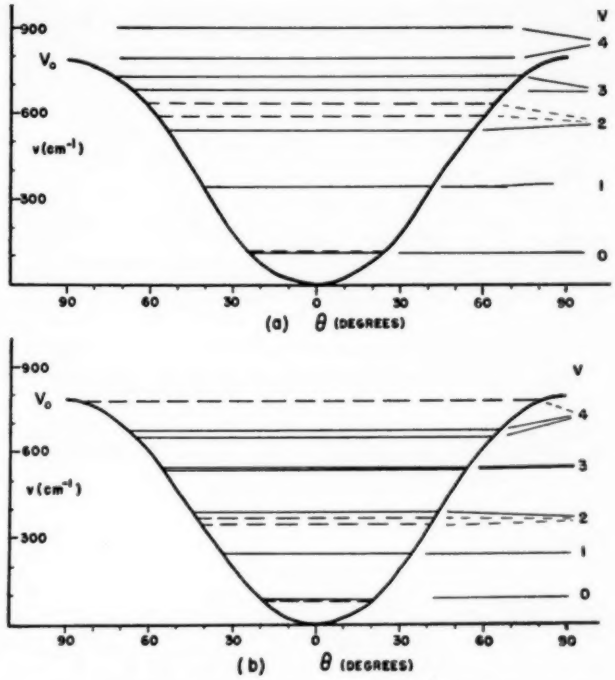

FIG. 4. Potential functions for the torsional oscillator-rotator (R state) in (a) C_2H_4 and (b) C_2D_4 for $v_2'=0$. The function $V=\frac{1}{2}V_0(1-\cos 2\theta)$ with $V_0=786$ cm^{-1} was used. Computed energy levels are the solid lines and observed levels are the dashed lines. The observed level for $v_4'=4$ in C_2D_4 was computed from the d band; the corresponding observed level in C_2H_4 is not shown but is well above the top of the barrier.

The Schroedinger equation for the system is

$$\frac{d^2\psi}{d\theta^2}+\frac{8\pi^2mr^2}{h^2}[W-\tfrac{1}{2}V_0+\tfrac{1}{2}V_0\cos 2\theta]\psi=0, \qquad (2)$$

where m is the mass of a hydrogen or deuterium atom, r is half the H to H distance in a CH_2 group, and W is the energy eigenvalue. If we write

$$\alpha=1/C[W-\tfrac{1}{2}V_0], \qquad (3)$$

and

$$V_0=8Cq, \qquad (4)$$

where

$$C=h^2/2\pi^2mr^2,$$

Eq. (2) reduces to Mathieu's equation:

$$\frac{d^2\psi}{d\theta^2}+[4\alpha+16q\cos 2\theta]\psi=0. \qquad (5)$$

Mathieu's equation has no closed analytical solution, but tables of α and q up to the second harmonic in α are available[30] for values of q up to 200. Tables of harmonics up to the fifth are also available[31] for a smaller range of q values. From Eqs. (3) and (4), the

[25] R. S. Mulliken and C. C. J. Roothaan, Chem. Revs. **41**, 219 (1947).

[26] Rabinovitch, Douglas, and Looney, J. Chem. Phys. **20**, 1807 (1952).

[27] Mulliken and Roothaan[25] estimated from their calculations that the potential barrier in the ionized state might even be negative, i.e., the perpendicular configuration might be slightly favored. Rydberg states should be very similar since the electron in a large Rydberg orbital should have very little influence on the potential function. This is well shown in some recent photoionization experiments on C_2H_4. [K. Watanabe, J. Chem. Phys. **22**, 1564 (1954).]

[28] H. H. Nielsen, Phys. Rev. **40**, 445 (1932).

[29] L. Pauling, Phys. Rev. **36**, 430 (1930).

[30] S. Goldstein, Trans. Cambridge Phil. Soc. **23**, 303 (1927).

[31] E. L. Ince, Proc. Roy. Soc. (Edinburgh) **52**, 355 (1932).

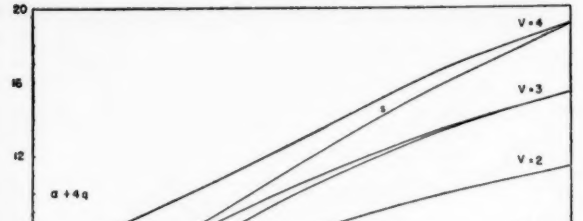

FIG. 5. Eigenvalues $(\alpha+4q)$ of Mathieu's equation against the parameter, q. Quantum numbers of torsional oscillation are given at the right (s=splitting).

eigenvalues

$$W=c(\alpha+4q), \tag{6}$$

for any given V_0 may be obtained.

If one assumes that the C−H distance and the H−C−H bond angle are the same in the R state as in the ground state, then one may make numerical calculations from (4) and (6). The assumptions made are probably fairly good (within 10% in the moment of inertia) provided the equilibrium configuration of the R state is planar. From the known moments of inertia of C_2H_4 and C_2D_4 in the ground state[32] $mr^2(=\frac{1}{4}I$ where I is the total moment of inertia about the figure axis) and the constant C may be obtained. By substitution of the numerical values Eqs. (6) and (4) become:

$$W_D=38.96(\alpha+4q)\ \text{cm}^{-1}, \tag{7a}$$

$$W_H=77.84(\alpha+4q)\ \text{cm}^{-1}, \tag{7b}$$

$$(V_0)_D=312q\ \text{cm}^{-1}, \tag{8a}$$

$$(V_0)_H=623q\ \text{cm}^{-1}. \tag{8b}$$

In Fig. 5 the eigenvalues $(\alpha+4q)$ of Mathieu's equation are plotted against q, which is proportional to the barrier height by Eqs. (8). The eigenvalues $(\alpha+4q)$ are related to the actual energy levels of C_2H_4 and C_2D_4 by Eqs. (7). To the right of Fig. 5 are given the quantum numbers of torsional oscillation. The treatment predicts a twofold splitting of the torsional oscillator-rotator levels. This is marked s in the figure and is seen to increase as the quantum number increases and as the barrier height decreases.

Application to the Experimental Data

The data necessary for the calculation of the barrier height are summarized in Table III. In column 4 of Table III are given the observed twisting levels from Table II for various v_2 and v_4 values. The zero of energy in each case is measured from the $R_{v_2,0}$ state. Values of q were obtained by dividing the $W(v_4)$ energies in column 4 by the factor 38.96 for C_2D_4 and by 77.84 for C_2H_4 to make them conform to the scale of Fig. 5 and fitting the reduced energy, $W(v_4)/C$, thus obtained, to the differences of the curves representing the zeroth and second and zeroth and fourth torsional energy levels. The barrier heights, were then calculated from these q values and equations (8) and are given in column 5. It is to be noted that the calculated barrier height for C_2H_4 agrees only roughly with that for C_2D_4 and that the values based on the d bands are much higher than those based on the second torsional level.

There is no reason why the actual barrier height should differ appreciably for the two isotopic molecules. Minor deviations in the apparent height could be expected from differences in zero point energies of the other vibrational degrees of freedom but close agreement in the calculated heights is expected only if the actual potential curve is of the form of Eq. (1).[33]

The potential barrier may also be estimated assuming a parabolic curve for V.[25] Then

$$\nu=\frac{1}{2\pi c}\left[\frac{k}{mr^2}\right]^{\frac{1}{2}}, \tag{9}$$

or

$$k=4\pi^2c^2mr^2\nu^2, \tag{10}$$

where k is the force constant for torsional oscillation, c is the velocity of light, and the other quantities are the

TABLE III. Calculations of the barrier hindering free rotation by various equations—Eqs. (8) and (11b). See text for discussion.

Molecule	v_2	v_4	W (cm^{-1}) observed	V_0 (cm^{-1}) Eq. (8)	V_0 (cm^{-1}) Eq. (11)	V_0 (cm^{-1}) average[a] Eq. (8)	W (cm^{-1}) calculated
C_2D_4	0	2	282	648	1030	786	315
	0	4	713	1085	2012		575
	1	2	275	617	980	739	305
	1	4	729	1135	2103		547
	2	2	274	617	970	739	305
	2	4	743	1166	2187		547
	3	2	273	598	960	729	302
	3	4	729	1135	2103		550
	4	2	271	600	961	742	307
	4	4	749	1184	2223		560
C_2H_4	0	2	472	923	1440	786	427
	0	4	1084	1401	2327		748
	1	2	459	860	1365	739	416
	1	4	1198	1650	2842		710
	2	2	458	860	1360	739	416
	2	4	1171	1607	2716		710
	3	2	459	860	1365	729	408
	3	4	1167	1594	2698		720
	4	2	462	883	1385	742	428
	4	4	1189	1631	2801		716

[a] Average V_0 for C_2H_4 and C_2D_4.

[32] See reference 15, page 437.

[33] However it is pertinent to inquire if the moment of inertia could be adjusted so that the experimentally observed ratio $(2\nu_4)_H/(2\nu_4)_D$ is reproduced with $(V_0)_H=(V_0)_D$. This results in a V_0 of 312 cm^{-1} for both molecules but requires an adjustment of the moment of inertia to a value 5½ times smaller than its value in the ground state which appears ridiculous.

same as before. The potential energy of the torsional harmonic oscillator is

$$V=\tfrac{1}{2}k\theta^2. \tag{11a}$$

At $\theta=\pi/2$:

$$V_0=\pi^2k/8. \tag{11b}$$

Values of V_0 computed from equation (11b) are given in column 6, Table III. It is to be noticed again that the barrier heights computed from (11b) do not agree very well for the two isotopic molecules, and, in general, they are higher than those computed from Eq. (8).

The harmonic oscillator equations (10) and (11) would not be expected to give the same V_0 values for both molecules since they predict an isotopic frequency ratio, $(\nu_4)_H/(\nu_4)_D$, of $2^{\frac{1}{2}}$.[34]

The average barriers for C_2D_4 and C_2H_4 are given in column 7 (Table III), from which the energies $W(v_4)$ may be computed. The results are given in column 8, and it is seen that the agreement with the experimental values (column 4) is poor. It may be seen that the observed energy level, $W(v_2,2)$ (column 4) lies below the average potential barrier, while $W(v_2,4)$ lies above the barrier for C_2H_4 but below it or only slightly above it for C_2D_4 (see also Fig. 5). This suggests that molecules in states corresponding to $W(v_2,2)$ energies are essentially "bound" or in torsional oscillation while those in states corresponding to $W(v_4,4)$ energies are so near the top or over the barrier that they are in free rotation. A pure free rotator would have an isotopic frequency ratio of 2.00 while a torsional harmonic oscillator would have a ratio of 1.414. For a very small hindering potential, one might expect that the torsional oscillator-rotator could become an intermediate case and that an isotopic frequency ratio of 1.67 would be possible. With the present potential curve (Eq. (1)), the barrier height is still too high for this to be realized.

The assignment of twice the twisting frequency, $2\nu_4$, to the separation of the Rydberg doublets in C_2H_4 (Fig. 3) is consistent with the fact that in the ground N^1B_{1u} state the twisting frequency is one of the lowest frequencies observed (1027 cm^{-1}).[24] The other low frequencies in the ground state are the out-of-plane bending vibrations, ν_7 and ν_8, and the in-plane deformation vibrations, ν_6 and ν_{10}. The experimentally observed ratios, ν_H/ν_D, for these ν_H/ν_D vibrations are as follows: 1.32, 1.21, 1.19, and 1.40, respectively, which may be predicted quite accurately by the theory of the isotope effect.[35] It is not clear how any of these vibrations could give an isotopic frequency ratio as high as 1.67 in the R state.

It is also possible that the equilibrium form of the R state of ethylene may not be planar but slightly twisted (corresponding to a negative V_0 (see reference 25), or even bent or staggered in some fashion. It is then conceivable that the "twisting" vibration would become mixed with a "rocking" or "wagging" vibration and that the experimentally observed isotopic frequency ratio could be understood on this model.

From all of the observed facts about the R state it is suggested that the actual barrier is between 600 and 1000 cm^{-1}. It is also suggested that the cosine potential curve used (Eq. (1)) is not adequate to describe the R state and that the shape of the actual barrier is considerably different from this or Eq. (11a).

The *d* Bands

The d bands in C_2H_4 and C_2D_4 (Fig. 1, Table I) have not been very satisfactorily accounted for by the theory of the torsional oscillator-rotator and yet they appear to belong to the $R\leftarrow N$ transition. They definitely are not "hot" bands, as may be seen from their intensity distribution, and the fact that they do not give the correct ground state fundamental.

It is not now possible to reach any certain conclusion concerning the origin of the d bands although it seems likely, as assumed above, that they are $v_4''=4$ bands arising from a highly perturbed R state. An alternate possibility might be that they arise from excitation of one of the nontotally symmetrical ν_7 or ν_{10} vibrations, but the observed frequencies (with average values of 1162 cm^{-1} and 736 cm^{-1} for C_2H_4 and C_2D_4 corresponding to $2\omega_7''$ or $2\omega_{10}''$) are much higher than expected since a strongly antibonding state is predicted from the observed frequencies of the ν_4'' vibration.

V. THE *V* STATE OF ETHYLENE

Introduction

The strong apparent continuum of ethylene with maximum at 1620 A is believed on theoretical grounds[36] to belong to a $V\leftarrow N(^1B_{1u}-{}^1A_{1g})$ transition closely analogous to the $V\leftarrow N(^3\Sigma_u^-\!-\!{}^3\Sigma_g^-)$ transition of oxygen. The latter takes the form of an extensive series of bands increasing in intensity from longer to shorter wavelengths and converging to a dissociation limit which is the beginning of an intense continuum with a maximum at 1420 A. These bands and continuum constitute the well-known Schumann-Runge system, of which the 0,0 band at 2026 A is very weak.

In ethylene, after allowing for the relatively sharp superposed $R\leftarrow N$ bands which extend from about 1750 A to shorter wavelengths, what remains (see Fig. 2) appears to be very closely analogous to the Schumann-Runge system. Namely, there is in C_2H_4 a

[34] One might ask whether the splitting in the second member of the first and second pairs of Rydberg doublets (marked s in Figs. 1 and 3 and Table I) can be interpreted as torsional splitting. In Fig. 4, the observed splitting in the torsional levels (dotted lines) is much larger than the theoretical predicted torsional splitting (solid lines). Furthermore, if one computes the barrier heights from the observed splittings by use of Fig. 5 and Eqs. (7) and (8), unreasonably low barriers are obtained. It seems much more reasonable to interpret the splitting as due to rotational structure (see Sec. III).

[35] See reference 15, page 232.

[36] R. S. Mulliken, J. Chem. Phys. 7, 29 (1939).

long series of broad diffuse bands of rapidly rising intensity [(1), (2), (3), (7)], extending from at least 2069 A (exceedingly weak) down to at least 1750 A, where the bands disappear under the strong $R \leftarrow N$ bands and/or merge into the apparent continuum which rises slowly to a maximum at 1620 A. Although some authors[37] have attributed the series of broad diffuse bands to a different electronic transition than the broad continuum, it seems altogether more probable that the bands and continuum together belong to the $V \leftarrow N$ transition of ethylene.[36,4] Recent photometric data embodied in Fig. 2 show a smooth continuity of intensity between bands and apparent continuum which is very convincing. Analogous to the long series of V^1-0 stretching Schumann-Runge bands, one would expect and may interpret the long series of bands in C_2H_4 as corresponding to excitation of the C=C stretching vibration.

That the C_2H_4 bands are diffuse is not surprising, since according to theory (38) the V state should have an energy maximum for a planar molecule and a minimum for a 90° twisted molecule. Hence, one would expect transitions to an agglomeration of twisting (and other) vibration levels to be combined with the transition to each stretching vibration level to give a diffuse or even continuous appearance. The fact that the series seems to stop at about 1750 A (where the $R \leftarrow N$ bands begin), even though the series has not yet by any means reached a convergence limit, is understandable as a consequence of either or probably both of two considerations: (1) the very strong and relatively sharp $R \leftarrow N$ bands may mask the much more diffuse $V \leftarrow N$ bands, (2) the diffuseness of the $V \leftarrow N$ bands in this region may be increasing to the point of giving an apparent continuum, because of increasing importance or closeness of spacing of twisting bands and perhaps other vibrational substructure; or this diffuseness perhaps also can occur because of onset of actual dissociation or predissociation by indirect mechanisms involving more than one vibrational degree of freedom even when direct dissociation by stretching alone does not occur.

The interpretation of the diffuseness of the long series of C_2H_4 bands as due to substructure is confirmed by the fact, reported here for the first time, that in the corresponding C_2D_4 bands such a substructure becomes clearly apparent (see Fig. 2 and discussion below).

Additional evidence that the long wavelength bands are associated with the $V \leftarrow N$ continuum and that the $R \leftarrow N$ transition is truly separate may be seen in the absorption spectra of the methyl ethylenes. When one to four methyl groups are successively substituted for the ethylene hydrogen atoms,[38,39,4,9] a progressive red shift occurs in the $R \leftarrow N$ bands of the substituted ethylenes analogous to the 1550–1745 A $R \leftarrow N$ bands of ethylene. Simultaneously, the $V \leftarrow N$ apparent continuum together with its series of bands at longer wavelengths shifts, but not so much.

[37] E. g., D. P. Craig, Proc. Roy. Soc. (London) **A200**, 272 (1950).
[38] W. J. Potts, J. Chem. Phys. **23**, 65 (1955).
[39] E. P. Carr and H. Stücklen, J. Chem. Phys. **4**, 760 (1936); J. Am. Chem. Soc. **59**, 2138 (1937); J. Chem. Phys. **7**, 631 (1939).

Experimental Data

The objection, frequently raised, that the longest wavelength bands are due to impurities, and not to C_2H_4 itself, has long needed checking. In particular, contamination with oxygen to form a molecular complex has been suggested as remotely possible. In this laboratory, ethylene was prepared as previously described, stored over sodium to remove all traces of residual oxygen, and flowed through a Pyrex absorption cell at a rate fast enough to sweep out desorbing impurities. Furthermore, photographs in a flowing system and in a static system as well as observations on four different preparations of the original gas disclosed no differences in the spectrum or the relative absorption intensities. It is concluded that the weak long wavelength bands are truly ethylene bands and that the Zelikoff and Watanabe data are reliable.

From the photoelectric measurements of the absorption coefficients of the $V \leftarrow N$ C_2H_4 bands by Zelikoff and Watanabe[7] and from photographic estimates on the additional bands reported here,[40] the absorption curve in Fig. 2 was constructed. In addition, rough estimates of the absorption coefficients of the $V \leftarrow N$ bands of C_2D_4 are plotted in the figure. These latter were taken completely from photographic density measurements and may be in considerable error although they appear consistent in a relative sense from a direct study of the densitometer traces. For C_2H_4 in Fig. 2, the sharp peaks of the $R \leftarrow N$ transition are drawn in with dotted lines and the solid base line under the peaks is the estimated position of the $V \leftarrow N$ continuum.

The wavelengths of eleven of the $V \leftarrow N$ absorption bands as photographed on the 21-foot vacuum spectrograph and using the hydrogen continuum as a background are given in Table IV, column 5. These are peak intensity positions as measured from microphotometer tracings and since the bands in C_2H_4 are quite broad and diffuse, these wavelengths cannot be taken as better than ±0.2 A in accuracy. For comparison, the wavelengths as measured by other observers are listed in columns 2, 3, and 4.

Columns 6 and 7 (Table IV) give the band frequencies and frequency differences, respectively. These latter may be taken to be $\Delta_1 G(v_2)$ values and show a gradual convergence as the region of continuous absorption is approached, but the trend is not consistent

[40] Dr. Watanabe has very kindly supplied us with his measurements of the absorption coefficients of the 1971 A and 2001 A bands which were not published in the original work.[7] These values are 0.18 cm^{-1} and 0.055 cm^{-1} which agree well with the present estimates of 0.15 cm^{-1} and 0.050 cm^{-1} obtained photographically (Fig. 2). In addition, he has confirmed the existence of the 1752 A and 2035 A bands.

TABLE IV. Absorption bands in C_2H_4 and C_2D_4—$V \leftarrow N$ transition.

	C_2H_4						C_2D_4				
v_2	λ(A)[a] ±2 A	λ[b](A)	λ(A)[c] ±4 A	λ(A) this work ±0.2 A	ν cm^{-1} ±6 cm^{-1}	$\Delta_1G(v_2)$ cm^{-1}	λ(A) ±0.1 A	ν cm^{-1} ±3 cm^{-1}	$\Delta_1G(v_2)$ cm^{-1}	$\Delta_1G(v_4)$ cm^{-1}	$\frac{\Delta_1G(v_2)_H}{\Delta_1G(v_2)_D}$	Isotope shift cm^{-1}
10		2069			(48 333)	(817)						
11	(2035)[d]	2032		2035.0	49 140	836						
12	(2004)[d]	2000		2000.7	49 976	768						
13	(1972)[d]	1970	1976	1970.7	50 744	858						
14	1938	1935	1935	1937.9	51 602	889						
15	1907		1905	1905.1	52 491	667	1925.7	51 929	664	546	1.00	562
							1921.3	52 047				
16	1881		1878	1881.2	53 158	816	1901.4	52 593	732		1.11	565
							1893.7	52 806		188		
							1887.0	52 994		177		
							1880.7	53 171		154		
17	1854		1852	1852.8	53 974	805	1875.3	53 325	774		1.04	649
							1869.0	53 504		214		
							1861.7	53 718		211		
							1854.3	53 929		170		
18	1826		1825	1825.5	54 779	763	1848.5	54 099	678		1.12	680
							1843.5	54 247		172		
							1837.5	54 419		195		
							1831.0	54 614		163		
19	1802		1800	1800.4	55 542	755	1825.6	54 777	709		1.06	765
							1818.5	54 991		182		
							1812.4	55 173		313		
20	1778		1777	1776.3	56 297	775	1802.3	55 486	714		1.04	811
							1795.0	55 709		175		
							1789.0	55 884		151		
							1784.6	56 035		165		
21	(1755)[d]		1756	1752.2	57 072		1779.4	56 200	741			872
							1772.5	56 418		137		
							1768.2	56 555		386		
22							1756.2	56 941				

[a] M. Zelikoff and K. Watanabe, J. Opt. Soc. Am. **43**, 756 (1953).
[b] C. P. Snow and C. B. Allsopp, Trans. Faraday Soc. **30**, 93 (1934).
[c] G. Scheibe and H. Grieneisen, Z. physik. Chem. **25B**, 52 (1934).
[d] See reference 39.

and the deviations appear well outside the experimental error. The bands in C_2D_4 are more numerous, considerably sharper and lie closer together than in C_2H_4; these are listed by wavelengths and frequencies in Table IV and are shown in Fig. 2. This is the first reported observation of the $V \leftarrow N$ bands in C_2D_4.

Vibrational Analysis

Since the $V \leftarrow N$ transition in ethylene is very similar to oxygen, with which it is isoelectronic, the long wavelength ethylene bands would be expected to show the C=C ν_2 stretching vibration of the V state. In the complicated C_2D_4 spectrum certain frequency intervals (Table IV, column 10) may be found which show the expected isotopic frequency ratio of 1.06 when compared with corresponding intervals in C_2H_4. Since the 0−0 band has never been observed, it is not possible to establish the vibrational numbering directly. However, if the isotope shift of corresponding bands (Table IV, column 13) is plotted against a preliminary quantum number assignment, the result may be extrapolated to a reasonable value for the isotope shift of the 0−0 band. Since this 0−0 band shift is the sum of the differences between all of the zero point energies in the upper and lower states, a reasonable value of -285 cm^{-1} was chosen (the same as in the $R \leftarrow N$ transition), and a tentative quantum number assignment was made (Table IV, column 1).

Using this tentative assignment, the following empirical equations were derived:

$$(C_2H_4): \quad \nu = 40\,015 + 852v - 1.9v^2 \qquad (12a)$$

$$(C_2D_4): \quad \nu = 40\,300 + 797v - 1.8v^2 \qquad (12b)$$

which fit the experimental data fairly well (Table V). Of course, if the isotope shift of the 0−0 band or the vibrational numbering is in error, then the vibrational constants will also be in error.

Equations (12a) and (12b) would locate the 0,0 bands at 2499 A and 2461 A for C_2H_4 and C_2D_4, respectively. If these figures are at all nearly correct, the bands observed by C. Reid[41] in the 2600 A−3350 A region probably do not belong to the $V \leftarrow N$ transition, but rather to the corresponding intersystem transition ($^3B_{1u} \leftarrow {}^1A_{1g}$).[42]

It is of interest to compare $\omega_2{}^0$ obtained for the V state of C_2D_4 with ω_0 for the $^3\Sigma_u^-$ state of oxygen (equal masses).[43] For oxygen, $\omega_0 = 692.4$ cm^{-1}. For the

[41] C. Reid, J. Chem. Phys. **18**, 1299 (1950).
[42] Professor Reid has suggested in a private communication that since these bands were found in a long path (1.5–2.5 meters) of liquid ethylene, they might possibly be impurity bands.
[43] H. P. Knauss and S. S. Ballard, Phys. Rev. **48**, 796 (1935); P. Brix and G. Herzberg, J. Chem. Phys. **21**, 2240 (1953); Can. J. Phys. **32**, 110 (1954). G. Herzberg, *Spectra of Diatomic Molecules* (D. Van Nostrand Company, Inc., New York, 1950), p. 560.

TABLE V. Experimental frequencies of the $V \leftarrow N$ bands of C_2H_4 and C_2D_4 compared with Eqs. (12a) and (12b).

	C_2H_4		C_2D_4	
v_4'	Eq. (12a) (calc'd) cm^{-1}	(Exp'tal) cm^{-1}	Eq. (12b) (calc'd) cm^{-1}	(Exp'tal) cm^{-1}
10	48 345	48 333		
11	49 157	49 140		
12	49 965	49 976		
13	50 770	50 774		
14	51 571	51 602		
15	52 367	52 491	51 850	51 929
16	53 161	53 158	52 591	52 593
17	53 950	53 974	53 327	53 325
18	54 735	54 779	54 063	54 099
19	55 517	55 542	54 793	54 777
20	56 295	56 297	55 520	55 486
21	57 069	57 072	56 245	56 200
22	57 839		56 963	56 941
23	58 605		57 679	
24	59 367		58 391	

best comparison, this value should be multiplied by the factor $\omega_0(^1A_{1g})/\omega_0(^3\Sigma_g^-)=1623/1580$ (the ground state ω_0's of the two molecules), which gives 717 cm^{-1} as compared to 797 cm^{-1} (by Eq. (12b)) for C_2D_4. From the estimated ω_0 of the V state, the C=C distance, r_0, may be calculated by use of the well-known empirical equation, $r_0^n\omega_0=\text{const}$,[22] using for n the value 2.88 which fits the $B^3\Sigma_u^-$ and $X^3\Sigma_g^-$ states of oxygen. One obtains $r_0=1.69$ A for the V state of ethylene which may be compared with the ground state r_0 of 1.353 A. The 0—0 vibrational band in the $V \leftarrow N$ transition would then correspond to an increase of 0.34 A in equilibrium distance which, by the Franck-Condon principle, would explain why this band and others with low quantum numbers are not observed under the present experimental conditions. The intensity distribution would be very analogous to that in the oxygen Schumann-Runge bands with $r_e''=1.207$ A and $r_e'=1.604$ A.

The oscillator strength of the $V \leftarrow N$ transition in C_2H_4 has been the subject of considerable experimental interest[5–7,9] and has also been treated theoretically[44] in a semiempirical LCAO calculation. The various measured values agree pretty well (0.3) and the theoretical prediction is also in line. The oscillator strength of the $V \leftarrow N$ system of oxygen (0.2) is somewhat smaller but of the same order of magnitude. The analogy between the $V \leftarrow N$ systems of oxygen and ethylene is very apparent. The differences may reasonably be attributed mainly to the greater complexity of the ethylene molecule rather than to any basic difference in electronic structure.

The V State as a Torsional Oscillator-Rotator

The observed fine structure in the $V \leftarrow N$ bands of C_2D_4 tempts one to treat these as torsional oscillations in a manner similar to the "R" state. The main difference is that the equilibrium form of the V state is believed to be no longer planar like the R and N states, but with the CH_2 (or CD_2) groups now twisted in planes at right angles to each other. However, Walsh[10] has given reasons for supposing that in the V state each carbon atom may also be "slightly out of the mirror plane bisecting the H—C—H angle of the other CH_2 group."

Transitions to states of torsional oscillation must now obey different selection rules than in the $R \leftarrow N$ transition, since changes in torsional quantum numbers of 0, 1, 2, 3, etc. would now be permitted. A "vertical" transition with very little change in torsion angle should be the most intense while a transition with a larger change in torsion angle is "Franck-Condon forbidden" and should result in weaker absorption. Thus the C_2D_4 bands in Fig. 2 which are labeled 22–0, 21–0, 20–0, etc. might correspond to transitions from a planar configuration in the N state to a nearly planar configuration in the V state while the discrete bands forming a small group to slightly longer wavelengths in each case would correspond to small changes in instantaneous torsional angle during the electronic jump and should be weaker than the first band in the group, as is in general observed. Transitions only to states of high torsional quantum numbers should be observed; those to low torsional quantum numbers have a low probability because of the large changes in instantaneous torsional angle involved. However, overlapping of the torsional states of different stretching quantum numbers is to be expected, and, consequently, absolute identification of each individual absorption band in Fig. 2 is not possible.

In column 11 of Table IV frequency differences, $\Delta_1G(v_4)$, are given which may correspond to separations of the higher torsional levels. The average separation is about 175 cm^{-1} but some levels appear to be missing.

The Dissociation Energy of Ethylene

The dissociation energy of the V state of ethylene cannot be estimated reliably by a Birge-Sponer extrapolation of the $V \leftarrow N$ bands because the observable bands do not converge rapidly enough. Since the observed $V \leftarrow N$ continuum is very probably a superposition of very complicated twisting bands (pseudo-continuum) on a true dissociation continuum with also a possibility of a predissociation continuum, the precise dissociation energy cannot be determined. The probability that the CH_2 radicals, produced as dissociation products, have considerable rotational energy also complicates the interpretation.

However, it is plausible to suppose that the dissociation limit occurs somewhere in the broad $V \leftarrow N$ con-

[44] R. S. Mulliken, J. Chem. Phys. 7, 29 (1939); R. S. Mulliken and C. A. Rieke, Repts. Progr. in Phys. 8, 249 (1941).

tinuum, probably on the longer wavelength side of the $V \leftarrow N$ maximum at 1620 A (in analogy with the $V \leftarrow N$ system in oxygen). It is suggested tentatively that the dissociation limit is about halfway between the last observable $V \leftarrow N$ band (57 071 cm^{-1}) and the maximum of the continuum (61 728 cm^{-1}), giving an energy of 59 400 cm^{-1} or 7.26±0.30 electron volts with the state of excitation of the CH_2 radicals being unknown.

ACKNOWLEDGMENT

The authors are especially indebted to Professor J. R. Platt for suggesting the torsional oscillator-rotator treatment and the interpretation of the *d*-bands and to Professor C. Reid for many stimulating discussions. The authors are also indebted to Mr. Ivar Kalberg of the Ryerson Machine Shop for construction of the slit mechanism and grating controls.

THE JOURNAL OF CHEMICAL PHYSICS VOLUME 23, NUMBER 10 OCTOBER, 1955

Infrared and Raman Spectra of 1,1,2,2-Tetrachloroethane; Calculation of Normal Vibrations

KAZUO NAITO,* ICHIRO NAKAGAWA, KENJI KURATANI, ISAO ICHISHIMA, AND SAN-ICHIRO MIZUSHIMA
Chemical Laboratory, Faculty of Science, Tokyo University, Hongo, Tokyo, Japan

(Received December 28, 1954)

Infrared spectra of 1,1,2,2-tetrachloroethane have been measured in the gaseous, liquid, and solid states and in solutions. Raman spectra of the same substance have been observed in the liquid and solid states. From the experimental results the equilibrium molecular forms of the rotational isomers have been determined. The normal vibrations of the molecule in the *trans*- and *gauche*-forms have been calculated as an 8-body problem, and the assignment of the observed infrared and Raman frequencies in all the states of aggregation has been made.

INTRODUCTION

THE Raman and infrared spectra of 1,1,2,2-tetrachloroethane have been studied by many authors.[1–6] The recent investigation, by Kagarise and Rank, in the liquid state has cleared up many doubtful points so far present in the experimental results of the previous investigations in the liquid state, but there still remain problems to be solved, especially those concerning the change of the spectra with state of aggregation and the assignment of Raman and infrared bands. We have remeasured the Raman spectra of this substance in the liquid and solid states and have also made the infrared measurements in the gaseous, liquid, and solid states, as well as in solutions. Furthermore, the normal modes of vibration have been calculated as an 8-body problem.

EXPERIMENTAL RESULTS

The infrared spectra have been measured with the spectrometer of our own construction[7] and with the Baird instrument. The Raman spectra were photographed with the spectrograph of high luminosity (height of prisms 15 cm), also of our own construction.[7]

The results are shown in Table I. The Raman spectrum observed in the liquid state is in good agreement with that obtained by Kagarise and Rank.[4] It is readily seen that some of the Raman lines and the infrared absorption bands, which are present with fairly strong intensity in the liquid spectra, disappeared completely in the solid spectra. This bears an important relation to the molecular structure of this substance, as we have often reported in the case of dihalogenoethanes.[7]

Some infrared bands observed in the liquid state have not been detected in the gaseous state. However, all of these bands have very weak intensity or just correspond to shoulders of the absorption curve and, consequently, could easily escape detection in the gaseous spectrum. It can, therefore, be concluded that so far as the number of absorption bands is concerned, the liquid and gaseous spectra are essentially identical, whereas both of them are quite different from the spectrum observed in the solid state.

We have also observed the relative intensities of some of the infrared absorption bands in different solutions, choosing *n*-heptane and CS_2 as nonpolar solvents and nitromethane and acetonitrile as polar solvents. The intensity ratio $I(756)/I(739)$ has been found as 0.96, 0.68, 0.19, and 0.15 in *n*-heptane, CS_2, nitromethane and acetonitrile, respectively. This shows that the strong liquid band at 756 cm^{-1}, which disappears in the solid spectrum, becomes weaker in a more polar solution,

* Present address: Governmental Industrial Research Institute, Osaka, Japan.

[1] Mizushima, Morino, and Kozima, Sci. Papers Inst. Phys. Chem. Research **29**, 111 (1936).
[2] K. W. F. Kohlrausch and Gr. P. Ypsilanti, Z. physik. Chem. **B29**, 274 (1935).
[3] A. Langseth and H. J. Bernstein, J. Chem. Phys. **8**, 410 (1940).
[4] R. E. Kagarise and D. H. Rank, Trans. Faraday Soc. **48**, 394 (1952).
[5] J. Powling and H. J. Bernstein, J. Am. Chem. Soc. **73**, 1815 (1951).
[6] E. K. Plyler, J. Chem. Phys. **17**, 218 (1949).
[7] S. Mizushima, *Structure of Molecules and Internal Rotation* (Academic Press, Inc., New York, 1954).

TABLE I. Infrared and Raman wave numbers of $CHCl_2-CHCl_2$ in cm^{-1}.

Infrared			Raman	
Gas	Liquid	Solid	Liquid	Solid
			89 (9)	90 (3)
			173 (8)	173 (4)
			225 (3)	
			242 (7)	249 (4)
			290 (7)	289 (4)
			300 (4)	
			353 (10)	352 (6)
			367 (5)	
	546 m	545 m	546 (5)	551 (3)
654 m[a]	650 m	647 m	649 (9)	657 (5)
722 s	716 m			
745 s	739 s	741 s		
761 s	756 s			
			766 (4)	
795 s	794 s	793 s		
802 s	800 sh	801 s	801 (10)	800 (6)
	813 vw?	813 vw?	814 (3)	
	837 sh	833 sh		
	888 vw			
	902 vw	905 vw		
978 w	973 w	984 m		
1018 s	1017 s	1018 ms	1019 (2)	1019 (0)
			1047 (0)	
1090 w	1088 w	1092 w		
	1188 sh			
1200 s	1202 s	1203 s	1202 (1)	
	1216 sh	1215 s	1217 (4)	1214 (4)
1247 m	1243 m	1245 s	1246 (3)	1241 (3)
1282 s	1279 s	1279 s	1280 (3)	1268 (2)
	1304 sh		1308 (2)	
	1340 w	1339 vw		
	1383 vw	1394 vw		
	1416 vw	1426 w		
	1440 w	1458 w		
2990 m	2990 s	2985 m	2989 (6)	2989 (6)

[a] Estimated relative intensity (s = strong, m = medium, w = weak, v = very); sh = shoulder; and uncertain data are indicated by ?.

whereas the other strong liquid band at 739 cm^{-1}, which appears in both the liquid and solid spectra, becomes weaker in a nonpolar solution.

The temperature dependence of $I(739)/I(756)$ also has been measured in the liquid state. At higher temperatures the 739 band becomes weaker while the 756 band becomes stronger.

ROTATIONAL ISOMERS

The experimental results described above can be explained from the existence of rotational isomers. From the comparison of the number of absorption bands or Raman lines observed in the liquid and solid states it can be concluded that the molecules exist in 2 forms in the liquid state and in only 1 form in the solid state. It is also seen that the band at 756 cm^{-1}, observed only in the liquid state, arises from one of the 2 forms, while the band at 739 cm^{-1}, observed in both liquid and solid states, corresponds to the other molecular form.

Since the 756 cm^{-1} band increases considerably in intensity in nonpolar solvents, it should be assigned to the less polar form which, as will be shown later by the normal vibration calculation, corresponds to the *trans*-form with a center of symmetry (C_{2h}). This is compatible with the fact that for the infrared and Raman bands observed only in the liquid state the mutual exclusion rule is satisfied.

On the other hand, the band at 739 cm^{-1} which decreases in intensity in nonpolar solvents should be assigned to the more polar form which will be shown to correspond to the *gauche*-form (C_2). Since this band is observed in both the liquid and solid states, the molecular form present in the solid state is concluded to be the more polar *gauche* form. In other words, in the liquid state are present both the *trans*- and *gauche*-forms, of which only the *gauche*-form exists in the solid state. This is in contradistinction to the result obtained in the case of 1,2-dihalogenoethanes for which the *trans*-form was the only form present in the solid state.[7]

In the liquid state the intensity ratio $I(739)/I(756)$ has been found to decrease at higher temperatures. Therefore, the *gauche*-form is concluded to be the more stable form in this state in conformity with the result of Kagarise and Rank.[4] However, it should be realized that the energy difference in the free state (gaseous state) is different from that in the liquid state which includes the interaction with the neighboring molecules.[8]

THE CALCULATION OF NORMAL MODES OF VIBRATION

The calculation of normal modes of vibration has been made as an 8-body problem, in which the vibration of H atoms also has been taken into account.

The potential function used is of the Urey-Bradley type, with which many calculations have been made in our laboratory.[9] The force constants used are shown in Table II, where K and H denote the constants for the

TABLE II. Force constants in 10^5 dynes/cm.

$K(C-C)=2.80$	$H(Cl-C-C)=0.10$	$F(C\cdots Cl)=0.60$
$K(C-Cl)=1.81$	$H(C-C-H)=0.15$	$F(C\cdots H)=0.40$
$K(C-H)=3.90$	$H(Cl-C-H)=0.05$	$F(Cl\cdots H)=0.80$
	$H(Cl-C-Cl)=0.10$	$F(Cl\cdots Cl)=0.64$
		$F'=-\frac{1}{10}F$

TABLE III. Types of vibrations.

Trans-form (C_{2h})				*Gauche*-form (C_2)			
Type	Number of vibrations	Activity Raman	Activity Infrared	Type	Number of vibrations	Activity Raman	Activity Infrared
A_g	6	+	−				
A_u	4	−	+	A	10	+	+
B_g	3	+	−				
B_u	5	−	+	B	8	+	+

[8] Watanabe, Mizushima, and Masiko, Sci. Papers Inst. Phys. Chem. Research Tokyo **40**, 425 (1943). See also reference 7.

[9] See, e.g., T. Shimanouchi, J. Chem. Phys. **17**, 245, 734, 848 (1949); See also reference 7.

bond-stretching and deformation vibrations and F and F' refer to the interaction between non-bonded atoms. The intramolecular tension k is taken as 0.10×10^{-11} dynes·cm. These values are exactly the same as those used in the calculation of normal vibrations of 1,2-dichloroethane except for $K(C-H)$, $H(Cl-C-Cl)$, and $F(Cl\cdots Cl)$, the latter two having no corresponding quantities in that case.

The calculations have been made for the *trans* form C_{2h} and the *gauche*-form C_2. The latter differs from the former in internal rotation about the C—C axis by 120°. The 18 normal vibrations are grouped into various types shown in Table III, which includes the selection rules for infrared and Raman spectra. The symmetry coordinates used in these calculations are shown in Table IV.

TABLE IV. Symmetry coordinates and vibrational types.

Vibrational type	Symmetry coordinates	Type
	$\Delta S_1=\Delta R$	CC stretching
	$\Delta S_2=\frac{1}{\sqrt{2}}\Delta(r_1+r_1')$	CH stretching
	$\Delta S_3=\frac{1}{2}\Delta(r_2+r_3+r_2'+r_3')$	CCl stretching
A_g (*trans*) A (*gauche*)	$\Delta S_4=\frac{1}{\sqrt{24}}\Delta(\beta_2+\beta_3+\alpha_{12}+\alpha_{13}-2\beta_1-2\alpha_{23}+\beta_2'+\beta_3'+\alpha_{12}'+\alpha_{13}'-2\beta_1'-2\alpha_{23}')$	
	$\Delta S_5=\frac{1}{2\sqrt{2}}\Delta(\beta_2+\beta_3-\alpha_{12}-\alpha_{13}+\beta_2'+\beta_3'-\alpha_{12}'-\alpha_{13}')$	CCl_2 wagging
	$\Delta S_6=\frac{1}{2}\Delta(\beta_1-\alpha_{23}+\beta_1'-\alpha_{23}')$	
	$\Delta S_7=\frac{1}{2}\Delta(r_2-r_3-r_2'+r_3')$	CCl stretching
A_u (*trans*) A (*gauche*)	$\Delta S_8=\frac{1}{2\sqrt{2}}\Delta(\beta_2-\beta_3-\alpha_{12}+\alpha_{13}-\beta_2'+\beta_3'+\alpha_{12}'-\alpha_{13}')$	CCl_2 twisting
	$\Delta S_9=\frac{1}{2\sqrt{2}}\Delta(\beta_2-\beta_3+\alpha_{12}-\alpha_{13}-\beta_2'+\beta_3'-\alpha_{12}'+\alpha_{13}')$	CH bending
	$\Delta S_{10}=\frac{1}{2}\Delta(r_2-r_3+r_2'-r_3')$	CCl stretching
B_g (*trans*) B (*gauche*)	$\Delta S_{11}=\frac{1}{2\sqrt{2}}\Delta(\beta_2-\beta_3-\alpha_{12}+\alpha_{13}+\beta_2'-\beta_3'-\alpha_{12}'+\alpha_{13}')$	CCl_2 twisting
	$\Delta S_{12}=\frac{1}{2\sqrt{2}}\Delta(\beta_2-\beta_3+\alpha_{12}-\alpha_{13}+\beta_2'-\beta_3'+\alpha_{12}'-\alpha_{13}')$	CH bending
	$\Delta S_{13}=\frac{1}{\sqrt{2}}\Delta(r_1-r_1')$	CH stretching
	$\Delta S_{14}=\frac{1}{2}\Delta(r_2+r_3-r_2'-r_3')$	CCl stretching
B_u (*trans*) B (*gauche*)	$\Delta S_{15}=\frac{1}{\sqrt{24}}\Delta(\beta_2+\beta_3+\alpha_{12}+\alpha_{13}-2\beta_1-2\alpha_{23}-\beta_2'-\beta_3'-\alpha_{12}'-\alpha_{13}'+2\beta_1'+2\alpha_{23}')$	
	$\Delta S_{16}=\frac{1}{2\sqrt{2}}\Delta(\beta_2+\beta_3-\alpha_{12}-\alpha_{13}-\beta_2'-\beta_3'+\alpha_{12}'+\alpha_{13}')$	CCl_2 wagging
	$\Delta S_{17}=\frac{1}{2}\Delta(\beta_1-\alpha_{23}-\beta_1'+\alpha_{23}')$	

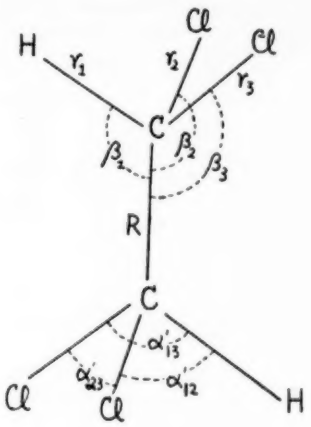

FIG. 1. Equilibrium values whose changes constitute the internal coordinates.

The significance of the notations is clear from Fig. 1. With these symmetry coordinates the secular equation can be written as a product of factors corresponding to each symmetry type. By putting each of the factors equal to zero, the wave numbers are calculated as shown in Table V. The computed values are in good agreement with those observed in the infrared and Raman spectra.

The assignment made in Table V can be checked by the sum rule derived in our previous paper.[10] The sum of squares of all the frequencies assigned to the *trans*-form† was found as 2.805×10^7 which compares favorably with that for the *gauche*-form, 2.789×10^7. This shows that the assignment of the observed frequencies to the *trans*- and *gauche*-forms is correct.

In Tables IV and V, rough characterizations have been made as CCl stretching vibration, CH bending vibration, etc. In order to discuss this problem more precisely, we have to calculate the relative amplitude for each of the internal coordinates (e.g., change of bond lengths or bond angles), or of the internal symmetry coordinates in a given normal mode of vibration. The internal coordinates R or the internal symmetry coordinates S are related linearly to the normal coordinates Q through the matrix expressions

$$\mathbf{R}=\mathbf{L}\mathbf{Q}$$

and

$$\mathbf{S}=\mathbf{L}'\mathbf{Q}.$$

If, therefore, we calculate the elements of the L matrix or of the L' matrix for a given normal vibration, we can determine the relative amplitude for each internal coordinate or for each internal symmetry coordinate. Such a calculation has been made by us and the result will be published elsewhere. All the conclusions derived in this paper are compatible with this result.

The assignment of the vibrations of type A_g of the *trans*-form and of type A of the *gauche*-form has also been made by Kagarise and Rank.[4] The wave numbers

[10] Mizushima, Shimanouchi, Nakagawa, and Miyake, J. Chem. Phys. **21**, 215 (1953).

† For ν_9, ν_{17}, and ν_{18} we used calculated values as we have no observed ones.

TABLE V. Calculated and observed wave numbers in cm^{-1}.

	Trans form Type of vibration	Calc.	Obs.		*Gauche* form Calc.	Obs.
	ν_1 CH stretching	2930	2989		ν_1' 2930	2989
	ν_2 CH bending	1200	1202		ν_2' 1190	1217
A_g	ν_3 CC stretching	1029	1047		ν_3' 1035	1019
	ν_4 CCl stretching	747	766		ν_4' 640	649
	ν_5 CCl_2 wagging	348	367		ν_5' 144	173
	ν_6 CCl_2 bending	191	225	A	ν_6' 318	353
	ν_7 CH bending	1250	1304		ν_7' 1260	1280
A_u	ν_8 CCl stretching	738	756		ν_8' 818	801
	ν_9 CCl_2 twisting	125	···		ν_9' 224	242
	ν_{10} torsional	···	···		ν_{10}' ···	89
	ν_{11} CH bending	1260	1308		ν_{11}' 1250	1243
B_g	ν_{12} CCl stretching	837	814		ν_{12}' 773	794
	ν_{13} CCl_2 twisting	276	300		ν_{13}' 144	173
	ν_{14} CH stretching	2940	2990	B	ν_{14}' 2940	2990
	ν_{15} CH bending	1190	1188		ν_{15}' 1200	1202
B_u	ν_{16} CCl stretching	718	716		ν_{16}' 727	739
	ν_{17} CCl_2 wagging	316	···		ν_{17}' 493	546
	ν_{18} CCl_2 bending	288	···		ν_{18}' 288	290

814 and 1306 cm^{-1} assigned to ν_{12} (CCl stretching) and ν_{11} (CH bending) of B_g in Table V have been assigned by them to ν_3 (CC stretching) and ν_2 (CH bending) of A_g. However, the calculation of normal frequencies and of the L matrix shows that our assignment is more reasonable.

The Raman line at *ca* 90 cm^{-1} in both the liquid and solid states has been assigned to the torsional oscillation about the C−C axis of the *gauche* form, in conformity with the assignment of Kagarise and Rank. (This oscillation has not been treated in our calculation, since, in the potential function of the molecule, the azimuthal angle of the internal rotation about the C−C axis has not been included as an internal coordinate and the interaction between the two movable groups $-CHCl_2$ has been neglected.) This line is reported to be depolarized and may not be compatible with its assignment as the A vibration of C_2. However, it should be realized that a Raman line reported as depolarized may belong to a polarized type, because the polarization factor of a symmetric vibration may have any value up to the limiting one expected for a depolarized line. Furthermore, the experimental value is not always reliable, unless the line is isolated and sufficiently intense.

As shown in Table IV the bands at 739 and 794 cm^{-1} observed in the infrared absorption have been assigned to C−Cl stretching vibrations of the *gauche*-form. These vibrations should, therefore, be allowed in the Raman effect, although we did not show them in the Raman column of Table I. A weak line shifted by 740 cm^{-1} from Hg−k has been assigned as $i-546$, but it is possible to assign this line as the superposition of $i-546$ and $k-740$.‡ As to the other Raman line at 794 cm^{-1}, the detection would be difficult, because in the close vicinity (at 801 cm^{-1}) a strong Raman line has been observed. At any rate an inspection of the L matrices for these vibrations shows that they must be weak lines. It is, therefore, understandable that we did not observe these Raman lines clearly.

In conclusion we could show that the vapor and the liquid of 1,1,2,2-tetrachloroethane contains both the *trans*- and the *gauche* forms, whereas the solid contains only the *gauche*-form. All the infrared and Raman frequencies observed in the gaseous, liquid, and solid states can be brought into agreement with the calculated normal frequencies of the *trans*- and the *gauche*-forms.

‡ The wavelengths of Hg−k and $-i$ are 4047 A and 4078 A.

Internal Pressure of Carbon Tetrachloride between −7° and 70°

HARM BENNINGA AND ROBERT L. SCOTT
Department of Chemistry, University of California, Los Angeles, California
(Received January 13, 1955)

Measurements of $(\partial P/\partial T)_V$ of carbon tetrachloride at ten different temperatures between −7° and 70°C yield an equation for the internal pressure $(\partial E/\partial V)_T = 3346[1-2.97\times10^{-3}(t-25)-12.6\times10^{-6}(t-25)^2]$ atmospheres.

Comparison with the cohesive energy density $(\Delta E^v/V)$ confirms previous observations (Hildebrand and co-workers) that the ratio of the internal pressure to the cohesive energy density is approximately unity and further shows this ratio to be remarkably constant over the entire 77° range of temperature.

The experimental data on the internal pressure are in marked disagreement with the predictions of "free-volume theory" (Lennard-Jones and Devonshire, Hirschfelder and co-workers).

INTRODUCTION

THE relation between the internal energy and the molar volume is of considerable importance in the theory of the liquid state. Pure thermodynamics gives the following relation, sometimes called the "thermodynamic equation of state".[1]

$$(\partial E/\partial V)_T = T(\partial P/\partial T)_V - P. \quad (1)$$

Although $(\partial P/\partial T)_V$ can be calculated from the coefficient of thermal expansion and the isothermal compressibility, Hildebrand and co-workers[2–4] have shown that more reliable results are obtained by direct measurements. Their experiments indicate that $(\partial P/\partial T)_V$ is constant along a constant volume line up to pressures of more than 150 atmospheres.

The external pressure P is negligible compared with the internal pressure $T(\partial P/\partial T)_V$ which is 2000–8000 atmospheres:

$$(\partial E/\partial V)_T = T_{P=0}(\partial P/\partial T)_T \cong T_{P=1\ \text{atmos}}(\partial P/\partial T)_V. \quad (2)$$

Hildebrand[5] compared $V^2(\partial E/\partial V)_T$ with $V\Delta E^V$, where ΔE^V is the energy of vaporization, and found for several nonpolar liquids a slightly greater value of the first quantity. Remembering that ΔE^V at low pressures is practically equal to $-E$, the energy of vaporization to an ideal gas, we may write:

$$(\partial E/\partial V)_T \cong -E/V. \quad (3)$$

Frank[6] has proposed to represent the volume dependence of E over a small range of volumes as $E = a/V^n$, which gives for $(\partial E/\partial V)_T$:

$$(\partial E/\partial V)_T = -nE/V. \quad (4)$$

Hildebrand's results indicate that for nonpolar liquids under normal conditions n is slightly greater than one, the value for a van der Waals liquid

In recent years the Lennard-Jones and Devonshire cell method[7] has found many applications in the theory of liquids and solutions. The exact comparison of the results of this so-called free volume theory with experiment has been greatly facilitated by the compilation of extensive tables of reduced "free volume" thermodynamic quantities by Wentorf, Buehler, Hirschfelder, and Curtiss[8] and by Salsburg and Kirkwood.[9] In this paper we evaluate the internal pressure $(\partial E/\partial V)_T$ for carbon tetrachloride over a large range of temperatures (75% of its liquid range at atmospheric pressure). Carbon tetrachloride, with its pseudo-spherical molecules, should fit the assumptions of free volume theory as well as any substance liquid at room temperature. This allows us on the one hand to establish the accurate relation between internal pressure and cohesive energy density for CCl_4, and provides on the other hand a test for the validity of the free volume theory.

EXPERIMENTAL

Apparatus and procedure were very similar to those described by Alder, Haycock, Hildebrand, and Watts.[4] The volume of our thermoregulator was about 40 cm,[3] the pressure was applied from a cylinder with dry nitrogen. An improvement over earlier methods was the measurement of the temperature inside the bomb by means of a Western Electric thermistor (#14). The resistance at 25° was about 100 kΩ, the temperature coefficient 4% per degree. The resistance of the thermistor was determined in a Wheatstone bridge with a Helipot potentiometer which allowed for readings of two parts in 10 000. The thermistor was calibrated between −10° and +80°C against a platinum resist-

[1] J. H. Hildebrand and R. L. Scott, *Solubility of Nonelectrolytes* (Reinhold Publishing Corporation, New York, 1950), third edition.
[2] Westwater, Frantz, and Hildebrand, Phys. Rev. **31**, 135 (1928).
[3] J. H. Hildebrand and J. M. Carter, J. Am. Chem. Soc. **54**, 3592 (1932).
[4] Alder, Haycock, Hildebrand, and Watts, J. Chem. Phys. **22**, 1060 (1954).
[5] J. H. Hildebrand, Phys. Rev. **34**, 984 (1929).
[6] H. S. Frank, J. Chem. Phys. **13**, 493 (1945).
[7] J. E. Lennard-Jones and A. F. Devonshire, Proc. Roy. Soc. (London) **A163**, 53 (1937).
[8] Wentorf, Buehler, Hirschfelder, and Curtiss, J. Chem. Phys. **18**, 1484 (1950). See also: Hirschfelder, Curtiss, and Bird, *Molecular Theory of Gases and Liquids* (John Wiley and Sons, Inc., New York, 1954).
[9] Z. W. Salsburg and J. G. Kirkwood, J. Chem. Phys. **21**, 2169 (1953).

ance thermometer; the calibration points were about 5 degrees apart.

The measurement of the pressure was done with a standard dead weight gauge (#9010) of the Refinery Supply Company. Excess pressures between 5 and 1000 psi, e.g., between 0.34 and 68.05 atmospheres, could be determined to within about 0.01 atmosphere.

Reagent grade carbon tetrachloride (Baker Chemical Company) was used without further purification, its density was $d_4^{25}=1.5843\pm0.0002$.

RESULTS

In the first series of experiments the P–t relationship at constant volume was reinvestigated. The results of ten experiments between 1 and 60 atmos could be represented by a linear equation with a standard deviation of 0.01°C in t:

$$P=11.153t-331.15 \text{ atmos.} \quad (5)$$

Equating the right-hand side of Eq. (5) to zero gave the t value at zero pressure: $t_p=0=29.69$°C. Only three points were determined in each of the other nine series. Equations similar to Eq. (5) were calculated, the deviation of the calculated from the observed temperature was never more than 0.02°C. All $\Delta P/\Delta T$ values finally had to be corrected for the small volume changes of the glass[2]:

$$(\partial P/\partial T)_V=\Delta P/\Delta t(1-0.032)+0.10 \text{ atmos deg}^{-1}. \quad (6)$$

This formula was obtained using compressibilities of Pyrex glass and CCl_4 from Landolt-Börnstein and the thermal expansion coefficient of Pyrex from the I.C.T.

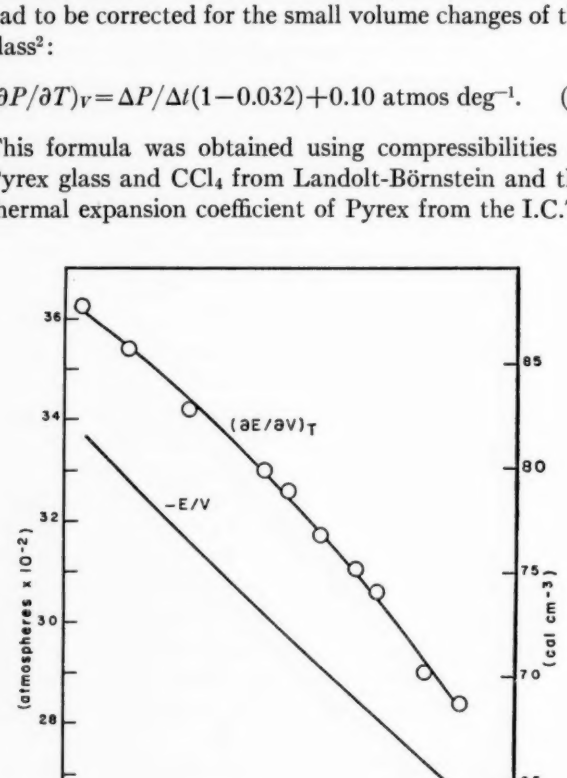

FIG. 1. Internal pressure and cohesive energy density of carbon tetrachloride.

From the corrected $(\partial P/\partial T)_V$ values and the corresponding zero pressure temperatures a quadratic expression was found by means of the method of least squares:

$$(\partial P/\partial T)_V=11.224[1-6.36\times10^{-3}(t-25)+8.3\times10^{-6}(t-25)^2] \text{ atmos deg}^{-1} \quad (7)$$

with a standard deviation of 0.06 atmos deg^{-1} in $(\partial P/\partial T)_V$.

Our values for $(\partial P/\partial T)_V$ are in general about 1.5% greater than the values obtained by Westwater, Frantz, and Hildebrand[2] and by Hildebrand and Carter.[3] The two values of Alder, Haycock, Hildebrand, and Watts[4] agree with Eq. (7) within our standard deviation.

DISCUSSION

Internal Pressure and Cohesive Energy Density

The equation for the internal pressure calculated from the original data with the method of least squares is:

$$(\partial E/\partial V)_T=3346[1-2.97\times10^{-3}(t-25)-12.6(t-25)^2] \text{ atmos.} \quad (8)$$

TABLE I. Values of n and a for CCl_4.

t (°C)	V (cm³)	n	a (atmos liter²)
− 5	93.66	1.07	31.6
+ 5	94.77	1.08	31.7
+15	95.91	1.09	31.6
+25	97.09	1.09	31.5
+35	98.30	1.09	31.3
+45	99.55	1.09	31.0
+55	100.85	1.08	30.6
+65	102.19	1.07	30.1

The curve corresponding to this equation has been plotted in Fig. 1, together with the curve representing the cohesive energy density $(-E/V)$ of CCl_4 *versus* temperature in the same region.

The relationship between cohesive energy density and temperature of carbon tetrachloride has been calculated in the following way: An equation for the heat of vaporization to zero pressure was obtained from the heat of vaporization at 25°C, as given by "Selected values of chemical thermodynamic properties",[10] and specific heat data given by Hicks, Hooley, and Stephenson,[11] by Stull,[12] and by Vold[13]:

$$\Delta H^V=7800-11.5(t-25)+0.008(t-25)^2 \text{ cal mole}^{-1}, \quad (9)$$

[10] "Selected values of chemical thermodynamic properties", Circular of the National Bureau of Standards #500, Washington, D. C. 1952.

[11] Hicks, Hooley, and Stephenson, J. Am. Chem. Soc. **66**, 1064 (1944).

[12] D. R. Stull, J. Am. Chem. Soc. **59**, 2726 (1937).

[13] R. D. Vold, J. Am. Chem. Soc. **57**, 1192 (1935).

which gave for the energy of vaporization to ideal gas:

$$-E=E^V=H^V-RT=7200[1-1.88\times10^{-3}(t-25)+1.1\times10^{-6}(t-25)^2]\text{ cal mole}^{-1}. \quad (10)$$

The temperature dependence of the specific volume of CCl_4 between 15° and 75° has been determined very accurately by Gibson and Loeffler,[14] recalculated for molar volumes their equation reads:

$$V=97.086[1+1.227\times10^{-3}(t-25)+1.90\times10^{-6}(t-25)^2+7\times10^{-9}(t-25)^3]\text{cm}^3. \quad (11)$$

We have applied Eq. (14) also between $-10°$ and $+15°$C, since the error involved is probably smaller than the errors we would make in taking data from other sources.

The cohesive energy density, finally, is the quotient from expressions (10) and (11):

$$-E/V=3063[1-3.14\times10^{-3}(t-25)+3.0\times10^{-6}(t-25)^2]\text{atmos}. \quad (12)$$

TABLE II. Reduced internal pressures and cohesive energy densities for a free volume liquid. (W.B.H.C.)

T^*	V^*	P^*	$-E^*$	$-E^*/V^*$	$\partial E^*/\partial V^*$
0.70	1.04	0	7.29	7.03	5.0_0
0.80	1.06	0	7.09	6.65	5.3_6
0.90	1.10	0	6.77	6.17	5.6_0
1.00	1.16	0.06	6.45	5.63	5.7_2
1.10	1.21	0.14	5.97	4.96	5.6_4
1.20	1.30	0.240	5.41	4.17	5.0_4
1.30	1.77	0.434	3.75	2.12	2.4

We are now in a position to evaluate the parameter n in Eq. (14):

$$n=1.092[1+0.12\times10^{-3}(t-25)-16\times10^{-6}(t-25)^2] \quad (13)$$

and van der Waals' constant:

$$a=V^2(\partial E/\partial V)_T=31.54\times[1-0.51\times10^{-3}(t-25)-15\times10^{-6}(t-25)^2]\text{ atmos liter}^2. \quad (14)$$

Both parameters are remarkably constant, although a decreases slightly as the temperature approaches the boiling point (Table I).

Comparison with the Free Volume Theory

The reduced thermodynamic quantities in the free volume theory are reduced by means of the parameters ϵ_m and r_0 of the Lennard-Jones potential function, which expresses the interaction energy for a pair of symmetrical, nonpolar molecules:

$$\epsilon(r)=4\epsilon_m[(r_0/r)^{12}-(r_0/r)^6]. \quad (15)$$

[14] R. E. Gibson and O. H. Loeffler, J. Am. Chem. Soc. **63**, 898 (1941).

TABLE III. Reduced internal pressures and cohesive energy densities for a free volume liquid (S.K.).

T^*	V^*	$-E^*$	$-E^*/V^*$	$\partial E^*/\partial V^*$
0.1840	0.94	8.320	8.851	1.6_9
0.5315	1.00	7.664	7.664	4.2_3
0.6250	1.02	7.466	7.320	4.7_1
0.7700	1.06	7.096	6.694	5.3_7
0.8819	1.10	6.761	6.146	5.4_8
0.9989	1.16	6.311	5.441	5.5_7

Here ϵ_m is the maximum energy of interaction, r_0 is the low temperature collision diameter; related to r_0 is a volume $V_0=Nr_0^3$, where N is Avogadro's constant.

The theoretical values of the reduced internal pressure and cohesive energy density were obtained in the following way:

(a) From the tables of Wentorf, Buehler, Hirschfelder, and Curtiss,[8] tables of reduced cohesive energy densities ($-E^*/V^*=-EV_0/N\epsilon_mV$) and reduced pressures ($P^*=PV_0/N\epsilon$) were calculated for temperatures from $T^*=kT/\epsilon_m=0.70$ to $T^*=1.30$ (the theoretical critical point) and for volumes from $V^*=V/V_0=0.9899$ to $V^*=1.8385$. The cohesive energy densities in the coexistence region were determined graphically in a plot of the $-E^*/V^*$ *versus* P^* isotherms. The following values of the reduced vapor pressure in this region were used: $P^*=0.434$ for $T^*=1.30$; $P^*=0.240$ for $T^*=1.20$; $P^*=0.14$ for $T^*=1.10$; $P^*=0.06$ for $T^*=1.00$; and $P^*=0$ for all lower isotherms. The first two pressure values are given by W.B.H.C., the others we have estimated. The next step was a determination of the V^*'s corresponding with these ($-E^*/V^*$) values from a ($-E^*/V^*$) *vs* V^* diagram. The volume dependence of the reduced internal energy finally was obtained from energy-volume isotherms with the aid of a tangent meter. All these quantities are listed in Table II.

(b) The paper of Salsburg and Kirkwood[9] contains a table of reduced thermodynamic quantities at zero reduced pressure. The values of $\partial E^*/\partial V^*$ in our Table III were calculated from formula (13) of S.K.

In the range ($T=0.70$ to 1.00) where both papers report calculations, the two sets of values are not in complete agreement, but the discrepancies are not large enough to concern us here.

The difficulties involved in the determination of the Lennard-Jones parameters are discussed by S.K. The most appropriate values in our case are doubtless the values computed from the experimental heat of vaporization and molar volume at a temperature in our temperature range, using the free volume expressions for the thermodynamic functions. For CCl_4 the S.K. values are:

$\epsilon/k=485.7°$K; $r_0=5.411$ A, which means

$V_0=95.37$ cm^3 mole^{-1}.

In Fig. 2, the experimental results for $-E/V$ and $(\partial E/\partial V)_T$, cast in reduced form, are compared with

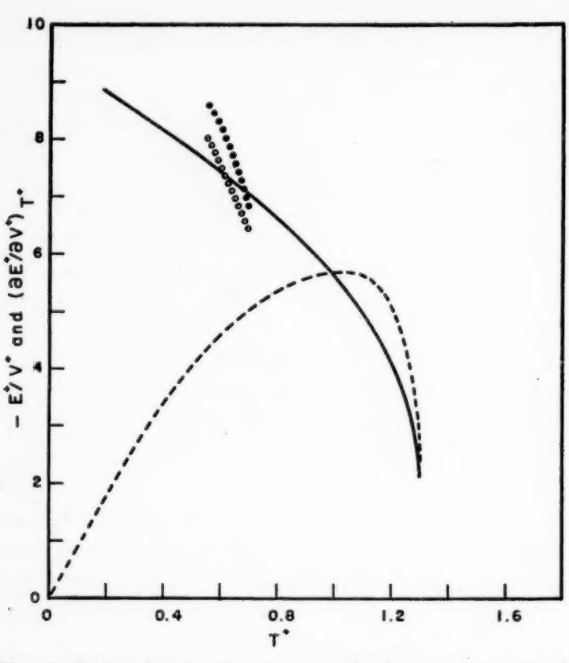

FIG. 2. Reduced internal pressure and cohesive energy density as functions of reduced temperature. $(\partial E^*/\partial V^*)_{T^*}$, free volume theory ----; $(\partial E^*/\partial V^*)_{T^*}$, smoothed curve from experimental points for CCl_4 ●●●●; $-E^*/V^*$, free volume theory——; $-E^*/V^*$, calculated for CCl_4 from experimental heat of vaporization and specific heat data○○○○○.

the predictions of the free-volume or cell theory. Since the Lennard-Jones parameters were evaluated from experimental data for the liquid at 25°C, the experimental and theoretical values of the cohesive energy density are identical at this temperature. The variation with temperature is, however, not satisfactorily treated by the theory, for the experimental slope is about three times the theoretical. (If $-E/V$ is plotted against V, the agreement is much better, since the experimental $(\partial V/\partial T)_P$ is also about three times the theoretical.)

There is, however, no agreement at all between the internal pressure functions. The experimental values are slightly greater than the cohesive energy densities, instead of being much smaller, and they are decreasing with T (and V), whereas the theoretical internal pressures are increasing. Consequently the theoretical value of n is entirely wrong. Only in the region of the critical point, far above the expected boiling point, do the theoretical values of $(\partial E/\partial V)_T$ and n approach the behavior observed experimentally in the normal liquid range.

We are of course aware that the cell theory as used includes a spherically symmetric Lennard-Jones 6–12 potential, and carbon tetrachloride would be expected to show a steeper repulsive potential (i.e., a repulsive exponent greater than 12), and some angular dependence. Until measurements of the kind we have made on carbon tetrachloride can be made on liquid argon, krypton, or methane, or until calculations have been made for the cell model with other potential functions, the effect of this cannot be predicted with certainty. We feel, however, that the effect of changing the potential function to fit a molecule like carbon tetrachloride, is distinctly secondary to the error introduced in the cell model by assuming single occupancy of all cells.

It is evident that energy-volume-temperature relations for liquids present a severe and sensitive test for a theory of liquids. The Lennard-Jones and Devonshire "free volume" or cell model, even as subsequently refined fails badly here (at least for carbon tetrachloride) as do most other treatments. An adequate theory of liquids must account for the approximate equality $(n \approx 1)$ of the internal pressure and the cohesive energy density of a normal liquid over the entire normal liquid range of temperatures.

ACKNOWLEDGMENT

We wish to express our thanks to the California Research Corporation for its grant-in-aid to our research program on liquids and solutions.

High-Temperature Equation of State by a Perturbation Method. II. Polar Gases*

ROBERT W. ZWANZIG†
Sterling Chemistry Laboratory,‡ Yale University, New Haven, Connecticut
(Received January 4, 1955)

The perturbation theory described in a previous article is applied to the calculation of the equation of state at high temperature of a polar gas. The electrostatic dipolar potential is considered to be a perturbation on the nonpolar Lennard-Jones potential. The dipole contribution to the equation of state is expressed in terms of properties of the unperturbed system. These properties are obtained from experimental data on argon and xenon. Numerical tables of the reduced equation of state of the polar gas, over a wide temperature and density range, are presented. The theory is tested on water vapor and on methyl fluoride. Theoretical predictions of the pressure agree with experimental data over a wide density range (up to 0.25 g/cc for water) to within several percent.

I

IN A previous article[1] we showed how the equation of state of a nonpolar gas (illustrated by argon and nitrogen) may easily be computed for high temperatures and a wide range of densities, by adding to the equation of state of a rigid sphere fluid a correction due to the perturbing effect of a Lennard-Jones potential. In this article, we shall describe similiar computations, whereby the high temperature equation of state of a polar gas (illustrated by water and methyl fluoride) is obtained by correcting the observed equation of state of a nonpolar gas for the perturbing effects of an electrostatic dipole potential.

Pople[2] has described an attack on the problem of dipolar liquids which begins very much like ours. Instead of applying the dipole correction to the observed equation of state of a nonpolar substance, he applied the correction to the equation of state predicted by the free volume theory of liquids. By keeping the dipole moment of a molecule as an adjustable parameter, he discovered that in order to obtain satisfactory values of, for example, the latent heat of vaporization, it was necessary to use apparent dipole moments considerably larger than the actual moments. We shall see later that if only first order perturbing effects of the dipoles are included, this type of theory can generally work only at temperatures somewhat above the critical temperature, so that Pople's application to condensed phases was perhaps too ambitious.

II

The thermodynamic properties of a substance are determined, in statistical mechanics, by the potentials of intermolecular force. Little is known quantitatively about the forces between unsymmetrical molecules. Their computation quantum-mechanically is difficult, only a few systems have been studied in detail, and the results are complex even for the interaction between two hydrogen molecules. For this reason, if one wishes to develop a statistical mechanical theory involving unsymmetrical molecules it is necessary to assume some convenient approximate intermolecular potential, and see whether it leads to satisfactory computed thermodynamic properties. A commonly used approximation for simple polar molecules is the Stockmayer potential[3,4] which is the superposition of a spherically symmetric potential of the type which occurs between noble gas atoms and an electrostatic point dipole potential,

$$V_{jk}=\epsilon\gamma\left(\frac{R_{jk}}{a}\right)+\boldsymbol{\mu}_j\boldsymbol{\mu}_k:\left(\mathbf{1}-\frac{3\mathbf{R}_{jk}\mathbf{R}_{jk}}{R_{jk}^2}\right)\frac{1}{R_{jk}^3}, \quad (1)$$

where $\mathbf{R}_{jk}$ is the vector separation of the centers of the molecules j and k, ϵ and a are parameters characteristic of the type of molecule, $\boldsymbol{\mu}_k$ is the vector dipole moment of the kth molecule, $\mathbf{1}$ is the unit dyad, and $\gamma(x)$ is a function which is assumed to be the same for all molecules being considered. (For nonpolar molecules, $\mu=0$, this potential leads to the well-known principle of corresponding states.) The approximations contained in the potential which may be serious are (1) the van der Waals forces of attraction and the forces of repulsion are assumed to be spherically symmetric, and (2) the electrostatic forces are assumed to be due to point dipoles only. For methyl fluoride, which is one of our examples, these approximations are probably not bad: we shall see that the agreement between our theory and experiment is fairly good. For water, which is our other example, both approximations are undoubtedly serious: the water molecule certainly has an appreciable quadrupole moment, it is quite unsymmetrical, and hydrogen bonding is a further complication. However, we shall find that at high temperature, the Stockmayer potential does lead to reasonably good results for water. We shall indicate in the next paragraph how this might have come about.

* This work was supported by the U. S. Office of Naval Research, under Contract Nonr-410(00) with Yale University.
† Present address: Department of Chemistry, The Johns Hopkins University, Baltimore 18, Maryland.
‡ Contribution No. 1257 from the Sterling Chemistry Laboratory, Yale University.
[1] R. W. Zwanzig, J. Chem. Phys. **22**, 1420 (1954).
[2] J. A. Pople, Proc. Roy. Soc. (London) **A215**, 67 (1952).
[3] W. H. Stockmayer, J. Chem. Phys. **9**, 398 (1941).
[4] Hirschfelder, Curtiss, and Bird, *Molecular Theory of Gases and Liquids* (John Wiley and Sons, Inc., New York, 1954), p. 211, 248.

The parameters ϵ and a which appear in the nonpolar part of the Stockmayer potential may be determined by an analysis of experimental second virial coefficient data of the gas in question, provided that a suitable potential $\gamma(x)$ has been chosen. The customary choice is the Lennard-Jones 6–12 potential,

$$\gamma(x)=4(x^{-12}-x^{-6}), \tag{2}$$

and we shall use this in our computations. The dipole moment μ may also be determined in this way, but it is easier to obtain μ by some independent method, and then to use it as a given parameter in the determination of ϵ and a. If the Stockmayer potential is a good approximation, a fixed ϵ and a will lead to good agreement between computed and experimental second virial coefficients over a wide temperature range. We have observed that when this analysis is performed for water, then one must use an ϵ and a which depend on temperature. This dependence indicates that the Stockmayer potential is not a good approximation over a wide temperature range. However, if one uses second virial data in the temperature range in which one is interested, then the Stockmayer potential with ϵ and a determined in that temperature range may be reliable for the computation of other properties in the same temperature range. The approximations in the potential may be accounted for, at least partially, by using the appropriate ϵ and a.

Another source of difficulty with the Stockmayer potential, which has been discussed by Pople[2] is that it takes no account of molecular polarizabilities. The electric fields due to the permanent dipoles induce extra dipole moments if the molecules are polarizable, so that the actual moment may be quite different from the permanent moment. To correct for this effect, the μ in the Stockmayer potential should be the actual dipole moment at the density and temperature under consideration. Another way of correcting for this effect would be to add to the Stockmayer potential an extra contribution due to the electrostatic potential energy stored in each molecule because of its polarizability. We shall later estimate the magnitude of the correction, but for the time being, this effect will be neglected.

III

We shall consider a one-component system of N molecules in a volume v. The pressure p in this system may be obtained from the configurational energy $\bar{A}_N$,

$$p=-(\partial\bar{A}_N/\partial v)_T. \tag{3}$$

The configurational free energy is defined by

$$\exp(-\bar{A}_N/kT)=\int\cdots\int d\tau_1\cdots d\tau_N \times\exp(-V_N/kT) \tag{4}$$

where T is the absolute temperature, $\int d\tau_k$ is an integral over the complete configuration space of the kth molecule, and V_N is the total potential energy of a configuration,

$$V_N=\sum_{j<k}^{N} V_{jk}.$$

The Stockmayer potential may be rewritten in the form

$$V_{jk}/\epsilon=\left\{\gamma\left(\frac{R_{jk}}{a}\right)+\left(\frac{\mu^2}{\epsilon a^3}\right)^2 \times\left(\frac{a}{R_{jk}}\right)^3\left(1-\frac{3\mathbf{R}_{jk}\mathbf{R}_{jk}}{R^2_{jk}}\right):\mathbf{v}_j\mathbf{v}_k\right\}; \tag{5}$$

$\mu^2/\epsilon a^3$ is a dimensionless parameter characteristic of the molecule, and $\mathbf{v}_k$ is a unit vector $\boldsymbol{\mu}_k/\mu$ in the direction of the kth dipole. We shall find it convenient to use the reduced or dimensionless variables

$$\begin{aligned}\mathbf{x}_k&=\mathbf{R}_k/a\\ p^*&=p\epsilon/a^3\\ v^*&=v/Na^3\\ T^*&=Tk/\epsilon.\end{aligned} \tag{6}$$

It is easily seen that the reduced thermodynamic variables satisfy an equation of state,

$$p^*=p^*(T^*,v^*;\,\mu^2/\epsilon a^3). \tag{7}$$

This equation contains a statement of the principle of corresponding states for polar molecules:[4] an additional variable, $\mu^2/\epsilon a^3$, is needed to compare the properties of different polar molecules. The functional dependence of p^* on T^*, v^*, and $\mu^2/\epsilon a^3$ involves only the form of the potential $\gamma(x)$, and is therefore the same for all systems whose molecules interact with the same Stockmayer potential.

We may expand p^* in powers of $\mu^2/\epsilon a^3$,

$$p^*=p_0^*(T^*,v^*)+\frac{\mu^2}{\epsilon a^3}p_1^*(T^*,v^*) +\left(\frac{\mu^2}{\epsilon a^3}\right)^2 p_2^*(T^*,v^*)+\cdots. \tag{8}$$

The coefficients of the powers of $\mu^2/\epsilon a^3$ are determined entirely by the form of $\gamma(x)$. When the dipole moment is zero, the reduced equation of state is that of the simple nonpolar systems (e.g., argon), if $\gamma(x)$ is a good approximation to the intermolecular potential in those systems. Thus, p_0^* may be obtained from known experimental data. It turns out that p_1^* vanishes. When $\gamma(x)$ is chosen to be the Lennard-Jones potential, we shall see that p_2^* may be computed directly in terms of p_0^*. In this way, we may calculate the pressure of a polar system from information about nonpolar systems and from the molecular parameters μ, ϵ, and a, provided that $\mu^2/\epsilon a^3$ is small enough.

The expansion of p in powers of $\mu^2/\epsilon a^3$ is easily obtained by the general perturbation theory developed in reference 1. To use this theory, we must split the po-

tential energy into an unperturbed part $V_N^{(0)}$ and a perturbation $V_N^{(1)}$. We shall do it in this way:

$$V_N^{(0)}=\epsilon\sum_{j<k}^{N}\gamma\left(\frac{R_{jk}}{a}\right)$$

$$V_N^{(1)}=\sum_{j<k}^{N}V^{(1)}(j,k); \tag{9}$$

$$V^{(1)}(j,k)=\epsilon\frac{\mu^2}{\epsilon a^3}\left(\frac{a}{R_{jk}}\right)^3\left(1-3\frac{\mathbf{R}_{jk}\mathbf{R}_{jk}}{R_{jk}^2}\right):\mathbf{v}_j\mathbf{v}_k. \tag{10}$$

The configurational free energy of the unperturbed system is $\bar{A}_N^{(0)}$ and the effect of the perturbation is given by

$$\exp(-(\bar{A}_N-\bar{A}_N^{(0)}/kT)=\langle\exp(-V_N^{(1)}/kT)\rangle_0 \tag{11}$$

where the average is performed over an ensemble of the unperturbed systems. When a semi-invariant expansion is performed, we get

$$\bar{A}_N=\bar{A}_N^{(0)}+\omega_1-\omega_2/2kT+O(1/kT)^2 \tag{12}$$

in which the quantities ω_1 and ω_2 are defined as averages of various combinations of $V^{(1)}$ over the unperturbed system. We shall need the distribution function $P_0^{(n)}(1,\cdots,n)$, for $n=1,2,3$, and 4. $P_0^{(n)}$ is the probability density in the configuration space of a set of n specified molecules, averaged over the configuration space of the remaining $N-n$ molecules. Since $P_0^{(n)}$ is a distribution function for the unperturbed system, in which molecular interactions are spherically symmetric, it does not depend on the orientations. In particular, $P_0^{(2)}(1,2)=g_0^{(2)}(R_{12})/(4\pi v)^2$ where $g_0^{(2)}(R_{12})$ is the radial distribution function in the unperturbed system. In terms of the $P_0^{(n)}$, ω_1 and ω_2 are given by

$$\omega_1=N^2\int\int d\tau_1 d\tau_2 P_0^{(2)}(1,2)V^{(1)}(1,2) \tag{13}$$

and

$$\omega_2=\frac{N^4}{4}\int\int\int\int d\tau_1 d\tau_2 d\tau_3 d\tau_4[P_0^{(4)}(1,2,3,4)$$
$$-P_0^{(2)}(1,2)P_0^{(2)}(3,4)]V^{(1)}(1,2)V^{(1)}(3,4)$$
$$+N^3\int\int\int d\tau_1 d\tau_2 d\tau_3 P_0^{(3)}(1,2,3)V^{(1)}(1,2)V^{(1)}(2,3)$$
$$+\frac{N^2}{2}\int\int d\tau_1 d\tau_2 P_0^{(2)}(1,2)[V^{(1)}(1,2)]^2. \tag{14}$$

Since $P_0^{(n)}$ does not depend on orientations, the integrations over orientations may be performed directly,

$$\int d\mathbf{v}_1 V^{(1)}(1,2)=\int d\mathbf{v}_2 V^{(1)}(1,2)=0$$

$$\int\int d\mathbf{v}_1 d\mathbf{v}_2[V^{(1)}(1,2)]^2 \tag{15}$$
$$=(4\pi)^2\epsilon^2\cdot\tfrac{2}{3}\left(\frac{\mu^2}{\epsilon a^3}\right)^2\left(\frac{a}{R_{12}}\right)^6.$$

We see that $\omega_1=0$ and that ω_2 simplifies to

$$\omega_2=N^2\epsilon^2\frac{1}{3}\left(\frac{\mu^2}{\epsilon a^3}\right)^2\frac{1}{v^2}$$
$$\times\int_v\int_v d^3R_1 d^3R_2\frac{1}{R_{12}^6}g_0^{(2)}(R_{12}). \tag{16}$$

If the volume v is large compared with the range of the intermolecular potential γ, we may perform one integration over volume directly and then extend the other integral over all space, so that

$$\frac{\omega_2}{N\epsilon}=\epsilon\frac{4\pi}{3}\left(\frac{\mu^2}{\epsilon a^3}\right)^2\frac{N}{v}\int_0^\infty\frac{1}{R^4}g_0^{(2)}(R)dR. \tag{17}$$

The free energy of the perturbed system, to this order of approximation is

$$\bar{A}_N/N\epsilon=\bar{A}_N^{(0)}/N\epsilon$$
$$-\frac{2\pi}{3}\left(\frac{\mu^2}{\epsilon a^3}\right)^2\frac{1}{T^*v^*}\int_0^\infty\frac{1}{x^4}g_0^{(2)}(x)dx$$
$$+O\left(\frac{\mu^2}{\epsilon a^3}\right)^3\left(\frac{1}{T^*}\right)^2 \tag{18}$$

when we replace R/a by x and use $g_0^{(2)}(x)$ in reduced units. This equation may be differentiated to yield the reduced pressure,

$$p^*=p_0^*+\left(\frac{\mu^2}{\epsilon a^3}\right)^2$$
$$\times\left\{\frac{2\pi}{3T^*}\frac{\partial}{\partial v^*}\frac{1}{v^*}\int_0^\infty\frac{1}{x^4}g_0^{(2)}(x)dx\right\}$$
$$+O\left(\frac{\mu^2}{\epsilon a^3}\right)^3 \tag{19}$$

so that we now have an expression for p_2^* in terms of properties of the unperturbed system.

We shall now relate p_2^* to p_0^*. To do this, we shall specialize $\gamma(x)$ to the Lennard-Jones 6–12 potential,

$$\gamma(x)=4(x^{-12}-x^{-6}). \tag{20}$$

The key to the discussion is that the pressure p_0^* and the excess internal energy $\bar{E}^*$ may be expressed[5] as integrals of products of $g_0^{(2)}(x)$ and $x^3\gamma'$ or $x^2\gamma$,

$$\frac{p_0^*v^*}{T^*}=\frac{p_0v}{NkT}=\Phi_0=1-\frac{2\pi}{3v^*T^*}\int_0^\infty x^3\gamma'(x)g_0^{(2)}(x)dx \tag{21}$$

[5] Zwanzig, Kirkwood, Stripp, and Oppenheim, J. Chem. Phys. **21**, 1268 (1953).

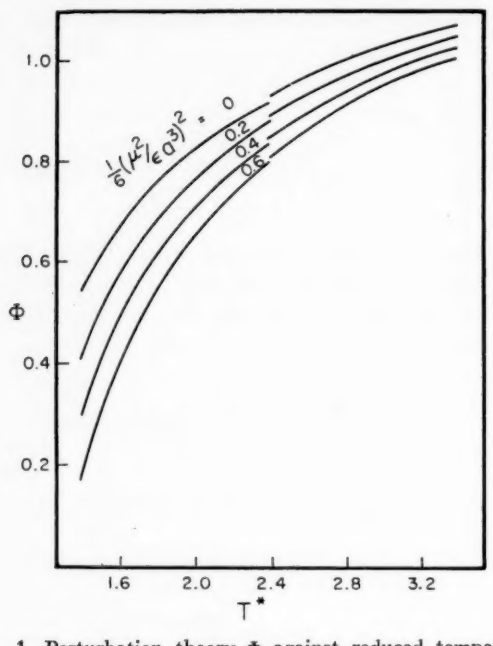

FIG. 1. Perturbation theory Φ against reduced temperature T^*, at constant density $1/v^*=0.2$, for various values of the perturbation parameter.

and

$$\bar{E}^* = (E-3NkT/2)/N\epsilon$$
$$= \frac{2\pi}{3v^*}\int_0^\infty x^2\gamma(x)g_0^{(2)}(x)dx. \tag{22}$$

We note that

$$\begin{aligned} x^2\gamma(x) &\quad 4x^{-10}-4x^{-4} \\ x^3\gamma'(x) &= -48x^{-10}+24x^{-4} \end{aligned} \tag{23}$$

so that x^{-4} may be expressed as a linear combination of $x^2\gamma$ and $x^3\gamma'$. Thus,

$$J=\frac{1}{v^*}\int_0^\infty x^{-4}g_0^{(2)}(x)dx=\frac{1}{4\pi}\left\{\frac{T^*}{4}(\Phi_0-1)-\bar{E}^*\right\} \tag{24}$$

and

$$\frac{\partial J}{\partial v^*}=\frac{1}{4\pi}\left\{\frac{T^*}{4}\frac{\partial\Phi_0}{\partial v^*}-\frac{\partial\bar{E}^*}{\partial v^*}\right\}. \tag{25}$$

The derivative of the energy may be expressed in terms of p_0^* by the well-known thermodynamic relation

$$\left(\frac{\partial E}{\partial v}\right)_T=-p+T\left(\frac{\partial p}{\partial T}\right)_v. \tag{26}$$

If we let

$$\Phi=p^*v^*/T^*=pv/NkT \tag{27}$$

for the perturbed system, we obtain finally

$$\Phi=\Phi_0+\frac{1}{6}\left(\frac{\mu^2}{\epsilon a^3}\right)^2\frac{1}{T^*}\Psi(T^*,v^*)+\cdots \tag{28}$$

where

$$\Psi=\frac{1}{4}v^*\frac{\partial\Phi_0}{\partial v^*}-T^*\frac{\partial\Phi_0}{\partial T^*}. \tag{29}$$

Thus we have accomplished the expression of p_2^* in terms of p_0^*. It is clear that the same discussion could be carried through for the potential $\gamma(x)=C_1x^{-m}-C_2x^{-6}$, and that the results will be different in detail, but of the same general form. Since the 6–12 potential is so widely used, we shall not investigate this generalization.

If we assume that the theoretical equation of state is accurate for all densities and temperatures, we may in principle compute such quantities as the vapor pressure curve. A simple calculation of the critical constants indicates how reliable the results may be. The critical temperature $T^{*(c)}$, volume $v^{*(c)}$ and pressure $p^{*(c)}$ are defined as the solution of the equations

$$\left(\frac{\partial p^*}{\partial v^*}\right)_{T^*}=0=\left(\frac{\partial^2 p^*}{\partial v^{*2}}\right)_{T^*}. \tag{30}$$

If the critical constants for the unperturbed system are $T_0^{*(c)}$, $v_0^{*(c)}$, and $p_0^{*(c)}$, and if we retain only terms of the order of $(\mu^2/\epsilon a^3)^2$, we get

$$\begin{aligned} T^{*(c)} &= T_0^{*(c)}+\frac{1}{6}\left(\frac{\mu^2}{\epsilon a^3}\right)^2+\cdots \\ v^{*(c)} &= v_0^{*(c)}-\frac{1}{24}\left(\frac{\mu^2}{\epsilon a^3}\right)^2+\cdots \\ p^{*(c)} &= p_0^{*(c)}+\frac{5}{24}\left(\frac{\mu^2}{\epsilon a^3}\right)^2+\cdots. \end{aligned} \tag{31}$$

The critical ratio

$$\Phi^{(c)}=p^{*(c)}v^{*(c)}/T^{*(c)} \tag{32}$$

is independent of any choice of ϵ and a for a nonpolar system, and depends only on $\mu^2/\epsilon a^3$ for the polar system with a Stockmayer potential. We see that

$$\Phi^{(c)}=\Phi_0{}^{(c)}\{1+O(\mu^2/\epsilon a^3)^3\} \tag{33}$$

so that in our approximation the critical ratio should be the same for a polar as for a nonpolar system. This is not borne out by experiment except in systems like carbon monoxide, where the dipole effects are entirely negligible. Of course, if this approximation leads to an incorrect critical ratio, it can hardly be trusted to lead to a reliable vapor pressure curve.

TABLE I. Φ_0 (from xenon data).

	T^*					
$1/v^*$	1.4	1.6	1.8	2.0	2.2	2.4
0	1	1	1	1	1	1
0.05	0.826	0.897	0.922	0.940	0.955	0.967
0.10	0.741	0.807	0.854	0.890	0.918	0.938
0.15	0.637	0.731	0.801	0.851	0.891	0.925
0.20	0.550	0.669	0.756	0.823	0.875	0.919
0.25	0.482	0.621	0.726	0.808	0.870	0.925
0.30	0.429	0.581	0.709	0.805	0.879	0.944
0.35	0.389	0.567	0.707	0.818	0.902	0.976
0.40	0.364	0.562	0.720	0.846	0.942	···

An experimental test of the theory falls naturally into two parts, the calculation of the functions Φ_0 and Ψ (which needs to be done only once), and the determination of the parameters μ, ϵ, and a for each system being studied.

Any system in which the Lennard-Jones 6–12 potential is a good approximation may be used to obtain Φ_0 and Ψ. The systems which are most likely to be reliable in this way are the heavy noble gases argon, krypton, and xenon. Fortunately, there is available a considerable amount of experimental equation of state data on these gases, covering a wide range of reduced temperatures and densities. The temperature ranges, in reduced units, of the data on argon[6] and xenon[7] overlap somewhat, with krypton overlapping both. Therefore, only the argon and xenon data were used. The Lennard-Jones parameters for these systems have been determined by analysis of experimental second virial coefficient data, using the 6–12 potential. They are

$$\text{Argon}^6\text{: } \epsilon/k = 119.8^\circ\text{K}, \quad Na^3 = 23.78 \text{ cc.}$$
$$\text{Xenon}^7\text{: } \epsilon/k = 224.5^\circ\text{K}, \quad Na^3 = 40.42 \text{ cc.}$$

The experimental temperatures and densities were converted to reduced variables T^* and $1/v^*$, and the product $\Phi_0 = p_0 v/NkT$ was interpolated to convenient values of T^* and $1/v^*$. The results are given in Tables I and II. The tables overlap at the temperature $T^* = 2.4$. The xenon data covers the region of the critical point. Because of the interpolation, the last digit in each value may be in error by a few units.

To compute the perturbation Ψ, the derivatives

$$v^* \frac{\partial \Phi_0}{\partial v^*} = -\frac{1}{v} \frac{\partial \Phi_0}{\partial 1/v} \tag{34}$$

and

$$T^* \partial \Phi_0/\partial T^* = T \partial \Phi_0/\partial T \tag{35}$$

TABLE II. Φ_0 (from argon data).

	T^*					
$1/v^*$	2.4	2.6	2.8	3.0	3.2	3.4
1	1	1	1	1	1	1
0.05	0.976	0.977	0.985	0.993	0.998	1.004
0.10	0.945	0.964	0.980	0.994	1.006	1.116
0.15	0.933	0.961	0.985	1.005	1.023	1.038
0.20	0.933	0.971	1.002	1.028	1.051	1.071
0.25	0.947	0.992	1.031	1.064	1.092	1.116
0.30	0.976	1.030	1.076	1.114	1.148	1.177
0.35	1.023	1.086	1.139	1.184	1.222	1.256
0.40	1.094	1.165	1.225	1.275	1.318	1.356
0.45	1.192	1.271	1.338	1.393	1.441	1.482
0.50	1.325	1.411	1.484	1.544	1.595	1.639
0.55	1.502	1.594	1.671	1.735	1.788	1.834
0.60	1.732	1.828	1.907	1.972	2.027	2.072

[6] Michels, Wijker, and Wijker, Physica **15**, 627 (1949).
[7] Beattie, Barriault, and Brierly, J. Chem. Phys. **19**, 1219, 1222 (1951).

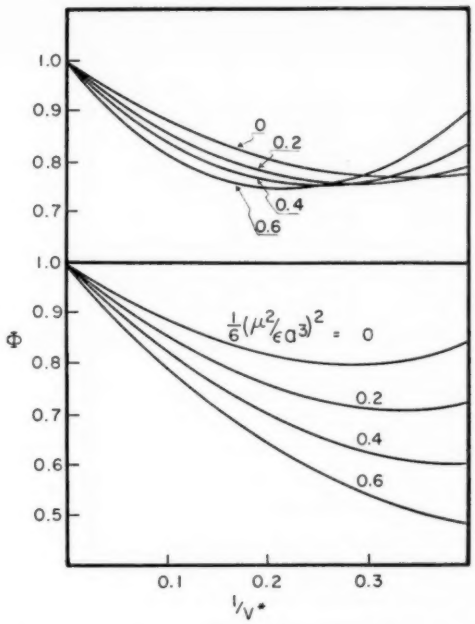

FIG. 2. Lower curves: perturbation theory Φ against reduced density $1/v^*$, at constant temperature $T^* = 2.0$, for various values of the perturbation parameter. Upper curves: Φ computed with second and third virial coefficients, under identical conditions.

were needed. The differentiations were performed numerically on the original data, before interpolation and before conversion to reduced units, by the method of Rutledge.[8] The results were then interpolated to the same values of T^* and $1/v^*$ as for Φ_0. Again, the last digit reported is possibly in error by several units.

As an illustration of the theoretical reduced equation of state obtained in this way, we have plotted in Fig. 1 the quantity $\Phi(\mu^2/\epsilon a^3)$ against T^*, for $1/v^* = 0.2$, and for various values of $(\mu^2/\epsilon a^3)^2/6$. The apparent discontinuity at $T^* = 2.4$ reflects discrepancies between the experimental data on argon and xenon, and indicates that even in this very favorable case, the principle of corresponding states is not reliable to better than a few percent. In Fig. 2 we have plotted (lower curves) Φ against $1/v^*$ at $T^* = 2.0$, for various values of $(\mu^2/\epsilon a^3)^2/6$. This figure also contains (upper curves) Φ, under the same conditions, computed using the virial expansion of the equation of state, including the second and third virial coefficients.[9] It is clear that our treatment predicts entirely different results than the third order virial expansion, at high densities. This comes about because the virial expansion is valid at all temperatures, for only sufficiently low densities, while our theory is valid presumably at all densities, for only sufficiently high temperatures.

In order to test this theory, we must have experimental equation of state date for polar gases, subject to certain restrictions. First of all, the parameter $\mu^2/\epsilon a^3$ must not be too large, or the higher order terms

[8] G. Rutledge, Phys. Rev. **40**, 262 (1932).
[9] See reference 4, pp. 1142–1154.

TABLE III. $-\Psi$ (from xenon data).

			T^*			
$1/v^*$	1.4	1.6	1.8	2.0	2.2	2.4
0	0	0	0	0	0	0
0.05	0.249	0.203	0.169	0.150	0.137	0.127
0.10	0.485	0.390	0.334	0.291	0.266	0.245
0.15	0.695	0.569	0.487	0.433	0.395	0.355
0.20	0.882	0.731	0.636	0.565	0.520	0.475
0.25	1.043	0.887	0.785	0.706	0.654	0.599
0.30	1.186	1.046	0.939	0.856	0.785	0.733
0.35	1.326	1.218	1.104	1.015	0.914	0.899
0.40	1.491	1.405	1.289	1.192	1.039	···

in the perturbation expansion, which we have neglected, may be important. It must also not be too small, or the effects of the dipoles will be negligible. (This is the case with carbon monoxide, whose dipole moment is 0.12 debye. The perturbation parameter is $\mu^2/\epsilon a^3 \approx 0.02$, and $(\mu^2/\epsilon a^3)^2/6 \approx 0.0001$ multiplies the perturbation function Ψ.) Another restriction is that the molecule should be reasonably symmetrical, so that the Lennard-Jones potential can be used for the unperturbed system. Also, the range of temperature must be such that T^* falls between 1.4 and 3.4, so that our basic tables can be used. Finally, the range of densities should be greater than that for which the third order virial expansion is sufficient, or else there would be no point in testing our theory.§ Experimental data satisfying these conditions are remarkably scarce: methyl fluoride seems to be the only dipole gas for which data satisfying the above restrictions are available. We have also applied our theory to water, partly because of the abundance of data and partly because of the intrinsic interest in the properties of water. As we have already indicated, it is optimistic to expect this theory to hold for water.

Experimental equation of state data for methyl fluoride have been obtained by Michels and co-workers.[10]

TABLE IV. $-\Psi$ (from argon data).

			T^*			
$1/v^*$	2.4	2.6	2.8	3.0	3.2	3.4
0	0	0	0	0	0	0
0.05	0.117	0.111	0.104	0.097	0.090	0.086
0.10	0.245	0.224	0.207	0.193	0.181	0.172
0.15	0.366	0.338	0.313	0.292	0.274	0.261
0.20	0.492	0.456	0.423	0.396	0.374	0.359
0.25	0.622	0.580	0.540	0.506	0.479	0.456
0.30	0.762	0.714	0.667	0.627	0.594	0.564
0.35	0.920	0.862	0.807	0.760	0.720	0.680
0.40	1.096	1.027	0.963	0.908	0.860	0.817
0.45	1.295	1.213	1.137	1.071	1.015	0.964
0.50	1.518	1.422	1.332	1.254	1.188	1.126
0.55	1.769	1.657	1.551	1.459	1.379	1.305
0.60	2.050	1.920	1.795	1.676	1.588	1.496

§ If a virial expansion is carried out on the equation of state predicted by our theory, the resulting virial coefficients are identical, to terms of order $(\mu^2/\epsilon a^3)^2$, with those obtained by direct integration using the same potential energy function.

[10] Michels, Visser, Lunbeck, and Wolkers, Physica **18**, 114 (1952).

Lunbeck and ten Seldam[11] have determined the Lennard-Jones parameters for methyl fluoride,

$$\mu = 1.82 \text{ debye}$$
$$\epsilon/k = 207°\text{K}$$
$$Na^3 = 22.9 \text{ cc.}$$
$$(\mu^2/\epsilon a^3)^2/6 = 1.554.$$

The experimental data, converted to reduced units, and compared with the predictions of our theory, is presented in Table V. At the lower densities, the pressure predicted by this theory is in error by at most a few percent. At a density of $1/v^* \approx 0.1$ (about 100 amagat units) the error is of the order of 10%, and is decreasing as the temperature increases. The error is always in the same direction: our theory over-corrects for the effect of the dipoles. (Discussion of possible causes of the error will be reserved for a later section of this article.) The highest temperature and pressure reached in this data are 150°C and 150 atmos.

Let us now consider the test of this theory on water vapor. Although the Lennard-Jones parameters for water vapor have already been determined,[12] we repeated this calculation to see how precise the results may be. The dipole moment of the water molecule (in vacuum) was recomputed from the data of Stranathan[13] using recent values of Avogadro's number, the Boltzmann constant, and the molecular weight M of water,

$$N = 6.024 \times 10^{23}$$
$$k = 1.3802 \times 10^{-16}$$
$$M = 18.015.$$

We used the expression

$$\mu^2 = 9kMb/4\pi N \tag{36}$$

and Stranathan's value

$$b = 1149.6 \pm 7.8$$

to obtain

$$\mu = 1.844 \pm 0.008.$$

It is desirable to know the dipole moment as accurately as possible, because it enters the perturbation formulae as the fourth power of μ. The procedure described by Hirschfelder *et al.*[4] for determining a and ϵ may be applied at a single temperature, provided that the experimental second virial coefficient $B_0(T)$ and its temperature derivative are known. If the Stockmayer 6–12 potential is reliable, the computed values of a and ϵ will not vary with temperature. We used the empirical equation of Keyes, Smith, and Gerry[14] for the second virial coefficient (converted from mass to mole units)

$$B_0 = 34.05 - 47591(1/T)\exp(186210/T^2) \tag{37}$$

[11] R. J. Lunbeck and C. A. ten Seldam, Physica **17**, 788 (1951).
[12] J. S. Rowlinson, Trans. Faraday Soc. **45**, 980 (1949).
[13] J. D. Stranathan, Phys. Rev. **48**, 538 (1935).
[14] N. E. Dorsey, *Properties of Ordinary Water Substance* (Reinhold Publishing Corporation, New York, 1940), pp. 78–80.

over the temperature range $T=333°K$ to $600°K$, and obtained a and ϵ at six temperatures in the range. The results were expressed by a least squares analysis as

$$\epsilon/k=310.5+19.3(10^3/T)°K \tag{38}$$

and

$$\frac{2\pi Na^3}{3}=23.85+0.32\left(\frac{10^3}{T}\right)\text{cc.} \tag{39}$$

The equation for ϵ/k is accurate to within about 1°K and the equation for $2\pi Na^3/3$ to within about 0.1 cc. Because of this variation, we may conclude that the second virial coefficient calculated with the Stockmayer 6-12 potential does not represent the experimental data over a wide temperature range.

The average of ϵ/k over the six temperatures at which this computation was performed is 358°K and the corresponding volume factor is $Na^3=11.31$ cc. Using these parameters to compute a single theoretical second virial curve, the average percentage deviation from Keyes' empirical curve is less than 1%. It is likely that some slightly different ϵ/k and its corresponding Na^3 will be just as good. This is implied by the observation of Hirschfelder *et al.*[15] that if one makes calculations of second virial coefficients with different potential energy functions $V(r)$, choosing parameters such that the integral $\int_0^\infty V(r)dr$ is about the same, then the agreement between calculations and experiment is about the same.

The perturbation parameter is

$$(\mu^2/\epsilon a^3)^2/6=2.24.$$

Figure 3 contains a comparison of the experimental equation of state of water,[14] as a function of the reduced density $1/v^*$, at a temperature $T^*=2.0$ (443°C), with the predictions of various theories. Curve A was computed from this perturbation theory. Curve B is the equation of state with the second virial coefficient only, and curve C is the equation of state with the second and third virial coefficients. At the reduced density $1/v^*=0.15$, which corresponds to an actual density of about 0.25 g/cc, the perturbation theory predicts a pressure that is about 20% too low. At lower densities, the agreement is much better.

The comparison with experimental data on water at high temperature[16] (up to 1000°C) is more uncertain. If we compute the perturbation at high temperatures using the same ϵ/k and Na^3 as at low temperatures, agreement with experiment is poor. The equation of Keyes, Smith, and Gerry for the second virial coefficient cannot be used with reliance above temperatures of about 500°C, and there is no available second virial data at higher temperatures. It is tempting to use the empirical Eqs. (38) and (39) for the variation of ϵ/k and Na^3 with temperature to perform an extrapolation to high temperatures, but there is no guarantee that this is valid. Indeed, the results obtained in this way are also poor.

[15] See reference 4, p. 206.

[16] G. C. Kennedy, Am. J. Sci. **248**, 540 (1950).

TABLE V. Test of theory on CH_3F. $\Phi^{(t)}$ (theoretical) and $\Phi^{(e)}$ (experimental) at various values of T^* and v^*.

$1/v^*$	T^*	1.66	1.77	1.89	2.00
0.036	(*e*)	0.78	0.81	0.84	0.86
	(*t*)	0.78	0.81	0.84	0.86
0.061	(*e*)	0.69	0.74	0.77	0.80
	(*t*)	0.67	0.72	0.76	0.79
0.081	(*e*)	0.62	0.67	0.72	0.76
	(*t*)	0.57	0.63	0.68	0.72
0.101	(*e*)	0.56	0.62	0.67	0.72
	(*t*)	0.48	0.55	0.61	0.66
0.121	(*e*)	0.50	0.57	0.63	0.68
	(*t*)	0.38	0.47	0.54	0.60
0.142	(*e*)	0.46	0.54	0.60	0.66
	(*t*)	0.29	0.39	0.48	0.54

In the absence of a satisfactory method of independently obtaining ϵ/k and Na^3, it was decided that the best procedure is to regard these parameters as adjustable, and to select their values so that the best over-all agreement is obtained between the perturbation theory and experiment. This procedure requires an involved sequence of interpolations and successive approximations, since the perturbation parameter $\mu^2/\epsilon a^3$ depends on ϵ and a. (We have kept the dipole moment μ as a given constant, so that this is strictly

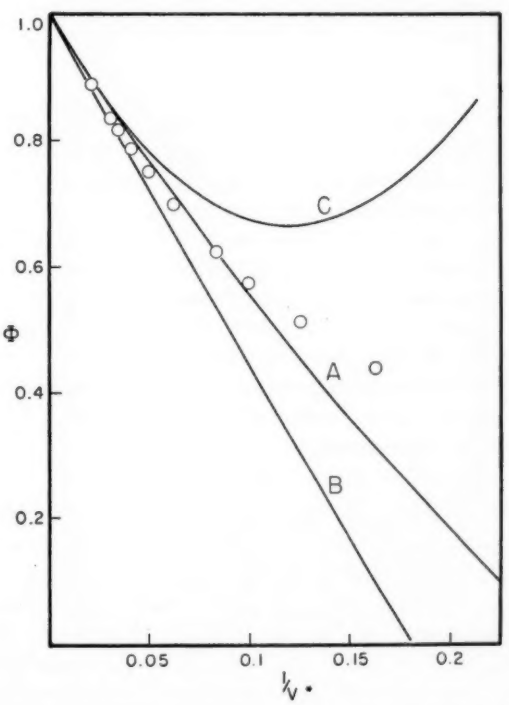

FIG. 3. Comparison of experimental (circled) and theoretical equations of state of water, at $T^*=2.0$. Curve A is perturbation theory; Curve B was computed with theoretical second virial coefficient; Curve C was computed with theoretical second and third virial coefficients.

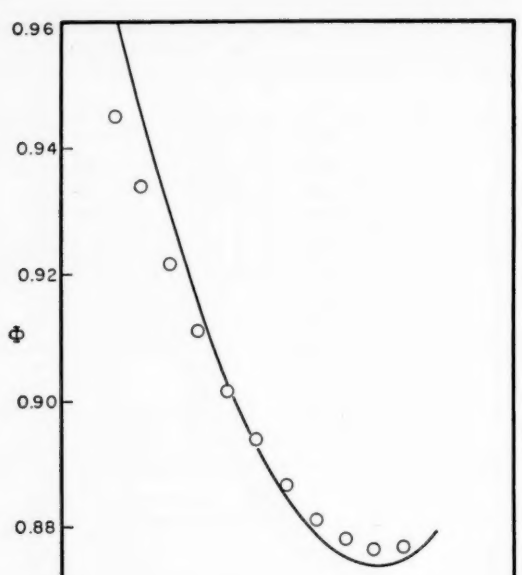

FIG. 4. Comparison of experimental (circled) and perturbation theory equations of state of water, at $T^*=3.0$.

a two-parameter approach.) Without going into the details of this computation, the results are:

$$\epsilon/k = 351°\text{K}$$
$$Na^3 = 17.0 \text{ cc}$$
$$(\mu^2/\epsilon a^3)^2/6 = 0.388$$

at the temperature $T^*=3.0 (T=1053°\text{K})$. The temperature factor ϵ/k has not been changed appreciably, but the volume factor Na^3 is 50 percent higher than at the lower temperatures, and the perturbation parameter, which varies as the square of Na^3 is quite different. The theoretical and experimental equations of state are compared in Fig. 4. The agreement is good; the computed pressure deviates from the experimental pressure by less than 1% over most of the density range. The poorer agreement at very low densities is due in part to the choice of the a and ϵ which give the best over-all agreement.

IV

We have already discussed some of the reasons why the perturbation theory might fail. We shall now consider these reasons in the light of the actual agreement between theory and experiment. First, the Stockmayer potential may not be reliable. It undoubtedly is not, in the case of water, for reasons which have already been discussed. For methyl fluoride, one might expect the potential to be good. The quadrupole moment is probably negligible, the molecule is roughly spherical, and there are no specific interactions of the hydrogen bond type. The perturbation parameters for the two molecules differ by less than an order of magnitude, so that the perturbation series expansions should converge about equally fast. It appears, then, that the apparent inadequacy of the Stockmayer potential for water is not serious at $T^*=2$, since the final results for water and methyl fluoride are about equally good.

At the temperature $T^*=2$, the perturbation theory deviates from experiment at high densities. If the Stockmayer potential is applicable at all densities, and if the spherically symmetric Lennard-Jones 6–12 potential is valid for argon and xenon at all densities, then the perturbation theory should be exact at all densities, provided that the temperature is sufficiently high. We do not know that the rate of convergence of the perturbation series is the same at all densities, and our results indicate that it is slower at high densities. This point will arise in all applications of the general statistical mechanical perturbation theory, and should be investigated further.

Another possible cause of the poorer agreement between our calculations and experiment at high densities is that we have not taken account of molecular polarizabilities. One way of doing this, which is not rigorous but which is easy to accomplish, is to put into the Stockmayer potential the actual dipole moment of the molecule, which is different from the vacuum moment because of intermolecular interactions. We have made some rough calculations, using Onsager's[17] theory of dielectrics. We first compute the dielectric constant D according to

$$D-n^2=\frac{3D}{2D+n^2}\frac{4\pi N_0}{3kT}\left(\frac{n^2+2}{3}\right)^2\mu^2 \qquad (40)$$

where μ is the vacuum moment and n is the index of refraction (obtainable using the Clausius-Mosotti equation). We then compute the actual moment μ',

$$\mu'=\frac{2D+1}{2D+n^2}\frac{n^2+2}{3}\mu. \qquad (41)$$

The actual moment μ' increases with density. For example, at a temperature $T^*=3.4$ and a density $1/v^*=0.2$, μ' of water is about three percent higher than its vacuum value. This means that the perturbation parameter increases with density. We have observed that at high densities the perturbation theory already overcorrects for the effect of the dipoles: the polarizability correction makes the situation still worse. Although it is theoretically more satisfactory to make this correction, agreement is better when it is omitted.

ACKNOWLEDGMENT

Many of the computations described in this article were performed by Theodore Einwohner and Richard J. Plock.

[17] H. Frohlich, *Theory of Dielectrics* (Oxford University Press, London, 1949), pp. 32–35.

Liquid Metals. II. X-Ray Diffraction by Liquid Mercury and the Distance of Closest Atomic Approach

JOSEPH S. LUKESH, WILLIAM H. HOWLAND, LEO F. EPSTEIN, AND MARION D. POWERS*
General Electric Company, Knolls Atomic Power Laboratory,† Schenectady, New York

(Received January 10, 1955)

The distance of closest approach in mercury determined from vapor viscosity data, 3.25 A, differs considerably from the value found by x-ray and neutron diffraction studies on liquid Hg, 3.00 A. This x-ray value has been confirmed using a balanced filter-spectrometer technique and all the essential features of the intensity *versus* Bragg angle curve observed in previous studies have been verified except the low angle peak reported by Campbell and Hildebrand. The discrepancy between the two r_0 values is attributed to the probable persistence of the asymmetrical structure known to exist in the solid into the liquid phase, and its subsequent vanishing in the vapor state.

IN the first paper of this series[1] a detailed study of mercury, both liquid and vapor, led to the conclusion that the vapor viscosity, equation of state, and other properties of this material could be adequately represented by a Lennard-Jones 6–9 potential function with $\epsilon/k=775\pm20°$K and $r_0=3.25\pm0.04$ A. This last figure, the equilibrium distance of closest approach in Hg, is in excellent agreement with the value, 3.23 A, found in the classical x-ray diffraction studies on the liquid by Debye and Menke,[2] but differs considerably from the results found in subsequent x-ray studies. Boyd and Wakeham[3] obtained 2.87 A; Campbell and Hildebrand,[4] 3.00 A; Kerr and Lund's[5] analysis of Campbell and Hildebrand's data, 2.97 A; Hendus[6] has also recently found 3.0 A. It will be noted that there is some disagreement between these various x-ray measurements. Further, all of them with the exception of the Debye and Menke figure lie far below the value of 3.25 A obtained from the potential function derived from the mercury vapor viscosity. In previous comparisons of this sort with other substances, x-ray studies and measurements of the vapor properties have led to excellent agreement: with argon, for example, the Eisenstein and Gingrich (x-ray) data[7] yield an r_0 of 3.76 to 3.80 A, depending upon the technique of evaluation; while Hirschfelder, Bird, and Spotz[8] from viscosity data obtained 3.827 A. Because of the differences among the various results with mercury, it was felt desirable to repeat the x-ray diffraction work, using a Geiger-counter technique.

High purity mercury (seven times distilled) was contained at a constant temperature of $50\pm0.1°$C in a cell adapted to a Philips diffractometer. The cell consisted of a copper block equipped with "Calrod" heating units and water cooling tubes mounted so that the surface of a pool of mercury held in a recess in the copper block (to prevent contamination of the mercury, the recess was lined with a steel cup) was aligned with the axis of rotation of the goniometer. The mercury was covered with a 0.15 mm sheet of beryllium. A flat surface of mercury was thus presented to the x-ray beam at all angles and in the correct position for proper focusing.

The intensity of the diffracted radiation was measured over the entire significant range of $\sin\theta/\lambda=0.056$ to about 0.800. The principal radiation used was molybdenum, monochromatized by use of a balanced filter system of zirconium and strontium oxide. For very small values of 2θ, copper radiation filtered with nickel foil was employed. (Although filter techniques eliminate the harmonics of the K_α line, the applied potential was kept low enough to prevent their excitation.) It is of interest to note that the fluorescent radiation excited in mercury by the molybdenum K_α line constituted no problem in this work since the diffracted x-rays were detected with a Krypton filled Geiger tube. Krypton has an absorption edge at 0.8637 A, thus eliminating all of the long-wave fluorescent radiation.

The diffraction pattern obtained under the conditions described above did not differ significantly from that of Hendus or from that of Campbell and Hildebrand, with one exception to be discussed below. Because of the close agreement, it was considered unnecessary to calculate the radial distribution function. It may be concluded that the experimentally determined distance of closest approach, 3.0 A, is correct. The early determination of Debye and Menke may be discounted because of the improved experimental techniques used by later investigators and because of the agreement of the independent investigations of Campbell and Hildebrand, Hendus, and this study. In addition, the more

* Present address: Remington-Rand Corporation, New York, New York.

† The Knolls Atomic Power Laboratory is operated by the General Electric Company for the United States Atomic Energy Commission under Contract No. W-31-109 Eng. 52.

[1] L. F. Epstein and M. D. Powers, J. Phys. Chem. **57**, 336 (1953).

[2] P. Debye and H. Menke, Ergeb. d. tech. Rontgenk II 1 (1931). See also N. S. Gingrich, Revs. Modern Phys. **15**, 90 (1943).

[3] R. N. Boyd and H. R. R. Wakeham, J. Chem. Phys. **7**, 958 (1939). See also Hildebrand, Wakeham, and Boyd, J. Chem. Phys. **7**, 1094 (1939).

[4] J. A. Campbell and J. H. Hildebrand, J. Chem. Phys. **11**, 330 (1943).

[5] R. H. Kerr and L. H. Lund, J. Chem. Phys. **19**, 50 (1951).

[6] H. Hendus, Z. Naturforsch. **3A**, 416 (1948).

[7] A. S. Eisenstein and N. S. Gingrich, Phys. Rev. **62**, 261 (1942).

[8] Hirschfelder, Bird, and Spotz, Trans. Am. Soc. Mech. Engrs. **71**, 921 (1949).

recent work of Vineyard[9] by neutron diffraction leads to the same result of 3.00 A.

Campbell and Hildebrand[4] report two main peaks in their intensity curve, one at $\sin\theta/\lambda$ approximately equal to 0.100, and a more pronounced one at 0.191. Hendus[6] did not observe the weaker peak, nor did Vineyard[9] in his neutron diffraction study of liquid mercury. Gingrich and Gamertsfelder[10] are reported to have observed the low angle maximum. Gingrich[11] questions its reality however. It was about one-third to one-fourth as large as Campbell and Hildebrand found, and the pattern was obtained under conditions which would enhance a spurious peak. Such peaks have been discussed by Gregg and Gingrich.[12] No evidence for the 0.100 maximum was found in the present study, but the position of the peak at 0.191 has been confirmed.

The discrepancy between the vapor viscosity value of $r_0=3.25$ A and the experimental x-ray result 3.00 A probably arises because of the assumption, in the theoretical analysis that Hg consists of a radially symmetrical structure. Solid Hg has been shown to be rhombohedral,[13] with six nearest neighbors at a distance of 3.00 A and six next nearest neighbors at 3.47 A, and is therefore highly asymmetrical. In the liquid, at low temperatures, it is to be expected that some remnants of the solid structure will persist, and this is confirmed by the close agreement between the liquid and the solid values of r_0. The radial distribution function obtained by Hendus[6] also shows a small peak at about 3.47 A, although this has not been confirmed by other workers. Solid structure may persist even in the vapor, and the latter may be thought of as an equimolar mixture of two species, one with $r_0^{(1)}=3.00$ A, the second with $r_0^{(2)}=3.47$ A. The usual technique in the computation $r_0^{(12)}$, the parameter for a mixture of two gases, 1 and 2, is to use the arithmetic mean,[14] which is in this case

$$r_0^{(12)}=\tfrac{1}{2}[r_0^{(1)}+r_0^{(2)}]=3.24 \text{ A},$$

and this will be seen to give excellent agreement with observation. Alternately, it may be postulated that in the vapor at high temperatures (on which the potential function computations are for the most part based) thermal agitation is quite effective in redistributing the atoms, so that a radially symmetrical model with an $r_0^{(12)}$ which is the mean of the two distances obtained in the solid is found. It will be noted that these two alternative hypotheses—(1) persistence of the solid configuration into the vapor phase and (2) complete elimination of asymmetrical solid structure in the gas—both lead to identically the same result so far as $r_0^{(12)}$ is concerned, and there appears to be no basis for objectively deciding between them from the present observations. But the persistence of the radial asymmetry of the mercury atoms, which exists in the solid and possibly the liquid, into the vapor phase seems rather unlikely, and the alternative hypothesis above, i.e., complete obliteration of the radial anisotropy in the gas, appears to be a far more palatable postulate. In solid argon, which is cubic with $r_0=3.82$ A, there is no radial asymmetry in the solid, liquid, or gas, and the agreement between the r_0 values obtained in x-ray and other types of measurement on these phases is a direct consequence of the simple spherically symmetrical configuration of the atoms in this material.

[9] G. H. Vineyard, J. Chem. Phys. **22**, 1665 (1954).
[10] N. S. Gingrich and C. C. Gamertsfelder, private communication quoted by Campbell and Hildebrand in reference 4.
[11] N. S. Gingrich, private communication.
[12] R. Q. Gregg and N. S. Gingrich, Rev. Sci. Instr. **11**, 305 (1940).
[13] R. W. G. Wyckoff, *Crystal Structures* (Interscience Publishers, Inc., New York, 1948), Vol. I. Chap. II, p. 7.
[14] J. A. Beattie and W. H. Stockmayer, Repts. Progr. in Phys. **VII**, 195 (1940).

Grüneisen's Constant for Some Metals

J. J. GILVARRY
The RAND Corporation, Santa Monica, California
(Received December 29, 1954)

The Grüneisen constants, as evaluated from compressibility parameters, are redetermined for the alkali metals Li, Na, and K and are determined for Rb and Cs from experimental data of Bridgman, and are shown to be in good agreement with the corresponding values as evaluated from Grüneisen's law. In the cases of Au, Mo, Ta, and Mn, previous work by Slater had shown a large discrepancy between these two evaluations of the Grüneisen constant. The discrepancy is largely removed for Au by a redetermination of the Grüneisen constant from more recent compressibility data of Bridgman. The disagreement persists for Mo (to some degree), and for Ta (where the disparity is large); the results for Mn are inconclusive. A redetermination for Al brings closer agreement than previously between the two evaluations of the constant. The bearing of the results for compressibility parameters on some semiempirical equations of state is indicated.

THE Grüneisen constant γ is the negative exponent of the volume v in the statement of the approximation that the normal frequencies of vibration of a crystal all vary as $v^{-\gamma}$. On this assumption, Grüneisen[1] has derived the equation (Grüneisen's law)

$$\gamma=\alpha v/aC_v, \tag{1}$$

where α is the coefficient of thermal expansion, a is the compressibility, and C_v is the heat capacity at constant volume v. Experimental values of γ derived from the relation (1) will be designated by γ_G. Slater[2,3] has shown that γ can be evaluated likewise from compressibility parameters as

$$\gamma=b/a^2-2/3, \tag{2}$$

where the coefficient b is defined by the equation of state

$$-(v-v_0)/v_0=aP-bP^2+\cdots, \tag{3}$$

in which P is the pressure and v_0 is the normal volume. The coefficients a, b, $\cdots$ are functions of temperature, in general, but Eq. (2) should hold regardless of this fact, since γ is nearly independent of temperature.[4] The notation γ_S will be used for experimental values of γ derived from compressibility parameters by means of Eq. (2).

Prior to 1940, agreement was very poor in the case of the less compressible metals[4] between values of γ_G and values of γ_S derived from experimental data of Bridgman. In that year, a redetermination by Bridgman[5] of the coefficient b for the fiducial material iron permitted Slater[2] to correct Bridgman's values of b for the less compressible metals. Essential agreement between γ_G and the revised value of γ_S was obtained in nearly all cases. The outstanding exceptions were gold, molybdenum, tantalum, and manganese. This work led Slater to conclude that experimental values of the coefficients a and b should be questioned if the corresponding γ_S differed violently from γ_G (exact agreement is not demanded by theory).

In Slater's tabulation, the agreement of γ_S and γ_G for the alkali element Li is merely fair (they differ by a factor nearly $\frac{1}{2}$). Values of γ_S for the alkali elements Rb and Cs are omitted, presumably because of disagreement between γ_S and γ_G. Since the time of Slater's work Bridgman has redetermined the compressions of the alkali metals to higher accuracy. Furthermore, he has redetermined to higher accuracy the compressions of the discrepant elements Au, Mo, and Ta, and of the element Al for which agreement is only fair (γ_S differs from γ_G by a factor nearly $\frac{1}{2}$ in Slater's list). A redetermination, but not to as high an accuracy as for the other elements mentioned, has been carried out likewise for Mn. The purpose of this note is to examine the implications of this later experimental work of Bridgman on the validity of Grüneisen's law, with respect to the alkali metals and the discrepant elements in Slater's compilation.

In Table I, the values of a (old) and b (old) obtained by Slater are tabulated for the elements in question,

TABLE I. Old values of compressibility parameters and Grüneisen constants.

	a (old) bar^{-1}	b (old)[a] bar^{-2}	γ_S (old)[a]	γ_G[c]	a_G[c] bar^{-1}
Li	8.70×10^{-6}[a]	98.0×10^{-12}	0.63	1.17	8.9×10^{-6}
Na	15.6[a]	610.	1.83	1.25	15.8
K	36.[a]	4100.	2.55	1.34	33
Rb	53.0[b]	...	...	1.48	40
Cs	71.0[b]	...	...	1.29	61
Al	1.32[a]	3.37	1.27	2.17	1.37
Au	0.578[a]	$\binom{0.8}{1.8}$	$\binom{1.8}{4.8}$	3.03	0.59
Mo	0.347[a]	(−0.1)	(−1.5)	1.57	0.36
Ta	0.478[a]	(−1.1)	(−5.)	1.75	0.49
Mn	0.806[a]	(4.0)	(5.8)	2.42	0.84

[a] Slater (references 2 and 3).
[b] Birch, Schairer, and Spicer, *Handbook of Physical Constants* (Geological Society of America, New York, 1942), p. 43 (values refer to 50°C).
[c] Grüneisen (reference 1).

[1] E. Grüneisen, in *Handbuch der Physik* (Springer-Verlag, Berlin, Germany, 1926), Vol. X, p. 27.
[2] J. C. Slater, Phys. Rev. **57**, 744 (1940).
[3] J. C. Slater, *Introduction to Chemical Physics* (McGraw-Hill Book Company, Inc., New York, 1939), p. 450.
[4] N. F. Mott and H. Jones, *Properties of Metals and Alloys* (Oxford University Press, London, 1936), p. 20.
[5] P. W. Bridgman, Phys. Rev. **57**, 235 (1940). The redetermination was confirmed in later work [P. W. Bridgman, Proc. Am. Acad. Arts Sci. **77**, 187 (1949)].

TABLE II. Revised values of compressibility parameters and Grüneisen constants.

	a (bar^{-1})	b (bar^{-2})	γ_S[a]	γ_G(rev.)	$2b/a^{2}$[a]
Li	$8.65_0\times10^{-6}$	$164._3\times10^{-12}$	1.53_0	1.20	4.39_3
Na	14.4_7	$388._3$	1.18_8	1.37	3.70_9
K	31.4_8	194_4.	1.29_5	1.41	3.92_4
Rb	31.8_0	158_5.	0.900_7	1.86	3.13_5
Cs	49.2_8	439_4.	1.14_2	1.60	3.61_8
Al	1.38_6	5.05_9	1.96_7	2.15	5.26_8
Au	0.577_5	0.831_6	1.82_7	3.10	4.98_7
Mo	0.36_7	0.16_0	0.52_3	1.54	2.3_8
Ta (99.9% pure)	0.49_9	0.23_9	0.29_6	1.72	1.9_2
(99.95+% pure)	0.49_5	0.10_7	(-0.23_2)	1.73	0.87_0
(2:1 average)	0.49_8	0.19_5	0.12_2	1.72	1.5_8
Mn	$(1._{68})$	$(8._{45})$	$(2._{34})$	(1.21)	$(6._{02})$

[a] Rounded after computation from unrounded a and b.

with the corresponding values of γ_S (old). The value of γ_G from Grüneisen is likewise shown, as is a_G, the value of a used by Grüneisen in evaluating γ_G. Parenthetic values of b and γ_S correspond to discrepant elements. The tabulated values of b for Mo and Ta are Bridgman's values with Slater's correction; the corrected values are negative (which Slater viewed as implausible), as is γ_S. The two values of b for Au correspond to measurements on two different specimens.

Bridgman[6] gives the compressions of the alkali metals to four figures at main intervals of $5\cdot10^3$ kg/cm^2 over a pressure range up to $4\cdot10^4$ kg/cm^2 (in the case of Cs, the useful pressure range extends up to $2\cdot10^4$ kg/cm^2 only, since a polymorphic transition exists at 23 300 kg/cm^2). These data[7] have been fitted to a polynomial in P of the form (3), by means of a least-squares procedure.[8] The coefficients a and b corresponding to P in bars are tabulated in Table II for each alkali element, with the corresponding value of γ_S and a revised value γ_G (rev.) of γ_G defined by $(a_G/a)\gamma_G$. One notes that the revised values of the compressibility parameters reduce the percentage difference between γ_S and γ_G for the three cases Li, Na, and K in which values of γ_S were given by Slater, and that γ_S and γ_G are in reasonable agreement for Cs and in fair agreement for Rb. The values of a and b for Rb seem out of sequence in the progression of values in the alkali metal family, and values of the parameters for Rb are open to some doubt on this score.

From a set of relatively accurate experiments, designed specially to measure the deviation of the compression from linearity with pressure, Bridgman reports compression values[9] to three (or four) figures for the elements Al, Au, Mo, and Ta, at intervals of $5\cdot10^3$ kg/cm^2 over a pressure range up to $3\cdot10^4$ kg/cm^2. The coefficients a and b for these elements[10] with the corresponding values of γ_S and γ_G (rev.), are tabulated in Table II. One notes that the agreement for Al is improved. The values of b and γ_S for Au coincide with the smaller of the two previous values in each case; the value of γ_S is in reasonable agreement with γ_G.

The revised coefficients b are positive for both Mo and Ta. The value of γ_S is positive for a specimen of Ta reported to Bridgman as 99.9% pure, but the value for a specimen reported 99.95+% pure is negative. Bridgman states it is "probable that the second-order term of the less pure specimen should be given greater significance," on grounds of the treatment and behavior of the two specimens in the experiment. On this basis the two values of a and b for Ta have been averaged with a weight of two to one in favor of the less pure specimen, to yield the averages and corresponding value of γ_S tabulated in Table II. Note that an average with equal weight for the two specimens would yield a positive γ_S also. Aside from this question of sign, the value of γ_S for Ta corresponding to the average in Table II disagrees strongly (by a factor of about $\frac{1}{15}$) from γ_G. The value of γ_S for Mo is somewhat in disagreement (by a factor about $\frac{1}{3}$) from γ_G.

It is clear that the large discrepancy between γ_S and γ_G for Ta is of a different order of magnitude than the relatively small differences between these quantities for the other elements (except Mo) tabulated. The disagreement does not seem traceable purely to the smallness of the coefficients a and b in this case, since Au, for which a and b are not greatly different from

[6] P. W. Bridgman, Proc. Am. Acad. Arts Sci. **76**, 71 (1948).

[7] Unless otherwise noted, all data quoted correspond to room temperature (20 to 26°C).

[8] The values of a and b obviously depend on the number n of terms taken in Eq. (3). Use of Gauss' criterion [A. G. Worthing and J. Geffer, *Treatment of Experimental Data* (John Wiley and Sons, Inc., New York, 1943), p. 260] to determine n was deemed inadvisable, since it assigns equal weight to each data point, whereas coefficients evaluated at zero pressure are desired. To prevent over-emphasis of the higher pressures, the value $a(n)$ of a as a function of n was compared with the value obtained by numerical differentiation of the data. It was found that $a(n)$ converged toward the value obtained by numerical differentiation and then diverged, in general. The value of n corresponding to the stationary point was taken; the value was 6, 7, 9, 8, and 4 in the cases Li, Na, K, Rb, and Cs, respectively, as against the values 5, 4, 5, 7, and 5, respectively, corresponding to use of Gauss' criterion. However, the values of a, and of b, on the two criteria are not very different. The fractional error in the fit, defined as the ratio of the root-mean-square error in $-(v-v_0)/v_0$ to the average value, was about 0.3% on the average.

[9] P. W. Bridgman, Proc. Am. Acad. Arts Sci. **77**, 187 (1949).

[10] A two-term fit was made (the fractional error in the fit was about 0.1% on the average).

those for Ta, yields a value of γ_S in reasonable agreement with γ_G. The unusually small magnitude of b for Ta (and Mo) seems consistent with the fact that previous determination yielded the sign as negative. Hence, the possibility exists that Grüneisen's γ_G is in error in the sense of being too large. Tantalum and molybdenum are the metallic elements of lowest thermal expansion, exclusive of tungsten; hence experimental inaccuracy in the small coefficient may possibly be the source of the discrepancy. It is impossible to say, therefore, whether there exists a real failure of Grüneisen's law for Ta (or Mo).

In the case of manganese, Bridgman gives compressions[11] to two figures at a pressure of $25\cdot10^3$ kg/cm^2 and at intervals of 10^4 kg/cm^2 over a pressure range from $3\cdot10^4$ to $10\cdot10^4$ kg/cm^2. The coefficients a and b are given[12] in Table II. The value of a differs from a (old) by a factor of somewhat more than two. Since the values of a and a (old) show only small differences in all other cases (except Rb), this fact makes the values of a and b uncertain (as indicated by parenthetic entries in the table). In spite of this discrepancy, the values of γ_S and γ_G (rev.) are in fair agreement.

It should be pointed out that an evaluation of γ from compressibility parameters, differing from that of Slater, has been given by Dugdale and MacDonald.[13] Their result can be expressed as $\gamma_S-\frac{1}{3}$ in terms of Slater's value (2) of γ. One notes that this result would yield a negative value of γ from both specimens of Ta. Further, its use would reduce sharply the over-all agreement with γ_G in Table II. Another evaluation of γ from compressibility parameters (as $\gamma_S+\frac{1}{2}$) has been given likewise by Mott and Jones[4]; one can note that this result would bring all values in Table II within at least roughly fair agreement with γ_G, and would retain reasonable agreement for the other elements in Slater's tables.

The last column of Table II contains a tabulation of the quantity $2b/a^2$ for each element. This dimensionless parameter is of some importance in connection with semiempirical equations of state. From Murnaghan's theory of finite strain,[14] Birch[15] has derived the equation of state

$$P=(3/2a)[(v_0/v)^{7/3}-(v_0/v)^{5/3}], \qquad (4)$$

which he has used widely in geophysical applications to extrapolate compression data for many elements and compounds beyond the experimental range.[16] In large part, he has justified this procedure in the case of the less compressible metals from the fact that Eq. (4) represents well the data of Bridgman for the highly compressible alkali metals. Birch's equation predicts $2b/a^2=5$, which coincides with the average value of this parameter (over most materials) given by Slater as 5. However, the average value of $2b/a^2$ for the alkali metals is 3.76 from Table II.

In Eq. (4), a factor $1-\xi[(v_0/v)^{2/3}-1]$ in P, arising from higher order terms, is neglected; this factor must be retained to obtain agreement with the data in the cases of solid hydrogen and deuterium[17] and of some compounds. If the disposable constant ξ is chosen to yield $2b/a^2=3.76$ for the alkali metals, one obtains $\xi\sim1$, with which value the corrected equation yields pressures too low by a factor of about one-half at the highest compressions. Thus, Birch's equation can not be made fully consistent with the data for these metals. Further, a semiempirical equation of state

$$P=(3/a)[(v_0/v)^{5/3}-(v_0/v)^{4/3}], \qquad (5)$$

proposed by Bardeen[18] on quantum-mechanical grounds for the alkali metals, yields $2b/a^2=4$, which is close to the average noted above for the alkali metals. Some objection has been raised to the universality of application, as made by Birch, of Eq. (4) to different metals and compounds.[19] The considerations here seem to indicate that Bardeen's equation is preferable to Birch's for small compressions of the alkali metals, and thus sustain to some degree the objection mentioned.

In conclusion, it appears that tantalum is the only metal showing violent disagreement with Grüneisen's law, on the basis of present data. A minor discrepancy persists for molybdenum, and no statement can be made for manganese. This work leads to significant revisions of the compressibility parameters of a number of elements, and the corresponding values in the compilation of Waser and Pauling[20] should be revised accordingly.

The author wishes to thank Professor W. G. McMillan of the University of California, Los Angeles, and Dr. R. Latter of the RAND Corporation, for a number of helpful discussions. Thanks are due to Miss E. Force for the computational work.

[11] P. W. Bridgman, Proc. Am. Acad. Arts Sci. **76**, 55 (1948).
[12] A two-term fit was made (the fractional error in the fit was about 0.3%). As a check, an attempt was made to fit the data with $a=a$ (old) but b disposable in Eq. (3); it proved impossible to obtain even a rough two-term or three-term fit in this manner. Because of the high incompressibility of this metal, the lack of data below a pressure of $25\cdot10^3$ kg/cm^2 should not affect the value of a seriously.
[13] J. S. Dugdale and D. K. C. MacDonald, Phys. Rev. **89**, 832 (1953).
[14] F. D. Murnaghan, Am. J. Math. **59**, 235 (1937); Proc. Natl. Acad. Sci. **30**, 244 (1944).
[15] F. Birch, Phys. Rev. **71**, 809 (1947).
[16] F. Birch, J. Geophys. Research **57**, 227 (1952).
[17] J. W. Stewart and C. A. Swenson, Phys. Rev. **94**, 1069 (1954).
[18] J. Bardeen, J. Chem. Phys. **6**, 372 (1938). A factor nearly unity has been neglected in Eq. (5) above.
[19] J. Verhoogen, J. Geophys. Research **58**, 337 (1953).
[20] J. Waser and L. Pauling, J. Chem. Phys. **18**, 747 (1950).

Steady-State Burning of a Liquid Droplet. I. Monopropellant Flame*

JACK LORELL AND HENRY WISE†
Jet Propulsion Laboratory, California Institute of Technology, Pasadena 3, California
(Received December 13, 1954)

The flame equations corresponding to the steady-state combustion of a liquid droplet are presented and adapted to the case of a monopropellant system with chemical reaction diffused throughout the gas phase. The theoretical analysis is applied to the case of a liquid hydrazine monopropellant flame.

1. INTRODUCTION

THE subject of steady-state flame propagation in homogeneous media has been studied rather intensively in recent years, culminating in the work of Boys and Corner[1,2] and Hirschfelder.[3,4] These investigators concentrated on the linear one-dimensional steady flame in a duct of constant cross-sectional area. Extension of this work to the study of flame propagation in heterogeneous media, i.e., liquid or solid spheres in a gaseous atmosphere, involves two points of departure from the homogeneous case: the linear one-dimensional model is replaced by a three-dimensional, spherically symmetric one, and a finite cold boundary corresponding to a liquid-vapor or solid-vapor interface exists which replaces Hirschfelder's flame holder[3,4] required for mathematical reasons rather than physical necessity.

Two cases of droplet combustion are investigated, (1) a one-component system in which the reactant evaporates from a spherical droplet and then gradually decomposes exothermically in the vapor phase, and (2) a two-component system‡ in which one reactant evaporates from a spherical droplet into an atmosphere containing the other, resulting in a diffusion flame located at some distance from the liquid surface.

The mathematical formulation of the heterogeneous monopropellant combustion process differs from that of the one-dimensional, homogeneous flame propagation,[2] because of the spherical symmetry and the cold boundary conditions of the present model. The development is simplified to the extent that the effects of variable heat capacity and thermal conductivity are not included. It is felt that such effects are secondary in importance to the basic simplifying assumptions for the model. Thus, the emphasis in the present development is on mathematical simplicity consistent with the accuracy of the physical model.

2. GENERAL FLOW EQUATIONS

The physical systems to be studied are essentially gas-phase, steady-state flow, multicomponent systems with diffusion of species and transfer of energy by heat conduction. In addition, heat generation throughout the gaseous medium occurs, as a result of the exothermic chemical reactions. For simplicity the discussion is limited to the one-dimensional variable area flow case, i.e., a system in which the properties of the fluid are functions of a single-space coordinate r, and therefore uniform over parallel planes. However, as formulated, this analysis includes the two-dimensional, cylindrically symmetric, and the three-dimensional, spherically symmetric systems since these last two cases depend on only one independent space variable.

In Fig. 1, the three types of one-dimensional flow are illustrated. In a coordinate system fixed with respect to the cold boundary, the gases flow from the cold boundary at $r=r_l$ outward towards infinity ($r=r_0$) where the properties of the fluid are indicated by a subscript zero. At an arbitrary surface with coordinate r, the transport of mass and enthalpy is determined by

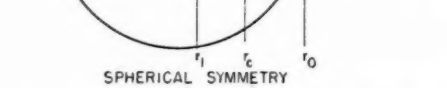

ONE-DIMENSIONAL FLAME

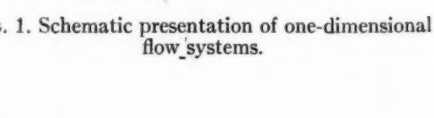

CYLINDRICAL SYMMETRY

SPHERICAL SYMMETRY

FIG. 1. Schematic presentation of one-dimensional flow systems.

* This paper presents the results of one phase of research carried out at the Jet Propulsion Laboratory, California Institute of Technology, under Contract No. DA-04-495-ORD 18, sponsored by the Department of Army, Ordnance Corps.
† Present address: Stanford Research Institute, Menlo Park, California.
[1] Boys and Corner, Proc. Roy. Soc. (London) **A197**, 90 (1949).
[2] J. Corner, Proc. Roy. Soc. (London) **A198**, 388 (1949).
[3] Hirschfelder and Curtiss, J. Phys. & Colloid Chem. **55**, 774 (1951).
[4] Hirschfelder and Curtiss, J. Chem. Phys. **17**, 1076 (1949).
‡ See paper II in this series (to be published).

the hydrodynamical equations for the conservation of mass and energy.§

$$\dot{m}_j=\dot{M}_j+\dot{m}z_j=A\rho v(Y_j-D_jY'_j/v)\ j=1,2,\cdots n \quad (2.1)$$

$$\sum_{j=1}^{n}\dot{m}_jh_j-A\lambda t'=\text{constant} \quad (2.2)$$

in which $\dot{m}_j$ is the mass flow rate of species j at position r; $\dot{m}$, the total mass flow rate, and $\dot{M}_j$, the mass flow rate of j at the liquid surface, a constant determined by the boundary conditions.

The variables in Eqs. (2.1) and (2.2) are subject to the restraints

$$\sum Y_j=1;\ 0\leq Y_j. \quad (2.3)$$

The weight fraction of flow contributed by component j is given by the sum $(Y_j-D_jY'_j/v)$ composed of the mass transport by movement of the fluid and mass transfer by diffusion. The parameter z_j represents the weight fraction of component j resulting from chemical reaction in the region from r_l to r; thus,

$$z_j=\int_{r_l}^{r}(R_j/v)dr \quad (2.4)$$

where R_j represents the rate of chemical production of species j, i.e., following the motion of an element of fluid, the reaction rate is $R_j=Dz_j/D\tau=\partial z_j/\partial\tau+v\partial z_j/\partial r=v\partial z_j/\partial r$ under steady-state conditions. In the linear case, with constant area, A is constant. In the cylindrical and spherical cases, $A=2\pi r$ and $A=4\pi r^2$, respectively.

Since the pressure remains practically constant, the transport parameters will generally depend on the local temperature and chemical composition. However as a first approximation the coefficients D_j and λ_j are considered independent of species. Nevertheless different values of the transport parameters in different regions of the flow system (see Fig. 1) may be chosen. In the analysis to be presented the diffusion of main reactants is taken into account. However the diffusion of labile species, such as radicals and atoms, is not taken into consideration.

Except for the simpler form used for the diffusion coefficients, Eqs. (2.1) and (2.2) are suggestive of those used in the study of linear flame propagation.[4] However, no attempt is made in this analysis to include complex chemical kinetics involving a series of consecutive reactions. It will be assumed that the kinetics can be represented in terms of an over-all rate, R. Such an assumption is strictly applicable only to a unimolecular reaction with negligible reverse reaction. However, such a system is particularly attractive because of the smaller number of equations and functions involved. Nevertheless, the general equations presented can be applied to more complex reaction systems with variable transport coefficients and activation energies.

§ The conditions of isobaric deflegration permit the approximation of neglecting the equation for conservation of momentum.

3. MONOPROPELLANT FLAME

Flame propagation in a heterogeneous medium is analyzed herein in terms of the steady-state combustion of a single, liquid droplet immersed in a gaseous, inert atmosphere. For the monopropellant flame, the material transfer of a single reactant is involved, which in its passage from the liquid surface undergoes exothermic chemical transformation at a rate governed by the chemical kinetics. Therefore, the problem of a monopropellant droplet deals with the steady-state transport of material and energy in a system containing heat sources distributed throughout the medium. The effects of dynamic forces on the droplet and other types of interaction between different droplets are neglected in this analysis.

In order to give the model mathematical definition the following assumptions are made: (a) The droplet is spherically symmetric, i.e., $A=4\pi r^2$; (b) The system contains at most three gaseous species, which will be referred to as fuel—F, products—P, and inert gas—G; (c) The source of fuel vapor is a liquid surface at its boiling point; the energy L (including the enthalpy of the liquid phase) is absorbed in the vaporization process; (d) The fuel vapor decomposes exothermically into product gases at a rate $R(t, Y_F)$ dependent on temperature and weight fraction of fuel vapor; (e) The outermost boundary is at an infinite distance from the liquid surface. As the outer boundary is approached, the weight fraction of fuel tends to zero, and the temperature tends to a preassigned value, t_0. (f) The total pressure of the system remains constant.

These assumptions, together with a knowledge of the chemical kinetics and the gas properties of the system including an equation of state (described by the ideal gas law) are sufficient to permit the calulation of the flame characteristics. However, the kinetics of the combustion process are not known in sufficient detail to warrant high precision computing. Nor does the inclusion of the variations of the transport and thermodynamic parameters with temperature and composition appear justified. Consequently, the quantities D, λ, ρ, and C are taken to be independent of temperature and composition, and the relation $\lambda=C\rho D$ is assumed to hold throughout the system.¶

The conservation equations of Sec. 2 applied to this system are:

$$Y_F+Y_P+Y_G=1 \quad (3.1)$$

$$\dot{m}_F=A\rho(vY_F-DY'_F)=\dot{M}(1-z) \quad (3.2)$$

¶ This approximation representing the Lewis number as unity is valid for most of the stable chemical species in the system under consideration. (The Lewis number is defined as the ratio of the Schmidt to Prandtl numbers.)

$$\dot{m}_P = A\rho(vY_P - DY'_P) = \dot{M}z \tag{3.3}$$

$$\dot{m}_G = A\rho(vY_G - DY'_G) = 0 \tag{3.4}$$

$$\dot{m} = \dot{m}_F + \dot{m}_P + \dot{m}_G = A\rho v = \dot{M} \tag{3.5}$$

$$\dot{m}_F h_F + \dot{m}_P h_P - A\lambda t' = \dot{M}(1-z)h_F + \dot{M}zh_P - A\lambda t' = \dot{M}q - A_1\lambda t'_l \tag{3.6}$$

in which the progress of the reaction is indicated by the variable

$$z = \int_{r_l}^{r} (R/v)dr \tag{3.7}$$

which measures the weight fraction of product produced by chemical reaction in the region between the liquid surface and a given point in the system. Since the fuel flow varies continuously with r, it is necessary to use the special notation $\dot{M}$ in these equations for the mass flow rate of fuel at the liquid surface.

Equation (3.4) can be integrated independently. Thus, in the case of spherical symmetry the distribution is given by:

$$Y_G = Y_{GO} \exp\left(-\frac{\dot{M}}{4\pi\rho D}\cdot\frac{1}{r}\right) r_l \leq r \leq \infty. \tag{3.8}$$

The energy relations applicable to this system are:

$$\left.\begin{aligned} h_F &= q + C_F t = q + Ct \\ h_P &= C_P t = Ct \end{aligned}\right\} \tag{3.9}$$

and in addition

$$\dot{M}L = A_1\lambda t'_l \tag{3.10}$$

since all the heat transferred into the droplet is used for vaporization and heating of the liquid material to its boiling point.**

Based on these relations Eq. (3.6) may be expressed as:

$$t' = \frac{\dot{M}}{A\lambda}(Ct - qz + L). \tag{3.11}$$

Of the remaining equations (3.1) to (3.6), only (3.2) is of further interest, since the variables v, Y_P and Y_G can be eliminated by means of the other equations. One obtains, therefore,

$$Y'_F = \frac{\dot{M}}{A\rho D}(Y_F + z - 1) \tag{3.12}$$

and by Eq. (3.7)

$$z' = \frac{A\rho}{\dot{M}} R(Y_F, t) = \frac{A\rho Y_F}{\dot{M}} Be^{-E/RT}. \tag{3.13}$$

** During the burning process an increase in the average temperature of the liquid occurs as a result of heat transfer into the interior of the droplet. However, this effect is relatively small for liquids which exhibit a high mass burning rate and therefore a relatively short lifetime.

The system of equations to be integrated is (3.11), (3.12), and (3.13), with the following boundary conditions:

$$r = r_l,\ t = 0,\ z = 0,\ t'_l = \dot{M}L/\lambda A_l \tag{3.14}$$

$$r = r_0,\ t = t_0,\ z = 1. \tag{3.15}$$

Obviously, this is an eigenvalue problem with two independent eigenvalues to be determined, namely $\dot{M}$ and Y_{F1}.†† It could be solved in this form by trial and error. However, there is a simplification available, based on the relation $\lambda = C\rho D$. Using this relation combined with Eqs. (3.11) and (3.12), one obtains

$$(Ct + qY_F)' = \frac{\dot{M}}{A\rho D}(Ct + qY_F - q + L)$$

which can be integrated from the outer boundary at which $r = \infty$ and $t = t_0$ to give

$$Ct + qY_F = q - L - (q - L - Ct_0)\exp\left(-\frac{\dot{M}}{4\pi\rho D}\cdot\frac{1}{r}\right). \tag{3.16}$$

The weight fraction of fuel at the liquid surface is therefore

$$Y_{F_l} = \frac{q-L}{q} - \left(\frac{q - L - Ct_0}{q}\right) \times \exp\left(-\frac{\dot{M}}{4\pi\rho D}\cdot\frac{1}{r_l}\right) \tag{3.17}$$

and one of the eigenvalues is thereby determined, while $\dot{M}$ has to be calculated by trial and error.

A considerable reduction in the numerical work is effected by a change to dimensionless variables as shown in the Appendix.

In regard to the method of solution of the differential equations, the present method differs from that used by Corner[2] because of the introduction of spherical symmetry and the cold boundary at the liquid droplet surface. Corner[2] is able to write his equations in a form entirely independent of r, thus making it possible to integrate back from the hot boundary. Neither the spherical nor the cylindrical models permit this method of attack. Thus, in the present development it is necessary to integrate from the cold boundary.

4. NUMERICAL ANALYSIS

The equations and boundary conditions which describe the steady-state burning of a liquid droplet sustained by its exothermic heat of reaction (i.e., a monopropellant) have been applied to the thermal decomposition of hydrazine. Flames produced by the thermal degradation of this substance have been

†† With two first-order equations, a single eigenvalue is to be determined, while with three first-order equations, two eigenvalues are required.

studied.[5,6] However, the kinetics of this reaction are not known in detail. Experimentally it has been found[7] that the first step in the thermal decomposition of hydrazine is the unimolecular reaction $N_2H_4 \rightarrow 2NH_2$ with a rate constant $k=4\times10^{12}\exp(-60\,000/RT)\text{sec}^{-1}$. In the numerical analysis to be presented only the kinetics of the initial step of the decomposition leading to NH_2 radicals is considered. The subsequent reactions of this radical to final products are not taken into account.

Based on thermochemical considerations and the experimental measurement of flame temperature by Murray and Hall[5] one obtains an average specific heat of 0.58 cal/g deg. The average diffusion coefficient[8] and average density of the system as listed in Table I fix the average value of the thermal conductivity by means of the previously used relationship $\lambda=C\rho D$. A summary of the parameters and the boundary conditions used in these calculations is presented in Table I. The mass burning rate of a droplet of hydrazine 0.2 cm in radius

TABLE I. Parameters used in calculation of mass burning rate of hydrazine droplet.[a]

Heat of combustion[b]	1000 cal/g
Heat of vaporization[c,d]	380 cal/g
Average specific heat	0.58 cal/g°K
Average diffusion coefficient	1.8 cm²/sec
Average thermal conductivity	5×10^{-4} cal/cm sec°K
Average density	4.8×10^{-4} g/cc
Reaction rate constant[e]	$4\times10^{12}\exp(-60\,000/RT)\text{sec}^{-1}$
Boundary conditions:	
$r_l=0.2$ cm	
$T_l=387$°K	
$T_0=1460$°K	

[a] The physical properties are evaluated at an average temperature of 950°K.
[b] See reference 5.
[c] This figure includes the enthalpy of the liquid phase.
[d] C. C. Clark, *Hydrazine* (Mathieson Chemical Corporation, Baltimore, 1951).
[e] See reference 7.

was computed with the boiling point of the liquid as the cold boundary and the adiabatic flame temperature as the hot boundary.

In Fig. 2, a series of trial solutions are shown based on Eqs. (3.11) and (3.13) combined with the simplified form of Eq. (3.16) i.e., $Ct+qY_F=q-L$, which is obtained by setting t_0 equal to the adiabatic flame temperature $[t_0=(q-L)/c]$. The correct solution is identified as that curve which fits the hot boundary condition imposed by physical considerations; i.e., $z=1$ and $t=1073$°K. The limiting line marked $t=1724z-655$ is the locus of points at which the integral curves are vertical $(dz/dt=\infty)$. A schematic illustration of the behavior of the solution is shown in Fig. 3. Continuation

[5] Murray and Hall, Trans. Faraday Soc. **47**, 743 (1951).
[6] Adams and Stocks, *Fourth Symposium on Combustion, Cambridge, Massachusetts* (Williams and Wilkins, Baltimore, 1953).
[7] M. Szwarc, J. Chem. Phys. **17**, 505 (1949).
[8] Hirschfelder and Curtiss, Naval Research Laboratory Report No. CM-756, University of Wisconsin (November, 1952).

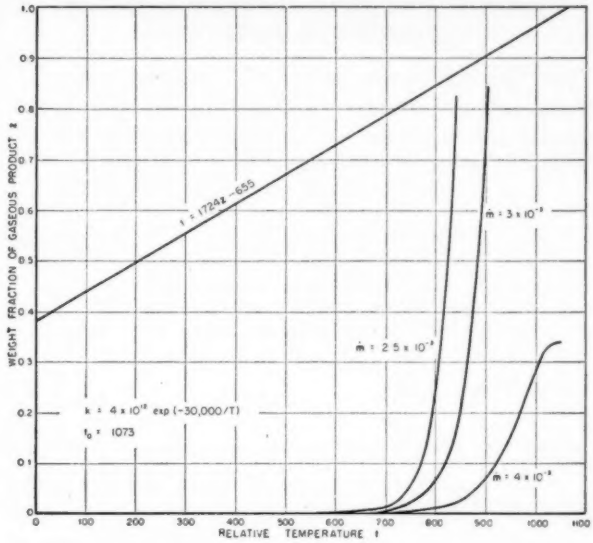

FIG. 2. Mathematical solution of mass burning rate of liquid hydrazine droplet (radius=0.2 cm).

of a particular curve (curve *a*) above this limiting line leads to decreasing values of t, a solution which is physically insignificant. Such a curve corresponds therefore to trial values of the mass burning rate which are less than the eigenvalue $\dot{M}$ for this system. On the other hand, if the trial value chosen is in excess of the true $\dot{M}$ (curve *c*, Fig. 3), the curves fail to reach the limiting line. The correct solution is shown schematically by curve *b* (Fig. 3).

It is apparent therefore from the curves of Fig. 2 that the correct mass burning rate for this system is between 3×10^{-3} and 4×10^{-3} g/sec. Assuming a mean value of 3.5×10^{-3} g/sec corresponding to a linear burning rate of 5.7×10^{-3} cm/sec, one obtains from Eq. (3.11) for the temperature gradient at the liquid surface 5.75×10^3°K/cm. The value of the mass burning rate is of the same order of magnitude as that observed for many fuel droplets burning in air.[9,10]

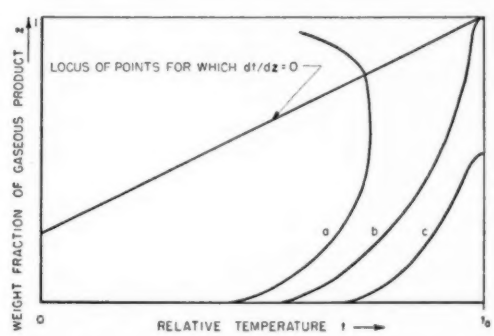

FIG. 3. Schematic presentation of trial solutions for mass burning rate of liquid droplet.

[9] G. A. E. Godsave, *Fourth Symposium on Combustion* (Williams and Wilkins Company, Baltimore 1953), Paper No. 103.
[10] Wise, Lorell, and Wood, *Fifth Symposium on Combustion* (Reinhold Publishing Corporation, New York, 1955), Paper No. 8.

APPENDIX. NUMERICAL INTEGRATION OF DIFFERENTIAL EQUATIONS

For the spherico-symmetrical case the change to dimensionless variables (denoted by bars) and the introduction of a new independent variable η leads to the following set of equations:

$$r=\frac{\dot{M}}{4\pi\rho D}\bar{r} \tag{3.18}$$

$$t=\frac{q-L}{C}\bar{t} \tag{3.19}$$

$$Y_F=\bar{Y} \tag{3.20}$$

$$z=\bar{z} \tag{3.21}$$

$$\eta=1/\bar{r} \tag{3.22}$$

$$\frac{d\bar{Y}}{d\eta}=1-\bar{Y}-\bar{z} \tag{3.23}$$

$$\frac{d\bar{t}}{d\eta}=\frac{C\rho D}{\lambda}\left(-\bar{t}+\frac{q\bar{z}}{q-L}-\frac{L}{q-L}\right) \tag{3.24}$$

$$\frac{d\bar{z}}{d\eta}=\frac{1}{\eta^4 D}\left(\frac{\dot{M}}{4\pi\rho D}\right)^2\cdot\bar{R}(\bar{Y},\bar{t}) \tag{3.25}$$

and the corresponding boundary conditions

$$\eta_l=\frac{1}{r_l}\frac{\dot{M}}{4\pi\rho D} \tag{3.26}$$

$$\eta_l=\eta:\ \bar{t}=0,\bar{z}=0,\ \bar{Y}_l$$

$$=\frac{q-L}{q}\left\{1-(1-\bar{t}_0)\exp(-\eta_l)\right\} \tag{3.27}$$

$$\eta=0:\ \bar{t}=\bar{t}_0,\ \bar{z}=1. \tag{3.28}$$

If the relation $\lambda=C\rho D$ is used in Eq. (3.24) for the integration, the system simplifies further since Eq. (3.23) may be replaced by:

$$\bar{Y}+\frac{q-L}{q}\bar{t}=\frac{q-L}{q}\left\{1-(1-\bar{t}_0)e^{-\eta}\right\}. \tag{3.29}$$

NOTATION

A Area of section normal to flow
B Pre-exponential coefficient in equation for reaction rate constant
C Isobaric heat capacity per unit mass
D Diffusion coefficient
h Enthalpy per unit mass of specified component relative to boiling point of liquid reactant
L Latent heat of vaporization plus enthalpy of liquid reactant
$\dot{m}$ Total mass flow rate
$\dot{m}_j$ Mass flow rate of species j in vapor phase
$\dot{M}$ Liquid mass flow rate
q Heat of reaction per unit mass of fuel vapor
r Space coordinate
R_j Rate of production of component j by chemical reaction
T Temperature
T_l Boiling point of liquid reactant
t Relative temperature with respect to T_l, i.e., $t=T-T_l$
v Flow velocity
Y Weight fraction of specified component at any point r
z Weight fraction of specified component generated by chemical reaction in the region from r_l to any point
η $1/\bar{r}$
λ Thermal conductivity of gas mixture
ρ Density of gas mixture
τ Time

Subscripts

c Flame front
j Component j
l Liquid surface
o Outer boundary
F Fuel
G Inert gas
P Product
X Oxidizer
x Region x
f Region f

New Form of Molecular Potential Function for Use in Molecular Vibrational Analysis

EMIL J. SLOWINSKI, JR.
University of Connecticut, Storrs, Connecticut
(Received August 10, 1953)

A molecular potential function which takes simple and direct account of intramolecular strains is proposed. The parameters in the function are the conventional bond-stretching and angle-bending force constants and the strain-free magnitudes of the bond lengths and bond angles.

The function is applied to the analysis of the vibrations of XY_2 molecules with C_{2v} symmetry. Calculations based on the zero-order frequencies of H_2O and D_2O indicate that a three-parameter function is adequate for these molecules. All molecules studied with the function show a moderate attraction between the end atoms of the molecules, resulting in a decrease in the size of the bond angle from the strain-free value. For compounds of the oxygen family with hydrogen the bond angle at zero strain appears to have a constant value equal to 120°.

CLASSICAL mechanics offers several methods for the analysis of the vibrations of linearly-coupled systems. These methods involve the expression of the potential and kinetic energies of the system in terms of suitable coordinates. Given a system (see Fig. 1) consisting of several masses connected by conventional springs, one can immediately express the potential energy:

$$V=\tfrac{1}{2}\sum k_{il}(L_{il}-\lambda_{ilo})^2+\tfrac{1}{2}\sum k_j(A_j-\alpha_{jo})^2, \qquad (1)$$

where the first sum is taken over springs between masses, and the second over springs in the angles. k_{il} is the force constant of the spring between the ith and lth masses, L_{il} is the instantaneous distance between them, and λ_{ilo} is the distance in the event that there is no strain in the spring. Similarly, k_j is the force constant of the spring in the jth angle, A_j is its instantaneous magnitude, and α_{jo} its magnitude when there is no strain in the spring.

The form of the function is obvious, given the system. It allows for all possible strains within the system at equilibrium, and, indeed, one would not consider expressing the potential energy in the classical problem in any other way.

The methods used in present-day problems in molecular vibrational analysis are essentially classical; atoms are considered to be mass points in a linearly-coupled force field and are assumed to move only infinitesimally from their equilibrium positions. This approach has been shown to be consistent with results as obtained from direct use of quantum-mechanical reasoning, and is almost universally employed.

However, the potential functions which have been assumed for molecules are not of the form (1), which we would like to propose as being a reasonable function, but rather (in the simplest case) are of the following type:

$$V=\tfrac{1}{2}\sum k_{il}\Delta L_{il}^2+\tfrac{1}{2}\sum k_j\Delta A_j^2, \qquad (2)$$

where the sums are taken in the same way as in (1), but ΔL_{il} and ΔA_j are infinitesimal changes in bond length and angle from the equilibrium configuration, rather than finite changes from the strain-free configuration. Basically, function (2) assumes what function (1) does not; namely, that at equilibrium, there is no potential energy in the molecule and hence no intramolecular strain. Therefore, even if the molecular force field were of the simple form shown in Fig. 1, function (2) would not be directly applicable to the vibrational analysis problem, except in the special situation where the molecule existed at equilibrium under no strain.

To improve correlation between calculated and observed vibrational frequencies function (2) has been modified in various ways. One of the most successful has been a function of the type suggested by Urey and Bradley,[1] which takes essentially the following form:

$$V=\tfrac{1}{2}\sum k_{il}\Delta L_{il}^2+\sum k_{il}'\Delta L_{il}+\tfrac{1}{2}\sum k_j\Delta A_j^2+\sum k_j'\Delta A_j. \qquad (3)$$

In this function the terms have the same meaning as before, and k_{il}' and k_j' have the appropriate dimensions.

One finds on investigating the k' terms that they depend on intramolecular strains in the equilibrium configuration. In this sense one can say that functions (1) and (3) are similar. Where function (1) introduces the strain terms into the sums involving the fundamental force constants, function (3) adds terms taking account of strain to the previously-existing ones.

On comparing the two functions it seems reasonable to suggest that those of form (1) have some advantages not possessed by those of the Urey-Bradley type. The parameters in the proposed function have a direct and easily-visualized significance, being either conventional force constants or strain-free magnitudes of bond lengths

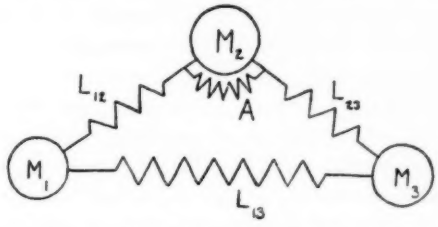

FIG. 1. A simple linearly-coupled system.

[1] H. C. Urey and C. A. Bradley, Phys. Rev. 38, 1969 (1931).

and angles. The (k')'s have no such simple meaning. Simanouti,[2] in a treatment of a group of molecules with a Urey-Bradley field, never reports some of the k' values at all, but rather goes directly to the intramolecular forces. Also, the proposed function (1) attributes, in the first instance at least, intramolecular strain to the inability of the bond lengths and angles in the molecule to fit easily together, where the Urey-Bradley field introduces strain terms in a more formal way. Generalizing, one might say that the proposed function makes a more literal interpretation of the familiar model for the molecule than does the Urey-Bradley field.

Application of the proposed function to problems of molecular vibrations yields some interesting results. The approach for XY_2 molecules of the H_2O type, shown in Fig. 1, will be outlined. The Lagrangian method is used with Cartesian displacement coordinates.

The potential energy of the XY_2 molecule is taken to be, according to (1):

$$V=\tfrac{1}{2}k_{XY}[(L_{12}-\lambda_{120})^2+(L_{23}-\lambda_{230})^2]+\tfrac{1}{2}k_{YY}(L_{13}-\lambda_{130})^2+\tfrac{1}{2}k_s(A_s-\alpha_{so})^2.$$

Applying the Lagrangian equations to the system, and noting that at equilibrium a balance of forces exists within the molecule, we obtain for the generating equation for the secular determinants (general form):

$$w^2m_u\Delta q_u=\sum k_{il}\Delta L_{il}\frac{\partial L_{il}}{\partial q_u}+\sum k_{il}(L_{ilo}-\lambda_{ilo})\left(\frac{\partial L_{il}}{\partial q_u}-\frac{\partial L_{il}}{\partial q_u}\right]_{\text{equil.}}\Bigg)+\sum k_j\Delta A_j\frac{\partial A_j}{\partial q_u}+\sum k_j(A_{jo}-\alpha_{jo})\times\left(\frac{\partial A_j}{\partial q_u}-\frac{\partial A_j}{\partial q_u}\right]_{\text{equil.}}\Bigg), \quad (4)$$

where m_u is the mass of the uth atom, Δq_u is one of its Cartesian displacement coordinates, L_{ilo} and A_{jo} are magnitudes of bond lengths and angles at equilibrium, derivatives are taken in the instantaneous or, as noted, in the equilibrium configuration, and all other terms are as previously defined. From this equation it is apparent that the inclusion of possible strain has simply introduced extra terms into the force Eq. (4), and that in the absence of strain the equation reduces immediately, as expected, to the one obtained by application of the Lagrangian to function (2).

[2] T. Simanouti, J. Chem. Phys. **17**, 848 (1949).

For the XY_2 molecule Eq. (4) takes the form:

$$\begin{aligned}w^2m_u\Delta q_u=&k_{XY}\left[\Delta L_{12}\frac{\partial L_{12}}{\partial q_u}+\Delta L_{23}\frac{\partial L_{23}}{\partial q_u}\right]\\&+k_{XY}\left[(L_{120}-\lambda_{120})\left(\frac{\partial L_{12}}{\partial q_u}-\frac{\partial L_{12}}{\partial q_u}\right]_{\text{equil.}}\right)\Bigg]\\&+k_{XY}\left[(L_{230}-\lambda_{230})\left(\frac{\partial L_{23}}{\partial q_u}-\frac{\partial L_{23}}{\partial q_u}\right]_{\text{equil.}}\right)\Bigg]\\&+k_{YY}\Delta L_{13}\frac{\partial L_{13}}{\partial q_u}+k_{YY}\left[(L_{130}-\lambda_{130})\right.\\&\left.\times\left(\frac{\partial L_{13}}{\partial q_u}-\frac{\partial L_{13}}{\partial q_u}\right]_{\text{equil.}}\right)\Bigg]+k_s\Delta A_s\frac{\partial A_s}{\partial q_u}\\&+k_s\left[(A_{so}-\alpha_{so})\left(\frac{\partial A_s}{\partial q_u}-\frac{\partial A_s}{\partial q_u}\right]_{\text{equil.}}\right)\Bigg].\end{aligned}$$

The ΔL's, ΔA_s, and the various associated derivatives are fairly easily expressed in terms of the Cartesian displacement coordinates by means of well-known or readily-derived formulas and the secular determinants thereby formed.

For the totally-symmetric class the resulting frequency equations are:

$$\begin{aligned}(w_1^2+w_2^2)m_Y=&k_{XY}\left[1+\frac{2m_Y}{m_X}D^2\right.\\&\left.+\left(1+\frac{2m_Y}{m_X}C^2\right)\left(1-\frac{\lambda_{120}}{L_{120}}\right)\right]+2k_{YY}\\&+\frac{2k_s}{L_{120}^2}\left[1+\frac{2m_Y}{m_X}(C^2+CD[A_{so}-\alpha_{so}])\right]\end{aligned}$$

$$\begin{aligned}w_1^2w_2^2\frac{m_Y^2m_X}{m_X+2m_Y}=&k_{XY}^2\left[1-\frac{\lambda_{120}}{L_{120}}\right]\\&-\frac{k_s^2}{L_{120}^4}[A_{so}-\alpha_{so}]^2+\frac{2k_{XY}k_s}{L_{120}^2}\\&+2k_{YY}k_{XY}\left[D^2+C^2\left(1-\frac{\lambda_{120}}{L_{120}}\right)\right]\\&+\frac{4k_{YY}k_s}{L_{120}^2}[C^2+CD(A_{so}-\alpha_{so})].\end{aligned}$$

For the B_2 class the equation is

$$\begin{aligned}w_3^2m_Y=&k_{XY}\left[1+\frac{2m_Y}{m_X}C^2+\left(1+\frac{2m_Y}{m_X}D^2\right)\left(1-\frac{\lambda_{120}}{L_{120}}\right)\right]\\&-\frac{4k_s}{L_{120}^2}CD(A_{so}-\alpha_{so})\frac{m_Y}{m_X}+2k_{YY}\left(1-\frac{\lambda_{130}}{L_{130}}\right),\end{aligned}$$

where $C=\sin(A_{s0}/2)$; $D=\cos(A_{s0}/2)$; $\lambda_{120}=\lambda_{230}$; $L_{120}=L_{230}$.

From the condition that a balance of forces must exist at equilibrium we obtain:

$$\frac{k_s}{L_{120}^2}(A_{s0}-\alpha_{s0})=k_{XY}\frac{D}{C}\left(1-\frac{\lambda_{120}}{L_{120}}\right)$$

and

$$k_{XY}\left(1-\frac{\lambda_{120}}{L_{120}}\right)+2k_{YY}C^2\left(1-\frac{\lambda_{130}}{L_{130}}\right)=0.$$

This system is one with three conditions on four independent parameters. To solve for the parameters one needs to use the frequencies of isotopic pairs. One such pair of molecules is represented by H_2O and D_2O, where there is the added advantage that the zero-order frequencies are known. These frequencies were used to determine the parameters for the water molecule, with one notable result. The value of k_{YY}, the force constant for the distance between nonbonded atoms was found to have a value of about 0.09×10^5 dynes per cm, which is only about one percent of the O—H bond-stretching force constant. In the equations in which they appear the contributions of terms in k_{YY} is also small, being about 1.5% in one case and about 5% in the other. The value of k_{YY} is very sensitive to the vibrational frequencies which are used, and a change of one or two wave numbers in a single frequency is sufficient to change its size by a factor of two.

This very small calculated size and effect of k_{YY} has led to the postulate that in these molecules this force constant may reasonably be taken to be zero, though the force between the end atoms is not zero. This assumption, suggested by the results with the water molecule, has been extended to other XY_2 molecules. Since that assumption reduces the number of independent parameters by one, it becomes possible to calculate the vibrational parameters for a molecule in terms of its vibrational frequencies, with no need for the use of isotopic pairs.

TABLE I. Vibrational parameters for H_2O-D_2O isotopic pair, determined from zero-order frequencies.[a]

	ν_1	ν_2	ν_3	A_{s0}^0	k_{XY}	$\frac{k_s}{L_{120}^2}$	α_{s0}^0
H_2O	3825.32	1653.91	3935.59	104°27′	8.317	0.931	121.0°
D_2O	2758.06	1210.25	2883.79	104°27′	8.293	0.956	122.6°
D_2O (calc)	2763.3	1208.0	2883.6				
	cm^{-1}				$\times10^5$ dynes/cm		

[a] Vibrational frequencies are those reported by Darling and Dennison, Phys. Rev. **57**, 128 (1940).

TABLE II. Vibrational parameters of XY_2 molecules determined from fundamental frequencies.[a]

Molecule	ν_1	ν_2	ν_3	A_{s0}^0	k_{XY}	$\frac{k_s}{L_{120}^2}$	α_{s0}^0	$\frac{\lambda_{120}}{L_{120}}-1$
H_2O	3652	1595	3756	105	7.5823	0.8544	120.5	0.0397
D_2O	2666	1179	2789	105	7.7075	0.8986	122.7	0.0470
H_2Se	2260	1074	2350	90	2.9716	0.4852	121.3	0.0893
D_2Se	1630	745	1696	90	3.0412	0.4651	122.7	0.0874
F_2O	830	490	1110	104	4.7565	1.4262	145.9	0.2805
Cl_2O	680	330	973	111	4.4255	1.0241	150.8	0.2337
SO_2	1151	519	1361	120	9.8886	0.9442	129.9	0.0285
		cm^{-1}			$\times10^5$ dynes/cm			

[a] Vibrational frequencies are taken from G. Herzberg *Infrared and Raman Spectra* (D. Van Nostrand Company, Inc., New York, 1945).

The results of such calculations are given in Tables I and II. In Table I, the parameters for H_2O and D_2O have been independently determined on the basis of the three-parameter function and the zero-order frequencies of the molecules. In the last line of the table the parameters of H_2O as obtained above have been used to calculate the zero-order frequencies of D_2O. The mean deviation from the reported frequencies is 0.13%.

In Table II, the parameters for several molecules are given on the basis of the fundamental frequencies and the three-parameter function. It is to be noted that in all cases studied, the bond angle in the molecule at equilibrium is found to be smaller than the angle would be in its strain-free state, indicating a moderate attraction exists between the nonbonded atoms in these molecules. In all calculations involving water and hydrogen selenide the strain-free bond angle α_{s0} appears to have the same value, about 120°, although the angle magnitudes at equilibrium are known to differ by 15°. Decrease in bond length due to the attraction between end atoms varies from about 4% for water to about 28% for F_2O.

The approach to molecular properties through the proposed potential energy function shows, we believe, some promise, and at present work is progressing on the application of the function to the vibrations of NH_3- and CH_4-type molecules.

Theory of the Faradaic Admittance. III. Application of Diffusion Theory to Current-Interrupter Studies

WILLIAM T. SCOTT
Department of Chemistry, Amherst College, Amherst, Massachusetts, and Department of Physics, Smith College, Northampton, Massachusetts

(Received October 26, 1954)

The problem of predicting and interpreting the potential *vs* time curves obtained in current-interrupter studies of electrochemical reactions is considered with reference to those cases in which diffusion in one or both phases plays a major role. Fick's laws of diffusion are solved in such a way as to provide a complete set of equations governing the current and potential across the interface and the concentrations of the active substances at the interface. These solutions are given for a plane, finite or effectively infinite, unstirred or boundary layer in which diffusion takes place, and for initially uniform or arbitrary gradients. Application is made to the case of a simple uncomplicated reaction and to the hydrogen discharge case, and the mathematical complexity of the latter is made evident. Some efforts are made to discuss the solution of the potential-time equation, and a procedure is given in the simpler case for evaluating the parameters of the process from experimental data. A mathematical appendix gives the application of the Laplace transform method to the solving of Fick's laws under transient conditions and to related aspects of the problem.

1. INTRODUCTION

IN the second of two recent theoretical papers on the Faradaic admittance,[1] D. C. Grahame presented a mathematical analysis of a technique of investigation of the properties of a metal-solution interface known as the current-interrupter method. The present paper, which constitutes the third of the series, contains an extension of that analysis, with particular reference to the role of diffusion. We also discuss further the problem of obtaining numerical values for the various parameters of a given system from the experimental data.

As a consequence of the mathematical analysis here presented it appears evident that a correct application of data obtained by the current-interrupter method must overcome very formidable computational and experimental difficulties. The value of this analysis of the problem depends chiefly upon the fact that it provides definitive, if sometimes complicated, answers to questions which have long been dealt with in unsatisfactory ways.

Current-interrupter studies of metal-solution interfaces involve the establishment of steady-state currents followed by a rapid reduction of the current in the circuit to zero. A study of the variation of potential with time following the moment of interruption is used to obtain information concerning the electrochemical reactions which discharge the double layer. The interpretation of these potential changes requires an adequate theory of the time behavior of the various phenomena involved.

The following assumptions will be used in the treatment that follows:

1. The surfaces are smooth, homogeneous, clean, and plane.

2. There is only one component of the solution that undergoes electrochemical reaction and discharges the double layer after the current interruption.

3. The solution contains a large excess of an inert or "supporting" electrolyte.

4. The concentration of the discharging ions is governed by diffusion—that is, we have either no stirring and no convection, or stirring that is effective only outside a diffusion-supporting boundary layer.[2]

5. The discharged, neutral atoms have a concentration that is either constant or controlled by diffusion (case I), or controlled by a second-order combination reaction (Case II), as in the case of the reaction $H+H\rightarrow H_2$.[3] They may also undergo a reverse reaction or participate in a secondary discharge reaction ($H+H^+ + e \rightarrow H_2$).

6. The primary and secondary discharge currents in either direction at the interface are proportional to the concentrations of the respective reacting substances on the respective sides of the interface, and depend on the potential difference that encourages the reactions through terms of the form $\exp(\alpha n \mathfrak{F} E/RT)$, where α is a constant between 0 and 1, n is the number of electrons transferred, and $\mathfrak{F}$ is the Faraday.

7. The only assumptions made concerning mechanisms or relative rates are that the rate of the discharge reaction is independent of changes in the surface concentration of discharged atoms, and that ordinary second order chemical kinetics govern the combination reaction mentioned in assumption 5.

8. The differential capacity C of the electrical double layer will be considered to be either a constant or a function of the potential difference E that encourages the primary discharge current, measured with respect to any convenient reference electrode in the solution.

9. Diffusion in either phase is governed by Fick's laws of diffusion with a constant value ϵ of the diffusion coefficient for each substance considered.

[1] D. C. Grahame, J. Phys. Chem. **57**, 257 (1953). This paper will be referred to as part II.

[2] See, e.g., B. Levich, Discussions Faraday Soc. **1**, 37 (1947).

[3] That is, we deal with substances of classes II and III as defined in Part I of this series: D. C. Grahame, J. Electrochem. Soc. **99**, 370C (1952).

We can now write equations for the current in its dependence on concentration and potential. We treat two cases. In case I there is considered to be only a single discharge reaction and a single reverse (ionization) reaction. In case II, that of hydrogen ion discharge, there is a primary discharge reaction dependent only on the ion concentration, a secondary discharge reaction dependent on the concentration of neutral atoms, and a combination reaction $H+H\rightarrow H_2$ (nomenclature of Part I). The primary discharge reaction is one in which protons (from water or hydronium ions) are discharged and become adsorbed hydrogen atoms on the metal surface. The secondary discharge is one in which a proton is discharged directly on an adsorbed atom, thus forming a hydrogen molecule. The primary reverse current ($H\rightarrow H^+ + e$) will then depend on the concentration of adsorbed hydrogen atoms, and any secondary reverse current ($H_2\rightarrow H+H^+ + e$) would be proportional to the concentration of molecular hydrogen on the surface. Although in most cases the molecular hydrogen probably bubbles off or dissolves in the solution, a term including it will be inserted for completeness.

For case I we have (see Eqs. (7)–(9) of part II)[3a]

$$i=i^f-i^r=n\mathfrak{F}w_1k_1\exp(\alpha n\mathfrak{F}E/RT) - n\mathfrak{F}w_2k_2\exp[-(1-\alpha)n\mathfrak{F}E/RT] \quad (1)$$

and for case II

$$\begin{aligned} i&=i_p^f+i_s^f-i_p^r-i_s^r \\ &=n\mathfrak{F}w_1k_1\exp(\alpha n\mathfrak{F}E/RT)+n\mathfrak{F}w_1w_2k_{12}\exp(\alpha_{12}n\mathfrak{F}E/RT) \\ &\quad -n\mathfrak{F}w_2k_2\exp[-(1-\alpha)n\mathfrak{F}E/RT] \\ &\quad -n\mathfrak{F}w_3k_3\exp[-(1-\alpha_{12})n\mathfrak{F}E/RT]. \end{aligned} \quad (2)$$

We measure current here in amperes/cm^2, and concentrations in moles/cm^3 or moles/cm^2 depending on circumstances (volume concentrations must be used if diffusion effects are important). We use the symbol w for concentrations at the boundaries of the respective phases, and shall denote by the symbol u or $u(x,t)$ the concentrations in the interiors of phases at time t and distance x from the boundary. Thus $w(t)=u(0,t)$, or more rigorously, $w(t)$ is the extrapolated value, $\lim_{x\rightarrow 0}u(x,t)$.[4] Subscript 1 refers to the ionic or oxidized material, subscript 2 to the neutral or reduced material, and subscript 3 refers to combined molecules of the reduced material, measured in terms of moles of the uncombined units. α is the constant that gives the fraction of the potential difference E responsible for the forward reaction (primary forward reaction in case II), and α_{12} is the corresponding constant for the secondary forward reaction in case II. k_1, k_2, k_{12}, and k_3 are reaction rate constants that depend on the reference potential and are otherwise assumed to be constant for the given solution and metal (assumption 7 above implies that k_1 is independent of w_2). The symbols i^f and i^r refer to the (positive) magnitudes of the forward and reverse currents, respectively. Subscripts p and s refer to primary and secondary currents.

The characteristic of the interrupter method is that the current in Eqs. (1) and (2) is entirely a double-layer current. That is, we assume that the conduction current in the body of the solution has dropped to zero sufficiently fast on interruption that even at the shortest times of observation the faradaic current i can come only from discharge of the double layer. Then we must have

$$i=-C(E)dE/dt. \quad (3)$$

Now if all the w's were constant, we would have enough equations to determine the variation of E with time as shown in part II. However, if diffusion occurs, w_1 will at least be a function of the time, and a third equation is needed in addition to (1) and (3) or (2) and (3).

The third equation is to be derived from the fact that the ions of substance 1 must come to the boundary by diffusion, and the decrease of current with time after the interruption will involve a change in the diffusion rate and a change in w_1. Since the net flow of ions of substance 1 *across* the interface is equal to the current i, there must be a flow of ions *at* the boundary of this amount, which means a local concentration gradient sufficient to provide it by diffusion. The presence of the inert electrolyte means that this flow of ions will be accompanied by an equal flow of inert ions of opposite sign, since there is no current outside the double layer. We can therefore treat the ionic diffusion as if each species were separately governed by a diffusion constant, even though only neutral substances actually can diffuse without destroying electrical neutrality. Fick's first law then reads

$$i=n\mathfrak{F}\epsilon_1(\partial u_1/\partial x)_{x=0}=n\mathfrak{F}\epsilon_1 g_1(t), \quad (4)$$

introducing the symbols $g_1(t)$ and $g_2(t)$ for the gradient at the interface on either side. The inert electrolyte also eliminates concentration polarization of the kind which is responsible for the formation of liquid junction potentials which would otherwise arise at the interface.

Furthermore, if the reduced substance diffuses into the metallic phase, a similar result must hold for that side also:

$$i=n\mathfrak{F}\epsilon_2(\partial u_2/\partial x)_{x=0}=n\mathfrak{F}\epsilon_2 g_2(t). \quad (5)$$

We shall take x on each side of the boundary as a dis-

[3a] This equation was first given by J. A. V. Butler, Trans. Faraday Soc. **28**, 379 (1932), Eq. (5).

[4] The character of the extrapolation is discussed further in part I. It is clear that the rate of an electrochemical reaction actually depends not upon the extrapolated value of $u(x,t)$ but upon the concentration of the reacting species at its distance of closest approach to the interface, i.e., within the double layer. These two concentrations will tend to be different if there is any considerable tendency for the electric fields in the double layer to affect the positions of the ions. [See, e.g., A. N. Frumkin, J. Phys. Chem. U.S.S.R. **24**, 244 (1950) and Nikolaeva *et al.*, Doklady Akad. Nauk S.S.S.R. **86**, 581 (1954).] However, Frumkin and Florianovich showed theoretically and experimentally that the above-mentioned tendency is negligible when there is an excess of inert electrolyte present. [A. N. Frumkin and G. M. Florianovich Doklady Acad. Nauk S.S.S.R. **80**, 907 (1951).]

tance measured positively away from the interface (the two sides are completely independent of each other).

Equations (4) and (5) do not yet provide the necessary equations relating the w's to i; such relations are to be found by solving for $u(x,t)$ from Fick's second law for suitable initial conditions and an undetermined variation of w with time. This will be done in section 2 below.

For case II, w_2 and w_3 are not controlled by diffusion. We can write a combination-reaction equation for w_2:

$$dw_2/dt = -Kw_2^2 + (i_p^f - i_s^f - i_p^r + i_s^r)/n\mathfrak{F}, \quad (6)$$

where the various components of the current can be identified in Eq. (2). Note that this equation assumes no particular reaction mechanism since K or i_s^f and i_s^r can be zero. If the variation of w_3 is to be considered, we can write

$$dw_3/dt = \tfrac{1}{2}Kw_2^2 + (i_s^f - i_s^r)/n\mathfrak{F} - D(w_3), \quad (7)$$

where $D(w_3)$ is the rate at which the combined molecules bubble off or diffuse into the solution. For the steady state in which the derivatives are zero, Eqs. (6) and (7) yield Faraday's law, namely, that the rate of production of molecular hydrogen is proportional to one-half the net current:

$$D(w_3) = \tfrac{1}{2}(i_p^f + i_s^f - i_p^r - i_s^r)/n\mathfrak{F} = \tfrac{1}{2}i/n\mathfrak{F}. \quad (8)$$

Initial Conditions

At the time of interruption of the current, some sort of steady state must have been established, and it is this steady state that determines the initial conditions for Eqs. (1) to (7). Since the double layer cannot discharge itself instantaneously, E right after interruption must equal its value E_0 just before. This quantity is measurable, in principle at least, by the usual interrupter technique. Since concentrations also cannot change instantaneously, the current just after interruption must by Eq. (1) or (2) be equal to its steady-state value i_0. Because we have assumed a large excess of inert electrolyte, we must consider that all of the current in the body of the solution is carried by ions of this inert electrolyte. That is, the transference number for substance 1 is essentially zero:

$$\tau_1 = 0. \quad (9)$$

Since all of the current i_0 is carried across the double layer by ions of substance 1, this current must be equal to the rate of flow of this substance by diffusion.[5] In other words, Eq. (4) holds for the steady state, and we shall write it

$$i_0 = n\mathfrak{F}\epsilon_1 G_1, \quad (10)$$

where G_1 denotes the initial gradient at the boundary,

$$G_1 = (\partial u_1/\partial x)_{x=0,\, t=0} = g_1(0). \quad (11)$$

We shall denote the initial values of w_1 and w_2 by w_{10} and w_{20}, respectively. They are not susceptible of direct measurement, but constitute quantities whose evaluation is to be attempted by an analysis of the time variation of E. Finally we have dw_2/dt and dw_3/dt both equal to zero at $t=0$, since the right sides of Eqs. (6) and (7) cannot change abruptly.

The question of the concentrations w_1 and w_2 in the body of the solution and in the metallic phase respectively, at the initial time is more complicated. A steady-state current involves a steady diffusion of material toward the interface on one side and away from it on the other. Thus material must be continually added on one side and taken away on the other—a condition hard to realize in a steady way. Perhaps the simplest initial state to consider is one in which there is a constant concentration gradient at time $t=0$ from the boundary $x=0$ to some region at a distance l from the interface, where l is large enough that the periodic on and off times of the interrupter fail to have appreciable effects on the concentration at $x=l$. We shall see that once l is suitably large, it may be set equal to infinity in the formulas for the solution of the problem, without appreciable error. In general, l corresponds to the diffusion boundary-layer thickness δ' of Levich's treatment of mass transfer at electrodes.[2]

To illustrate specifically how the initial conditions are related to the conditions of the experiment, suppose that the solution is stirred in such a way that outside a boundary layer of thickness l, the concentration is constant during the transient period:

$$u_1(l,t) = u_{10}(l). \quad (12)$$

Then the initial value w_{10} is given by

$$w_{10} = u_{10}(l) - lG_1 = u_{10}(l) - i_0 l/n\mathfrak{F}\epsilon_1. \quad (13)$$

Suppose further that a potential difference V_0 (referred to the reference electrode) is established across the cell and that the ohmic resistance of the cell is r, so that $E_0 = V_0 - i_0 r$. Let us also assume that w_2 is a constant w_{20}, determined by the preparation of the electrode surface. We can then write for Eq. (1) just before interruption

$$i_0 = n\mathfrak{F}w_{10}k_1 \exp(\alpha n\mathfrak{F}E_0/RT) - n\mathfrak{F}w_{20}k_2 \times \exp[-(1-\alpha)n\mathfrak{F}E_0/RT], \quad (14)$$

$$i_0 = [u_{10}(l) - i_0 l/n\mathfrak{F}\epsilon_1]n\mathfrak{F}k_1 \exp(\alpha n\mathfrak{F}E_0/RT) - n\mathfrak{F}w_{20}k_2 \exp[-(1-\alpha)n\mathfrak{F}E_0/RT]. \quad (15)$$

This equation shows that i_0 is determined by the experimental conditions mentioned, as are w_{10} and E_0. It is important to note that w_{10} (and possibly w_{20}) depends on the chosen i_0 and E_0, whereas k_1 and k_2 are constants that do not depend on i_0 and E_0.

We proceed in the next section to give the above-mentioned solutions of Fick's law and to indicate certain generalizations of them. Section 3 will make use of these

[5] We are describing the situation with volume concentrations only. Without surface concentrations there can be no build-up of material *at* the boundary. See for instance, D. C. Grahame and B. A. Soderberg, J. Chem. Phys. 22, 449 (1954), footnote 9.

solutions in Eqs. (4) and (5) to establish completely the equations governing the time variation of E, and we shall in fact derive expressions for the solution for small values of t. Possible methods of handling experimental data will be suggested in Sec. 4. Finally Sec. 5 will give a complete mathematical derivation of the results quoted in Secs. 2 and 3.

2. SOLUTION OF THE DIFFUSION EQUATION[6]

As stated in Sec. 1, we shall let u refer to the concentration at any point in the interior of the phase in question, and u_0 refer to the value at any point at $t=0$. We shall deal only with the plane case, but the case of complete spherical symmetry can be handled by similar methods. For plane diffusion problems Fick's second law reads

$$\epsilon\partial^2u/\partial x^2=\partial u/\partial t. \tag{16}$$

The value of $u(x,t)$ is clearly determined if its value is known for all values of x at $t=0$ and also for all values of t at $x=0$ and at $x=l$. We shall assume that the value at $x=l$ is constant. The conditions on Eq. (16) then become

$$u(x,0)=u_0(x)=w_0+Gx, \tag{17a}$$

$$u(0,t)=w(t), \tag{17b}$$

$$u(l,t)=w_0+Gl. \tag{17c}$$

We have here taken the initial condition to be one of constant gradient G out to the point $x=l$.

The solution of Eq. (16) subject to the conditions of Eqs. (17a)–(17c) can then be written as follows[7]:

$$u(x,t)=w_0+Gx+\frac{1}{(\pi\epsilon)^{\frac{1}{2}}}\int_0^t\frac{dt'[w(t')-w_0]}{(t-t')^{\frac{1}{2}}}\sum_{n=-\infty}^{n=\infty}(nl+\tfrac{1}{2}x)\times\exp[-(nl+\tfrac{1}{2}x)^2/\epsilon(t-t')]. \tag{18a}$$

This solution is readily shown to satisfy Eq. (16) by direct substitution, noting that the integrand becomes zero as $\exp(-\infty)$ when $t'\to t$. Furthermore, when $x=l$ the series vanishes, since for every positive value of n, say $n=m$, there is another term for negative n that cancels it, namely the term for $n=-m-1$, and Eq. (17c) is satisfied. When $t=0$ the integral vanishes, satisfying Eq. (17a).

[6] Subscripts referring to the two different phases will be omitted in this section.

[7] In this and the following equations we use t' and t'' as variables of integration, to distinguish them from the fixed time t that also appears. The reader will observe that we have made several uses of the following convenient change of variables: let $t'=t-\tau$. Then $dt'=-d\tau$. The limit $t'=0$ becomes $\tau=t$; the limit $t'=t$ becomes $\tau=0$. Thus $\int_0^t F(t,t')dt'=\int_0^t F(t,t-\tau)d\tau$ where we have interchanged the limits after the substitution, to remove the negative sign. Now in the latter integral we may set $\tau=t'$ without changing the result, since the symbol used as integration variable disappears when the integral is calculated. The same type of change can be made with respect to t''. The other variable changes that we use below,

$$\xi^2=x^2/4\epsilon t' \quad\text{or}\quad \xi^2=x^2/4\epsilon(t-t')$$

are more complicated but thereby less confusing.

To show that Eq. (17b) is also satisfied, note that except for the term with $n=0$, the series vanishes when $x=0$. (Compare terms with $n=m$ and with $n=-m$.) The $x=0$ term contains an integrand that becomes infinite instead of zero when $t'\to t$, if x is *first* put equal to zero. To avoid this difficulty, write $x^2/4\epsilon(t-t')=\xi^2$, where ξ is a new variable of integration to be used in place of t'. We can write then

$$u(x,t)=w_0+Gx+(2/\pi^{\frac{1}{2}})\times\int_{x/2(\epsilon t)^{\frac{1}{2}}}^{\infty}d\xi[w(t-x^2/4\epsilon\xi^2)-w_0]\exp(-\xi^2)+\text{terms for } n=\pm1,\pm2,\pm3,\cdots. \tag{18b}$$

Now since $\int_0^\infty\exp(-\xi^2)d\xi=\frac{1}{2}\pi^{\frac{1}{2}}$, it is quite clear that when $x=0$ we get $u(x,0)=w(t)$.

Some of the terms of the series in Eq. (18a) will turn out to be negligible if the exponents are sufficiently large negative quantities. The smallest absolute value of the exponent in any term, which yields the largest value of the term itself, occurs when $t'=0$, namely $n^2l^2/\epsilon t$. Hence if conditions are such that l is much larger than $(\epsilon t_{\max})^{\frac{1}{2}}$, where $t_{\max}$ is the longest time after interruption that observations are of interest, all the terms with $n\neq0$ will be negligible, and only the $n=0$ terms will be important. It seems not unlikely that these conditions can be met in practice, so that no appreciable error will be made if we take l to be infinite, even though a continuous, constant gradient out to infinity is plainly nonphysical, and Levich's δ' may in fact be quite small. When we take l infinite, we must replace condition (17c) with

$$u(x,t)/u_0(x)\to1 \text{ as } x\to\infty. \tag{17d}$$

The resulting solution can then be written in the two alternate forms

$$u(x,t)=w_0+Gx+\frac{x}{2(\pi\epsilon)^{\frac{1}{2}}}\int_0^t dt'\frac{[w(t')-w_0]}{(t-t')^{\frac{3}{2}}}\times\exp[-x^2/4\epsilon(t-t')], \tag{19a}$$

$$u(x,t)=w_0+Gx+(2/\pi^{\frac{1}{2}})\int_{x/2(\epsilon t)^{\frac{1}{2}}}^{\infty}d\xi[w(t-x^2/4\epsilon\xi^2)-w_0]\exp(-\xi^2), \tag{19b}$$

where the first form is convenient for testing Eqs. (16) and (17a), and the second form is convenient for testing Eqs. (17a), (17b), and (17d).

Now our only interest in these solutions lies in the conditions at the boundary. The gradient at the boundary will give us the current, and thus establish a relation determining the current in terms of the concentration $w(t)$. It may be desirable, however, to find the concentration in terms of the current. We wish to show that both these relations are readily established. We shall

use the solutions (19), and later indicate the modifications introduced by a finite value of l.

From Eq. (19b) we find, on differentiating with respect to x (time derivatives will be denoted by superior dots: $dw/dt=\dot{w}$, etc.),

$$\partial u(x,t)/\partial x=G-(x/\epsilon\pi^{\frac{1}{2}})\int_{x/2(\epsilon t)^{\frac{1}{2}}}^{\infty} d\xi\dot{w}(t-x^2/4\epsilon\xi^2)\times\exp(-\xi^2)/\xi^2. \quad (20a)$$

On changing variables again, now letting $\xi^2=x^2/4\epsilon t'$, we find

$$\partial u(x,t)/\partial x=G-(\pi\epsilon)^{-\frac{1}{2}}\times\int_0^t dt'\dot{w}(t-t')\exp(-x^2/4\epsilon t')/t'^{\frac{1}{2}}. \quad (20b)$$

As in the previous section, we shall denote the value of the gradient at $x=0$ by $g(t)$. Then we have from Eq. (20b)

$$g(t)=G-(\pi\epsilon)^{-\frac{1}{2}}\int_0^t dt'\dot{w}(t-t')/(t')^{\frac{1}{2}}$$

$$=G-(\pi\epsilon)^{-\frac{1}{2}}\int_0^t dt'\dot{w}(t')/(t-t')^{\frac{1}{2}}. \quad (21)$$

This equation tells us the value of the gradient at the boundary at any time t in terms of the initial gradient G and the values of $dw/dt=\dot{w}$ for all times from 0 to t.

Suppose now that $g(t)$ is known through Fick's first law. Can we solve Eq. (21) for $w(t)$? The answer is yes, and we give the solution below, postponing the derivation to section 5, but verifying the result here. The solution is

$$w(t)=w_0-(\epsilon/\pi)^{\frac{1}{2}}\int_0^t dt''[g(t'')-G]/(t-t'')^{\frac{1}{2}}$$

$$=w_0-(\epsilon/\pi)^{\frac{1}{2}}\int_0^t dt''[g(t-t'')-G]/(t'')^{\frac{1}{2}}. \quad (22)$$

From the second of these two forms we can derive $\dot{w}$:

$$\dot{w}(t)=-(\epsilon/\pi)^{\frac{1}{2}}\int_0^t dt''\dot{g}(t-t'')/(t'')^{\frac{1}{2}}. \quad (23)$$

Now let us substitute Eq. (23) into Eq. (21), using the second form of the latter, and writing[7] t'' for $t-t''$ (sic!) in Eq. (23):

$$g(t)=G+\frac{1}{\pi}\int_0^t\frac{dt'}{(t-t')^{\frac{1}{2}}}\int_0^{t'}\dot{g}(t'')\frac{dt''}{(t'-t'')^{\frac{1}{2}}}.$$

Interchanging the order of the t' and t'' integrations in accordance with the usual rules, we have

$$g(t)=G+\frac{1}{\pi}\int_0^t dt''\dot{g}(t'')\int_{t''}^t\frac{dt'}{(t-t')^{\frac{1}{2}}(t'-t'')^{\frac{1}{2}}}.$$

The t' integral is equal to π:

$$\int_{t''}^t\frac{dt'}{(t-t')^{\frac{1}{2}}(t'-t'')^{\frac{1}{2}}}=2\tan^{-1}\left(\frac{t'-t''}{t-t'}\right)^{\frac{1}{2}}\Bigg|_{t'=t''}^{t'=t}=\pi.$$

As a result the t'' integral is straightforward, and we have

$$g(t)=G+g(t)-G,$$

thus proving our assertion that Eq. (22) is a solution of Eq. (21).

The solution to Eq. (16) for $u(x,t)$ was found on the assumption that values of u at the boundary $x=0$ were known for all times from 0 to t. If, however, we consider the gradient to be known instead, we can readily obtain the solution by use of Eq. (22). The result of substitution of Eq. (22) into Eq. (19a) is

$$u(x,t)=w_0+Gx-(\epsilon/\pi)^{\frac{1}{2}}\int_0^t dt'[g(t')-G]\times\exp[-x^2/4\epsilon(t-t')]/(t-t')^{\frac{1}{2}} \quad (24)$$

an expression which is readily verified as having the correct properties. (The substitution is most easily carried out by use of Eqs. (A-8) and (A-12) of section 5.)

Our working equations, however, are those relating $w(t)$ and $g(t)$. While the relations given by Eqs. (21) and (22) are probably sufficiently accurate in view of the simplifying assumptions involved in any case which can be treated by this method, it may be useful to generalize them in ways which demonstrate their range of validity. Consequently we quote here results from Sec. 5 involving two generalizations: the quantity l may be any arbitrary value and the initial concentration u_0 may have any arbitrary variation with x. For completeness the simplest case is repeated in the following list:

1. l infinite, special initial value $u_0=w_0+Gx$

$$g(t)=G-(\pi\epsilon)^{-\frac{1}{2}}\int_0^t dt'\dot{w}(t-t')/(t')^{\frac{1}{2}}, \quad (21)$$

$$w(t)=w_0-(\epsilon/\pi)^{\frac{1}{2}}\int_0^t dt''[g(t'')-G]/(t-t'')^{\frac{1}{2}}. \quad (22)$$

2. l finite, special initial value $u_0=w_0+Gx$

$$g(t)=G-(\pi\epsilon)^{-\frac{1}{2}}\int_0^t dt'\dot{w}(t-t')(t')^{-\frac{1}{2}}\times\sum_{n=-\infty}^{n=\infty}\exp(-n^2l^2/\epsilon t'), \quad (25)$$

$$w(l)=w_0-(\epsilon/\pi)^{\frac{1}{2}}\int_0^t dt''[g(t-t'')-G](t'')^{-\frac{1}{2}}\times\sum_{n=-\infty}^{n=\infty}(-1)^n\exp(-n^2l^2/\epsilon t''). \quad (26)$$

3. l finite, general $u_0(x)$. The symbol G will denote here $g(0)=u_0'(0)$, and $w_0=u_0(0)$. The deviation from linearity of $u_0(x)$ can be measured by the value of $u_0''(x)$; or by the value of $u_0'(x)-u_0'(0)=u_0'(x)-G$; or by the value of $u_0(x)-u_0(0)-xu_0'(0)=u_0(x)-w_0-Gx$.

$$g(t)=G-(\pi\epsilon)^{-\frac{1}{2}}\int_0^t dt'\dot{w}(t-t')(t')^{-\frac{1}{2}} \times\sum_{n=-\infty}^{n=\infty}\exp(-n^2l^2/\epsilon t') +(\epsilon\pi t)^{-\frac{1}{2}}\int_0^l dx'[u_0'(x')-G] \times\sum_{n=-\infty}^{n=\infty}\exp[-(nl+x'/2)^2/\epsilon t], \quad (27)$$

$$w(t)=w_0-(\epsilon/\pi)^{\frac{1}{2}}\int_0^t dt''[g(t-t'')-G](t'')^{-\frac{1}{2}} \times\sum_{n=-\infty}^{n=\infty}(-1)^n\exp(-n^2l^2/\epsilon t'') +t^{\frac{1}{2}}\int_0^l dx'[u_0'(x')-G]\sum_{n=0}^{n=\infty}2\pi^{-\frac{1}{2}} \times\int_{(nl+x'/2)/(\epsilon t)^{\frac{1}{2}}}^{[(n+1)l-x'/2]/(\epsilon t)^{\frac{1}{2}}}d\xi\exp(-\xi^2) \quad (28)$$

or the equivalent

$$w(t)=w_0-(\epsilon/\pi)^{\frac{1}{2}}\int_0^t dt''[g(t-t'')-G](t'')^{-\frac{1}{2}} \times\sum_{n=-\infty}^{n=\infty}(-1)^n\exp[-n^2l^2/\epsilon t''] +(\epsilon\pi t)^{-\frac{1}{2}}\int_0^l dx'[u_0(x')-w_0-Gx'] \times\sum_{n=-\infty}^{n=\infty}(-1)^n\exp[-(nl+x'/2)^2/\epsilon t]. \quad (29)$$

4. When l is taken as infinite, formulas (27), (28), and (29) become

$$g(t)=G-(\pi\epsilon)^{-\frac{1}{2}}\int_0^t dt'\dot{w}(t-t')(t')^{-\frac{1}{2}} +(\epsilon\pi t)^{-\frac{1}{2}}\int_0^\infty dx'[u_0'(x')-G]\exp(-x'^2/4\epsilon t), \quad (30)$$

$$w(t)=w_0-(\epsilon/\pi)^{\frac{1}{2}}\int_0^t dt''[g(t-t'')-G)](t'')^{-\frac{1}{2}} +(\epsilon\pi)^{-\frac{1}{2}}\int_0^\infty dx'[u_0'(x')-G)] \times\int_{x'}^\infty dx''\exp(-x''^2/4\epsilon t), \quad (31)$$

$$w(t)=w_0-(\epsilon/\pi)^{\frac{1}{2}}\int_0^t dt''[g(t-t'')-G)](t'')^{-\frac{1}{2}} +(\epsilon\pi t)^{-\frac{1}{2}}\int_0^\infty dx''\exp(-x''^2/4\epsilon t) \times[u_0(x'')-w_0-Gx'']. \quad (32)$$

For future reference we give the most general form of $u(x,t)$, corresponding to a finite l, plane surface, and arbitrary $u(x,0)=u_0(x)$:

$$u(x,t)=u_0(x)+(\pi\epsilon)^{-\frac{1}{2}}\int_0^t dt'[w(t-t')-w_0)] \times(t')^{-\frac{1}{2}}\sum_{n=-\infty}^{n=\infty}(nl+\tfrac{1}{2}x)\exp[-(nl+\tfrac{1}{2}x)^2/\epsilon t'] +\tfrac{1}{2}(\epsilon/\pi)^{\frac{1}{2}}\int_0^l dx'u_0''(x')\int_0^t dt'(t')^{-\frac{1}{2}} \times\sum_{n=-\infty}^{n=\infty}\{\exp[-(nl+\tfrac{1}{2}x-\tfrac{1}{2}x')^2/\epsilon t'] -\exp[-(nl+\tfrac{1}{2}x+\tfrac{1}{2}x')^2/\epsilon t']\}, \quad (33)$$

which satisfies the conditions

$$\left.\begin{aligned}\epsilon(\partial^2u/\partial x^2)&=\partial u/\partial t\\ u(x,0)&=u_0(x)\\ u(0,t)&=w(t)\\ u(l,t)&=u_0(l).\end{aligned}\right\} \quad (34)$$

3. COMPLETE SETS OF EQUATIONS AND APPROXIMATE SOLUTIONS

We are now in a position to relate the current to the concentration at the boundary by means of the equations of Sec. II. Let us write down a complete set of equations for the current, potential difference, and concentration, choosing as our main example our case I, with the concentration of reduced substance w_2 taken as a constant. We shall set $w_2=w_{20}$, its initial value, in appropriate equations for this case. We shall also assume that l for the boundary layer can be set equal to infinity in the formulas, and that the initial concentration gradient is uniform in x.

From Eqs. (1), (2), and (4) we have

$$i=n\mathfrak{F}w_1k_1\exp(\alpha n\mathfrak{F}E/RT) -n\mathfrak{F}w_2k_2\exp[-(1-\alpha)n\mathfrak{F}E/RT], \quad (35)$$

$$i=-C(E)dE/dt, \quad (36)$$

$$i=n\mathfrak{F}\epsilon_1g_1(t). \quad (37)$$

Equation (21) becomes

$$i/n\mathfrak{F}=\epsilon_1G_1-(\epsilon_1/\pi)^{\frac{1}{2}}\int_0^t dt'\dot{w}_1(t)(t-t')^{-\frac{1}{2}}, \quad (38)$$

while (22) can be written in the form

$$w_1(t)=w_{10}-\frac{1}{n\mathfrak{F}(\pi\epsilon_1)^{\frac{1}{2}}}\int_0^t dt'[i(t')-i_0][t-t']^{-\frac{1}{2}}. \quad (39)$$

From (39) we can get by differentiation

$$\dot{w}_1(t)=-\frac{1}{n\mathfrak{F}(\pi\epsilon_1)^{\frac{1}{2}}}\int_0^t dt'\dot{i}(t-t')(t')^{-\frac{1}{2}}. \quad (40)$$

Now, if we substitute (36) into (39), and put the result along with (36) itself into (35), we will have an equation in E that involves dE/dt and an integral expression, but contains no other variable quantities. This equation has the character of a first-order differential equation as far as initial conditions are concerned. Specification of E at $t=0$ will therefore completely determine the solution. Thus we have obtained a complete set of equations for determlning i, E, and w, as functions of the time.

Let us now analyze the behavior of these functions for small values of t. The initial value of dE/dt by (36) will be

$$(dE/dt)_{t=0}=-i_0/C(E_0)=-i_0/C_0, \quad (41)$$

where $C(E_0)$ is written C_0 for brevity.

This means that $E(t)$ must have the form

$$E(t)=E_0-i_0t/C_0+E^*(t), \quad (42)$$

where $E^*(t)$ is small for small times, and has a derivative that vanishes when $t=0$. In terms of E^*, we have for the current

$$i(t)=-C(E)[-i_0/C_0+\dot{E}^*(t)]. \quad (43)$$

Since C is not a constant, we can write, approximately,

$$\begin{aligned}C(E)&=C(E_0)+(E-E_0)C_0'+\tfrac{1}{2}(E-E_0)^2C_0''+\cdots\\&=C_0+[-i_0t/C_0+E^*(t)]C_0'\\&\quad+\tfrac{1}{2}[-i_0t/C_0+E^*]^2C_0''+\cdots, \quad (44)\end{aligned}$$

where C_0', $C_0''\cdots$ signify the values of dC/dE, $d^2C/dE^2\cdots$ for $E=E_0$.

Before we carry out an expansion of (43) for the current, with use of (44), we must make note of the relation between an expansion for the current in powers of t and one for the concentration. If $i-i_0$ is written as a series of powers of t, and one of them is a_mt^m, Eq. (39) will give a term for $n\mathfrak{F}(w_1-w_{10})$ equal to

$$\begin{aligned}&-\frac{a_m}{(\pi\epsilon_1)^{\frac{1}{2}}}\int_0^t\frac{t'^m dt'}{(t-t')^{\frac{1}{2}}}\\&=-\frac{a_m}{(\pi\epsilon_1)^{\frac{1}{2}}}\cdot 2\frac{2\cdot4\cdot6\cdots(2m)t^{m+\frac{1}{2}}}{1\cdot3\cdot5\cdots(2m+1)}\\&=-\frac{a_m(m!)^2 2^{2m+1}t^{m+\frac{1}{2}}}{(\pi\epsilon_1)^{\frac{1}{2}}(2m+1)!}\ (2m \text{ an even integer}), \quad (45)\end{aligned}$$

$$\begin{aligned}&=-\frac{a_m}{(\pi\epsilon_1)^{\frac{1}{2}}}\frac{1\cdot3\cdot5\cdots(2m)\pi t^{m+\frac{1}{2}}}{2\cdot4\cdot6\cdots(2m+1)}\\&=-\frac{a_m(2m+1)!\pi t^{m+\frac{1}{2}}}{(\pi\epsilon_1)^{\frac{1}{2}}[(m+\frac{1}{2})!]^2 2^{2m+1}}\ (2m \text{ an odd integer}), \quad (46)\end{aligned}$$

where the integral may be reduced to a standard definite integral[8] either by the substitution $t'=t\sin^2\theta$ or by the substitution $t'=tx$. Thus integral powers 1, t, t^2, $t^3\cdots$ in the series for the current become half-integral powers for the concentration, $t^{\frac{1}{2}}$, $t^{\frac{3}{2}}$, $t^{5/2}$, $t^{7/2}\cdots$, and vice versa, $t^{\frac{1}{2}}$, $t^{\frac{3}{2}}\cdots$ become t, $t^2\cdots$.

We conclude that expansions in series of integral powers alone will not solve our problem. That is, we have functions which cannot be expanded by Taylor's theorem in the ordinary way. Considerable mathematical caution is needed in order to obtain conclusive information on the variations of the functions for small t.

A suitable procedure is the following. $i(t)-i_0$ is a small quantity for small t. Let us temporarily call it $\Delta i(t)$ and let us similarly set $E-E_0=\Delta E(t)$. Then we put Δi in Eq. (39), and substitute the result into (35). Let us also put (42) into the exponents in (35), and expand the exponentials with respect to ΔE. After the expansion, we multiply out and retain only those terms that do not have the product of two or more Δ's. The terms without any Δ's combine, of course, to give i_0. The result is

$$\begin{aligned}\Delta i(t)&=-k_1(\pi\epsilon_1)^{-\frac{1}{2}}\exp(\alpha n\mathfrak{F}E_0/RT)\\&\quad\times\int_0^t\Delta i(t')(t-t')^{-\frac{1}{2}}dt'+\{w_{10}k_1\alpha n^2\mathfrak{F}^2\\&\quad\times\exp(\alpha n\mathfrak{F}E_0/RT)+w_{20}k_2(1-\alpha)n^2\mathfrak{F}^2\\&\quad\times\exp[-(1-\alpha)n\mathfrak{F}E_0/RT]\}\Delta E(t)/RT. \quad (47)\end{aligned}$$

We see that the slowest variation of Δi with t must come from ΔE, since the result of carrying out the integration on $\Delta i(t')$ is to give a more rapid variation, by a factor $t^{\frac{1}{2}}$, than that of Δi itself.

ΔE, by (42), contains a first-power term in t and a term of more rapid variation. Therefore Δi must have both a term in t and a term from the integral in $t^{\frac{1}{2}}$ but no terms of lower power than the first. This information if used in Eqs. (43) shows that $\dot{E}^*$ might contain terms in t and $t^{\frac{1}{2}}$; this implies that E^* would have terms in t^2, $t^{5/2}$, $\cdots$ but none of lower power. Examination of (44) shows that part of the first-power term for i comes from the term $-i_0C_0't/C_0$, but that the $t^{\frac{1}{2}}$ cannot be found in (44) and *must* be found in $\dot{E}^*$.

Let us calculate the coefficients of t^2 and $t^{5/2}$ in $E^*(t)$, and of t and $t^{\frac{3}{2}}$ in $\Delta i(t)$. To shorten the writing, we define

[8] This integral may be found, for instance, in any recent edition of the *Handbook of Chemistry and Physics* (Chemical Rubber Company, Cleveland, Ohio).

A_1 and B as the coefficients in Eq. (47):

$$A_1=k_1(\pi\epsilon_1)^{-\frac{1}{2}}\exp(\alpha n\mathfrak{F}E_0/RT), \tag{48}$$

$$B=(1/RT)\{w_{10}k_1\alpha n^2\mathfrak{F}^2\exp(\alpha n\mathfrak{F}E_0/RT) +w_{20}k_2(1-\alpha)n^2\mathfrak{F}^2\exp[-(1-\alpha)n\mathfrak{F}E_0/RT]\}. \tag{49}$$

(B is ξ of part II evaluated for $t=0$) so that, getting ΔE from (42),

$$\Delta i=-A_1\int_0^t \Delta i(t')dt'/(t-t')^{\frac{1}{2}} +B[-i_0t/C_0+E^*(t)]. \tag{50}$$

The coefficient of t in Δi is then $-i_0B/C_0$. Inserting $-i_0Bt/C_0$ into the integral, and using (45), we find that the coefficient of $t^{\frac{1}{2}}$ is $4i_0A_1B/3C_0$, so we have found that

$$i(t)=i_0+\Delta i=i_0-i_0Bt/C_0+4i_0A_1Bt^{\frac{3}{2}}/3C_0+\cdots. \tag{51}$$

To find the coefficients for E^*, let us compare (51) with (43), equating coefficients of t and $t^{\frac{1}{2}}$ in each equation. For this purpose, we only need two terms from (44), and can write (43) as

$$i=-[C_0-(i_0C_0'/C_0)t+\cdots][-i_0/C_0+\dot{E}^*(t)]. \tag{52}$$

We readily find for the first two terms in $\dot{E}^*(t)$:

$$\dot{E}^*(t)=[(i_0B/C_0^2)-(i_0^2C_0'/C_0^3)]t -[4i_0A_1Bt^{\frac{3}{2}}/3C_0^2]+\cdots. \tag{53}$$

On integration, remembering that $E^*(0)=0$, we finally arrive at

$$E(t)=E_0-(i_0t/C_0)+E^*(t)=E_0-(i_0t/C_0) +(i_0/2C_0^2)[B-(i_0C_0'/C_0)]t^2 -[8i_0A_1Bt^{5/2}/15C_0^2]+\cdots. \tag{54}$$

It is clear that further terms in each of these series could be found by repetition of this calculation, and that each will proceed with further powers of $t^{\frac{1}{2}}$. It would be necessary in this case to expand the exponential containing ΔE in Eq. (35) to higher powers than the first.

Let us consider next the case in which w_2 is also controlled by diffusion. The results given already will need only a slight modification.

In addition to Eq. (39), we have a relation between w_2 and i:

$$w_2(t)=w_{20}-(\pi\epsilon_2)^{-\frac{1}{2}}\int_0^t dt'[i(t')-i_0]/(t-t')^{\frac{1}{2}}. \tag{55}$$

w_{20} will be determined at $t=0$ in a way similar to w_{10}. Equation (47) for small changes Δi and ΔE will now become

$$\Delta i(t)=(A_2-A_1)\int_0^t \Delta i(t')dt'/(t-t')^{\frac{1}{2}} +B[-(i_0t/C_0)+E^*(t)], \tag{56}$$

where A_2 arises from substitution of (55) into (35) and is given by

$$A_2=k_2(\pi\epsilon_2)^{-\frac{1}{2}}\exp[-(1-\alpha)n\mathfrak{F}E_0/RT]. \tag{57}$$

Equations (43) and (44) are still valid, so that we can obtain equations for i and E^* for this case from Eqs. (51) and (54) by replacing A_1 by A_1-A_2:

$$i=i_0-[i_0Bt/C_0] +[4i_0(A_1-A_2)Bt^{\frac{3}{2}}/3C_0]+\cdots, \tag{58}$$

$$E^*(t)=(i_0/2C_0^2)[B-(i_0C_0'/C_0)]t^2 -[8i_0(A_1-A_2)Bt^{5/2}/15C_0^2]+\cdots. \tag{59}$$

In part II it is stated without proof that dw_1/dt, dw_2/dt etc. are zero at $t=0$. For the case (I) as treated above, this result follows at once. Since Δi varies as t, di/dt has an initial constant value, with its next term proportional to $t^{\frac{1}{2}}$, so that by (40) and (45), each $\dot{w}$, has terms in $t^{\frac{1}{2}}$, t, etc., and vanishes when $t\to 0$. On the other hand, d^2w/dt^2 will behave like $t^{-\frac{1}{2}}$ and become infinite as $t\to 0$.

Let us now consider case II. We shall not pursue the calculation to the point of evaluating coefficients of powers of t, but shall content ourselves with identifying the nature of the expansions. A complete set of equations for case II consists of Eqs. (2), (3), (6), (7), and (39). Eliminating i and w_1 from the set as we did for case I, we have a set of three equations in E, w_2, and w_3 and their first derivatives, which has a unique solution if the three initial values E_0, w_{20}, and w_{30} are given. The latter two must be determined in some fashion from the surface conditions on the electrode.

Now we may use an approximate analysis for small times, using Δi and ΔE as before, and in addition $\Delta w_2=w_2-w_{20}$ and $\Delta w_3=w_3-w_{30}$.

After introducing these quantities into the three equations and expanding to first powers only, we will have a set of equations which can be written

$$\Delta i=a_{10}\Delta E+a_{11}\int_0^t dt'\Delta i(t')(t-t')^{-\frac{1}{2}} +a_{12}\Delta w_2+a_{13}\Delta w_3, \tag{60}$$

$$\Delta\dot{w}_2=a_{20}\Delta E+a_{21}\int_0^t dt'\Delta i(t')(t-t')^{-\frac{1}{2}} +a_{22}\Delta w_2+a_{23}\Delta w_3, \tag{61}$$

$$\Delta\dot{w}_3=a_{30}\Delta E+a_{31}\int_0^t dt'\Delta i(t')(t-t')^{-\frac{1}{2}} +a_{32}\Delta w_2+a_{33}\Delta w_3, \tag{62}$$

where the coefficients a_{10}, $a_{11}\cdots a_{32}$, and a_{33} are similar to A_1, A_2, and B, and can be found in a straightforward manner. As before, we know that the lowest term of ΔE is of the first power in t. Furthermore, since dw_2/dt and dw_3/dt vanish for $t=0$, Δw_2 and Δw_3 must involve higher powers than the first. Thus from Eq. (60) we see that Δi starts with the first power, and also has a $\frac{3}{2}$ power term.

Equation (61) and (62) then tell us that $\Delta\dot{w}_2$ and $\Delta\dot{w}_3$ start with terms in t and have terms in $t^{\frac{1}{2}}$. By integration we see that Δw_2 and Δw_3 start with t^2 terms and have $t^{5/2}$ terms and of course all higher integral and half-integral powers. Again we can only get two terms in the various series without considering higher powers of the Δ's than the first.

The same arguments as before can be used to show that E^* starts with terms in t^2, $t^{5/2}\cdots$, and that $\dot{w}_1$ starts with $t^{\frac{1}{2}}$, t, $\cdots$. The vanishing of all the dw/dt's is thus proved for case II.

A general analytic solution of the equations cannot be obtained because of their transcendental nature. We shall limit ourselves to a few remarks on possible procedures for numerical calculation, for case I only with w_2 constant.

Let us use a dimensionless variable x in place of E in Eqs. (35) and (36), given by

$$x=\alpha n\mathfrak{F}E/RT. \tag{63}$$

Let us also set

$$(RT/\alpha n\mathfrak{F})C(E)=c(x). \tag{64}$$

Elimination of i and w_1 from Eq. (35) by means of (36) and (39) then yields (after integration of the term in i_0)

$$-c(x)dx/dt=n\mathfrak{F}w_{10}k_1e^x+k_1(\pi\epsilon_1)^{-\frac{1}{2}}e^x \times\int_{x_0}^{x}dx'c(x')/(t-t')^{\frac{1}{2}} -2k_1i_0t^{\frac{1}{2}}(\pi\epsilon_1)^{-\frac{1}{2}}e^x-n\mathfrak{F}w_2k_2e^{-x}, \tag{65}$$

with the initial condition

$$x=x_0=\alpha n\mathfrak{F}E_0/RT \quad \text{when} \quad t=0, \tag{66}$$

and the relation

$$i_0=n\mathfrak{F}[w_{10}k_1e^{x_0}-w_2k_2e^{-x_0}]=-c(x_0)(dx/dt)_{t=0}. \tag{67}$$

Equation (65) determines x as a function of t. The meaning of t' is given below. Four constants enter the solution as parameters, namely the quantities $n\mathfrak{F}w_{10}k_1$, $k_1\epsilon_1^{-\frac{1}{2}}$, $n\mathfrak{F}w_2k_2$, and x_0. α must also be known, but can often be taken as equal to 0.50. In addition, $c(x)$ must be known. In the simplest case, that of constant differential capacity, the value of c is a fifth parameter. With so many parameters entering, a numerical computation would not seem to be worthwhile until considerable information is available concerning the probable values of the parameters.

Even if all the parameters were known, Eq. (65) is not easy to handle. One simplification is to find t as a function of x, rather than the reverse. In this case, the unknown function $t(x)$ appears in the derivative $dx/dt=(dt/dx)^{-1}$, in the term with $[t(x)]^{\frac{1}{2}}$, and in the denominator under the integral sign, which must be written $[t(x)-t(x')]^{\frac{1}{2}}$, with x' the integration variable and x the upper limit as indicated.

The quantity $t(x')$ is written t' in Eq. (65).

Now, whether diffusion plays a large or small role in the determination of $x(t)$ or $t(x)$, the current will be influenced more by the exponential factor than by the variation of w_1, since the latter only varies by the difference of i and i_0. Therefore it will always be an appropriate method of approximation to treat w_1 as a constant, as a first step.

Suppose for instance we take $c(x)$ to be a constant and solve for the relation between t and x on the assumption that w_1 is also a constant. This problem was solved in part II, but in that paper it could be assumed that E is measured with respect to the equilibrium potential, so that $w_{10}k_1=w_2k_2$. We cannot make this assumption here, since w_{10} depends on i_0. However, we can write for the first approximation

$$\begin{aligned}-cdx/dt&=n\mathfrak{F}[w_{10}k_1e^x-w_2k_2e^{-x}]\\&=n\mathfrak{F}(w_{10}k_1w_2k_2)^{\frac{1}{2}}[e^{x+x_c}-e^{-(x+x_c)}]\\&=2n\mathfrak{F}(w_{10}k_1w_2k_2)^{\frac{1}{2}}\sinh(x+x_c),\end{aligned} \tag{68}$$

where x_c is given by

$$e^{x_c}=(w_{10}k_1/w_2k_2)^{\frac{1}{2}}. \tag{69}$$

The solution to (68) is then

$$t(x)=-\frac{c}{2n\mathfrak{F}(w_{10}k_1w_2k_2)^{\frac{1}{2}}}\ln\left[\frac{\tanh\frac{1}{2}(x+x_c)}{\tanh\frac{1}{2}(x_0+x_c)}\right] \tag{70}$$

or

$$x(t)=\ln\frac{1+\tanh\frac{1}{2}(x_0+x_c)\exp[-2n\mathfrak{F}(w_{10}k_1w_2k_2)^{\frac{1}{2}}t/c]}{1-\tanh\frac{1}{2}(x_0+x_c)\exp[-2n\mathfrak{F}(w_{10}k_1w_2k_2)^{\frac{1}{2}}t/c]}, \tag{71}$$

where the constant of integration denoted by t' in part II has been evaluated by setting $t=0$ when $x=x_0$.

Now we can substitute (70) into the right-hand side of (65), and assume that the approximation involved in (70) makes a small error in the result because it enters in the relatively small terms of (65). The integral $\int c(x')dx'(t-t')^{-\frac{1}{2}}$ has to be evaluated numerically. Calling the resulting right side of (65) $f(x)$, one can calculate a second solution for $t(x)$ by integrating (65) in the form

$$dt=-c\int dx/f(x). \tag{72}$$

One more step can be performed analytically in the event that E is large enough to make the reverse current negligible, which means that

$$e^{x+x_c}\gg 1 \tag{73}$$

for some chosen period of time. Then, since $\tanh\frac{1}{2}(x+x_c)\simeq 1-2e^{-(x+x_c)}$ when (73) holds, and $\ln(1+y)\simeq y$ for small y, we have

$$t(x)\simeq(-c/n\mathfrak{F})(w_{10}k_1w_2k_2)^{-\frac{1}{2}}[e^{-(x+x_c)}-e^{-(x_0+x_c)}], \tag{74}$$

which is equivalent to Eq. (23) of part II.

If (74) is substituted into (65), the integral $\int cdx'(t-t')^{-\frac{1}{2}}$ can be evaluated analytically by use of the identity

$$\int dx'(1-e^{x-x'})^{-\frac{1}{2}}=-x'-2\ln[1-(1-e^{x-x'})^{\frac{1}{2}}]. \quad (75)$$

It will still be necessary to calculate the next approximation by numerical integration.

If c is not a constant, then the integral $c\int dx\ \mathrm{csch}\frac{1}{2}(x+x_c)$ that leads to (70) is to be replaced by $\int c(x)dx\ \mathrm{csch}\frac{1}{2}(x+x_c)$ which will in most cases involve still another step of numerical computation.

Case II is sufficiently more complex that we shall not attempt to discuss its solution in the above fashion.

4. EVALUATION OF PARAMETERS FROM EXPERIMENTAL RESULTS

It is evident from the results of the last section that the best use of the theory at present would be to try evaluating the various parameters directly from the experimental results.

As Grahame[1] has pointed out, the interrupter method probably does not give any information on the differential capacity that is not available by the bridge method. Let us assume therefore that $C(E)$ can be taken as an experimentally known function of E. Then the experimental results for E as a function of t can be directly transformed into knowledge of i as a function of t.

Two methods of handling this information can be proposed on the basis of the equations of Sec. III. In the first place, we can attempt the evaluation of the coefficients in Eqs. (51) and (54). For instance, straight lines fitted to the i and E curves at $t=0$ will give E_0, i_0, and B and some information on $C_0=C(E_0)$. Independent information on the latter, however, should probably be used to improve the data for times near $t=0$. Subtraction of the equation of the best-fitted straight line from (51) and (54) will yield curves that should fit expressions starting with $t^{\frac{1}{2}}$ and t^2, respectively. If the resulting data are divided by these respective powers of t, and new straight lines fitted, the next two higher coefficients in each series are obtained. There are, of course, numerous other numerical procedures for fitting the equations to the data.

If the quantity B is found for several values of E_0, not too different from each other and large enough to make the reverse current quite small, a value of α can be obtained in the usual way from a semilogarithmic plot, since the variation of w_{10} with E_0 will not greatly disturb the determination of the exponent.

The other procedure that suggests itself is to fit Eq. (65) as it stands to the data. If we have or can obtain α, we then know $x(t)$ or $t(x)$, and can calculate all the variable terms in Eq. (65). It then becomes a matter of setting one known function, say

$$F_1(x)=-c(x)dx/dt, \quad (76a)$$

equal to a sum of three others with unknown coefficients. That is, let

$$F_2(x)=e^x, \quad (76b)$$

$$F_3(x)=e^x\int_{x_0}^{x}\frac{c(x')-i_0(dt/dx')}{[t(x)-t(x')]^{\frac{1}{2}}}dx', \quad (76c)$$

$$F_4(x)=e^{-x} \quad (76d)$$

and we have

$$F_1(x)=n\mathfrak{F}w_{10}k_1F_2(x)+k_1(\pi\epsilon_1)^{-\frac{1}{2}}F_3(x)-n\mathfrak{F}w_2k_2F_4(x). \quad (77)$$

It now becomes a matter of using standard curve-fitting procedures to find "best" values of the three coefficients in (77) from suitable data.

If ϵ_1 is available from polarographic experiments, as is usually true, we have a method for evaluating k_1 and hence w_{10}, as functions of E_0 and i_0.

Let us consider case II. The evaluation of the coefficients in the expansions for i and E corresponding to (51) and (54) involves nothing new, but the coefficients will be more complicated and more terms will be needed to get significant results. Fitting data to an equation like (77) is, however, not a simple matter. Let us assume (1) that we know the values of α and α_{12}, and (2) that the reverse currents are negligible. Then w_3 does not enter Eq. (2) and we can eliminate it from consideration.

The chief complication is the variation of w_2, determined by Eq. (6). Let us use F's for the known functions in Eqs. (2) and (6), as we did for Eq. (77). However, we shall use t as the independent variable.

$$F_1(t)=n\mathfrak{F}w_{10}k_1F_2(t)+k_1F_3(t)(\pi\epsilon_1)^{-\frac{1}{2}}+[n\mathfrak{F}w_{10}k_1F_4(t)+k_1(\pi\epsilon_1)^{-\frac{1}{2}}F_5(t)]w_2(t), \quad (78)$$

$$dw_2/dt=-Kw_2(t)^2+n\mathfrak{F}w_{10}k_1F_2(t)+k_1(\pi\epsilon_1)^{-\frac{1}{2}}F_3(t)-[n\mathfrak{F}w_{10}k_1F_4(t)+k_1(\pi\epsilon_1)^{-\frac{1}{2}}F_5(t)]w_2(t), \quad (79)$$

with $dw_2/dt=0$ when $t=0$.

If we could solve (79) explicitly for w_2 in terms of the known functions F_2, F_3, F_4, and F_5, we could substitute in (78) and get an expression to be fitted to $F(t)$ by adjustment of the parameters. Equation (79) can be made linear by writing

$$w_2=\frac{1}{Kv}\frac{dv}{dt}. \quad (80)$$

If (79) is written in the form

$$dw_2/dt=-Kw_2^2+g(t)-h(t)w_2(t), \quad (81)$$

then the equation for v is

$$d^2v/dt^2+h(t)dv/dt+Kg(t)v=0. \quad (82)$$

There are standard methods for solving (82) if $h(t)$ and $g(t)$ are known, but they are complicated, and only

numerical methods will work if h and g do not have simple forms.

The problem of obtaining parameters from the data in the hydrogen discharge case is thus seen to be extremely complicated and difficult, although not impossible. The main reason for dealing with case II in this paper was to demonstrate this complexity.

5. MATHEMATICAL APPENDIX

The various results given in this paper can all be verified by straightforward, elementary calculation, but their derivation from the differential equations is complicated. Since further work in this field will most likely involve developing the solution of other but similar equations, it seems appropriate to give here a brief outline of the method of Laplace transforms which so readily yields the results of Secs. 2 and 3. We shall quote from the theory of this method only those mathematical assertions which are directly relevant.[9]

The Laplace transform of any arbitrary function $F(t)$ of any variable ranging from 0 to ∞ is a new function $\varphi(s)$ given by

$$\varphi(s)=\int_0^\infty e^{-st}F(t)dt\equiv\mathfrak{L}\{F(t)\}. \tag{A-1}$$

Provided the integral is suitably convergent, there is a unique relationship between F and φ; several tables of pairs of such functions are available.[10] An equation for F can be turned into one for φ; frequently the latter is easy to solve, whence F can be found from a table.

It is not always certain that a given $\varphi(s)$ is the Laplace transform of any $F(t)$. However, if an F can be found such that φ is derivable from it by (A-1), the doubts are erased. There is one criterion of a negative sort, however, which is quite general and is needed in the present case. Any $\varphi(s)$ calculated from (A-1) must go to zero, as $s\rightarrow+\infty$. Thus if a function of s is found that does not go to zero as $s\rightarrow+\infty$, there can be no $F(t)$ corresponding to it, and we are thereby warned to search for a mistake or another solution.

The Laplace transform obeys in particular the following properties:

(a) The relation between φ and F is linear.

(b) If $\varphi_1(s)=\mathfrak{L}\{F_1(t)\}$ and $\varphi_2(s)=\mathfrak{L}\{F_2(t)\}$ then

$$\mathfrak{L}\left\{\int_0^t F_1(t')F_2(t-t')dt'\right\}=\varphi_1(s)\varphi_2(s). \tag{A-2}$$

(c) $$\mathfrak{L}\{dF(t)/dt\}=s\varphi(s)-F(0). \tag{A-3}$$

Let us now consider the simplest case of Sec. 2—namely that to which Eqs. (16), (17a), (17b), and (17d) apply. We shall write $v(x,s)$ for the transform of $u(x,t)$:

$$v(x,s)=\int_0^\infty e^{-st}u(x,t)dt, \tag{A-4}$$

where x is treated as a constant with respect to the integration. Now let us multiply both sides of Eq. (16) by $e^{-st}dt$ and integrate from 0 to ∞. We have then using (A-3) and (17a),

$$\epsilon\partial^2v/\partial x^2=sv(s,t)-u(x,0)=sv(s,t)-w_0-Gx. \tag{A-5}$$

Letting the transform of $w(t)$ be denoted by $\omega(s)$, (17b) and (17d) become

$$v(0,s)=\omega(s), \tag{A-6}$$

$$v(x,s)/(w_0+Gx)\rightarrow 1/s \quad \text{as} \quad x\rightarrow\infty. \tag{A-7}$$

Equation (A-5) is an ordinary differential equation in x, of the second order with constant coefficients. It is easily soluble by standard methods, and the particular solution that satisfies (A-6) and (A-7) is

$$v(x,s)=[\omega(s)-w_0/s]\exp[-x(s/\epsilon)^{\frac{1}{2}}]+(w_0+Gx)/s. \tag{A-8}$$

The expression in (A-8) can now be recognized from tables and (A-2), as the transform of

$$u(x,t)=w_0+Gx+\int_0^t \frac{dt'w(t-t')x\exp(-x^2/4\epsilon t')}{2(\pi\epsilon t'^3)^{\frac{1}{2}}} -2w_0\pi^{-\frac{1}{2}}\int_{x/2(\epsilon t)^{\frac{1}{2}}}^\infty \exp(-\xi^2)d\xi, \tag{A-9}$$

which can be recognized as being Eq. (19), partly in the form (19a) and partly in the form (19b).

However, the relations we are most interested in are those between $w(t)$ and $g(t)$. Since $g(t)=(\partial u/\partial x)_{x=0}$, the transform of g, say $\gamma(s)$, is given by

$$\gamma(s)=[\partial v(x,s)/\partial x]_{x=0}. \tag{A-10}$$

From (A-8) we have (after some rearranging)

$$\gamma(s)=(G/s)-[s\omega(s)-w_0](s\epsilon)^{-\frac{1}{2}}. \tag{A-11}$$

[9] Of the many treatments of Laplace transforms in the literature, the following are especially useful as references for the material of this section: H. S. Carslaw and J. C. Jaeger, *Conduction of Heat in Solids* (Oxford University Press, London, 1947), Chap. XI; and G. Doetsch, *Tabellen zur Laplace-Transformation und Anleitung zum Gebrauch* (Springer-Verlag, Berlin and Göttingen, 1947), out of print. See also H. S. Carslaw and J. C. Jaeger, *Operational Methods in Applied Mathematics* (Oxford, University Press, New York, 1941); P. Delahay, *New Instrumental Methods in Electrochemistry* (Interscience Publishers, Inc., New York, 1954), pp. 415–419; R. V. Churchill, *Modern Operational Mathematics in Engineering* (McGraw-Hill Book Company, Inc., New York, 1944); L. A. Pipes, *Applied Mathematics for Engineers and Physicists* (McGraw-Hill Book Company, Inc., New York, 1946), pp. 119–140 and Chap. XXI. Pipes uses $s\mathfrak{L}\{(t)\}$ as the Laplace transform of $f(t)$.

[10] The most extensive lists are contained in the following: A. Erdélyi *et al.*, *Tables of Integral Transforms* (McGraw-Hill Book Company, Inc., New York, 1954), Vol. I; G. Doetsch, cited in previous footnote; N. W. McLachlan and P. Humbert, *Formulaire pour le Calcul Symbolique* (Gauthier-Villars, Paris, 1941 and 1950), Nos. 100 and 113 of the series "Memorial des Sciences Mathématiques." This last reference uses $s\mathfrak{L}\{f(t)\}$ as the Laplace transform.

Since $s\omega(s)-w_0$ is the transform of $dw/dt=\dot{w}(t)$, and $s^{-\frac{1}{2}}$ is the transform of $(\pi t)^{-\frac{1}{2}}$, we immediately have Eq. (21).

Now, (A-11) can be easily solved for $\omega(s)$:

$$\omega(s)=(w_0/s)-[\gamma(s)-G/s](\epsilon/s)^{\frac{1}{2}}. \quad \text{(A-12)}$$

Since $\gamma(s)-(G/s)$ is the transform of $g(t)-G$, we immediately have Eq. (22).

The more complicated cases of Sec. 2 can all be derived in a similar fashion. For instance, if we take l finite, and use (17c) in place of (17d), we must replace (A-7) by

$$v(l,s)=(w_0+Gl)/s. \quad \text{(A-13)}$$

The solution of (A-5) now becomes

$$v(x,s)=\frac{s\omega(s)-w_0}{s\sinh l(s/\epsilon)^{\frac{1}{2}}}\sinh(l-x)(s/\epsilon)^{\frac{1}{2}} + (w_0+Gx)/s. \quad \text{(A-14)}$$

Equations (A-11) and (A-12) become

$$\gamma(s)=\frac{G}{s}-\frac{\coth l(s/\epsilon)^{\frac{1}{2}}}{(\epsilon s)^{\frac{1}{2}}}[s\omega(s)-w_0] \quad \text{(A-15)}$$

and

$$\omega(s)=w_0/s-(\epsilon/s)^{\frac{1}{2}}[\tanh l(s/\epsilon)^{\frac{1}{2}}][\gamma(s)-G/s]. \quad \text{(A-16)}$$

The inversion of Eqs. (A-14), (A-15), and (A-16), involves the hyperbolic functions, given in Doetsch,[9] table 5, and Erdélyi,[10] table 5.9. (The relation that $\varphi(as)$ is the transform of $F(t/a)/a$, with $a>0$, is also needed in using the tables.) The series forms given in Eqs. (18), (25), and (26) may be derived, however by the following consideration. All the hyperbolic functions that can appear must have denominators of the form $\exp(bs^{\frac{1}{2}})\pm\exp(-bs^{\frac{1}{2}})$ if the necessary relation $\varphi(s)\to 0$ as $s\to\infty$ is to hold. Such a denominator can be expanded by the binomial series as follows:

$$\frac{1}{\exp(bs^{\frac{1}{2}})\pm\exp(-bs^{\frac{1}{2}})} = \frac{\exp(-bs^{\frac{1}{2}})}{1\pm\exp(-2bs^{\frac{1}{2}})} = \exp(-bs^{\frac{1}{2}}) \times\sum_{n=0}^{\infty}(\mp 1)^n[\exp(-2bs^{\frac{1}{2}})]^n, \quad \text{(A-17)}$$

whence the simpler exponential functions used in deriving (A-9) appear.

To derive the most general solution given for $u(x,l)$—Eq. (33)—we solve Eq. (A-5) for the most general conditions, namely, that $u(x,0)$ is an arbitrary function $u_0(x)$, that $v(0,s)=\omega(s)$ and $v(l,s)=u_0(l)/s$. The solution, as can be readily verified, is

$$\begin{aligned} v(x,s)=&[s\omega(s)-w_0][\sinh(l-x)(s/\epsilon)^{\frac{1}{2}}/s\sinh l(s/\epsilon)^{\frac{1}{2}}] \\ &+[u_0(x)/s]+[(\epsilon/s^3)^{\frac{1}{2}}/2\sinh l(s/\epsilon)^{\frac{1}{2}}] \\ &\times\left\{\int_0^l d\xi u_0''(\xi)\cosh[(l+x-\xi)(s/\epsilon)^{\frac{1}{2}}]\right. \\ &-\int_0^l d\xi u_0''(\xi)\cosh[(l-x-\xi)(s/\epsilon)^{\frac{1}{2}}] \\ &\left.+\int_0^x d\xi u_0''(\xi)\cosh[(l-x+\xi)(s/\epsilon)^{\frac{1}{2}}]\right\}. \end{aligned} \quad \text{(A-18)}$$

In inverting this solution, care must be taken to see that the various ratios of hyperbolic functions approach zero as $s\to\infty$. It will be found that appropriate combinations of the integrals must be taken, and that then the relatively simple form of Eq. (33) can be obtained. The other equations given in Sec. 2 can also be obtained from (A-18).

Another use of the Laplace transform method is to give an alternative and more systematic way of developing the expansions in powers of t of Sec. 3. If the linear equations in Δi, ΔE etc. are transformed, algebraic equations in the transforms of these functions are obtained and easily solved. The results appear cumbersome, but since an expansion in positive powers and half-powers of t corresponds to a development in *negative* powers and half-powers of s, it is only necessary to expand these cumbersome solutions in inverse powers of s and in fact only to two or three terms, since the linear equations in the Δ's are only valid for two or three terms in t.

Finally, it might prove desirable to fit various analytic functions other than powers to the experimental data. If it is desired to find functions which yield simple or at least known expressions when subjected to the operation

$$\int_0^t F(t-t')(t')^{-\frac{1}{2}}dt'$$

an extensive table of Laplace transforms can be used to find functions with this property. The operation just given corresponds, with respect to the transforms, to multiplication by $(\pi/s)^{\frac{1}{2}}$. Therefore one seeks to find functions in the table of transforms that are given with arbitrary negative powers of s, or are given in pairs that differ only by a factor $s^{-\frac{1}{2}}$. As one example of such pairs, we have $(1/\pi)\sin\alpha t^{\frac{1}{2}}$ whose transform is $(\alpha^3/4\pi s^3)^{\frac{1}{2}}\exp(-\alpha^2/4s)$, and $t^{\frac{1}{2}}J_1(\alpha t^{\frac{1}{2}})$ whose transform is $(\alpha/2s^2)\exp(-\alpha^2/4s)$. ($J_1(x)$ is a Bessel function.) The two functions are related by

$$t^{\frac{1}{2}}J_1(\alpha t^{\frac{1}{2}})=(1/\pi)\int_0^t t'^{-\frac{1}{2}}\sin\alpha(t-t')^{\frac{1}{2}}dt'.$$

It is easy to show from the material of this section that if

$$f(t)=\int_0^t t'^{-\frac{1}{2}}F(t-t')dt',$$

with $f(0)=0$, as is required by this expression, then

$$F(t)=(1/\pi)\int_0^t t'^{-\frac{1}{2}}\dot{f}(t')dt'.$$

Therefore, any pair of functions used in one way in the integral relation we are considering can be inverted by taking the derivative of one of them and dividing by π as we have indicated.

Notes added in proof.—

1. Tachi and Kambara (Bull. Chem. Soc. Japan **27**, 523–524 (1954), and **28**, 25–31 (1955)) have carried out a treatment somewhat similar to that of this article, from a different point of view. In particular, they do not consider the period of interruption to be long in comparison to the transient decay times.

2. Vol. II of the book of Erdelyi et al.[10] contains in its section 13.1 several pairs of functions related as $f(t)$ and $F(t)$ above.

The author wishes to acknowledge with gratitude the support of the Office of Naval Research. He wishes to thank Professor D. C. Grahame for his courtesy in making it possible for the author to participate in his project, and for many stimulating discussions.

THE JOURNAL OF CHEMICAL PHYSICS VOLUME 23, NUMBER 10 OCTOBER, 1955

Effects of Oxygen on PbS Films*

HENRY T. MINDEN
Chicago Midway Laboratories, Chicago, Illinois
(Received December 28, 1954)

The effect of oxygen on the conductivity of vacuum evaporated PbS films has been experimentally investigated. When outgassed these films are *n*-type semiconductors. If they are exposed to oxygen at temperatures below about 200°C, the conductivity decreases with increasing pressure and then increases again. The thermoelectric power changes from negative to positive, but less than 10^{-3} moleO_2/molePbS is sorbed by the film.

Above 200°C the conductivity merely decreases when oxygen is admitted, and the thermoelectric power becomes small. The film gradually absorbs all the oxygen in the vacuum system and evolves a good deal of SO_2. When the reaction is complete, the conductivity returns to its initial value, and the thermoelectric power is once again negative. The film can repeatedly absorb large amounts of oxygen without there being any permanent change in electrical properties.

It is concluded that these films are composed of two layers. Next to the substrate there is a conducting layer that chemisorbs oxygen but does not react with it. The chemisorbed oxygen acceptors are responsible for the observed changes in conductivity. The upper layer of the film is nonconducting and reacts to completion with oxygen, possibly forming $PbSO_3$:PbO, and evolving SO_2.

INTRODUCTION

IT is well known that lead sulfide type films which are evaporated in vacuum can be rendered photoconductive by treatment with oxygen. The exact nature of this treatment and its theoretical basis are still not well understood, however.

PbS type films which have been evaporated in vacuum seem always to be *n*-type semiconductors. Levenstein and Bode[1] have discovered that PbTe films can be reversibly changed from *n*- to *p*-type by mere exposure to oxygen at room temperature. They found that maximum photosensitivity occurred when the resistance is greatest and the thermoelectric power is zero. Scanlon and Humphrey[2] have made a similar observation with PbSe films. Finally, in their original work on PbS films Sosnowski and his co-workers[3] reported the same findings, but they were quite obscure as to the nature of the oxygen treatment.

On the basis of his work Sosnowski[4] advanced the theory that oxygen reacts with the surface of the *n*-type microcrystals of the film. A surface *p*-region is thus formed, and the resulting micro *p-n* junctions are the sites of the photoeffect.

The chemistry proposed for these surface reactions is quite complex. By using electron diffraction techniques, Wilman[5] in England, and later Lark-Horovitz and his group[6] in America were able to identify a lanarkite ($PbO:PbSO_4$) phase in the film. Brockway[7]

* This work was supported in full by the United States Air Force under contract number AF 33(038)–25913.

[1] D. Bode and H. Levenstein, Phys. Rev. **96**, 259 (1954).

[2] Private communication.

[3] Sosnowski, Starkiewicz, and Simpson, Nature **159**, 818 (1947).

[4] L. Sosnowski, Phys. Rev. **72**, 641 (1947).

[5] H. Wilman, Proc. Roy. Soc. (London) **60**, 117 (1948).

[6] K. Lark-Horovitz *et al.*, Phys. Rev. **79**, 203 (1950).

[7] Private communication.

has recently discovered other oxidized phases in PbS films.

Such oxidized phases as have been discovered, however, should not be p-type conductors, but rather, insulators. Moreover, insofar as can be determined, these phases have been formed at temperatures and oxygen pressures much higher than needed for photosensitization.

In the present work the kinetics and stoichiometry of oxidation have been quantitatively investigated. The resistance changes caused by exposure of the film to oxygen have been correlated with the nature of the treatment. It is believed that the results of this investigation shed a new light on the nature of Sosnowski's surface p-region, and that the general character of the complex oxidation chemistry has been somewhat elucidated.

EXPERIMENTAL METHODS

Evaporation Cell

The lead sulfide used in this work was synthesized from specially purified lead and sulfur and grown into single crystals by vapor phase deposition.[8] The films were prepared by the evaporation of small weighed amounts of the ground up single crystals; the residual pressure during evaporation was not more than 10^{-5} mm. Figure 1 illustrates the Pyrex glass cell in which the films were evaporated. A weighed amount of lead sulfide A is introduced through the sidearm B onto the quartz evaporation head C, which is located close to the center of the sphere G. D is a quartz to Pyrex graded seal. The sidearm B is sealed off, and the cell is evacuated through the tubulation E to a pressure of 10^{-6} mm, the ultimate vacuum attainable by the system used. The cell is outgassed in a furnace at 300°C, after which the lead sulfide is evaporated onto G by means of the removable heater F. In this manner a fairly uniform film is produced on a hemispherical surface. The thickness $\tau = sm$ where m is the weight of PbS used and s is a constant depending on the dimensions of the cell, the density of the PbS microcrystals, and the shape and packing of these microcrystals on the substrate (close-packed spheres, cubes, etc.). Depending on the film structure assumed, s varies by not more than about 30%.

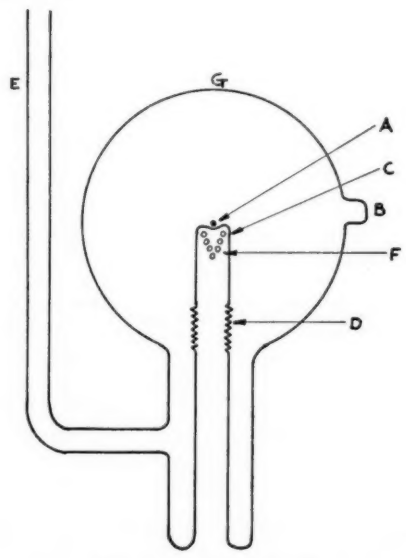

FIG. 1. Evaporation cell.

[8] F. Pizzarello, J. Appl. Phys. **25**, 805 (1953).

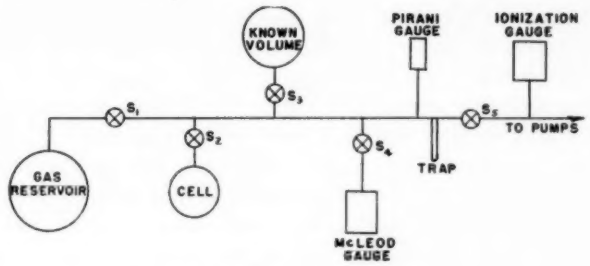

FIG. 2. Gas handling system.

Not shown in the figure are graphite electrodes. These are painted along meridians 180° apart and are separated at the north pole by a 1 mm gap. Most of the current flows around parallels of lattitude; thus a weighted conductivity of the whole film is measured. Two tungsten wires are sealed through the cell wall below the equator; each wire has a platinum strip spot welded to the inside end. The platinum strips are in turn sealed to the inside of the cell wall, and the graphite electrodes are painted over the strip. Neither the platinum nor the tungsten ever come into contact with the PbS.

The over-all dimensions of the cell were not more than $2\frac{1}{2} \times 3\frac{1}{2}$ inches, so it could readily be placed in a simple furnace. The cell temperature was measured by fastening a calibrated thermocouple to the outside of the cell dome by means of wet asbestos paper, which dried hard during the outgassing.

Gas Handling System

The vacuum system is shown in Fig. 2. Pressure from 1μ to 800μ was measured by a Pirani gauge, which was part of a special oscillator circuit.[9] The McLeod gauge was used for calibration only. The ionization gauge was used for measuring low pressures in a kinetic system.

The known volume was measured by weighing the water the vessel contained. The volumes of the rest of the system were measured by observing the pressure change due to the expansion of helium from the known volume.

Sorption Measurements

During the oxygen sorption measurements S_3 and S_4 (Fig. 2) were normally closed. The rest of the system to the right of S_1 was pumped out; S_2 and S_5 were then

[9] G. von Dardel, J. Sci. Instr. **30**, 114 (1953).

closed. The trap T was usually immersed in liquid nitrogen to freeze out condensable gas evolved by the film during sorption. Oxygen was introduced from the gas reservoir through the leak S_1. When the desired pressure in the manifold and gauge was reached, S_1 was closed and S_2 opened, admitting gas to the cell. From the pressure changes which slowly occurred, the amount of gas sorbed at any time could be calculated. Blank runs were made with no film in the cell, but the sorption was zero within the sensitivity of the method. The minimum sorption which could be detected was about 5×10^{-8} mole of gas; this was also the experimental error in the sorptions which were observed.

The gas condensed in T during the oxygen sorption process was found to be SO_2 and the Pirani gauge was calibrated for this gas as well as for oxygen. At the end of each sorption run the system was pumped out through S_5 with T still immersed in liquid nitrogen. (Usually there was a negligible amount of gas to pump out.) S_5 and S_2 were closed and T was allowed to warm to room temperature. From the pressure in the gauge and manifold the amount of SO_2 evolved during the oxygen sorption was determined.

Some experiments were done at low constant pressures in a kinetic system. S_2 and S_5 were open, and the leak S_1 was partially open. The pressure was monitored by the ionization gauge, or the Pirani gauge.

Conductivity Measurements

Conductance was measured using 60 cycle ac, partly for convenience and partly to minimize the effect of thermal emf's. A regulated 1 volt, low resistance source was used and the ammeter circuit had negligible resistance compared with that of the cell. The device was regularly calibrated against a standard resistance box.

Several assumptions and approximations have been made to permit the conversion of the conductance readings into conductivities. As was mentioned above, the current measured by the ammeter spreads through the whole film, not through just a small portion of it as is usual in PbS photocells. The prime assumption is, then, that the conductivity is indeed uniform throughout the film. Although inhomogeneities were hard to detect, the nature of the results indicated that the conductivity did not vary by more than a factor of 2 or 3 over the area of the film.

Since experiments with gold and with graphite electrodes gave identical results, it is probable that no error is introduced by the assumption that the electrodes contribute negligibly to the cell resistance, either in themselves or at the electrode-film interface.

Because of slight variations in the preparation of each cell blank, the evaporation head (C, Fig. 1) was not always located in the center of the hemisphere G. This introduced a possible variation in film thickness of $\pm0.2\mu$ over the area of the hemisphere. From the subsequent discussion it will become evident, however, that the important thickness in determining the conductivity is not the total thickness of the film (about 0.5μ), but rather the thickness of a conducting layer, assumed to be 0.1μ. This thickness may be low by as much as 100% which would make the calculated conductivity high by a factor of 2.

The model of current flow around parallels of lattitude is incorrect near the gap at the north pole of the cell. The approximation is improved by adding a current which is assumed to flow straight across the gap at the north pole. The errors introduced by this model would be fairly small were it easily possible to paint the electrodes correctly and to measure the dimensions of the gap precisely. In practice the errors so introduced might make the calculated value of the conductivity off by a factor of 2. In all, the calculated conductivities ought not to be incorrect by more than a factor of five.

Thermoelectric Power

Only the sign of the thermoelectric power was determined. A sensitive galvanometer was used, and one electrode of the heated cell was gently and briefly cooled with an air stream, or alternatively, one electrode of the cell at room temperature was heated slightly with a flame.

EXPERIMENTAL RESULTS

General Properties of the Films

Viewed through the glass substrate, the films had a shiny mirror-like appearance. Films thinner than about 0.1μ also appeared shiny when viewed from the side away from the substrate. The films used in this work were 0.5μ to 0.7μ thick. These films appeared dull on the side away from the substrate. Moreover, after oxidation this side of the film took on a whitish patina, while the mirror-like substrate side remained untarnished.

When the films were thoroughly outgassed, the conductance seemed to be more or less independent of film thickness. Only one film which was 0.026μ thick had an appreciably lower conductance than the rest. Moreover, the thermoelectric power was always negative. It is

TABLE I. Conductivity of PbS films.

Film	Weight PbS (mg)	σ^a (ohm-cm)$^{-1}$	N_d^b (10^{17} donors/cm^3)	N_{tot} (10^{-9} mole)	σ_{min} (ohm-cm)$^{-1}$
A–1[c]	0.70	7.9	0.99	0.115	0.178
A–2	17.7	19.4	2.42	0.95	0.090
A–3	14.6	13.5	1.70	0.545	
A–4	17.3	43.5	5.45	2.09	
A–5	9.4	14.0	1.75	0.364	
A–6	16.7	323	40.4	14.9	2.23
A–7	19.3	46	5.7	2.44	
A–8	15.8	44	5.5	1.93	

[a] When the film is outgassed. Assuming the conducting layer is 0.1μ thick.
[b] μ_n is assumed to be 500 cm^2/volt sec. (See S. J. Silverman and H. Levenstein, Phys. Rev. 94, 876 (1954).)
[c] Film thickness was 0.026μ.

assumed that the contacts between the microcrystals of the film are perfect. When the film is outgassed the resistance is due solely to the bulk properties of the microcrystals. The high conductivities observed tend to support the validity of this assumption.

When outgassed, then, the films behave like very impure electronic semiconductors. For such substances the conductivity $\sigma = qN_d\mu_n$ where q is the electronic charge, N_d is the concentration of donor impurities, and μ_n is the electron mobility, here assumed to be 500 cm²/volt sec. From the observed value of the conductivity when the film is outgassed, a value of N_d can be calculated. Table I shows σ and N_d for the films which were investigated.

Effects of Oxygen Not Accompanied by Detectable Sorption

When oxygen is admitted to contact with the film, the conductance decreased by one to three orders of magnitude. There was no detectable oxygen sorption accompanying these conductance changes. Figure 3 illustrates the typical variation of the conductivity σ with the pressure for three films at different temperatures. This effect showed considerable hysteresis in the conductance in going from low to high pressures and back down again. At low temperatures there was a definite minimum in the conductivity; near this minimum there was a change from negative to positive thermoelectric power. Above about 200°C the conductivity merely leveled off; when the conductivity was low, the thermoelectric power was substantially zero.

Figure 4 shows the change in conductivity with the time when oxygen was admitted to contact with a film. The pressure was 7μ and the temperature 90°C. Here again the typical minimum in conductivity was observed. The higher the pressure (above about 2μ) and the higher the temperature (up to about 200°C) the more quickly was the minimum reached. Below 2μ or above 200°C there was no minimum, as is evident from Fig. 3. Table I shows the minimum conductivity σ_{min}

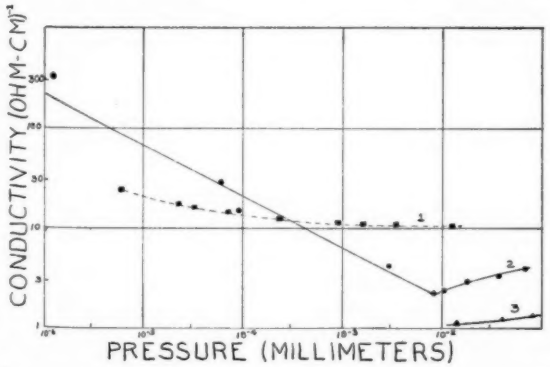

FIG. 3. Variation of conductivity with oxygen pressure. Curve 1, film A–7, 310°C. Curve 2, film A–6, 155°C. Curve 3, film A–3, 200°C.

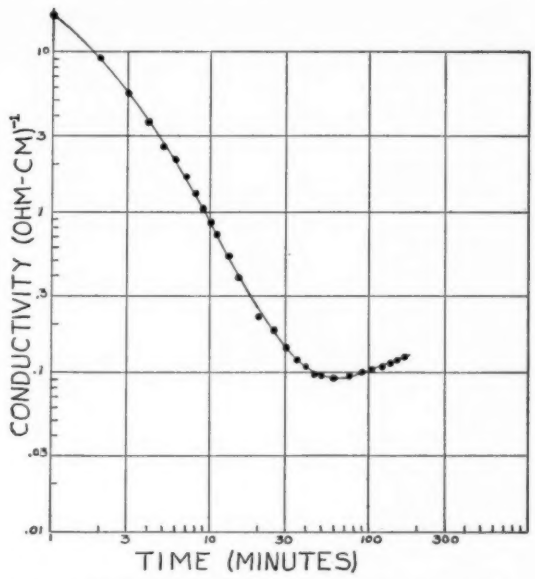

FIG. 4. Variation of conductivity with time, film A–2. Oxygen pressure, 7μ; temperature, 90°C.

observed in the presence of oxygen below 200°C for three of the films investigated.

Figure 5 shows the variation of the conductance g with temperature at several oxygen pressures. Again, there is considerable hysteresis in the temperature cycle. Nonetheless, the qualitative features of the curves are readily reproducible. At higher pressures there is always a conductance minimum in the neighborhood of room temperature, while at low pressures the temperature coefficient of conductance is very small and positive.

It was definitely established that the above effects were caused by the specific action of oxygen on PbS. Neither helium, nitrogen, nor sulfur dioxide had any effect on the conductance, nor were any of these gases sorbed by the film. Furthermore, no effects occurred when oxygen was admitted to cells having no films.

Several films were vacuum evaporated onto a cooled substrate; the pressure during evaporation was held below 10^{-5} mm. The film was then heated slowly from room temperature to 300°C under vacuum. As the temperature rose there was a considerable amount of outgassing. In one typical case (Fig. 6) the conductance increased slightly and then reached a maximum while the temperature was still below 80°C. With further heating the conductance decreased, reached a minimum (less than the initial value) and then rose over an order of magnitude. The film was baked at 300°C until gas evolution ceased and the conductance was constant; then the film was slowly cooled to room temperature. The conductance decreased only slightly, and there were no reversals in the cooling curve. Levenstein and Bode[10] have made a similar observation on PbTe films.

[10] Private communication.

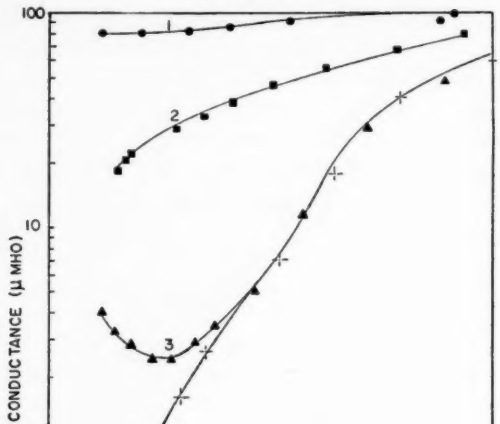

FIG. 5. Variation of conductance with temperature in the presence of oxygen, film A–1. Oxygen pressures—Curve 1, 6×10^{-6} mm; Curve 2, 2×10^{-4} mm; Curve 3, 1×10^{-3}mm; Curve 4, 2×10^{-3}mm.

Sorption of Oxygen

When oxygen was admitted to contact with PbS films at temperatures above about 200°C, there was immediately a sudden decrease in conductance. The thermoelectric power, which had initially been quite negative, all but vanished. Simultaneously the pressure in the system began to fall. If T (Fig. 2) was immersed in liquid nitrogen, the oxygen pressure invariably fell to zero over a period of time. The behavior of the conductance and the pressure as a function of time is shown in Fig. 7. On warming the trap at the end of the run (as described above) the condensed gas was evaporated. It was identified as SO_2 by vapor pressure measurements.† The above sequence of events could be repeated at will merely by introducing more oxygen, whether or not the SO_2 was pumped out. Sorption runs could have been made almost indefinitely, were it not for the fact that the sorption rate decreased with each successive run, until it became excessively small.

The amount of O_2 sorbed and the amount of SO_2 evolved was determined for each run. When the SO_2 was frozen out during the run, the average mole ratio O_2 sorbed to SO_2 evolved was 2.15 ± 0.22. This ratio was surprisingly independent of the film temperature, the initial oxygen pressure, and the particular film used. On the other hand, when the SO_2 was not frozen out but rather allowed to remain in contact with the film during the sorption, comparatively little SO_2 was evolved; the above ratio in these cases averaged about 15.

One film, having 65.9μ moles PbS, sorbed a total of 31.5μ moles O_2 and evolved 12.9μ moles SO_2 in the course of nine runs, during each of which the SO_2 was frozen out.

The sorption rate decreased markedly with decreasing temperature until it was almost negligible below 200°C. Since the rate of sorption depended strongly on the history of the film, however, it was not readily feasible to determine the temperature coefficient of the sorption rate.

The kinetics of oxygen sorption were investigated for the case in which the SO_2 evolved was frozen out during the run. Figure 8 is a semilogarithmic graph of pressure versus time for the last sorption run of the film mentioned above. Within experimental error the reaction was first order in the oxygen pressure.

As the oxygen pressure approached zero at the end of a run, the conductance began to increase until it ultimately reached its initial value before the introduction of the oxygen (see Fig. 6); moreover, the thermoelectric power became once again negative. In no case was there observed a permanent change in the conductivity or thermoelectric power.

DISCUSSION

General Structure of the Film

Although the films absorbed a great deal of oxygen, they remained n-type semiconductors in the absence of

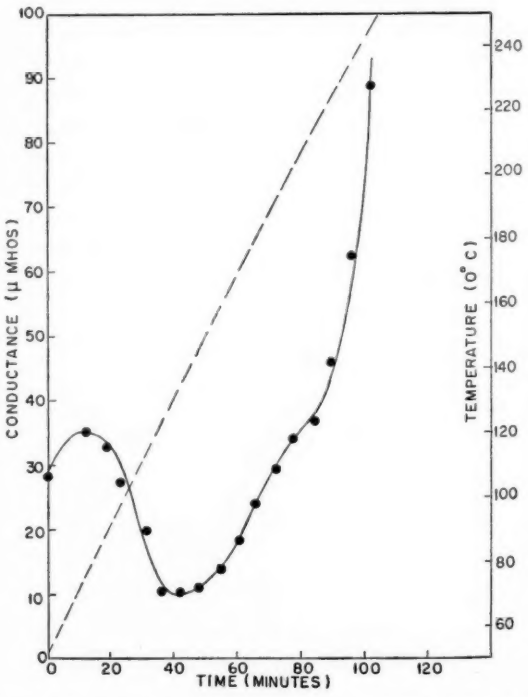

FIG. 6. Changes in conductance during outgassing, film A–3. Solid curve, conductance; dashed curve, temperature.

† The author is indebted to R. Harada for making the determination.

oxygen. Furthermore, the magnitude of the conductivity was never permanently altered by the sorption of oxygen. Finally the mirror-like layer next to the substrate was not tarnished by the oxidation of the films.

These facts strongly suggest that the films were not homogeneous throughout their thickness. It is proposed here that the mirror-like layer next to the substrate is responsible for almost all of the electrical conductivity of the film. Experience has shown that this mirror-like layer is roughly 0.1μ thick. On top of this substrate layer is a thicker, nonconducting, dull layer, which readily reacts with oxygen.

Harada[11] has shown that the true surface area of evaporated PbS films varies linearly with film thickness. This seems to be true for films as thin as 0.05μ up to thicknesses of 5μ. For annealed films the ratio of the true area to the apparent area (roughness factor) increases by a factor of 45 for every micron increase in film thickness. It was concluded that the films are quite porous. The calculated average size of the microcrystals composing the film is about 0.1μ in agreement with electron microscope data.[5] In the subsequent discussion the particle size for both layers will be assumed to be 0.1μ, and the surface areas will be calculated from Harada's work.

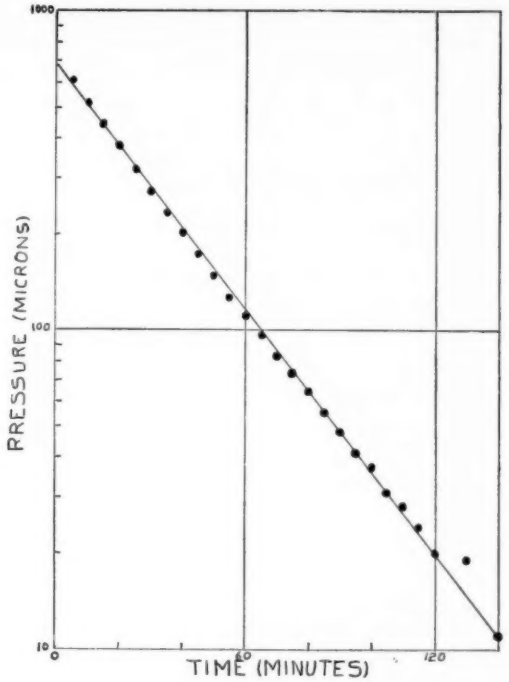

FIG. 8. Sorption of oxygen showing first-order reaction kinetics, film A–8.

The Conducting Layer

The conducting layer gives rise to almost the entire conductivity of the film. On this assumption, a free electron concentration of about 10^{17} was calculated from the conductivity of films when they were completely outgassed (see Table I). If this was also the free electron concentration of the nonconducting layer, the total free electron content (N_{tot} Table I) of the films prepared for this investigation (about 16 mg PbS) was in the neighborhood of 10^{-9} mole.

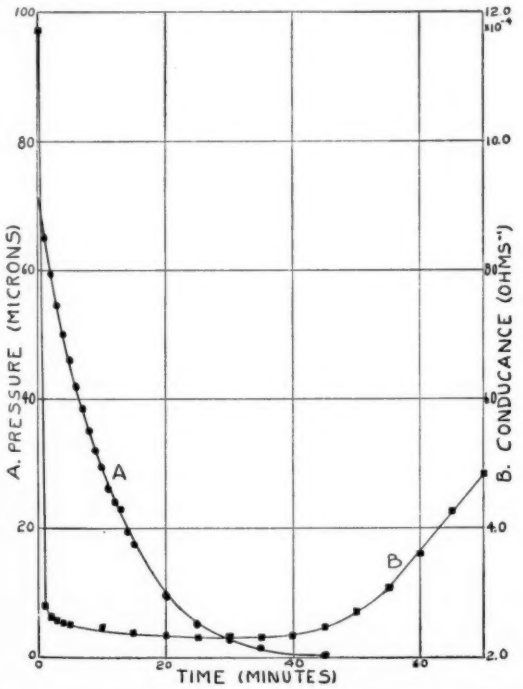

FIG. 7. Sorption of oxygen and accompanying conductance changes, film A–8. Curve A, pressure; Curve B, conductance.

When the oxygen gas is admitted in contact with the film, oxygen is chemisorbed as atoms onto the microcrystaline surfaces of the film. There the atoms act as low energy electron acceptors. The total surface area of the films was about 1000 cm²; the area occupied by a single oxygen molecule is 20 A². Thus the surface of the film can accommodate 6×10^{-7} mole of oxygen molecules close packed. This is over 100 times more oxygen acceptors than are needed to trap out the entire free electron content of the film. Furthermore, the amount of oxygen just needed to trap out the free electrons (10^{-9} mole) is less than 1/10th the minimum sorption which could be detected in this investigation (5×10^{-8} mole). This is why the conductivity was affected without there having been any detectable sorption.

The positive evidence for oxygen chemisoprtion rather than bulk diffusion into the microcrystals is twofold. First, the rate at which the oxygen affects the conductivity is fairly rapid at all temperatures. Second, the changes in conductivity brought about by the oxygen are readily and repeatedly reversible. What hysteresis there is in the conductivity versus temperature and pressure curves is attributed to the slowness of

[11] R. Harada, J. Chem. Phys. (to be published).

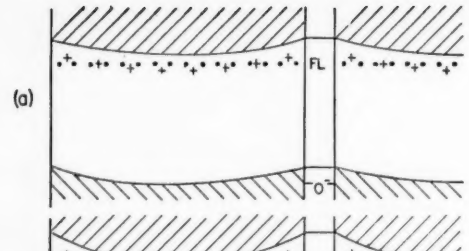

FIG. 9. Band model of oxygen chemisorption. FL Fermi level; +donors; 0^- surface oxygen acceptors. (a) No oxygen present; conduction is *n*-type. (b) Space-charge barrier; conduction is "intrinsic." (c) Development of *p*-type conducting region near surface.

oxygen migration along the grain boundaries between the microcrystals of the conducting layer (see Fig. 4).

Figure 9 illustrates the band theory of the effect of oxygen on the conductivity. The fresh film is highly conducting and *n*-type (Fig. 9(a)). Chemisorbed oxygen causes the formation of a positive space-charge region with a compensating negative surface states' charge (Fig. 9(b)). The potential barrier arising from the positive space charge produces a large decrease in electron conductivity (see Fig. 3). If enough oxygen is chemisorbed (Fig. 9(c)), the surface region of each particle is effectively converted to *p*-type material. The *n*-type interior is short circuited by the surface region, so that the conductivity of the film increases slightly and is *p*-type, as was observed. If the temperature is above 200°C, however, the intrinsic free electron concentration is sufficiently high to prevent the Fermi level at the surface (Fig. 9) from dropping much below the midpoint of the energy gap with any reasonable density of surface states. The *p*-region near the surface does not develop, so that the conductivity does not increase at the higher oxygen pressures; moreover, the thermoelectric power merely remains close to zero.

The scheme of Fig. 9 can be used to explain the experiment illustrated in Fig. 5. If a film is cooled from 350°C in the presence of a high enough pressure of oxygen, chemisorption will occur to an increasing extent during the cooling. The changes in conductance should be similar to those occurring when the oxygen pressure is increased at a constant temperature below 200°C.

If it is assumed that when PbS is evaporated onto a cooled substrate even at pressures of 10^{-5} mm, the film acquires a chemisorbed layer of oxygen, the effects of outgassing the film can be explained (see Fig. 6). Upon raising the temperature of the film initially, more electrons gain enough energy to surmount the surface potential barrier, so that the conductance increases slightly. As the temperature is still further increased, however, oxygen desorbs, leaving electrons which recombine with holes in the surface *p*-region. This accounts for the observed decrease in conductivity. Finally, when enough oxygen is desorbed, the space charge induced barrier disappears; the conductivity increases greatly, and is *n*-type, of course.

Chemical Reaction

It has been proposed here that only about 20% of a 0.5μ thick film contributes to electronic conduction. This layer is influenced by the chemisorption of oxygen, but is much less susceptible to reaction with oxygen than is the nonconducting layer. Nonetheless, on several films the amount of oxygen atoms sorbed at high temperatures (above 200°C) was equal to or greater than the total number of PbS molecules in the entire film. Clearly then, the chemical reaction cannot involve only one oxygen atom per PbS molecule. A plausible reaction is

$$O_2+\tfrac{2}{3}PbS\rightarrow\tfrac{2}{3}PbSO_3. \quad (1)$$

This is not the only chemical reaction which can take place, and it is possible that it is not even a correct one, since $PbO:PbSO_4$ has been previously reported as an oxidation product of PbS films. Reaction (1) most simply explains the results of this investigation, however, and it will be used for the sake of discussion. Any general conclusion reached on the basis of this reaction will apply also to the formation of higher oxidation products.

In the example quoted in the results, a film composed of 65.9μ moles PbS had absorbed 31.5μ moles O_2. For this amount of absorbed oxygen the stoichiometry of reaction (1) demands that $(\frac{2}{3})\times 31.5=21.0\mu$ moles of PbS be converted into $PbSO_3$; hence on the assumption of reaction (1) $21.0/65.9=32\%$ of the film was converted.

On the other hand, even after this 32% of the film had reacted, the reaction rate was becoming extremely slow. Figure 7 is the last sorption run for the above film. It will be noted that this run took some $2\frac{1}{2}$ hours, while earlier runs took less than 15 minutes. So it is quite possible that the outer layers of the film can be saturated by a great deal of oxygen without the inner, conducting layer being at all affected under the conditions of the experiment.

The evolution of SO_2 can be readily explained in terms of the well-known decomposition

$$PbSO_3\rightarrow PbO+SO_2. \quad (2)$$

When the SO_2 is frozen out, the mole ratio of O_2 sorbed to SO_2 evolved is very nearly 2. A combined reaction can be proposed for this case.

$$6O_2+4PbS\rightarrow PbSO_3+3PbO+3SO_2. \quad (3)$$

It is doubtful whether this reaction has much significance, since $PbSO_3$:3PbO does not seem to be a known compound. Reaction (3) is mentioned only because the 2:1 ratio of O_2 to SO_2 occurred under a surprisingly wide range of conditions. When the SO_2 is not frozen out, however, its presence in contact with the film seems to inhibit greatly reaction (2).

When the oxygen is first admitted to the cell, the conductivity decreases, and it is almost intrinsic, as described above. As the oxidation of the film progresses, the oxygen pressure in the cell decreases. The pressure goes so low, in fact, that at the end of the reaction the oxygen adsorbed on the conducting layer desorbs and reacts with the nonconducting layer. In this manner the conductivity of the film eventually should and does in fact rise to its original value. Furthermore, in spite of repeated oxidation, the final conductivity was always *n*-type, as would be predicted from this model.

CONCLUSIONS

Lead sulfide films which are evaporated in vacuum onto a smooth glass substrate are composed of two layers. Next to the substrate there is a 0.1μ thick mirror-like layer which is responsible for almost the entire electrical conductivity of the film. The conductivity of this layer is affected by oxygen, but there is no permanent oxidation. On top of this conducting layer there is a nonconducting layer which is readily oxidized.

The microcrystals of the conducting layer can reversibly chemisorb oxygen. The oxygen forms surface acceptor states on the *n*-type particles, and a positive space-charge barrier is produced. This barrier greatly reduces the conductivity of the film. If enough oxygen is chemisorbed, however, the space charge *p*-region can be sufficiently well developed to provide a shorting *p*-type conduction path around the *n*-type interior of the microcrystal.

When the temperature of the film is above about 200°C, in addition to being adsorbed by the conducting layer, the oxygen reacts chemically with the upper, nonconducting layer of the film. This reaction involves the absorption of relatively large amounts of oxygen and also the evolution of SO_2. The reaction goes so far to completion that oxygen is desorbed from the conducting layer with a consequent rise in *n*-type conductivity. Under the conditions of these experiments the conducting layer is not affected by the oxidation process.

It is concluded that when lead sulfide films are baked in oxygen, two relatively unrelated physico-chemical processes occur. A nonconducting layer of the film undergoes a gross chemical reaction with oxygen. The chemical changes produced in this layer by oxidation have little or no effect on the electrical properties of the film. The observed presence of macroscopic sulfate and oxide phases[5–7] is not a relevant condition for alterations in the electrical conductivity or for photosensitization.

On the other hand, even without gross exidation of the film, the electrical properties are readily affected by chemisorption of oxygen on the conducting layer of the film. Chemisorption also occurs during the gross oxidation process. The role of chemisorption in changing the conductivity has been described in this paper and will be elaborated upon in a subsequent theoretical paper.

Letters to the Editor

THIS section will accept reports of new work, provided these are terse and contain few figures, and especially few half-tone cuts. The Editorial Board will not hold itself responsible for opinions expressed by the correspondents. Contributions to this section should not exceed 600 words in length and must reach the office of the Editor not later than the 15th of the second month preceding that of the issue in which the Letter is to appear. No proof will be sent to the authors. The publication charge for Letters is $25 per page, with a minimum of $25 per Letter. If honored, the Institution will be entitled to 100 reprints without covers.

Chemical Shifts of Nitrogen

B. E. HOLDER AND M. P. KLEIN
University of California Radiation Laboratory, Livermore Site, California
(Received July 12, 1955)

THE large chemical shifts of the nuclear magnetic resonance of nitrogen[1,2] and the difficulty encountered in chemically analyzing for various nitrogenous compounds suggests that nuclear magnetic resonance may serve as a useful analytical method for nitrogen.

Employing a Varian V-4200 nuclear induction spectrometer and a 12-inch electromagnet, we measured the nitrogen shifts in a variety of compounds. The samples were in aqueous solution except for the compounds which are liquids. Figure 1 is a plot of the shifts in gauss with respect to the NO_2^- ion. All shifts are positive and are normalized to exactly 10 000 gauss.

Since it was previously reported[1] and verified in these experiments that the relative shifts for the two nitrogen isotopes are the same, only the abundant species, N^{14}, was studied.

Ramsey has developed theoretical expressions for the magnetic shielding of nuclei in molecules.[3-6] These expressions divide the shielding into two parts, the first of which is a diamagnetic term which is essentially the Lamb[7] shift. The second term considers the second-order paramagnetism resulting from orbital angular momentum. *S*-electrons dominate the diamagnetic term for nitrogen and, since the *s*-electrons enter into the chemical bonding only slightly if at all, it is considered that the shifts in nitrogen can be attributed almost entirely to the paramagnetic contributions. Variations in chemical bonding influence the orbital angular momentum, and such variations would produce chemical shifts. Saika and Slichter[8] have presented a calculation of the shift between F_2 and F^- based on this mechanism that agrees quite well with experiment.

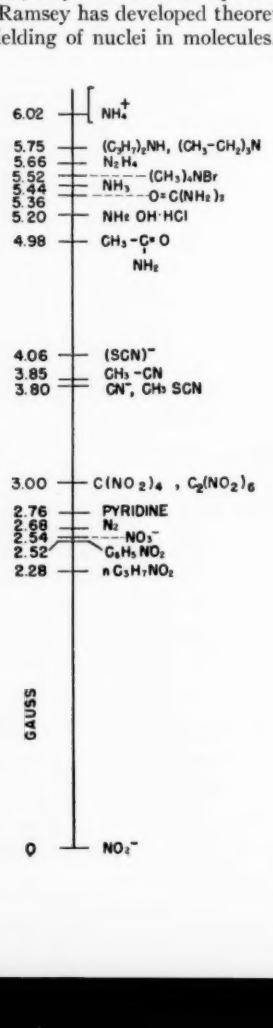

FIG. 1. Tabulation of chemical shifts taken relative to nitrite ion is in gauss. All shifts are positive—toward higher fields.

An atom that has a closed shell possesses zero angular momentum, and on this basis it is suggested that since the electronic environment of the nitrogen atom in the ammonium ion has most nearly the noble-gas structure, the contribution of second-order paramagnetism is least in all the compounds studied. As the electronegativity of the atoms or groups bonded to the nitrogen increases there is a progressive decrease in the ionic character of the nitrogen atom. The loss of ionic character and increase of covalency leads to asymmetries in the electronic structure, with consequent increase in orbital angular momentum resulting in paramagnetic shifts toward lower values of applied field. The order in which the species occur is in qualitative agreement with this concept. The shifts of the nitrate, nitrite, and ammonium ions are both concentration- and *p*H-dependent. From the concentration dependence certain facts concerning the state of dissociation and exchange rates of the ions may be deduced.[2,9,10]

All compounds were measured without addition of paramagnetic catalysts, the interaction between the nuclear quadrupole moment and the intramolecular electric field gradients providing the thermal relaxation mechanism.

The results presented here and in the accompanying letter of Weaver *et al.*, indicate that in order to explain the magnitudes and directions of the shifts in molecules were both oxygen and nitrogen occur, it will be necessary to consider in detail the variation in electronic wave functions and the manner in which bond types and hybridization influence the wave functions. Since hydrogen, nitrogen, and oxygen frequently occur together in the same molecule, a detailed study of the chemical shifts of each of these nuclides as they occur in a variety of molecules may provide a useful means for elucidating bond information. We have outlined methods for the determination of isotope abundance ratios by nuclear magnetic resonance,[11] and these same techniques are applicable to quantitative determinations of chemically nonequivalent nuclear species. Details will be presented in a future paper.

We acknowledge with thanks the aid of Dr. E. Bissell for many of the samples. This work was performed under the auspices of the U. S. Atomic Energy Commission.

[1] W. G. Procter and F. C. Yu, Phys. Rev. **77**, 716 (1950).
[2] Y. Masuda and T. Kanda, J. Phys. Soc. Japan **8**, 432 (1953).
[3] N. F. Ramsey, Phys. Rev. **77**, 569 (1950).
[4] N. F. Ramsey, Phys. Rev. **78**, 699 (1950).
[5] N. F. Ramsey, Phys. Rev. **83**, 540 (1951).
[6] N. F. Ramsey, Phys. Rev. **86**, 243 (1952).
[7] W. C. Dickenson, Phys. Rev. **81**, 717 (1951).
[8] A. Saika and C. P. Slichter, J. Chem. Phys. **22**, 26 (1954).
[9] H. S. Gutowsky and A. Saika, J. Chem. Phys. **21**, 1688 (1953).
[10] Hood, Redlich, and Reilly, J. Chem. Phys. **22**, 2067 (1954).
[11] B. E. Holder and M. P. Klein, Phys. Rev. **98**, 265(A) (1955).

Observation of Chemical Shifts of O^{17} Nuclei in Various Chemical Environments

H. E. WEAVER, *Varian Associates, Palo Alto, California*
AND
B. M. TOLBERT AND R. C. LA FORCE, *Radiation Laboratory and Chemistry Department, University of California, Berkeley, California*
(Received June 18, 1955)

THE dependence of the measured value of the gyromagnetic ratio of any nucleus upon the chemical environment of the nucleus is well known. Alder and Yu[1] in their measurement of

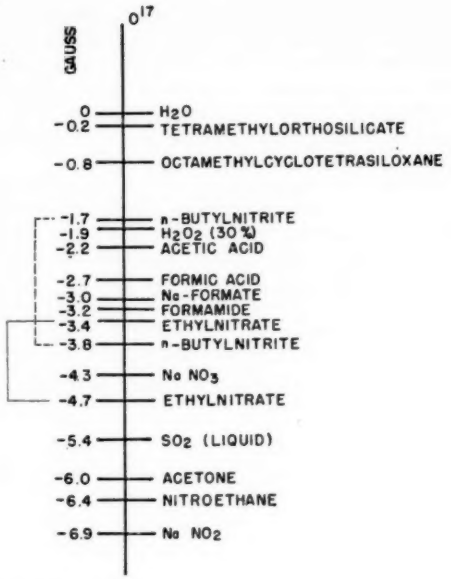

FIG. 1. The chemical shifts are taken relative to water and are based on a resonant field of 10 000 gauss. The brackets to the left of the vertical listing indicate those compounds in which a double resonance was observed. The dashed bracket indicates that the measurement was hampered by very low S/N for this compound.

$\mu(O^{17})$ reported observing chemical shifts of the order of 1/4000 for O^{17} resonance in acetic acid relative to water. The very low abundance (0.04%) of the O^{17} isotope and the resulting limitations in signal-to-noise of their apparatus were large factors which, until just recently, discouraged a more comprehensive study of chemical shifts associated with the O^{17} nuclear resonance.

Employing a Varian V-4200 Spectrometer and associated twelve-inch magnet system, $n-m-r$ signals of O^{17} in water may be obtained with an amplitude up to 50 times that of the random noise. This value of S/N is sufficient to permit observation of resonances in a wide variety of compounds with much lower oxygen content, without artificial enrichment. With few exceptions, the natural thermal relaxation time (T_1) of the O^{17} nucleus was sufficiently short as to provide the experimental conditions necessary for "slow-passage"[2] observation of the resonance. On the average, the line width of the O^{17} resonances was observed to be of the order of 3/10 of a gauss. The dispersion mode[2] was employed for the reason that the optimum value of the rf field, H_1, need not be so exactly chosen for maximum signal.

Of the liquids thus far studied none has yielded an O^{17} resonance which occurs at a higher field than that of water. For this reason, the water signal was taken as reference and all measurements are relative to this compound.

In the tabulated series of chemical shifts of Fig. 1, of particular interest are the two O^{17} signals of ethyl nitrate which occurred in an intensity ratio of roughly 1:2. These signals may be associated, respectively, with the oxygen in the C—O—N and 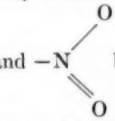 bonds of the ethyl nitrate molecule and provide a rather graphic illustration of the magnetic nonequivalence of these two types of bond situations of the oxygen atom.

The relative shifts of the O^{17} resonance in NO_3^- and NO_2^- are also interesting, since these shifts may be readily compared with the N^{14} data (see preceding letter, Klein *et al.*). The direction of the relative shift for N^{14} and O^{17} is indicative of the magnetic behavior of the electrons involved in the bonding of the ion. The fact that the magnitude of the relative shift for N^{14} and O^{17} in the NO_3^- and NO_2^- is identical, within the experimental error, is probably coincidental, and a more detailed theoretical picture is necessary before any significance may be attached to this result.

The fact that the oxygen resonance in water occurs at the highest field relative to all other bond situations thus far observed may lend itself to interpretation in light of the mechanism proposed by Ramsey[3] (see also Saika and Slichter[4]). As a result of the partial ionic character of the O—H bonds, the valence electrons of the oxygen atom probably form a system of high symmetry and under this condition of high symmetry, a lower amount of second-order paramagnetic and a higher amount of diamagnetic shielding would result, thus placing the resonance at the highest relative field. This interpretation is consistent with, for example, the occurrence of the O^{17} resonance in H_2O_2.

The authors wish to express their appreciation of Professor M. Calvin's interest in this work. Thanks are also due Dr. Malcolm Thaine of the Radiation Laboratories of the University of California.

[1] F. Alder and F. C. Yu, Phys. Rev. **81**, 1067 (1951).
[2] F. Bloch, Phys. Rev. **70**, 460 (1950).
[3] N. F. Ramsey, Phys. Rev. **86**, 243 (1952).
[4] A. Saika and C. P. Slichter, J. Chem. Phys. **22**, 26 (1954).

Note on the Interaction and Configuration in Chlorine-Benzene Complex

HIDEO MURAKAMI
Department of Chemistry, Faculty of Science, Osaka University, Osaka, Japan
(Received July 15, 1955)

RECENTLY, Collin and D'Or[1] discovered a broad infrared band at 526 cm^{-1} in solution of Cl_2 in benzene and assigned to the modified band of the fundamental vibration frequency of Cl_2 at 557 cm^{-1}. As discussed by them, the infrared activity of this band requires the appearance of electric moment in Cl_2 and consequently the existence of the relative configurations between Cl_2 and benzene in which two Cl atoms in the former component are electronically interacting with the latter component nonequivalently.

In order to explain such configurations, previously considered improbable, from the viewpoint of charge-transfer interaction, Mulliken[2] expected the exceptional situation which seems to be incompatible with the usual theoretical concept, that is, he expected the contribution of the more highly excited dative structures as well as the lowest energy dative term.

On the other hand, the present author[3] concluded, by the analysis of the relative intensity of ultraviolet charge-transfer spectra, that the contribution of charge-transfer interaction to the total binding energy between two components is much smaller than that of van der Waals type interaction.* If so, the required configuration should be explained from the viewpoints of van der Waals type interaction, packing condition, and statistical distribution.

First, the author points out that the infrared measurement was performed as the mixture of two components, benzene and Cl_2, without using any other inert solvent. Under such a condition as above, the dissolved Cl_2 molecule may be contacting with several (at least two) benzene molecules. Consequently, one can reasonably expect that such configurations as realizing the condition of the equivalent interaction among one Cl_2 and several benzene are highly improbable from the statistical point of view. That is, even when two Cl atoms in chlorine molecule are interacting with one benzene equivalently, they may be interacting with the other benzene nonequivalently.†

Second, the author points out the importance of the smaller molecular size of Cl_2 than I_2. It is reasonable to expect that the energy difference of van der Waals type interaction between the most stable configuration (the most compact one) and any other configurations is considerably reduced in Cl_2·benzene complex than in I_2·benzene complex on account of the smaller

molecular size of Cl_2. This sitation may increase the distribution probability of the latter configurations even in case of the isolated 1:1 complex in dilute solution system. It is obvious that the major part of the latter ones realize the condition of nonequivalent interaction.

From the statistical point of view, the observed absorption intensity ϵ_c of the ultraviolet charge-transfer spectra and also that of infrared band of fundamental vibration frequency in Cl_2 are both given by

$$\epsilon_c = \Sigma_i \bar{w}_i \epsilon_i / \Sigma_i \bar{w}_i, \quad (1)$$

where $\bar{w}_i$ is the distribution probability of any configuration i and ϵ_i is the absorption intensity in that configuration. In case of the aforementioned infrared band of Cl_2, ϵ_i of such configurations as satisfying the condition of equivalent interaction are vanish and Eq. (1) becomes as follows:

$$\epsilon_c = \Sigma_n' \bar{w}_n \epsilon_n / \Sigma_i \bar{w}_i. \quad (2)$$

Here the summation in the numerator extends over all configurations n which realize the condition of nonequivalent interaction. In practice, any one of $\bar{w}_n$ may not be equal to zero although it may be rather small,‡ and ϵ_c comes to have appreciable value since the summation extends over numerous terms. Moreover, the situation pointed out before make the ratio $\Sigma_n' \bar{w}_n / \Sigma_i \bar{w}_i$ and hence ϵ_c considerably larger. That is, one can expect the strong infrared activity even if the Mulliken's expectation is not realized. The broadness of the observed band is also in harmony with the statistical situation as discussed in the foregoing. The quantitative examination of the problem is a task for future study.

[1] J. Collin and L. D'Or, J. Chem. Phys. **23**, 397 (1955).
[2] R. S. Mulliken, J. Chem. Phys. **23**, 397 (1955).
[3] H. Murakami, Bull. Chem. Soc. Japan **26**, 441 (1953); **27**, 268 (1954); **28** (to be published).

* If the donor-character of one component is localized in one or a few oxygen or nitrogen atoms, the charge-transfer interaction amounts to considerable magnitude. For example, pyridine-iodine complex [C. Reid and R. S. Mulliken, J. Am. Chem. Soc. **76**, 3869 (1954)]. In this case, the situation is rather close to the usual covalent bond.

† Although the molecular arrangement in liquid benzene seems to have some regularity in the local and instantaneous meaning, the introduction of Cl_2 may cause considerable irregularity at least in the neighborhood of it.

‡ If one or more methyl groups are introduced into benzene ring, $\bar{w}_i$ of the unsymmetrical configurations may increase remarkably. (See reference 3.)

Phosphorescence of Solids Containing the Manganous or Ferric Ions

L. E. Orgel
Laboratory of Molecular Structure and Spectra, Department of Physics, The University of Chicago, Chicago 37, Illinois
(Received May 6, 1955)

We have recently identified the six lowest transitions of the hydrated manganous ion and have shown that the one at longest wavelength is from the ^6S ground state to the $^4G(T_{1g})$ state.[1] The theory is applicable to other tetrahedrally or octahedrally coordinated manganous ions. It is therefore probable that the same $^6S - ^4G(T_{1g})$ transition is responsible for the emission of manganese-activated phosphors.

Red phosphorescence at about 6100 A is produced by octahedrally coordinated manganese.[2] The rather large separations between the emission maxima and the nearest absorption maxima at about 5080 A[3] may be explained in the following way. The ^6S ground state of the manganous ion has the d-electron configuration $(t_{2g})^3(e_g)^2$ while the upper state has the configuration $(t_{2g})^4(e_g)^1$.[4] It has been shown that the radius of a transition-metal ion depends on the number of electrons in the e_g d-orbitals, decreasing as the latter decreases.[5] The internuclear distance in the excited state is, therefore, smaller than in the ground state, and so the value of Dq needed to calculate the position of the emission maximum is greater than that found in the ground state. In fact Dq for the excited state of Mn^{++} should very roughly equal that for the ground state of Cr^{++}, which has the configuration $(t_{2g})^3(e_g)$.[1] From the energy-level diagram, and from the known Dq values of Mn^{++} (780 cm^{-1}) and Cr^{++} (1200 cm^{-1}), we predict a separation of about 4800 cm^{-1} for the hydrated ion. This is larger than that observed in the phosphors (3200 cm^{-1}). The difference may be the result of the different Dq's appropriate to oxygen atoms in a solid lattice or to the inadequacy of the approximated Dq taken for the excited state. The experimental data is best fitted by $Dq = 1100$ cm^{-1} in the excited state, a quite reasonable value.

In the tetrahedral complexes the crystal fields are generally much weaker than in similar octahedral complexes so that both absorption and emission should occur at longer wavelengths. This theoretical result supports Weyl's conclusion[2] that in the phosphors which emit green light the manganese is tetrahedrally coordinated.

The energy-level diagram for the ferric ion is similar to that for the manganous ion. The phosphorescence, if it occurs, is predicted to be in the near infrared. It would be interesting to know if the quenching of visible phosphorescence by the ferric ion is accompanied by infrared emission.

[1] L. E. Orgel, J. Chem. Phys. **23**, 1824 (1955).
[2] S. H. Linwood and W. A. Weyl, J. Opt. Soc. Am. **32**, 443 (1942).
[3] F. A. Kröger, *Some Aspects of the Luminescence of Solids* (Elsevier Publishing Company, Inc., Houston, Texas, 1948).
[4] For an explanation of this notation see L. E. Orgel, J. Chem. Soc. 4756 (1952).
[5] J. H. van Santen and J. S. van Wieringen, Rec. trav. chim. **71**, 420 (1952).

Molecular Association and Proton Resonance in Propionic Acid

B. N. Bhar and G. Lindström
Nobel Institute for Physics, Stockholm, Sweden
(Received August 8, 1955)

By the help of the high-resolution nuclear magnetic resonance technique some interesting features of the proton spectra of propionic acid and its aqueous solution have been observed. The spectra were observed at 3285 gauss corresponding to the stimulating radio-frequency field of 13.997 Mc/sec to proton resonance and the resolution being 1 part in 2 millions. We believe that by virtue of the property of molecular association through a hydrogen bridge (bond) of the type $O-H\cdots O$, propionic acid, like acetic acid, exists as double molecules, which can be represented as

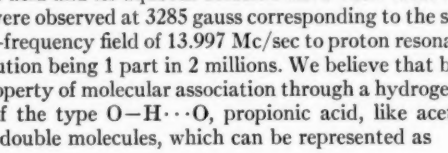

The proton resonance absorption spectrum of the acid revealed only two peaks with no further details, according to the present resolution of our apparatus as mentioned above, the one occurring at the lower value of the externally applied magnetic field is due to bridge protons of the COOH group and the other one due to protons of the CH_3 and CH_2 groups as it seems that their natural line widths are greater than their separation. In aqueous solution the protons of water and COOH groups will constitute a common line. By adding water to the acid the dimers will break up to monomers and there will also be an alternative formation of hydrogen bond with water and a rapid exchange of protons between the water and the COOH group of the acid. If the correlation time of the associated and unassociated states of the propionic acid is sufficiently small, the proton resonance of the COOH group will be observed at a frequency corresponding to the average diamagnetic shielding for the two states. Since the dilution will alter the distribution between associated and unassociated states, the resonance frequency of the COOH group, and hence its chemical shift would be dependent upon dilution. It was observed that on increasing the dilution the common peak due to COOH group and water progressively shifted to higher values of the externally applied magnetic field, but near the region where the concentration of the acid was 50% by volume some "irregular-

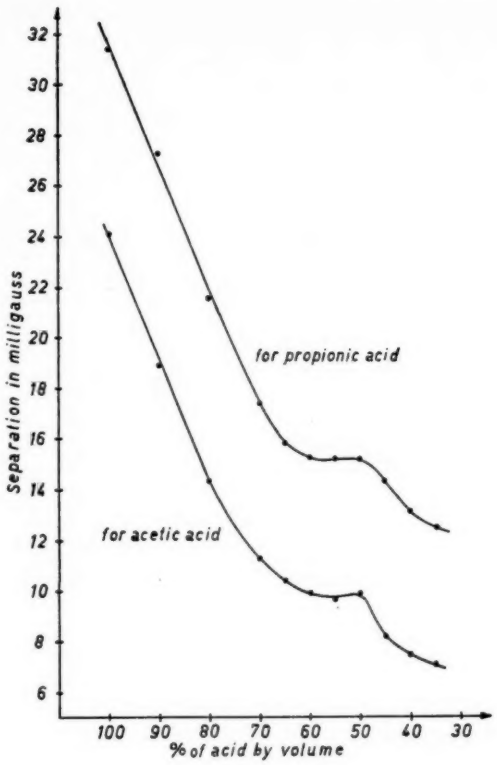

FIG. 1.

ities" of the shift was observed. When the separation of the dilution dependent COOH proton peak from the peak due to CH_3-CH_2 was plotted against the concentration of the acid by volume, as shown in the accompanying curve in Fig. 1, a "hump" was observed and the nature of the curve seemed to be similar to isothermals ($p-v$ curves) of gases obeying van der Waals' equation of state. This nature of the curve was also observed in the case of acetic acid-water system.[1] That curve is also presented here. The nature of the curve has recently been confirmed by Dr. J. N. Shoolery of Varian Associates, Palo Alto, California.[2] We believe that not only acetic acid and propionic acid but all chemical compounds which can exist in the associated state in the liquid phase (and hence suitable for high resolution $n-m-r$ work) by virtue of a hydrogen bond will present the same nature of the proton chemical shift curve when the extent of association is being altered by active solvents.

[1] Bhar, Forsling, and Lindström, Arkiv Fysik (to be published).
[2] Private communication.

Line-Width Transition of the Proton Magnetic Resonance in Polymers

AKIRA ODAJIMA, JUNKICHI SOHMA, AND MITSURU KOIKE
Research Institute of Applied Electricity, Hokkaido University, Sapporo, Japan
(Received July 1, 1955)

TO detect how the side chains of the polymers behave in their glassy to rubbery transitions, proton magnetic resonance studies have been carried on.

All lines showed no fine structure and simple bell-shaped curves. The line for polymethyl methacrylate (PMMA), however, has a central narrowing, plausibly interpreted to come from the rotation of the three-proton system of the methyl groups.[1] The second moments observed for the several polymers at room temperature, at which they are supposed to be in the rigid states, are shown in the first column of Table I. The second moment for a monomer are estimated and these values are given in the second column.

TABLE I. Observed and theoretical values of the second moments for the polymers.

Sample	(1) Observed	(2) Theoretical
Polystyrene	12.5 gauss[2]	6.8 gauss[2]
PMMA	8.5	7.8[a]
PVC	14.5	11.5

[a] The CH_3 groups contained in these polymers rotate about their C_3 axis at room temperature. In this case the contribution of these groups to the second moment is one-fourth as great as in the rigid state.

The samples we used have all large side chains except polyvinyl chloride (PVC). In the cases of PMMA and polystyrene, the line-width transitions occur in a two step process. In contrast with these cases, the line-width transition of PVC, which has small side chains, occurs in not two steps but only one step at the higher temperature. In Fig. 1 $\Delta H_{\frac{1}{2}}$ of the absorption lines are plotted against the temperature for PMMA, and PVC, respectively.

For PMMA, after the first narrowing the curve enters into the second step of an abrupt decreasing, followed probably by a leveling off. The values of the line width in the higher temperature region, however, may be greater than the true ones because of the modulation broadening. Concerning the line-width transition in the higher temperature region, it should seem reasonable that this corresponds to the transition which appears in the same temperature region in measuring the elastic and dielectric constants of this material at audio-frequencies or less.[2] On the other hand, the transition at the lower temperature should be supposed to correspond to the inflexion point of the ultrasonic velocity *vs* temperature curve for PMMA.[3]

Recently, Kubo and Tomita[4] presented the expression for $\Delta H_{\frac{1}{2}}$ caused by motional narrowing, being a modified form of BPP one.

$$(\Delta H_{\frac{1}{2}})^2=\frac{4\log 2}{\pi}\langle\Delta H_0^2\rangle\tan^{-1}\left(\frac{\pi\tau}{4\log 2}\gamma\Delta H_{\frac{1}{2}}\right), \qquad (1)$$

where $\langle\Delta H_0^2\rangle$ stands for second moment of the rigid state, τ for the correlation time of the Brownian motion, and γ for gyromagnetic ratio. If the intramolecular motion of the polymer is divided into two groups characterized by two different correlation times, we can adjust Eq. (1) to match the observed curve in Fig. 1. It would seem reasonable that one of these correlation times corresponds to the second step and is associated with the "hindered rotation" of the main chain. Concerning the other, we are inclined to consider it might correspond to the "hindered rotation" of the side chains. In the case of PVC, the curve is represented satisfactorily by Eq. (1).

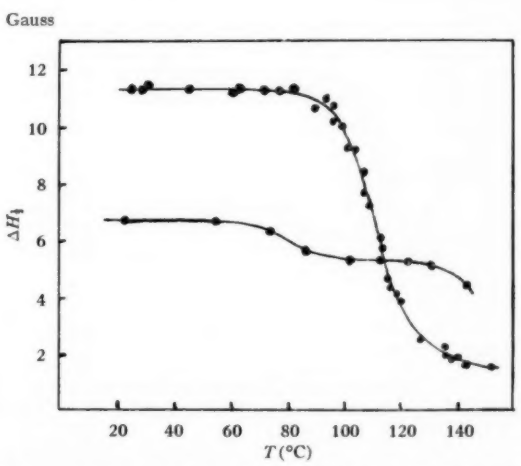

FIG. 1. Temperature dependence of the line width in PMMA (lower curve) and PVC (upper curve).

For PMMA, the only possible configuration of the carboxyl group in the side chain is the *trans*-form.[5] In this configuration, the rotation of the methyl group in the side chain are restricted about the only two axes, the C−C axis and the C_3 symmetry one. Its rotation about C−C axis causes little reduction in the broadening contributed from the two neighbors in the CH_3 group, because the C−C axis makes only small angle with the C_3 one. The rotation, however, reduces the additional broadening by the external protons, as it is discussed by Poweles and Gutowsky.[2] The above consideration leads us to the conclusion that the first step narrowing is probably attributed to the rotation of the side chain.

A more detailed account of this work as well as our results will be submitted for publication in the near future.

[1] J. G. Poweles and H. S. Gutowsky, J. Chem. Phys. **21**, 1695, 1704 (1953).
[2] S. Iwayanagi and T. Hideshima, J. Phys. Soc. Japan **8**, 368 (1953).
[3] S. V. Subrahayam, J. Chem. Phys. **22**, 1564 (1954).
[4] R. Kubo and K. Tomita, J. Phys. Soc. Japan **9**, 888 (1954).
[5] S. Mizushima, *Structure of Molecules and Internal Rotation* (Academic Press, Inc., New York, New York, 1954).

Order-Disorder Transitions in the Alkali Borohydrides

C. C. Stephenson, D. W. Rice, and W. H. Stockmayer
Department of Chemistry, Massachusetts Institute of Technology, Cambridge, Massachusetts
(Received August 8, 1955)

A λ POINT occurring[1] in anhydrous sodium borohydride at 190°K has been interpreted[2] as an order-disorder transition involving the orientations of the tetrahedral BH_4^- ions. The disordered crystal above 190°K is face-centered cubic,[3] while the low temperature ordered form has been found[4] to have the predicted[2] tetragonal structure. Since the borohydrides of potassium, rubidium, and cesium also have the face-centered cubic structure at room temperature,[4] entirely similar transitions are to be expected in these materials, at progressively lower temperatures as the lattice constant increases and the interactions between borohydride ions become weaker. We have now detected the expected transitions from cooling and warming curves: KBH_4 76°K±1°, $RbBH_4$ 44°K±3°, $CsBH_4$ 27°K±1°. For the last two salts a cooling bath of liquid helium was used.

In Fig. 1, a plot of the logarithms of the transition temperatures T_c against the corresponding values[4] of the distance r between the centers of neighboring borohydride ions is seen to give a fairly straight line. This is just the result to be expected if, as previously suggested,[2] the higher energy of the disordered phase ($\Delta E \cong RT_c \ln 2$ per mole) is due principally to increased overlap energy, which should vary approximately as $\exp(-r/\rho)$. The slope of the line in Fig. 1 gives $\rho \cong 0.45$ A, which is quite a reasonable value, though somewhat larger than the familiar Born-Mayer[5] figure of 0.35 A for the alkali halides.* Alternatively, a plot of $\log T_c$ against $\log r$, corresponding to an inverse-power law for the overlap energy, has a negative slope of about 10, which is again a reasonable figure for this power. However, some contribution to ΔE from electrostatic interaction between the octupolar charge distributions of neighboring BH_4^- ions, which would vary as r^{-7}, cannot be excluded.

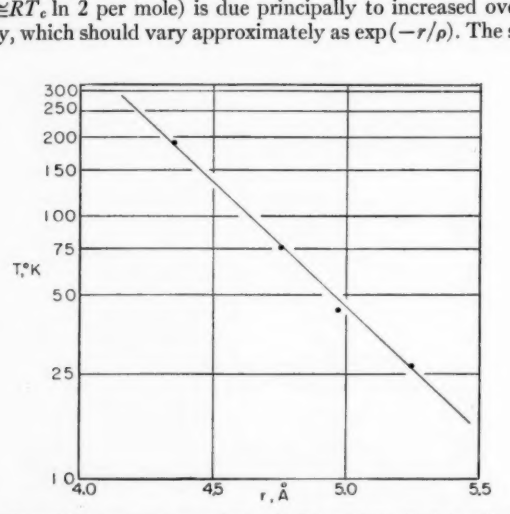

FIG. 1. Transition temperatures of Na, K, Rb, and Cs alkali borohydrides as a function of the distance between neighboring borohydride ions.

We thank Dr. M. D. Banus of Metal Hydrides, Incorporated, for the samples of the higher alkali borohydrides, which were the same ones used in the x-ray investigation,[4] and R. P. Cavileer, D. R. Bentz, D. A. Stevenson, and J. C. Morrow for experimental assistance.

[1] H. L. Johnston and N. C. Hallett, J. Am. Chem. Soc. **75**, 1467 (1953).
[2] W. H. Stockmayer and C. C. Stephenson, J. Chem. Phys. **21**, 1311 (1953).
[3] A. M. Soldate, J. Am. Chem. Soc. **69**, 987 (1947).
[4] S. C. Abrahams and J. Kalnajs, J. Chem. Phys. **22**, 434 (1954).
[5] M. Born and J. E. Mayer, Z. Physik **75**, 1 (1932).
* In Fig. 1 we have had to use values of r at room temperature instead of at T_c. Use of the latter would decrease ρ somewhat.

Energy Excitation of Vibrations in Halo-Methane Gases

Robert Amme and Sam Legvold
*Department of Physics, Iowa State College, Ames, Iowa**
(Received August 8, 1955)

ROSSING and Legvold have reported the collision lifetimes of molecular vibrations for fourteen halo-methanes at 300°K.[1] These they have plotted against the lowest vibrational modes for the molecules, along with data of other investigators taken at different temperatures. Theoretical lines were drawn according to the equation

$$Z_{10}=\frac{1}{\alpha(\epsilon^*/kT+1)}\exp(\epsilon^*/kT). \tag{1}$$

α is called the steric factor, and ϵ^* is some minimum relative translational energy which must be exceeded to produce de-excitation. It appeared that ϵ^* is proportional to the energy of the lowest mode: $\epsilon^*=nh\nu_1$.

If, however, one wishes to consider the relative translational energy along the line of centers, it is then necessary to consider the component of the relative velocity along this line.[2] One then obtains alternatively the number of collisions per molecule per second in which the relative translational energy along the line of centers at the moment of contact exceeds a specified value ϵ^*:

$$\Re \exp(-\epsilon^*/kT), \tag{2}$$

where $\Re$ is the collision rate per molecule.

We assume now that the probability p_{10} in a given collision of de-exciting the molecule is a constant, α, when the relative energy along the line of centers is equal to or greater than the deactivation energy ϵ^* and is zero otherwise. If α is thought to be determined by the geometry of the particular molecule and therefore not a function of translational energy, the total number of collisions per second which the average molecule suffers causing de-excitation is simply $\alpha\Re\exp(-\epsilon^*/kT)$. The average probability p_{10} in a single collision that de-excitation occurs is therefore

$$\alpha\exp(-\epsilon^*/kT).$$

For $\epsilon^*=nh\nu_1$ the corresponding expression for the average collision lifetime of the first excited state is, in place of (1),

$$Z_{10}=1/p_{10}=(1/\alpha)\exp(nh\nu_1/kT). \tag{3}$$

This expression is similar to the empirical relationship given by Fogg, Hanks, and Lambert.[3]

It is interesting to examine the data of Rossing and Legvold on this new basis. Points numbered 1 through 7 in Fig. 1 show their results on the study of methane derivatives in which no hydrogen

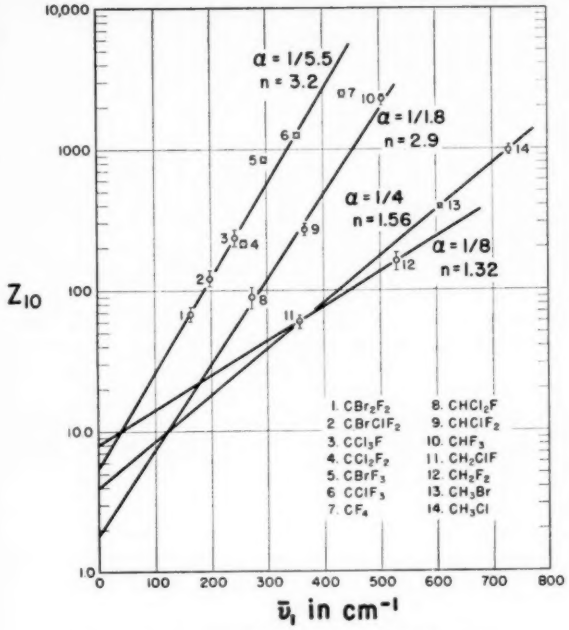

FIG. 1. Z_{10} interpreted by energy excitation theory.

atoms remain. These points approximate a straight line drawn using (3) with $n=3.2$ and $\alpha=1/5.5$, the value 5.5 being the intercept in this case. Thus one may still retain the association of the constant n with the number of hydrogen atoms replaced. Points 8, 9, and 10 represent molecules with one hydrogen remaining, and are seen to fall along a line drawn with $n=2.9$ and $\alpha=1/1.8$. Sette, Busala, and Hubbard[4] reported $Z_{10}=110$ for $CHCl_3$ at 303°K which approaches this line. ($\bar{\nu}=260$ cm^{-1}.)

Similar lines have been drawn through the pairs of molecules having two and one substitutions, but a single line might do well in locating both of these groups. Sette *et al.* have found multiple dispersion in CH_2Cl_2, and suggest that the mode of lowest frequency, 283 cm^{-1}, gives rise to the faster relaxation process. This short relaxation time corresponds to $Z_{10}=32$ at 300°K. This point falls in line with CH_2 ClF, CH_3Br, and CH_3Cl.

Judging from this interpretation, the steric factor cannot be easily taken as constant for the entire methane group, but does not appear to vary greatly; it ranges from around $\frac{1}{2}$ to $\frac{1}{6}$ in place of $\frac{1}{12}$ used by Rossing and Legvold. Inadequate data exist at the present time to test (3) well under temperature variation. When this equation is used to correct the data of Fogg *et al.* for CH_3Cl and CH_3Br, the resulting values of Z_{10} are, as for CF_4, about 20% high.

* Work done in cooperation with the Iowa State College Engineering Experiment Station and sponsored by the National Advisory Committee for Aeronautics and by the Air Research and Development Command.

[1] Rossing and Legvold, J. Chem. Phys. **23**, 1118 (1955).
[2] Fowler and Guggenheim, *Statistical Thermodynamics* (The Macmillan Company, New York, 1939), paragraph 1201.
[3] Fogg, Hanks, and Lambert, Proc. Roy. Soc. (London) **A219**, 490 (1953).
[4] Sette, Busala, and Hubbard, J. Chem. Phys. **23**, 787 (1955).

Erratum: Equation of State and the Thermal Dependence of the Elastic Coefficient of Crystalline Argon

[J. Chem. Phys. **23**, 681 (1955)]

JOHN H. HENKEL
Field Research Laboratories, Magnolia Petroleum Company, Dallas, Texas

THIS paper is based on a thesis submitted in partial fulfillment of the requirements for the degree of Doctor of Philosophy at Brown University, June, 1954.

Effect of Proton Irradiation upon the Rate of Solution of Fe_2O_3 in Hydrochloric Acid

M. SIMNAD AND R. SMOLUCHOWSKI
Carnegie Institute of Technology, Pittsburgh, Pennsylvania
(Received July 20, 1955)

THE influence of the crystal structure of metal compounds upon their behavior in aqueous solutions is known to be appreciable. An outstanding example of this is provided in the recent work of Pryor and Evans[1] on the solubility of ferric oxide, Fe_2O_3, in hydrochloric acid solutions. Their results show that, at *p*H values below 2, the rate of reductive dissolution of ferric oxide is controlled by the ionic surface conductivity of the oxide and hence by the number of surface defects. This is based on the observation that specimens annealed at high temperatures had a greater resistance to attack by acid solutions than those prepared at low temperatures which had more lattice defects.

Nuclear irradiation which, as recently shown, affects the chemical behavior of tungsten,[2] may be expected to alter the chemical properties of ferric oxide if a sufficient concentration of lattice imperfections is produced by the irradiation. As a preliminary study we have measured the influence of proton irradiation upon the solution rate of Fe_2O_3 in *N* hydrochloric acid. The specimens of ferric oxide were prepared by heating pure iron sheet, 10×15×1 mm, in dry oxygen at 1200°C for one week. The rates of solution of the oxides were measured in hydrochloric acid solutions which were kept in a thermostat at 30°C. The solutions were stirred vigorously, and small aliquot portions were removed at regular intervals in order to determine the iron concentration as a function of time. The reproducibility of the results was good. Three of the oxide specimens were then irradiated with 260-Mev protons of a total flux of 10^{16} protons per cm^2, and their dissolution rates were measured. The results obtained are shown in Fig. 1 The experiments indicate that proton irradiation significantly increases the solution rate of ferric oxide in hydrochloric acid. The initial rates increase slowly and there is only a very small difference between the irradiated and nonirradiated specimens. After 7 hours immersion in the acid solution, however, there is a rapid increase in the solution rate of the irradiated samples, as compared to the nonirradiated specimens.

The effect of proton irradiation upon the chemical properties of ferric oxide may be ascribed to the production of lattice defects, such as vacancies, displaced atoms, and dislocations. Recent work on radiation effects in ionic crystals[3] indicates that even above room temperature some of these defects can be quite stable and thus the magnitude of the effect observed on Fe_2O_3 is not surprising. On the other hand defects located near the surface have a good chance to diffuse out and to disappear and this may account for the rapid increase in the dissolution rate when a surface layre about 6000 A thick is removed.

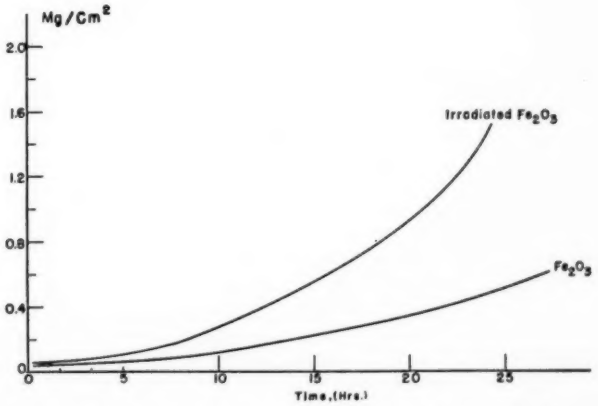

[[FIG. 1. Rate of dissolution of Fe_2O_3 (in terms of dissolved Fe) in *N* hydrocholric acid.

In view of the fact that the resistance of most metals to chemical attack is governed largely by the properties of thin surface oxide films, these results are pertinent to the problem of chemical attack on metals subjected to nuclear irradiation. Even if the metal itself suffers little radiation damage, the films formed on its surface may be disrupted sufficiently to lead to an increased attack in corrosive environments.

The authors wish to acknowledge the assistance of Dr. E. Pearlstein, who irradiated the specimens at the Carnegie Institute of Technology synchrocyclotron, and of Mrs. Aija Spilners in measuring the dissolution rates. Support of this work has been given by a research program sponsored by the U. S. Atomic Energy Commisson.

[1] M. J. Pryor and U. R. Evans, J. Chem. Soc. 1259 (1950).
[2] M. Simnad and R. Smoluchowski, Phys. Rev. (to be published).
[3] See for instance, R. Smoluchowski, Proc. Intern. Conf. on Peace Uses of Atomic Energy, Geneva, 1955.

Photoionization Efficiencies and Cross Sections in N_2O and NO†

W. C. WALKER AND G. L. WEISSLER
Department of Physics, University of Southern California, Los Angeles 7, California
(Received July 25, 1955)

PRELIMINARY measurements of total absorption cross sections, photoionization efficiencies, and ionization cross sections of N_2O and NO have been obtained for radiation in the region between the ionization onset and 687 A using techniques previously described.[1] For N_2O absorption spectra have been obtained down to 850 A[2] and absorption coefficients[3] measured to 1000 A. However, there appear to be no absolute measurements published for the region of the ionization continuum. In the case of NO, absolute absorption and ionization measurements in the region from the ionization onset to 1080 A have been reported by Watanabe,[4] but there seem to exist no previous ionization measurements at shorter wavelengths.

In the present investigation absorption and ionization measurements within the ionization continuum were obtained for commercial tank gases which had been purified by distillation with liquid nitrogen and frozen alcohol cold traps. The photoionization efficiencies of N_2O are presented in Fig. 1(a) in percent or ion-pairs per 100 absorbed photons. An ionization onset was found at 965±5 A corresponding to 12.83±0.07 ev, in agreement with the ionization potential of 12.9±0.5 ev obtained by Smyth and Stueckelberg[5] using electron impact methods and the value of 12.66 ev obtained by Duncan[2] from Rydberg series. Absorption and ionization cross sections of N_2O are shown in Fig. 1(b). An estimate of the accuracy of these data indicated a probable error of 5 to 10% in the absorption cross section and 15 to 20% in the ionization cross section. The cross sections were found to be independent of pressure except for four lines at 770, 787, 833, and 843 A. For these lines the cross sections were found to increase with decreasing pressure. A pressure range of a factor of four between 10 to 100 microns produced at most a variation of about a factor of two in the cross sections. The values shown in Fig. 1(b) for these lines are the largest values obtained, corresponding to the lowest pressure used. This apparent pressure variation suggests the presence of sharp bands in this region since it is known[6] that rapid fluctuations in the cross section over a wavelength range comparable with the width of the radiation band passed by the exit slit (5 A in the present case) produce such apparent pressure effects. By disregarding the values corresponding to these sharp bands the contour of the ionization continuum was established; this is shown in Fig. 1(b) by the broken line.

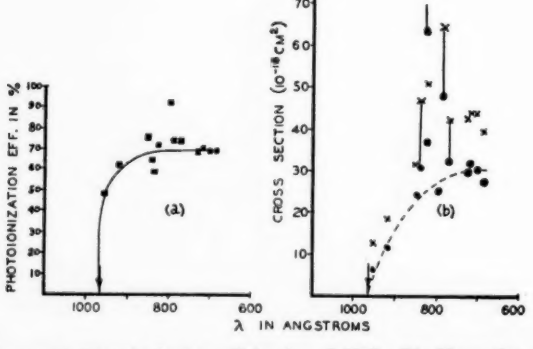

FIG. 1. (a) Photoionization efficiencies of N_2O. (b) Absorption and photoionization cross sections of N_2O. × Absorption cross sections, ○ ionization cross sections. Data were taken with 3 cm ionization chambers and a 5 A resolution.[1] The first ionization potential at 12.83±0.07 ev is shown by an arrow.

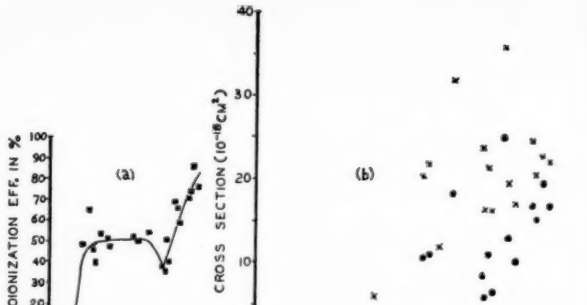

FIG. 2. (a) Photoionization efficiencies of NO. (b) Absorption and photoionization cross sections of NO. × Absorption cross sections, ● ionization cross sections. Data were taken with 3 cm ionization chambers and a 5 A resolution.[1] The first ionization potential at 9.20±0.03 ev is shown by an arrow.

The ionization efficiencies and the corresponding absorption and ionization cross sections of NO are shown in Figs. 2(a) and 2(b). An ionization onset was found at 1347±5 A corresponding to 9.20±0.03 ev. This is in agreement with the 9.25±0.02 ev obtained by Watanabe[4] and the electron impact value of 9.4±0.2 ev by Hagstrum.[7] The absorption cross sections were found to be independent of pressure over a pressure range of a factor of three for the region studied. Fluctuations in the cross sections with wavelength, however, indicated the presence of diffuse bands in the region below 1000 A, in agreement with the absorption spectra obtained by Tanaka.[8] Because of these fluctuations it was not possible to establish with any degree of certainty the contour of the ionization continuum; it is likely that more than one continuum is present in this region. The ionization cross sections obtained by Watanabe[4] are shown in Fig. 2(b) by the solid line. Within the experimental error his data agree with those obtained in the present investigation.

† The aid of the Office of Naval Research is gratefully acknowledged.
[1] Wainfan, Walker, and Weissler, J. Appl. Phys. **24**, 1318 (1953) and Phys. Rev. July 15 (1955).
[2] A. B. F. Duncan, J. Chem. Phys. **4**, 638 (1936).
[3] Zelikoff, Watanabe, and Inn, J. Chem. Phys. **21**, 1643 (1953).
[4] K. Watanabe, J. Chem. Phys. **22**, 1564 (1954); and Watanabe, Zelikoff, and Inn, A.F.C.R.C. Technical Report No. 53-23, Geophysics Research Directorate, Air Force Cambridge Research Center, Cambridge, Massachusetts.
[5] H. D. Smyth and E. C. G. Stueckelberg, Phys. Rev. **36**, 478 (1930).
[6] Nielsen, Thorton, and Dale, Revs. Modern Phys. **16**, 307 (1949).
[7] H. D. Hagstrum, Revs. Modern Phys. **23**, 185 (1951); J. Chem. Phys. **23**, 1178 (L) (1955).
[8] Y. Tanaka, J. Sci. Research Inst. (Tokyo) **43**, 160 (1949).

Nuclear Quadrupole Resonances in Solid Iodine Compounds

S. KOJIMA, K. TSUKADA, S. OGAWA, AND A. SHIMAUCHI
Department of Physics, Tokyo University of Education, Otsuka, Tokyo, Japan
(Received August 9, 1955)

THE iodine nuclei of spin $\frac{5}{2}$ give rise to two resonances corresponding to the transitions, $m_s=\pm\frac{1}{2}\leftrightarrow\pm\frac{3}{2}$ and $\pm\frac{3}{2}\leftrightarrow\pm\frac{5}{2}$. The frequency of the first resonance, ν_1, is approximately a half of the frequency of the second resonance, ν_2. We observed both resonance frequencies on ICl, I_2O_5, HgI_2, and NH_4I_3 and determined the coupling constants and the asymmetry parameters using the formulas given by Dehmelt and Krüger.[1] Beside these samples, ZnI_2, $N(CH_3)_4I_3$, and $N(CH_3)_4I_5$ were also studied. We could measure only one of the two resonances for each sample.

For most of the experiment the spectrometers mentioned before[2,3] were used. For the frequency range between 700 Mc and 1000 Mc a coaxial cavity spectrometer[4] was applied.

Samples of ICl were made from I_2 and SO_2Cl_2 and purified by repeating crystallization. NH_4I_3 was prepared from I_2 and NH_4I by the method reported by Johnson.[5] $N(CH_3)_4I_3$ and $N(CH_3)_4I_5$ were prepared from $N(CH_3)I$ and I_2 by the method mentioned by Hach and Rundle.[6] For HgI_2, I_2O_5, and ZnI_2, commercial samples were used.

The typical results of the experiment are listed in Tables I and II. ICl was measured in α state, which was achieved by slow crystallization at about 20°C. The first resonance line, which was already observed by Dehmelt at liquid air temperature,[7] was a doublet, one of which was strong and the other weak. The weak line of the second resonance doublet was not observed. The constants listed in Table I were calculated for the strong line of the doublet. The resonance of Cl^{35} in ICl was also measured as 37.184 Mc at +20°C which was approximately agreed with the Bray's 37.2 mc at liquid-nitrogen temperature of β state.[8] One of the resonances of I_2O_5 was reported by Shimomura *et al.*[9] The present experiment revealed that their value was the frequency of the first resonance. This resonance seemed to be a composed line, but the second resonance line was definitely a triplet. The constants were calculated for mean values. I_2O_5 gave rise to a piezoelectric absorption line[10] in the frequency range of the observation of the first resonance at liquid-nitrogen temperature.

The resonances in HgI_2 were observed between the liquid-air temperature and the transition point of +126°C where the sample changed from red to yellow. The observed ratio of the two resonance frequencies yielded very large asymmetry parameter. The mercury atom combines with four iodine atoms and the iodine atom combines with two mercury atoms. The bond angle between Hg−I−Hg is calculated from the crystal structure[11] as 103°8′. The situation of the iodine atoms is truly analogous to the case of AsI_3, which was treated with the concept of resonance switching of fifty percent.[3] Applying the same analysis, we obtained the bond angle from the asymmetry parameter to be 100°6′, which agreed well with the crystallographic value, and the coupling constant for the single bond of Hg−I to be 1600 Mc, which indicated ionic character of about 30%.

In the NH_4I_3 crystal three iodine atoms are arranged in almost linear fashion, where the angle between I−I−I is 176°. The iodine atoms at both ends are connected to the central atom by a covalent bond. The observed resonances seem to be caused by these atoms. The obtained coupling constant, 2441 Mc, is larger than 2292 Mc which was obtained by the atomic beam method.[12] The discrepancy between these values seems to indicate the effect of overlap integral.[13]

The observed resonance frequencies of $N(CH_3)_4I_3$ and $N(CH_3)_4I_5$ were very near to the first resonance frequency of NH_4I_3, so that these are the frequencies of the first resonances.

On ZnI_2 only one resonance which was resolved in a triplet was observed between room temperature and the liquid-air temperature.

TABLE I. Nuclear quadrupole resonances of I^{127}.

Sample	T (°C)	ν_1 (Mc)	ν_2 (Mc)	eQq (Mc)	η (%)
ICl	20	451.46±0.01	902.46±0.02	3008.3	2.0
		440.9 ±0.3[a]	———	———	—
	− 26	453.56±0.01	905.84±0.02	3020.1	3.3
		446.41±0.05[a]	———	———	—
	−196	457.39±0.01	———	———	—
		460.17±0.01[a]	———	———	—
I_2O_5	18	177.47±0.03	303.75±0.03	1056.0	35.0
			312.45±0.03		
			313.64±0.03		
	− 58	177.75±0.03	305.63±0.01	1061.0	34.0
			314.14±0.01		
			315.85±0.01		
	−196	178.01±0.03	307.80±0.01	1068.0	33.0
			316.10±0.01		
			318.05±0.01		
HgI_2	11	151.12±0.05	229.47±0.02	799.0	52.7
	− 24	151.25±0.05	230.03±0.02	800.7	52.5
NH_4I_3	25	366.23±0.01	732.13±0.02	2440.6	1.8
	− 40	367.06±0.02	733.81±0.02	2446.2	1.8
	−196	368.81±0.01	———	———	—

[a] Weak line.

TABLE II. Nuclear quadrupole resonances of I^{127}.

Sample	Temperature (°C)	Frequency (Mc)
$N(CH_3)_4I_3$	liquid air	361.70±0.40
$N(CH_3)_4I_5$	31	356.14±0.02
	−54	358.62±0.02
	liquid air	361.50±0.40
ZnI_2	23	184.99±0.05
		179.54±0.05
		176.52±0.05
	−55	186.55±0.05
		181.19±0.05
		178.65±0.05
	liquid air	188.88±0.05
		183.75±0.05
		182.18±0.05

In the NH_4I_3 crystal three iodine atoms are arranged in almost linear fashion, where the angle between I−I−I is 176°. The iodine atoms at both ends are connected to the central atom by a covalent bond. The observed resonances seem to be caused by these atoms. The obtained coupling constant, 2441 Mc, is larger than 2292 Mc which was obtained by the atomic beam method.[12] The discrepancy between these values seems to indicate the effect of overlap integral.[13]

The observed resonance frequencies of $N(CH_3)_4I_3$ and $N(CH_3)_4I_5$ were very near to the first resonance frequency of NH_4I_3, so that these are the frequencies of the first resonances.

On ZnI_2 only one resonance which was resolved in a triplet was observed between room temperature and the liquid-air temperature.

[1] H. G. Dehmelt and H. Krüger, Z. Physik **130**, 385 (1951).
[2] Kojima, Tsukada, Shimauchi, and Hinaga, J. Phys. Soc. Japan **9**, 795 (1954).
[3] Kojima, Tsukada, Ogawa, Shimauchi, and Abe, J. Phys. Soc. Japan **9**, 805 (1954).
[4] Kojima, Shimauchi, Hagiwara, and Abe, J. Phys. Soc. Japan (to be published).
[5] G. S. Johnson, J. Chem. Soc. **33**, 397 (1838).
[6] R. J. Hach and R. E. Rundle, J. Am. Chem. Soc. **73**, 4321 (1951).
[7] H. G. Dehmelt, Z. Physik **130**, 356 (1951).
[8] P. J. Bray, J. Chem. Phys. **23**, 703 (1955).
[9] Shimomura, Kushida, Inoue, and Imaeda, J. Chem. Phys. **22**, 350 (1954).
[10] Kojima, Tsukada, Ogawa, Shimauchi, and Matsumiya, J. Phys. Soc. Japan **10**, 265 (1955).
[11] R. W. G. Wyckoff, *Crystal Structures* (Interscience Publishers, Inc., New York, 1948).
[12] Jaccarino, King, and Stroke, see Robinson, Dehmelt, and Gordy, J. Chem. Phys. **22**, 511 (1954).
[13] K. Tsukada, J. Phys. Soc. Japan **9**, 872 (1954).

New Modification of Solid Nitrogen

C. A. SWENSON*
Cryogenic Engineering Laboratory, Massachusetts Institute of Technology, Cambridge, Massachusetts
(Received August 1, 1955)

THE existence of a first-order transformation in solid nitrogen at 35.6°K has been established both from x-ray and calorimetric studies.[1,2] These experiments, however, give no idea as to the density change during the transformation, or of the nature of the slope of the transition line between the two phases. Techniques for studying volume changes as a function of high pressures at low temperature have been worked out recently,[3,4] and this letter gives preliminary results on the phase diagram of solid nitrogen, and reports the existence of a third, γ, phase which exists only at low temperatures.

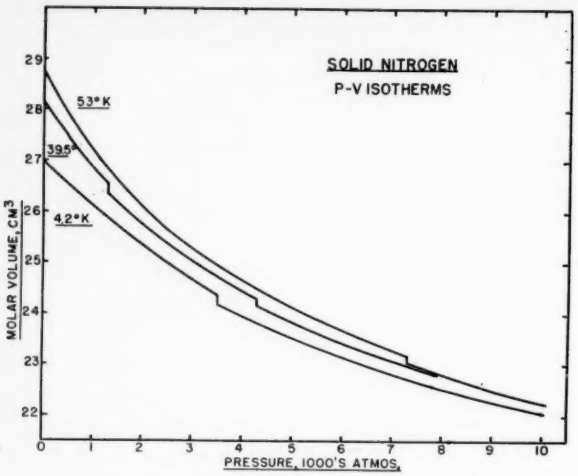

FIG. 1. Typical pressure-volume isotherms as obtained in this work. The transitions shown are, respectively, the $\beta \rightarrow \gamma$ at 53°, the $\beta \rightarrow \alpha$ and $\alpha \rightarrow \gamma$ at 39.5°, and the $\alpha \rightarrow \gamma$ at 4.2°K.

The high-pressure equipment and sample holder used for these measurements is similar to that described by Stewart,[3] with a special cryostat[5] being used to maintain the sample holder at any desired temperature, with fluctuations of less than 0.1°. All temperatures were measured with a copper-constantan thermocouple, calibrated in this laboratory.

Figure 1 shows three of the $P-V$ isotherms which were obtained, plotted in terms of molar volume. The results of seven such isotherms are summarized in Fig. 2 as the proposed phase diagram for solid nitrogen.

The transitions shown in Fig. 1 are quite idealized, and were in practice spread out over two or three hundred atmospheres. The occurrence of the transitions was always quite unambiguous on both the pressure-increasing and pressure-decreasing curves, but the exact pressure was difficult to determine, due both to quite large friction effects (especially below 30°K) and the need for an over pressure of about 500 atmospheres to make the transitions run. The transition pressure was taken as the mean of the pressures needed to initiate the transition in first the forward direction and then in the reverse direction. The actual volume changes could be measured to about 20%. The large friction at 4.2°K is probably the reason why Stewart failed to observe this transition in his earlier work.[3]

In Fig. 1, the variation of the volume of solid nitrogen at zero pressure was estimated from incomplete published measurements due to various workers.[6] The initial compressibilities shown are uncertain since they are the result of an extrapolation.

The volume changes (ΔV) and the entropy changes ($\Delta S = \Delta V dP/dT$) deduced from the ΔV's and the slopes of the transition lines are given for the triple point (44.5°K, 4650 atmos) in Fig. 2. This point has been chosen, along with the ΔV's, so that the data are thermodynamically consistent. The observed data for $\Delta V_{\beta\alpha}$ was used to estimate the volume change at zero pressure, and this was used with the known entropy change (1.536 cal/mole-deg)[1] to calculate the initial slope shown. $\Delta V_{\beta\alpha}$ decreases rapidly along this curve (see Fig. 2), as does $\Delta V_{\beta\gamma}$ with increasing pressure, although $\Delta V_{\alpha\gamma}$ is constant within experimental error. In general, the phase existing at the higher pressure has the lower compressibility by about 20%. These results are as yet quite preliminary in nature and it is hoped to continue this work in the near future with an improved setup.

The exact structure of the γ phase cannot be determined easily. Nitrogen crystallizes as a molecular crystal, with the α phase molecules lying on the points of a face centered cubic lattice, and the β phase having a hexagonal structure in which the individual molecules rotate or precess about their center of gravity. Neither structure is close packed, so the effect of pressure probably produces a close-packed structure. Similar results should be obtained for solid CO, which behaves much like solid N_2 at zero pressure.[2]

The author wishes to express his appreciation to Dr. J. J. M. Beenakker and to Dr. Z. S. Basinski for their assistance and discussions. This work was performed under a contract with the U. S. Army Office of Ordnance Research.

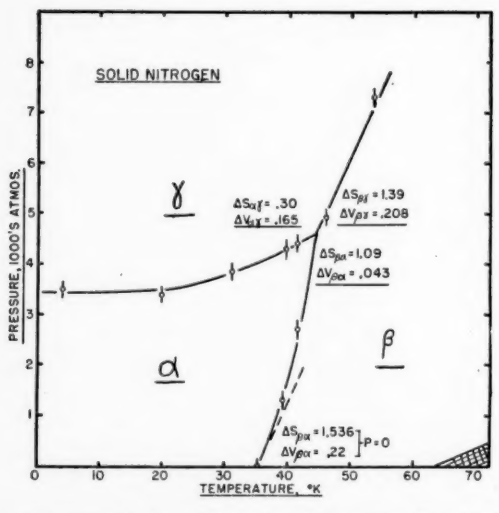

FIG. 2. The proposed phase diagram for solid nitrogen. The shaded area in the lower right is the liquid region. The values of the volume and entropy changes around the triple point and at zero pressure are given in cc/mole and cal/mole-deg, respectively. The coordinates of the triple point are 44.5°K and 4650 atmos.

* Present address: Physics Department, Iowa State College, Ames, Iowa.

[1] W. F. Giauque and J. O. Clayton, J. Am. Chem. Soc. **55**, 4875 (1933).
[2] For a summary of the x-ray data and other references to them, see L. Vergard, Z. Physik **88**, 240 (1934).
[3] J. W. Stewart, Phys. Rev. **97**, 578 (1955).
[4] C. A. Swenson, Phys. Rev. (to be published).
[5] C. A. Swenson and R. H. Stahl, Rev. Sci. Instr. **25**, 608–611 (1954).
[6] For a summary of the density measurements on solid nitrogen see Dokoupil, van Soest, and Swenker, Appl. Sci. Research **5**, 204 (1955).

Errata: Free Electron Treatment of the Orientation of Substituents in Aromatic Molecules

[J. Chem. Phys. **22**, 1952 (1954)]

SADHAN BASU
Department of Chemistry, University of Calcutta, Calcutta 9, India

IN the calculation of ω values for the model V some mistake has been made. The state $\omega=0$ is absent, and the $\pi/2$ state is not degenerate. Further, if usual assumptions for free electron treatment are introduced, i.e., the box dimension extends half bond beyond the free end, the π-electron energy difference for the various positions comes out as follows:

$$\begin{array}{c} \Delta E_\pi \\ o-0.13 \text{ K} \\ m-0.56 \\ p-0.20. \end{array}$$

This also shows that the substitution will be o,p but with o predominating. However, the slight advantage may be well compensated by the familiar o effect.

The author's sincere thanks are due Dr. L. S. Bartell and Dr. R. A. Bonham of Iowa State College, Ames, Iowa, for drawing attention to the error.

Note on Imperfect Gas Theory

FRANK E. HARRIS
Department of Chemistry, Harvard University, Cambridge, Massachusetts
(Received July 18, 1955)

IN the theory of imperfect gases,[1] two types of cluster integrals are ordinarily introduced, the first of which, b_l, represents contributions from all possible connected clusters of l molecules. The equation of state expressed in terms of the b_l involves the series

$$\sum_{l=1}^{\infty} b_l z^l,$$

with z defined by

$$\sum_{l=1}^{\infty} l b_l z^0 = v^{-1},$$

where v is the volume per molecule. The second type of cluster integral, β_k, involves only contributions from totally multiply connected (i.e., "irreducible") clusters of $k+1$ molecules and permits explicit expression of the equation of state as a power series in v^{-1}. The β_k and the b_l are related by

$$l^2 b_l = \sum_{\{m_k\}} \prod_k \frac{(l\beta_k)^{m_k}}{m_k!}, \quad \sum_{k=1}^{\infty} k m_k = l-1. \tag{1}$$

The usual analysis relating $\Sigma b_l z^l$ to a power series in v^{-1} is a bit tedious.[2] We here present a more direct procedure. Converting Eq. (1) into a contour integral in y, multiplying by z^l, and summing over l,

$$\sum_{l=1}^{\infty} l^2 b_l z^l = \sum_{l=1}^{\infty} \frac{1}{2\pi i} \oint dy z^l y^{-l} \exp\Big(l \sum_{k=1}^{\infty} \beta_k y^k\Big). \tag{2}$$

The contour encloses the origin in a counter clockwise sense. Interchanging summation and integration, then performing both operations,

$$\sum_{l=1}^{\infty} l^2 b_l z^l = \frac{y}{1 - \sum_{k=1}^{\infty} k\beta_k y^k}, \tag{3}$$

where the value of y appearing in Eq. (3) is that at the residue,

$$y = ze \sum_{k=1}^{\infty} \beta_k y^k. \tag{4}$$

It is possible to choose z so that the analysis leading to Eqs. (3) and (4) is valid. By successive applications of the operator $\int_0^z dz/z$ to both sides of Eq. (3), simplifying the resultant expressions with the aid of (4), one may obtain the well-known relations

$$\sum_{l=1}^{\infty} l b_l z^l = y \tag{5}$$

$$\sum_{l=1}^{\infty} b_l z^l = y\Big(0.1 - \sum_{k=1}^{\infty} \beta_k y^k\Big). \tag{6}$$

From Eq. (5), y may be identified as v^{-1}, and (6) provides the connection necessary to write the equation of state,

$$p/kT = \sum_{l=1}^{\infty} b_l z^l = \frac{1}{V}\Big(1 - \sum_{k=1}^{\infty} \frac{k}{k+1} \beta_k v^{-k}\Big). \tag{7}$$

The essential simplification afforded by the procedure here outlined is the direct passage to Eqs. (3) and (4).

[1] Imperfect gas theory is discussed extensively in J. E. Mayer and M. G. Mayer, *Statistical Mechanics* (John Wiley and Sons, Inc., New York, 1940). See particularly Chap. 12, appendices X and XI, and the references therein.

[2] We are here concerned with proof of the relation between the irreducible clusters and the coefficients of the series in v^{-1}. An elegant method is available for constructing the series in v^{-1} [see D. Ter Haar, *Statistical Mechanics* (Rinehart and Company, Inc., New York, 1954), p. 176], but it does not identify the coefficients with the β_k.

Electrical Conductivity of Hydrocarbon Cracking Catalyst

P. B. WEISZ, C. D. PRATER, AND K. D. RITTENHOUSE
Socony Mobil Laboratories (A Division of Socony Mobil Oil Company, Incorporated), Research and Development Department, Paulsboro, New Jersey
(Received July 28, 1955)

IN a previous letter[1] measurements were reported of the electrical conductivity of silica-alumina hydrocarbon cracking catalysts of varying alumina content. The conductivities increased with increasing alumina concentration and suggested an electronic conduction mechanism.

Further investigations now lead to the conclusion that the observed conductivities are clearly related to the residual *sodium* content and *not* to the amount of alumina contained in the silica. Figure 1 shows the electrical conductivities, alumina and sodium content, of two samples, A and B, before and after the Na concentration was decreased by extensive (18 days) base exchanging. This was done with 0.3 molar NH_4Cl solution followed by washing in distilled H_2O (15 days) and calcining (at 600°C for 1 hour) to remove ammonia. This treatment removed no measurable amounts of alumina. These data show that the conductivities in each pair are nearly proportional to the Na content.

The residual Na content of the above samples originated from the Na silicate and aluminate salts used in their original preparation. Samples of silica-aluminas were also prepared by gelation of ethyl silicate/aluminum nitrate mixtures. Data for these samples, virtually free of Na, are shown as C and D on Fig. 1. They show low values of conductivity consistent with their low Na content.

We have also shown that addition of Na to a catalyst increases its conductivity. Samples were prepared by ion exchanging with 0.5 molar solution of NaCl (30-hour contact), washing for several days with distilled water until no Cl^- ion could be detected with $AgNO_3$, drying, and calcining. At 462°C the electrical conductances were 5.6×10^{-8} and 3.2×10^{-7} ohm^{-1} before and after addition of Na from 0.08 wt % to 0.32 wt %. In contrast to this the addition of potassium from a solution of KCL showed no increase

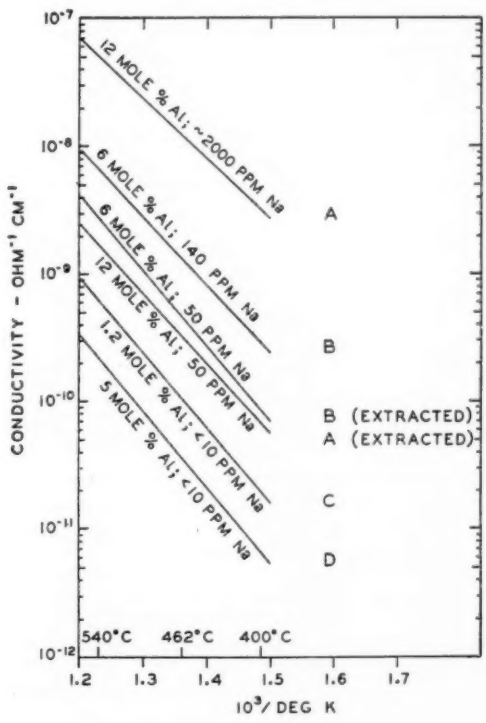

FIG. 1.

in conductivity. (By an error this experiment was, in the previous letter[1] reported as using NaCl.)

The conductivity behavior in respect to Na and K is very similar to that observed for glasses,[2] where ionic conductivity of Na has been demonstrated.

Some electrode polarization is observed. However, the polarization voltage remains below the value of the applied voltage, indicating that if the conductivity is ionic a discharge mechanism exists at the electrodes.

[1] Weisz, Prater, and Rittenhouse, J. Chem. Phys. **21**, 2236–2237 (1953).
[2] See George W. Morey, *The Properties of Glass* (Reinhold Publishing Corporation, New York, 1954), second edition, Chap. XVII.

Microwave Spectrum of Imine-Deuterated Ethylenimine

T. E. Turner, Verna C. Fiora, and W. M. Kendrick
Ballistic Research Laboratories, Aberdeen Proving Ground, Maryland
(Received August 8, 1955)

THE microwave spectrum of the ordinary isotopic species of ethylenimine has been reported previously by a number of investigators,[1–3] and their results are in quite good agreement. We continued the study of this molecule by analyzing the pure rotational spectrum of C_2H_4ND and improving on the structure determination.

The C_2H_4ND was readily obtained by introducing equal pressures of D_2O and C_2H_4NH vapors into the wave-guide cell of the spectrometer. Even at total pressures as low as 10 microns of mercury, the intensity of the C_2H_4ND spectrum reached a maximum within a few seconds after D_2O admission, indicating that the deuterium exchange proceeded quite rapidly. We also noticed that D_2O persisted in the wave guide for several weeks even after considerable pumping, with the consequence that C_2H_4ND was formed whenever C_2H_4NH was admitted to the wave guide. C_2D_4NH or C_2D_4ND were not observed and indeed would not be expected to be formed by exchange with D_2O.

The spectral frequencies and transition assignments are given in Table I. The rotational constants as determined by the best fit to the measured spectrum are listed in Table II. These constants were used to obtain the calculated frequencies included in Table I. The influence of centrifugal distortion can readily be noticed by comparing the measured and calculated frequencies. The nuclear quadrupole moment of the nitrogen nucleus gives rise to a hyperfine structure of which two components were resolved in several instances as indicated in Table I. It is of interest to note that C_2H_4ND is almost an oblate symmetric top and the assigned transitions follow *a*-axis selection rules whereas the C_2H_4NH spectrum follows from *b*-axis selection rules.

TABLE I. Assignments in the spectrum of C_2H_4ND.

Transition	Measured	Calculated
$2_{1,2} \rightarrow 2_{1,1}$	23 359.5 ±0.5 mc/sec	23 357.80 mc/sec
	23 356.3	
$3_{2,2} \rightarrow 3_{2,1}$	23 217.1	23 217.08
$4_{3,2} \rightarrow 4_{3,1}$	23 028.2	23 029.80
$5_{4,2} \rightarrow 5_{4,1}$	22 792.3	22 796.26
$6_{5,2} \rightarrow 6_{5,1}$	22 509.5	22 516.87
$7_{6,2} \rightarrow 7_{6,1}$	22 181.1	22 192.13
$8_{7,2} \rightarrow 8_{7,1}$	21 805.9	21 822.67
$9_{8,2} \rightarrow 9_{8,1}$	21 385.1	21 409.28
$10_{9,2} \rightarrow 10_{9,1}$	20 918.5	20 952.88
$11_{10,2} \rightarrow 11_{10,1}$	20 410 ±10	20 454.60
$12_{11,2} \rightarrow 12_{11,1}$	19 860	19 915.75
$2_{0,2} \rightarrow 2_{2,1}$	23 643.6 ±0.5	23 641.15
	23 638.6	
$3_{1,2} \rightarrow 3_{3,1}$	23 787.8	23 786.32
	23 784.8	
$4_{2,2} \rightarrow 4_{4,1}$	23 985.1	23 984.17
	23 983.1	
$5_{3,2} \rightarrow 5_{5,1}$	24 239.1	24 238.33
	24 237.5	
$6_{4,2} \rightarrow 6_{6,1}$	24 554.6	24 553.31
	24 553.2	
$7_{5,2} \rightarrow 7_{7,1}$	24 937.3	24 934.46
	24 936.3	
$8_{6,2} \rightarrow 8_{8,1}$	25 393.3	25 387.89
$9_{7,2} \rightarrow 9_{9,1}$	25 920 ±10	25 920.38
$0_{0,0} \rightarrow 1_{0,1}$	33 420 ±20	

TABLE II. Ethylenimine rotational constants.

	Measured	Calculated	Species
$(a+c)/2$	18 059.7 ±0.25 mc/sec	18 067.54 mc/sec	
$(a-c)/2$	4676.0 ±0.25	4669.48	C_2H_4NH
κ	0.6700 ±0.0001	0.668987	
$(a+c)/2$	16 757 ±10 mc/sec	16 758.69 mc/sec	
$(a-c)/2$	3940.05 ±0.10	3945.50	C_2H_4ND
κ	0.97610 ±0.00005	0.978468	

Changes in the rotational constant combinations $(a \pm c)/2$ and κ were expressed as a first-order Taylor expansion in terms of the derivatives of these combinations with respect to the various structural parameters involved. The derivatives (actually differences) were evaluated in the neighborhood of a reasonable ethylenimine structural model using the calculation[4] of the rotational constant combinations made for a number of assumed structures. When the rotational constant combinations for the ordinary and imine-deuterated isotopic species were included in the expansions, an essentially linear system of algebraic equations resulted which when solved on the ORDVAC gave the structural corrections to be applied to the originally chosen model. Since only six of the necessary seven rotational constant combinations were measured, it was necessary to assume the value for one of the structural parameters and the N–H distance was chosen as 1.000 A after it had been shown that variations of this parameter had the least effect on the rotational constants. The structure obtained in this manner (Table III) was used to calculate the rotational constant combinations (Table II) on the assumption that the parameters are unaffected by isotopic substitution. Further work was done to show that zero-point vibrational effects give rise to an uncertainty in the last decimal place of the structural parameter values, but these uncertainties cannot be specified until experimental data on other isotopic species of ethylenimine are obtained.

TABLE III. Structural parameters for ethylenimine.

C–C distance	1.480 A
C–N distance	1.488 A
C–H distance	1.083 A
C_2NH angle	112°
H_2CC angle	159° 25′
HCH angle	116° 41′

[1] Wilcox, Brannock, DeMore, and Goldstein, J. Chem. Phys. **21**, 563 (1953).
[2] Turner, Fiora, Kendrick, and Hicks, J. Chem. Phys. **21**, 564 (1953).
[3] Johnson, Myers, and Gwinn, J. Chem. Phys. **21**, 1425 (1953).
[4] Hicks, Turner, and Widule, J. Chem. Phys. **21**, 564 (1953).

New Model for a Two-Dimensional Standard State

H. Leon Harter, Paul R. Rider, and Pierce M. Williamson
Wright Air Development Center, Air Research and Development Command, Wright-Patterson Air Force Base, Ohio
(Received August 10, 1955)

IN the region of linear relationship between the two-dimensional pressure of an adsorbed gas and its equilibrium three-dimensional pressure, a standard state of the adsorbed gas is needed for entropy calculations. Kemball and Rideal[1] arrive at a statement of the standard state after assigning an arbitrary thickness of 6 A to the adsorbed layer, which is one molecular diameter of the gas used. Two-dimensional pressure is converted to three-dimensional pressure by means of a model barrier one molecule high. de Boer[2] bases a two-dimensional standard on the condition

that the average distance between the molecules is the same as the average distance in the three-dimensional standard state (0°C, 1 atmos).

It appears that de Boer's model may be conceptually improved by changing the condition of equal distance to that of equal freedom of movement, i.e., assume $(V-b)/V=(A-b_2)/A$. If this is done, an appealingly simple relation between the two-dimensional pressure, p_2, and the three-dimensional pressure, p, may be shown.

The evaluation of p_2/p is reached in two stages. The first consists in changing Leonard B. Loeb [*The Kinetic Theory of Gases* (McGraw-Hill Book Company, Inc., New York and London, 1934), Second Edition, Sections 14 and 15] to represent the two-dimensional situation. The result is an evaluation of the ratio of the two-dimensional collisions per centimeter of container to the three-dimensional collisions per square centimeter of container.

$$\frac{n_2}{n}=\frac{8r}{3\pi}\cdot\frac{\bar{u}}{\bar{v}},$$

where r = radius of molecule, $\bar{u}$ = average two-dimensional velocity, and $\bar{v}$ = average three-dimensional velocity. Also,

$$\frac{p_2}{p}=\frac{3}{2}\cdot\frac{n_2}{n}=\frac{4r}{\pi}\cdot\frac{\bar{u}}{\bar{v}}.$$

The second stage consists in changing Section 3 of the chapter on "Atomic Theory of Heat" by J. de Boer [in R. Kronig, *Textbook of Physics* (Interscience Publishers, Inc., New York and London, 1954)] to represent two-dimensional conditions. The ratio $\bar{u}/\bar{v}$ comes out equal to $\pi/4$. $\therefore\ p_2/p=r$.

The implication of the Kemball and Rideal expedient is that $p_2/p=2r$. In turn, the implication of the value r for p_2/p is that the pressure conversion barrier of Kemball and Rideal should not be higher than r. The de Boer model yields a value of p_2/p greater than that from the equal freedom model by one order of magnitude.

Either the Kemball and Rideal two-dimensional standard state or that of de Boer will serve the purposes of thermodynamic calculations. Nevertheless, the equal freedom model may seem to interested persons to be based on a less arbitrary and a more esthetically satisfying condition.

[1] C. Kemball and E. K. Rideal, Proc. Roy. Soc. (London) **A187**, 53–73 (1946).
[2] J. H. de Boer, *The Dynamical Character of Adsorption* (Clarendon Press, Oxford, 1953), p. 112.

Structure of Ferrocene

E. A. Seibold and L. E. Sutton
Physical Chemistry Laboratory, Oxford University, England
(Received August 11, 1955)

THE results of an electron diffraction study of ferrocene[1] are presented in Table I. The analysis was carried out by a modified visual method[2] details of which will be presented elsewhere.

Table I. Bond length results[a] for ferrocene.

Bond	Length and error in A	$\langle l_{ij}^2\rangle^{\frac{1}{2}}$ in A
Fe−C	2.03±0.02	0.080 ass.
C−C	1.43±0.03	0.055 ass.
C−H	1.09 ass.	0.070 ass.

[a] The average amplitudes of vibration are indicated by $\langle l_{ij}^2\rangle^{\frac{1}{2}}$. See I. L. Karle and J. Karle, J. Chem. Phys. **17**, 1052 (1949).

The results are in excellent agreement with the highly symmetrical "sandwich" structure proposed by Wilkinson *et al.*,[3] although it must be added that no other configuration was tried because all available evidence indicates such a structure.[3–6(a),7–9] The experimental results are best satisfied by a molecular scattering intensity curve which is the average of intensity curves calculated for staggered and eclipsed configurations of the cyclopentadienyl rings. The s_{calc}/s_{obs} ratios for the best staggered, eclipsed, and average configurations are 1.000±0.003, 1.000 ±0.004, and 1.000±0.001, respectively. This may be deemed to indicate that at the vapor temperature (approximately 400°C) the rings rotate freely about the common orthogonal axis. This result may be compared with the observation by Eiland and Pepinsky[5] of a staggered configuration in the crystal state, and that by Lippincott and Nelson[9] of a restricted rotation configuration for ferrocene in solution (both presumably at room temperature). The electronic structure of ferrocene has been considered by Dunitz and Orgel[6(a),(b)] and independently by Jaffé[10] and by Moffitt.[11] All of these authors have stated that no major barrier exists against free rotation of the cyclopentadienyl rings around the orthogonal axis. According to Moffitt, the electron densities of the bonding iron orbitals are axially directional but rotationally nondirectional. A small barrier to rotation might arise from the H−H, H−C, and C−C interactions between the cyclopentadienyl rings which are not considered in these theoretical descriptions. However, it is noteworthy that the separation of the rings (3.25 A) is also very similar to that in graphite (3.35 A). Thus, there is little direct binding between the rings.

The Fe−C distance (2.03±0.02 A) observed is much larger than the Fe−C bond (1.84±0.03 A) in iron carbonyl reported by Ewens and Lister,[12] but the latter probably has a bond order greater than one. It is exactly equal to the sum of the covalent radii of carbon (0.77 A) and iron with a coordination number of 12 (1.26 A), but is slightly greater than would correspond to the sum (2.00 A) for an iron coordination number of 8.

The C−C distance (1.43±0.03 A) observed is between the value (1.54 A) for a single bond and the value (1.34 A) for a double bond. It can be compared with the value (1.393 A) for benzene and (1.42 A) for graphite and so corresponds to a bond character of 1.29 on Pauling's[13] scale.

[1] T. J. Kealy and P. L. Pauson, Nature **168**, 1039 (1951).
[2] E. A. Seibold, D. Phil. thesis, Oxford (1955).
[3] Wilkinson, Rosenblum, Whiting, and Woodward, J. Am. Chem. Soc. **74**, 2125 (1952).
[4] E. O. Fischer and W. Pfab, Z. Naturforsch. **7b**, 377 (1952).
[5] P. F. Eiland and R. Pepinsky, J. Am. Chem. Soc. **74**, 4971 (1952).
[6] (a) J. D. Dunitz and L. E. Orgel, Nature **171**, 121 (1953); (b) J. Chem. Phys. **23**, 954 (1955).
[7] Woodward, Rosenblum, and Whiting, J. Am. Chem. Soc. **74**, 3458 (1952).
[8] Kaplan, Kester, and Katz, J. Am. Chem. Soc. **74**, 5531 (1952).
[9] E. R. Lippincott and R. D. Nelson, J. Chem. Phys. **21**, 1307 (1953).
[10] H. H. Jaffé, J. Chem. Phys. **21**, 156 (1953).
[11] W. Moffitt, J. Am. Chem. Soc. **76**, 3386 (1954).
[12] R. V. G. Ewens and M. W. Lister, Trans. Faraday Soc. **35**, 681 (1939).
[13] L. Pauling, *The Nature of the Chemical Bond* (Cornell University Press, Ithaca, New York, 1948).

Paramagnetic Resonance of Color Centers in $NaNO_3$†

William B. Ard, Jr.‡
Department of Physics, Duke University, Durham, North Carolina
(Received August 8, 1955)

PARAMAGNETIC resonance has been observed in single crystals of $NaNO_3$ irradiated at 20°C for about twenty-four hours with 50 kv x-rays. Two sets of lines are observed. One group consists of three equal-intensity, equally spaced lines with a total separation of 135±5 gauss. The spacings of these lines are not dependent either upon the value of the external magnetic field or upon its orientation relative to the crystal. The width of these lines is 10 gauss at 20°C, but it decreases to 3 gauss at 77°K. The g value of the center line is 2.000±0.003.

The other set of lines changes with crystal orientation in the magnetic field. When the shorter diagonal of the crystal is parallel to the external magnetic field one line is observed at a g value of about 2.00. When the longer crystal diagonal is parallel to the external field, three lines are observed with g values of 2.013

± 0.003, 2.020 ± 0.003, and 2.026 ± 0.003. These lines have a width of about 3 gauss at both 20°C and 77°K. The line at $g = 2.026$ is the strongest, and the line at $g = 2.013$ the weakest. The weakest line is about half the intensity of the strongest line. The intensity of the one line observed when the shorter diagonal is parallel to the field is about equal to the sum of the intensities of the three lines observed when the longer diagonal is parallel to the field. Each of the lines in the first group has about the same intensity as the weakest line in the second group.

If the $NaNO_3$ crystal is x-rayed for two hours at 77°K and examined for paramagnetic resonance without being allowed to warm, one very strong line is observed instead of the second group of lines. The first group of three lines is found but is much weaker than the strong line. Where the sample is allowed to warm to 20°C and then recooled to 77°K the same type of resonance is round that is found if the crystal has been x-rayed at 20°C for an hour or two.

The three equally spaced, equal-intensity lines are interpreted as hyperfine structure due to the coupling with the N^{14} nucleus. This resonance might be the result of either NO_2 or NO_3 molecules. Since the g value of the center of the triplet is about 2.00 and the line widths are very small, the effective orbital angular momentum of the molecule or radical must be very nearly zero. However, some small residual orbital momentum would result in a shorter spin-lattice relaxation time at higher temperature, accounting for the greater line width at 20°C than at 77°K. Hybridization of the nitrogen orbitals could give an appreciable amount of $2s$ character to the unpaired electron which would account for the observed 135 gauss separation. This is much larger than the 7.5 gauss separation reported for the $^4S_{\frac{3}{2}}$ ground state of atomic nitrogen by Heald and Beringer.[1]

Pringsheim[2] reports an anisotropic absorption in the optical region by x-rayed $NaNO_3$ crystals. This absorption is considered due to F centers. The paramagnetic resonance lines observed with anisotropic g values might be correlated with these F centers. However, the 3 gauss width observed for these lines makes their interpretation as F centers rather unlikely, since F centers so far observed give broad paramagnetic resonance lines, of the order of 50 gauss or more.

† This work is supported by the Office of Ordnance Research, Department of the Army.
‡ Present address: Department of Physics, University of Alabama, University, Alabama.
[1] Mark A. Heald and Robert Beringer, Phys. Rev. **96**, 645 (1954).
[2] P. Pringsheim, J. Chem. Phys. **23**, 369 (1955).

Reaction of Methyl Radicals with Nitric Oxide

W. A. Bryce and K. U. Ingold
Department of Chemistry, University of British Columbia, Vancouver, British Columbia, Canada
(Received August 5, 1955)

THE products and collision efficiency of the reaction of methyl with nitric oxide

$$CH_3 + NO \rightarrow CH_3NO$$

have been examined by the method previously reported.[1] Methyl was produced by passing a low pressure of mercury dimethyl in a stream of helium over a short movable furnace. Nitric oxide was added to the gas stream just below the furnace. The concentration of the products was measured by continuous analysis of the gases with a mass spectrometer. A small portion of the gas entered the ionization chamber of the spectrometer through a small leak in a quartz cone projecting into the stream.

With a reaction time of 5×10^{-2} sec the following products were detected: NH_3, H_2O, HCN, CO, N_2, CO_2, CH_3CN, and a peak at mass 45 (CH_3NO) which may have been the result of either nitroso-methane or formaldoxime. Methane, ethane, and methyl were also present as products of the $Hg(CH_3)_2$ decomposition. No $(CH_3NO)_2$ or $(CH_2NOH)_3$ were found.

The reaction time could be decreased, and the average temperature increased, by moving the furnace closer to the leak. When this was done, secondary products diminished markedly, and the only product left in appreciable concentration was CH_3NO. With these shorter reaction times the extent of reaction could be measured either by the formation of CH_3NO or by the decrease in the amount of ethane formed when the nitric oxide concentration was changed. Since ethane and nitric oxide have the same mass, the 29 peak ($C_2H_5^+$ from C_2H_6) was used to measure the change in the ethane concentration. At 900°C, and with a reaction time of 1.2×10^{-4} sec, mean values of 3.4×10^{-4} for the collision efficiency and 1.4×10^{11} $(moles/cc)^{-1}$ sec^{-1} for the rate constant were obtained by these two methods.[2] At 480°C, and with a reaction time of 4×10^{-4} sec, a collision efficiency of 3.9×10^{-4} and a rate constant of 1.3×10^{11} $(moles/cc)^{-1}$ sec^{-1} were obtained. Since the helium carrier gas pressures used were of the order of 1 cm, it is probable that third-body restrictions are coming into play, and that the collision efficiencies and rate constants at higher pressures will be larger than these values. The present results agree closely with the results obtained by earlier workers at different temperatures[3] which indicates that the activation energy of the reaction is approximately zero.

We are grateful to the Defence Research Board of Canada for financial assistance.

[1] K. U. Ingold and W. A. Bryce, J. Chem. Phys. (to be published).
[2] The mean molecular diameter was taken as 3.75×10^{-8} cm.
[3] E. W. R. Steacie, *Atomic and Free Radical Reactions* (Reinhold Publishing Corporation, New York, 1954), second edition, p. 646.

Structure of Hexamethyldisilane

Hiromu Murata and Kazuhiro Shimizu
Osaka Municipal Technical Research Institute, Osaka, Japan
(Received August 9, 1955)

FOR hexamethylethane Cleveland, Lamport, and Mitchell[1] concluded that the staggered model (symmetry D_{3d}) seems to be more probable than the eclipsed (symmetry D_{3h}) or the free rotation (symmetry D_{3h}'). In order to decide the configuration of hexamethyldisilane, skeletal fundamental frequencies were calculated for an ethane-like, octa-atomic molecule assuming methyl groups as one particle, using the method given by Shimanouchi[2] and potential constants given in Table I. Tetrahedral

Table I. Potential constants for hexamethyldisilane (10^5 dynes/cm).

Type	Set I[a]	Set II[b]
KSi$-$CH$_3$	2.35	2.60
KSi$-$Si	0.68	0.75
HCH$_3-$Si$-$CH$_3$	0.05	0.10
HSi$-$Si$-$CH$_3$	0.18	0.18
F'CH$_3\cdots$CH$_3$	−0.01	−0.02
F'Si$\cdots$CH$_3$	−0.04	−0.04
F'CH$_3\cdots$CH$_3'$ [c]	0.00	0.00
FCH$_3\cdots$CH$_3$	0.20	0.03
FSi$\cdots$CH$_3$	0.10	0.10
FCH$_3\cdots$CH$_3'$	0.00	0.00
κ	0.04	0.04

[a] Of these constants, KSi$-$CH$_3$, HCH$_3-$Si$-$CH$_3$, F'CH$_3$CH$_3$, and FCH$_3$CH$_3$ were obtained directly from the normal frequencies of Si$(CH_3)_4$. ($\nu_1 = 598$, $\nu_2 = 202$, $\nu_3 = 696$, and $\nu_4 = 239$.)
[b] HCH$_3-$Si$-$CH$_3$, F'CH$_3$CH$_3$, and FCH$_3$CH$_3$ were those given by Shimanouchi (see reference 2).
[c] $'$ denotes CH$_3$ attached to a different Si atom.

angles were assumed and the equilibrium values of the bond distances were taken as Si−Si=2.34 A, and Si−CH_3=1.90 A. The Raman and infrared spectral data, calculated wave numbers, and assignments are given in Table II. In general, the assignment

TABLE II. Raman and infrared spectral data, calculated wave numbers, and assignments for hexamethyldisilane.[a]

Description	M-K	Raman C-L-B	PS	Infrared C-L-B	Probable values	Calculated wave number Set I	Set II	Assignment	D_{3d}	Type D_{3h}	D_{3h}'
δ(Si−CH_3)	178	180	D		180	183	183	ν_9	e_u	e'	e
		190	D		190	208	203	ν_{12}	e_g	e''	$\tilde{e}$
		200	P		200	181	181	ν_3	a_{1g}	a_1'	a_1
	250	251	D	244	250	221	222	ν_8	e_u	e'	e
		305	D		305	301	306	ν_{11}	e_g	e''	$\tilde{e}$
				328	328	325	332	ν_6	a_{2u}	a_2''	$\tilde{a}_2$
ν(Si−Si)	403	404	P		404	400	403	ν_2	a_{1g}	a_1'	a_1
				610	610	616	618	ν_5	a_{2u}	a_2''	$\tilde{a}_2$
ν(Si−CH_3)	638	638	P		638	619	617	ν_1	a_{1g}	a_1'	a_1
	689	686	D	690	690	721	690	ν_7	e_u	e'	e
	754	753	D		754	753	722	ν_{10}	e_g	e''	$\tilde{e}$
δ(C−H)	833	830	D	834	834						
	883	883	P		883						
	1245	1241	D	1245	1245						
	1317	1315	P		1316						
	1373	1372	D		1373						
ν(C−H)	2893	2898	P	2898	2898						
	2955	2957	D	2957	2957						

[a] M-K = Murata, Kumada [H. Murata and M. Kumada, J. Chem. Phys. 21, 945 (1953)] C-L-B = Cerato, Lauer, Beachell[3]; PS = polarization state; (P = polarized, D = depolarized).

is quite satisfactory. If the most stable structure of this molecule is that corresponding to point group D_{3d}, the type e_u frequencies should be allowed only in the infrared spectrum. Thus, it seems to indicate clearly that the equilibrium configuration for this molecule is D_{3h} or D_{3h}', in agreement with the conclusion of Cerato, Lauer, and Beachell.[3]

[1] Cleveland, Lamport, and Mitchell, J. Chem. Phys. **18**, 1321 (1950).
[2] T. Shimanouchi, J. Chem. Phys. **17**, 245, 848 (1949).
[3] Cerato, Lauer, and Beachell, J. Chem. Phys. **22**, 1 (1954).

Nuclear Quadrupole Resonance of γ-Irradiated *Para*-Dichlorobenzene

JULES DUCHESNE AND ANDRÉ MONFILS,*
Institut d'Astrophysique, University of Liège, Belgium
AND
JULIEN GARSOU†
Institut de Radiologie, University of Liège, Belgium
(Received August 8, 1955)

IT was recently discovered[1] that mixed crystals in which one of the components is present even in very low concentrations (one part in one thousand) give rise to a decrease in the intensity of the nuclear quadrupole resonance line of the main component. One could expect therefore that any ionizing radiation able to create imperfections in the crystal lattices would produce a similar effect. The present work was undertaken to confirm this and it was decided to irradiate *p*-dichlorobenzene at 20°C with gamma rays from Co^{60}.

A frequency-modulated super-regenerative oscillator was used and the spectra were automatically recorded after phase sensitive detection of the signals. The observations made at 20°C showed that the height of the line corresponding to Cl^{35} was decreased by about 25 and 37% for irradiations of 1.4×10^8 and 2.7×10^8 roentgen, respectively. We have not been able to detect any shift in the line greater than the mean errors of measurement (±1 kc). A decay of the unstable molecular species formed during the irradiation was indicated by a partial reappearance of the normal intensity of the line after a period of some hours. It was noted that the irradiated crystals were greenish in color, and that they became gradually yellow when the sample was heated up to 50°C. If one can assume that the effect on the quadrupole line of the particles created by the irradiation is roughly the same as that of impurities,[1] then the proportion of particles should be of the order of one part in one thousand and 1.6 part in one thousand, respectively, in the two cases considered.

This new method, which appears to be of wide application, may be invaluable in the study of the detailed mechanism of the damage produced in matter by irradiation of different kinds. Further research concerned with this, and identification of the particles, is being carried out in our laboratories.

We are greatly indebted to Professor Paul Desaive of the Institute of Radiology for his kind hospitality and for having put at our disposal the source of gamma rays.

* Chargé de Recherches du Fonds National de la Recherche Scientifique.
† Chercheur agréé de l'Institut Interuniversitaire des Sciences Nucléaires.
[1] J. Duchesne and A. Monfils, Compt. rend. **238**, 1801 (1954).

Luminescence Quenching by Oxygen: Cyclohexane-Benzene-*p*-Terphenyl*

P. J. BERRY† AND MILTON BURTON
Department of Chemistry, University of Notre Dame, Notre Dame, Indiana
(Received July 29, 1955)

QUALITATIVELY, the quenching effect of oxygen in "liquid scintillation" solutions has been known for some time.[1] Recently, a quantitative study of (cobalt-60) gamma-induced luminescence in a solution of *p*-terphenyl (mole fraction 6.1×10^{-4}) in solvent of varying relative concentrations of cyclohexane and benzene has given results summarized by the "degassed" and "66 cm" curves of Fig. 1.[2] Evidently, while there is no inflection

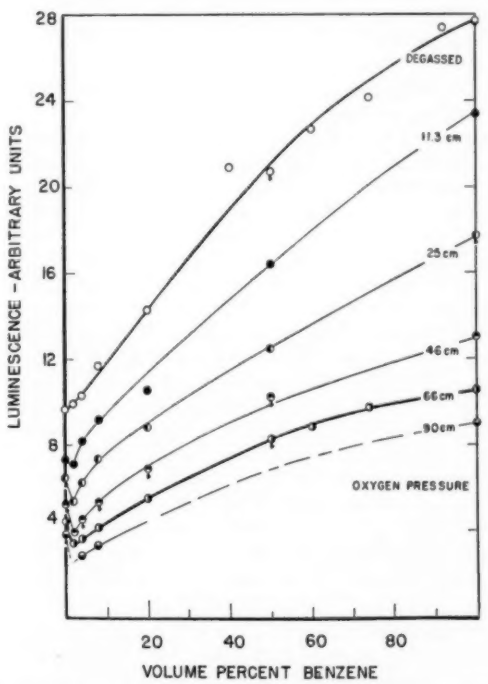

FIG. 1. Effect of oxygen on gamma-induced luminescence of *p*-terphenyl in cyclohexane-benzene solvent. Flagged points are taken from experimental curves in which luminescence in a solution of particular relative concentration of solvents was determined as a function of oxygen pressures but for which points corresponding to the precise values required for this figure were not determined. All available and pertinent data are shown. Mole-fraction *p*-terphenyl = 6.1×10^{-4}.

in the curve for the degassed solution, there is a definite minimum when oxygen is present at 66 cm pressure. The other curves in the diagram represent results of new work designed to establish the quenching effect of oxygen as a function of pressure; the technique of the measurements is that previously employed.[2]

The work is inadequate for determination of the precise location of a minimum in the luminescence of oxygenated solutions; nevertheless the minima evidently lie at, or below, about 2 volume percent (practically the same, in this case, as 2 electron percent) of benzene. The greater the oxygen concentration the more pronounced is the effect.

Regarding the validity of the points at zero volume percent benzene, there is reason to suspect that the "pure" cyclohexane employed contained traces of impurity,[2] probably benzenoid in character. If the last traces of such impurity were removed, the effect would be as if the zero percent ordinate were removed to the left; i.e., to make the zero percent benzene points on the degassed curve slightly lower and on the oxygenated curves slightly higher. There is thus no question of the reality of the minima at all oxygen pressures.

In terms of a Stern-Volmer plot, i.e. I_0/I *vs* concentration of quenching material, where I_0 is the luminescence with no quenching material present, the slope of the curve, γ, at any point is the quenching constant. Table I presents quenching constants for

TABLE I. Quenching constants in oxygenated mixtures: Cyclohexane and benzene with added *p*-terphenyl.

% Benzene	0	2	4	8	20	50	60	74	100
Solubility[a] 1 mole^{-1}	11 104	10.9 231	10.8 196	10.7 192	10.2 190	9.07 189	8.69 206	8.15 211	7.15 266

[a] Oxygen solubility is expressed in units of mole 1^{-1} atmos^{-1} $\times 10^3$.

several mixtures of cyclohexane-benzene with added constant *p*-terphenyl concentration of 6.1×10^{-4} mole fraction (corresponding to 1.58 grams per liter in benzene). In this table, the solubility of oxygen in mixtures of cyclohexane and benzene is assumed to be a linear function of the constitution of the mixture; the solubility of oxygen in benzene is taken from Pringsheim,[3] and that for oxygen in cyclohexane interpolated from data tabulated in Hildebrand for other gases in cyclohexane.[4]

Oxygen quenching of gamma-ray induced luminescence from solutions of a solute such as *p*-terphenyl in a single solvent seems to be mostly ascribable to quenching of excited states of the solvent, rather than excited states of the solute.[5] The minimum results because a mixture near 2% benzene and 98% cyclohexane is quenched much more efficiently than pure cyclohexane. Chemical evidence has been presented that energy transfer takes place with high efficiency from cyclohexane to benzene in the radiolysis of mixtures of the two.[6] Since excited states of benzene are apparently quenched considerably more efficiently than excited states of cyclohexane (the quenching constant for benzene-*p*-terphenyl is more than twice that for cyclohexane-*p*-terphenyl[2]), one reasonable explanation for the minimum is that energy transfer takes place efficiently from excited states of cyclohexane to excited states of benzene in the mixed solvent, and that quenching then involves mainly excited states of benzene, despite the fact that the solution may contain a much higher concentration of cyclohexane. Other possible explanations depend on the mechanism by which energy is transferred, specifically on the contribution of ionic species.

* Contribution from the Radiation Project of the University of Notre Dame, supported in part under U. S. Atomic Energy Commission contract AT(11-1)-38 and Navy equipment loan contract Nonr-06900.
† Monsanto Fellow, University of Notre Dame 1954–1955.
[1] Pringle, Black, Funt, and Sobering, Phys. Rev. **92**, 1582 (1953).
[2] Burton, Berry, Lipsky, J. Chim. Phys. (to be published).
[3] P. Pringsheim, *Fluorescence and Phosphorescence* (Interscience Publishers, Inc., New York-London, 1949), p. 332.
[4] J. H. Hildebrand, *Solubility of Nonelectrolytes* (Reinhold Publishing Corporation, New York, 1940), second edition, p. 78.
[5] M. Furst and H. Kallman, Phys. Rev. **97**, 583 (1955).
[6] J. P. Manion and M. Burton, J. Phys. Chem. **56**, 560 (1952).

Specific Heat of Graphite at Very Low Temperatures*†

WARREN DESORBO
General Electric Research Laboratory, Schenectady, New York
(Received July 21, 1955)

A COMPARISON of some specific heat data of graphite recently reported by Bergenlid *et al.*[1] (1.5–90°K) with those reported by DeSorbo and Tyler[2] (13–300°K) showed deviations between the two studies in the region 13–25°K.[1] It has been suggested that[3] in addition to gaseous adsorbates, there are other factors that can affect the specific heat of graphite. The influence of particle size, the influence of lattice irregularities (such as turbostatic structures, faulting, twinning, edge effects, lattice strain, etc.), and the influence of intergranular carbon on the specific heat of graphite have not been evaluated.

We have recently measured the specific heat of a graphite sample (H−CS−II) in the temperature region 1.5–20°K. The data are in good agreement with those presented by Bergenlid *et al.*[1] X-ray analysis[4] show this sample to have the $L(A)=240$ A (i.e., the "apparent crystallite size" in the C direction). The sample was found to be "slightly faulted." Total ash content was found to be 0.4% by weight. Gas evolved by this sample when heated to 600°C amounted to 50 ppm by weight.

In the temperature region 1.5–3°K, the specific heat data of sample, H−CS−II, fit equally well (considering root-mean-square deviations) the equations

$$C=aT^3+\gamma T, \quad (1.5\text{–}3^\circ\text{K}) \tag{1}$$

$$C=bT^{2.4}, \quad (1.5\text{–}4.2^\circ\text{K}). \tag{2}$$

Equation (1) is suggestive of the presence of both a lattice and an electronic component of the total specific heat of graphite. The coefficient of the linear term γ is smaller than that found for metals (see Fig. 1). If we assume that the linear term is due to the specific heat of the "free electrons" for graphite, a "lattice" specific heat C_L, for this sample of graphite can be evaluated. A plot of $\log C_L$ *vs* $\log T$ reveals that the exponential of T in the equation

$$C_L=kT^n \tag{3}$$

is decreasing with increasing temperature from a value $n\cong3$ at ~3°K to $n\cong2$ at ~20°K.

We have recently studied the specific heat of another graphite sample, SA-25,[5] in the temperature region 1.5–4.2°K. The x-ray analysis shows this sample to be "highly faulted" with an

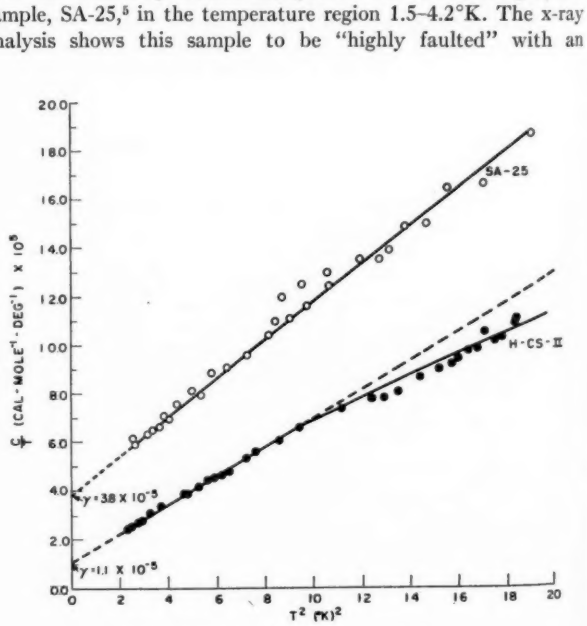

FIG. 1. c/T *vs* T^2 for two different samples of graphite.

$L(A) = 110$ A. As reported tentatively by J. C. Bowman, National Carbon Company, the gas content is set at an upper limit of 100 ppm by weight. The total ash content is less than 0.05% by weight. The specific heat of this sample (SA-25) was found to be significantly greater throughout the temperature region studied by us when compared with the specific heat data of sample H−CS−II, in spite of the fact that the ash content of sample SA-25 is less than that of H−CS−II. The data for SA-25 can be described by Eq. (1) in the temperature region 1.5–4.2°K. The constants a and γ vary from those derived from the data of sample H−CS−II (Fig. 1).

It is important to note that the specific heat data of graphite that is to be compared with various theoretical models (for a bibliography on the theories of the specific heat of graphite, see latest two reports.[6,7]) recently proposed for describing this property of graphite, should be that data obtained for a high purity graphite sample of "large" crystallite size and one free of lattice faults and defects.

The details of the experimental techniques—including those which protect the sample from any possible gaseous contamination during the experiment—and data will be published shortly. (Latest corrections proposed[8] to the 1948 liquid helium vapor pressure-temperature scale have been incorporated in the data.)

The author wishes to thank Dr. J. A. Krumhansl (National Carbon Company) and Dr. W. L. Roth for their continued interest in this work.

* Presented in part before the U. S. Atomic Energy Commission Off-Site Conference on Solid State Metallurgy, Carnegie Institute of Technology, June 20–21, 1955.

† Work supported in part by U. S. Atomic Energy Commission, Contract No. W-31-109-Eng.-52.

[1] Bergenlid, Hill, Webb, and Wilks, Phil. Mag. **45**, 851 (1954).

[2] W. DeSorbo and W. W. Tyler, J. Chem. Phys. **21**, 1660 (1953).

[3] W. DeSorbo, "Low temperature heat capacity of Ceylon graphite," General Electric Research Laboratory Report No. RL-1202 November, 1954 (also in press J. Am. Chem. Soc.); Twenty-fourth Quarterly Report General Electric Research Laboratory Report No. 1237 U. S. Atomic Energy Commission Contract No. W-31-109-Eng.-52, January, 1955.

[4] Performed by Dr. W. L. Roth of the General Electric Research Laboratory.

[5] Supplied to us by Dr. J. A. Krumhansl, National Carbon Company, Cleveland, Ohio.

[6] G. F. Newell, "Vibration spectrum of graphite and boron nitride. I. The two dimensional spectrum," Technical Report Contract No. Nonr-562(08), May 15, 1955, The Metals Research Laboratory, Brown University.

[7] K. Komatsu, J. Phys. Soc. (Japan) **10**, 346 (1955).

[8] Clement, Logan, and Gaffney, "An examination of the 1948 liquid helium vapor pressure-temperature scale," Naval Research Laboratory Report No. 4542.

Overvoltages in Melted Electrolytes

R. PIONTELLI AND G. STERNHEIM
*Laboratory of Electrochemistry, Chemical Physics and Metallurgy, Politecnico of Milan, Milan, Italy**

(Received August 1, 1955)

PRECEDING papers from this Laboratory concern the experimental methods realized here for measuring electrode overvoltages of melted metals against metal electrolytes[1] and the anodic and cathodic behavior of the electrode $Pb/PbCl_2$ at 520°C ÷ 530°C.[2] These methods have been extended with suitable improvements and adaptations to the electrodes: (a) $Pb/PbCl_2$ +KCl (various amounts) at 560°C ÷ 670°C; (b) $Cd/CdCl_2$ and $Cd/CdCl_2$+KCl (i.d.: 590°C); (c) $Sn/SnCl_2$ and $Sn/SnCl_2$+KCl (i.d.: 350°C); (d) $Zn/ZnCl_2$ and $Zn/ZnCl_2$+KCl (i.d.: 490°C).

Figures 1–3 give some examples of the results thus obtained. ξ is the value (mv) of the voltage changes in the "tensiometric cell" formed by the studied electrode coupled with a reference electrode,[3] determined in a way to practically exclude the concentration polarization; i_a and i_c are the current densities (A/dm^2) carried by the studied electrode when it acts as anode, or as cathode, respectively, in the electrolysis cell; d is the mean distance (mm) between reference electrode and studied electrode. KCl amounts are given in weight percent.

The measured overvoltages for all of the studied systems, and both from anodic and cathodic side have character of pure ohmic drop. Correcting these results by subtracting the ohmic drop in the layer between reference electrode and polarized electrode, the remaining "true overvoltage" is zero, in the order of approxima-

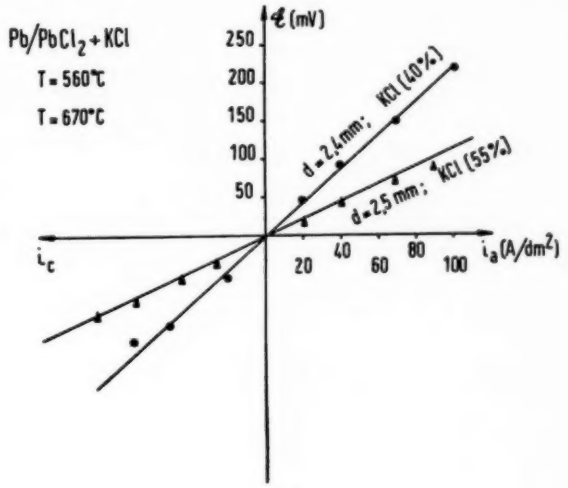

FIG. 1.

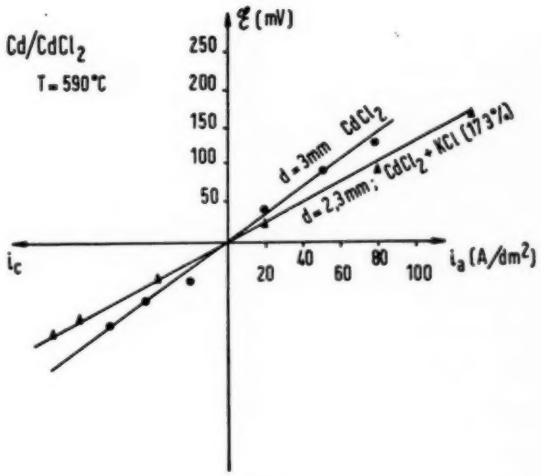

FIG. 2.

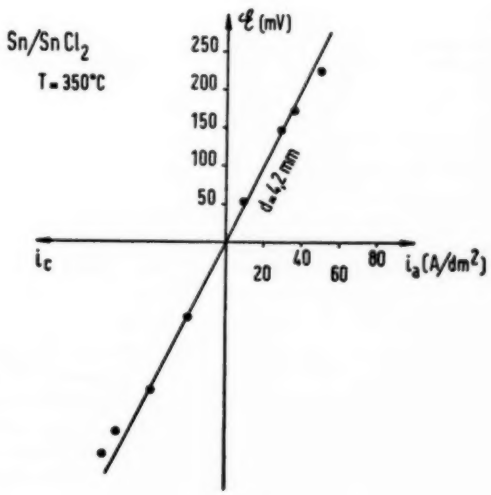

FIG. 3.

tion allowed by the experiment and by accuracy of the existing data on the conductivity of the baths employed.[4]

Other experiments, recently carried out and in progress confirm the wide validity of this conclusion for the electrodes at which ions of low melting metals (whose behavior is "normal" also in aqueous solutions[5]) are exchanged.[6]

For these electrodes, only "concentration overvoltages," intervening when the baths contain several components, seem significant in practice. The quantitative aspects of this contribution are now studied in this Laboratory.

Mr. Consonni has given very valuable help in the experiments.

* The researches reported in this paper have been sponsored in part by the Air Research and Development Command U. S. Air Force under Contract No. AF 61 (514) 733 C through the European Office, ARDC.

[1] (a) R. Piontelli, Gazz. chim. ital. **83**, 357, 370 (1953); Rend. Ist. lombardo sci. **88**, 51 (1955). (b) R. Piontelli *et al.*, Z. Elektrochem. **56**, 86 (1952); **58**, 54 (1954); **59**, 64 (1955). R. Piontelli and G. Montanelli, Alluminio **22**, 672 (1953); J. Chem. Phys. **22**, 1981 (1954).

[2] Piontelli, Rivolta, and Montanelli, Z. Elektrochem. **59**, 64 (1955); R. Piontelli and G. Sternheim, J. Chem. Phys. **23** (1955) (to be published).

[3] The reference electrode is made of silver and is arranged as previously described.[2]

[4] See in particular: H. Bloom and E. Heymann, Proc. Roy. Soc. (London) **188**, 392 (1947). P. Drossbach, *Elektrochemie geschmolzener Salze* (Springer Verlag, 1938). Measurements of conductivity are now also performed by us.

[5] R. Piontelli, Z. Elektrochem. **55**, 128 (1951).

[6] Experiments now in preparation will indicate if this conclusion applies also to the high melting metals, for which, on the contrary the overvoltages in aqueous solutions are high, as a rule.[5] The behavior of the electrodes where gases are evolved seems, on the basis of the existing evidence, largely different, also under conditions far from those of the so-called "anode effect."

On Proton Chemical Shift in Ammonia

B. N. Bhar
Nobel Institute of Physics, Stockholm, Sweden
(Received August 15, 1955)

REVIEWING our suggestion that the chemical shift of proton resonance lines of COOH group of carboxylic acids and of OH group of alcohols should be dependent upon pressure,[1] it appears that the suggestion of pressure dependence of chemical shift of proton resonance should also hold in all compounds endowed with the property of molecular association by virtue of hydrogen bonding. The association is most explicitly manifested in cases where hydrogen atoms are bonded with most electronegative elements like flourine, oxygen, nitrogen, etc. by the bond of the type F−H···F, O−H···O, N−H···N. The vicinity of electronegative elements to hydrogen reduces the normal diamagnetic shielding of the hydrogen nucleus. The diamagnetic shielding of protons in case of associated compounds will depend upon the extent of association. If the correlation time in the associated and unassociated states are extremely short then the diamagnetic shielding will be an average over the two states.[2] The proton resonance in such cases will be observed at a frequency corresponding to the average shielding for the two states, and therefore upon the extent of association. It seems that any parameter affecting the extent of association would alter the average diamagnetic shielding and, hence, also the chemical shift of proton resonance. Since pressure, like temperature, does alter the extent of association, it seems logical that the chemical shift of proton resonance should be pressure dependent. At increased pressure the extent of association will be increased and, hence, the average diamagnetic shielding would be less and, as a result, the proton resonance will occur at lower values of the externally applied magnetic field. At reduced pressure the extent of association will be reduced and therefore the average diamagnetic shielding would be greater and the proton resonance will occur at higher values of the externally applied magnetic field. Now let us consider the proton resonance of a chemical compound endowed with the property of association by virtue of hydrogen bonding, in its liquid and gaseous phase. As the liquid can be considered as a "highly compressed gas," the extent of association in liquid will therefore be greater than that in vapor and the proton resonance, according to arguments presented above, will occur at a value of the externally applied magnetic field which is lower than that required for resonance in the gaseous phase. Otherwise stated the proton resonance in vapor will occur at a higher value of the externally applied magnetic field. It appears that Ogg's observation[3] of proton resonance in vapor ammonia occurring at a *higher* value of the externally applied magnetic field seems to be compatible with our suggestion.

[1] Bhar, Forsling, and Lindström, Arkiv Fysik (to be published).
[2] U. Liddel and N. F. Ramsey, J. Chem. Phys. **19**, 1608 (1951).
[3] R. A. Ogg, J. Chem. Phys. **22**, 560 (1954).

Alternative Method for Calculating SCF Orbitals

H. Brion and R. Lefebvre, *Centre de Chimie Théorique de France, 155 Rue de Sèvres, Paris 15°*
and
C. M. Moser, *Pavillon Pasteur de l'Institut du Radium, 11 rue Pierre Curie, Paris 5°*
(Received July 18, 1955)

REPEATED iterations performed with a method recently published[1] make it possible to calculate the orbitals which minimize the energy associated with certain orbital-type wave functions. If approximate orbitals are known, they can be improved by diagonalizing a limited configuration interaction matrix, and the process is repeated until certain elements of the matrix become zero. Then no further improvement of the orbitals can be made. The relationship between self-consistency and the partial vanishing of the CI matrix has been known for a long time[2] for one determinant WF's, but this can be extended to cases where more than one determinant is needed.

This procedure, which avoids the introduction of multipliers to guarantee the orthogonality of the orbitals, can be particularly useful for problems where approximate orbitals have been derived by simplified methods, and we report here our findings concerning the LCAO MO's of certain states of unsaturated alternant hydrocarbons.

For the closed-shell ground state of even alternant hydrocarbons, many simplifications result from the use of semiempirical assumptions[3,4] and, as expected,[4] the final bonding and antibonding orbitals show the property of being related by pairs. There is no compensation here to the drawback of having a rather large matrix to solve at each iteration, as the orbitals can be made automatically orthogonal in the usual procedure.[5] *Trans*-butadiene and naphthalene have been reconsidered along these lines.

For odd alternant hydrocarbons, a ground state WF with all orbitals except one doubly occupied has been considered. If the restrictions quoted above are introduced, there is self-consistency of the assumption that the orbitals behave as in the Hückel theory (that is with bonding and antibonding orbitals related by pairs, and the singly occupied orbital with one set of coefficient zero). Allyl and pentadienyl have been studied as examples of this class of compounds.

As an application to functions made of more than one determinant, the lowest triplet and singlet B_u states of *trans*-butadiene have been considered, in the representation where two molecular orbitals are singled occupied. The procedure converges satisfactorily, and in the semiempirical approximation the final orbitals present the interesting particularity of being related by pairs, as are those of the ground state.

One of us (C.M.M.) wishes to acknowledge the receipt of a U. S. Public Health Service Fellowship in support of this work.

[1] R. Lefebvre, Compt. rend. **240**, 1094 (1955).
[2] L. Brillouin, Actualités sci. et ind. **159** (1934).
[3] R. Pariser and R. G. Parr, J. Chem. Phys. **21**, 466, 767 (1953).
[4] J. A. Pople, Trans. Faraday Soc. **49**, 1375 (1953).
[5] C. C. J. Roothaan, Revs. Modern Phys. **23**, 69 (1951).

Polarized Spectra of Anthracene Crystals and Davydov Splitting

L. E. LYONS
Physical Chemistry Department, University of Sydney, New South Wales, Australia
(Received July 28, 1955)

DIFFICULTIES in interpreting the spectra of molecular crystals of the anthracene type have arisen from the interactions between molecules in the crystal lattice. One way of overcoming this problem has been to work with solid solutions[1] of the substance of interest in a dispersing medium. However the more fundamental problem of understanding the spectra of pure crystals remains, and in this connection Davydov's theory has proved most fruitful.[2] Predictions[3] have been made on this basis of this theory in connection with anthracene crystals, and some of them have not previously been tested fully by experiment.

It is the purpose of this note to list some unpublished experimental results which provide striking confirmation of some of the predictions.

(1) Davydov's theory predicts[3] that the anthracene second main absorption system (A_g-B_{3u}) will be split in the crystal, by an estimated 16 000 cm^{-1}. Since the component parallel to the b crystal axis occurs at about 2680 A, the a component is expected about 1900 A. Experiments[4] made with a vacuum spectrograph and polarized light showed that absorption bands actually occur with a maximum at 1890 A and 2200 A and that the absorption in each case is greater in a direction perpendicular to the b axis than parallel to it. It is therefore possible to interpret the 1890 A absorption as the a component of the vapor A_g-B_{3u} transition, polarized along the longer molecular in-plane axis.

(2) Other experiments[5] have given precise information about molar extinction coefficients in crystals, the thickness being measured by interferometric methods. Here too the interpretation of the 2680 A absorption is confirmed. The assignment of the molecular transition as A_g-B_{3u} enabled[3] a calculation by first-order perturbation theory of the intensity expected for the b component absorption. The predicted value of the molar extinction coefficient, ϵ_b, was 9100±500 for the crystal, taking the solution extinction coefficient as 232 000. The experimental value we found as 9450.

(3) Similar experiments to (2) done on the 3920 A crystal transition confirm the assignment of A_g-B_{2u} to a transition polarized along the short molecular axis. The intensity expected is 21 000; for ϵ_b, while the experimental value[5] is 22 800.

The correlation between theory and experiment in (2) and (3) would not be obtained unless pronounced Davydov splitting occurred and consequently the results are direct evidence for the reality of the splitting phenomenon.

[1] D. S. McClure, J. Chem. Phys. **22**, 1256 (1954).
[2] A. Davydov, Zhur. Eksptl. i Teort. Fiz. **18**, 210 (1948).
[3] D. P. Craig and P. C. Hobbins, J. Chem. Soc. 539 (1955); D. P. Craig, J. Chem. Soc. (1955).
[4] T. M. Dunn and L. E. Lyons (unpublished).
[5] A. Bree and L. E. Lyons (to be submitted to J. Chem. Soc.).

Infrared Spectrum and Molecular Structure of Succinonitrile

GEORGE J. JANZ AND WARREN E. FITZGERALD
Department of Chemistry, Rensselaer Polytechnic Institute, Troy, New York
(Received August 4, 1955)

FOR n-butane[1] and 1,2-dihaloethanes,[2] simplifications of the vibrational spectra, upon transition from the gaseous to the solid state, have been interpreted in the light of rotational isomerism. The present note reports the results of a similar investigation for succinonitrile, $NC-CH_2-CH_2-CN$. A comparison of n-butane, 1,2-dichloroethane, and succinonitrile with reference to rotation about the central carbon-carbon bond is shown in Fig. 1.

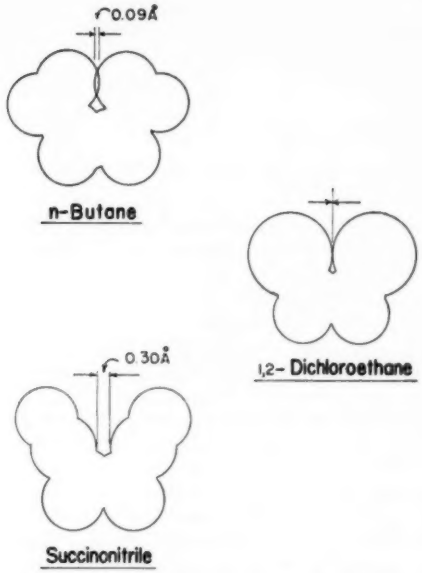

FIG. 1. Molecular silhouettes of n-butane, 1,2-dichloroethane, and succinonitrile.

The molecular silhouettes for the *cis*-configuration, using Van der Waals' radii, show that for the former two, the substituents overlap, (0.09 and 0.00 A, respectively) while for the latter there is no steric interference. A free rotation about the central C−C bond, however, is not very probable considering the polar nature of the cyano groups and the electrostatic repulsion in the *cis*-configuration of succinonitrile.

The results of the experimental investigations[3] are summarized in Fig. 2 which shows the infrared spectrum for succinonitrile at three temperatures. No changes in the vibrational spectrum were observed for the transition from liquid to solid (55–57°C) or with cooling until the temperature of −43.7±0.8°C was reached. Inspection of the data in Fig. 2 shows that the frequencies, 1270, 917, 760, and 530 cm^{-1} disappear, and a splitting occurs at 2240 and 818 cm^{-1} at the lower temperature leaving still fourteen strong bands. These data are in accord with the presence of rotational isomers in succinonitrile.

The line splitting is attributed to the existence of succinonitrile entirely in one form below −43.7°C. Above this temperature a second component is contributing to this band contour. Like

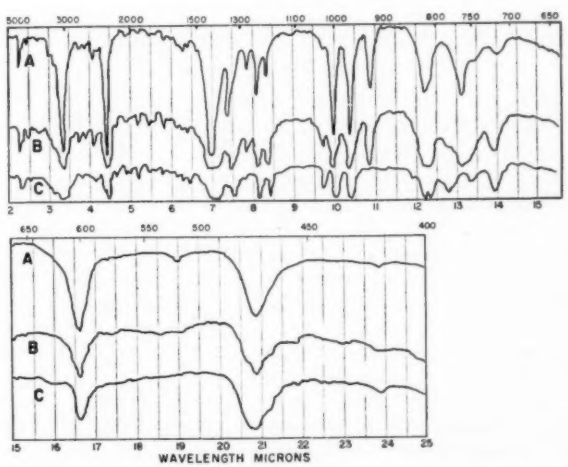

FIG. 2. Infrared spectra for succinonitrile. *A* is liquid, 60°C; *B* is solid, −40°C; and *C* is solid, −45°C.

TABLE I.

Vibration	Descriptive assignment	Type vibration and activity		
		C_{2v}	C_{2h}	C_2
ν_6	C−C−C bend	A_1(R., I.)	A_g(R.)	A(R., I.)
ν_{22}	C−C−C bend	B_2(R., I.)	B_u(I.)	B(R., I.)

n-butane[1] and the 1,2-dihaloethanes,[2] succinonitrile can assume three rotationally isomeric configurations, *cis*, *trans*, and *gauche*. The vibrational assignment[3] of the spectrum at −45°C is in accord with a structure of C_2 symmetry (*gauche*), rather than C_{2h} or C_{2v} (*trans* and *cis*, respectively). Consideration of the selection rules shows that of the 24 vibrational modes, 19, 9, and 16 are predicted infrared active in the region 3000 to 400 cm^{-1} for the *gauche*-, *trans*-, and *cis*-forms. The *cis*-isomer is predicted the least stable of the three configurations from steric considerations, the polar nature of the two cyano groups, and by analogy with related molecules.[1,2] Restricting the consideration to the *trans*- and *gauche*-forms, the small but definite simplification in the spectrum on cooling to −45°C favors the *gauche*-form as the more stable isomer. The identity of this is confirmed in the assignment of the two C−C−C bending modes found in the 600 to 400 cm^{-1} region and summarized in Table I. Only ν_{22} is predicted infrared active for the *trans*-form, whereas ν_6 and ν_{22} are infrared active for the *gauche*-isomer. Two strong bands, 601 and 478 cm^{-1}, are present in the infrared spectrum at −45°C (Fig. 2). Above −43.7°C as evidenced by the appearance of new bands, and change in band contour, the molecule exists as a mixture of isomers, with the *gauche*-form predominating. Succinonitrile, thus, like *n*-butane and the dihaloethanes, exhibits rotational isomerism, but differs in that the most stable form at low temperatures is not the *trans*-, but rather the *gauche*-configuration.

Acknowledgments.—Support of this research through grants-in-aid from the Research Corporation, New York, and the Trustees Research Committee, Rensselaer Polytechnic Institute is gratefully acknowledged. The authors wish to thank Dr. H. J. Bernstein and Dr. J. Lancaster for helpful discussion and continued interest in this work.

[1] Szasz, Sheppard, and Rank, J. Chem. Phys. **16**, 704 (1948); D. W. E Axford and D. H. Rank, J. Chem. Phys. **17**, 403 (1949).
[2] Mizushima, Morina, and Higasi, Sci. Papers Inst. Phys. Chem. Research (Tokyo) **25**, 159 (1934); Mizushima, Morina, and Kozima, Sci. Papers Inst. Phys. Chem. Research (Tokyo) **29**, 111 (1936); K. Kozima and S. Mizushima, Sci. Papers Inst. Phys. Chem. Research (Tokyo) **31**, 296 (1937); W. F. Edgell and G. Glocker, J. Chem. Phys. **9**, 357 (1941); H. J. Bernstein, J. Chem. Phys. **17**, 258 (1949).
[3] To be described elsewhere in detail.

Dynamic Equilibrium of Inverted Isomers in a Crystalline Phase

TSUNEO YOSHINO
Tokyo Institute of Technology, Oh-okayama, Meguro-ku, Tokyo, Japan
(Received August 15, 1955)

THE fact that the compound having rotational isomers in gaseous and liquid states takes one form in the solid has long been used as a useful technique to study the molecular structure of the compound. However it has been known in our laboratory that the isomeric forms of such compounds as 1,2-dichloro-4,5-dibromocyclohexane[1] and 1,2-dichloro-1,2-dibromoethane[2] persist even in solid states. But it is not without doubt whether these solids are crystalline or amorphous. If they are crystalline, it is uncertain whether they are homogeneous or not.

Trans-1,4-dichlorocyclohexane (m.p. 102°C) has two isomeric forms in solutions, and the abundance ratio of the isomers varies with changing solvents.[3] The infrared absorption bands were measured in various solutions by a Perkin-Elmer Model 112 spectrometer, and were assigned to the *ee* and *aa* forms by the use of the change of the abundance ratio. The infrared measurement of the crystal of the compound was also made by the KBr disk technique, and the bands of both forms were found in the spectrum. The frequencies of the bands below 800 cm^{-1} were smaller by 5∼10 cm^{-1} than those in solutions, as ordinarily found for the crystals of the other compounds. The coexistence of both forms in the crystal is not due to the distortion of the crystal lattice in making the KBr disk, because the same spectrum was obtained for the unpressed crystal deposited from cyclohexane or ethyl alcohol solution.

As shown in our previous paper[3] the mole fractions of the *ee* and *aa* forms are nearly the same in solutions. Comparing the intensity ratios of the absorption bands of the both forms in the crystal with those in solutions, we can estimate the *aa*/*ee* mole ratio in the crystal to be about $\frac{1}{3}$ at room temperature.

With the rise of temperature of the KBr disk the absorption intensities of the *aa* form remarkably increase, while those of the *ee* form decrease. When the disk returns to room temperature the intensities also return to their original magnitudes. At −80°C the bands of *aa* form disappear, and they recover their intensities when the disk returns to room temperature. We see, therefore, that the change of the mole ratio with temperature is not due to a transition from a metastable phase to a stable one, but the two forms stand in an equilibrium in a stable homogeneous phase as if they were in liquid. Because of the small mole ratio of *aa* form at low temperature and the difficulty of the measurement of Raman spectra of solids, we have failed to notice the Raman lines of the *aa* form in our previous work.[3]

The temperature dependency of the abundance ratio of two isomers in the crystal was obtained by measuring the peak intensity ratios of 468 cm^{-1} band of *ee* form and 557 cm^{-1} band of *aa* form for different temperatures. They are suitable for the measurement because they are perfectly apart from the other bands and from each other. The mole ratio at 70°C was four times that of the ratio at 4°C. We see, therefore, that in the solid of this compound the phase changes continuously with such a large change of mole ratio as those not observed for liquids. A detailed report will be published in the near future.

It will be of interest to mention here that the crystal of *trans*-1,4-dibromocyclohexane takes only the *ee* form at room temperature.

The author would like to express his appreciation to Professor K. Kozima for his kind advice.

[1] Kozima, Yoshino, Sakashita, Maéda, and Tsumori, presented at the meeting for the molecular structure held by the Chemical Society of Japan, October, 1953.
[2] Kozima, Tsubomura, and Hamano, presented at the fourth meeting of the Chemical Society of Japan, April, 1951.
[3] K. Kozima and T. Yoshino, J. Am. Chem. Soc. **75**, 166 (1953).

OH, HO_2, and H_2O_2 Production in the Reaction of Atomic Hydrogen with Molecular Oxygen*

S. N. FONER AND R. L. HUDSON
Applied Physics Laboratory, The Johns Hopkins University, Silver Spring, Maryland
(Received August 5, 1955)

WHEN atomic hydrogen and molecular oxygen react at low pressures the products condensed in a liquid nitrogen trap are hydrogen peroxide and water.[1,2] As the trap temperature is raised the yield of peroxide decreases steadily becoming unobservable experimentally above −80°C.[2] The identity of the radicals condensing at low temperatures to form H_2O_2 has not hitherto been definitely established.

We have used a mass spectrometer with a molecular beam sampling system[3] to identify the components in the room temperature reaction of atomic hydrogen with oxygen and to observe the formation of peroxide at liquid nitrogen temperature. The Pyrex reactor used in this work is shown in Fig. 1. For most of the ex-

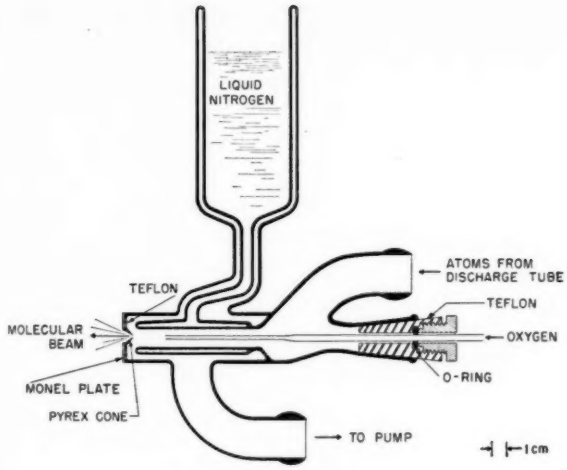

FIG. 1. Experimental arrangement.

periments the inner surface of the reactor was coated with phosphoric acid. A Teflon liner could be inserted in the cylindrical reaction region to check the effect of surface condition on the room temperature reaction, low temperature experiments being prevented by the poor thermal contact between the Teflon liner and the liquid nitrogen bath.

In the room temperature, low-pressure (~1 mm) reaction between hydrogen atoms and oxygen molecules, independent of surface conditions, water was observed as the principal product with no measurable amount of H_2O_2, in agreement with the results of Boehm and Bonhoeffer,[1] Geib and Harteck,[2] Frost and Oldenberg,[4] and Badin,[5] although in disagreement with the recent mass spectrometric experiments of Robertson.[6] While no HO_2 radicals were found under these conditions (i.e., HO_2 less than 0.01% of O_2), substantial quantities of OH radicals, approximately 1% of the O_2 concentration, were observed. Since OH radicals are observed even at very low pressures and cannot be formed in bimolecular reactions for energetic reasons, they must be produced in a surface reaction, quite possibly by the mechanism proposed by Badin[5]: $H+O_2+W\rightarrow HO_2+W$ on the wall, followed by $H+HO_2+W\rightarrow[HO-OH]^*+W$, the excited peroxide complex dissociating into OH radicals when the wall temperature is above 200°K.

In our original experiments on HO_2 production[7] at much higher pressures (~30 mm) the occurrence of OH radicals was puzzling because OH formation in the gas phase apparently required the presence of unstabilized HO_2^* complexes which reacted with hydrogen molecules according to: $H_2+HO_2^*\rightarrow OH+H_2O$, the excitation energy of the HO_2^* being used to overcome the activation barrier for the reaction. Since much more OH was produced than HO_2, this required in addition that collisional deactivation of HO_2^* was a slo process. The most plausible explanation for the OH radicals measured at high pressures, in light of the experiments reported here, is that they were likewise formed on the surface of the reactor and diffused back into the gas stream. Since HO_2 was present in the gas phase, it is, of course, possible that some OH was also produced in the homogeneous reaction:

$$H+HO_2\rightarrow[H_2O_2]^*\rightarrow 2OH.$$

At low pressures, cooling the reactor to liquid nitrogen temperature causes the OH intensity to drop to zero and only the consumption of hydrogen and oxygen is measured by the mass spectrometer. The integrated production of H_2O_2 at liquid nitrogen temperature was obtained by warming up the reactor and recording the evolution of H_2O_2. A plot of H_2O_2 intensity after running the discharge tube about 20 minutes is shown in Fig. 2. The pressure in the reactor was 1.7 mm consisting of $O_2=0.15$ mm, $H_2=0.70$ mm. about 10% of the hydrogen being dissociated, and He=0.85 mm.

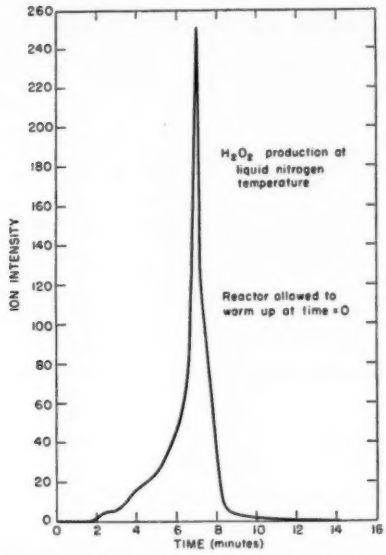

FIG. 2. Hydrogen peroxide production at liquid nitrogen temperature measured by warming up reactor to room temperature.

Helium was added to the hydrogen stream to prevent back diffusion of reactants into the discharge tube. The gas velocity in the reactor was about 500 cm/sec. The average production rate of H_2O_2 at liquid nitrogen temperature is at least 150 times the room temperature rate. The high yield of H_2O_2 at liquid nitrogen temperature is in accord with independent chemical observations.[1,2,5] The observed H_2O_2 production can be accounted for by assuming that most of the hydrogen atoms react at low temperature to form peroxide.

The color and phase change of the glassy deposits trapped at liquid nitrogen temperature have been ascribed[8] to HO_2 radicals condensed from the vapor phase and stabilized on the cold surface. Our experiments indicate that if HO_2 is present in the glassy deposit, it is formed on the surface.

* This research was supported by the Bureau of Ordnance, Department of the Navy, under NOrd 7386.

[1] E. Boehm and K. F. Bonhoeffer, Z. physik. Chem. **119**, 385 (1926).
[2] K. H. Geib and P. Hartek, Z. physik. Chem. **170A**, 1 (1934).
[3] S. N. Foner and R. L. Hudson, J. Chem. Phys. **21**, 1374 (1953).
[4] A. A. Frost and O. Oldenberg, J. Chem. Phys. **4**, 642, 781 (1936).
[5] E. J. Badin, J. Am. Chem. Soc. **70**, 3651 (1948); *Third Symposium on Combustion, Flame and Explosion Phenomena* (Williams and Wilkins, Baltimore, 1949), p. 382.
[6] A. J. B. Robertson, *Applied Mass Spectrometry* (Institute of Petroleum, London, 1954), p. 112.
[7] S. N. Foner and R. L. Hudson, J. Chem. Phys. **21**, 1608 (1953).
[8] P. A. Giguère, J. Chem. Phys. **22**, 2085 (1954).

Paramagnetic Resonance in Semiquinone Ions of Substituted *o*-Benzoquinones

RAYMOND HOSKINS
The Dow Chemical Company, Midland, Michigan
(Received August 11, 1955)

THE detection of the semiquinone ions of *o*- and *p*-benzoquinone by the technique of paramagnetic resonance has recently been reported by Blois.[1] The hyperfine structure reported by Venkataraman and Fraenkel[2] for the *p*-benzosemiquinone ion in alkaline alcoholic solution was not observed by Blois[1] for either the *o*- or the *p*-benzosemiquinone ion in aqueous solution. We wish to report observations made on *o*-benzosemiquinone ions derived from the air oxidation of some substituted 1,2-benzenediols in alkaline alcoholic solution. The paramagnetic resonance experiments were carried out at a frequency of about 9000 mc/sec using a magic-T bridge. The absorptions were detected by the method of magnetic field modulation. The magnetic field is believed to have

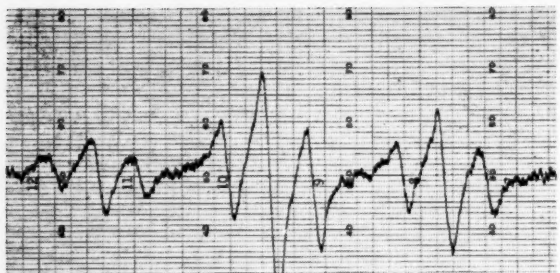

FIG. 1. Derivative of the absorption spectrum of the *o*-benzosemiquinone ion.

been homogeneous to better than 0.1 oersted over the area of the sample.

The derivative of the absorption spectrum of *o*-benzosemiquinone, the semiquinone ion derived from 1,2-benzenediol, is shown in Fig. 1. It is seen to consist of three sets of three lines each. The splitting is attributed to hyperfine interaction of the unpaired electron spin with the protons on the ring. The two equivalent protons *para* to the oxygens split the line into three parts with relative intensities (1,2,1). These three lines are further split into three lines each by the two equivalent protons *ortho* to the oxygens again with relative intensity ratios (1,2,1). The interval for the *para*-proton splitting is 4.0 oersteds and for the *ortho*-proton splitting is 1.0 oersted. The assignment of the larger splitting to the *para*-protons is made on the basis of the observations made on the substituted compounds below.

The spectrum of the semiquinone ion of 4-tert. butyl-1,2-benzenediol is shown in Fig. 2. The spectrum is seen to consist of a broad doublet envelope of incompletely resolved smaller splittings. The doublet splitting is about 4.1 oersteds and is attributed to the proton on position 5. The further splitting is due to the remaining two ring protons and the protons on the substituted group. Incomplete resolution prevents an exact assignment of the individual peaks. We have also examined the spectra of the semiquinone ions of 4-phenyl-1,2-benzenediol and 3,6-dially-4-tert. butyl-1,2-benzenediol. These spectra (not shown) also show a doublet envelope of incompletely resolved smaller splittings. The doublet splitting amounts to 3.4 oersteds in the former and 3.6 oersteds in the latter.

The semiquinone ion of 3-phenyl-1,2-benzenediol exhibits three groups of lines as shown in Fig. 3. The central group is a triplet and the outer groups are doublets. This pattern can be explained if the splitting by the three ring protons is in the ratio of (1,4,5); the smallest splitting being 0.7 oersted. This model predicts seven lines in three groups with relative intensities (1,1) (1,2,1) (1,1). It seems reasonable, on the basis of the above spectra, to attribute the smallest splitting to the proton *para* to the phenyl group, but no conclusion can be drawn from the spectrum alone as to which of the remaining two protons contributes the larger splitting.

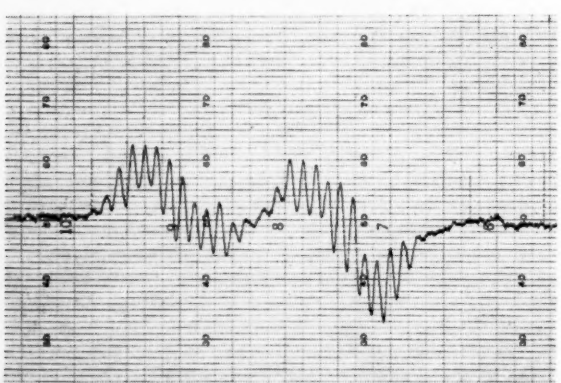

FIG. 2. Derivative of the absorption spectrum of the semiquinone ion derived from 4-tert. butyl-1,2-benzenediol.

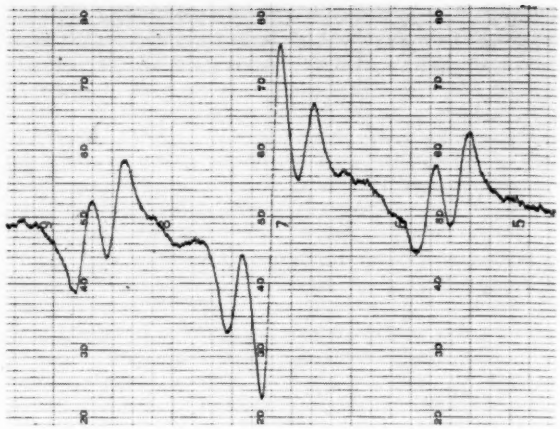

FIG. 3. Derivative of the absorption spectrum of the semiquinone ion derived from 3-phenyl-1,2-benzenediol.

In Figs. 1 and 2 it will be noted that the intensity of the spectrum is not symmetrical about the center of gravity of the spectrum. This is due to a decrease in the concentration of free radicals in the sample during the time taken to sweep the magnetic field through the resonance. This time is of the order of three minutes.

The author wishes to thank Dr. E. B. Baker for helpful discussion and Mr. B. R. Loy for valuable assistance in the preparation of samples.

[1] Blois, J. Chem. Phys. **23**, 1351 (1955).
[2] B. Venkataraman and G. R. Fraenkel, J. Chem. Phys. **23**, 588 (1955).

Thermoluminescence of Zinc Sulfide Phosphors Doubly Activated with Copper and Manganese

SHIGEO SHIONOYA
Faculty of Engineering, Yokohama National University, Yokohama, Japan
(Received August 8, 1955)

THE emission of manganese incorporated in zinc sulfide is sensitized by copper incorporated as a sensitizer, as has been mentioned in the previous letter.[1] ZnS: (Cu+Mn) phosphors have two kinds of the excitation band, similar to ZnS:Cu phosphors, the one due to the absorption of host crystal (located near 3400 A) and the other due to the absorption of Cu impurity (located about 3800 A); and Mn emission is caused by the absorption of Cu as well as that of the host crystal. In this letter, the thermoluminescences were studied for both the Cu and Mn emissions after the excitation by both the host and Cu absorption.

The samples used were the same as used in the previous letter. An ordinary 100 w tungsten incandescent lamp was used as the excitation source, selecting only the necessary wavelength region for the host or Cu excitation with filters; namely, Matsuda UV–D1 plus nickel sulfate solution filter, which transmits 3000–3750 A, for the host excitation, and Matsuda UV–D1 plus V–B2, which transmits 3700–4000 A, for the Cu excitation. The thermoluminescences were measured with a specially designed Dewar vessel, using liquid air as a coolant. The phosphors were excited up to the saturated emission intensities at a liquid air temperature, and then heated with a constant rate 0.22°K/sec after allowing the emission to decay for 6 min, detecting glow intensities with a photomultiplier attached to a sensitive amplifier. The Cu and Mn emissions were isolated from each other with filters; namely, Matsuda V–Y1 plus V–B2 for Cu and V–O2 or V–R3 for Mn.

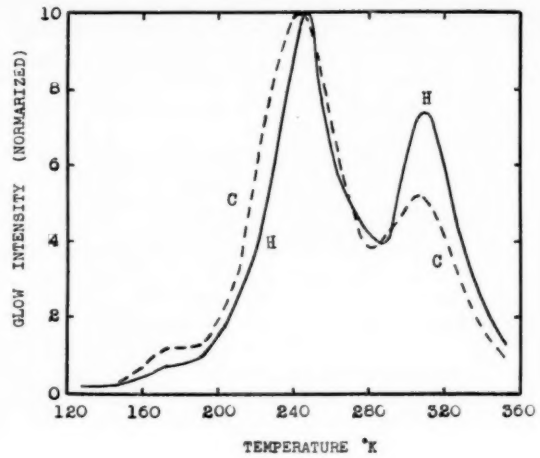

(a)

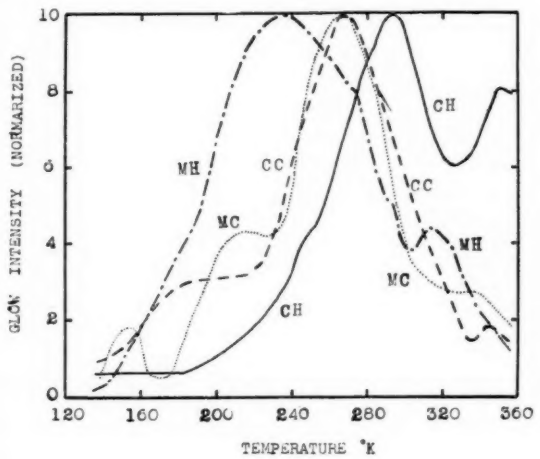

(b)

FIG. 1. (a) Glow curves for the Cu emission of ZnSμCu (containing Cu of 3×10^{-5} g/gZnS, and fired at 1200°C for 1 hr). *H*: after the host excitation, *C*: after the Cu excitation. (b) Glow curves for the Cu and Mn emissions of ZnS:(Cu+Mn) (containing Cu of 3×10^{-5} g/gZnS and Mn of 8×10^{-4} g/gZnS, and fired at 1200°C for 1 hr). *CH*:Cu glow after the host excitation. *CC*:Cu glow after the Cu excitation. *MH*:Mn glow after the host excitation. *MC*:Mn glow after the Cu excitation.

Examples for the glow curves for ZnS:Cu and ZnS:(Cu+Mn) are shown in Fig. 1. It should be strongly noticed that the glow curves for the Cu and Mn emissions of ZnS:(Cu+Mn) after the Cu excitation are very similar to each other, whereas those after the host excitation are remarkably different from each other. Analyses for the main glow peaks were carried out in the usual manner,[2,3] based on the assumption that the electron in a single trap is released with the monomolecular kinetics and that the retrapping is negligible. The trap depths and frequency factors for the thermal release thus calculated are given in Table I.

The trap depths for the Cu main peaks are 0.21–0.23 ev, irrespective of either the host or Cu excitation. The frequency factors for those are made a bit smaller by the incorporation of Mn. The trap depth for the Mn main peak after the Cu excitation shows a similar value to that for Cu, whereas that after the host excitation shows a considerably different value from that for Cu, namely, a smaller one 0.15 ev.

TABLE I. Trap depths and frequency factors for the main glow peaks.

Phosphors	Emission	Excitation	Trap depth (ev)	Frequency factor (sec^{-1})
ZnS:Cu	Cu	host	0.23	4×10^2
		Cu	0.23	6×10^2
ZnS:(Cu+Mn)	Cu	host	0.21	2×10
		Cu	0.21	6×10
	Mn	host	0.15	1×10
		Cu	0.23	2×10^2

If an assumption is made that there exists two kinds of the main traps in these phosphors, the deep one associated to Cu and the shallow one associated to Mn, the aforementioned results may be reasonably explained by the following inference. Under the Cu excitation, the freed electron from Cu center enters only into the Cu associated trap, and the thermal release from it is the rate-determining step for both of the Cu and Mn main glow peaks. On the other hand, under the host excitation, the freed electron from the host lattice enters, probably through the conduction band, into either of the Cu and Mn associated traps, and the thermal release from each of them is the rate-determining step for each of the Cu and Mn main glow peaks.

A detailed report of this work will appear soon.

The author is grateful to Professor S. Makishima, Mr. Y. Kotera, and Assistant Professor K. Oshima for their discussions, and to Mr. K. Amano for his assistance.

[1] Shigeo Shionoya, J. Chem. Phys. **23**, 1173 (1955).
[2] J. T. Randall and M. H. F. Wilkins, Proc. Roy. Soc. (London) **A184**, 347, 365, 390 (1945).
[3] H. Eyring and F. E. Williams, J. Chem. Phys. **15**, 289 (1947).

Interaction of an Electron with a Physical Dipole

GEORGE S. HANDLER
Department of Chemistry, University of Pittsburgh, Pittsburgh 13, Pennsylvania
(Received August 5, 1955)

IT has perhaps not been realized that the solution of a rather amusing problem in quantum mechanics can be had as a special case of the general two-center solutions as presented by Baber and Hassé.[1] The nomenclature used here is theirs. Unprimed equations are reproductions of theirs, and primed equations are alterations suitable for our case.

The wave equation for the general two-center problem was separated by Baber and Hassé[1] in prolate spheroidal coordinates, leading to

$$\frac{d}{d\lambda}\left[(\lambda^2-1)\frac{d\psi}{d\lambda}\right]+\psi\left[A-p^2\lambda^2+R(N_1+N_2)\lambda-\frac{m^2}{\lambda^2-1}\right]=0, \quad (4)$$

$$\frac{d}{d\mu}\left[(1-\mu^2)\frac{d\psi}{d\mu}\right]+\psi\left[-A+p^2\mu^2-R(N_1-N_2)\mu-\frac{m^2}{1-\mu^2}\right]=0, \quad (5)$$

where A is the separation constant, $p^2=-\frac{1}{4}R^2E'$, E' is the electronic energy, and N_1 and N_2 are the charges on the nuclei. There seems to be nothing in the nature of the problem or the solution that requires N_1 and N_2 to be positive. Let us set $N_2=-N_1=N$ and $NR=\xi$, the dipole moment; (4) and (5) become

$$\frac{d}{d\lambda}\left[(\lambda^2-1)\frac{d\psi}{d\lambda}\right]+\left[A-p^2\lambda^2-\frac{m^2}{\lambda^2-1}\right]=0, \quad (4')$$

$$\frac{d}{d\mu}\left[(1-\mu^2)\frac{d\psi}{d\mu}\right]+\psi\left[-A+p^2\mu^2-2\xi\mu-\frac{m^2}{1-\mu^2}\right]=0. \quad (5')$$

As we have assigned the charges, the negative charge is on the right. Now the region to the right of the negative charge is a region of positive, though finite, potential. Since the wave function cannot be zero everywhere in such a region it follows from the separability of Schroedinger's equation that the wave function cannot be zero at the negative charge. A similar argument for the ground state, buttressed by the known behavior of an electron near a positive charge, indicates that we expect no inflection points anywhere. Figure 1 shows the wave function and the charge distribution, plotted on arbitrary scales, in the region of interest.

Subject to the restriction that ξ is constant, there is no explicit dependence on R in these equations. As a consequence, p^2 is a function only of ξ and E' varies as $-1/R^2$.

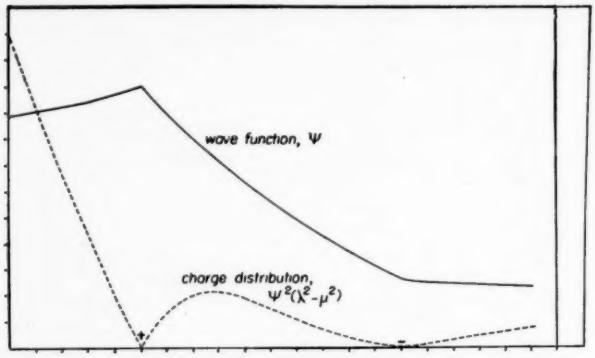

FIG. 1. Wave function and charge distribution along dipole axis.

A few further remarks may be of interest. As there is no R dependence at constant moment, the coefficients of the terms of the series that are the wave functions likewise are independent of R. The first terms of the series give, approximately, aside from a normalization factor

$$\psi \sim e^{-p(\lambda+\mu)}.$$

This, from the definition of λ and μ, is

$$\psi \sim e^{-p r_1/R},$$

a hydrogen-like orbital on the positive charge. The effective charge parameter varies as $1/R$, as indeed it should. On this basis it appears reasonable that the electronic energy should approach $-\infty$, since the electron may stay in the left half of space, and thus be in the region of a high positive potential, as R approaches zero.

It is worth noting that a mathematical dipole potential is extraordinary in this respect. Representing a general multipole potential as

$$V=-(q_n/r^n)P_{n-1}(\cos\theta),$$

where $n=2$ for a dipole, 3 for a quadrupole, etc., and a trial eigenfunction as

$$\psi=r^m e^{-\alpha r} f(\theta)$$

on dimensional grounds, the kinetic energy is of the form $a\alpha^2$, and the potential energy $-b\alpha^n$. We have

$$E=a\alpha^2-b\alpha^n.$$

Minimizing with respect to α,

$$\alpha^{n-2}=2a/nb,$$

which misbehaves for $n=2$. This argument implies nothing about the higher multipoles, as the variation theorem provides only an upper bound to the energy.

E' was calculated for various values of ξ using appropriate expressions from the Baber and Hassé paper.[1] Calculations were performed for the ground state only and are good to about 10%.

Dipole moment, ξ		$4p^2$	
Atomic units	Debyes	Atomic units (R in Bohr radii)	cgs units (R in A)
0	0	1 0	0
0.3	0.76	1.4×10^{-6}	1.1×10^{-5}
0.5	1.27	2.1×10^{-5}	1.6×10^{-4}
0.7	1.78	1.2×10^{-4}	9.1×10^{-4}

[1] Baber and Hassé, Proc. Cambridge Phil. Soc. 31, 564 (1935).

Photosensitized Decomposition of Acetyl Peroxide

C. LUNER AND M. SZWARC
Chemistry Department, State University of New York, College of Forestry, Syracuse 10, New York

(Received July 25, 1955)

IT appears that aromatic hydrocarbons may act as photosensitizers for a variety of reactions proceeding in solution. For example, West and Miller[1] have shown that certain aromatic hydrocarbons may sensitize the decomposition of alkyl halides in hexane solution. Recently, a number of papers[2-4] dealing with the sensitized fluorescence of aromatic hydrocarbons with ultraviolet and γ rays have appeared. In this note, the decomposition of dilute solutions of acetyl peroxide photosensitized by aromatic hydrocarbons is reported.

When a degassed solution of acetyl peroxide in benzene (10^{-3} M) was irradiated with light of the wavelength 2537 A, obtained from a mercury resonance lamp combined with a Corning 7910 filter, acetyl peroxide was decomposed. Similar results were obtained by irradiating with the 3650 A line dilute solutions of acetyl peroxide in iso-octane containing small amount of anthracene or naphthacene. Since at 2537 A, benzene essentially absorbs all the exciting radiation, while at 3650 A only the aromatic hydrocarbon absorbs the radiation (acetyl peroxide does not absorb in this region), it must be concluded that the aromatic hydrocarbon sensitizes the decomposition of acetyl peroxide.

Preliminary quantitative experiments were performed with anthracene as the sensitizer and the 3650 A Hg line as the exciting radiation. The data are given in Table I. The rate of decomposition of acetyl peroxide, measured by the rate of formation of carbon dioxide, seems to be proportional to the concentrations of acetyl peroxide and anthracene. This relation is shown in Fig. 1. However, at concentration of anthracene exceeding $1\cdot10^{-4}$ M, the rate of decomposition levels off. It was calculated from the extinction coefficient of anthracene at 3650 A, that 99% of the radiation is absorbed at the concentration of $1.5\cdot10^{-4}$ M. It should, therefore, be expected that at higher concentrations of anthracene, the rate of decomposition would be independent of its concentration.

Table I shows that the CH_4/CO_2 ratio decreases with increasing concentration of anthracene. This effect is similar to that observed by Levy and Szwarc[5] who studied the thermal decomposition of acetyl peroxide in the presence of aromatic hydrocarbons, and showed that the decrease in the ratio was due to the addition of methyl radicals to the aromatic compounds. A similar interpretation would apply here.

In many photochemical or photosensitized reactions, radicals are formed in the primary process. The rate of such reactions is usually deduced from the rate of formation of specific products resulting from the subsequent reactions of the radical. The present investigation shows how misleading such a conclusion might be if the rates were based on the rate of formation of methane. In this investigation, complications of such a nature are avoided by using the rate of formation of CO_2 as a measure of the rate of decomposition of the peroxide.

While the ratio CH_4/CO_2 decreases considerably with increasing anthracene concentration, the ratio C_2H_6/CO_2 remains essentially constant, independent of acetyl peroxide and anthracene concentration, and of light intensity. These results indicate that ethane is formed by a cage reaction. Similar results were obtained in the thermal decomposition of acetyl peroxide in the presence of a variety of scavengers.[6] In the latter work, the ratio of C_2H_6/CO_2 was found to be 0.084 at 65°C and 0.045 at 85°C, while an average value of 0.13 at 25°C was found in the present study. This result is in accord with the concept of a cage reaction, the higher ratio

TABLE I. Photosensitized decomposition of acetyl peroxide in iso-octane at 25°C.

Acetyl peroxide M×10³	Anthracene M×10⁴	R_{CO_2} M/hr×10⁶	$\frac{CH_4}{CO_2}$	$\frac{C_2H_6}{CO_2}$
1.6	0.28	0.20	0.62	0.11
1.6	0.72	0.58	0.58	0.12
1.6	1.45	0.90	0.59	0.13
1.6	4.35	1.17	0.46	0.12
3.2	4.35	1.80	0.54?	···
7.2	4.35	3.54	0.45	0.13
7.2	9.43	3.21	0.43	0.13
7.2	18.8	3.10	0.39	0.13
1.6[a]	0.72	0.25	0.61	0.14

[a] Incident intensity reduced by 38%.

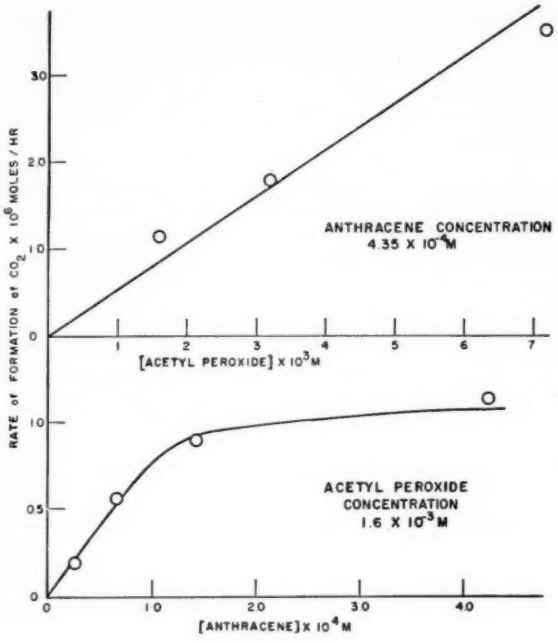

FIG. 1.

obtained at 25°C reflects the greater probability of cage recombination of radicals at lower temperatures. It would thus appear that the photosensitized decomposition of acetyl peroxide involves a mechanism similar to that operating in the thermal decomposition.

Further experiments are in progress and will be reported at a later date.

[1] W. West and W. E. Miller, J. Chem. Phys. **8**, 849 (1940).
[2] A. Weinreb and S. G. Cohen, Phys. Rev. **93**, 1117 (1954).
[3] H. Kallmann and M. Furst, Phys. Rev. **79**, 857 (1950).
[4] E. J. Bowen and R. Livingston, J. Am. Chem. Soc. **76**, 6300 (1954).
[5] M. Levy and M. Szwarc, J. Am. Chem. Soc. **77**, 1949 (1955).
[6] A. Rembaum and M. Swarc, J. Am. Chem. Soc. **77**, 3486 (1955).

Supplementary Comments on the "Electronic Structure of the Amylose-Iodine Complex"

HIDEO MURAKAMI
Department of Chemistry, Faculty of Science, Osaka University, Osaka, Japan
(Received July 15, 1955)

IN a previous paper,[1] the author discussed the charge transfer from hydroxyl- or bridge-oxygen atoms into the iodine chain with respect to the electronic structure of the colored molecular complexes between iodine and oxygen-containing organic molecules such as amylose,[2(a)] α-dextrin (cyclohexaamylose),[3] pyrone derivative,[3] and polyvinyl alcohol.[4] As can easily be inferred, the electronic interaction between oxygen and iodine amounts to appreciable value only when the relative configuration between two components allows the sufficient approach of these atoms. In case of polyvinyl alcohol- or pyrone derivative-iodine complex, it seems to be no apparent difficulty to realize the required relative configuration between two components.

On the other hand, in case of amylose- or α-dextrin-iodine complex, it was found such an ambiguity as follows on this point. In a previous paper, the author adopted one of the possible chair forms of pyranose ring in the glucose residue* [chair form (I), see Fig. 1 (b) in reference 1]. According to the result of x-ray analysis, however, the pyranose ring in the crystalline sucrose exists as another chair form (II).[5] If the latter form (II) is adopted into the helical amylose, the distance between the internal iodine and hydroxyl oxygen in the primary alcoholic group (or bridge oxygen in the pyranose ring) becomes considerably larger compared with the author's previous model. Consequently, one can scarcely expect the electronic interaction between iodine and these oxygens.

One should notice, however, the existence of the other oxygen atoms of which one can expect some amount of electronic interaction with the internal iodine. These oxygen atoms exist as the connecting bridge between neighboring pyranose rings (glucosidic oxygen). At present, the experimental data are not sufficient to predict the very accurate atomic coordinates in the helical amylose even when the stereochemical form of the pyranose ring is postulated as chair form (II). Consequently, the geometry of helical amylose is examined by using the following two idealized models.†

Model (1): the bond angles of all the carbon (and oxygen) in the pyranose ring are assumed to be tetrahedral angle. In this case, all the strain is comcentrated into the bond angle of glucosidic oxygen and makes it abnormally large. (The projected value of this angle on the plane which is normal to the helical axis is about 127°, and the actual bond angle slightly exceeds 130°.) The projected figure shows that the internal surface of helix is dominated by hydrogen atoms and oxygen atoms cannot contact with the internal iodine. (The exterior van der Waals' diameter of this helix is estimated as 13.7 A[2(b)].)

Model (2): the actual (not projected) bond angle of glucosidic oxygen is kept to tetrahedral angle and the major part of the strain is transferred into the other parts of amylose. By adjusting the valence angles of carbon atoms within the reasonable range so as to give the observed exterior van der Waals' diameter 13 A,[2(c)] the dominance of hydrogen atoms in the internal surface of helix is removed and the oxygen atoms are brought on the contact with iodine.

Consequently, if the actual geometry of helical amylose is close to model (2), one can expect the electronic interaction even when the chair form (II) is adopted. Here, one should consider that such a configuration as model (2) is stabilized by the electronic interaction energy between oxygen and iodine even if it includes some amount of strain. In this configuration, the hydroxyl oxygen in the secondary alcoholic group (CH_2OH) may also be able to contact with the internal iodine more or less. Thus, the essential part of the previous paper seems to retain its validity. The detailed study on the geometry of helical amylose will be reported elsewhere.

[1] H. Murakami, J. Chem. Phys. **22**, 367 (1954).
[2] (a) R. S. Stein and R. E. Rundle, J. Chem. Phys. **16**, 195 (1948). See also R. J. Hach and R. E. Rundle, J. Am. Chem. Soc. **73**, 4321 (1951). (b) R. E. Rundle and F. C. Edwards, J. Am. Chem. Soc. **65**, 2200 (1943). (c) R. E. Rundle and D. French, J. Am. Chem. Soc. **65**, 1707 (1943).
[3] F. Cramer, Chem. Ber. **84**, 855 (1951); H. v. Dietrich and F. Cramer, Chem. Ber. **87**, 806 (1954). See also F. Cramer, Chem. Ber. **86**, 1576, 1582 (1953).
[4] C. D. West, J. Chem. Phys. **15**, 689 (1947).
* The author's previous statement is due to the oversight of some of the *trans*-configurations and is not correct.
[5] C. A. Beevers and W. Cochran, Proc. Roy. Soc. (London) **A190**, 257 (1947).
† In the present examination, it was assumed that the helical amylose contains exactly the six glucose residues per turn although slight deviation from this statement seems to be permissible.

Sensitivity of Explosives to Pure Shocks

WILLIAM A. GEY AND ARTHUR L. BENNETT
U. S. Naval Ordnance Test Station, China Lake, California
(Received May 12, 1955)

THE "influence" test of sensitivity of explosives to explosive shocks is a valuable criterion for determining the suitability of explosive components in explosive applications.[1]

We have undertaken an investigation of the initiation of reaction of explosive materials by uniform shocks in a shock tube. The use of the forward facing shock in an inert atmosphere appears to provide a reproducible experimental determination of

the relation between the energy density, temperature, and pressure requirements for initiation of very small samples.

The shock tube is 6.5 cm² cross section, the high pressure end being an 11 cm long cylinder and the low pressure chamber a 75 cm long square section with observation windows 23 cm in length at the downstream end. Hydrogen is used as the driver gas, argon as the inert atmosphere. The explosive is contained in a metal cup facing the diaphragm and positioned on the axis of the expansion chamber in the end of a rod supported from the closed end of the tube. The axial dimensions of the tube and the positioning of the samples are designed to expose the explosive to the head-on shock of Mach 5 to 7 for periods of 60 to 120 μsec, and to cool the heated argon by the rarifaction wave before the shock reflected from the closed end of the expansion chamber reaches the sample. Calculations according to Lobb[2] were carried carried out on IBM 701 equipment to obtain for each of eight shock strengths (pressure ratio across the shock) between Mach 5.67 and Mach 6.83, the particle velocity, shock zone duration, shock zone temperature, and speed of the reflected shock.

The explosive holder is necessarily small to avoid excessive interference with the shock wave and damage by the reaction of the explosive. The sample sizes varied with the loading pressure, but were of the order of 2.5, 4.0, and 9 mg, weighed to ± 0.1 mg after loading. The explosives were loaded by pressing with a ram slightly smaller than the inside diameter of the cup. The largest cup was loaded at uniform density by one pressing in a loading jig, the excess being cut off level.

The luminosity of the interaction of the shock front with the target and of the reaction products was photographed by a drum camera focused on the sample cup through a 1 mm slit parallel to the tube axis.

Lead styphnate, 4,6-dinitrobenzene-2-diazo-1-oxide (DDNP), tetracene, nitrosoguanidine, lead azide, and nitroglycerin have been subjected to the shock tests. Lead styphnate appears to be the most sensitive, being initiated by shocks of Mach 4 to 4.5. Next in sensitivity is DDNP which has been extensively studied. It is reproducibly initiated by shocks of Mach 5.5 to 6.3. Shocks of this strength are sometimes bright enough for photographic recording.

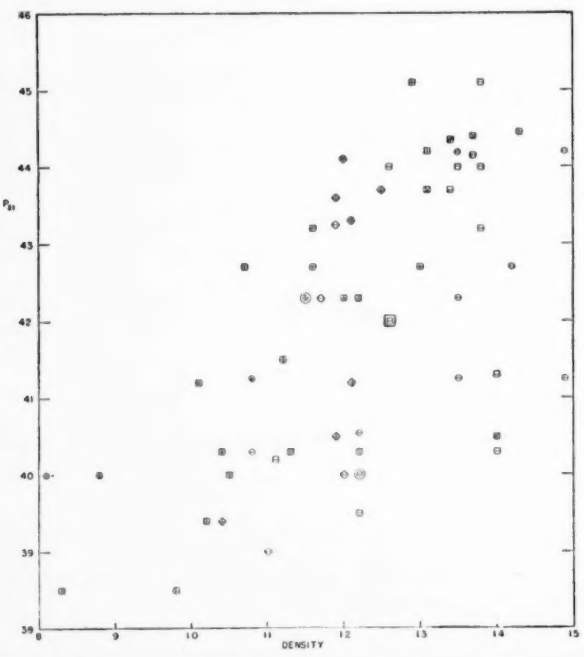

FIG. 1. Sensitivity of DDNP as a function of density at initial pressure. $P_1 = 50$ mm. ○ = 1.54 mm, □ = 2.34 mm, ◇ = 2.72-mm target cups. + denotes go; −, no go; ×, partial.

The sensitivity, expressed as go or no-go results as a function of the shock strength, is essentially independent of the exposed area of the sample. As expected from Eyring's treatment,[1] sensitivity is dependent on the density of the explosive. Figure 1 shows the relation for one log of DDNP; other lots have been found to be less sensitive.

A study of the relation between sensitivity and energy density in the shock zone is being undertaken, since the absolute pressure in the shock can be varied while holding other parameters constant. Results to date indicate that as the energy density is decreased, the shock strength must be increased to obtain initiation. Photographic data indicate that initiation occurs at the shock impact.

[1] H. Eyring *et al.*, Chem. Revs. **45**, 69 (1949), treats this calibrated shock sensitivity test in detail.
[2] R. K. Lobb, NOLM 10494. U. S. Naval Ordnance Laboratory Memorandum. "On the length of a shock tube." July, 17 1950. U. S. Naval Ordnance Laboratory, White Oak, Silver Spring, Maryland; UTIA Report No. 4, "On the length of a shock tube," by R. K. Lobb.

Infrared Spectrum of Ammonia Adsorbed on Porous Silica Glass

D. J. C. YATES, N. SHEPPARD, AND C. L. ANGELL
Department of Colloid Science, Free School Lane, Cambridge, England
(Received August 15, 1955)

POROUS silica glass[1] is a high area adsorbent with optical properties similar to that of fused silica, and is an excellent material for use in the study of the infrared spectra of physically adsorbed molecules.

An evacuable metal cell with rocksalt windows was constructed in which a tube of porous glass was mounted in contact with a nickel plated copper block slotted to let infrared radiation pass through. The temperature could be varied between 320°C and −180°C by electrical heating, or by contact with refrigerant.

The glass tube in the absorption cell was pumped for a period of 30 hours at gradually increasing temperature until a vacuum of 10^{-5} mm was reached at 320°C. Under these conditions all physically adsorbed molecules, principally water adsorbed from the atmosphere, were entirely removed. A reference spectrum of the clean glass *in vacuo* at room temperature was measured between 2 and 5μ. The spectra of the glass with a series of measured doses of

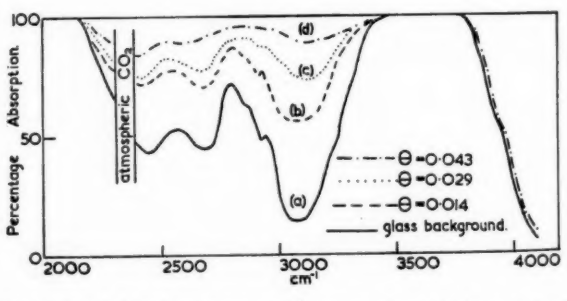

FIG. 1. The infrared spectrum of (a) porous glass (thickness 2.6 mm) (b), (c), and (d) porous glass with ammonia adsorbed at indicated surface coverages θ. (The weak maxima at 2870 and 2940 cm^{-1} appeared only after NH_3 had been adsorbed to $\theta = 0.05$ and removed once again.)

physically adsorbed ammonia were then recorded and are shown in Fig. 1. Fractional surface coverages range from about 1/70 to 1/20 of a monolayer. The coverages (θ) were calculated using monolayer capacity values (v_m) determined in a conventional adsorption apparatus by techniques described elsewhere.[2] The specific surface of the sample was approximately 190 meters² per gram.

The spectrum of the clean glass shows an extremely strong blackout band centered near 3600 cm^{-1} due to the bond stretching (νOH) frequency of OH groups on the surface, presumably co-

valently bound to silicon atoms. The spectrum of an equivalent thickness of sintered porous glass differs only in that this bond is reduced to a sharp peak near 3650 cm^{-1}.

Adsorption of ammonia resulted in an increase in the absorption of radiation throughout the accessible region at lower frequencies than the νOH band but not on the higher frequency side. The first dose of ammonia ($\theta=0.014$) caused an almost uniform increase in absorption between 3400 and 2150 cm^{-1} presumably due to the utilization of a range of sites of different activity; subsequent additions showed more pronounced increases in the higher frequency end of this region and a broad maximum in absorption occurred at 2850–2900 cm^{-1} for $\theta=0.043$.

This value is much lower than the strong νNH frequency of ammonia in the solid state[3] (3378 cm^{-1}) or of the νOH fundamental of the surface (or of NH_4^+)[4] and it seems certain that strong hydrogen bonding has occurred between ammonia and the surface of the glass. This is indicated by the shift in frequency and by the breadth of the maximum. Such strong bonding is more likely to be of the O—H···N rather than the N—H···O type,[5] i.e. the new absorption is interpreted as shifted νOH band, and the νNH bands of the adsorbate are presumed to occur with little change in frequency in the masked 3400–3600 cm^{-1} region. Sidorova,[6] using unspecified surface coverages and much thinner layers of porous glass has indeed reported the νNH band of adsorbed ammonia near 3400 cm^{-1}; her pathlength appears however to have been too small to detect the new 2900 cm^{-1} band. Few previous attempts[7] have been made to obtain the infrared spectra of adsorbed molecules at known surface coverages, and these have been much nearer to $\theta=1$. The adsorption of a number of other small polyatomic gases have been studied by the present technique, and the results will be reported later.

[1] M. E. Nordberg, J. Am. Ceram. Soc. **27**, 299 (1944).
[2] D. J. C. Yates, Proc. Roy. Soc. (London) A, **224**, 526 (1954).
[3] F. P. Reding and D. F. Hornig, J. Chem. Phys. **19**, 594 (1951).
[4] E. L. Wagner and D. F. Hornig, J. Chem. Phys. **18**, 296 (1950); L. F. H. Bovey, J. Chem. Phys. **18**, 1684 (1950).
[5] W. Gordy, J. Chem. Phys. **7**, 93, 167 (1939).
[6] A. N. Sidorova, Doklady Akad. Nauk. SSSR **95**, 1235 (1954).
[7] Pimentel, Garland, and Jura, J. Am. Chem. Soc. **75**, 803 (1953).

Nuclear Magnetic Resonance Spectra of Methyl Pyridines

EDWARD B. BAKER
The Dow Chemical Company, Midland, Michigan
(Received August 15, 1955)

THE nuclear magnetic resonance spectra of pyridine and a number of methyl-substituted pyridines were examined. It was found that the structure of pyridine qualitatively resembles that of nitrobenzene[1] but that the ring nitrogen is a much stronger electron sink than the nitro group. The α ring protons are shifted 1.5 ppm from the β and γ protons and always appear well resolved from them. In nitrobenzene it was shown[1] that the *para* proton was nearly equivalent to *meta*, but slightly closer to *ortho*. This

TABLE I. Chemical shifts relative to H_2O (ppm) and spin-spin coupling constants (cps).

Compounds	αH	βH	γH	αCH_3	βCH_3	γCH_3	$J_{\alpha\beta}$	$J_{\beta\gamma}$
pyridine	−3.4	−2.0						
α-picoline	−3.2	−1.9		+2.6				
β-picoline	−3.2	−2.0			+3.0			
γ-picoline	−3.2	−1.7				+3.0	4.1	
αα′-lutidine		−1.7	−2.1	+2.4				6
αβ-lutidine	−3.3	−2.0		+2.5	+2.9			
αγ-lutidine	−2.9	−1.6		+2.7		+3.0	4.1	
αγ/α′-collidine		−1.7		+2.4		+2.7		
Average	−3.2	−1.7	−2.1	+2.5	+3.0	+2.9	4.1	6
Toluene		−1.58			+3.19			

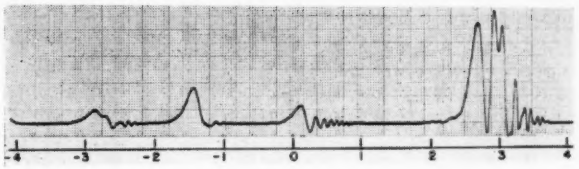

FIG. 1. Entire proton spectrum of αγ-lutidine at 30 Mc.

effect is much more pronounced in the pyridines and the alternation in charge (*o,p,m*) is clearly demonstrated.

The numerical results are given in Table I. Dissolved water was used as an internal standard, and its line is shifted +0.1 ppm from an external water standard. The values listed are based on the latter as zero. In all cases relative line intensities agree with

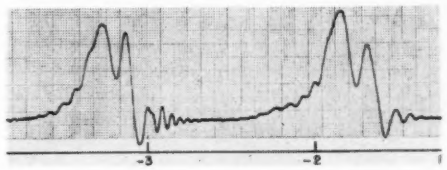

FIG. 2. Ring proton spectrum of γ-picoline at 30 Mc.

those expected from the compound structures, and it is quite simple to identify the pure isomers from NMR spectra. Note that

$$\tfrac{1}{3}(\alpha H-\beta H)=(\alpha CH_3-\beta CH_3)$$
$$\tfrac{1}{3}(\beta H-\gamma H)=(\beta CH_3-\gamma CH_3)$$

within 0.1 ppm, which would be true under the crude assumption that each proton of CH_3 loses $\frac{1}{3}$ the charge of a single proton at the same ring position.

The relative value of $J_{\alpha\beta}$ and $J_{\beta\gamma}$ are in accord with the premise that the electron density is greater in the C—C bonds *meta-para* than in *ortho-meta*.

Figure 1 shows the spectrum of αγ-lutidine. At higher resolution the doublet at −2.9 ppm due to $\alpha' H$ is well resolved showing no

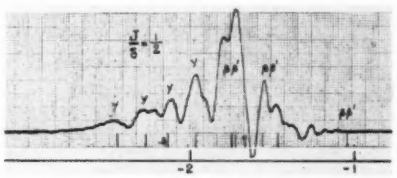

FIG. 3. Ring proton spectrum of αα′-lutidine at 30 Mc.

splitting due to βH, whereas the line at −1.6 ppm, is a superposition of split $\beta' H$ and unsplit βH.

Figure 2 shows the ring proton spectrum of γ-picoline, which is particularly simple due to symmetry, and qualitatively the same as for *p*-nitrocumene.[1]

The αα′ protons are absent in αα′-lutidine (see Fig. 3) and therefore the ββ′ protons are not split by them as in γ-picoline. The presence of the nearly equivalent γ proton presents an interesting case in which $J/\delta \sim \frac{1}{2}$. The lines predicted by Hahn and Maxwell[2]

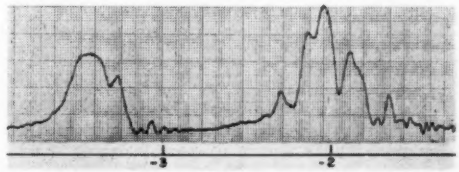

FIG. 4. Proton spectrum of pyridine at 30 Mc.

for this case are marked on the figure. The intensities are quite reasonable since the envelope of the lines must become bell shaped as J/δ increases, finally collapsing to a single line. The largest line and all others on the high-field side belong to the two $\beta\beta'$ protons, those on the low-field side to the γ proton. By this comparison with the theoretical pattern, J and δ may be determined.

In pyridine itself (see Fig. 4) there appears to be sufficient $\alpha\gamma$ coupling to prevent good resolution of the αH doublet, which is also true in all other cases except those in which the γ proton has been replaced by methyl ($\alpha\gamma$-lutidine and γ picoline). The $\alpha\gamma$ coupling also further complicates the $\beta\gamma\beta'$ line beyond that in $\alpha\alpha'$-lutidine (Fig. 3). The spectrum of $\alpha\gamma\alpha'$-collidine shows only the single $\beta\beta'$ line with no observable $\beta\beta'$ splitting, as expected from symmetry.

[1] E. B. Baker, J. Chem. Phys. **23**, 984 (1955).
[2] E. L. Hahn and D. E. Maxwell, Phys. Rev. **88**, 1077 (1952), Fig. 6. In this figure E_6 should be $(\hbar/2)(3H_0+h_1+2h_2)-J(K/2)$.

Magnitude of Diffusive Displacements in Liquids

RICHARD M. NOYES
Department of Chemistry, Columbia University, New York 27, New York
(Received July 15, 1955)

THE diffusion coefficient of a molecule is written[1]

$$D=\tfrac{1}{6}\nu\sigma^2, \tag{1}$$

where ν is the frequency of diffusive displacements and σ is the root-mean-square displacement distance. If molecules are small and do not have strong specific interactions, D is customarily somewhat larger than 10^{-5} cm^2/sec. Because no unequivocal additional information is available for evaluation of ν and σ, two rather different models of molecular motion in liquids have developed.

One model proposed by Rabinowitch[2] assumes that displacements are of the order of a molecular diameter or $3\text{–}5\times10^{-8}$ cm. Then ν is of the order of 10^{11} sec^{-1} and a molecule makes several quasi-vibrational motions in a "cage" before it is able to surmount the potential barrier hindering displacement. Eyring[3] has applied transition state theory to this model and obtained

$$D=\lambda^2\frac{kT}{h}e^{\Delta S^{\neq}/R}e^{-\Delta H^{\neq}/RT}, \tag{2}$$

where his λ is at least very nearly equivalent to σ above.

An alternative model by Collins[4] assumes continuous motion with no net potential barrier to diffusive displacements. If $\nu\sigma$ is of the order of gas-phase translational speeds, then ν is of the order of 10^{13} sec^{-1} and σ is between 10^{-9} and 10^{-8} cm.

We have previously thought the temperature dependence of diffusion coefficient indicated a potential barrier of a few kcal/mole and supported the Rabinowitch-Eyring model. However, a recent paper by Watts, Alder, and Hildebrand[5] showed that at constant pressure the temperature coefficient for self-diffusion in carbon tetrachloride corresponded to an Arrhenius activation energy of 3300 cal/mole, but at constant volume it was only 1070 cal/mole, or about $\frac{3}{2}RT$. These data imply that D increases with temperature chiefly because expansion of the liquid increases λ. If λ is independent of temperature at constant volume, the data suggest that $\Delta H^{\neq}$ (which is RT less than the Arrhenius activation energy) is only about $\frac{1}{2}RT$. This small value is intermediate between the two models but is much closer to that of Collins than of Eyring.

Studies of diffusion-controlled reactions should be helpful, although rate data as such are not very useful. Thus, the rate of recombination of iodine atoms requires that diffusive displacements be 0.2 molecular diameter or larger, but it does not provide the support for the Rabinowitch-Eyring model we once thought.[6] Even the change of reactivity of a molecule with time does not contribute to the question; a detailed theoretical treatment will be submitted for publication soon.

However, studies of diffusive recombination of original partners offer considerable promise. Roy, Williams, and Hamill[7] concluded from such studies that diffusive displacements were 0.3–0.5 molecular diameter, and new work[8] suggests figures as low as 0.2 diameter in some cases. The data of Lampe and Noyes[9] on quantum yields for photodissociation of iodine indicated a considerable increase with temperature. The excess kinetic energy of the dissociating atoms was so large compared to kT that small changes in temperature could hardly have had much influence on the average separation at which random diffusion started. If diffusive displacements were of the order of a molecular diameter, it is hard to explain the temperature dependence of the escaping tendency, but our observations are consistent with a small average displacement that increases with temperature.

We believe that the proper choice of model is fundamental to an understanding of transport processes in liquids and that a decision will be possible from studies of diffusive recombination reactions now going on in several laboratories. Studies of temperature coefficients at constant volume (instead of constant pressure) should be of particular value in the decision.

This work was supported in part by the U. S. Atomic Energy Commission under Contract No. AT(30-1)-1314.

[1] A. Einstein, Ann. Physik **17**, 549 (1905).
[2] E. Rabinowitch, Trans. Faraday Soc. **33**, 1225 (1937).
[3] Glasstone, Laidler, and Eyring, *The Theory of Rate Processes* (McGraw-Hill Book Company, Inc., New York, 1941), p. 524.
[4] F. C. Collins and H. Raffel, J. Chem. Phys. (to be published).
[5] Watts, Alder, and Hildebrand, J. Chem. Phys. **23**, 659 (1955).
[6] R. M. Noyes, J. Chem. Phys. **22**, 1349 (1954).
[7] Roy, Williams, and Hamill, J. Am. Chem. Soc. **76**, 3274 (1954).
[8] W. H. Hamill (private communication).
[9] F. W. Lampe and R. M. Noyes, J. Am. Chem. Soc. **76**, 2140 (1954).